

AD-A199 171

DTIC FILE COPY

2

AGARD-CP-427

AGARD-CP-427

# AGARD

ADVISORY GROUP FOR AEROSPACE RESEARCH & DEVELOPMENT

7 RUE ANCELLE 92200 NEUILLY SUR SEINE FRANCE

AGARD CONFERENCE PROCEEDINGS No.427

## Behaviour and Analysis of Mechanically Fastened Joints in Composite Structures

DISTRIBUTION STATEMENT A

Approved for public release  
Distribution Unlimited

DTIC  
ELECTE  
JUL 28 1988  
S Co D

NORTH ATLANTIC TREATY ORGANIZATION



DISTRIBUTION AND AVAILABILITY  
ON BACK COVER

88

4

AGARD-CP-427

NORTH ATLANTIC TREATY ORGANIZATION  
ADVISORY GROUP FOR AEROSPACE RESEARCH AND DEVELOPMENT  
(ORGANISATION DU TRAITE DE L'ATLANTIQUE NORD)

AGARD Conference Proceedings No.427  
BEHAVIOUR AND ANALYSIS OF MECHANICALLY FASTENED  
JOINTS IN COMPOSITE STRUCTURES

Accession For	
NTIS GRA&I	<input checked="" type="checkbox"/>
DTIC TAB	<input type="checkbox"/>
Unannounced	<input type="checkbox"/>
Justification	
By	
Distribution	
Availability Codes	
Dist	Availability and/or Special
A-1	



Papers presented at the Structures and Materials Panel Specialists' Meeting held in Madrid, Spain on 27-29 April 1987.

## THE MISSION OF AGARD

According to its Charter, the mission of AGARD is to bring together the leading personalities of the NATO nations in the fields of science and technology relating to aerospace for the following purposes:

- Recommending effective ways for the member nations to use their research and development capabilities for the common benefit of the NATO community;
- Providing scientific and technical advice and assistance to the Military Committee in the field of aerospace research and development (with particular regard to its military application);
- Continuously stimulating advances in the aerospace sciences relevant to strengthening the common defence posture;
- Improving the co-operation among member nations in aerospace research and development;
- Exchange of scientific and technical information;
- Providing assistance to member nations for the purpose of increasing their scientific and technical potential;
- Rendering scientific and technical assistance, as requested, to other NATO bodies and to member nations in connection with research and development problems in the aerospace field.

The highest authority within AGARD is the National Delegates Board consisting of officially appointed senior representatives from each member nation. The mission of AGARD is carried out through the Panels which are composed of experts appointed by the National Delegates, the Consultant and Exchange Programme and the Aerospace Applications Studies Programme. The results of AGARD work are reported to the member nations and the NATO Authorities through the AGARD series of publications of which this is one.

Participation in AGARD activities is by invitation only and is normally limited to citizens of the NATO nations.

The content of this publication has been reproduced  
directly from material supplied by AGARD or the authors.

Published March 1988

Copyright © AGARD 1988  
All Rights Reserved

ISBN 92-835-0431-3



Printed by *Specialised Printing Services Limited*  
40 Chigwell Lane, Loughton, Essex IG10 3TZ

## PREFACE

The rapidly increasing use of composite structures in NATO aerospace has intensified interest in methods of strength, and life analysis. At the same time the introduction of new tough resins has increased the static strength of composite joints with implications for the corresponding strength in fatigue. A number of NATO nations have built up data bases and developed methods for strength and life analysis; in order to take advantage of these resources the Structures and Materials Panel held a Specialists' Meeting, in conjunction with the 64th Panel Meeting, in Madrid, Spain on 27th—29th April 1987, under the chairmanship of Professor Vittorio Giavotto, to provide a focus for methods of analysis and the identification of research needs. This volume contains the papers presented at this Specialists' Meeting.

\* \* \*

L'emploi de plus en plus fréquent de matériaux composites dans le cadre des activités aérospatiales de l'OTAN est à l'origine d'un regain d'intérêt dans les méthodes d'analyse de la résistance et de la durée de vie des composants. Parallèlement, l'arrivée de nouvelles résines hautement résistantes a eu pour effet d'augmenter la résistance statique des joints composites; phénomène non sans importance pour la résistance en fatigue correspondante. Un certain nombre de pays membres de l'OTAN ont constitué des bases de données et ont élaboré des méthodes pour l'analyse de la résistance et de la durée de vie des composants. Souhaitant tirer profit de ces moyens, le Panel des Matériaux et Structures a organisé une réunion de spécialistes à l'occasion du 64ème Réunion du Panel à Madrid en Espagne, le 27—29 avril 1987, présidée par le professeur Vittorio Giavotto, afin d'orienter les méthodes d'analyse et de permettre l'identification des besoins en matière de recherche. Le présent volume présente des présentations faites lors de cette réunion de spécialistes.

## CONTENTS

	Page
<b>PREFACE</b>	iii
<b><u>SESSION I</u></b>	
<b>LITERATURE REVIEW ON THE DESIGN OF MECHANICALLY FASTENED COMPOSITE JOINTS</b> by C.Poon	1
<b>COMPARISON OF EXPERIMENTAL RESULTS AND ANALYTICALLY PREDICTED DATA FOR DOUBLE SHEAR FASTENED JOINTS</b> by J.Bauer and E.Menale	2
<b>RECENT STUDIES ON BOLTED JOINTS IN COMPOSITE STRUCTURES</b> by V.B.Venkayya, R.L.Ramkumar, V.A.Tischler, B.D.Snyder and J.G.Burns	3
<b>DAMAGE GROWTH IN COMPOSITE BOLTED JOINTS</b> by V.Giavotto, C.Caprile and G.Sala	4
<b>STRESSES IN PINLOADED ANISOTROPIC PLATES</b> by Th. de Jong	5
<b><u>SESSION II</u></b>	
<b>AN ANALYSIS METHOD FOR BOLTED JOINTS IN PRIMARY COMPOSITE AIRCRAFT STRUCTURE</b> by I.Eriksson	6
<b>STRENGTH ANALYSIS OF MECHANICALLY FASTENED COMPOSITE STRUCTURES</b> by R.L.Ramkumar, E.S.Saether, K.Appa and V.B.Venkayya	7
<b>TYPICAL JOINTS IN A WING STRUCTURE</b> by D.Rose, M.Rother and H.Schelling	8
<b>MISE AU POINT D'ELEMENTS DE FIXATION SPECIFIQUES POUR ASSEMBLAGES DES STRUCTURES COMPOSITES</b> par L.Raymond	9
<b>A STUDY TO OPTIMIZE THE CFRP-AI MECHANICAL JOINT IN ORDER TO REDUCE THE ELECTRICAL RESISTANCE</b> by F.Cipri and M.Pelosi	10
<b><u>SESSION III</u></b>	
<b>TEST SPECIMENS FOR BEARING AND BY-PASS STRESS INTERACTION IN CARBON FIBRE REINFORCED PLASTIC LAMINATES</b> by M.B.Snell and G.P.Burkitt	11
<b>Paper 12 withdrawn</b>	
<b>BEARING-BYPASS LOADING ON BOLTED COMPOSITE JOINTS</b> by J.H.Crews, Jr and R.A.Naik	13
<b>BOLTED JOINTS IN COMPOSITES PRIMARY STRUCTURES</b> by A.Ruiz	14
<b>THE STATIC STRENGTH OF BOLTED JOINTS IN FIBRE REINFORCED PLASTICS</b> by F.L.Matthews	15
<b><u>SESSION IV</u></b>	
<b>MECHANISM OF SINGLE SHEAR FASTENED JOINTS</b> by J.Bauer	16

	<b>Page</b>
<b>JOINING OF CARBON FIBER COMPOSITE WITH FASTENERS</b> by S. Pagliuso	<b>17</b>
<b>ENTURES BOULONNEES EN MATERIAUX COMPOSITE CARBONE: COMPARAISON ENTRE MONTAGES A INTERFERENCE ET MONTAGE A JEU</b> par D. Chaumette	<b>18</b>
<b>EFFECT OF ENVIRONMENT AND IMPROVEMENT MEASURES ON STATIC AND FATIGUE STRENGTH OF BOLTED CFRP-JOINTS</b> by J.J. Gerharz and H. Huth	<b>19</b>
<b>STIFFNESS AND RESIDUAL STRENGTH VARIATIONS ON MECHANICAL JOINTS IN FRP SPECIMENS IN CYCLING LOADING</b> by C. Caprile and G. Sala	<b>20</b>
<b>BEHAVIOUR OF MECHANICALLY FASTENED JOINTS IN ADVANCED COMPOSITES</b> by C. Poon and R. Gould	<b>21</b>

## LITERATURE REVIEW ON THE DESIGN OF MECHANICALLY FASTENED COMPOSITE JOINTS

by

C. Poon

Structures and Materials Laboratory  
National Aero-nautical Establishment  
National Research Council Canada  
Ottawa, Ontario, K1A 0R6

### SUMMARY

This report presents a literature review of the state-of-the-art analytical and experimental methodologies adopted in the aerospace industry for the design of mechanically fastened joints in composite structures. Results and conclusions obtained from the published literature relating to the effects of critical parameters, which include composite material system, fastener configuration and joint geometry, on the mechanical behaviour and failure modes of composite mechanically fastened joints are discussed. Further research required to improve the design of composite mechanically fastened joints is identified as a result of this review.

### 1.0 INTRODUCTION

The purpose of this literature review is to assess the state-of-the-art analytical and experimental methodologies for the design of composite mechanically fastened joints. This review aims at providing a basis for identifying further research in these areas.

Joints that require mechanical fasteners such as bolts, rivets or pins to connect two or more parts in a structure where the transfer of loads is provided by the fasteners are generically described as mechanically fastened joints. This is in contrast to adhesively bonded joints where the connecting and load transfer medium is the adhesive layer. Mechanically fastened joints are required in cases where the need for component disassembly is entailed.

One of the more challenging aspects of composite mechanically fastened joints is that the well-established design procedures for metal joints, that are based on years of experience with isotropic and homogeneous materials, have to be changed in order to accommodate the anisotropic and nonhomogeneous properties of composite materials. Also, advanced composites have practically none of the forgiving capabilities of metals which yield to redistribute loads and thus reduce the sensitivity to local stress concentrations. The inherent matrix weaknesses of composites, especially organic matrix composites, render the joints susceptible to interlaminar shear failures as a result of matrix stresses.

Analytical procedures for the prediction of static strength and fatigue life of composite mechanically fastened joints are presented in Section 2. The application of finite element and two-dimensional elasticity methods in stress analyses and the adoption of failure criteria in static strength predictions are discussed. Current methods for fatigue life prediction are also discussed.

Experiments investigating the effects of important parameters on the mechanical performance of composite mechanically fastened joints are presented in Section 3. Of principal interest in the results discussed are stress concentrations at the fastener hole as a function of fastener configurations and material parameters, and the relationship between failure modes and joint configuration, fastener pattern, lay-up, etc. The special topic of environmental effects is not included in this review.

Further research in improving the design of composite mechanically fastened joint is discussed in the last section. This includes the analytical effort required to improve the accuracy and reliability of both static and fatigue strength prediction methodologies as well as the experimental work required to provide a data base which is essential for the application of advanced high strain/tough resin composites. Also, the development of failure models based on physical damage phenomena is needed for the prediction of delamination and gross bearing failure modes.

### 2.0 ANALYTICAL METHODOLOGIES FOR STRENGTH PREDICTIONS

A typical analytical procedure for the evaluation of the static strength of composite mechanically fastened joints involves four basic steps: first, the load distribution in the vicinity of the fastener holes is determined by an overall analysis of the structural component; second, the fastener load and the by-pass load at individual fastener holes are determined; third, the detailed stress distribution in the vicinity of an individual fastener hole is evaluated based on the fastener load and by-pass load; and fourth, the joint strength is assessed by applying appropriate material failure criteria. These analytical steps for composite bolted joint strength evaluation are illustrated in Figure 1. Methodologies adopted in each of the steps are discussed in the following sub-sections.

#### 2.1 Overall Structural Analysis

An overall structural analysis to determine the internal load distributions is performed, generally, by finite element methods. Because of economic limitations, it is common practice for a component finite element model to consider overall geometric and material properties to determine stiffness parameters and to exclude fastener flexibility under the assumption that the contributions of bolts and local joint structures to the overall structural deformation are quite small (1). When the bolt flexibility is considered to have an effect on the overall response to loads, the inclusion of fastener effects in the general model is necessary for accurate analysis (2,3). In Reference 2, the finite element analysis of the Space Shuttle payload bay doors clearly demonstrated that the analysis of joint behaviour was required to be an integral part of the overall structural analysis. Also Reference 3 shows that the flexibility of the fasteners was required in the local root area of the overall finite element model of the B-1 horizontal stabilizer. Baumann (4) presented a method incorporating the effects of fastener representation. He discussed various modelling techniques for the fastener effect and demonstrated excellent correlation with test results by allowing the fastener (beam elements) end constraints to be flexible rather than rigidly fixed against rotation.

## 2.2 Analysis of Load Distribution at Fastener Hole

The overall structural analysis discussed in the previous sub-section can, in most cases, even though fasteners are not modeled, provide an estimation of loads acting on complex joints. One dimensional analytical methods for redundant structures (5) are commonly used to determine the load carried by each row of fasteners in a complex joint. These methods include analytical closed form procedures for simple lap-joint configurations, and numerical procedures capable of handling more complex geometries and joints with multiple shear faces. Engineering idealizations employed in one dimensional analysis are based upon gross assumptions regarding the plate flexibility between successive fastener rows, the bolt flexibility due to shear and bending effects, and the local flexibility associated with the complex stress and deflection pattern in the immediate vicinity of the hole (5,36). As illustrated in Figure 2, rows of fasteners are represented by fastener shear elements in the structural joint idealization.

In order to determine individual fastener loads accurately, it is important to account for the contribution of each fastener to joint flexibility. This contribution is dependent upon fastener stiffness, joint member stiffness, and load eccentricity. Joint flexibilities, which are obtained experimentally from load-deflection tests upon single fastener specimens, are required for the analysis. In metals, this type of data is available for a wide variety of fasteners, sheet materials and thicknesses (6). In composites, however, this data is not as prevalent and is usually generated on a "need" basis for specific conditions. When data is not available, it is common to obtain estimates of composite joint flexibility by comparison to existing isotropic metal data or by calculations using formulae developed for thin sheet metals (3,7). An extensive experimental investigation was performed by Huth (111) to determine the fastener flexibility for a wide range of joints of practical interest. A formula for predicting load transfer in multiple-row joints based on fastener flexibility was derived from test results. It can be used with a variety of fastener systems and joint materials which include graphite/epoxy systems to improve the prediction of stress and fatigue performance in mechanically fastened joints.

## 2.3 Effect of Friction on Bolted Joint Load Distribution

The effect of friction is commonly ignored in the analytical work published in the literature. Friction between plate surfaces can, however, significantly affect joint bolt load distribution. Experimental work by Wittmeyer and Smode (8) and the survey report by Munse (9) both indicate that the clamp-up force resulting from bolt tightening relieves the joint load transmitted by fastener shear. However, in most design situations, this beneficial effect of friction in relieving fastener load is conservatively ignored because it is felt that the bolt torque cannot be maintained due to the viscoelastic property of resin-based laminates which allows bolt clamp-up relaxation (108) to occur during the life of the structure.

In fatigue tests using aluminium single-shear dog-bone specimens with steel Huck rivets, Hooson and Baker (10) reported that failures of specimens occurred not at the fastener hole where the stress concentration is highest, but outside the region of peak clamp-up pressure between plates. Significant fretting was observed in the region of failure. This observation led to the belief that failure was the result of the propagation of cracks which were initiated by a fretting mechanism.

In composites, this contact problem in the faying plate surfaces is further complicated by the fact that the behaviour of friction and wear is a function of varying fiber orientations with respect to the sliding direction. Sung and Suh (11) measured the friction coefficient and wear volume of composites as a function of sliding distance for three different fiber orientations, perpendicular, transverse and longitudinal to the sliding direction (see Figure 3). As illustrated in Figure 4, which presents their results for graphite epoxy composite (Thornel 300/SP-288), both wear and friction coefficients were a minimum when the fiber orientation was normal to the sliding surface, and both wear and friction coefficients were a maximum when the sliding was transverse to the fiber axis. Different failure modes for different fiber orientations with respect to sliding direction were observed in their experiments (Figure 3).

Sandifer (106) investigated the effect of fretting fatigue on graphite/epoxy composites and found that fretting has no significant effect on the fatigue life of graphite/epoxy material when fretted against aluminium, titanium, or graphite/epoxy of the same type. Fatigue life was actually found to be increased by a factor of four under tension-tension cyclic loading due to the clamping of the fretting pad in the test section of the unnotched specimen. It was noted that, during cycling testing, the specimens began to delaminate in the thickness plane between the grips and clamped pads. However, such delamination never occurred in the clamped regions. This observation led to the conclusion that the pads act as a stabilizing point holding the plies together and thus a longer fatigue life is achieved. Sandifer further mentioned that the application of a common test technique where buckling guides or stabilizing fixtures are mounted at specimen mid-point may lead to non-conservative fatigue life results.

The effect of friction in the faying plate surfaces can be included in the stress analysis if the clamping is known. Both finite difference and finite element methods have been applied successfully in calculating the clamp-up pressure for isotropic plates (12, 13, 14). A typical idealization of a bolted joint used to determine the contact pressure between plates is illustrated in Figure 5. The effects of clamping pressure and lateral constraint were investigated experimentally by Stockdale and Matthews (15) on glass/epoxy and by Collings (16) on carbon/epoxy. It was concluded that increasing the bolt torque increases the bearing strength. Semi-empirical equations, which account for friction effects and lateral constraints at the bolt hole, were established by Collings (17) to predict bearing strength and failure mode of carbon fiber-reinforced plastics.

The through-thickness effects for a multi-orientation laminate as a result of fastener/plate interaction are very complicated because the coefficient of friction varies through the thickness, from ply to ply, at the edge of the hole. Also, under compressive and frictional loading, complicated failure modes, such as fibers debonding from matrix and fiber buckling, are encountered. To treat these effects analytically, three dimensional methods and suitable failure criteria are required.

## 2.4 Detailed Stress Analysis and Static Strength Prediction

The detailed stress or strain distribution in the vicinity of the loaded bolt hole in a composite joint is determined by means of finite element methods, elastic anisotropic analysis based on complex variable formulation and fracture mechanics analysis. The prediction of static strength and failure mode is accomplished by the application of anisotropic material failure criteria based on unidirectional laminate properties.

The failure of a composite laminate is assessed on a ply-by-ply basis. At the edge of the fastener hole where a high stress concentration is present, strength prediction is based on stresses at a "characteristic dimension" from the edge of the hole (18). In this way, the non-linear material behaviour in the region immediately surrounding the fastener hole is avoided. This approach, as illustrated in Figure 6, has been commonly applied in the failure analysis of composite bolted joints (19,20). The establishment of the "characteristic dimension" is based on experimental data obtained by test procedures discussed in References 19-21.

Failure modes in composite bolted joints can be very complex and quite different from those of metal joints because composites exhibit anisotropic properties, lack of ductility and inherent interlaminar weakness. Various failure modes for composite bolted joints are illustrated in Figure 7. Many failure criteria have been developed essentially by modifying isotropic criteria to allow for anisotropic effects in predicting these failure modes and strengths of composite bolted joints. In developing these failure criteria, sufficient arbitrary parameters are introduced so that various failure modes can be incorporated.

#### 2.4.1 Static strength failure criteria

Sandhu (22) published a survey of failure criteria for anisotropic materials in 1972. He broadly categorized these criteria according to their capability to account for failure mode interactions. Failure criteria that do not account for failure mode interactions include maximum stress (23), maximum strain (24), and maximum shear criteria (25). In applying these criteria, failure is precipitated when any one of the longitudinal, transverse, and shear stresses/strains exceed the material limits determined by tests. In the other category of failure criteria where failure mode interactions are accounted for, expressions mainly of a quadratic form that yield a smooth and continuous quadratic failure envelope in each load quadrant, are included. The expressions are either generalizations of Von Mises' criterion, such as those developed by Hill (26), Tsai (27) and Hoffman (28), or have been developed explicitly in quadratic form using the stress tensor approach which satisfies the invariant requirements for coordinate transformation, such as the Tsai-Wu criterion (29). Tennyson (30) adopted the cubic form of the stress tensor polynomial criterion to predict failure strength of graphite/epoxy under biaxial loads and obtained more accurate predictions than with the quadratic form. Experimental procedures required to obtain these parameters for various failure criteria are discussed in Reference 31.

#### 2.4.2 Static strength prediction based on fracture mechanics

Eisenmann (32) established a bolted joint static strength prediction model based on fracture mechanics for composite materials. The failure criterion is:

$$K_i^2 = K_0^2$$

where  $K_i$  is the Mode I stress intensity factor at location  $i$  on the fastener hole boundary and  $K_0$  is the corresponding

fracture toughness. This fracture mechanics concept is similar to the "characteristic dimension" concept of Whitney and Nuismer (18) except that the characteristic dimension,  $a_i$ , is taken as the length of a through crack extending radially outward from location  $i$  on the hole boundary. The determination of  $a_i$  is based on laminate strength and fracture toughness obtained by tests discussed in Reference 33. Eight potential crack initiation positions on the hole boundary (1-8) are selected based on an examination of many failed joint test specimens. Values of laminate tensile strength and Mode I fracture toughness at these locations are determined by tests using tensile coupons and edge-notched beam specimens fabricated in a manner such that they represent laminate properties in the direction tangential to the hole boundary. Once the laminate tensile strength and Mode I fracture toughness have been determined, the characteristic dimension,  $a_i$ , can be calculated for each of the eight selected locations by the following equations:

$$a_i = \frac{1}{\pi} \left( \frac{K_0^2}{\sigma_{uh}^2} \right)^2$$

The established dimension,  $a_i$ , is then used to calculate the Mode I stress intensity at each of the eight locations and for each of the five specific load cases that consist of the tension loads in the X and Y directions, the bolt bearing loads in the X and Y directions and the shear loads, as illustrated in Figure 8 for location  $i = 2$ . The Mode I stress intensity factor for the general load case at location  $i$  is obtained by adopting linear superposition of all five Mode I stress intensity factors for specific load cases.

The validity of this fracture mechanics model has been verified by successful correlation of experimental results. Experimental data consisting of measured failure loads and observed failure locations from a series of forty-eight static tensile tests were used (32). The application of this model, however, is limited by the requirement of an extensive data base and is only valid for tensile strength predictions.

#### 2.4.3 Static strength prediction using finite element method

The two dimensional finite element model is by far the most common method in composite mechanically fastened joint analysis (34-49). The major limitation of two dimensional analyses is that three dimensional effects, such as thickness deformation related to bearing failures, interlaminar shear resulting from ply-to-ply displacement incompatibilities, through-the-thickness friction effects between the fastener and the hole, and lateral constraint at the fastener hole as a result of clamping of washer and nut face on the plates that are joined together, are not accounted for. However, in most design situations, two-dimensional methods are chosen over three-dimensional ones because of their relative simplicity and economy.

A two-dimensional finite element method solution predicting bolted joint strength was published by Waszczak and Cruse (34) in 1971. A cosine-distributed radial pressure acting along the semi-circular boundary was used to simulate the load from a rigid and frictionless pin. Orthotropic laminates, which were mid-plane symmetric, were considered. The maximum stress criterion, the maximum strain criterion and the Tsai-Hill distortional energy failure criterion were applied to predict the laminate failure strength and failure mode. For cases where lay-ups were  $\pm 45^\circ$ , this analysis resulted in failure strength predictions which were 30% conservative.

Chang et al. (35, 36) investigated the same problem using similar techniques. Improved correlations in failure strength and failure mode with experimental results were obtained by adopting the Yamada-Sun shear strength failure

criterion (37) in conjunction with a proposed failure hypothesis (36) that predicts failure based on stresses at a characteristic distance from the pin-hole interface in order to minimize three-dimensional effects. Wong and Matthews (38) used the FINEL code to calculate the strains at the pin-loaded holes of mid-plane symmetric and balanced laminates. The layers of a laminate were treated as being homogeneous and orthotropic. One half of the joint was modelled based on symmetry. The load applied by the pin was represented by a sinusoidally distributed pressure as well as by a uniform vertical displacement at the hole boundary on the loaded side of the hole. Only insignificant differences were found between these two techniques of pin load representation. Experimental correlations of results are included in the investigation.

An alternative technique to simulate the frictionless rigid pin joint is to apply zero radial displacements along the semi-circular boundary and to apply force at the far end (39,41,42). Agarwal (39) used this technique and the NASTRAN code to determine the stress distribution around the fastener hole of a double-shear bolt bearing specimen. The composite plate, which was assumed to be orthotropic and mid-plane symmetric, was idealized by 284 CQMEMI elements which are isoparametric membrane elements and do not include any bending. The plate was assumed to be symmetric about the X axis and only half of the plate was modelled (see Figure 9). The Grimes-Whitney (maximum strain) first ply failure criterion (40) was applied to predict the unnotched laminate strength and the Whitney-Nuismer average stress criterion (19,20) was applied to predict the mechanically fastened joint strength and failure mode. Soti (41) used the same NASTRAN code and the boundary conditions but adopted the Tsai-Wu tensor polynomial failure criterion (29) for the strength analysis of pin-loaded plate. The ultimate laminate failure strength was based on the last ply failure stress. The results obtained by both investigations were conservative by a factor of two for lay-ups which were predominately 45° when compared with corresponding experimental results.

York et al. (42) used the Structural Analysis Program SAP V and the modified "point stress" failure criterion (43) to predict the net tension strength of composite mechanically fastened joints. Application of the modified "point stress" failure criterion requires the empirical determination of two notch sensitivity parameters,  $m$  and  $c$ , for a particular material system and laminate configuration. Accurate strength predictions were achieved based on experimental net tension strength data for Hercules AS/3501-6 graphite/epoxy with a laminate configuration of (45/0/-45/02/-45/0/45/02/90).

Crews et al. (44) presented another technique to simulate frictionless pin loading in their two-dimensional finite element analysis where the pin was also modelled. The pin was loaded at its center and was connected to the laminate by short, stiff spring elements which had no transverse stiffness and as a result they transferred only radial loads and thereby produced the desired frictionless interface. An iterative procedure was adopted to determine the contact boundary between the pin and the hole. When a spring was computed to have a tensile force, its radial stiffness was set to zero and the analysis was repeated until convergence was reached. Stress concentration factors, based on nominal bearing stress, for finite size orthotropic laminates of different lay-ups and geometries were established using this analytical technique.

The above methods ignore the effects of friction and the length of contact of the fastener with the boundary of the hole in the laminate. Oplinger (45,46) adopted an accurate treatment of boundary conditions at the fastener hole by modelling fastener/plate interactions in his finite element analysis. This treatment involves the use of a displacement boundary condition to represent the effect of the fastener moving against the hole boundary. The use of displacement conditions in the contact region leads to successful modelling of changes in contact length with increasing by-pass load, a condition which exists in a complex joint with multiple rows of fasteners. The analytical results showing the effect of friction on radial and shear stress distributions around the fastener hole are given in Figure 13. A departure from the commonly assumed half-cosine radial stress distribution as a result of friction is noted in Figure 10.

Wilkinson et al. (47) used an incremental finite element method to determine the stresses and strains around pin-loaded holes in orthotropic plates. The numerical solution provided by the analysis accounts for friction along the contact surface between the pin, which is assumed rigid, and the plate, and determines the region of slip and nonslip. This analytical method was later extended to provide numerical solutions for multiple-bolted joints (48). The effects of variations in friction, material properties, load distribution among the bolts and bolt/plate contact were considered. A condition of nonslip existed at a point on the hole boundary if:

$$\mu \sigma_r > \tau_{\theta}$$

where  $\mu$  = coefficient of friction,  $\sigma_r$  = radial stress, and  $\tau_{\theta}$  = tangential shear stress. An incremental loading with an

iterative procedure was performed to obtain the results at the final specified load level. The effect of friction on the radial stress between the bolt and the contacting hole boundary of a wooden joint obtained from Reference 48 is presented in Figure 11. This figure shows that the total absence of friction ( $\mu = 0$ ) allows the relatively low modulus wood to "wrap" around the rigid pin and thereby distribute the pressure more evenly. For stiffer orthotropic materials, such as glass composite, a change in the contact coefficient of friction from  $\mu = 0.7$  to  $\mu = 0.4$  has little effect on the radial stress on the boundary of the hole (Figure 12). However, this relative insensitivity of the stress distribution as shown in Figure 12 to moderate changes in friction is fortuitous since, even at a fixed position around a loaded pin, the coefficient of friction for a stacked fiber-reinforced laminate could vary from ply to ply depending on the particular ply's orientation relative to that of the pin in the contact region. The treatment of the through-the-thickness friction effect requires very complicated three-dimensional analysis. No work has been published in this area.

The effects of pin elasticity, clearance, and friction on the stress distributions around a hole in a pin loaded orthotropic plate were investigated by Hyer and Kiang (112). Numerical results, computed by using two-dimensional techniques for a (0/24/3) graphite/epoxy laminate, indicated that pin elasticity does not have a significant effect on stress distribution while pin clearance influences the arc of contact and the radial stress. As a result of a reduced arc of contact due to increased clearance, the radial stress was found to be higher. The effect of friction was found to decrease the bearing stress and increase the hoop stress. Both the no-slip region and the contact angle were found to increase with friction.

In a two-dimensional, elasto-plastic finite element analysis, Tsujimoto and Wilson (113) investigated the effect of including frictional forces along the fastener hole interface on the strength of composite bolted joints. It was found that for a conventional graphite/epoxy material, the net tensile failure is relatively insensitive to friction effects while

bearing and shearout failures are sensitive. The failure strength for the bearing and the shearout mode was found to increase when the coefficient of friction is increased. However, when comparing predicted results with experimental results, a condition of no friction gave the best correlation. Therefore this condition was used in subsequent elasto-plastic analysis. The special capability of this incremental elasto-plastic analysis is that it provides the details of the damage progression and employs a cumulative damage concept to predict failure. In a separate report, Wilson and Tsujimoto (114) presented a damage mapping study performed by using a laminate deply technique developed by Freeman (115). After a quasi-isotropic laminate was loaded to ultimate tensile strength by a pin in a double lap joint, it was deplyed and the damage was documented photographically. The damage maps determined in this way were found to correlate well in a qualitative sense with those predicted using the elasto-plastic analysis. The development of quantitative failure criteria based on damage mechanics is being pursued by exploiting the present capability of the elasto-plastic model in an extension of the research described in Reference 113.

In order to predict bearing and delamination failure and to account for the effect of clamping pressure created by bolt torque in composite mechanically fastened joints, the distribution of stresses around the loaded hole in three directions has to be evaluated. Matthews et al. (89) performed a three-dimensional finite element analysis on a single composite bolted joint by using a new element derived from a standard 20-noded, isoparametric 'brick' element. This modified element can represent several layers of the composite without serious loss of accuracy. The results for three clamping cases were discussed: (1) Pin-loaded hole case where lateral constraint is excluded; (2) finger-tight washer case where lateral constraint is provided; and (3) bolted joint case where a compressive displacement to all the surface nodes under the washer is imposed. The effect of friction was ignored in the analysis. It was observed that when the laminate is loaded via a bolt with finger-tight washers, the most noticeable change from the pin-loaded case is a reduction of the through-the-thickness tensile stress. This observation was consistent with the increase in failure load obtained experimentally. For the bolt loading with a fully clamped washer, a significant increase in the direct stress,  $\sigma_{zz}$ , under the washer and the interlaminar shear stress,  $\sigma_{zx}$ , at the edge of the washer in the outer plies, was noticed. Again this is consistent with experimental results where failure was found to occur by delamination at the washer edge. A suitable failure criterion has not been combined with the stress analysis to predict the actual failure loads and failure modes.

#### 2.4.4 Static strength prediction using elastic anisotropic analysis

These methods are principally formulated from two-dimensional anisotropic elasticity theory (50). In these methods, the stress distributions around a hole in an infinite orthotropic laminate are determined and various ways of correcting these stresses for finite laminate widths and lengths have been applied (51,52). There are two common techniques of modelling fastener radial load distributions: (1) a radial stress boundary condition varying in a cosine distribution (52,53,55) and (2) a radial displacement boundary condition corresponding to rigid displacements of the fastener coupled with a solution of the associated contact problem (58,59). In most cases, fastener frictional shear forces at the hole boundary have been ignored.

Waszczak and Cruse (53) solved the problem of an infinite anisotropic plate containing a circular cut-out. The plate was loaded by the bolt load, which was represented by a cosine distribution of normal stress and was subjected to a uniform stress field caused by tension loads applied at two far ends of the plate. The method of superposition was used to generate the solution to the problem of interest by combining two infinite plate solutions. One case contained the bolt loading only while the other case contained the tension loading only. A series solution based on the theory of anisotropic elasticity was derived for the bolt loading case. The solution to the case of a plate with a hole under tension loading was obtained from Reference 54. Both infinite plate solutions for the two cases were corrected for the effects of finite specimen size using anisotropic correction factors generated by Boundary Integral Equation methods (51) prior to their superposition. Pin/plate interaction was assumed to be frictionless. It was noted that the use of correction factors to modify the infinite plate solutions produced a stress field which no longer strictly satisfies overall equilibrium requirements.

The maximum stress, the maximum strain and the Tsai-Hill criteria were considered for static joint strength predictions based on a first ply failure hypothesis. Conservative predictions of failure loads were obtained. The degree of conservatism was found to be a function of specimen lay-ups varying from 2% for a (0g/45°) boron-epoxy laminate to 33% for a (45°) boron-epoxy laminate where large shear deformation occurred. Prediction of failure locations was found to be satisfactory.

De Jong (52) presented a solution of the stress distribution around a pin loaded hole in an orthotropic plate. The approach used by De Jong was similar to that used by Waszczak and Cruse (53) except that the normal stresses carrying over the fastener loading force on the boundary of the hole were represented by a sine series where the coefficients of this series were calculated from the boundary conditions for the displacements of the loaded section at the edge of the hole. Waszczak and Cruse (53) only used the first term of the cosine series as a stress boundary condition and the possibility of determining the normal edge stresses in relation to material properties by means of a displacement boundary condition was not exploited. A superposition technique was then adopted to estimate the stresses in the plates of finite widths from infinite plate results. The prediction of joint strength by failure criteria was not investigated. One of the conclusions reached by De Jong was that although the pin has a neat fit in the hole, there is a clearance, resulting from elastic deformations of the plate material, not only between the pin and the unloaded side of the hole, but also between the pin and a small region of the loaded side as well.

Garbo and Ogonowski (55,56) developed a Bolted Joint Stress Field Model (BJSFM) which utilizes two-dimensional elastic anisotropic theory to determine laminate stress distributions around an unloaded or loaded fastener hole in orthotropic materials. The principle of elastic superposition was used to obtain laminate stress distributions due to the combined bearing and by-pass loading. Loaded hole analysis was performed by specifying a radial stress boundary condition varying as a cosine function over half of the hole. The stress solutions obtained are valid for mid-plane symmetric laminates only. Strain distributions are calculated using material compliance constitutive relations. Laminate compliance coefficients were derived from classical lamination plate theory (57) with unidirectional material elastic constants, ply angular orientations, and ply thicknesses. Strains for individual plies along lamina principle material axes were calculated using coordinate transformations. Finite width effects were accounted for by the superposition technique adopted by De Jong (52). To minimize the effect of nonlinear material behaviour at the hole boundary, the "characteristic dimension" hypothesis of Whitney and Nuismer (18) has been adopted in BJSFM. Laminate failure was predicted by comparing elastic stress distributions with material failure criteria on a ply-by-ply basis. Various material failure criteria, such as Tsai-Hill (27), Hoffman (28), Tsai-Wu (29), maximum stress (23), and maximum

strain (24), were incorporated in the BJSFM. Analytical predictions of joint strengths provided by the BJSFM have been extensively calibrated against experimental results (55,56).

Oplinger and Gandhi (58) presented the results of stress distributions around a hole in a pin loaded orthotropic plate by using a two-dimensional anisotropic elastic analysis which employed a least-squares boundary collocation scheme. The mode of interaction between the pin and the plate was described by a radial displacement boundary condition corresponding to a rigid displacement of the pin in the region of contact together with a condition of zero radial pressure outside the contact region. Iteration techniques were used to solve the non-linear contact boundary conditions of this problem. In a related investigation by Oplinger and Gandhi (59), results are presented which describe the effect of Coulomb friction between the pin and plate on the radial and shear stress distributions around fastener hole. These results are illustrated in Figure 10 for friction coefficients ranging from 0 to 0.5. Significant effects of friction on stress distributions are displayed in Figure 10.

### 2.3 Fatigue Life Prediction Methodology

There are basically four methodologies adopted for predicting composite fatigue behaviour. These methodologies are: (1) empirical correlation, (2) cumulative damage model, (3) residual strength degradation model, and (4) tensor polynomial failure criterion. The empirical approach has been extensively applied in fatigue life prediction of mechanically fastened joints in composite structures. Only limited experimental verifications of the accuracy of fatigue life prediction for composite mechanically fastened joints have been carried out for the remaining three methodologies. A review of the four fatigue life prediction methodologies is presented in the following:

(1) Empirical methods - current state-of-the-art fatigue verification approaches for composite structures employ spectrum fatigue tests on components/specimens representative of specific design details (60). These empirical methods are extensively applied due to a lack of confidence in existing analytical composite fatigue life prediction procedures which still require more experimental calibration. In all modern military aircraft that contain extensive composite contents in their primary and secondary structural components (e.g. B-1, F-15, F-16, F-18, AV-8B), empirical methods have been used extensively to assess the effects of cyclic loading on composite fatigue life in order to comply with various military durability specifications such as MIL-A-8866, MIL-A-83444 and MIL-STD-1530A (61-66). It has been postulated that sufficient fatigue life can be achieved by composite structures designed to satisfy static strength requirements (63). For the composite wings of the F-18 and the advanced Harrier aircraft (AV-8B), the maximum design strain level has been limited by McDonnell Douglas Aircraft Company in the range of 4000 to 5000  $\mu\text{m/m}$ . These design strain levels have been developed to accommodate the stress concentration effects of fastener holes and also serve to provide an inherent damage tolerant structure (63).

Most research and development programs on composite fatigue have also emphasized experimental investigations. Conclusions and recommendations reached in these studies have been based on empirical curves fitted through data. Generally, physical understanding of the failure mechanism involved is not included. This makes the extrapolation of curves very difficult or even meaningless. Most published fatigue data have been on unnotched laminates or laminates with an unloaded hole. Relatively little fatigue data exist on composite mechanically fastened joints. Of the existing data, results are often for specialized specimen design, lay-up, or test conditions (67,68).

(2) Cumulative damage model - Miner's linear cumulative damage rule is the most commonly applied cumulative method for analyzing composites because of its relative simplicity. This method requires only constant amplitude fatigue data (S-N curves) for the applied stress ratios in the spectrum in order to predict fatigue life. A simplistic spectrum fatigue life prediction procedure for composites using Miner's rule is illustrated in Figure 13.

There are disagreements reported in the literature regarding the accuracy of the composite fatigue life prediction using Miner's rule. In some cases, it has been reported that Miner's rule is grossly unconservative in predicting life of composite materials (69,70). Others have found it to be an adequate technique for preliminary design studies (71). An investigation at McDonnell Douglas Aircraft Company (1) has found that Miner's rule is adequate to gauge the severity of spectra variations.

The large amount of scatter in composite fatigue life may be the main reason for unreliable analytical predictions that have led to disputable conclusions. One of the major difficulties in developing a composite fatigue life prediction method is to provide sufficient replicate testing in order to establish statistical scatter factors to account for the variability of composite fatigue life.

(3) Residual strength degradation model - Yang (72) derived a residual strength degradation model to predict the fatigue life of composites. This model was derived based on the assumption that residual strength is a monotonically decreasing function of the applied load cycles. Weibull statistical procedures are used in this model to predict residual strength and fatigue life. Parameters required in the analysis are derived from static and constant amplitude fatigue (S-N curves) test data. Once these parameters are derived, probability of survival curves can be generated. The major limitation of this approach is in the basic assumption of continuously decreasing residual strength which makes the model incapable of accounting for initial strength increases that have been observed in many investigations on fatigue of composites (73).

(4) Tensor polynomial failure criterion - Tennyson et al. (30) have extended the application of the tensor polynomial failure criterion from static strength prediction to the fatigue life prediction of composite laminates. Unlike static strength parameters, the fatigue strength parameters are not constants, but rather are functions of the frequency of loading ( $n$ ), the number of cycles ( $N$ ) and the stress ratio  $R = \sigma_{\text{min}}/\sigma_{\text{max}}$ , i.e.  $F = F(n, N, R)$ . "Fatigue functions" required to predict the fatigue life of a laminate under uniaxial tension and compression cyclic loading conditions with constant frequency and  $R$  ratio have been established for the plane stress condition and implemented into a quadratic formulation of the tensor polynomial failure criterion (30). These fatigue functions were established based on results from tension and compression tests in both the fiber (1) and transverse (2) directions, as well as pure shear in the 1-2 plane. Applications of this model to predict fatigue life of "flawed" and "unflawed" graphite/epoxy laminates for uniaxial load cases in hot/wet environments with thermal-splice cycles were attempted and some encouraging results were reported (30). Current work involves applying this model to predict the fatigue life of graphite/epoxy laminates under random FALSTAFF loading conditions. Some experimental data using a four point bending specimen have been generated.

Rotem (74) has established a general fatigue failure criterion also based on experimentally determined "fatigue functions" for multidirectional laminates. "Fatigue functions" that account for delamination have also been developed. The effect of temperature is accounted for by experimentally determined "shifting factors" for the "fatigue functions" (75).

Presently, it is uncertain which methodologies provide the most reliable predictions, and under what conditions they are reliable. Thus it is important for the reliability aspects of the fatigue prediction methodologies discussed earlier to be evaluated. Until this is complete, it remains a difficult task for designers or researchers to select a methodology that can provide reliable fatigue life predictions under their specific requirements and conditions of interest.

### 3.0 EXPERIMENTAL INVESTIGATIONS

In the process of preparing this review, it was observed that the majority of the published work on composite mechanically fastened joints included comparisons of experimental results. This is mainly due to the fact that experimental investigations are often required to characterize the complicated behaviour of composite mechanically fastened joints which cannot be treated solely by the analytical methodologies described in the previous section.

State-of-the-art empirical approaches in composite joint strength analysis represent an alternative, often regarded as an expensive one, to the detailed stress distribution analysis described in the previous section. Through tests on design oriented composite specimens, the failure strength of a specific mechanically fastened joint as influenced by parameters such as geometry, lay-up, percent of load transferred in joint through bearing and by-pass etc., is assessed. However, it is obvious, in view of the very large number of variables involved, and their effect on each other, that a complete characterization of a general joint behaviour is impractical. Rather, the current approach is to determine as thoroughly as possible the behaviour of a few basic joints in a limited number of material systems and to hopefully infer the influence of the more important parameters from which the behaviour of other joints and materials can be predicted by empirical design methods. Hart-Smith's work is an example of a comprehensive experimental investigation of some mechanically fastened joints in graphite/epoxy composites where experimental results were generated to establish empirical formulae and design-analysis procedures (76).

Experimental results are also generated in order to complement/verify analytical results obtained by methodologies described in the previous section. The advantage of this is that once an analytical methodology has been well calibrated against experimental results, it can be used to predict composite mechanically fastened joint strengths and thus reduce the high cost of experimental assessment in new design applications.

In the following sub-sections, experimental results and conclusions obtained from published literature relating to the effects of various parameters on composite mechanically fastened joints are presented and discussed. For convenience, the parameters are arbitrarily divided into three groups:

- (1) Material parameters: fiber type and form (unidirectional, woven fabric etc.), resin type, fiber orientation and stacking sequence.
- (2) Fastener parameters: fastener type, fastener size, clamping force, washer size, hole size, and tolerance.
- (3) Design parameters: joint type, laminate thickness, geometry (pitch, edge distance, hole pattern, etc.) load direction, load mode (static or cyclic), and failure definition.

#### 3.1 Material Parameters

Fibrous composites, in most secondary and primary aeronautical applications, are generally manufactured by stacking layers of prepreg consisting of reinforcing fibers embedded in a resin matrix. Graphite, Kevlar or glass fibers and epoxy resins are common ingredients used in producing laminates. The reinforcing fibers are arranged in either unidirectional or woven format in a single ply of prepreg where they are saturated with resin material. This resin matrix serves to bind the fibers together and transfer loads to the fibers.

The mechanical behaviour and failure mode of composite mechanically fastened joints are dependent upon the orientation and stacking sequence of plies in the laminates. In their work on unloaded holes in laminates, Rybicki and Schmuerer (79), and Pagano and Pipes (80) demonstrated that the stacking sequence of plies affects the interlaminar normal and shear stresses around the unloaded hole and hence, by inference, the strength of a loaded hole in a composite mechanically fastened joint. In order to reduce these matrix stresses which are responsible for delamination at the fastener hole or other free edges, it is important to intersperse the ply orientations thoroughly in the laminates such that the number of parallel adjacent plies are minimized (76).

The effect of stacking sequence on the bearing strength of composite bolted joints was investigated experimentally by Garbo and Ogonowski (56) and Ramkumar and Tossavainen (77) by grouping plies with the same fiber orientation together in the laminates. Both groups of investigators found that the bearing strength decreased when the percentage of the parallel adjacent plies with the same fiber orientation was increased. Quinn and Matthews (78) investigated the effect of stacking sequence in glass fiber-reinforced plastics. They showed that placing 90° plies perpendicular to the load direction at or near the surface improved the pin bearing strength.

The effect of orientation of plies or lay-up on the bearing strength of composite mechanically fastened joints has been investigated by several authors. Collins (81), whose work covers bolted joints in graphite/epoxy composites, concluded that for optimum bearing properties, more than 55% but less than 80% of 0° plies (i.e. parallel to the load) are required, the balance being made up of ±45° plies to provide transverse integrity to the composite bolted joint. He also concluded that optimum tensile properties were obtained when the ratio of 0° to 45° plies was 2:1 whilst optimum shear strengths required a ratio of 1:1. Matthews et al. (83) performed tests on composite riveted joints and concluded that the bearing strength is significantly higher for the 0°/±45° lay-up than for the 90°/±45° lay-up.

Ramkumar and Tossavainen (77) investigated the effect of lay-up on the strength of laminates that were bolted to metallic plates using a single fastener. They tested laminates that were fabricated using nonwoven AS1/3501-6 graphite/epoxy material with lay-ups that ranged from a fiber-dominated lay-up to a matrix-dominated lay-up. They

found that, under compression loading, the failure strain increased with an increase in the percentage of  $\pm 45^\circ$  plies while the gross compressive strength and bearing strength decreased with an increase of the percentage  $\pm 45^\circ$  plies. Their compression test results and tension test results are presented in Figure 14 and 15 respectively. They observed that the failure mode changed from the shear-out mode to local bearing failure mode when the percentage of  $\pm 45^\circ$  plies was increased from 40% to 60% under tension loading. However, under compression loading, they found that failure mode was insensitive to lay-up and specimens tested always failed in the local bearing mode.

The mode of failure is also influenced by joint geometry. This aspect will be discussed in sub-section 3.3.

It is recognized that a high stress concentration factor exists at the fastener hole of a composite mechanically fastened joint. Berg (83) emphasized that because most composite materials are incapable of yielding, local load redistribution at the fastener hole can only be achieved by brittle fracture. The distribution of stresses at the fastener hole is influenced by the lay-up of the laminates. Collings (84) suggested the inclusion of  $\pm 45^\circ$  plies in order to reduce the stress concentration at the fastener hole.

Hybrid laminates can also be used to reduce the sensitivity to stress concentration. Hart-Smith (76) replaced some of the graphite fibers which were aligned with the load direction with S-glass fibers. Mechanically fastened joint specimens fabricated from these glass/graphite hybrid laminates were consistently as strong or stronger than the equivalent all-graphite specimens when tested under tension loading. However, because of a lower modulus for the glass fibers with respect to the graphite fibers, the stabilization of compressively loaded joint specimens was found to be a problem. The failure mode of the glass/graphite was almost exclusively associated with local bearing failures rather than the potentially catastrophic tension-through-the-hole failure which was common for many of the all-graphite specimens.

The experimental results discussed here are essentially based on conventional material systems composed of graphite fibers of moderate modulus and first generation brittle resin materials (The classification of resin materials is according to Johnston (85)). Advanced composite material systems composed of high strain graphite fibers and second generation tough resin materials are now being manufactured by the composites industry. A survey was conducted by Canadair Ltd. (86) on the types of advanced material systems which are being examined by the aeronautical industry for the next generation of aircraft. As indicated by the survey report of Canadair Ltd., the tensile strengths and the compressive strengths of the advanced composite materials are significantly higher, by as much as 87% and 22% respectively, relative to those of the conventional baseline systems. The most important improvement of the newer composites over the conventional composites appears to be the post-impact performance. Unfortunately, there is no mechanically fastened joint data available currently in the published literature for these newer material systems.

### 3.2 Fastener Parameters

Many types of fastener are used in aerospace manufacturing. Some common types are screws, rivets and bolts. Each type of fasteners can be offered in a wide variety of dimensions, configurations and materials. The selection of fasteners depends on the type of applications. In general, screws give the lowest load-carrying capacity and tend to be of little use in a primary structural role. Both rivets and bolts offer adequate strength in composite joints for medium to high load transfer applications.

In composite structure, some parameters which affect the selection of fasteners are edge and side distances, hole diameter, laminate thickness, fiber orientation, laminate stacking sequence, and the type of material systems being used. For example, composite laminate thickness, material and location in an airframe structure are factors to be considered in determining whether a blind or two-piece fastener is selected. If the material stack-up has a thin top sheet, the hole countersink configuration and the head configuration of the fastener become important considerations.

Composite materials pose special problems for mechanical fastening because of their peculiar properties. In their survey report on fasteners for composite structures (88), Cole et al. identified four primary problems: (1) galvanic corrosion; (2) galling; (3) installation damage; and (4) low pull-through strength. The nature of these problems and the design of fasteners to circumvent them are discussed below:

(1) Galvanic corrosion: the basic force of the galvanic corrosion reaction is the difference in electrode potential between the graphite fibers and the metals. The less noble metals may corrode when mechanically fastened to graphite fiber composites. One solution is to cover the fastener with a protective coating. Prince (87) performed a comparison of the effectiveness of different coatings to protect against galvanic corrosion. He concluded that, when flawed, coatings are inadequate to provide protection against corrosion.

A more effective solution to the corrosion problem is to select compatible materials for the fasteners. For this purpose, a galvanic compatibility chart, shown in Figure 16, is used. This chart ranks nobility, or resistance to galvanic corrosion of fastener metals in a graphite based composite. Titanium is one of the most noble metals, and so titanium and titanium alloys offer excellent corrosion resistance when used with graphite composite.

A special composite fastener, made of both graphite/polyimide and glass/epoxy composites, has been developed to provide total compatibility, low weight, and low cost (88). The most serious disadvantage of this type of fastener is the lack of reliability of the adhesive bond which holds the two-piece fastener together.

(2) Galling - Galling problems are encountered when nuts fabricated with either titanium or A286 CRES steel are used with titanium bolts, such as the common Hi-Lok system (88). A lock-up situation occurs during installation prior to the development of the desired preload. McDonnell-Douglas has successfully eliminated this problem in the F-18 and AV-8B programs by applying suitable lubricants (88). Galling problems were also encountered in the Lockheed L1011 Advanced Composite Vertical Fin program. The solution was to use stainless steel nuts (Type 303) to replace A286 CRES steel or titanium nuts (88). Other solutions to the galling problem include the use of free running nuts, as in the Eddie Bolt system, and swaged collar fasteners such as the Groove Proportional Lockbolt (GPL) made by Huck Manufacturing Company.

(3) Installation damage: the procedure for installation of fasteners in metallic structures often uses high preload and interference-fit to obtain strength and durability improvements in the joint. Experience has shown that using the same fasteners and procedures in composite structures can produce unacceptable damage. Before the installation of

fasteners, holes must be cleanly drilled through the composite structure. This is not an easy task because composites are prone to fraying within the hole and to splintering on the exit side of the hole as a result of the drilling operation; consequently, special drill bits and procedure different from those used in metal drilling, are required in order to avoid introducing any local weakening of the composite structure. While the fastener is being installed into the hole, its rotation is not recommended because this would lead to breaking and lifting of fibers from the surface. Also, axial misalignment of fastener in the hole could lead to damage. For example, misalignment of a blind fastener during installation could cause the blind head to dig into the surface of the hidden side, crushing or delaminating the composite skin.

Several manufacturers have introduced fastener designs which have significantly facilitated their installation in composite structures. Figure 17 shows a typical design approach and installation sequence of a blind fastener. Normally, hydraulic or pneumatic tools are used to install the fastener after it has been inserted into a prepared hole. An axial pulling force is applied to cause a sleeve to form an expanded head on the blind side. This head expansion is accomplished by buckling the sleeve either against the composite structure or against a shoulder on the fastener shank. The fastener is designed to ensure hole fill-in and axial alignment during installation. Mechanical locking is achieved when the head is secured against the blind-side surface. A break groove is normally designed into the stem so that it fractures after a certain level of clamping force has been reached.

Figure 18 illustrates some unique features of a special blind fastener designed to overcome the problem of crushing the surface near the edge of the fastener hole as a result of buckling the sleeve directly against the composite structure. It has a washer element between the corebolt and the sleeve, and it is independent of both. The washer is driven over the tapered end of the nut and it expands to its final diameter. The formed washer is then seated against the joint surface by the continued advance of the sleeve and the corebolt. The unique feature of this fastener is that its blind head is formed by expanding its washer element to the desired diameter before engaging the sheet surface; consequently, there is no surface pressure brought to bear on the composite structure to cause any crushing damage. A straight axial load is applied to deliver the required clamping force, so there is no spinning action between fastener and structure which could cause fibers to separate.

Figure 19 illustrates the installation sequence of a two-piece lockbolt fastener for solid composite laminates. The fastening principle is based on the straight line tension/tension or swaged collar concept which minimizes the tendency of crushing the surface of the composite laminates. Furthermore, this swaging action fills the annular locking grooves on the pin with the collar material to form a permanent lock; thus the rotation of the nut is eliminated. This type of lockbolt fastener is designed for installation in clearance or interference fit conditions.

The nut tightening, collar swaging or tail forming during the installation of a fastener exerts a clamping force or preload on the composite sheets being joined. Because of the low through-the-thickness shear and compressive properties of composites, high preload may result in composite crushing. In order to achieve higher preloads to improve joint performance while minimizing the possibility of crushing damage, fasteners are designed with enlarged "footprints," which refer to the bearing area of the nut, collar or tail, and enlarged heads (Figure 20). Both serve to provide a larger area over which the preload can be spread. This increases the performance of the joint by allowing higher preloads to be achieved which lead to improved shear strengths to resist fastener cocking associated with eccentric loads and improved tensile strengths to prevent fastener pull-through. In addition, higher preloads increase the fatigue life of composite mechanically fastened joints (56).

The low interlaminar strength of composite materials often leads to delamination of the plies on the backside of the laminate when fasteners are forced into an interference-fit hole. Also, experience with fiberglass has shown that when rivets are installed to completely fill the hole by shank expansion, ply delamination and buckling occur at the hole boundary. These difficulties have led to the general requirement for all material systems that only clearance fit (-0.000 to +0.102 mm) fasteners are used in composite structures (88). However, interference fit is desirable in composite joints. Sendekyl and Richardson (89) demonstrated that increasing the level of interference in a graphite/epoxy joint increases the fatigue life. Interference is also required to increase the load-sharing capability in a joint with multiple rows of fasteners, to prevent fuel leakage in fuel tank area, and to provide the reactive torque needed for one-sided installations of blind fasteners.

Several manufacturers have produced special fasteners for interference installations. Grumman (88) developed the stress-wave rivet system for installation of titanium and A-286 CRES steel rivets in composite structure with up to .203 mm interference. The rivet deformation in the system is caused by a stress wave which causes the material to flow outward in all directions simultaneously. The damage is limited by this simultaneous tail formation and hole filling action. Huck Manufacturing Company has developed the HUCK-TITE titanium interference fit lockbolt. This fastener can be installed conveniently with standard installation tooling developed by Huck. The installation procedure is illustrated in Figure 19. The sleeve of this fastener is expanded into an interference fit hole during installation; consequently, an intimate contact is established between the fastener and the hole which forms a water intrusion barrier to prevent fuel leakage without the application of a sealant and also provides electrical continuity to prevent arcing.

(4) Low pull-through strength: the pull-through strength of a fastener for composite structures is shown to be a function of the size of the "footprint" and the outside diameter of the head as illustrated in Figure 20. An improvement in the pull-through strength can be achieved by using fasteners with enlarged "footprints" and enlarged heads. In the case of blind fasteners, many engineers feel that the blind head should be expanded 1.4 times the shank diameter instead of the 1.2 times used for typical metal fastening (108). The configuration of the head also has significant effect on the pull-through strength. Boeing has found that the 130° shear head can support 30% more load than the 100° shear head because of the improved bearing surface area (88). Lockheed-Georgia Company compared the performance of four head configurations (100° shear, 100° tension, 120° shear and 130° shear) on the basis of pull-through strength and fatigue. The results of the comparison indicated that, for sufficiently thick composite structure where the thickness is in excess of the fastener head height, the 100° tension flush head fastener is the best among the four configurations tested (88).

### 3.3 Design Parameters

In the primary and secondary structures of aircraft components that utilize composite materials, mechanically fastened joints of various composite-to-composite or composite-to-metal designs can be found (90, 91). Although these joints may be complex in appearance, each can be generically modeled as simple single or double lap specimen.

In selecting the type and configuration of a joint specimen, the following design parameters that reflect the structural joint requirements must be considered: (1) geometry, (2) hole pattern, (3) hole size, (4) laminate thickness, (5) load eccentricity, (6) fastener load direction, and (7) failure definition. The results of the survey with respect to these design parameters are presented in the following sub-sections.

### 3.3.1 Geometrical Effects

The convention adopted in this review, which is similar to that suggested as a standard by Kutscha and Hofer (92), is shown in Figure 21.

The effect of end distance ( $e$ ) has been investigated by a number of authors and they all agree that a certain minimum value of the  $e/d$  ratio is required to develop full bearing strength. Ramkumar and Tossavainen (77) investigated the strength of bolted laminates using AS1/3501-6 graphite/epoxy unidirectional prepreg material. They concluded that the bearing strength of all the lay-ups increases with  $e/d$  ratio to a value of 4 or 5, beyond which the bearing strength is relatively invariant. The 50/40/10 lay-up, where the number indicates the percentage of the 0°, +45° and 90° fiber orientation in the laminate respectively, exhibits a shear-out mode of failure when  $e/d \leq 3$ . For  $e/d > 3$ , the laminate exhibits a local bearing mode of failure. The 70/20/10 lay-up exhibits a total shear-out mode of failure for  $e/d$  values below 5. Collings (16) in his work on bolted joints in CFRP showed that for an all +45° lay-up, the minimum  $e/d$  ratio required for the development of full bearing strength in the laminate is 5, whereas for a pseudo-isotropic lay-up, the minimum  $e/d$  ratio is 3. MIL-HDBK 17A (93) quotes a minimum  $e/d$  ratio of 4.5 for 0/45° lay-up.

The width effects in single hole joint specimen have also been investigated in conjunction with the end effects. The results obtained from single hole joints are often used to predict the pitch distance effects in multi-hole arrangements. This is done by representing individual bolts isolated from a single row in a strip of a width equal to the bolt pitch. Ramkumar and Tossavainen (77) showed that for  $w/d > 6$ , the bearing strength remains relatively constant. When  $w/d < 4$ , the failure mode is primarily a net section failure across the hole. For  $w/d > 4$ , the failure mode is primarily a partial or a total shear-out of the 50/40/10 laminate. For the same  $w/d$  ratio, the 30/60/10 laminate fails in a local bearing mode. Collings (16) suggested minimum  $w/d$  of 8 and 5 for +45° and pseudo-isotropic lay-ups respectively, if full bearing strength is to be developed. Matthews et al (82) showed that for 0/+45° lay-ups in CFRP a minimum  $w/d$  of 4 is needed.

### 3.3.2 Hole Pattern

The preceding sections have dealt with single-bolt joints where failure can be defined uniquely in terms of bolt load alone. In most practical applications, however, this is not the case because the load is frequently transferred in multi-row fastener patterns, such as at a chordwise splice in a wing skin, or along a bolt seam aligned with the dominant load path, such as at a wing spar cap. In such more complex load situations, it is necessary to characterize both the bolt load and also the general stress field in which the particular bolt under consideration is located.

Geometrical parameters can influence the amounts of load transfer, as depicted in Figure 22 (110). The secondary bending is created by the load transfer in single shear or otherwise eccentric joints even if the external load is free from bending moment. Also, it is affected by geometrical changes. For a single shear joint with two rows of fasteners, it has been demonstrated that by increasing the distance between the rows from 4 cm to 8 cm, the secondary bending was reduced by 35% (110).

Agarwal (94) investigated the behaviour of multi-fastener bolted joints in AS/3501-5 graphite/epoxy. His experimental results indicated that the net tension failure stress of the joint is increased slightly (5 to 10 percent) by increasing the number of fastener rows. It was also noted that the net tension failure stress was reduced by up to 15 percent as the number of fasteners in a row was increased which was suggested to be caused by the specimen width effect. Hart-Smith (76), using T300/5208 graphite/epoxy, also demonstrated that for joint geometries producing tension failures for a single bolt, the addition of further rows of bolts generally increases the joint strength very little. He found that only when bearing failures occur do multi-row bolt patterns increase the joint strength significantly above the strength of a single bolt row. He observed that the transition between tension and bearing failure modes occurs in the range of bolt pitches between four and six times the diameter of the bolt hole.

Godwin et al (95) presented the experimental results of multi-bolt joints in glass-reinforced plastics. It was shown that bolts in a row develop full bearing strength at pitches of more than six diameters. At small values of pitch in a wide panel, it was suggested that the joint strength could be increased by increasing the end distance to suppress shear-out failure. It was also observed that no substantial improvement in strength is gained by using staggered rows of bolts. They suggested that the joint geometry that optimizes the joint strength is a single row of bolts, at a pitch of 2.5 diameters and an end distance of 5 diameters. At these values, joint strength is approximately half the gross panel strength, and the failure mode is in tension at the minimum section. They pointed out that increased safety can be gained by increasing the pitch to 5 or 6 diameters if there is bearing failure. In this case, the net joint strength is only about one-third of the gross panel strength. This value of pitch compares closely with that suggested by Hart-Smith for graphite/epoxy.

### 3.3.3 Hole Size

Garbo and Ogonowski (56) investigated the effects of hole size on composite bolted joint strength by applying tension to the two-fastener-in-tandem double shear specimens and loading to failure. It was shown that both bearing strength and gross joint failure strain decrease with increasing hole diameter over the range tested. It was observed that all specimens failed in bearing-shearout, regardless of hole size. Ramkumar and Tossavainen (77) investigated the effect of fastener diameter on the tensile response of a 20 ply, 50/40/10 lay-up graphite/epoxy laminate in a single lap configuration. It was shown that the gross tensile strength and the bearing strength of the laminate decrease when the fastener diameter is increased. A similar trend is also observed under static compression.

### 3.3.4 Laminate Thickness

Garbo and Ogonowski (56) also investigated the effects of laminate thickness and fastener countersink on graphite/epoxy laminate bearing strength. Their investigation covered a range of laminate thicknesses from 20 ply to 60 ply and three countersink depth-to-laminate thickness ratios (0.77, 0.38 and 0.26). Their test specimens were of a single

fastener in double shear configuration with 50/40/10 lay-up and were loaded to failure in both tension and compression. The bearing strength was shown to increase with increasing laminate thickness from 20 ply to 60 ply. Within data scatter, it was observed that the effects of countersink versus noncountersink on strength appear to be insignificant. For pin-loaded holes, i.e. no through-thickness clamping, Collings (17) showed that bearing strength reduces as  $d/t$  increases. Ramkumar and Tossavainen (77) showed that an increase in the thickness of a laminate in a single lap configuration introduces additional load eccentricity and bolt flexibility effects. Their experimental results from tests on 20-ply and 60-ply laminates with 50/40/10 lay-ups demonstrated that the thicker laminate strength was approximately 5 percent lower than that of the 20-ply laminates.

### 3.3.5 Load Eccentricity

In selecting a single lap joint specimen for an experimental program, joint eccentricity effects must be minimized or accounted for because significant bolt bending can lead to a lower joint strength due to the eccentricity in the load path. Ramkumar and Tossavainen (77) evaluated the load eccentricity effects by comparing single lap test results with double lap test results. The results of the comparison indicated as much as 17 percent and 20 percent increase in the gross tensile and bearing strengths and the gross compressive and bearing strengths of the laminate, respectively, are obtained by changing from a single shear to a double shear configuration. Hart-Smith (76) compared the experimental results between single lap and double lap joints and found a 20 percent decrease with respect to double-shear strengths. He suggested that due account should be taken of the differences between single and double shear bolted joints in the analysis of practical aerospace structures.

### 3.3.6 Fastener Load Direction

Because of the anisotropic nature of composites, the bearing strength of composite laminates will vary with load direction. This effect was investigated by Garbo and Ogonowski (56) and by Matthews and Hirst (96). All material systems evaluated by these investigators were sensitive to load direction. Figure 23 illustrates the changes in circumferential stress distributions around a loaded fastener hole in a laminate with 70/20/10 lay-up as a result of shifting the direction of load from  $\theta = 0^\circ$  to  $\theta = 45^\circ$ . The peak stresses no longer occur perpendicular to the load direction and the stress distribution is shifted and changed. The stress distribution for the isotropic case is included for comparison.

### 3.3.7 Failure Definition

For composite bolted joints, the determination of bearing strength depends on the definition of failure criterion which can vary widely from, simply, the maximum load sustained by the joint to a failure criterion based on the deformation of the hole. Johnson and Matthews (97), used typical load/extension plot of a composite bolted joint (see Figure 24), to suggest the following ways of defining failure load:

- (a) The maximum load - Usually considerable damage will have occurred in reaching this load (81).
- (b) The first peak in the load/extension plot - Damage sustained up to this load is not insignificant. Almost certainly cracks will have propagated outside of the washers (78).
- (c) The load corresponding to a specified amount of hole elongation - There is little agreement as to what value should be used. Dastin (98), Strauss (99) and Oleesky and Mohr (100) use a value of 4 percent of the hole diameter, for glass reinforced plastics; Webb (101) uses 1 percent for bolts and 2 percent for rivets in CFRP; Althof and Muller (102) use 0.5 percent for CFRP; and Johnson and Matthews (97) use 0.4 percent of the original diameter for glass fiber-reinforced plastics. They suggested the limit load corresponding to 0.4 percent elongation of hole diameter could be obtained from the maximum load by using a factor of safety of 2.
- (d) The load at which the load/extension curve first deviates from linearity - The point at which deviation from linearity occurs is usually difficult to establish. Also the slope of the load/extension curve may alter at more than one point (103).
- (e) The load at which cracking first becomes audible - Johnson and Matthews (97) examined specimens at this point and found a few visible cracks around the loaded side of the hole.
- (f) The load at which cracking is initiated - This load is probably quite low and very difficult to determine.
- (g) The load at which cracks become visible outside the washers - Only one side of the specimen is accessible for visual detection.

Some of the loads defined above (d to g) are subject to wide variability or are difficult to determine objectively. The majority of investigators adopt the first three approaches (a to c) to define failure load.

Hole elongation and overall joint compliance criteria based on data obtained from load-deflection hysteresis curves are often used in fatigue tests to indicate the amount of cyclic damage accumulation and failure (56, 77).

## 3.4 Fatigue Test Results

Relatively few experimental results relating to fatigue behaviour of composite bolted joints are available in the published literature. A brief reference to fatigue of glass fiber-reinforced plastics joints is available in MIL-HDBK 17A (93). Reliability of composite joints is discussed by Wolff and Lemon (104) and by Wolff and Wilkins (105). In a special fastener development program for composite structures, Cole et al. (88) obtained test results using a typical tension-dominated fighter load spectrum for composite laminates mechanically joined by fasteners with four different flush-head configurations. The 100° tension head fastener was found to yield significantly improved fatigue performance over the 100° shear, 120° shear and 130° shear type fasteners.

Crews (109) investigated the bolt-bearing fatigue strength of graphite/epoxy (T300/5208) laminates. In his study, fatigue tests were conducted for a wide range of bolt clamp-up torques using single fastener coupons. The specimen

width,  $w$ , and edge distance,  $e$ , were selected for  $w/d = 3$  and  $e/d = 4$ . These ratios assured bearing failure rather than net-tension or shear-out failures. During all fatigue tests, the hole elongation due to cyclic loads was monitored until each specimen failed in the bearing mode. Ultrasonic C-scan methods were used to examine the area around the bolt hole for delamination damage due to cyclic loads. Experimental results indicated that bolt clamp-up had a beneficial effect on the fatigue limit which was improved by as much as 100 percent compared to the pin-bearing case. The explanation for this improvement was found to be the through-the-thickness compressive stresses provided by the clamp-up loads. These loads also influenced the amount of bolt hole elongations. It was found that high clamp-up torques virtually eliminated hole elongation during fatigue loading. C-scan images of specimens were obtained after 20,000 cycles of 600 MPa maximum bearing stress. At this stage, the presence of delamination damage around the hole was recorded. Also, a slight elongation of the hole was measured. This evidence indicated the initiation and growth of delaminations as a result of fatigue. The permanent hole elongation was caused by localized delaminations which formed a soft region around the hole. The original stiffness of the laminate in this region was reduced significantly. The further growth of the delamination under cyclic loads led to a bearing failure of the laminates. In his investigation, Crews did not attempt to establish any failure criterion for the bearing mode. It appears that existing models cannot predict the initiation, growth and instability as a result of delamination under cyclic loads in composite laminates.

An evaluation of critical joint design variables on fatigue life was carried out by Garbo and Ogonowski (56). Seven design parameters which have significant effects on the static strength of composite bolted joints were selected for evaluation. Tension-tension ( $R = +0.1$ ), tension-compression ( $R = -1.0$ ) constant amplitude testing and spectrum testing were performed using a pure bearing double-lap test specimen. Hercules AS/3501-6 graphite/epoxy was used to fabricate the test specimens. A review of the effects of the seven variables on fatigue performance based on the work of Garbo and Ogonowski is summarized below:

(1) Lay-up - Three laminate variations were tested to determine the relative fatigue life in terms of the number of fatigue cycles required to produce a 0.51 mm elongation which is about 5.3 percent of the hole diameter. For tension-tension cycling, the results indicated similar fatigue life for all lay-ups. For  $R = -1.0$ , the two matrix-dominant lay-ups (19/6/5 and 30/60/10) sustained fewer load cycles prior to developing a 0.51 mm hole elongation, as compared to the 30/40/10 fiber-dominant lay-up (Figure 25). For spectrum fatigue tests, the results showed no measurable hole elongation for any of the tested lay-ups after testing to an equivalent of 16,000 service hours.

(2) Stacking Sequence - The effects of stacking sequence were found to be insignificant with respect to joint fatigue life under both constant amplitude and spectrum cycling.

(3) Fastener Preload - Significant increases in fatigue strength were obtained by increasing the fastener preload from 0 N.m to 18 N.m. Failure modes were observed to be the same for all the fastener torque-up levels.

(4) Joint Geometry - The effects of specimen geometry on joint life were evaluated for the 30/40/10 and 19/76/5 lay-ups using specimens with different edge distances and widths. Fatigue strength was not changed for the 30/40/10 lay-ups. For the matrix-dominant 19/76/5 lay-up, fatigue strength was found to increase when the  $w/d$  ratio was increased from 3 to 4. Further, a change of failure mode from bearing to net section occurred when  $w/d$  ratio was reduced from 4 to 3.

(5) Interference Fit - Fatigue tests were conducted to evaluate the effect of an interference fit of 0.127 mm on the fatigue life of no-torque and torqued joints. For  $R = +1$ , the results indicated that specimens with no preload and 0.127 mm interference fit failed at a lower fatigue life relative to neat-fit specimens with no preload. Associated with this lower life was a large data scatter. Standard pull-through installation techniques and fastener types were used. Some joint specimens were sectioned and examined. The presence of delamination at the fastener exit side as well as through-the-thickness of the hole in the laminate were discovered for joints with interference fits from .102 through .178 mm. Therefore, it was suspected that minor installation damage caused by inserting the interference fit fastener produced the wide scatter in data when no clamping constraint existed due to zero fastener preload. Limited fatigue testing of specimens with 18 N.m preload and 0.127 mm interference fit produced higher fatigue lives relative to neat-fit specimens with the same installation torque.

(6) Single-Shear Loading - The effect of bending stresses due to the single shear configuration resulted in a significant reduction in fatigue life. Further fatigue life reductions were exhibited by the countersunk fastener with its associated loss of direct bearing material and added fastener head flexibility relative to the protruding head fastener. Joint spring rates for the double-shear, non-countersunk single-shear, and countersunk single-shear specimens were found to be 49.35 MN/m, 60.77 MN/m, and 43.78 MN/m respectively.

(7) Porosity - Tests of specimens with moderate porosity resulted in no reduction in either static strength or joint fatigue life.

#### 4.0 CONCLUSIONS

Technical observations pertaining to composite mechanically fastened joint technology as a result of this review are summarized in the following:

(1) Similar directions have been followed throughout the technical community in the analysis of composite bolted joints in aircraft structural components. The analysis proceeds from an overall structural analysis, to localized joint idealization and bolt-load distribution analysis, and finally to an assessment of the static and/or fatigue strength through the utilization of joint failure analysis at individual fastener holes.

(2) Static joint failure analysis for composites, which represents the primary area of research activity in the literature reviewed, consists of detailed stress analysis performed at individual fastener holes and associated application of a failure criterion.

(3) State-of-the-art stress analysis methodologies include finite element, two-dimensional anisotropic elastic analysis and fracture mechanics. Three-dimensional analysis is needed for determining the through-the-thickness stress distribution around fastener holes in order to assess the role of bearing and interlaminar shear failures.

(4) Static strength is evaluated by applying anisotropic material failure criteria after the stresses at a "characteristic dimension" from the edge of the hole are determined. Quadratic failure surfaces, which account for failure mode interaction, have been demonstrated to be capable of predicting both failure load and failure mode accurately in composite bolted joints for most cases. A cubic formulation has been shown to yield more accurate predictions in biaxial loading cases.

(5) State-of-the-art fatigue life prediction methodologies require an extensive data base which, except for some specific cases, is not well established for composites. Predictions based on Miner's linear cumulative damage model have been found to be unconservative. The assumption of continuously decreasing residual strength in the residual strength degradation model restricts the model from general applications. "Fatigue function" models have achieved some preliminary success in correlating with experimental results. These models have been extended to include delamination and temperature effects. Empirical approaches are most common in predicting fatigue life of composites as well as in demonstrating compliance with military and commercial durability specifications.

(6) The effects of various design parameters on the static and fatigue behaviour of composite bolted joints have been examined. For quasi-isotropic lay-ups, minimum allowed edge distances and fastener spacings ranged respectively from 3-4 and 4-5 times fastener diameters in most design practices where full bearing strength is required of the joint. In general, the tensile and bearing strengths decrease with increasing hole diameter and decreasing laminate thickness. Load eccentricity in a single lap joint reduces both the static and fatigue strength significantly. Due to the anisotropic nature of composites, the bearing strength has been shown to vary with fastener load direction.

(7) Galvanic corrosion, galling, installation damage and low pull-through strength are recognized as the four basic problems where mechanical fastening of composite laminates is concerned. In general engineering practices, only tension head fasteners made of titanium are used with composites and no interference fit holes, hole filling fasteners, or vibration driving of rivets are recommended. Special fastener systems have been developed to allow for interference installation using appropriate toolings to minimize installation damage. It has been demonstrated that interference fit increases fatigue strength. The application of bolt torque to the optimum level has been accomplished by using fasteners with large "foot-print" or washers. Application of special lubricants and proper material selection eliminate galling problems. In general, high clamping forces increase static and fatigue strength of a composite bolted joint.

(8) There is currently no bolted joint data readily available for the advanced composite materials.

## 5.0 RECOMMENDATION - FURTHER RESEARCH

As a result of this review, the need for further research in the following areas is identified:

(1) The accuracy of the analytical prediction of the static strength of mechanically fastened joints depends strongly on the stress analysis and the failure criterion applied. In order to improve the accuracy of the strength prediction, further work is required in the three dimensional stress analysis of a joint to account for the through-the-thickness effects as a result of interference fit and preload. It is also deemed necessary to incorporate an elastic contact analysis with stick-slide behaviour in the three dimensional analysis in order to provide more sophisticated solutions which include frictional effects. Further work in the development of failure criteria based on physical damage phenomena to predict delamination and gross bearing failure modes is required.

(2) Further research is required in the development of fatigue life prediction methodologies. It appears that static strength prediction is sufficient in most cases because of the relative insensitivity of composite materials to fatigue. However, the initiation and growth of delaminations have been observed to take place under cyclic loading at free edges, especially at the edge of a fastener hole because of the stress concentration. This delamination creates a local region near the bolt hole where the original stiffness of the composite laminate has been reduced extensively. Consequently, the growth of delaminations can cause extensive elongation of the fastener hole. Further damage can be accumulated rapidly as a result of the pounding of a loose fastener in a hole when the load spectrum includes reversals ( $R < 0$ ). This can lead to the ultimate loss of the overall load-carrying capability of the composite component as a result of an extensive drop in stiffness or static strength. Further research is deemed necessary since methodologies available currently cannot predict initiation, growth and instability as a result of delamination under fatigue loading in composites.

(3) A critical evaluation is deemed necessary to compare and assess the reliability aspects of various existing fatigue life prediction methodologies and establish the specific conditions under which they are reliable. These specific conditions include: (a) operating conditions, e.g., temperature, environment, loading; (b) failure modes, e.g., delamination, bearing; (c) material parameters, e.g., ply orientation; and (d) specific assumptions, e.g., plane stress, continuously decreasing residual strength. This evaluation may provide a basis for the selection of methodologies to predict the fatigue life of composite mechanically fastened joints reliably under the conditions of interest.

(4) The application of advanced composite material systems should be investigated. These systems include high strain carbon fibers and tough resin matrix such as bismaleimide. Specifically, bearing properties and stress concentration sensitivity should be studied. Furthermore, the effects of the improved interlaminar normal and shear properties as a result of the tougher resin matrix on the clamping load and interference fit provided by the fastener systems should be investigated because, as indicated by the present literature review, enhanced static and durability performances of composite mechanically fastened joints could be obtained by increasing the clamping load and interference fit.

(5) No published data was found on the use of mechanical fasteners in high strain/tough resin composites. In order to design mechanically fastened joints using these high strain/tough resin composites, experimental work should be undertaken to generate design data similar to those generated based on conventional graphite/epoxy composites. The design data generated can be used to verify/establish the benefits of using these systems. For example, weight savings are predicted as a result of the improvement in the allowable design strain level provided by these advanced composites. Also, data is required to examine the applicability of the current analysis procedures and failure criteria based on conventional graphite/epoxy systems to predict the static and fatigue strengths and failure modes of mechanically fastened joints fabricated from these advanced composites.

## ACKNOWLEDGEMENTS

The work presented in this paper was supported by the Canadian Department of National Defence. The author would like to acknowledge the advice provided by Dr. W. Wallace and Mr. D.L. Simpson. Also, the technical support provided by Mr. T. Benak is gratefully acknowledged.

## REFERENCES

1. S.P. Garbo and J.M. Ogonowski, "Effect of Variances and Manufacturing Tolerances on the Design Strength and Life of Mechanically Fastened Composite Joints," AFFDL-TR-76-179, December 1978.
2. D. Garcia and C.E. Halstead, "Shuttle Orbiter-Graphite/Epoxy Payload Bay Doors," NASA TM X-3377, November 1975, pp. 115-130.
3. B. Whitman, P. Shyprykevich, and J. Whiteside, "Design of the B-1 Composite Horizontal Stabilizer Root Joint," NASA TM X-3377, November 1975, pp. 603-632.
4. E. Baumann, "Finite Element Analysis of Advanced Composite Structures Containing Mechanically Fastened Joints," Nuclear Engineering and Design, 70 (1982), pp. 67-83.
5. Ojalva, I.U., "Survey of Mechanically Fastened Splice-Joint Analysis," Proceedings of the 8th Army Materials Technology Conference, Boston, Massachusetts, 16-19 September, 1975, pp. 379-403.
6. MIL-HDBK-5C, "Military Standardization Handbook - Metallic Materials and Elements for Aerospace Vehicle Structures," 1976.
7. McCombs, W.F., McQueen, J.C. and Perry, J.L., "Analytical Design Methods for Aircraft Structural Joints," LTV Aerospace Corp., LTV Vought Aeronautics Division, Dallas, Texas, AFFDL-TR-67-184, January 1968.
8. Wittmeyer, H.M. and Smode, F.E., "Fatigue Resistant Fastener," in Aircraft Structures and Materials Application, Proceedings of the 1st National SAMPE Technical Conference, Seattle, Washington, September 9-11, 1969.
9. Munse, W.H., "Riveted and Bolted Structural Joints," University of Illinois, Urbana, Structural Series Report No. 365, August 1970.
10. Hoosan, R.E., and Baker, M., "Spectrum Fatigue of Single Shear Lap Joints," Grumman Aerospace Corporation, Bethpage, N.Y. Test Report No. MPLR43-74-95, October 1974.
11. Sung, N.H., and Suh, N.P., "Effect of Fiber Orientation on Friction and Wear of Fiber Reinforced Polymeric Composites," Wear, 53(1979), pp. 129-141.
12. Cullimore, M.S.G., and Upton, K.A., "The Distribution of Pressure Between Two Flat Plates Bolted Together," Int. J. Mech. Sci., 6(1964), pp. 13-25.
13. Gould, H.H. and Mikic, B.B., "Areas of Contact and Pressure Distribution in Bolted Joints," Trans. ASME, Ser. B, J. Eng. Ind., 94(1972), pp. 864-870.
14. Cullimore, M.S.G. and Eckhart, J.B., "Distribution of the Clamping Pressure in Friction - Bolted Joints," Struct. Eng., 52(1974), pp. 129-131.
15. Stockdale, J.H., and Matthews, F.L., "The effect of Clamping Pressure of Bolt Bearing Loads in Glass Fiber-Reinforced Plastics," Composites, Vol. 7, Jan 1971, pp. 34-38.
16. Collings, T.A., "The Strength of Bolted Joints in Multi-Directional CFRP Laminates," Composites, Vol. 8, No. 1, January 1977, pp. 43-55.
17. Collings, T.A., "On the Bearing Strengths of CFRP Laminates," Composites, July 1982, pp. 241-252.
18. Whitney, J.M., and Nuismer, R.J., "Stress Fracture Criteria for Laminated Composites Containing Stress Concentrations," Journal of Composite Materials, Vol. 8, July 1974, pp. 253-265.
19. Nuismer, R.J., and Labor, J.D., "Applications of the Average Stress Failure Criterion: Part I - Tension," J. Composite Materials, Vol. 12 (1978), p. 238.
20. Nuismer, R.J., and Labor, J.D., "Applications of the Average Stress Failure Criterion: Part II - Compression," J. Composite Materials, Vol. 13 (1979), pp. 49-60.
21. Chang, F.K., Scott, R.A., and Springer, G.S., "The Effect of Laminate Configuration on Characteristic Lengths and Rail Shear Strengths," J. Composite Materials, Vol. 18, May 1984, pp. 290-296.
22. Sandhu, R.S., "A Survey of Failure Theories of Isotropic and Anisotropic Materials," AFFDL-TR-72-71, 1972.
23. Kaminski, B.E., and Lantz, R.B., "Composite Materials: Testing and Design," ASTM STP 460, 1969.
24. Waddoups, M.E., "Advanced Composite Material Mechanics for the Design and Stress Analyst," General Dynamics, Ft. Worth Division, Report FZM-4763, 1967.
25. Lance, R.H., and Robinson, D.N., "A Maximum Shear Stress Theory of Plastic Failure of Fiber-Reinforced Materials," J. Mech. Phys. Solids, Vol. 19, 1971.
26. Hill, R., "A Theory of the Yielding and Plastic Flow of Anisotropic Metals," Proceedings of the Royal Society, Series A, Vol. 193, 1948, pp. 281-297.

27. Azzi, V.D., and Tsai, S.W., "Anisotropic Strength of Composites," *Experimental Mechanics*, Vol. 5, 1965, pp. 283-288.
28. Hoffman, O., "The Brittle Strength of Orthotropic Materials," *J. Composite Materials*, Vol. 1, 1967, pp. 200-206.
29. Tsai, S.W., and Wu, E.M., "A General Theory of Strength of Anisotropic Materials," *Journal of Composite Materials*, Vol. 5, 1971, pp. 58-80.
30. Tennyson, R.C., Hansen, G.E., Mabson, G.E., and Wharram, G.E., "Development of General Failure Model for CF-18 Graphite/Epoxy Laminates," *Proc. DND Composite Workshop*, Victoria, B.C., July 1983.
31. Wu, E.M., "Phenomenological Anisotropic Failure Criterion," *Composite Materials*, Volume 2, Academic Press, 1974, pp. 353-431.
32. Eisenmann, J.R., "Bolted Joint Static Strength Model for Composite Materials," *NASA TM-X-3377*, April 1976, pp. 563-602.
33. Cruse, T.A., "Tensile Strength of Notched Composites," *J. Composite Materials*, Vol. 7, 1973, p. 218.
34. Waszczak, J.P., and Cruse, T.A., "Failure Mode of Strength Predictions of Anisotropic Bolt Bearing Specimens," *Journal of Composite Materials*, Vol. 5, July 1971, pp. 421-423.
35. Cheng, F.K., Scott, R.A., and Springer, G.S., "Failure of Composite Laminates Containing Pin Loaded Holes - Method of Solution," *Journal of Composite Materials*, Vol. 18, 1984.
36. Chang, F.K., Scott, R.A., and Springer, G.S., "Design of Composite Laminates Containing Pin Loaded Hole," *Journal of Composite Materials*, Vol. 18, 1984, pp. 279-289.
37. Yamada, S.E., and Sun, C.T., "Analysis of Laminate Strength and Its Distributions," *Journal of Composite Materials*, Vol. 12, 1978, pp. 273-284.
38. Wong, C.M.S., and Matthews, F.L., "A Finite Element Analysis of Single and Two-Hole Bolted Joints in Fiber Reinforced Plastics," *Journal of Composite Materials*, Vol. 15, September 1981, pp. 481-491.
39. Agarwal, B.L., "Static Strength Prediction of Bolted Joint in Composite Material," *AIAA/ASME/ASCE/AHS, 20th Structure, Structural Dynamics and Materials Conference*, St. Louis, MD, April 1979, pp. 303-309.
40. Grimes, G.C., and Whitney, J.M., "Degradation of Graphite/Epoxy Composite Materials Because of Load Induced Micromechanical Damage," *SAMPE Quarterly*, July 1978, pp. 1-13.
41. Soni, S.R., "Failure Analysis of Composite Laminates with a Fastener Hole," *Joining of Composite Materials*, STP 749, American Society for Testing and Materials, Philadelphia, 1981, pp. 143-164.
42. York, J.L., Wilson, D.W., and Pipes, R.B., "Analysis of the Net Tension Failure Mode in Composite Bolted Joints," *Journal of Reinforced Plastics and Composites*, Vol. 1, April 1982, pp. 141-152.
42. Pipes, R.B., Wetherhold, R.C., and Gillespie, J.W., Jr., "Notched Strength of Composite Materials," *Journal of Composite Materials*, Vol. 13, April 1979, pp. 148-160.
44. Crews, J.H., Jr., Hong, C.S., and Jaju, L.S., "Stress Concentration Factors for Finite Orthotropic Laminates with a Pin-Loaded Hole," *NASA Technical Paper 1862*, May 1981.
45. Oplinger, D.W., "Behaviour of Mechanically Fastened Joints in Composite Structures," *Proceedings of a conference on Fibrous Composites in Structural Design*, San Diego, California, Nov. 14-17, 1978, pp. 575-602.
46. Oplinger, D.W., "Stress Analysis of Composite Joints," *Proceedings of the 4th Army Materials Technology Conference*, Boston, Massachusetts, 16-19 September, 1975, pp. 405-452.
47. Wilkinson, T.L., Rowlands, R.E., and Cook, R.D., "An Incremental Finite-Element Determination of Stresses Around Loaded Holes in Wood Plates," *Computer and Structures*, Vol. 14, No. 1-2, 1981, pp. 123-128.
48. Rowlands, R.E., Rahman, M.U., Wilkinson, T.L., and Chiang, Y.L., "Single- and Multiple- Bolted Joints in Orthotropic Materials," *Composites*, July 1982, pp. 273-279.
49. Matthews, F.L., Wong, C.M., and Chyrssafitis, S., "Stress Distribution Around a Single Bolt in Fiber-Reinforced Plastics," *Composites*, July 1982, pp. 316-322.
50. Lekhnitskii, S.G., *Anisotropic Plates*, Gordon and Breach Science Publishers, 1968.
51. Cruse, T.A., "Boundary-Integral Equation Solution Methods," *AFML-TR-71-268*, December 1971.
52. De Jong, T., "Stresses Around Pin-Loaded Holes in Elastically Orthotropic or Isotropic Plates," *Journal of Composite Materials*, Vol. 11, July 1977, pp. 313-331.
53. Waszczak, J.P., and Cruse, T.A., "A Synthesis Procedure for Mechanically Fastened Joints in Advanced Composite Materials," *AFML-TR-73-143*, Vol. II, September 1973.
54. Lekhnitskii, S.G., *Theory of Elasticity of an Anisotropic Elastic Body*, Holden Day, Inc., 1963.
55. Garbo, S.P., and Ogonowski, J.M., "Strength Predictions of Composite Laminates with Unloaded Fastener Holes," *AIAA Journal*, Vol. 18, No. 3, May 1980, pp. 585-589.

56. Garbo, S.P., and Ogonowski, J.M., "Effect of Variances and Manufacturing Tolerances on the Design Strength and Life of Mechanically Fastened Composite Joints," AFWAL-TR-81-3041, Air Force Wright Aeronautical Laboratory, Dayton, OH, Vol. 1 & 2, April 1981.
57. Ashton, J.E., and Whitney, J. A., Theory of Laminated Plates, Technomic Publishing Co., Inc., 1970.
58. Oplinger, D.W., and Gandhi, K.R., "Stresses in Mechanically Fastened Orthotropic Laminates," in Proceedings of the Conference on Fibrous Composites in Flight Vehicle Design, Dayton, Ohio, 21-24 May 1974, AFFDL-TR-74-103, pp. 811-842, September 1974.
59. Oplinger, D.W., and Gandhi, K.R., "Analytical Studies of Structural Performance in Mechanically Fastened Fiber-Reinforced Plates," in Proceedings of the Army Symposium on Solid Mechanics, 1974: The Role of Mechanics in Design - Structural Joints, Army Materials and Mechanics Research Center, AMMRC MS 74-8, pp. 211-242 (September 1974) (AD786343).
60. Wolff, R.V., and Wilkins, D.J., "Durability Evaluation of Highly Stressed Wing Box Structure," Proceedings of the Fourth Conference on Fibrous Composites in Structural Design held in San Diego, California, Nov. 14-17, 1978.
61. Goodman, J.W., Lincoln, J.W., and Bennett, T.H., "The Air Force Structural Integrity Program for Advanced Composite Structures," Proceedings of the 18th AIAA/ASME Structures, Structural Dynamics and Materials Conference held in San Diego, California, March 21-23, 1977.
62. Waggoner, G., and Erbacher, H., "Damage Tolerance Program for the B-1 Composite Stabilizer," AIAA Paper No. 77-464, 1977.
63. Weinberger, R.A., Somoroff, A.R., and Riley, B.L., "U.S. Navy Certification of Composite Wings for the F-18 and Advanced Harrier Aircraft," AIAA Paper No. 77-466, 1977.
64. "Airplane Strength and Rigidity Reliability Requirements, Repeated Loads and Fatigue," Military Specification MIL-A-038866B (USAF), 22 August 1975.
65. "Airplane Damage Tolerance Requirements," Military Specification MIL-A-83444 (USAF), 2 July 1974.
66. "Aircraft Structural Integrity Program, Airplane Requirements," Military Standard MIL-STD-1530A, 11 December 1975.
67. Kam, C.Y., "Bolt Hole Growth in Graphite-Epoxy Laminates for Clearance and Interference Fits When Subjected to Fatigue Loads," ASTM STP 723, American Society for Testing and Materials, 1981, pp. 21-30.
68. Schütz, D., Gerharz, J.J., and Alschweig, E., "Fatigue Properties of Unnotched, Notched, and Jointed Specimens of a Graphite/Epoxy Composite," ASTM STP 723, American Society for Testing and Materials, 1981, pp. 31-47.
69. Rosenfeld, M.S., and Gause, L.W., "Compression Fatigue Behaviour of Graphite/Epoxy in the Presence of Stress Raisers," ASTM STP 723, American Society for Testing and Materials, 1981, pp. 174-196.
70. Phillips, E.P., "Effects of Truncation of a Predominantly Compression Load Spectrum on the Life of a Notched Graphite/Epoxy Laminate," ASTM STP 723, American Society for Testing and Materials, 1981, pp. 197-212.
71. Harris, B., "Fatigue and Accumulation of Damage in Reinforced Plastics," Composites, Vol. 8, No. 4, 1972.
72. Yang, J.N., "Fatigue and Residual Strength Degradation for Graphite/Epoxy Composites Under Tension-Compression Cyclic Loadings," J. of Composite Materials, Vol. 12, 1978, pp. 19-29.
73. Yang, J.N., and Lin, M.D., "Residual Strength Degradation Model and Theory of Periodic Proof Tests for Graphite/Epoxy Laminates," J. of Composite Materials, Vol. 11, 1977, pp. 176-203.
74. Roten, A., "Fatigue Failure of Multidirectional Laminate," AIAA Journal, Vol. 17, No. 3, March 1979, pp. 271-277.
75. Kotem, A., and Nelson, H.G., "Fatigue Behaviour of Graphite-Epoxy Laminates at Elevated Temperatures," ASTM STP 723, American Society for Testing and Materials, 1981, pp. 152-173.
76. Hart Smith, L.J., "Bolted Joints in Graphite-Epoxy Composites," NASA-CR-144899, June 1976.
77. Ramkumar, R.L. and Tossavainen, F.W., "Strength and Lifetime of Bolted Laminates," ASTM STP 927, 1986, pp. 231-273.
78. Quinn, W.J., and Matthews F.L., "The Effect of Stacking Sequence on the Pin Bearing Strength in Glass fibre reinforced plastic," J. Composite Materials, 11, No. 2, April 1977, p. 139.
79. Rybicki, E.F., and Schuesser, D.W., "Effect of Stacking Sequence and Lay-Up Angle on Free Edge Stresses Around a Hole in a Laminated Plate under Tension," J. Composite Materials, 12, No. 3, July 1978, p. 307.
80. Pagano, N.J., and Pipes, R.B., "The Influence of Stacking Sequence on Laminate Strength," J. Composite Materials, 3, No. 1, January 1971, p. 50.
81. Collings, T.A., "The Strength of Bolted Joints in Multi-Directional CFRP Laminates," RAE Technical Report 73127, 1975.
82. Matthews, F.L., Nixon, A., and Want, G.R., "Bolting and Riveting in Fibre Reinforced Plastics," Proceedings of Reinforced Plastics Congress, British Plastics Federation, Brighton, November 1976.

83. Berg, K.R., "Problems in the Design of Joints and Attachments," in Mechanics of Composite Materials, Proceedings of the Fifth Symposium on Naval Structural Mechanics, 1967.
84. Collings, T.A., "The Strength of Bolted Joints in Multi-Directional CFRP Laminates," Composites, vol. 8, No. 1, January 1977, p.43.
85. Johnston, N.J., "Synthesis and Toughness Properties of Resins and Composites," ACBE Composite Structure Technology Conference, 13-16 August, 1984.
86. Lee, A., "A Material Selection Review for the P.I.P Contract on Development of Advanced Composite Materials Technology," Canadair Memorandum No. MCM-000-118, November 1984.
87. Prince, D.E., "Corrosion Behaviour of Metal Fasteners in Graphite-Epoxy Composites," AFML-TR-75-53, July 1975.
88. Cole, R.T., Bateh, E.J., and Potter, J., "Fasteners for Composite Structures," Composites, July 1982, pp. 233-240.
89. Sendekyl, G.P., and Richardson, M.D., "Fatigue Behaviour of a Graphite-Epoxy Laminate Loaded through an Interference Fit Pin," Proc. of 2nd Air Force Conference on Fibrous Composites in Flight Vehicle Design, AFFDL-TR-74-103, September 1974, pp. 469-520.
90. Vostean, L.F., "Composite Aircraft Structures," Proceedings of the Fourth Conference on Fibrous Composites in Structural Design, San Diego, California, November 14-17, 1978, pp. 7-24.
91. Huttrop, M.L., "Composite Wing Substructure Technology on the AV-8B Advanced Aircraft," Proceedings of the Fourth Conference on Fibrous Composites in Structural Design, San Diego, California, November 14-17, 1978, pp. 25-40.
92. Kutscha, D., and Hofer, K.E., Jr., "Feasibility of Joining Advanced Composite Flight Vehicle Structures," Technical Report AFML-TR-68-391.
93. Military Handbook MIL-HDBK-17A (U.S.A., Department of Defense), 1971.
94. Agarwal, B.L., "Behaviour of Multifastener Bolted Joints in Composite Materials," AIAA-80-0307, 1980.
95. Godwin, E.W., Matthews, F.L., and Kilty, P.F., "Strength of Multi-Bolt Joints in GRP," Composites, July 1982, pp. 268-272.
96. Matthews, F.L., and Hirst, I.R., "The Variation of Bearing Strength with Load Direction," Symposium: Joining in Fibre Reinforced Plastics, Imperial College, 1978 (IPC Press).
97. Johnson, M. and Matthews, F.L., "Determination of Safety Factors for Use When Designing Bolted Joints in GRP," Composites, April 1979, pp. 73-76.
98. Dastin, S., "Joining and Machining Techniques," Handbook of Fibreglass and Advanced Plastics Composites, edited by G. Lubin (Van Nostrand Reinhold), 1969.
99. Strauss, E.L., "Mechanical Joints in Reinforced Plastic Structures," Machine Design, Vol. 32, March 1960.
100. Oleesky, S.S., and Mohr, J.G., SPI Handbook of Reinforced Plastics, Reinhold, 1964.
101. Webb, J.N. and Smith, M.A., "The Fatigue and Residual Strength of a Multi-Bolt Joint Between Metal and Carbon Fibre Composite," Symposium: Joining in Fibre Reinforced Plastics, Imperial College, 1978 (IPC Press).
102. Althof, W., and Müller, J., "Investigations on Bonded and Demountable Joints Made from Fibre Reinforced Plastics," Sulzer Technical Review, Switzerland, 1975.
103. Stockdale, J.H. and Matthews, F.L., "The Effect of Clamping Pressure on Bolt Bearing Loads in Glass Fibre Reinforced Plastics," Composites, Vol. 7, No. 1, January 1976, p. 34.
104. Wolff, R.V., and Lemon, G.H., "Reliability Prediction for Composite Joints - Bonded and Bolted," AFML-TR-74-197, March, 1979.
105. Wolff, R. V. and Wilkins, D.J., "Durability Evaluation of Highly Stressed Wing Box Structure," Proceedings of the Fourth Conference on Fibrous Composites in Structural Design, San Diego, California, 14-17 November, 1978, pp. 761-769.
106. Sandifer, J.P., "Fretting Fatigue on Graphite/Epoxy Composites," AIAA Paper No. 77-418, 1977.
107. Shivakumar, K.M., and Crews, J.H., Jr., "An Equation for Bolt Clamp-up Relaxation in Transient Environments," NASA Technical Memorandum 84480, April, 1982.
108. Brahney, J.H., "Fasteners for Composite Structures," Aerospace Engineering, June 1985, pp.9-14.
109. Crews, J.H., Jr., "Bolt-bearing Fatigue of a Graphite/Epoxy Laminate," Joining of Composite Materials, ASTM STP 749, American Society for Testing and Materials, 1981, pp.131-144.
110. Jarfall, K.L., "Shear Loaded Fastener Installations," SAAB-Scania Rapport KH R-3360, 1983.
111. Huth, H., "Influence of Fastener Flexibility on the Prediction of Load Transfer and Fatigue Life for Multiple-Row Joints", ASTM STP 927, 1986, pp. 221-250.

112. Hyer, M.W. and Kiang, E.C., "Stresses Around Holes in Pin-Loaded Orthotropic Plates", *J. Aircraft*, Vol. 22, No. 12, December, 1985, pp. 1099-1101.
113. Tsujimoto, Y. and Wilson, D.W., "Elasto-Plastic Failure Analysis of Composite Bolted Joints", *Journal of Composite Materials*, Vol. 20, May, 1986, pp. 236-252.
114. Wilson, D.W. and Tsujimoto, Y., "On Phenomenological Failure Criteria for Composite Bolted Joint Analysis," *Composite Science and Technology*, 26, 1986, pp. 283-303.
115. Freeman, S.M., "Characterization of Lamina and Interlamina Damage in Graphite/Epoxy Composites by the Deply Technique," *ASTM STP 787*, 1982, pp. 30-62.

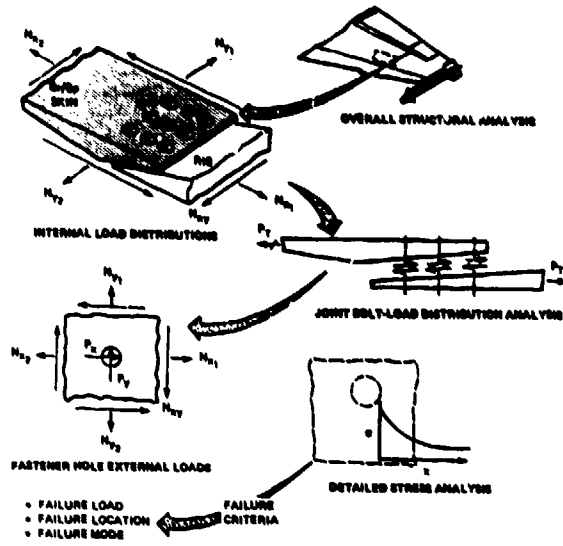


FIG. 1: JOINT FAILURE ANALYSIS (REF. 1)

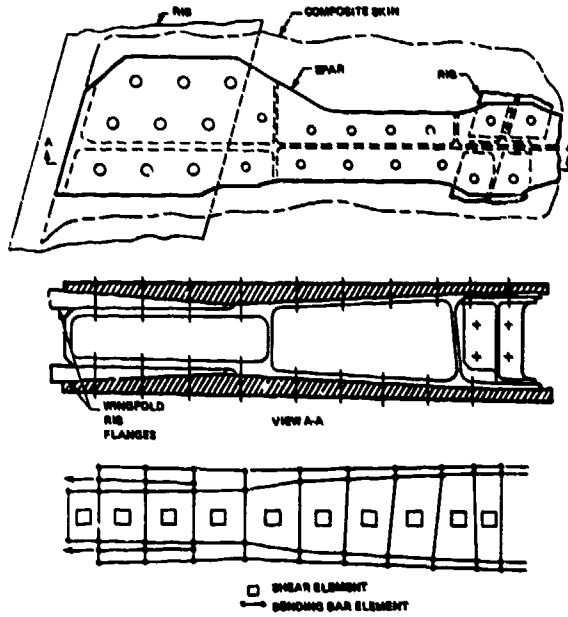


FIG. 2: WINGFOLD SPLICE JOINT IDEALIZATION (REF. 1)

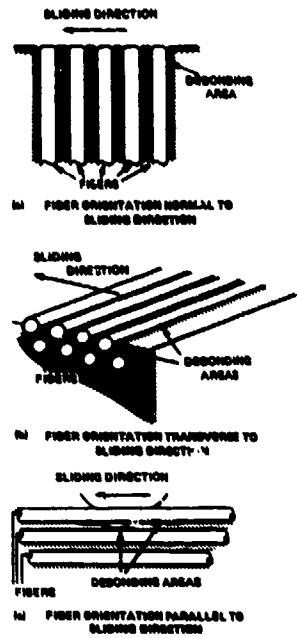


FIG. 3: SCHEMATIC REPRESENTATION OF FAILURE MODES IN UNIAXIAL CONTINUOUS FIBER REINFORCED COMPOSITE UNDER SLIDING SURFACE FIBER ORIENTATION NORMAL (a), TRANSVERSE (b) AND LONGITUDINAL (c) TO THE SLIDING DIRECTION (REF. 11)

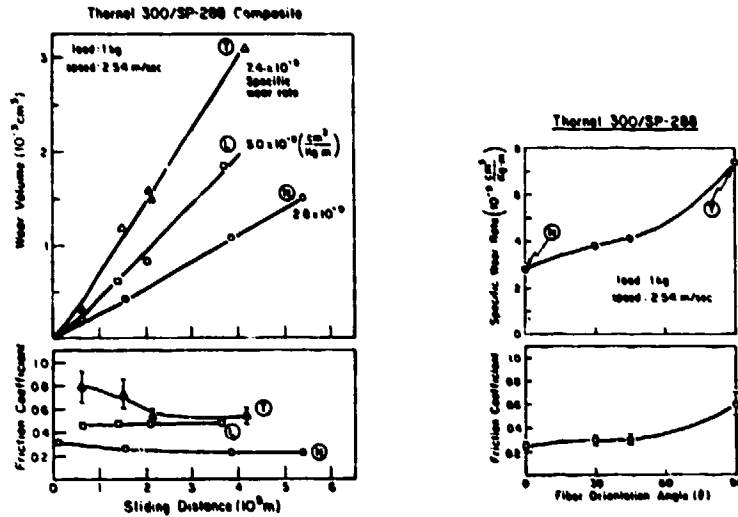


FIG. 4: FRICTION COEFFICIENTS AND WEAR VOLUME AS A FUNCTION OF SLIDING DISTANCE IN UNIAXIAL GRAPHITE FIBER-EPoxy COMPOSITE. SLIDING AGAINST S100 STEEL, WITH FIBER ORIENTATIONS NORMAL, LONGITUDINAL AND TRANSVERSE TO THE SLIDING DIRECTION (REF. 11)

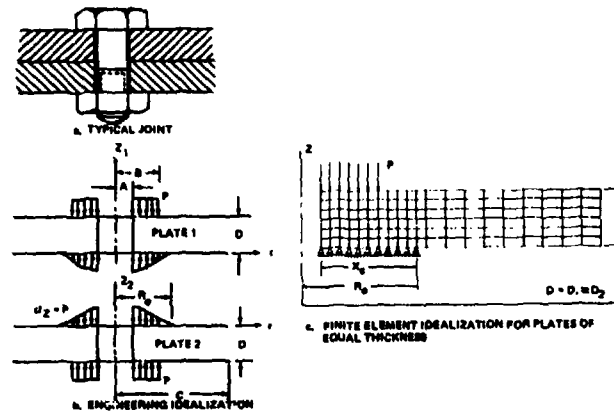


FIG. 5: IDEALIZATION OF TIGHTLY BOLTED JOINT TO DETERMINE CONTACT PRESSURE BETWEEN PLATES OF EQUAL THICKNESS (REF. 12)

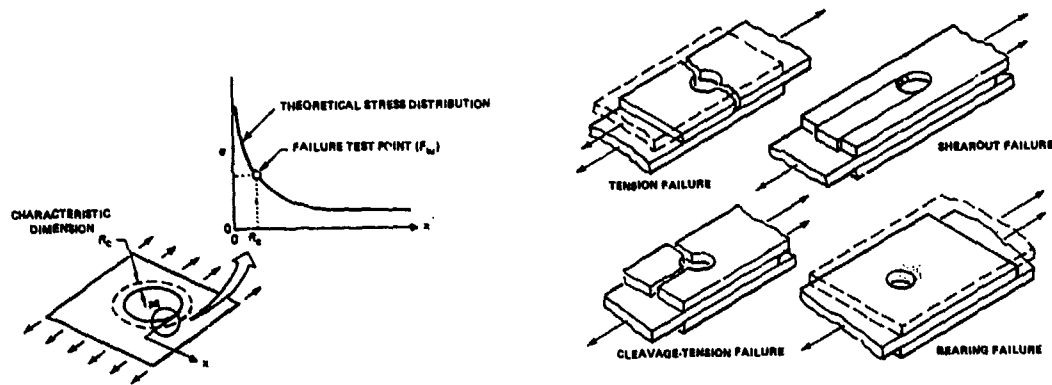
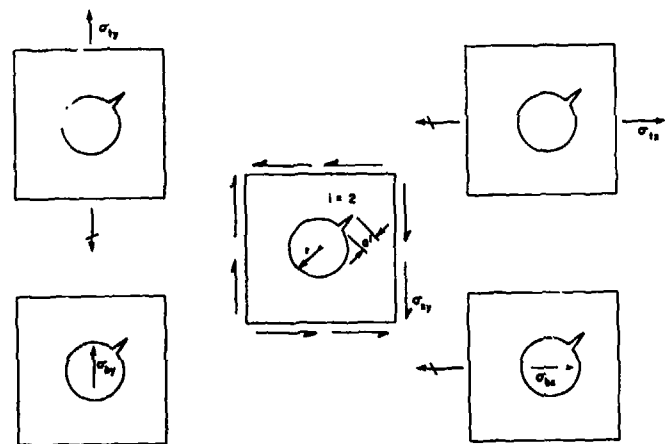


FIG. 6: FAILURE HYPOTHESIS (REF. 18)

FIG. 7: MODES OF FAILURE FOR BOLTED COMPOSITE JOINTS



$$K_I = \sqrt{\pi a} \left[ I \left( \frac{a}{r} \right)_{1x} \sigma_{1x} + I \left( \frac{a}{r} \right)_{1y} \sigma_{1y} + I \left( \frac{a}{r} \right)_{2y} \sigma_{2y} + I \left( \frac{a}{r} \right)_{2x} \sigma_{2x} + I \left( \frac{a}{r} \right)_{2y} \sigma_{2y} \right]$$

FAILURE CRITERION:  $K_I = K_{Ic}$

FIG. 8: COMPUTATION OF STRESS INTENSITY FACTOR USING LINEAR SUPERPOSITION (REF. 32)

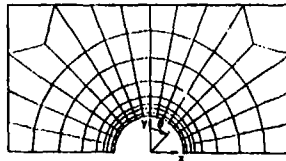
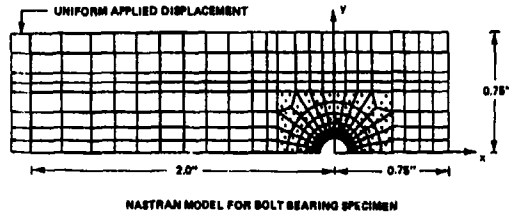
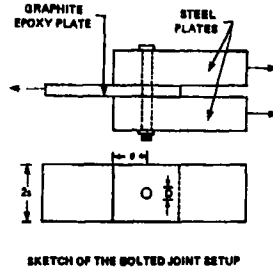


FIG. 9: NASTRAN MODEL OF THE REGION IN THE VICINITY OF THE FASTENER HOLE (REF. 39)

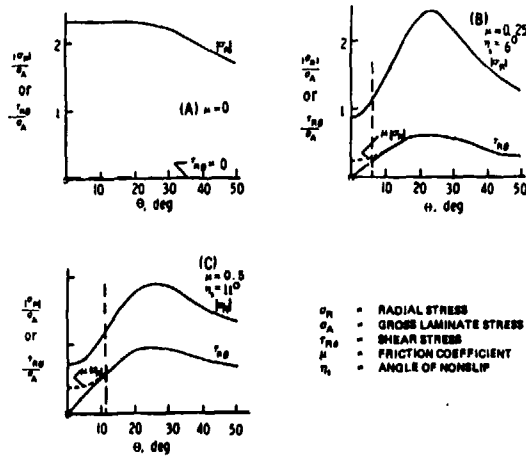


FIG. 10: EFFECT OF FRICTION ON RADIAL AND SHEAR STRESS DISTRIBUTION AROUND FASTENER HOLE,  $O_2 \pm 45$  GRAPHITE EPOXY,  $s/D = 4$ ,  $s/D = 1$  (MULTI-PIN) (REF. 39)

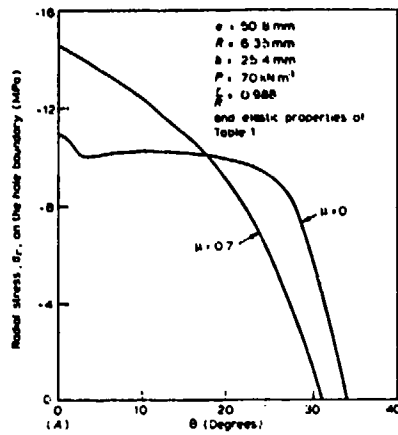


FIG. 11: EFFECT OF FRICTION ON THE RADIAL STRESS BETWEEN BOLT A AND WOOD OF A SINGLE FASTENER IN SITKA SPRUCE (REF. 48)

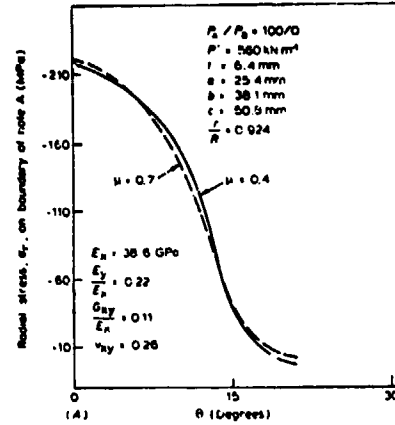


FIG. 12: THE RELATIVE INSENSITIVITY TO VARIATIONS IN FRICTION OF THE RADIAL STRESS BETWEEN BOLT A OF A DOUBLE FASTENER JOINT AND THE CONTACTING FIBREGLASS COMPOSITE (REF. 48)

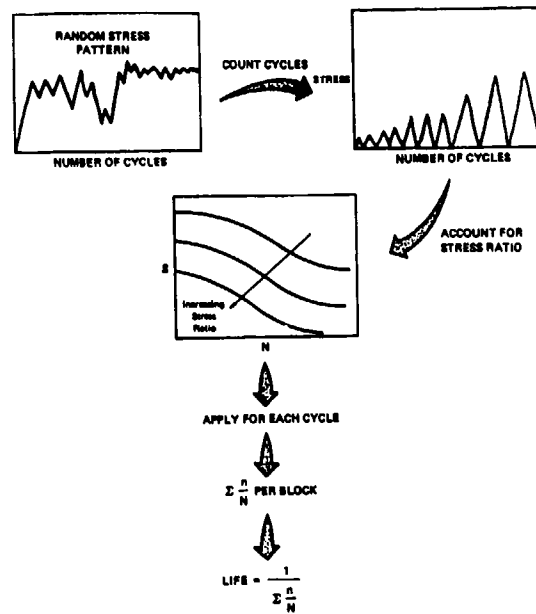


FIG. 13: MINER'S RULE APPLIED TO COMPOSITES

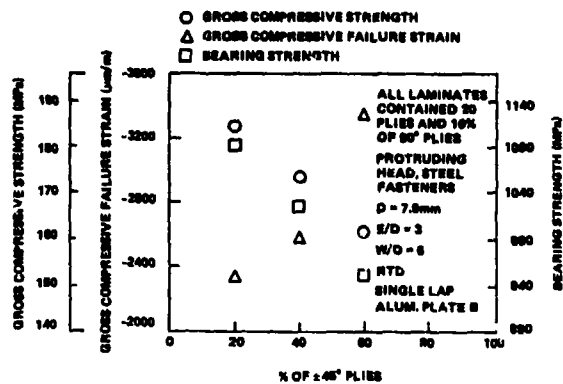


FIG. 14: EFFECT OF LAYUP ON THE COMPRESSIVE RESPONSE OF 20-PLY LAMINATES (REF. 77)

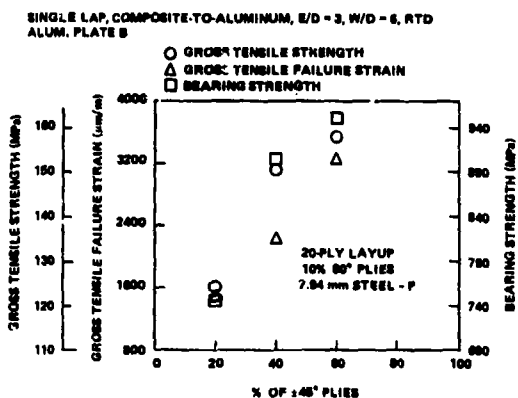
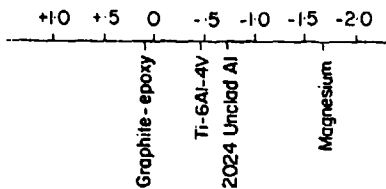


FIG. 15: EFFECT OF LAMINATE LAYUP ON THE TENSILE RESPONSE OF 20-PLY LAMINATES IN SINGLE SHEAR (REF. 77)

Galvanic potential (volts)

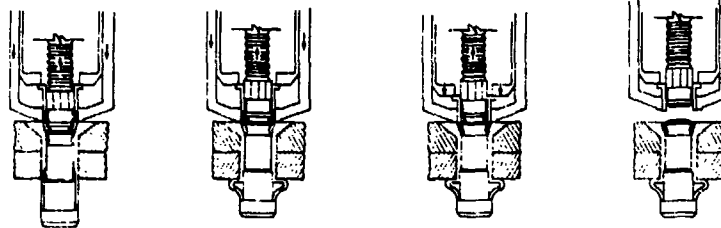


Comparison of galvanic potential of structural materials

Preference No	Material	Compatibility with graphite/epoxy
1	Titanium, Ti alloys, Ti-Nb	Compatible
2	MP-35N, Inco 600	Compatible
3	A286, PH13-8Mo	Marginally acceptable
4	Monel	Marginally acceptable
5	Low alloy steel; martensitic stainless steel	Not Compatible

Summary of NASC galvanic compatibility chart

FIG. 16: GALVANIC CORROSION RESULTS FROM DIFFERENCES IN POTENTIAL (REF. 58)



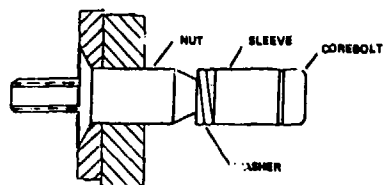
**Step 1.** During the initial part of the driving operation, the sleeve is squeezed between the head of the pin and the nose of the rivet tool.

**Step 2.** The head of the pin upsets the sleeve to form a strong, bulbous head on the blind side.

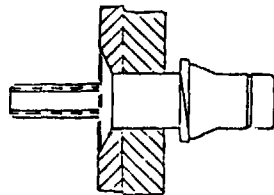
**Step 3.** When the blind head has been formed, the tool automatically forces the locking collar (at the pin end of the sleeve) into the conical space between the recess in the sleeve head and the locking groove in the pin. This locks the parts together permanently.

**Step 4.** Pin is broken off in tension at the break-neck groove, substantially flush with the head of the sleeve. There is no projecting pin left to be cut off in a separate operation.

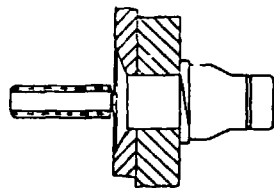
**FIG. 17: INSTALLATION SEQUENCE OF A TYPICAL BLIND FASTENER FOR SOLID COMPOSITE LAMINATES**



Using NAS 1675-type installation tooling, the nut is restrained from turning while the corebolt is driven.



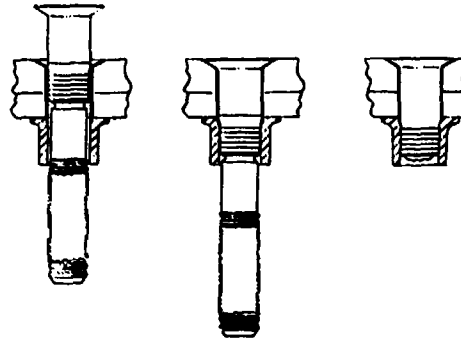
The advance of the corebolt forces the washer and sleeve over the taper, expanding and uncoiling the washer to its maximum diameter.



Continued advance of the corebolt draws the washer and sleeve against the joint surface, preloading the structure.

At a torque level controlled by the break groove, the slip bed portion of the corebolt separates, and installation is complete.

**FIG. 18: COMP-TITETM BLIND FASTENER INSTALLATION SEQUENCE**



**CIL INSTALLATION PROCEDURE**

- STEP 1. PLACE ASSEMBLY IN WORK STRUCTURE. INSERT COLLAR OVER PINTAIL. (GRIPS THRU 2D ONLY. SEE NOTE BELOW)
- STEP 2. TOOL PULLS ON PINTAIL AND DRAWS THE CIL PIN INTO THE SLEEVE WHICH EXPANDS THE SLEEVE TO COMPLETELY SEAL THE FASTENER IN THE WORK.
- STEP 3. AS THE PULL ON THE PIN INCREASES, TOOL ANVIL SWAGES COLLAR INTO LOCKING GROOVES AND A PERMANENT LOCK IS FORMED. TOOL CONTINUES TO PULL UNTIL THE PIN BREAKS AT THE BREAK-NECK GROOVE AND IS EJECTED. TOOL ANVIL DISENGAGES FROM SWAGED COLLAR.

NOTE: ABOVE 2D, IT IS NECESSARY TO PULL THE PIN/SLEEVE ASSEMBLY INTO THE WORK WITH A SPECIAL PULL IN TOOL. WHEN SEATED PUT THE COLLAR OVER THE PINTAIL AND INSTALL THE FASTENER USING THE STANDARD INSTALLATION TOOL. SEE ABOVE CHART FOR NOSE INSTALLATION INFORMATION AND PROCEDURES.

**FIG.19: INSTALLATION SEQUENCE OF A TWO-PIECE LOCKBOLT FASTENER FOR SOLID COMPOSITE LAMINATES**

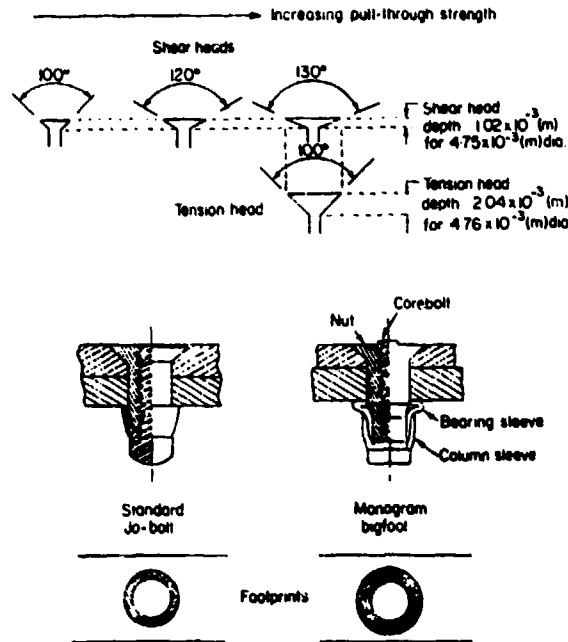


**FIG. 20: LARGER FLUSH HEAD DIAMETER AND FOOTPRINT INCREASE PULL-THROUGH STRENGTH (REF. 88)**

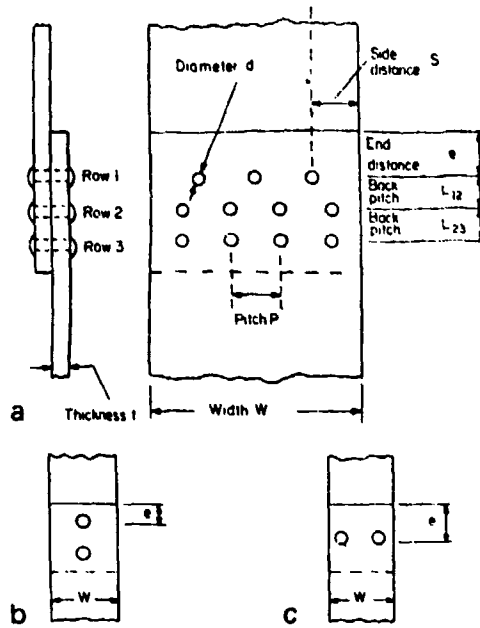


**FIG. 21: DEFINITION OF JOINT GEOMETRY: A) ROWS OF RIVETS (ROWS 1 AND 2 ARE STAGGERED, ROWS 2 AND 3 ARE IN UNIFORM RECTANGULAR PATTERN); B) 2 RIVETS IN TANDEM (LINE OF RIVETS); C) 2 RIVETS IN PARALLEL (ROW OF RIVETS) (REF. 82)**

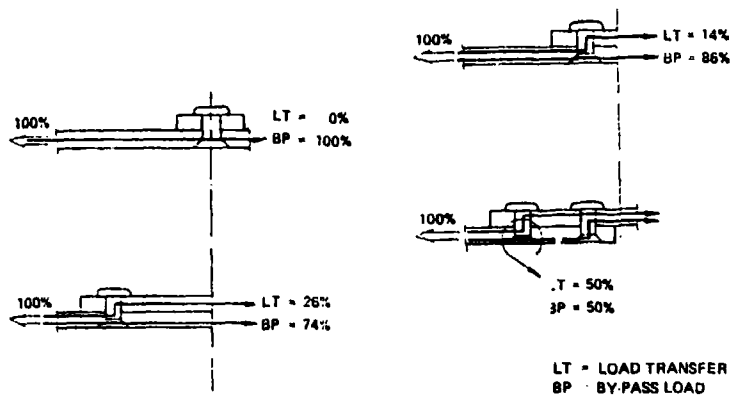


**FIG. 22: THE EFFECT ON THE AMOUNTS OF LOAD TRANSFERS AS A RESULT OF GEOMETRICAL CHANGES (REF. 110)**

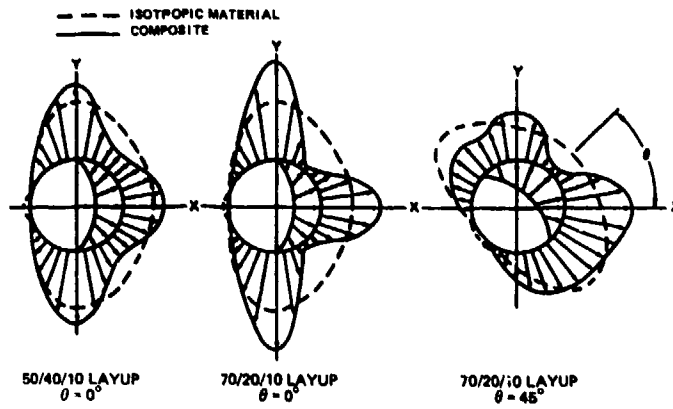


FIG. 23: THE EFFECTS ON CIRCUMFERENTIAL STRESS DISTRIBUTIONS AS A RESULT OF SHIFTING FASTENER LOAD DIRECTION (REF. 56)

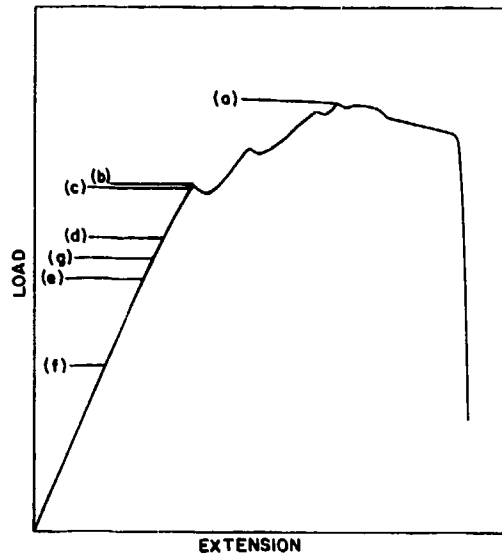


FIG. 24: TYPICAL LOAD/EXTENSION PLOT (REF. 67)

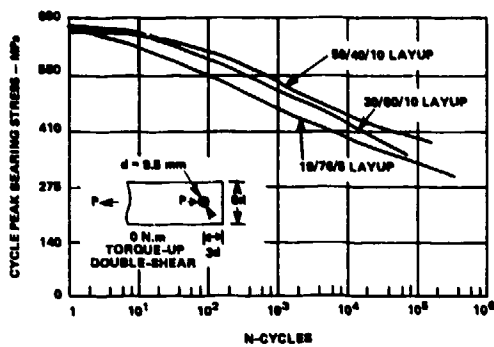


FIG. 25: COMPARISON OF R = -1.0 JOINT FATIGUE LIFE TRENDS (REF. 56)

COMPARISON OF EXPERIMENTAL RESULTS AND ANALYTICALLY  
PREDICTED DATA FOR DOUBLE SHEAR FASTENED JOINTS

J. Bauer, E. Mennle

MESSERSCHMITT-BÖLKOW-BLOHM GMBH  
Helicopter and Airplane Division  
8000 Munich 80, P.O. Box 801160, W-Germany

SUMMARY

Experimental tests were carried out to investigate the strength of open holes and pin loaded holes, as well as the combination of both. The material used was 914C/T300. The tests delivered enough information to represent the basis for the development of an analytic prediction method.

The prediction method is based on a linear analysis, which provides the stress field around a hole loaded with any type of loading. To make use of this information, in order to predict the strength, some empirical influence has to be taken into account to produce good correlation between experimental and theoretical data. The obtained accuracy is shown, as well as diagrams representing theoretically derived notch sensitivity and the double shear pin peeling strength.

INTRODUCTION

In aircraft structures the areas of local load introduction into CFRP parts require careful treatment during the design phase. To do good stressing and sizing of the load transferring parts special experience with composite materials is necessary. If an accurate prediction method for the strength of mechanically fastened joints is ready for use, there is every possibility to save weight, time and test costs. The problem of stressing bolted joints and notches in CFRP is much more complicated than with metal structures. The reason for this is the material non-homogenous nature, its orthotropic behaviour and its brittleness. Several prediction methods were discussed in the literature, for example the average stress criterion, the point stress criterion and the methods using stress concentration factors.

The prediction method discussed here calculates the stress distribution around the hole and evaluates the stresses point by point around it. This procedure gives the method its name: Point stress criterion. The input data required are: the unidirectional properties of the single layer and the geometric and loading conditions of the actual technical problem, as shown in Figure 1.

The overall purpose of the method is to be able to predict the strength of a single hole in CFRP laminates loaded with any type of loading. This includes for example a bolt load in any direction acting alone or by-pass stresses around an open hole or the most common case when both loading possibilities act superimposed together. This last case presents the biggest problems, but is needed for sizing complex aircraft structures and is therefore of great interest. Figure 2 clarifies the effect of the numerous different elastic and loading possibilities on the technical problem.

As a first step we must calculate the stress distributions around an open and pin loaded holes.

The second step and final challenge is to interpret the resulting stress distribution in such a manner, that good correlation with test results is obtained. In the following chapters an impression is given of the difficulties which arose during the development of the second step and the accuracy finally obtained.

PRINCIPLE OF THE MATHEMATICAL TREATMENT

The basis of our prediction method is the closed solution for the two-dimensional stress distributions around holes according to G.N. Savin, published 1966. Based on the starting point of stress functions, he provided solutions for open and for bolt-loaded holes, as shown in Figure 3. By superposition of these two solutions it is possible to obtain the stress distribution for the most general case (Figure 2) and to calculate the stress vector at any point around the hole independently from the kind of loading. A failure criterion is needed now to interpret the stresses point by point and to select the highest loaded one. If its failure load is regarded to be responsible for the failure of the laminate, then two items of information are received: the location where first failure occurs and the strength of the CFRP-laminate. In this way the failure of the hole, under the actual conditions, is analytically derived and the analysis is ready for verification by test results. Good correlation between theory and practice is required.

Following the assumption, that good correlation for the open hole problem plus good correlation for the loaded hole problem results as well in good correlation for the interaction of both, test series for open holes, double shear bearing strength and interaction of pin loaded holes with passing stresses are required for the development of a reliable prediction method.

## TESTS

To provide a good data base for comparisons with the calculation method, three different types of specimen configurations were tested: Open holes, double shear bearing and interaction of bearing and passing stresses. Figure 4 shows the configurations of the specimens used.

To avoid undesirable geometric influences of width, edge distance and hole diameter, the dimensions were kept constant for all the three specimens.

The necessary test parameters are

- the laminate lay-up
- off-axes loading
- RT and h/w conditions.

It is logical, that the accuracy and the reliability of the prediction method is dependent on number and selection of the available test points. This means a sufficient number of tests have to be performed to obtain good accuracy.

## CORRELATION OF TESTS AND PREDICTED DATA

The results of the experiments are shown on the load deflection curves (Figure 5). With reference to our linear-elastic analysis, the double shear pin bearing and the interaction tests show a behaviour, which causes difficulties. In Figure 5 is shown in principle, that a nonlinear range succeeds a linear one prior to failure. The problem which arises is that it is necessary, for the practical work of a stress office, to predict the ultimate failure and not the end of the linear range, which we could easily obtain with a linear elastic analysis. A second basic difficulty arises, because there exists no failure criterion, which is able to predict, with overall accuracy, the numerous failure mechanisms which might occur in CFRP-laminates and in the vicinity of a hole. To overcome these difficulties, there is no other choice, than to use the linear-elastic analysis, if a nonlinear one is not available and to influence the analysis semi-empirically, using test results.

The consequence is seen easily, that the test program has to cover a wide range of all technically practical applications. If the test points of the program are selected reasonably, the conditions for the development of a reliable prediction method are then available. In Figure 6 a summation of the different semi-empirical manipulations developed is shown.

The most important and generally used are characteristic distances. They result in the stresses being analysed at a certain distance away from the hole edge. This results in better correlation with the ultimate test failure loads but also in the disadvantage that the stress gradients in the vicinity of the hole cause a reduction of the accuracy.

This effect can be reduced if all unidirectional properties are increased by the same constant factor. Then the characteristic distances are able to be reduced and the evaluation of the stresses is done more close to the hole edge.

Every failure criteria has its specific advantages and disadvantages. We tried to avoid the imperfection of our ETL-failure hypothesis by the advantage of the YAMADA total failure criteria, in other words we used both.

By slightly increasing the unidirectional compression strength in the case of a 'filled hole' even better correlation with the test results is obtained. A good reason for influencing this is, that the bolt supports the laminate which has the effect of increasing the compression strength in the vicinity of the bolt.

All these empirical influences have to be co-ordinated with each other and in respect to the correlation between test results and the analytically predicted data. The achieved accuracy is represented by the diagrams of Figure 7. On the abscissa the predicted values are plotted and on the ordinate the test results. Every point on the diagrams represents a test point of usually six specimens of open hole, pin bearing and interaction tests. If the prediction is optimal, then the associated point lies on the angle bisector of the two lines. We tried to receive a final accuracy for our calculation method of +/-10 %. As seen in Figure 7 we had to accept less accuracy, but only when the predicted value was conservative in comparison to the test result. The accuracy shown was achieved by a lot of compromises between the three different items. Special attention was given to the accuracy of the interaction tests.

## CONCLUSIONS

The developed analysis is good enough to be used in aircraft design and offers the possibility to predict the strength of mechanically fastened joints in double shear.

Several possibilities are presented for using the analysis. In Figure 8 the strength of open holes in tension was calculated for all possible lay-up's and given in an overview. The same was done for the double shear pin bearing strength and is shown in the diagram of Figure 9.

Following from the more simple test cases presented to the more sophisticated ones, the possibility is available to investigate the influences of various loading conditions. This is advantageous, because experimental tests with complex loading are expensive and very difficult to perform.

If the input data of the unidirectional properties are varied, it is also possible to investigate material influences, but quantitative uncertainties have to be taken into account, because the semi-empirical manipulations were developed especially for the material 914C/T300. If other materials are used cross-checks by tests have to be carried out and the prediction method has to be modified.

#### REFERENCES

- 1) G.N. Savin  
Stress Distribution Around Holes  
NASA TT F-607
- 2) MBB/FE214/KLE/R/006  
J. Vilsmeier  
Grundlagenuntersuchungen für die Auslegung  
gebolzter Fügungen
- 3) Diplomarbeit, Institut für Flugzeugbau der Universität Stuttgart  
U. Sperling  
Literaturstudie über Kerben in CFK
- 4) S.G. Lekhnitskii  
Anisotropic Plates  
Gordon and Breach Science Publishers
- 5) F.K. Chang, R.A. Scott and G.S. Springer  
Design of Bolted Composite Joints  
28th National SAMPE Symposium, April 12-14, 1983

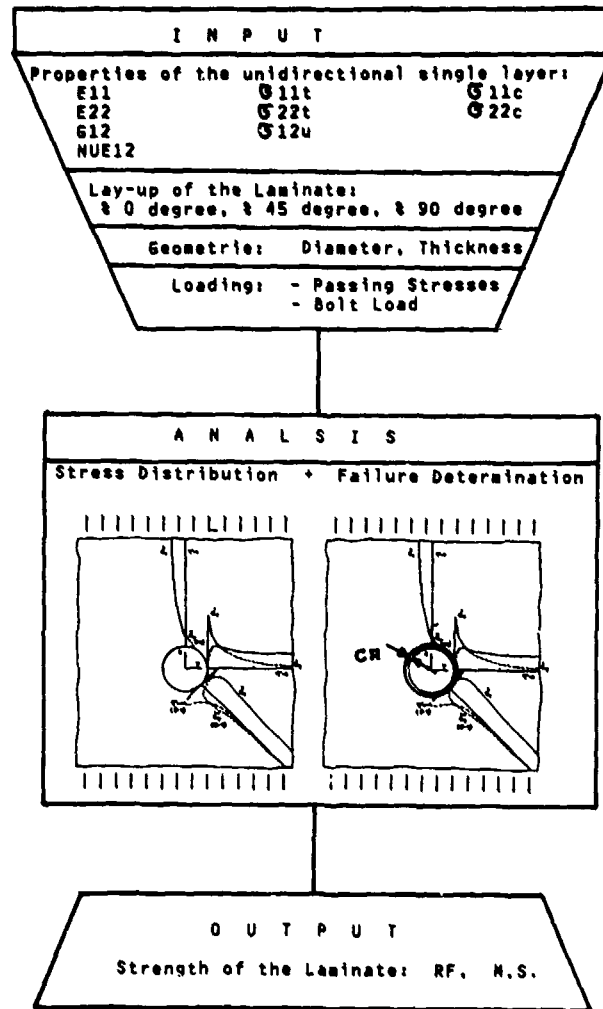


Figure 1 : Flow Chart of the Prediction Method

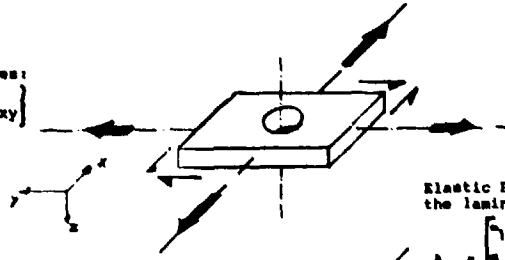
**MBB**

Figure 2 : Loading Possibilities of a Hole,  
Elastic Properties of an Orthotropic Plate

Open Hole

loaded by passing stresses:

$$/G / = \{ \sigma_x \quad \sigma_y \quad \sigma_{xy} \}$$



Elastic Properties of  
the laminate:

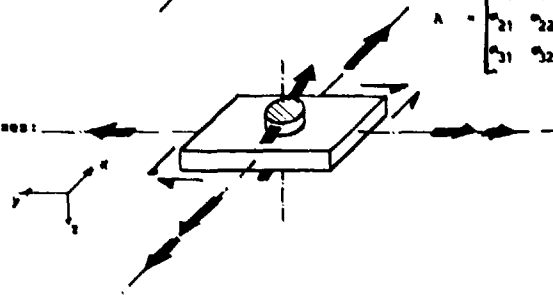
$$A = \begin{bmatrix} A_{11} & A_{12} & A_{13} \\ A_{21} & A_{22} & A_{23} \\ A_{31} & A_{32} & A_{33} \end{bmatrix}$$

Bolt Loaded Hole

loaded by passing stresses:

$$/G / = \{ \sigma_x \quad \sigma_y \quad \sigma_{xy} \}$$

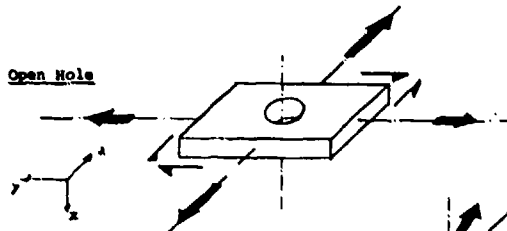
and a bolt load  $P$   
in direction  $\phi$



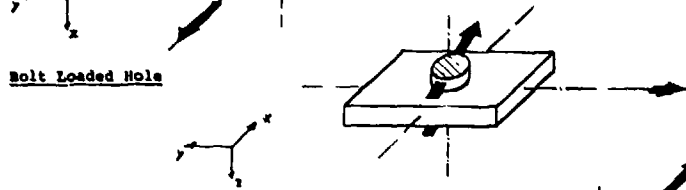
**MBB**

Figure 3 : Two-Dimensional Stress Distributions

Open Hole



Bolt Loaded Hole



Interaction

(of open and bolt-loaded hole)





Figure 4 : Specimen for Open Hole, Pin Bearing and Interaction Tests

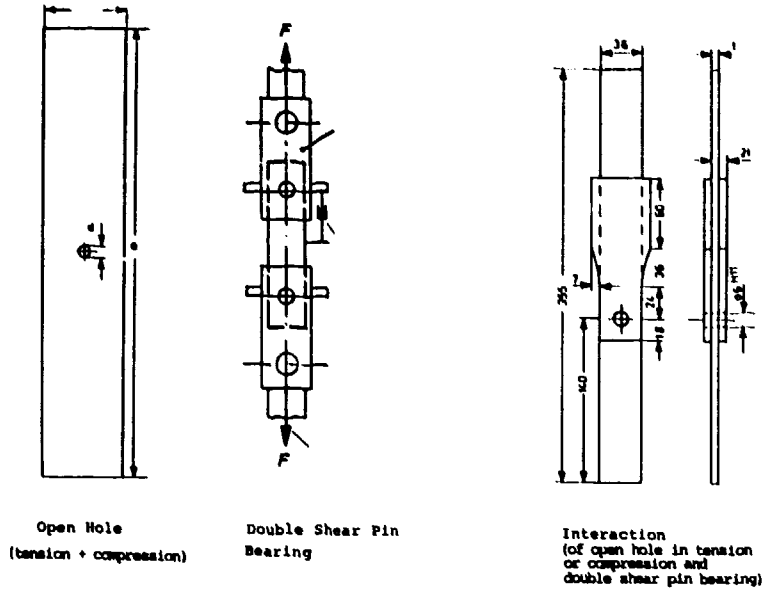
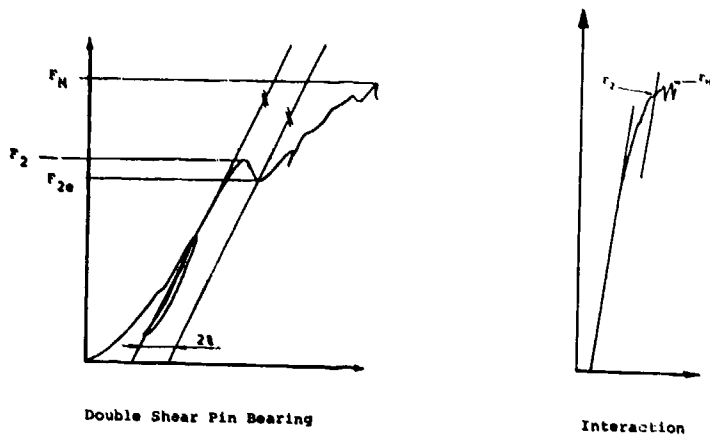


Figure 5 : Typical Load Deflection Curves



**MBB**

Fig. 6 : Semi-Empirical Influence

EMPIRICAL STEP	I	REASON
1.) CHARACTERISTIC DISTANCE	I	The first failure at the hole-contour doesn't represent the ultimate failure
2.) UNIDIRECTIONAL STRENGTHS	I	The stress-gradients in the vicinity of the hole contour decrease the accuracy of the stress-evaluation
3.) FAILURE CRITERIA	I	The imperfection of one failure criterion is avoided by the other one and vice versa
4.) COMPRESSION STRENGTH	I	In the vicinity of the bolt the compression strength is increased because of the support of the bolt

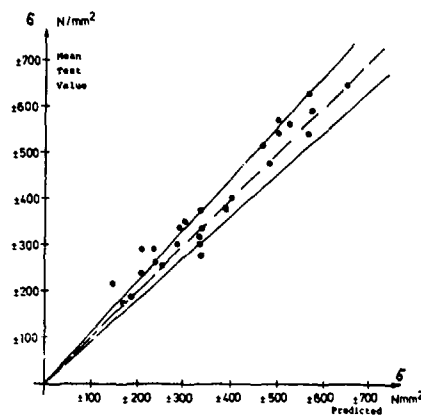


Figure 7a : Comparison of Open Hole Tension and Compression Tests with Predicted Data

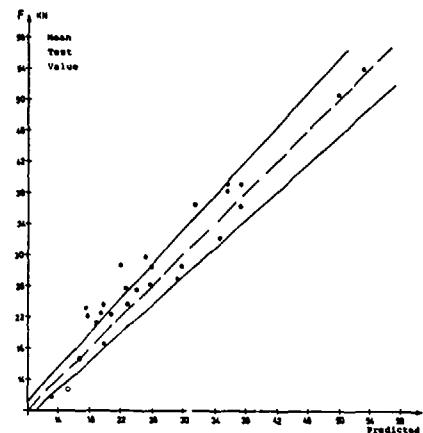


Figure 7b : Comparison of Double Shear Pin Bearing Strength Test Results with Predicted Data

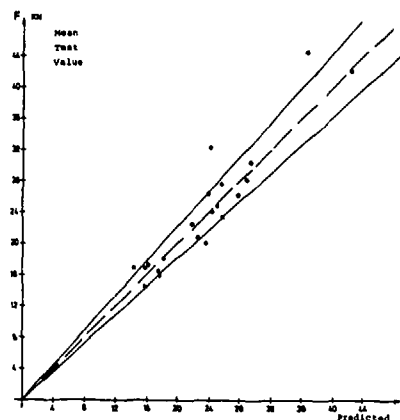


Figure 7c : Comparison of "Interaction" Test Results with Predicted Data

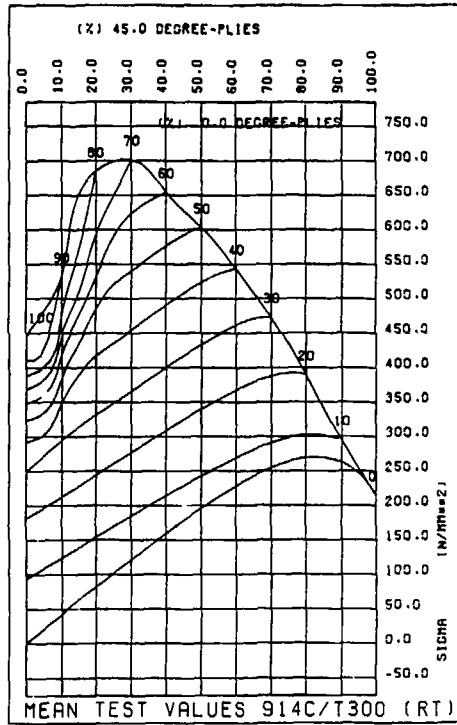


Figure 8 : Open Hole Tension Strength

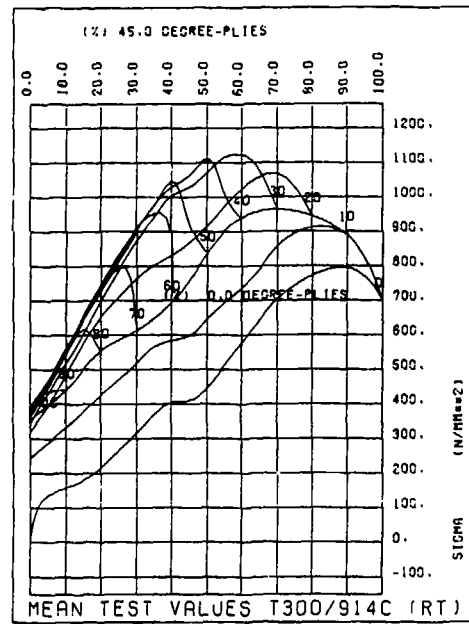


Figure 9 : Double Shear Pin Bearing Strength

## RECENT STUDIES ON BOLTED JOINTS IN COMPOSITE STRUCTURES

V.B. Venkayya\*, R.L.Ramkumar\*\*, V.A.Tischler\*, B.D. Snyder\*, J.G. Burns\*

### SUMMARY

A brief review of recent Air Force programs in bolted joints in composite structures was presented in this paper. The review included analytical methods development and experimental verification. Analytical methods addressed both single fastener and multifastener joints. A number of joint design variables, such as, finite geometry, fastener arrangement, joint service environment, and a number of relevant parameters were addressed in these programs. The test programs included static and fatigue specimens. Single fastener and multifastener joint tests were conducted to correlate the analysis results. Full scale test specimens were used to verify the overall analysis strategy. A comprehensive design guide was developed for the design and analysis of bolted joints in composite structures. This design guide is supported by four computer programs.

### 1. INTRODUCTION

Joints are the key elements in load transfer between aircraft components. They are also the weakest links in the overall performance of a structure. The major life cycle costs of an aircraft structure can be directly or indirectly traced to inadequately or improperly designed joints. Joining issues are particularly acute in composite structures because of the associated problems of delamination, anisotropy, absence of ductility and environmental effects. However, bolted composite joints, when properly designed, are reliable, structurally efficient and cost effective. The development of proper design procedures is the subject of a number of investigations by the Air Force, Navy, Army, NASA and industry. The purpose of this paper is to review some of the recent Air Force investigations and identify the key joint design issues.

The primary load carrying mechanism in joints is sliding of the joining elements (plates) which is prevented by the fasteners. In doing so the fastener transmits the load from one plate to the other. There are two elements in the failure of a joint: the fastener itself and failure of the components joined together by the fastener. The fasteners used in most aircraft construction are based on national aerospace standards, and the manufacturer is responsible for the design, specification and validation of their failure loads. Failure prediction of the component parts, however, is the responsibility of the joint designer. The interest of this paper is the design and failure prediction of component parts.

Joints can be in single shear (single lap) or in double shear (double lap) as shown in Fig. 1. Depending on certain joint parameters, the behavior of a single shear joint can be significantly different from a joint in double shear. A joint in double shear can be analyzed quite satisfactorily by a two dimensional analysis based on plane stress assumptions. The eccentricity in a single shear joint can introduce significant bending in the plates as well as in the fastener and invalidate the plane stress or two dimensional analysis. At the same time the behavior of a single lap is extremely complex, and an accurate three dimensional analysis is intractable. Modifications to account for the three dimensional effects are based on treating the fastener as a short beam, supported on an elastic foundation. Such an analysis with empirical estimates of the foundation stiffness can give reasonable results for the design.

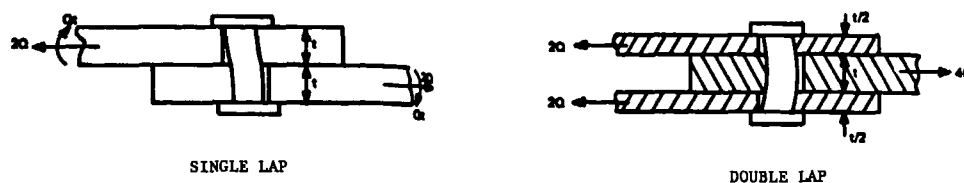


FIG 1: FASTENERS IN SINGLE AND DOUBLE SHEAR

The general failure modes in mechanically fastened joints are summarized in Fig. 2. There are some similarities in the failure of metal and composite joints. For instance, the basic failure modes, such as, net tension failure, bearing failure, shearout failure and cleavage-tension failure are not significantly different in both joints. However, there are many factors that are peculiar to the behavior of composite joints. The stress distribution around a hole is a function of the laminate layup and the load orientation. The stress concentrations are different for different layups. Similarly, the stress distribution

\* Aerospace Engineers, Flight Dynamics Laboratory, AFWAL, WPAFB OH 45433-6553

\*\* Northrop Corporation

around a loaded hole is different for different fiber orientations. The ductility of metals significantly reduces the danger of catastrophic failures. The tailored laminated composites exhibit unique failure modes because of their brittle behavior.

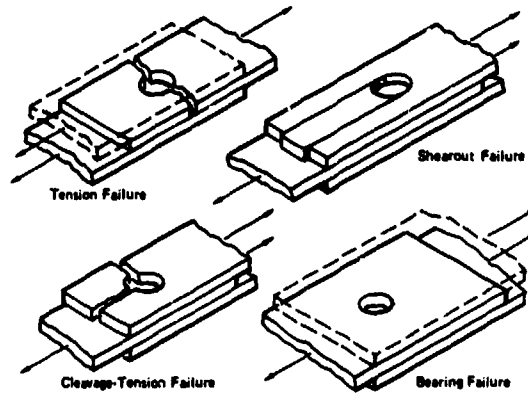


FIG 2: MODES OF FAILURE FOR BOLTED JOINTS  
REFERENCE 1

A number of steps precede a joint design in aircraft structures. The first step is to characterize the joints into simple load transfer mechanisms. The mechanism assumed in the joint design is not obvious from looking at an aircraft structure and its joints. The wing skin splices, the wing skin to spar/rib connection, the wing to fuselage connection, and the horizontal/vertical tail connection to the fuselage are some of the typical joints in aircraft construction. Figures 3 and 4 illustrate some of the joint configurations. The next step is the internal loads analysis. This step generally involves a finite element analysis of the aircraft structure. In this step details of the joints are not modeled, they are assumed to be an integral part of the structure. These models may be considered global models. The third step involves modeling the joints and their analysis. The next section presents a review of joint analysis methods.

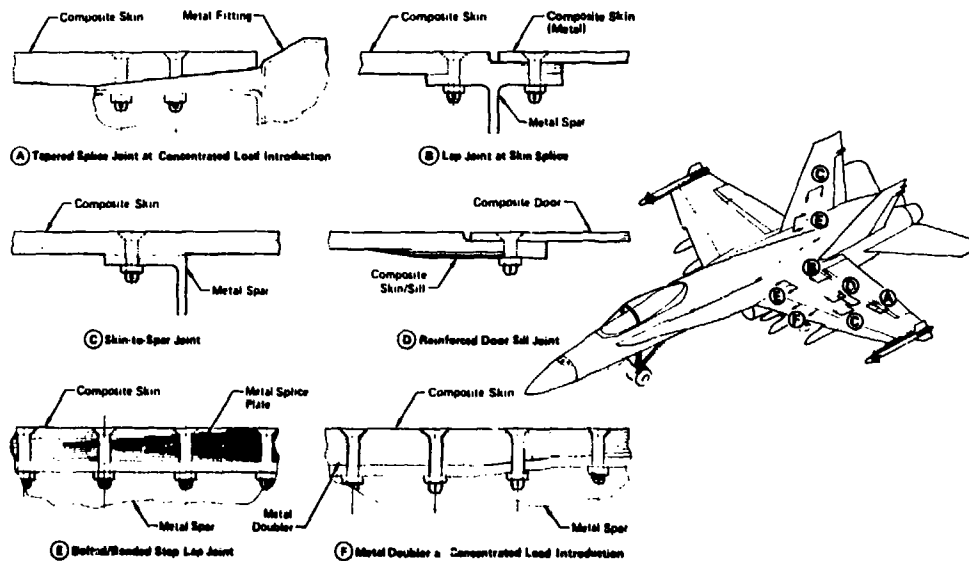


FIG 3: BOLTED COMPOSITE JOINTS  
REFERENCE 1

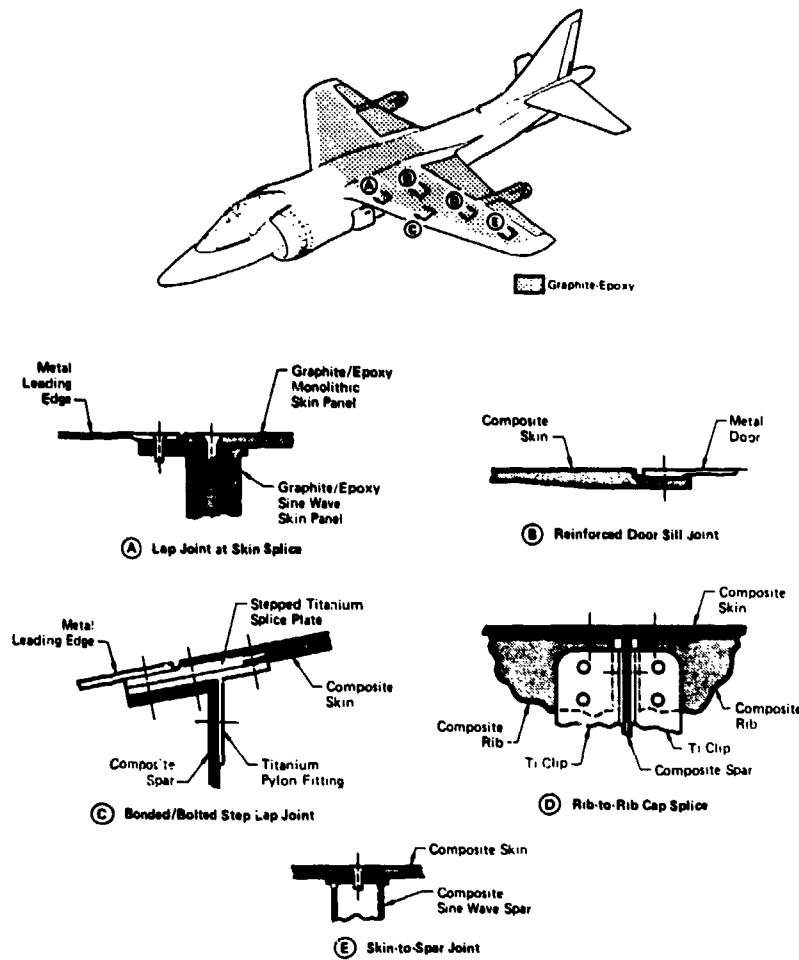


FIG 4: BOLTED COMPOSITE JOINTS  
REFERENCE 1

## 2. REVIEW OF JOINT ANALYSIS METHODS

The bolted joint failure load is determined by the stress analysis of single fastener joints. The basis for this analysis is two dimensional anisotropic plate theory<sup>(3)</sup>. This analysis is conducted in two steps<sup>(4,3,5)</sup>. First, an infinite plate with an unloaded hole is subjected to a uniaxial load. Then the same plate is analyzed with the loaded hole. Superposition of the two analyses gives the combined solution. Both analyses involve the solution of a fourth order differential equation in which the dependent variable is the Airy stress function,  $F$ , and the independent variables are the spatial coordinates  $(x,y)$ .

$$A_{22} \frac{\partial^4 F}{\partial x^4} - 2A_{26} \frac{\partial^4 F}{\partial x^3 \partial y} + (2A_{12} + A_{66}) \frac{\partial^4 F}{\partial x^2 \partial y^2} - 2A_{16} \frac{\partial^4 F}{\partial x \partial y^3} + A_{11} \frac{\partial^4 F}{\partial y^4} = 0 \quad (1)$$

The laminate compliance coefficients,  $A_{ij}$ , for the given symmetric laminate are given by

$$\xi = \mathbf{A} \mathbf{N} \quad (2)$$

where the matrices  $\xi$  and  $\mathbf{N}$  are the inplane strains and stress resultants, respectively, in an anisotropic plate. The complex stress function  $F$  can be written as

$$F(x,y) = 2\text{Re}[F_1(z_1) + F_2(z_2)] \quad (3)$$

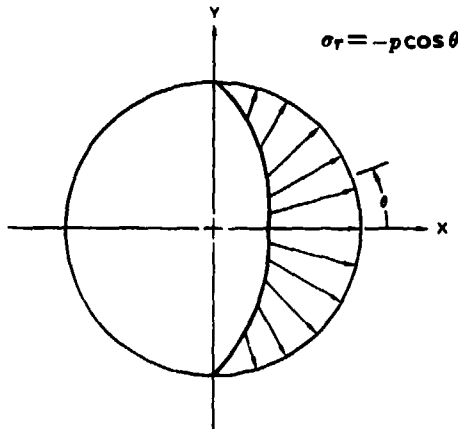
The complex stress functions  $F_1(z_1)$  and  $F_2(z_2)$  are analytic functions of the complex characteristic coordinates  $z_1$  and  $z_2$  respectively. The coordinates  $z_1$  and  $z_2$  are given by

$$z_1 = x + \mu_1 y \quad z_2 = x + \mu_2 y \quad (4)$$

The stresses and the stress function are related by

$$\sigma_x = \frac{\partial^2 F}{\partial y^2} \quad \sigma_y = \frac{\partial^2 F}{\partial x^2} \quad \tau_{xy} = -\frac{\partial^2 F}{\partial x \partial y} \quad (5)$$

An infinite plate with an open hole subjected to a uniaxial load will have a uniform stress  $\sigma_x$  everywhere except in the vicinity of the hole. The second analysis involves a plate with a loaded hole with stress free boundaries at infinity and an assumed radial stress distribution over half the hole varying as a cosine function. This analysis again gives the stress distribution around the hole and also assumes that the bolt-specimen interaction is frictionless. Superposition of these two linear elastic solutions gives the stress distribution in a single fastener joint. A summary of the superposition principle is shown in Fig. 5.



ASSUMED COSINE BOLT-LOAD DISTRIBUTION

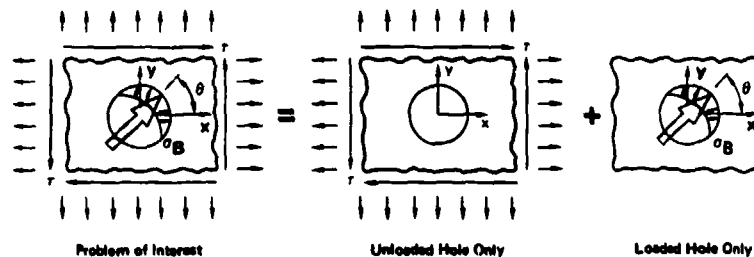


FIG 5: SUPERPOSITION OF LINEAR-ELASTIC STRESS SOLUTIONS  
REFERENCE 2

Substitution of Eq. (3) in Eq. (1) gives a characteristic equation in  $\mu$

$$A_{11}\mu^4 - 2A_{10}\mu^3 + (2A_{12} + A_{00})\mu^2 - 2A_{20}\mu + A_{22} = 0 \quad (6)$$

Solution of the characteristic Eq. (6) for  $\mu$  represents satisfaction of compatibility. The two infinite problems can be solved by using the complex stress function and an infinite series with unknown coefficients. The unknown coefficients can be determined approximately by matching the boundary conditions. Such solutions for an infinite plate with an open hole and a loaded hole are reported in Reference 4, and the results are summarized here.

For the open hole problem the stresses  $\sigma_r$ ,  $\sigma_\theta$  and  $\tau_{r\theta}$ , at two critical locations  $\theta = 0^\circ$  and  $90^\circ$ , are given by

$$\sigma_r = \tau_{r\theta} = 0 \quad (7)$$

The above solution is a consequence of the open hole being stress free. The hoop stress  $\sigma_\theta$  is given by

$$\sigma_\theta = \sigma_x \mu_1 \mu_2 \frac{A_{11}}{A_{22}} \quad \text{For } \theta = 0^\circ$$

$$\sigma_\theta = \sigma_x [1 - i(\mu_1 + \mu_2)] \quad \text{For } \theta = 90^\circ \quad (8)$$

where  $A_{11}$ ,  $A_{22}$  are the laminate compliance coefficients, and  $\mu_1$ ,  $\mu_2$  are the solutions of the characteristic equation that satisfies compatibility.  $\sigma_o$  is the nominal stress in the absence of the hole. From Eq. (8) the stress concentration factor  $K_o$  can be derived as

$$K_o = \frac{\sigma_\theta}{\sigma_o} = \mu_1 \mu_2 \frac{A_{11}}{A_{22}} \quad \text{at } \theta = 0^\circ$$

$$K_o = \frac{\sigma_\theta}{\sigma_o} = 1 - i(\mu_1 + \mu_2) \quad \text{at } \theta = 90^\circ \quad (9)$$

For an isotropic material the compliance coefficients are equal ( $A_{11} = A_{22}$ ) and  $\mu_1 = \mu_2 = i$ . Then the stress concentration factors are given by

$$K_o = -1.0 \quad \text{at } \theta = 0^\circ$$

$$K_o = 3.0 \quad \text{at } \theta = 90^\circ \quad (10)$$

Similarly for the loaded hole case the three stress components are given at the hole boundary by

$$\sigma_r = -p \quad \text{at } \theta = 0^\circ$$

$$\sigma_r = 0 \quad \text{at } \theta = 90^\circ \quad (11)$$

$$r_{,\theta} = 0 \quad \text{all around}$$

The hoop stress around the hole is given by

$$\sigma_\theta = \frac{A_{12}}{A_{22}} \frac{p}{4} + \frac{p}{4} \operatorname{Re} \left[ \frac{1 + i(\mu_1 + \mu_2)}{\mu_1 \mu_2} \right] + \frac{2p}{\pi} \operatorname{Re} \left[ \sum_{n=1,3,5,\dots} \frac{-(-1)^{\frac{n-1}{2}} 2 + in(\mu_1 + \mu_2)}{n(n^2 - 4)} \frac{1}{\mu_1 \mu_2} \right] \quad \text{at } \theta = 0^\circ$$

$$\sigma_\theta = \frac{A_{12}}{A_{11}} \frac{p}{4} - \frac{p}{4} \operatorname{Re} [\mu_1 + \mu_2 + i\mu_1 \mu_2] + \frac{2p}{\pi} \operatorname{Re} \left[ \sum_{n=1,3,5,\dots} \frac{i(2\mu_1 + 2\mu_2 + in\mu_1 \mu_2)}{n(n-2)(n+2)} \right] \quad \text{at } \theta = 90^\circ \quad (12)$$

The stress concentration for the loaded hole case is defined as

$$K_b = \frac{\sigma_\theta}{\sigma_b} \quad (13)$$

where  $\sigma_b$  is defined as

$$\sigma_b = \frac{\pi p}{4} \quad (14)$$

The stress concentration factor versus the percentage of  $0^\circ$  plies in a ( $0^\circ, \pm 45^\circ$ ) boron epoxy laminate is plotted in figures 6 and 7 for the open hole and loaded hole cases respectively. The following observations can be made from these curves (Ref. 4):

- The stress concentration in anisotropic materials can be significantly higher than in isotropic materials. It can be as much as four times in the loaded hole case and three times in the open hole case.
- For the case of 40%  $0^\circ$  plies, the stress field is nearly the same as that for an isotropic material in both the loaded and open hole cases.
- The hoop stress at  $\theta = 0^\circ$  and  $45^\circ$  goes through a stress reversal for the loaded hole case. This is not true for the open hole case. This stress reversal can have a significant impact on the failure mode of the joint.

The infinite plate solutions obtained from two dimensional anisotropic plate theory have to be corrected to account for a number of relevant design variables in an actual joint. Some of these variables are:

- The effects of finite geometry on the joint.
- Interference from adjacent joints and cutouts.
- Three dimensional effects coming from joint eccentricity.

The first two variables are accounted for in Reference 4 by using empirical correction factors. The corrected stress concentration factor is written as

$$K = \lambda_b K_b + \lambda_a \lambda_s K_o \quad (15)$$

where  $K_b$  and  $K_o$  are the stress concentration factors derived from infinite plate solutions for the loaded and open hole cases respectively. The correction factors  $\lambda_b$  and  $\lambda_s$  are to account for finite geometry effects, and  $\lambda_a$  is to account for adjacent fasteners. These correction factors were developed by using the Boundary Integral Equation (BIE) method. Extensive correction factor data for both the loaded and open hole cases in boron epoxy laminates ( $0^\circ, \pm 45^\circ$ ) is given in Ref. 4. Joint eccentricity (single lap joints) is not considered in this investigation.

So far only the single fastener analysis has been addressed in this discussion. In multifastener joints the load distribution among the individual fasteners is determined by an approximate load partitioning analysis<sup>(4)</sup>. After determining the

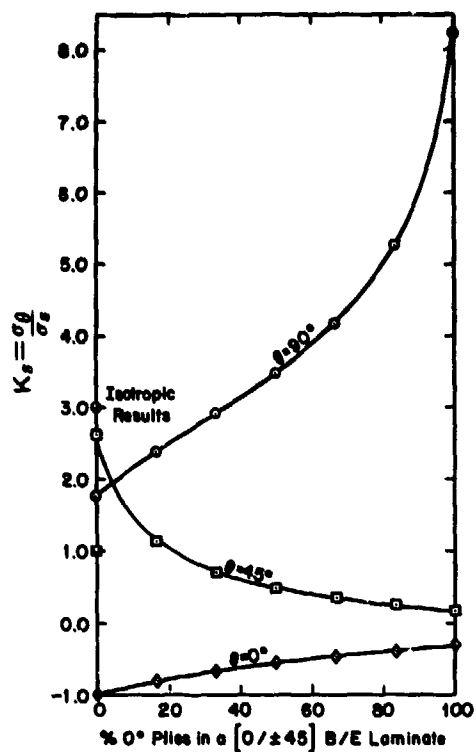


FIG 6: INFINITE PLATE STRESS CONCENTRATION FACTORS,  $K_s$ , FOR AN OPEN HOLE IN  $[0^\circ / \pm 45^\circ]$  BORON-EPOXY LAMINATES REFERENCE 4

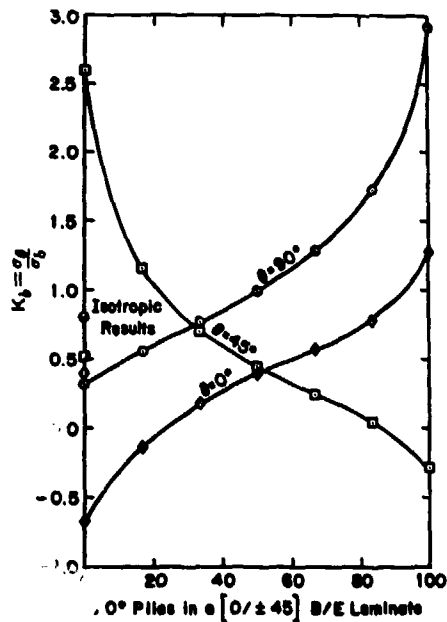


FIG 7: INFINITE PLATE STRESS CONCENTRATION FACTORS,  $K_b$ , FOR A LOADED HOLE IN  $[0^\circ / \pm 45^\circ]$  BORON-EPOXY LAMINATES REFERENCE 4

individual fastener loads, the multifastener joint is modeled as a series of single fastener coupons. The stresses in the individual fasteners are determined by the single fastener analysis outlined earlier. The load partitioning analysis for multifastener joints is based on an elongation matching technique. The distribution of fastener loads in a column of  $N$  fasteners is written as

$$\sum_{k=1}^N P_k = \frac{m}{m+s} \times F \quad (N-1) \text{ equations} \quad (16)$$

where  $P_k$  is the  $k^{\text{th}}$  fastener load from one end of the joint, and  $F$  is the total load carried by a column of fasteners. The factors  $m$  and  $s$  are integral functions of the modulus and cross-sectional areas of the main plate and the space plate respectively.

$$m = \int_{z_i}^{z_{i+1}} \frac{dz}{E_m(x)A_m(x)} \quad s = \int_{z_i}^{z_{i+1}} \frac{dz}{E_s(x)A_s(x)} \quad (17)$$

By considering equilibrium of the joint at each fastener location, Eq. (16) can be written. The overall equilibrium of the joint can be expressed as

$$\sum_{k=1}^N P_k = F \quad N^{\text{th}} \text{ equation} \quad (18)$$

With additional assumptions to evaluate the integrals in Eq. (17), the  $N$  equations can be solved for the  $N$  unknown fastener loads. Once the fastener loads are determined, the single fastener analysis provides stress information around the holes. Then the application of an appropriate failure criterion gives the fastener design load. The maximum ply stress, the maximum ply strain or some modification of the Von-Mises (Tsai-Hill) criterion is generally used in such failure analysis.

Following Waszczak's and Cruse's investigation, Garbo and Ogonowski (McAir) conducted both analytical and experimental investigations on single fastener joints in an Air Force program<sup>(1-2)</sup>. Their analysis is similar in the sense that it was based on two dimensional anisotropic plate theory with the superposition of results obtained from an infinite plate analysis with an open hole and a loaded hole. In addition, they have applied the characteristic dimension ( $R_C$ ) failure hypothesis, Fig. 8. This analysis was implemented in a computer program called BJSFM (*Bolted Joint Stress Field Model*). The failure criterion was applied on a ply-by-ply basis at a characteristic distance away from the hole boundary.

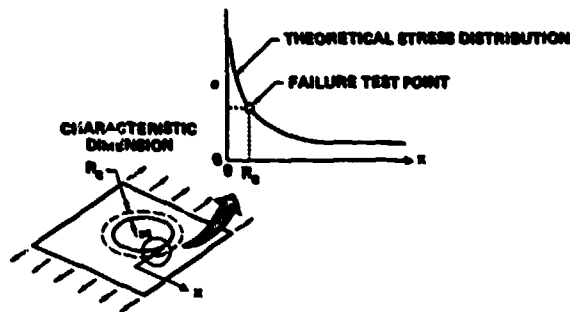


FIG 8: CHARACTERISTIC DIMENSION FAILURE HYPOTHESIS  
REFERENCE 2

A number of failure criterion options were provided in the program. The strength envelopes for various failure criteria for graphite epoxy (AS-3501-6) material, ignoring matrix failure, are shown in Fig. 9.

The stress distributions around the holes for open holes and loaded holes are shown in Figures 10 and 11. Stress concentrations in composite materials are affected by laminate layup and load orientation. Table 1 gives values of the stress concentration factors for some of the graphite epoxy layups.

Empirical estimates of the finite width effects are included in the BJSFM program. This program was used to address the effects of a number of joint design variables (Ref. 1):

- a. Joint anisotropy
- b. Hole size
- c. Finite width
- d. Characteristic dimension sensitivity
- e. Biaxial loading
- f. Pure bearing strength
- g. Environment

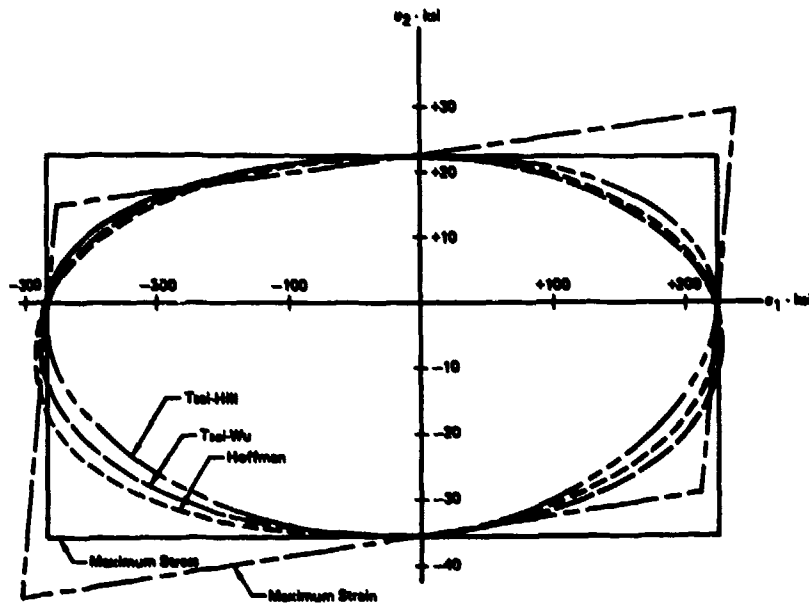


FIG 9: FAILURE CRITERIA COMPARISON  
REFERENCE 2

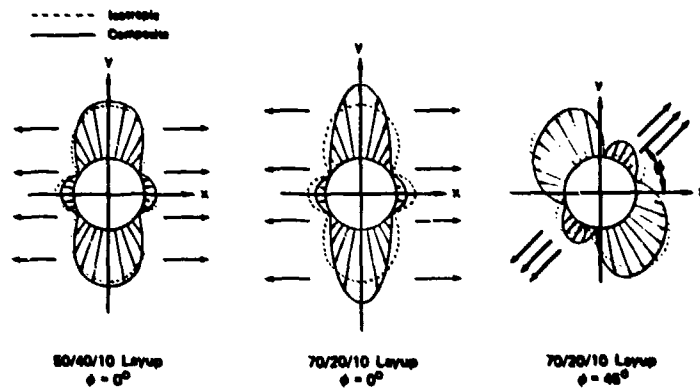


FIG 10: CIRCUMFERENTIAL STRESS SOLUTIONS AT UNLOADED HOLES  
REFERENCE 2

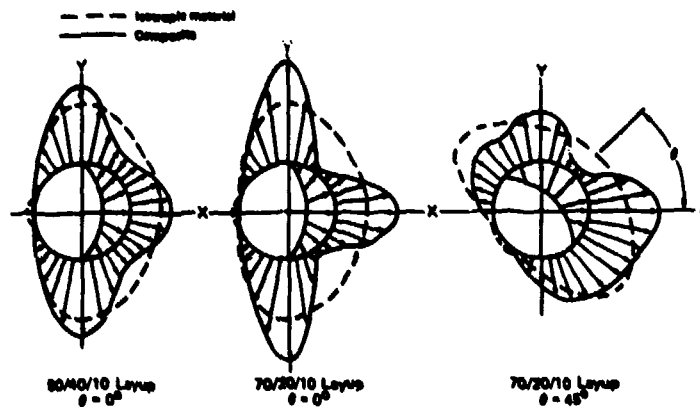


FIG 11: CIRCUMFERENTIAL STRESS SOLUTIONS AT LOADED HOLES  
REFERENCE 2

Laminate $\Delta$	Test Data	Theoretical		Theory Test
		Finite Element	Elasticity = Plane	
$(\pm 45^\circ)_{20}$	1.14	2.89	2.87	2.82
$(0^\circ, \pm 45^\circ, 0^\circ, \pm 45^\circ, 0^\circ, \pm 45^\circ, 90^\circ, 0^\circ)_1$	1.71	3.20	3.17	1.85
$(0^\circ, \pm 45^\circ, 90^\circ)_1$	1.51	3.00	3.00	1.99
$(0^\circ, \pm 45^\circ, 90^\circ, 0^\circ)_1$	1.54	3.42	3.41	2.21
$(0^\circ, \pm 45^\circ, 90^\circ, 0^\circ)_1$	1.56	3.72	3.71	2.38

$\Delta$  Uniaxial Loaded T300/E308 Coupon Specimens - Unloaded Open Hole

TABLE 1: THEORETICAL STRESS CONCENTRATION FACTOR IS CONSERVATIVE  
REFERENCE 1

The results of this study were reported in Ref. 2. Other finite geometry effects, such as, joint eccentricity, joint torque, multifastener joints, and interference from neighboring stress raisers (cut-outs) were not addressed in this investigation.

Another important bolted joint analysis program is A4EJ developed by Hart-Smith (Douglas Aircraft Company) for the Air Force<sup>(6)</sup>. This program is based on a semiempirical approach. The load transfer through the mechanical fasteners is explained in terms of the relative displacement between the members of each fastener station. The assumed mathematical model for the load transfer is shown in Fig. 12. The relative displacements between the members are explained in Fig. 13. The load sharing between the multirow fasteners is explained in Fig. 14.

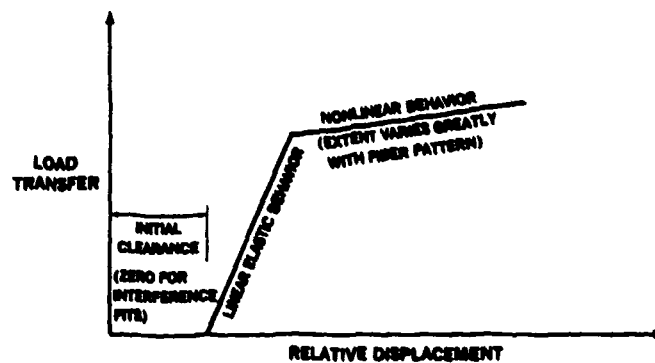


FIG 12: FASTENER LOAD-DEFLECTION CHARACTERISTICS  
REFERENCE 6



in single lap joints), environmental effects and durability are some of the important issues resolved in this task. The second task addressed the same issues for multifastener joints and stress concentration interactions. Both these tasks involved the development of new computer programs, SASCJ (Strength Analysis of Single fastener Composite Joints) and SAMCJ (Strength Analysis of Multifastener Composite Joints). These programs can be extremely effective tools for joint design. The details of these programs are provided in Refs. 8,12. Full scale verification of the analytical and experimental methods developed in the first two tasks constitutes the third task. At the end of these three tasks analytical tools were well defined for the analysis and design of representative bolted composite joints. These analytical methods and experiments addressed both fiber and matrix dominated cases in bearing and bypass loadings. A comprehensive design guide for bolted joints in composites was developed in the fourth task. The results of this investigation are reported in References 3,8-14.

The single fastener analysis implemented in SASCJ is also based on anisotropic plate theory. It is also a superposition of loaded and unloaded solutions. However, this solution is augmented by a least squares boundary collocation procedure to account for finite geometry effects. This procedure is a significant improvement over empirical estimates. The joint eccentricity problem (single lap joint) is solved by modeling fastener bending as a beam on an elastic foundation, the fastener being the beam and the plates on which it bears, acting as the foundation. In computing the three dimensional stress field at the fastener location, piecewise uniform moduli were assumed to represent various plies in a bolted laminate. The fastener is modeled as a Timoshenko beam to account for bending and shear deformations. To account for the reduced ply stiffness, after an initial damage, a bilinear contact load versus deflection curve was used to represent the foundation. At the head and nut locations of the fastener, rotational constraints were introduced. The applied torque and size of the washers affect the boundary conditions. Fastener torque also introduces friction forces on the bolted plates, thus reducing the load transferred by the fastener. If either of the bolted plates is a laminate, its stacking sequence will influence the fastener displacement and the load distribution in the thickness direction. The differential equation resulting from the beam on an elastic foundation analogy is solved by a finite difference approach using a central difference operator.

Using the SASCJ code a number of joint parameters were studied in Reference 5. The finite geometry variables, such as, width of the plate, edge distance and diameter of the hole affect the failure load, and the infinite plate solutions are generally not adequate for evaluating the joint strength. Joint variables, single and double shear load transfer, fastener size, fastener material, and the effect of laminate stacking sequence on the through the thickness load distribution are the parameters studied with reference to the joint eccentricity. They cannot be accounted for in a two dimensional analysis.

Options for a number of failure criteria were provided in the SASCJ program. These are expressed in terms of inplane stresses and strains: 1) point stress failure criterion, 2) average stress failure criterion, 3) maximum strain (fiber direction) criterion, 4) Hoffman criterion and 5) Tsai-Hill criterion. The first two criteria predict three modes of failure in each ply: net section, shear-out and bearing. The maximum strain criterion predicts ply failure based on fiber directional strain. The Hoffman and Tsai-Hill criteria predict ply failure accounting for biaxial stress interaction.

The SAMCJ program was developed for determining the fastener load distribution in a multifastener joint. The analysis is based on special finite elements. Four special finite elements were developed using a fastener analysis and a stress analysis that accounts for the finite laminate planform dimensions. These elements include a loaded hole element, an unloaded hole element, a plain element, and an effective fastener element. With the finite element model of the bolted joint, the fastener load distribution and the average stresses at the fastener and cut-out locations can be computed. The fastener load distribution, the critical fastener or cut-out location, the joint failure load and the corresponding failure mode are predicted by SAMCJ. SASCJ is an independent program as well as a subset of the SAMCJ program. More details of the analysis procedures in these programs are presented in References 8,12.

### 3. REVIEW OF EXPERIMENTAL PROGRAMS

The credibility of an analysis procedure is questionable without some experimental verification. This is particularly important in the case of nonhomogeneous materials such as laminated composites. The approximate two dimensional analysis developed in Ref. (4) has addressed little, if any, experimental verification. A few simple coupon tests reported in References 15 and 16 were used to compare the analysis results. These are geometrically similar graphite-epoxy bolt bearing specimens tested to failure. The specimens all failed in net tension. If the material is truly stress critical, it would be possible to predict the failure loads in all cases by analysis. However, this is not the case. It is generally believed that the analysis results exhibit consistent conservatism. This is particularly true in the case of the maximum ply stress failure criterion. The hole size offsets and characteristic distance hypothesis can explain the conservatism and help in predicting the joint failure load more accurately.

An extensive experimental program to verify the analysis results was conducted at McAir on an Air Force program<sup>(1,2)</sup>. This test program addressed both static strength and fatigue life issues in composites. However, the test program was limited to coupon tests. The effects of twelve joint design variables on static strength were experimentally evaluated. These variables are:

1. Fastener Torque
2. Stacking Sequence
3. Single Shear
4. Thickness
5. Countersunk Fasteners

6. Load Orientation-Off-Axis Loads-Bearing and Bypass Aligned
7. Hole Size
8. Edge Distance
9. Width
10. Layup
11. Fastener Patterns
12. Load Interaction - Bypass and Bearing Nonaligned

Four specimen configurations were used in this test program:

- a. A Single Bolt Pure Bearing
- b. A Two Bolt In Tandem (Load Sharing)
- c. A Four Bolt Fastener Pattern Specimen
- d. A Two Bolt Load Interaction Configuration

The analysis verification using the BJSFM program was limited to five of the twelve design variables. The other variables were beyond the scope of the analytical methods used in BJSFM. The five variables were layups, load interaction, off-axis loading, hole size and width. At first, the strength predictions from the analysis were correlated with data obtained from tests of specimens with unfilled fastener holes. Both tension and compression loading to failure were used in these tests. The characteristic dimension ( $R_C$ ) of 0.02 inch for tensile strength predictions and 0.025 inch for compressive strength predictions was empirically determined for a laminate made of Hercules AS/350-6 graphite-epoxy. The analysis results were correlated with the unloaded hole case for an extensive range of layup variations. The predicted results were within  $\pm 10\%$  of the experimental results.

This investigation addressed also the effects of manufacturing anomalies. The results of this study fell into two groups: 1) Porosity around the hole, improper fastener seating depth and tilted countersinks resulted in strength reductions of over 15 percent; 2) Out of round holes, broken fibers on the exit side of the hole, interference fit tolerances and removal and reinstallation anomalies resulted in less than 15 percent strength reduction.

Seven critical joint design variables on fatigue life were evaluated. Tests were performed to provide data on joint fatigue life performance, hole elongation and failure mode behavior. Single-fastener pure bearing specimens were cycled under tension-tension ( $R = + 0.1$ ) and tension-compression ( $R = -1.0$ ) constant amplitude fatigue loading and under spectrum fatigue loadings. During fatigue testing, load-deflection data was obtained at specified increments of accumulated hole elongation. Several tests were performed to determine the effect of environmental conditions. Static and residual strength tests were performed on selected specimens at each test condition.

Joint fatigue life was defined to occur at specimen failure or when hole elongations of 0.02 inches were measured. Little difference was noted in relative fatigue life between layups 50/40/10, 30/60/10 and 19/76/5 ( $0^\circ, \pm 45^\circ, 90^\circ$  respectively) under tension-tension ( $R = + 0.1$ ) cycling. Under fully reversed load cycling, ( $R = -1.0$ ), hole elongations of 0.02 inch occurred more rapidly in the matrix dominant 19/76/5 layup, followed by the 30/60/10 and 50/40/10 layups. Under spectrum fatigue tests of all three layups, no hole elongation occurred after 16000 spectrum hours at test limit loads of 89% of static strength values. This agreed with constant amplitude fatigue test results as well. At these load levels 16000 hours of spectrum loading did not produce enough cycles of high loads to produce hole elongation.

Effects of fastener torque-up on joint fatigue life were pronounced. Torque-up generally produced beneficial effects of increased strength and fatigue life for all layups in both tension-tension ( $R = + 0.1$ ) and tension-compression ( $R = -1.0$ ) loading. However, areas of damage were more pronounced for specimens with torque-up, and also failure occurred more abruptly (rates of hole elongation, once initiated, were faster).

Effects of joint eccentricity and geometry also influenced joint fatigue life characteristics. Single-shear specimens exhibited lower fatigue life than the baseline double shear configuration. Further reductions occurred with flush-head fasteners compared to protruding head fasteners due to increased fastener flexibility and specimen bending. For the 19/76/5 layup, changes in specimen width caused changes in the failure modes and significant changes in strength and fatigue life. However, for the 50/40/10 layup, variations in width and edge distance did not alter either failure modes or strength and fatigue life. Effects of the remaining variables on joint fatigue life were minor. The failure modes and durability were essentially the same as the baseline configurations.

The most comprehensive Air Force program on bolted joints in composite structures was conducted by Northrop Corporation<sup>(8, 9, 14)</sup>. The analytical developments in this program were outlined earlier. The single fastener analysis results were verified by extensive testing of single fastener composite-to-metal joint specimens of various configurations. About

450 coupon tests were made to verify the effects of various joint design variables. The results were documented in Ref. 9. Of the 450 tests 318 were static tests, and 132 were fatigue tests. The single lap and double lap configurations addressed composite-to-metal load transfer by a single fastener, and the bearing/bypass configuration addressed the effect of fractionally increasing bearing loads on the gross laminate strength and fatigue life. The material for this program was AS1/3501-6 graphite epoxy unidirectional tape, the prepreg containing approximately 35% resin by weight. The test variables were: laminate thickness, stacking sequence, fastener diameter (D), specimen width (W), edge distance (E), fastener material, fastener head type (protruding, tension head countersink and shear head countersink), type of loading, (tension or compression), bearing to total load ratio, joint configuration (single or double lap), fastener torque and the environment (RTD-room temperature, dry; RTW-room temperature, wet; 218W-218°F, wet).

The fatigue tests covered all the joint variables in the static test cases. Additional fatigue test variables were: type of loading (constant amplitude fatigue or blocks of constant amplitude fatigue loading at different mean intervals) and the minimum to maximum cyclic load ratio (R). Fatigue loads were imposed at a 10 Hertz frequency.

In addition to the single fastener joints, 160 composite-to-metal multifastener joints were tested to verify the multifastener joint analysis results from SAMCJ. A number of fastener arrangements were considered: two fasteners in tandem, two at an angle to the load direction, three fasteners in two arrangements, four fasteners in a rectangular pattern, five fasteners in tandem, three fasteners in each of two rows with an adjacent cut-out, and four fasteners in each of two rows with a cut-out either between or adjacent to the rows. A unique fastener load measurement technique, using strain-gaged bolts, was applied to every test case to compute the fractional fastener loads corresponding to the various test conditions. This information, in conjunction with photographic records of failed test specimens, was very useful in validating the strength of multifastener joints.

The final tests in this program consisted of representative full scale test specimens. The vertical tail root section of an aircraft was selected for full scale testing to verify the design and analysis programs developed. The test element was analyzed using the analytical methods developed in this program. Theoretical predictions correlated well with experimental results.

The Northrop program was concluded with the development of a comprehensive design guide<sup>(13)</sup>. Some details of this total program will be presented this afternoon by Dr Ramkumar<sup>(14)</sup>.

#### 4. CONCLUSIONS

The analysis and experimental verification programs reviewed in this paper are comprehensive and suitable for practical applications. Due to the empirical nature of some of the procedures, additional experimental programs are necessary to cover new material systems. Metal matrix composites and the materials coming out of the new powder metallurgy technology require augmentation to analysis and design procedures developed so far in these programs. This augmentation must be based on extensive experimental verification. Future high temperature joint applications require new investigations for analysis verifications. However, the programs developed so far will form a solid technology base for future investigations.

There are a number of industry and other government programs which could not be reviewed in this paper due to time limitations. Both the NAVY and NAFSA have bolted joint programs with industry (McAir, Northrop). Grumman, General Dynamics and Boeing have in-house projects in this area. A future review should consolidate the results of these programs.

#### REFERENCES

1. Garbo, S.P. and Ogonowski, J.M., "Effect of Variances and Manufacturing Tolerances on the Design Strength and Life of Mechanically Fastened Composite Joints," AFFDL-TR-78-179, 1978.
2. Garbo, S.P. and Ogonowski, J.M., "Effect of Variances and Manufacturing Tolerances on the Design Strength and Life of Mechanically Fastened Composite Joints," Volume I, II, and III, AFWAL-TR-81-3041, April 1981.
3. Lekhnitskii, S.G., "Anisotropic Plates," Gordon and Breach Science Publishers, 1968.
4. Waszczak, J.P. and Cruse, T.A., "A Synthesis Procedure for Mechanically Fastened Joints in Advanced Composite Materials," AFML-TR-73-145, Volume II, 1973.
5. Ramkumar, R.L., et al., "Strength Analysis of Composite and Metallic Plates Bolted Together by a Single Fastener," AFWAL-TR-85-3004, 1985.
6. Hart-Smith, L.J., "Design Methods for Bonded-Bolted Composite Joints," Vols I and II, AFWAL-TR-81-3154, 1981.
7. Chang, F., Scott, R.A. and Springer, G.S., "Strength of Bolted Joints in Laminated Composites," AFWAL-TR-84-4029, 1984.
8. Ramkumar, R.L., Kudva, N.J. et al., "Bolted Joints in Composite Structures: Design Analysis and Verification," AFWAL-TR-83-3093, 1983.
9. Ramkumar, R.L. and Tossavainen, E., "Bolted Joints in Composite Structures: Design, Analysis and Verification TASK I Test Results - Single Fastener Joints," AFWAL-TR-84-3047, 1984.

10. Ramkumar, R.L. and Tossavainen, E., "Bolted Joints in Composite Structures: Design, Analysis and Verification TASK II Test Results - Multifastener Joints," AFWAL-TR-85-3065.
11. Ramkumar, R.L., Saether, E.S. and Tossavainen, E., "Design, Fabrication, Testing and Analysis of Bolted Structural Elements," AFWAL-TR-86-3033, 1986.
12. Ramkumar, R.L., Saether, E.S. and Appa, K., "Stength Analysis of Laminated and Metallic Plates Bolted Together by Many Fasteners," AFWAL-TR-86-3034, 1986.
13. Ramkumar, R.L., Saether, E.S. and Cheng, D., "Design Guide for Bolted Joints in Composite Structures," AFWAL-TR-86-3035, 1986.
14. Ramkumar, R.L., Saether, E.S. and Venkaya, V.B., "Strength Analysis of Mechanically Fastened Composite Structures," AGARD Specialists' Meeting on Behavior and Analysis of Mechanically Fastened Joints in Composite Structures, 26 April - 1 May 1987, Madrid, Spain.
15. Waddoups, M.E., Eisenmann, J.R. and Kaminski, B.E., "Macroscopic Fracture Mechanics of Advanced Composite Materials," Convair Aerospace Division of General Dynamics, FZM-5670, (February 1971).
16. Eisenmann, J.R., Convair Aerospace Division of General Dynamics Corporation, Fort Worth, Texas, Private Communication (1971).

**DAMAGE GROWTH IN COMPOSITE BOLTED JOINTS**

by

V.Giavotto, C.Caprile & G.Sala  
Dipartimento di Ingegneria Aerospaziale  
Politecnico di Milano  
Italy

**Abstract**

Static and fatigue failures of composite joints are dominated by the growth and propagation of typical damages, up to some catastrophic condition.

Starting from experimental observations some typical damage propagation patterns are identified and analysed with simple models and finite element schemes.

This extension of the fracture mechanics approach, to a broader class of damages allows some insight into the intricate behaviour of FRP joints, and gives some suggestion for interpreting and correlating experimental data.

**1. INTRODUCTION**

Fatigue and failure of composite materials are still a difficult and intriguing problem, despite the large research effort devoted to them in the last years.

This apply even more strongly to bolted joints, where fatigue damage and static failure are likely to occur at lower load levels and with more complicated patterns.

There are several different reasons for this fact, the first being the real intricacy of the complex phenomena involved in composite failure, especially at a microscopic level. But definitely, another reason has been the unsuccessful attempt to transfer too literally the Fatigue and Fracture Mechanics approach, that was successful for metals.

In fact, in the early literature, composites were considered just as homogeneous (or homogenized) anisotropic media, prone to the macroscopic fatigue and fracture phenomena typical of metals.

So the study was dedicated to the stress concentration factors around a hole, and to the stress intensity factor at the tip of a through-the-thickness crack in anisotropic elastic solids.

On the other hand early fatigue tests were only in tension, with the main aim of measuring the number of load cycles to failure; this now is considered to be scarcely significant.

Nevertheless, even if not so quickly as it was expected, a large amount of experimental observation was carried on, which, produced and consolidated a substantial knowledge on the strength and fatigue of composite and composite joints.

Among the facts that are now clear, even if not all satisfactorily explained, the most significant are:

- a) the typical damage extending under fatigue loading is not a localized crack, but a system of intralaminar and interlaminar fractures (delaminations) distributed in a certain area or volume;
- b) The most significant damage parameter to be recorded in fatigue testing is the specimen stiffness (or elastic modulus) decrease;
- c) compression is generally producing higher damage extension rates through the mechanisms of microbuckling (buckling of single fibers) or minibuckling (buckling of relatively thin layers);
- d) in a bolted joint a positive clamp-up is essential for a good duration.

As it will be shown later point a) is essentially due to the fact that clamp-up prevents micro and minibuckling, even in areas of extended delamination.

Then, in composite fatigue, it is sensible to consider an extending damaged area, containing several fractures of different types, more than a single extending crack.

With this in mind the extension of the Fracture Mechanics approach to composites and composite joints can be very useful [1], [2].

Beside the concept of an extending damaged area, the single damage mechanisms should be investigated deeply to obtain a better understanding; this can be helped by the analysis of simple models, and may require well focused experiments.

This paper is dedicated to the study of simple models, with the aim of explaining some damage mechanics, and possibly to find some applicable results.

## 2. DELAMINATION MECHANICS

As it has been already suggested, the more suitable Delamination Mechanics parameter is the Energy Release Rate  $G$ , which can be defined as the decrease in the strain energy  $V$  for unit increase in the delamination area  $A$ , in a "Fixed Grip" condition, i.e.

$$G = - \left( \frac{\partial V}{\partial A} \right)_{F.G.}, \quad (1)$$

Let us consider a symmetrical delamination of the outer layers, at the 4 free edges of a prismatic coupon, as in figure 1, and call A and B the configurations corresponding to complete delamination and to null delamination, respectively (figure 2).

For a given strain  $\epsilon_x$  and coupon length  $l$ , if configuration A and B are both orthotropic respect to  $xy$ , the strain energies can be put as

$$V_A = \frac{1}{2} t b l E_A \epsilon_x^2; \quad V_B = \frac{1}{2} t b l E_B \epsilon_x^2, \quad (2)$$

and, in the configuration of figure 1:

$$V = \frac{2a}{b} V_A + \left( 1 - \frac{2a}{b} \right) V_B + 4V_D, \quad (3)$$

$V_D$  being the strain energy associated with the stress diffusion field near each of the 4 crack tips.

If diffusion length is small enough compared to crack length, an increase in  $a$  will only cause a displacement of each stress diffusion field without distorsion, so it can be assumed that  $\frac{\partial V_D}{\partial a} = 0$ , and then

$$G_E = \frac{1}{2b} (V_B - V_A) = \frac{t \epsilon_x^2}{4} \left( E_B - E_A \right), \quad (4)$$

the delaminated surface being  $A=4al$ .

If the outer delaminating layers are thin compared to the core of the laminate, the energy release rate (4) takes the simple form:

$$G_E = \frac{t E_y \epsilon_x^2}{2(1-\nu_x \nu_y)} (\nu_x - \tilde{\nu}_x)^2, \quad (5)$$

where  $E_y, \nu_x, \nu_y$  relate to the outer layers and  $\tilde{\nu}_x$  to the core.

It can be useful to define a non-dimensional energy release rate  $g$ , so that

$$G = \theta \frac{t E \epsilon^2}{2(1-\nu_x \nu_y)}; \quad (6)$$

in this case the non-dimensional energy release rate for the free edge delamination of an outer thin layer is:

$$\theta_E = (\nu_x - \tilde{\nu}_x)^2. \quad (7)$$

Let us now consider a thin outer layer delaminated from a thicker laminate, in a spot of length  $2a$  in  $x$  direction. If the laminate has a contraction  $\epsilon$ , the thin layer can undergo compression buckling, its critical strain being:

$$\epsilon_c = \frac{\pi^2}{12} \left( \frac{t}{a} \right)^2. \quad (8)$$

With reference to figure 3, since the normal displacement of the buckled layer is  $w$ , it is easy to demonstrate that

$$C = \frac{2a}{\pi} (\epsilon - \epsilon_c)^2, \quad \text{and} \quad V = \frac{E_x b t}{2(1-\nu_x \nu_y)} \left[ (L-2a)\epsilon^2 + 2a\epsilon_c^2 + \frac{t^2}{12} \int_{-a}^a w''^2 dx \right]$$

where  $b$  and  $L$  are a given width and length, respectively.

Since in this case the delaminated area to be considered is  $A=2ab$ , considering (1) and (6):

$$g = 1 + 2 \frac{\epsilon_c}{\epsilon} - 3 \left( \frac{\epsilon_c}{\epsilon} \right)^2. \quad (9)$$

It must be observed that the non-dimensional energy release rate (9) is the sum of a mode I and a mode II term, i.e.

$$g = g_I + g_{II}. \quad (10)$$

### 3. THE DUGDALE MODEL

The Dugdale's "yield strip" model can be useful to separate the energy release rates of the 2 modes 3, 4. It assumes for the interlaminar layer a rigid-plastic behaviour, i.e. a constant tension stress  $\sigma_Y$  in mode I opening (figure 4 and 5) and a constant shear stress  $\tau_Y$  in mode II opening (figure 6).

Calling  $u$  and  $w$ , respectively, the longitudinal and normal displacements, the Crack Opening Displacements are defined as  $\delta_I$  and  $\delta_{II}$ , and the energy release rates:

$$G_I = \sigma_Y COD_I \quad ; \quad G_{II} = \tau_Y COD_{II} \quad (11)$$

are independent from the values of  $\sigma_Y$  and  $\tau_Y$ , which therefore can be assumed arbitrarily.

The differential equations of the Dugdale model, in this case, are:

$$\begin{aligned} \text{for mode I} \quad & \frac{E \pi t^3}{12(1-\nu_x \nu_y)} W^{IV} = -\sigma_Y \quad , \text{and} \\ \text{for mode II} \quad & \frac{E \pi t}{1-\nu_x \nu_y} u'' = -\tau_Y \quad ; \quad (12) \end{aligned}$$

Applying the proper boundary conditions, considering  $J_I$  and  $J_{II}$  among the unknowns, and using the definition (6) of the non-dimensional energy release rate, from equations (12) and (11) it can be easily shown that

$$g_I = 4 \frac{\epsilon_c}{\epsilon} \left(1 - \frac{\epsilon_c}{\epsilon}\right) \quad \text{and,} \quad (13)$$

$$g_{II} = \left(1 - \frac{\epsilon_c}{\epsilon}\right)^2 \quad (14)$$

and then  $g_I + g_{II} = 1 + 2 \frac{\epsilon_c}{\epsilon} - 3 \left(\frac{\epsilon_c}{\epsilon}\right)^2$ , as was found in (9) with an entirely different approach.

Figure 7 shows diagrams of  $g$  and  $g_{II}$  versus  $\epsilon$ , computed with (9) and (14), for different values of  $a/t$ .

It must be observed that when buckling is well developed the total non-dimensional energy release rate  $g$  changes very little with  $a, t$  and  $\epsilon$ , all the curves remaining in the neighborhood of the maximum (4/3).

At low compression strain  $g_I$  can be much higher than  $g_{II}$ , while at higher strains this difference is much smaller. In any case both  $g$  and  $g_{II}$  are much higher than the Free Edge delamination  $g_E$  (7).

This is a simple but rational model that can explain, and possibly could be used to evaluate, the tendency of delamination to extend quite rapidly in compression buckled spots.

### 4. INSUFFICIENT CLAMP-UP

Around a bolt in a joint, in the side where bearing pressure is exerted, high compressive strains are likely to develop, and then a high damage propagation rate is likely to occur.

So a positive clamp-up, with a relatively large washer, is very beneficial, preventing buckling, and leaving possible delamination extension only to mode II.

But, if the bolt is not tight enough, some wear may occur due to the sliding of the joined parts, and then some small play may develop, then allowing for a certain amount of buckling.

In this case, if  $2h$  is a small normal gap between the delaminated layer and an ideally rigid wall (representing the washer), the buckling phases shown in figure 8 are occurring, in succession with increasing compressive strain; in the even phases all the wave crests are against the rigid wall, while in the odd ones there is at least one wave crest which is lower than the wall, and then which can still grow in the gap.

Following this model, in an odd phase with  $n$  waves, the wavelength is  $\lambda = a/n$ , and the critical strain

$$\epsilon_c = \frac{\pi^2}{12} \left(\frac{t}{\lambda}\right)^2 \quad . \quad (15)$$

The amplitude  $C$  of the wave that is not touching the wall is given by the equation:

$$C^2 (\pi-1) h^2 = n \left(\frac{2\lambda}{\pi}\right)^2 (\epsilon - \epsilon_c) \quad . \quad (16)$$

The strain energy is

$$V = \frac{E_x t}{2(1-\nu_x \nu_y)} \left\{ (L-2a)\epsilon^2 + 2a\epsilon_c^2 + \frac{\epsilon^2}{12} [(n-1)h^2 + C^2] \left(\frac{\pi}{\lambda}\right)^4 \lambda \right\}$$

and then:

$$g = 1 + 2 \frac{\epsilon_c}{\epsilon} - 3 \left(\frac{\epsilon_c}{\epsilon}\right)^2 \quad (17)$$

while  $g_{II}$  is still given by (14). It is worth noting that (17) is formally identical to (9), but  $\epsilon_c$  has a different value.

The phase  $2n-1$  changes into the following even phase  $2n$  when  $C > h$ , i.e. when

$$\epsilon - \epsilon_c \geq \left(\frac{n\pi}{2} \frac{h}{a}\right)^2 \quad (18)$$

After this point  $\lambda$  has the decreasing value

$$\lambda = \frac{n(\pi h)^2}{8a\epsilon} \left\{ 1 + \left[ 1 + \frac{16}{3} \left(\frac{a\epsilon}{n\pi h^2}\right)^2 \epsilon \right]^{\frac{1}{2}} \right\} \quad (19)$$

$$\text{and } g = 1 + \left(\frac{\epsilon_c}{\epsilon}\right)^2 \left\{ \left[ 4 \frac{a}{\lambda} + 16n \left(\frac{h}{\epsilon}\right)^2 \right] \frac{\partial \lambda}{\partial a} - 1 \right\} \quad (20)$$

$$\text{where } \frac{\partial \lambda}{\partial a} = -\frac{\lambda}{a} + \frac{2}{3n} \left(\frac{\epsilon}{h}\right)^2 \left[ 1 + \frac{16}{3} \left(\frac{a\epsilon}{n\pi h^2}\right)^2 \epsilon \right]^{-\frac{1}{2}} \quad (21)$$

$$\text{and } \epsilon_c = \frac{\pi^2}{12} \left(\frac{\epsilon}{\lambda}\right)^2$$

The mode II energy release rate is still given by (14).

The phase  $2n$  ends into a new odd  $2n+1$  phase, when a new wave can develop, i.e. when

$$\lambda \leq 2/(n+1) \quad (22)$$

Figure 9 and 10 show the trend of  $g$  and  $g_{II}$  versus  $\epsilon$ , for 3 values of  $a/t$  and 2 values of  $h/a$ .

It must be noted that  $g$  jumps passing from an odd to an even phase and viceversa, the even phases having much lower values. In the even phases (i.e. when all waves are against the wall)  $g_{II}$  is higher than  $g$ , and therefore  $g_I$  is negative. This means that delamination can still propagate by mode II while mode I is closing, as it can be easily seen in figure 8.

In this case the total energy release rate  $g$  is not adequate to correlate damage propagation, and the separation into its components  $g_I$  and  $g_{II}$  is essential.

Comparison of figure 9 and 10 shows that a reduction in the play  $h$  is beneficial because it reduces  $g_{II}$  and the amplitude of the strain intervals of even phases: but the peak values of  $g$  are only slightly modified.

So in an alternating load condition, going through all the values of the strain  $\epsilon$ , some of the peaks of  $g$  will be encountered at every cycle.

that means that even a very small amount of play can be detrimental, and that a good fatigue duration demands a high clamp-up.

## 5. A GLOBAL DAMAGE CONCEPT

In the previous analyses the mechanics of different delaminations was considered, through the evaluation of the rate of strain energy release for unit extension of the damage considered. There the measure of the damage was defined as the area of the delamination spot.

But experimentally this damage can be rather difficult to measure.

Figure 11 shows opaque penetrant enhanced radiography of damage extension in fatigue; the specimen is a coupon of quasi-isotropic (0/90/45/-45)s CFRP laminate in fatigue. The lamination at different levels are developing together with intralaminar cracking; experimentally it is quite difficult to separate such different damages, and it could be more sensible to evaluate the extension of a damaged area (or volume).

But with a bolted joint even this latter measure could be very uneasy.

In a specimen having a volume  $D$  the strain energy can be generally written as

$$V = \frac{1}{2} DE \epsilon^2 \quad ;$$

having defined a certain measure  $\psi$  of the damage, the energy release rate, or damage driving force, is consequently

$$G = -\frac{\partial V}{\partial \psi} = -\frac{1}{2} DE_0 \frac{\partial E}{\partial \psi} \quad (23)$$

Then a damage is such if it produces an appreciable change in the average modulus E, and it is sensible to adopt the following global damage definition:

$$\psi = \frac{E_0 - E}{rE_0} \quad (24)$$

where  $r \leq 1$  is the ratio of a typical damage area dimension and the corresponding specimen dimension, and  $E_0$  is the original value of E. For instance, in a specimen containing a single hole, r can be the ratio of hole diameter to specimen width.

In the case of point 2, since the free edge delamination may cover all the useful length of the specimen,  $r=1$ , and it is easily shown that the global damage measure  $\psi$  is proportional to the previously assumed damage width, being:

$$\psi = \left(1 - \frac{E}{E_0}\right) \frac{2a}{b}$$

Definition (24) in equation (23) gives the following global expression for the energy release rate

$$G = \frac{1}{2} r DE_0 E^2 = rV_0 \quad (25)$$

With this definitions the most essential measure to be taken in specimen tests is the trend of the modulus E versus the number N of strain cycles of amplitude .

Having recorded this measures it will be easy to evaluate  $\psi$  with (24) and

$$\frac{d\psi}{dN} = -\frac{1}{r} \frac{d}{dN} \left(\frac{E}{E_0}\right) \quad ; (26)$$

then correlation between G(25) and  $\frac{d\psi}{dN}$  (26) could be investigated.

In any case the measurement of specimen stiffness (or compliance) changes, as a measure of damage evolution appears to be mandatory.

## 6. FINITE ELEMENT ANALYSIS

The damage growth in figure 11 has been investigated with the Finite Element model in figure 12. Due to simmetry the model represents only half the thickness of the actual laminate, therefore only 4 layers, each layer containing 1 element and 3 nodes in the thickness.

Damage was assumed to be delamination of the 0° layer; the damage growth pattern has been taken from experimental evidence (shaded areas in figure 12).

Figure 13 shows the computed values of the global damage  $\psi$  (24) versus the total delaminated area A.

Since the 90° layer in the damaged area has a relatively high compressive stress, it may undergo buckling and possibly more severe conditions. This latter phenomenon can be important, if the clamp-up is insufficient, but it has not been yet investigated; it will be considered in the future.

## 7. CONCLUDING REMARKS

The extension of Fracture Mechanics approach to composite joint fatigue can be fruitful, but the damage concept must be broadened and detailed, to cope with the complex composite damage phenomenology.

On the other hand in specimen fatigue testing the most significant measurements are the applied strain history and the elastic modulus evolution.

## BIBLIOGRAFY

- 1- T.K.O'Brien, Characterization of Delamination Onset and Growth in a Composite Laminate, in Damage in Composite Materials, ASTM STP 775, 1982.
- 2- M.Caslini, C.Zanotti, T.K.O'Brien, Fracture Mechanics of Matrix Cracking and Delamination in Glass/Epoxy Laminates, NASA TM 89007, AVSCOM TR 86-B-3-1986.
- 3- D.S.Dugdale, Yielding of Steel Sheets Containing Slits. J.Mech.Phys.Sol. 8 (1960) pp. 100-104.
- 4- K.H.Schwalbe, The Crack Tip Opening Displacement in Elastic-Plastic Fracture Mechanics, Springer-Verlag, Berlin 1985.
- 5- D.Y.Konishi, Delamination Growth in composite Structures Under Inplane Compression Loading, in AGARD CP 335, 1983.

- 6- A.S.D.Wang, Fracture Mechanics of Sublaminar Cracks in Composite Laminates, in AGARD CP 335, 1983.  
 7- M.E.Roylance, W.W.Houghton, G.E.Foley, R.J.Shuford, G.R.Thomas, Characterization of Cumulative Damage in Composite during Service, in AGARD CP 335, 1983.  
 8- G.P.Sendeky, NDE Techniques for Composite Laminates, in AGARD CP 335, 1983.  
 9- R.Prinz, Growth of Delamination Under Fatigue Loading, in AGARD CP 335, 1983.

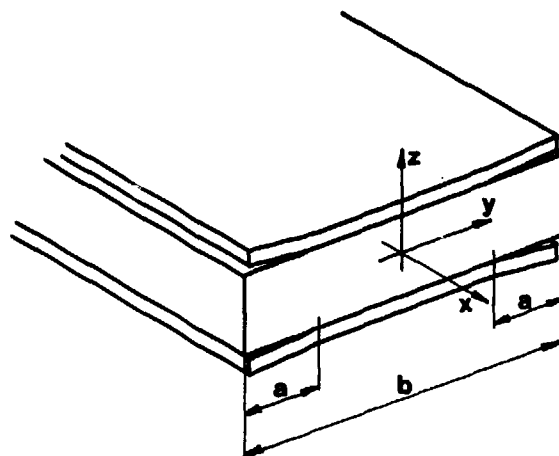


Figure 1: Free edge delamination.

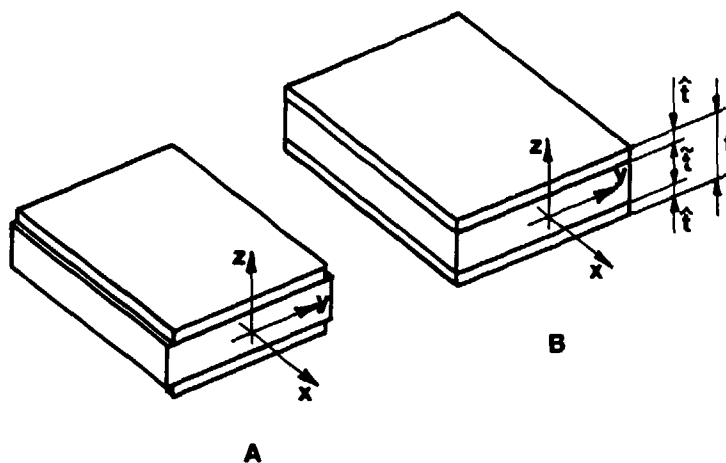


Figure 2: A: complete delamination  
 B: null delamination.

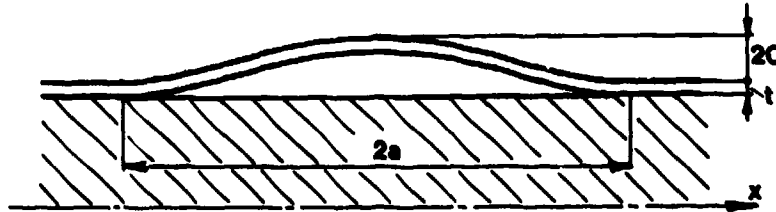


Figure 3: Buckling of a delaminated layer.

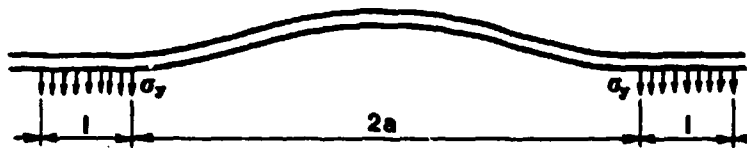


Figure 4: Dugdale's yield strip model for mode I.

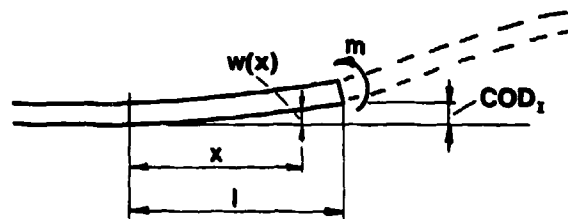


Figure 5: Dugdale's model: Crack Tip Opening Displacement.

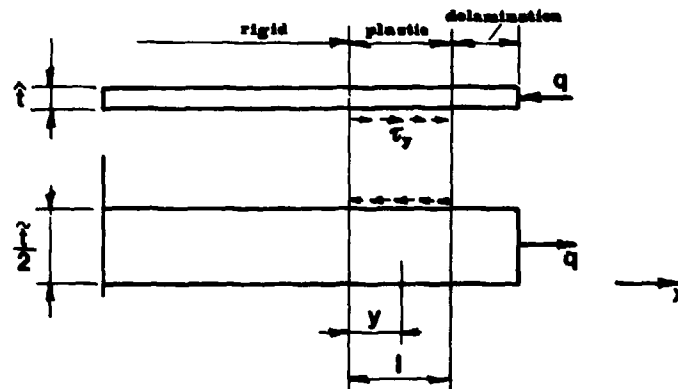


Figure 6: Dugdale's model: mode II.

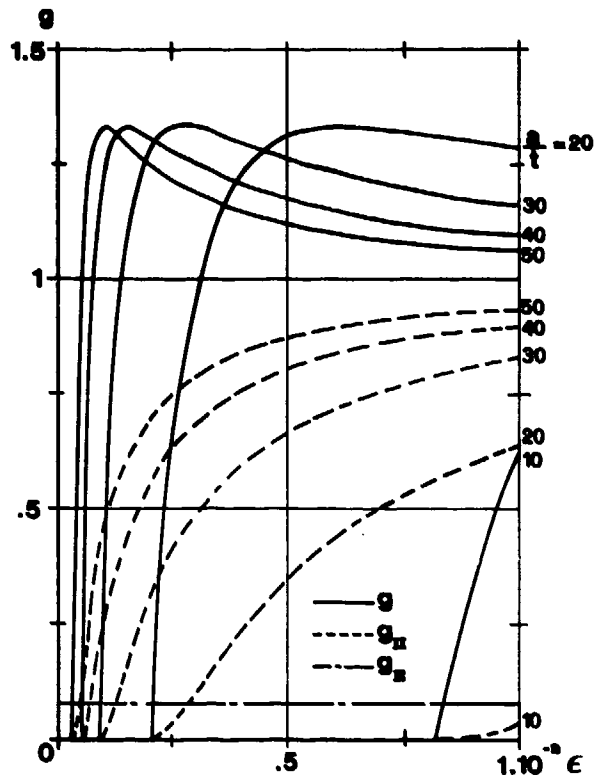


Figure 7: Non-dimensional energy release rate for a buckled layer.

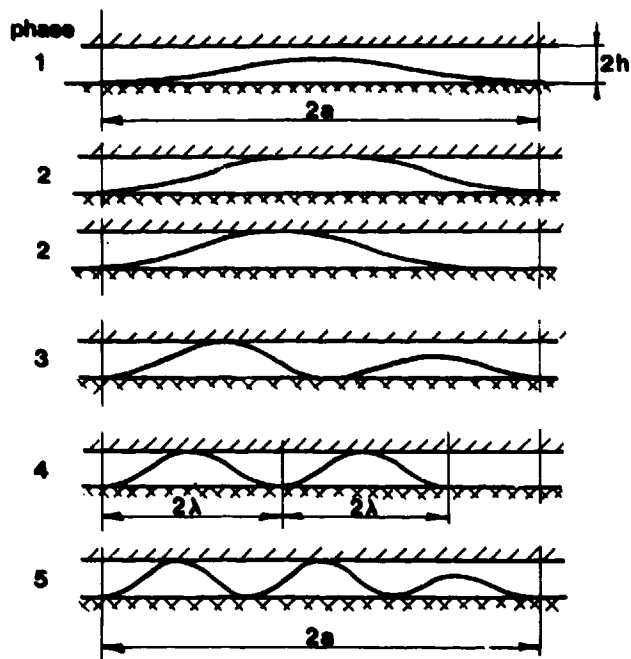


Figure 8: Delamination buckling within a narrow gap.

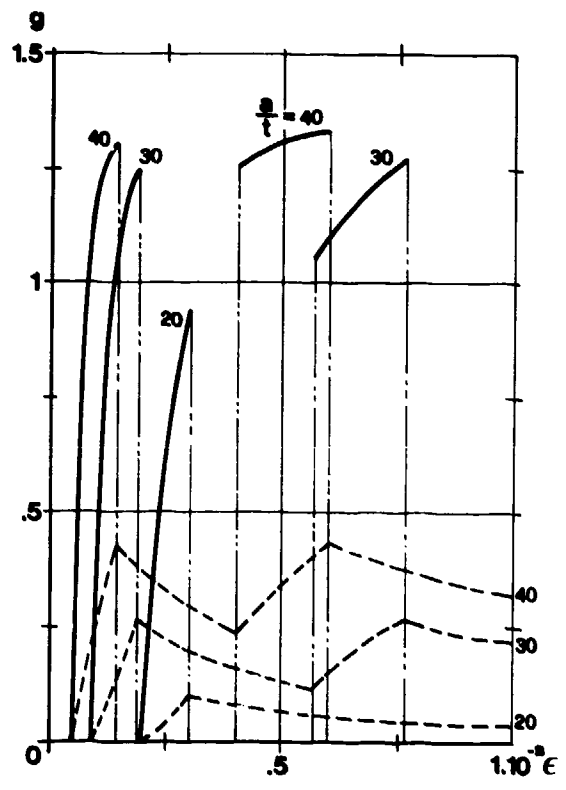


Figure 9: Delamination buckling within a narrow gap:  $h/a = .02$ .

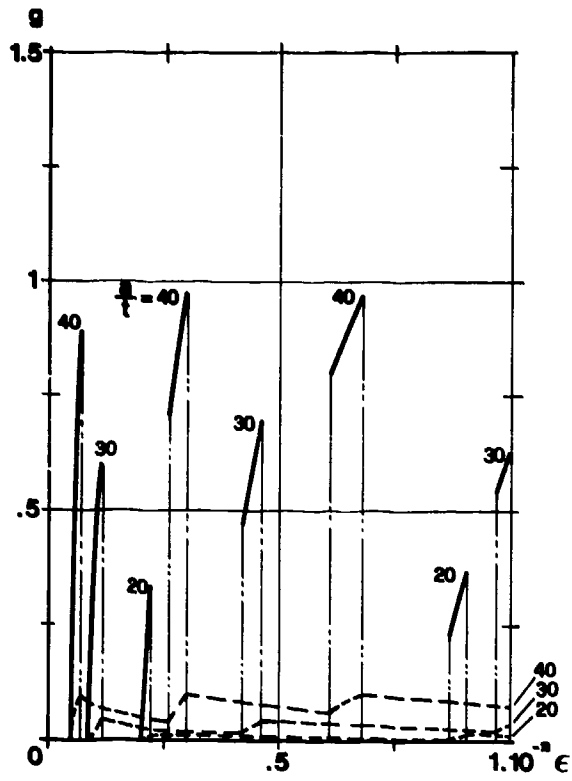


Figure 10: Delamination buckling within  
a narrow gap:  $h/a = .01$ .

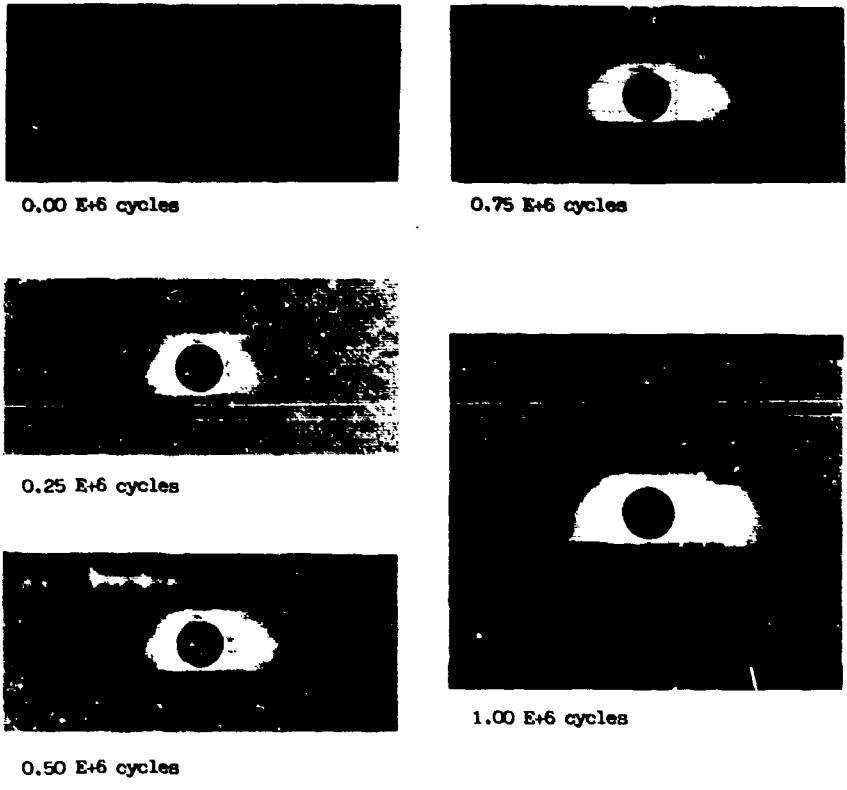


Figure 11: Delamination growth in a quasi-isotropic laminate.

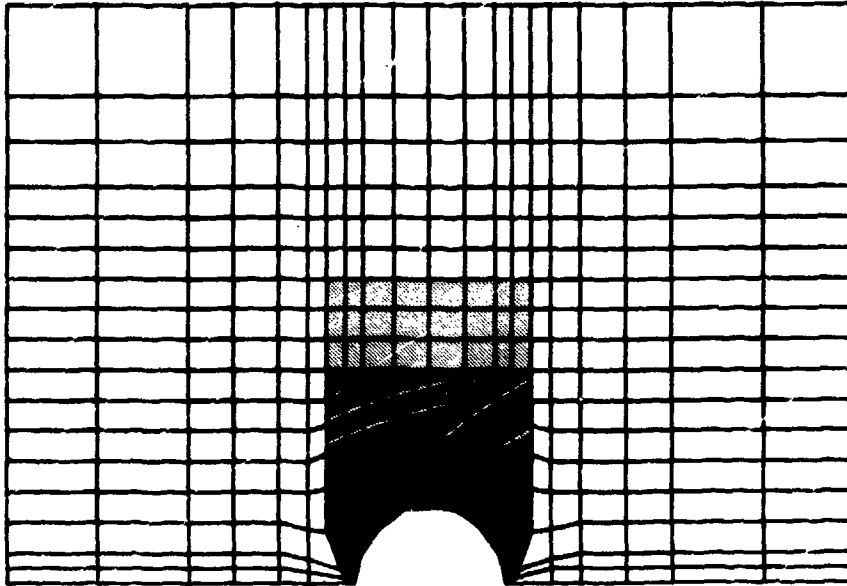


Figure 12: Finite Element model for a notched laminate.

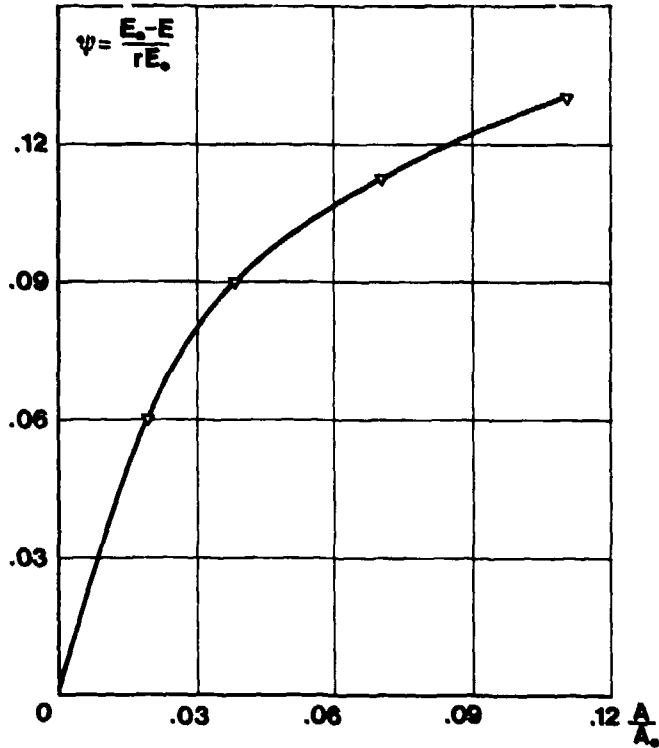


Figure 13: Damage versus damaged area from F.E.

## STRESSES IN PINLOADED ANISOTROPIC PLATES

by  
Th. de Jong  
Faculty of Aerospace Engineering  
Delft University of Technology  
Kluyverweg 1  
2629 HS Delft  
The Netherlands

## SUMMARY

A method is presented for the calculation of stresses in an anisotropic plate with a row of equally spaced, pin-loaded holes. The pin-plate configuration represents a practical joint in a composite laminate where load is transferred from a row of mechanical fasteners into the laminate. The pins fit without clearance in the holes and they are supposed to be infinitely rigid. Numerical results are presented showing various effects of geometrical and material parameters on the stress distribution.

The problem of a row of pin-loaded holes in an anisotropic plate is a complicated one of the mixed-boundary type. Several solutions can be found in literature based on simplifying assumptions regarding symmetry and geometry of the problem. The present solution is more general in those respects. It can be considered to be an application of Lekhnitskii's theory on stress distributions in anisotropic plates with holes. With this theory the determination of the stresses is reduced to the determination of two complex functions which must satisfy the specified boundary conditions of the problem.

## 1. INTRODUCTION

A major problem related to the use of composite materials in engineering is the design of reliable joints between composite parts and the remainder of a structure. Adhesive bonding has always been very popular for conventional composites and the advantages of continuous load transfer, fluid tightness and smoothness of the joint surface are well known. However, since the development of the so-called advanced composites there has been a growing interest in mechanically fastened joints. Advanced composites have potentially important applications in heavily loaded, primary structures and although mechanical joints have a relatively low structural efficiency they will most likely be preferred to adhesively bonded joints for use in those structures. An important reason is that high forces at the juncture of a bonded joint in composites may affect the structural integrity of the composite material itself because of its low interlaminar strength, a problem which does not occur in bonded joints between metal parts. Hence the load carrying capacity of bonded joints in composites is limited. Another, more general reason for application of mechanical joints is that bonded joints are often impracticable in view of disassembly and fabrication simplicity.

Due to the interest for many engineering areas the pin-plate configuration received considerable attention up till now. Unlike isotropic materials the pin bearing capacity of composites is strongly dependent on the design of the material itself and therefore joint optimization in composite plates requires knowledge of the local stresses around the fasteners. Two aspects of the theoretical work on pin-plate configurations are of special interest:

- the modelling of the joint as a pin-loaded anisotropic plate and the accurate analysis of the stresses;
- the prediction of failure in terms of the resulting stresses.

In the present work we emphasize on the first aspect. A solution is presented for the problem of an anisotropic plate with a row of equally spaced and equally loaded holes. It is based on Lekhnitskii's [1] continuum method of complex functions. The boundary conditions are fulfilled in the approximate sense using a numerical method of boundary collocation. Hence the solution is neither purely analytical, nor purely numerical.

The analysis of an anisotropic plate with a row of pin-loaded holes can be simplified considerably by assuming symmetry of the problem. It is then possible to model the plate as a finite width strip with a single pin and with known boundary conditions at the edges. Finite element methods are very appropriate for such problems. In real joints, however, the requirements regarding symmetry are not always met and we therefore will not assume it in advance. Hence modelling of the plate as a strip is not possible since the boundary conditions at the edges cannot be defined. Consequently we treat the problem as a plate problem with a periodic set of loaded holes.

All published analytical solutions for pin-loaded composite laminates contain the determination of Lekhnitskii's complex functions. A precondition for the application of Lekhnitskii's method is that the laminates are idealized to homogeneous, two-dimensional sheets with anisotropic elastic properties. Hence the laminate lay-up and related through thickness effects must be ignored. The pin-plate interaction is essentially different for different laminates and therefore the contact stresses between the pin and the plate are not known a priori. The evaluation of these stresses as part of the analysis requires the solution of a complicated mixed boundary value problem since at the contour of the hole restrictions are imposed to both the displacement and the forces. This aspect of the solution has been emphasized in the majority of the published work [2-16]. In most solutions the analysis is reduced to a boundary value problem involving a single body, namely the plate, only. Kiang [10] and Hyer and Kiang [11,12,13] were the first who explicitly modeled the pin and its interaction with the hole by including pin-elasticity. They showed that pin-elasticity is rather unimportant in stress predictions compared to clearance, friction and elastic properties of the plate material.

Published numerical results cover almost the whole field of parameters which are of interest for mechanical joints. The only exception is non-symmetry of finite-geometry problems. In the present work the theory of pin-loaded plates is therefore generalized to the problem of a row of pin loaded holes in a

composite plate where the centerline of the holes and the direction of the pin-loads are not necessarily coinciding with one of the material symmetry axes. As referred to before a purely numerical method of solution of this more general problem is difficult because of considerable problems in formulating the boundary conditions at the outer contour of the considered domain.

The solution of the problem is based on the consideration that in a practical joint the load transfer consists of two basic load systems, see Figure 1:

- a plate with a row of open, unloaded holes with a self-equilibrating load system at the outer contour;
- a plate with a row of pin-loaded holes, transferring the load from the pins into the plate. The load applied at the pins is reacted at the outer contour of the plate.

Lekhnitskii's complex functions corresponding to these two basic systems are derived separately and in a following step of the solution the functions together are made to satisfy the boundary conditions of the problem, using a simple collocation technique. This results in a set of linear equations in terms of the unknown coefficients of Lekhnitskii's functions for the pin-loaded plate. Finally the coefficients are evaluated and the stresses are calculated from the differentiated functions.

## 2. ELASTICITY SOLUTION

### The boundary conditions for the pin-plate interfaces

Figure 2 shows the different regions of the pin-plate interface. The contour of the hole is divided into:

- the region of separation, called the no-contact area, where the edge of the hole is free of tractions;
- the regions of slip, which are parts of the contact area between pin and plate. The difference in radial displacements of these parts of the edge of the hole with respect to the edge of the pin must be zero. In addition the friction force must obey a friction law;
- the region of no-slip, which is the rest of the contact area. Here the displacements of the edge of the hole are equal to the displacements of the corresponding part of the pin.

The extent of each of the regions of the interface between pin and plate depends on a number of parameters:

- the elastic properties of the pin and the plate, including the angle between principal material axes and load direction;
- the clearance between the pin and the edge of the hole;
- the pin displacement (the pin-loaded hole problem with clearance is non-linear);
- the coefficient of friction;
- the loading situation (there is an essential difference between loading, unloading and possibly static loading).

The actual extent of the regions must be determined iteratively by the requirement that tensile tractions are physically excluded and by the requirement that the friction force never can exceed the value dictated by a friction law.

The first detailed work discussing the effects of pin-flexibility, clearance and friction simultaneously was presented in [10]. The variation of these parameters was studied for a single, pin-loaded hole in an infinite plate. As already referred to in the introduction the results showed neglectable differences between steel, aluminium and infinitely rigid pins. Since pin-flexibility complicates the solution of the stress problem greatly and since the present study emphasizes on finite geometry effects we will consider infinitely rigid pins only.

In [10] clearance between pin and plate was shown to be very important. Clearance introduces non-linearity since the contact area will grow with the load. As a result the stress distribution is load-dependent. In the no-clearance or push-fit situation as it was also studied in [10] the contact area appeared to be load-independent which resulted in a linear relation between the load and the pin-displacement. This was confirmed experimentally in [17,18]. Lekhnitskii's complex functions of the present study can be used for the calculation of stresses in the non-linear clearance cases as well, utilizing Mangalgiri's [15] method of inverse formulation. Mangalgiri treats the non-linear problem by applying successively an essentially linear analysis to various configurations of contact and separation, in this way simulating the growing contact area during loading. We will restrict the calculations to no-clearance cases only; for more details on the effects of clearance the reader is referred to the work of Hyer and Kiang, Mangalgiri and Naidu et al. [16].

Because of the presence of friction between the pin and the edge of the hole a distinction must be made between the solutions for

- the loading situation; the load increases,
- the unloading situation; the load decreases with reversed friction forces,
- the static situation as it may occur at the end of the loading situation.

In the static situation the points of the edge of the hole do not displace with respect to the pin. Nevertheless friction forces will be present between the pin and the edge. The magnitude and the direction of these forces are unknown and therefore the boundary conditions cannot simply be defined. For that reason the static case will be excluded. It is noticed, however, that experimental values of stresses, which are measured during static situations, cannot agree exactly with theoretical stresses in the loading or unloading situation.

### The basic load systems

An important feature of the solution is the superposition of an infinite plate with a row of unloaded, open holes and an infinite plate with a row of pin-loaded holes. Figure 1 shows the superposition. With a suitable choice of the loads on the plate with the open holes the result of the superposition is a joint with a row of pins reacted at one side and with no by-pass of the load past the pins. Obviously the loads

on the plate with the open holes can also be chosen so that the result of the superposition is a joint where the load is partly by-passed, a situation which occurs in a multiple-row joint.

The method of solving Lekhnitskii's complex functions for a plate with a row of unloaded, open holes has been adopted from Ref. [19]. In this reference the elementary functions corresponding to an arbitrary, open hole at distance  $ps$  from the central hole are presented in the form

$$\phi_k^{(p)}(z_k - ps) = \sum_{n=1,3}^{\infty} g_n^{(k)}(z_k - ps)^{-n} \quad (1)$$

$$\begin{aligned} z_k &= x + \mu_k y & k &= 1, 2 \\ \mu_k &\text{ is a complex} & p &= -\infty \dots + \infty \\ \text{material parameter} & & p &= 0 \text{ excluded} \end{aligned}$$

In the neighbourhood of the central hole these functions are expanded in power series of  $z_k$ . The complex functions for the complete array of open holes then become

$$\phi_k^*(z_k) = \sum_{n=1,3}^{\infty} g_n^{(k)} z_k^{-n} + g_0^{(k)} z_k + 2 \sum_{p=1,2}^{\infty} \sum_{m=1,3}^{\infty} \frac{z_k^m}{m!} \sum_{n=1,3}^{\infty} (-n)(-n-1) \dots (-n-m+1) g_n^{(k)} (-ps)^{-n-m} \quad (2)$$

where the first series represents the influence of the central hole and the linear term corresponds with a homogeneous stress field.

By satisfying the boundary condition of zero tractions at the edge of the central hole a system of linear equations is obtained for the unknown coefficients of the complex functions. Solving a finite number of those equations results in an approximate solution. For a comprehensive treatment of this solution is referred to [19] where the convergency of the series expansions is discussed and numerical results are presented. It is emphasized that the expansions of the elementary functions of the individual holes have limited areas of convergence around the central hole. Therefore the solution for a plate with a row of unloaded, open holes is strictly limited to the edge of the central hole and its direct surrounding. Obviously the solution for the joint with a row of pin-loaded holes is confined to the same area.

The complex functions  $\phi_k^*(z_k)$  for a plate with a row of pin-loaded holes are adopted from Ref. [19] as well. The elementary functions  $\phi_k^{(p)}(z_k - ps)$  ( $k=1,2$ ) for an arbitrary, pin-loaded hole at distance  $ps$  from the central hole are corresponding with a radial load distribution on the edge of that hole

$$N(s) = \frac{4}{\pi} p_0 \left[ \frac{1}{2} \sum_{n=1,2}^{\infty} a_n \sin n\theta + \frac{1}{\pi} \left\{ \sum_{n=1,3}^{\infty} \frac{a_n}{n} + \sum_{m,n} \frac{2n a_n \cos m\theta}{n^2 - m^2} \right\} \right] \quad (3a)$$

and a friction force distribution

$$T(s) = \frac{4}{\pi} p_0 \left[ \frac{1}{2} \sum_{n=1,2}^{\infty} b_n \sin n\theta + \frac{1}{\pi} \left\{ \sum_{n=1,3}^{\infty} \frac{b_n}{n} + \sum_{m,n} \frac{2n b_n \cos m\theta}{n^2 - m^2} \right\} \right] \quad (3b)$$

where the dash indicates that in the double-series  $\sum_{m,n}$  only odd combinations of  $m$  and  $n$  have to be taken.

The elementary functions of the individual, pin-loaded holes are therefore completely defined in terms of the unknown load-coefficients  $a_n$  and  $b_n$  of (3a) and (3b) respectively. Expressions (3) yield loads on the upper part of the hole edge only. This implies that the elementary functions  $\phi_k^{(p)}(z_k - ps)$  of an individual, pin-loaded hole guarantee a traction free lower half of the hole to which they corresponds for every, arbitrary set of the coefficients  $a_n$  and  $b_n$ .

The total set of elementary functions  $\phi_k^{(p)}(z_k - ps)$  of the individual, pin-loaded holes will interfere and cannot represent the complex functions  $\phi_k^*(z_k)$  for a plate with a row of pin-loaded holes. Nevertheless the elementary functions of the individual holes are simply superimposed:

$$\phi_k^*(z_k) = \sum_{p=-\infty}^{\infty} \phi_k^{(p)}(z_k - ps) \quad (4)$$

As a result  $\phi_k^*(z_k)$  yield, physically impossible, normal and tangential shear stresses on the edge of the lower half of each hole. The elimination of these stresses requires the solution of an extra set of periodic functions  $\psi_k(z_k)$  of the type (2) from the load boundary conditions of the lower half of one of the holes.

The complex functions representing a joint as outlined in Figure 1 are now composed by superimposing the various functions as they are discussed in the previous paragraphs:

$$\phi_k(z_k) = \phi_k^0(z_k) + \phi_k^*(z_k) + \psi_k(z_k) \quad k = 1, 2 \quad (5)$$

- $\phi_k^0(z_k)$  correspond to a plate with a row of unloaded, open holes. They contain linear terms yielding homogeneous stresses which are used to modify the stresses in the far field in a plate with a row of pin-loaded holes. In this way realistic loading conditions can be simulated.
- $\phi_k^*(z_k)$  are the summed elementary functions corresponding to the individual pin-loaded holes. They contain the unknown load coefficients  $a_n$  and  $b_n$ .
- $\psi_k(z_k)$  are periodic functions which eliminate the tractions on the lower half of the holes resulting from  $\phi_k^*(z_k)$ . They disappear in the far field and therefore do not influence the equilibrium of the joint as it is shown in Figure 1.

The complex functions  $\phi_k(z_k)$  fulfil the load boundary conditions on all contours of the joint, independent of the values of  $a_n$  and  $b_n$ . Arbitrary coefficients, however, may not yield realistic displacements at the upper half of the holes. Therefore  $a_n$  and  $b_n$  are evaluated numerically from the displacement boundary conditions of the contact regions between pins and plate in connection with a friction law which couples the radial load (3a) and the friction force (3b). The displacements (also in terms of the unknown coefficients  $a_n$  and  $b_n$ ) can be found with the well-known expressions

$$u = 2\text{Re} [u_1 \phi_1(z_1) + u_2 \phi_2(z_2)] \quad (6a)$$

$$v = 2\text{Re} [v_1 \phi_1(z_1) + v_2 \phi_2(z_2)] \quad (6b)$$

where  $u_k$  and  $v_k$  ( $k=1,2$ ) are complex material parameters.

#### The evaluation of the load coefficients $a_n$ and $b_n$

The pins are given a displacement in a direction perpendicular to the centre line of the pin-loaded holes. This implies that in the general case of non-coinciding material axes and coordinate axes the direction of the resultant pin-load is not known and must follow from the calculations. The displacement of an arbitrary point of the contact area consists of two parts:

- a part equal to the displacement of the pin as a rigid body, say the displacement  $v_i$  of the point (0,1) in Y-direction;
- a tangential displacement relative to the pin with components  $u_r$  and  $v_r$ . The radial displacement of the points of the plate with respect to the pin must be zero for the contact area. For the no-slip region the relative tangential displacement is zero as well.

The displacement boundary condition for the slip regions is for small deformations

$$\frac{u_r}{v_r} = -\text{tg } \theta$$

or, with  $u = u_r$  and  $v = v_r + v_i$

$$u \cos \theta + (v - v_i) \sin \theta = 0 \quad (7)$$

The additional condition for the slip-regions is the requirement concerning the value of the friction force. Although a more general friction model could be used the simple Coulomb-law has been chosen. With  $\mu$  as the friction coefficient it is written as

$$T(s) = \pm \mu N(s) \quad (8)$$

where the choice of the + or - sign depends on the direction of the relative tangential displacement of the plate material, see Figure 2.

The relative displacements of the no-slip region both are zero, hence the conditions are for this area:

$$u = 0 \quad \text{and} \quad v - v_i = 0 \quad (9)$$

The displacement conditions and additional condition (8) are imposed on a finite number of points of the contact area, resulting in a homogeneous set of linear equations for the constants  $a_n$  and  $b_n$ . An extra non-homogeneous equation is added by giving the component  $R_y/p_0$  of the pin-load a specified value. Having solved the constants  $a_n$  and  $b_n$  the load distributions on the edge of the hole as well as the complex functions are completely known. After differentiation of the complex functions with respect to  $z_k$  the stresses are calculated with

$$\sigma_x = 2\text{Re} [\mu_1^2 \phi_1'(z_1) + \mu_2^2 \phi_2'(z_2)] \quad (10a)$$

$$\sigma_y = 2\text{Re} [\phi_1'(z_1) + \phi_2'(z_2)] \quad (10b)$$

$$\tau_{xy} = -2\text{Re} [\mu_1 \phi_1'(z_1) + \mu_2 \phi_2'(z_2)] \quad (10c)$$

### 3. NUMERICAL EVALUATION

#### Choice of the parameters

The following variables were chosen in the calculation presented in this section:

- the plate material ( $S_{ij\varphi}$ )
- the spacing of the holes (s/D)
- the angle between the principal material axes and the coordinate axes ( $\varphi$ )
- the mode of loading (loading or unloading)
- the coefficient of friction ( $\mu$ )
- by-pass of the load

The choice of the numerical values of the various parameters will shortly be discussed in the subsequent paragraphs.

#### The plate material

Four carbon fiber epoxy laminates with principal stacking sequences  $[0_4/\pm 45]_s$ ,  $[0_3/\pm 45]_s$ ,  $[0_2/\pm 45]_s$  and  $[\pm 45]_s$  are chosen because of their practical applicability. The index s refers to a symmetric stacking order. The stacking order itself, how important in practice it may be, is not relevant for this investigation. It is noted that generally the  $0^\circ$ -direction of a laminate has the highest Young's-modulus. In the calculations this direction coincides with the Y-axis or makes an angle  $\varphi$  with that axis. The engineering constants of the plate materials are listed in Table 1. The properties of the carbon fiber reinforced plastic (CFRP) laminates are measured values. They are taken from various publications for reference purposes. Hence there is no mutual relation between their properties in the sense of the classical laminate theory.

Table 1: The engineering constants used in the calculations.

Material	$E_{11}$	$E_{22}$	$\nu_{12}$	$G_{12}$
	GPa	GPa		GPa
CFRP $[0_4/\pm 45]_s$	20,43	111,70	0,12	16,95
$[0_3/\pm 45]_s$	18,00	92,00	0,12	14,00
$[0_2/\pm 45]_s$	17,44	63,17	0,20	17,37
$[\pm 45]_s$	20,33	20,33	0,73	27,74
alum. 7075-T6				
plane stress	71,72	71,69	0,33	26,89
plain strain	(80,69)	(80,65)	(0,50)	(26,89)

#### The spacing of the holes s/D

The calculations have been made for the following s/D-ratios:

- s/D = 1,5 the minimum ratio for which the solution still gives acceptably accurate stress values
- s/D = 3 generally accepted as the minimum ratio from a technical point of view
- s/D = ∞ which can be used for comparison with one-hole solutions

In some cases other values have been used for reference purposes.

#### The angle $\varphi$ between the principal material axes and the coordinate axes

From simple tensile tests on uni-directional composites it is known, that even a small angle of  $5^\circ$  between the direction of the load and the fiber direction decreases the strength considerably. It is therefore necessary to include this angle in the stress calculations for pin-loaded holes. To show the effect of  $\varphi$  the calculations have been made for  $\varphi = 0^\circ$  and  $\varphi = 30^\circ$ .

#### The mode of loading and coefficient of friction $\mu$

In the unloading mode the friction forces are reversed compared with the loading mode and hence the stresses in the unloading case can be calculated by giving the friction coefficient the opposite sign. The value  $\mu = .4$  is generally accepted as a good value for the friction between steel and carbon fiber epoxy. To show the effects of  $\mu$  on the stress distributions the friction coefficients  $\mu = 0$  and  $\mu = .2$  were chosen as well.

#### Clamping

An important effect may be due to the friction between the surfaces of the joined plates resulting from a possible clamping force of the fastener. In [20] it is shown that the joint strength depends strongly on that force. In certain cases the strength can be increased by a factor 2 to 3 by a proper tightening of the bolt. Composite laminates, however, behave visco-elastically in the direction of the clamping force. This visco-elasticity may relieve the clamping force and it is therefore questionable whether strength

predictions may include clamping. A finger-tightened bolt will not clamp the joined plates. Nevertheless it constrains the lateral expansion in thickness direction at the top of the hole and therefore influences the stress distribution and probably changes the failure mode. Hence the plane strain situation is supposed to represent the joint with finger-tightened bolts better than the plane stress situation for cases where the top of the hole is critical for failure. A complicating fact is that in plane strain calculations reduced material compliances are needed. These are difficult to calculate since the material properties in the thickness direction of a laminate are generally unknown. The reduced properties of isotropic materials, however, are easy to establish; hence the plane strain situation is considered for the aluminium only.

#### The load by-pass

As already discussed in Section 2 the homogeneous stresses loading the plate with a row of unloaded, open holes are used to modify the reaction of the pin-loads in the far field. In Figure 1 a situation is shown with no by-pass of the load on the joint past the pins. This situation represents a single row joint or the last row in a joint with two or more rows of pins. If the homogeneous stresses are multiplied by a factor 3 a situation is obtained where half of the load on the joint is by-passed. This situation represents the first row of a joint with two rows of equally loaded pins. Both situations are chosen because of their technical relevance. The method presented here does not include mutual interference of rows of pins. Therefore the numerical results in the cases with rows of pins are valid only for joints with sufficiently large spacing between the rows.

#### Numerical results

The stresses as presented in the various figures are made dimensionless with the classical bearing stress. With pin-loads  $P$  and the hole radii and plate thickness taken unity it is

$$p_0 = \frac{1}{2} P \quad (11)$$

#### The isotropic case

The maximum tangential stress as function of  $s/D$  is shown in Figure 3 for two values of the friction coefficient  $\mu$ . It is noticed that this stress does not always occur in the net area between the holes. Its location is sometimes shifted to a higher position on the contour of the holes. In the figure the results of the work of Frocht and Hill [21] and of the theoretical work of Schulz [22] are also shown. The measured stress concentrations refer to a single, closely fitting pin loading the specimen. The friction coefficient for the tests was unknown. It is obvious that the boundary conditions at the lateral edges of a single pin specimen are not identical to the conditions at the symmetry lines between the holes in the multiple hole analysis. The lateral edges are allowed to contract and prevention of the contraction in order to make the situation comparable with the multiple hole analysis needs extra normal tractions. These tractions would reduce the tangential stress in the net area slightly. Therefore a single pin test or analysis with finite dimensions will always yield somewhat higher stresses in the net area than the comparable multiple hole case. Nevertheless the results of Frocht and Hill are in fairly good agreement with the present results for  $\mu = .4$ . Frocht and Hill also showed that lubrication of the pin in order to decrease the friction induced small decreases in the maximum tangential stress. This is also in agreement with the present results.

Schulz [22] calculated the stress distribution around a row of pin-load holes in an infinite plate and superimposed the stresses in an infinite plate with a row of unloaded, open holes in order to balance the pin-loads at one side of the row. In [6] it is shown that the sinusoidal radial stress distribution which he used as pin-load yields lower maximum values of the tangential stress than a distribution which is evaluated from the displacement boundary conditions of the loaded part of the hole contour. In addition Schulz neglected friction between the pin and the plate material which also decreases the maximum value of the tangential stress. Schulz's results as shown in Figure 3 indeed are appreciable lower than the results of Frocht and Hill. Qualitatively, however, they are in rather good agreement with the present results for the frictionless case.

Nisida and Saito [23] investigated the stresses in a photo-elastic plate with a single, pin-loaded hole and  $s/D = 10$ . The friction coefficient in their test was unknown. They emphasized on the effects of the edge distance on the stress distribution around the fastener hole. Nisida and Saito compared their results with results of Frocht [24] for a large edge distance and found considerable differences. These differences were explained with a slight clearance between hole and pin in the tests of Frocht. In Figure 4 the stresses obtained by Nisida and Saito and by Frocht are compared with present results for friction coefficients  $\mu = 0$  and  $\mu = .2$ . As can be concluded from the figure our results compare better with the results of Nisida and Saito than with those of Frocht. Nisida and Saito lubricated the pin and worked with very low load levels. The stresses as shown in Figure 4 suggest that the friction coefficient of their test had the low value of about .1.

One of the specimens which Hyer and Liu [25,26] used for their photo-elastic measurements on a connector with a single, pin-loaded hole was made from a laminate with a quasi-isotropic lay-up. For purposes of comparison Hyer and Liu [26,27] tested also a homogeneous, isotropic plate. Figure 5 shows the stresses as they were evaluated from the tests, together with stresses calculated with the present method for the same ratio  $s/D = 4$  as Hyer and Liu used for the tests. The test results indicated very low friction coefficients. Therefore the calculations were done with  $\mu = 0$  and  $\mu = .2$ . Figure 5 shows a fairly well agreement between the various stress distributions, although discrepancies exist. Especially the sign of the friction shear stress in the quasi-isotropic plate opposite to the sign of the shear stresses in the other cases is striking.

Referring to tests on pin-loaded isotropic material it is noticed that the stresses in different materials are comparable only if those materials have identical Poisson's ratios. Nisida and Saito reported a value  $\nu = .41$  and Hyer and Liu mentioned  $\nu = .4$  for the isotropic material and  $\mu = .328$  for the quasi-isotropic laminate. In the analytical solution a ratio  $\nu = .33$  was used. The different values of  $\nu$  may be a reason for the discrepancies between the various stress distributions in Figures 4 and 5. A second possible

reason is that the described tests were obviously static tests where the friction forces between the pins and the surrounding plates certainly did not obey the simple friction-law of the theoretical analysis. This problem is discussed in Section 2. In the case of laminates with a quasi-isotropic lay-up a third possible reason for discrepancies is that the engineering constants of such laminates often do not yield values of Young's modulus  $E$  and the modulus of rigidity  $G$  which fulfil the typical isotropic relation  $E = G/2(1+\nu)$ . In other words: those laminates are often not isotropic at all although they have a quasi isotropic lay-up. The laminate of Hyer and Liu, however, yielded values of  $E$  and  $G$  which approximate the isotropic relation very closely and hence comparison of the laminate with other isotropic materials is legitimate in this respect.

Figure 6 and 7 represent graphs of the stresses  $\sigma_r$  and  $\sigma_t$  along the entire contour of the hole in the plane stress and the plane strain situation respectively. The friction shear stress  $\tau_{rt}$  and the stress in thickness direction in the plate in plane strain have not been plotted. The effects of load by-pass are shown in Figure 8 for two values of the ratio  $s/D$ .

Somizi [22] calculated the stress distribution around two rows of equally loaded holes in a staggered and in an in-line configuration for three values of  $s/D$  and friction coefficient  $\mu = 0$ . As in the case of a single row of pin-loaded holes the radial stress distribution along the contour of the hole was assumed to be sinusoidal. The maximum value of the tangential stress at the contour of the holes nearest to the applied load are compared with the present results in Figure 9. Hyer and Liu [28] tested relatively wide photo-elastic models of isotropic, double-lap connectors with two pins in tandem parallel to the load direction. The spacing of the holes was  $6D$ . In the isotropic case this seems to be sufficient to prevent interaction between the pin-loaded holes. In all tested models each pin reacted one half of the load as the load level increased. Although the friction coefficient of the tests was unknown the stresses at the edge of the hole nearest to the applied load are comparable with the calculated stresses of the present work. The maximum value of the measured tangential stress is shown in Figure 9 as well. As can be concluded from the figure the results are generally in agreement.

#### The orthotropic cases

The influence of the ratio  $s/D$  on the stress distribution in the  $[0_4/\pm 45]_3$ -laminate is shown in Figure 10 for  $\mu = .4$  and coinciding principal material axes and coordinate axes. The  $[0_4/\pm 45]_3$ -laminate represents the highest degree of orthotropy of the considered plates and it has the largest maximum tangential stress at the contour of the holes compared with corresponding cases in the other laminates. In Figure 11 the influence of the friction coefficient is shown for  $s/D = 3$ . Figure 12 and 13 show the stresses in the same laminate for an angle  $\varphi = 30^\circ$  between the material and coordinate axes. Figure 14 and 15 show the influence of the friction coefficient on the stresses in the  $[0_3/\pm 45]_3$ -laminate for  $s/D = 3$  and  $\varphi = 0$  and  $30^\circ$  respectively. The stresses in the  $[0_2/\pm 45]_3$ -laminate for various  $s/D$  ratios and  $\mu = .2$  are shown in Figure 16. Figure 17 refers to the  $[\pm 45]_3$ -laminate with  $\varphi = 0^\circ$  and  $30^\circ$  respectively and friction coefficient  $\mu = .4$ . It shows that the radial stress and the friction shear stress at the contour of a single pin-loaded hole in an infinite plate are independent of the angle  $\varphi$  if the plate material has identical Young's moduli in the principal material directions. This phenomenon is explained mathematically in [19]. It is, however, by no means obvious physically. Figure 18 shows the stresses in the same laminate with a row of pin-loaded holes with  $s/D = 3$ .

There have been several theoretical studies which aimed at the determination of the stresses in mechanically fastened joints in orthotropic materials as a basis for strength prediction. We will discuss here a few only. The first analytical investigation into the effects of joint geometry was presented by Oplinger and Gandhi [2,3]. The results of their study of a periodic array of pin-loaded holes should be comparable with the results of the present analysis. We therefore calculated the stresses in a laminate having the same engineering constants as Oplinger and Gandhi assumed for their calculations. The constants represent a  $[0_2/\pm 45]_3$ -laminate of high modulus carbon fiber reinforced epoxy. In agreement with Oplinger and Gandhi a pitch to hole diameter ratio  $s/D = 2$  and a friction coefficient  $\mu = .25$  were chosen. The results as shown in Figure 19 do not agree very well. Klang [10] and Hyer and Klang [11,12,13] used for their numerical evaluation a laminate with complex material parameters which were almost equal to the parameters of the  $[0_2/\pm 45]_3$ -laminate of the present work. Hyer and Klang studied infinitely large plates with a single, pin-loaded hole only. The stresses in the laminate of Hyer and Klang in the case of a rigid pin without clearance are therefore comparable with the present results for the  $[0_2/\pm 45]_3$ -laminate with  $s/D \rightarrow \infty$ . Figure 20 shows the results of both studies for  $\mu = .2$  and it is concluded that the agreement is very good.

The majority of published work on mechanically fastened joints in composite materials is related to the experimental investigation of the several parameters affecting the joint strength. Godwin and Matthews [29] gave an extended review of that work. Published work on the experimental determination of stress distributions are scarce. Based on their full field experiments on wood and glass fiber reinforced epoxies Wilkinson and Rowlands [30] and Rowlands et al. [31] gave general conclusions regarding the effects of the variation of friction coefficient, material properties, loading and geometry. Pabhakaran [32] tested birefringent glass-epoxy models which simulated bolted joints and presented the resulting fringe patterns in order to show the capability of the method. The patterns were not evaluated into stress distributions, however. Hyer and Liu [25,26,27] tested similar materials and did calculate the stress distributions from the fringe patterns. The technique utilized by Prabhakaran and Hyer and Liu requires the plate material to be transparent and therefore can be applied to glass reinforced epoxies only. The stresses in glass fiber laminates are obviously not representative for the stresses in pin-loaded plates composed of other materials.

## 4. DISCUSSION OF RESULTS

Some general remarks

The results of the investigation of several authors as they are presented in the previous section point out that the maximum values of the tangential stress generally agree very well. This may be important for isotropic materials since the maximum tangential stress is an essential indication for the fatigue strength of a mechanical joint in metal sheets. Nevertheless the numerical values of the maximum tangential stress are not necessarily representative for realistic situations, as will be indicated in the following paragraph. Here it is emphasized that for the prediction of the strength of a joint in a laminated material the whole stress distribution is of interest. The maximum tangential stress has no special significance there. Classical failure predictions in laminates are always made by combining stress predictions with one of the various failure rules. These are applied on a layer-by-layer basis to a great number of points in order to cover the whole stress field. Crack growth and resulting change of the stress distribution is not accounted for, neither for crack stopping effects because of adjacent layers bridging the crack. Therefore classical methods are only used for the prediction of crack initiation or the so-called first significant damage. The results indicate that failure of the laminate often initiates at places with large shear or transverse stress values in one of the layers. In laminates with loaded or unloaded holes these places are not associated primarily with the highest tangential stress concentrations at the hole boundary.

In Figures 3, 4 and 5 experimentally determined stresses are presented which agree well with theoretically determined stresses for very low values of the friction coefficient. These figures therefore may suggest that in real joints the friction forces between pin and plate generally are small. Some of the investigators indeed decreased the friction by lubricating the pin or by using specially treated, very smooth pins. Others did not and nevertheless got results corresponding with low friction forces as well. As shown in Figure 5 Hyer and Liu [26] even measured friction shear stresses in a quasi-isotropic laminate with signs opposite to the expected ones. A possible reason for the low friction stresses is already given in Sections 2. It is discussed there that statically measured stresses generally are not representative for dynamic situations with slip at the interface between pin and plate. Statically measured stress concentrations therefore may have limited significance with regard to dynamic loads.

In simple failure predictions of mechanical joints in metal plates the concept of bearing strength as material property is used. It is related to a specific type of failure, called the 'bearing failure', or to a certain degree of hole ovalization. The stresses and stress distributions presented in the previous chapter have been made dimensionless with a reference stress which is called the 'bearing stress' according to definition (11). If the pin-load  $P$  reaches a value at which the laminate fails the corresponding value of  $p_b$  is easy to calculate. Since it is the maximum value of  $p_b$  it is often referred to as the bearing strength of a laminate. The maximum value, however, will not only depend on the strength characteristics of the composite material but also on the whole set of parameters described in Section 3. Hence a concept of bearing strength as a material property related to mechanical joints is not justified for composite laminates. Composite materials exhibit several failure modes and the maximum value of the bearing stress is not necessarily associated with a specific one.

The plate material

As illustrated by several figures the radial stress distributions do not differ substantially for the various materials. They however differ essentially from the sinusoidal distribution as it is often assumed in literature. The tangential stress distributions show considerable differences. As expected the peak stresses increase with increasing degree of anisotropy. In the isotropic aluminium the stress distributions in the plane stress and the plane strain situation are almost similar, as Figures 6 and 7 show. Nevertheless they will result in different yield values of the bearing stress  $p_b$ . Although the present work does not emphasize on yielding or fracture the Von Mises yield value of  $p_b$  has been calculated in order to show that effect. The calculations were done with  $\sigma_{0.2} = 503$  MPa as the yield stress value of the aluminium. The results are given in Table 2, together with the place at the edge of the holes where first yielding is predicted.

Table 2: Yield values of the bearing stress  $p_b$  and places where first yielding occurs in the plane stress and in the plane strain situation. The material is Aluminium 7075-T6.

	s/D = 1.5		s/D = 3		s/D = ∞	
	$\bar{p}_b$ MPa	$\theta^\circ$	$\bar{p}_b$ MPa	$\theta^\circ$	$\bar{p}_b$ MPa	$\theta^\circ$
plane stress $\mu = .2$	154	5	308	7	406	55
plane strain $\mu = .2$	181	7	320	12	424	60

- The spacing of the holes

As expected the tangential stress concentration  $\sigma_t/p_b$  in the net-sections increase with decreasing s/D-ratio. At the top of the holes, however, they remain almost constant. At these tops the values of  $\sigma_t/p_b$  are very low or even slightly negative in all loading cases. The values of  $\sigma_t/p_b$  at  $\theta = 270^\circ$  is also slightly negative in most considered cases. A less expected effect of the spacing of the holes is that the radial stresses decrease at the upper part of the contact area with decreasing s/D-ratio. As a consequence they increase at the flanks of the hole. From the effects of the s/D-ratio on both the tangential stresses and the radial stresses it can be concluded that small pitch values are favourable for the stress situation at the top of the holes.

- The angle  $\phi$  between principal material axes and coordinate axes

Figures 12, 13 and 15 show effects of the angle  $\phi$  on the stress distributions. In general peak values of the tangential stress are generated in the vicinity of the points on the edge of a hole where the direction of the highest Young's modulus of the laminate is parallel to the hole boundary. Hence the maximum tangential stress does not necessarily occur in the plate net areas. An example of this phenomenon is shown in Figures 17 and 18 where the stress distributions are given in a non-rotated and a rotated  $[\pm 45]_2$ -laminate.

- The loading mode and the coefficient of friction  $\mu$

Figures 11 and 13 give the stress distributions in the  $[0_4/\pm 45]_2$ -laminate for  $\mu = .2$  in the loading and the unloading situation. The zero friction case is shown as well. The figures exhibit a predominant influence of the loading mode on the stress distribution near the point on the edge of a hole where the direction of the highest Young's modulus of the plate material is perpendicular to the hole boundary. Both the tangential stresses and the radial stresses at this place show a peak in the unloading situation. The peaks result from the reversed friction forces on the flanks of the hole. Apparently the unloading mode is very unfavourable for the top of the hole. It is remarked that the tangential stresses in the unloading and frictionless cases are positive for the whole contact area. The maximum tangential stresses are affected only marginally by the mode of loading.

The unloading mode has been simulated by giving the friction coefficient an opposite sign compared to the loading mode. This implies that there is no fundamental difference between the influence of the loading mode on the stress distributions and that of the friction coefficient. Figures 14 and 15 show that the stresses near the top of a hole decrease with increasing friction coefficient. In all considered loading cases the tangential stress at the top or near the top in the rotated laminates is negative for positive values of  $\mu$ . This was also noticed by Wilkinson and Rowlands [42] and several other investigators. Hence positive values of  $\mu$  relieve the top of the hole compared to the unloading and frictionless situation.

- The load by-pass

Load by-pass calculations are done for the isotropic aluminium only. Figure 8 shows the influence of load by-pass on the stress distributions for two values of s/D and  $\mu = .4$ . The joint consists of two rows of pins in line which are supposed to be equally loaded. The by-pass distributions in Figure 8 refer to the row on the stretched side of the joint. The no by-pass distributions represent the second row or a joint with a single row. From the figure it is clear that the influence of load by-pass on the tangential stress near the net areas is predominant. Figure 21 gives the maximum value of the gross stress  $\sigma_{gr}$  in the far field on the stretched side of the joint as function of D/s. It is calculated with

$\bar{p}_b$  D/s in the case of a single row and with  $2\bar{p}_b$  D/s in the case of two rows of pins.  $\bar{p}_b$  is the Von Mises yield value of the bearing stress. As in the plane stress and plane strain calculations it is the value of the bearing stress at which somewhere on the edge of the holes first yielding of the plate material occurs. Hence  $\bar{\sigma}_{gr}$  is a measure for the static loading capacity of the joint in terms of first yielding of the plate material around the fastener holes. The theoretical stress concentration factor  $K_t$  is presented in Figure 22 as function of D/s.  $K_t$  is defined here as the ratio of the maximum tangential stress at the hole boundary and the gross stress  $\sigma_{gr}$  in the far field. Figures 21 and 22 both show an optimum value of the ratio D/s. This value is .44 for the two rows of pins and .5 for the single row. Schulz [4] calculated almost the same values for the corresponding cases with  $\mu = 0$ . He also notified that in the limiting cases D/s = 0 and D/s = 1 the stress concentration factor  $K_t$  tends to infinity.

This corresponds with zero values of  $\bar{\sigma}_{gr}$  in Figure 21.

## 5. CONCLUDING REMARKS

In the present work an elasticity solution in combination with a numerical method has been used in order to study the stresses in an anisotropic plate with an infinite row of equally spaced and equally loaded pins. The loads are applied by giving the pins a displacement in a direction perpendicular to the center line of the holes. The center line does not necessarily coincide with one of the principal material axes. This implies that the direction of the pin-loads is not known a priori. The loads are balanced in the far field by uniform stresses, either on one side of the joint or on both sides. The last case represents by-pass of the load on the joint past the pins.

In the solution series expansions have been used with limited areas of convergency. Therefore the solution is confined to the edge of a hole and its direct vicinity. The solution represents a real joint with a sufficiently large number of pin-loaded holes and does not apply to a joint with only a few pins or to the end pins of a row.

In particular the effects of joint geometry, material parameters, load by-pass and friction at the interfaces between pins and plate have been studied. Pin elasticity and clearance were not considered. In the calculations a simple friction model with a constant friction coefficient was used.

The results of the calculations show predominant influences of friction and pitch to hole diameter ratio. In specific cases the results were compared with results from literature. From this comparison the conclusion seems to be justified that the present study provides an accurate description of the stresses in a pin-loaded, anisotropic plate.

## 6. REFERENCES

1. Lekhnitskii, S.G. (1956). Anisotropic Plates. Translated from the 2nd Russian edition by S.W. Tsai and T. Cheron, 1968, Gordon and Breach, London.
2. Oplinger, D.W. and Gandhi, K.R. (1974). Stresses in mechanically fastened orthotropic laminates, Proc. of the 2nd Conf. on Fibrous Composites in Flight Vehicle Design, Dayton, 813-841.
3. Oplinger, D.W. and Gandhi, K.R. (1974). Analytical studies of structural performance in mechanically fastened fiber reinforced plates. Army Symp. on Solid Mechanics, 211-240.
4. De Jong, Th. (1976). Spanningen rond een gat in een elastisch orthotrope of isotrope plaat, belast door een pen die zich daarin wrijvingsloos kan bewegen (Stresses in an elastically orthotropic or isotropic plate loaded by a frictionless pin). Report LR-223, Delft University of Technology.
5. De Jong, Th. and Beukers, A. (1977). Stresses around a pin-loaded hole in an elastically orthotropic or isotropic plate. Report LR-241, Delft University of Technology.
6. De Jong, Th. (1977). Stresses around pin-loaded holes in elastically orthotropic or isotropic plates. Journ. of Comp. Mat., Vol. 11, 313-331.
7. De Jong, Th. and Vuil, H.A. (1981). Stresses around pin-loaded holes in elastically orthotropic plates with arbitrary load direction. Report LR-333, Delft University of Technology.
8. De Jong, Th. (1982). The influence of friction on the theoretical strength of pin-loaded holes in orthotropic plates. Report LR-350, Delft University of Technology.
9. De Jong, Th. (1982). Stresses around pin-loaded holes in composite materials. Mechanics of Composite Materials Recent Advances, Pergamon Press, New York, 339-353.
10. Klang, E.C. (1983). The stress distribution in pin-loaded orthotropic plates. Thesis VPI and SU, Blacksburg.
11. Hyer, M.W. and Klang, E.C. (1984). Contact stresses in pin-loaded orthotropic plates. Report VPI-E-84-14, CCMS, VPI and SU, Blacksburg.
12. Hyer, M.W. and Klang, E.C. (1984). Stresses around holes in pin-loaded orthotropic plates. 25th Struct., Structural Dyn. and Mat. Conf. of the AIAA, ASME, ASCE and AHS, Palm Springs, 232-242.
13. Hyer, M.W. and Klang, E.C. (1985). Contact stresses in pin-loaded orthotropic plates. Int. Journ. of Solids and Struct., vol. 21, 9, 957-975.
14. Zhang, K.D. and Ueng, C.E.S. (1984). Stresses around a pin-loaded hole in orthotropic plates. Journ. of Comp. Mat., vol. 18, 432-446.
15. Mangalgiri, P.D. (1984). Pin-loaded holes in large orthotropic plates. AIAA-Journal, vol. 22, 10, 1478-1484.
16. Naidu, A.C.B., Dattaguru, B., Mangalgiri, P.D. and Ramamurthy, T.S. (1985). Analysis of a finite composite plate with smooth, rigid pin. Composite Structures, 4, 197-216.
17. De Jong, Th. and Klang, E.C. (1985). Pinned connections in composite materials: Theory and experiment. Report LR-445, Delft University of Technology.
18. Klang, E.C. and De Jong, Th. (1985). Elastic response and damage accumulation of composite materials used in pinned connections. Mechanical Characterization of Load Bearing Fibre Composite Laminates, Elsevier, London, 132-138.
19. De Jong, Th. (1987). On the calculation of stresses in pin-loaded anisotropic plates. LR-report, Delft University of Technology. To be published.
20. Collings, T.A. (1982). On the bearing strength of C.F.R.P. laminates. Composites, vol. 13, 3, 241-252.
21. Frocht, M.M. and Hill, H.N. (1940). Stress concentration factors around a central circular hole in a plate loaded through pin in the hole. Journ. of Appl. Mech., vol. 7, 1, A5-A9.
22. Schulz, K.J. (1941). Over den spanningstoestand in doorboorde platen (On the state of stress in perforated plates). Thesis, Delft University of Technology.
23. Nisida, M. and Saito, H. (1966). Stress distributions in a semi-infinite plate due to a pin determined by interferometric method. Experimental Mechanics, vol. 6, 5, 273-279.
24. Frocht, M.M. (1941). Photoelasticity I, 4th pr. 1957, Wiley and Sons, 309-322.
25. Hyer, M.W. and Liu, D. (1984). Stresses in a quasi-isotropic pin-loaded connector using photoelasticity. Experimental Mechanics, vol. 24, 1, 48-53.
26. Hyer, M.W. and Liu, D. (1985). Stresses in pin-loaded plates. Mechanical Characterization of Load Bearing Fibre Composite Laminates, Elsevier, London, 179-190.
27. Hyer, M.W. and Liu, D. (1985). Stresses in pin-loaded orthotropic plates: Photoelastic results. Journ. of Comp. Mat., vol. 19, 2, 138-153.
28. Hyer, M.W. and Liu, D.H. (1983). Photoelastic determination of stresses in multiple-pin connectors. Experimental Mechanics, vol. 23, 3, 249-256.
29. Godwin, E.W. and Matthews, F.L. (1980). A review of the strength of joints in fibre-reinforced plastics. Composites, vol. 11, 3, 155-160.
30. Wilkinson, T.L. and Rowlands, R.E. (1981). Analysis of mechanical joints in wood. Experimental Mechanics, vol. 21, 11, 408-414.
31. Rowlands, R.E., Rahman, M.U., Wilkinson, T.L. and Chiang, Y.I. (1982). Single- and multiple-bolted joints in orthotropic materials. Composites, vol. 13, 3, 273-279.
32. Prabhakaran, R. (1982). Photoelastic investigation of bolted joints in composites. Composites, vol. 13, 3, 253-256.

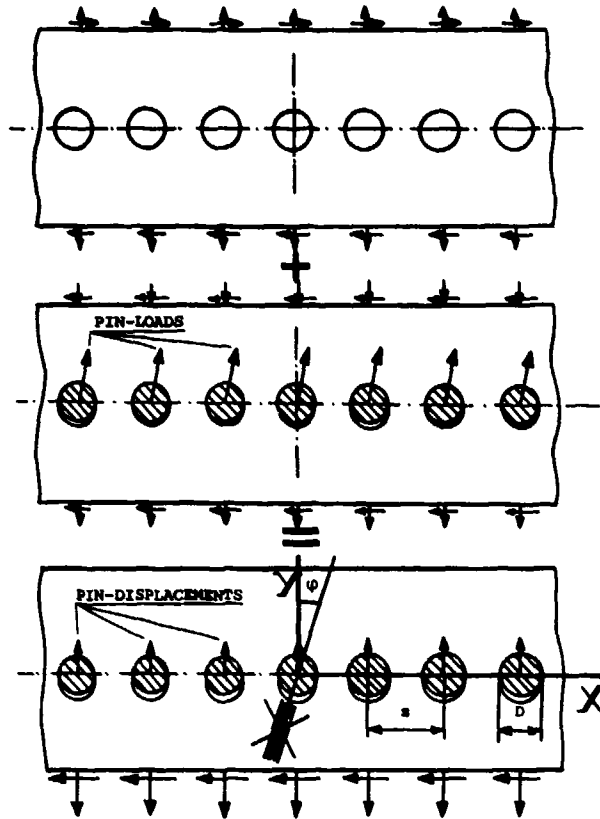


Figure 1: The basic load systems of a joint.

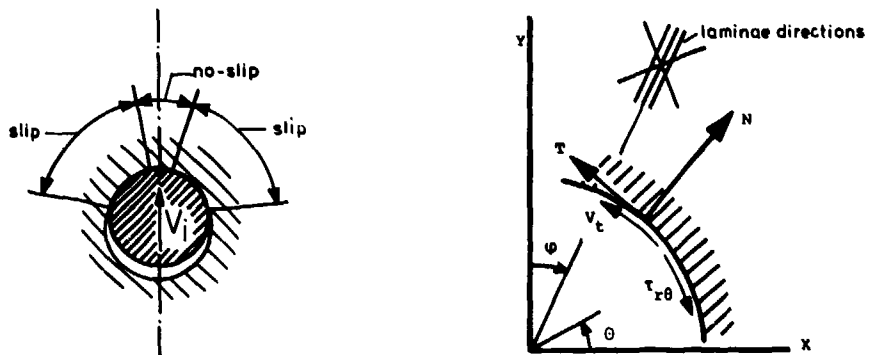


Figure 2: The different regions of the pin-plate interface and the positive directions of forces, stresses, displacements and angles.

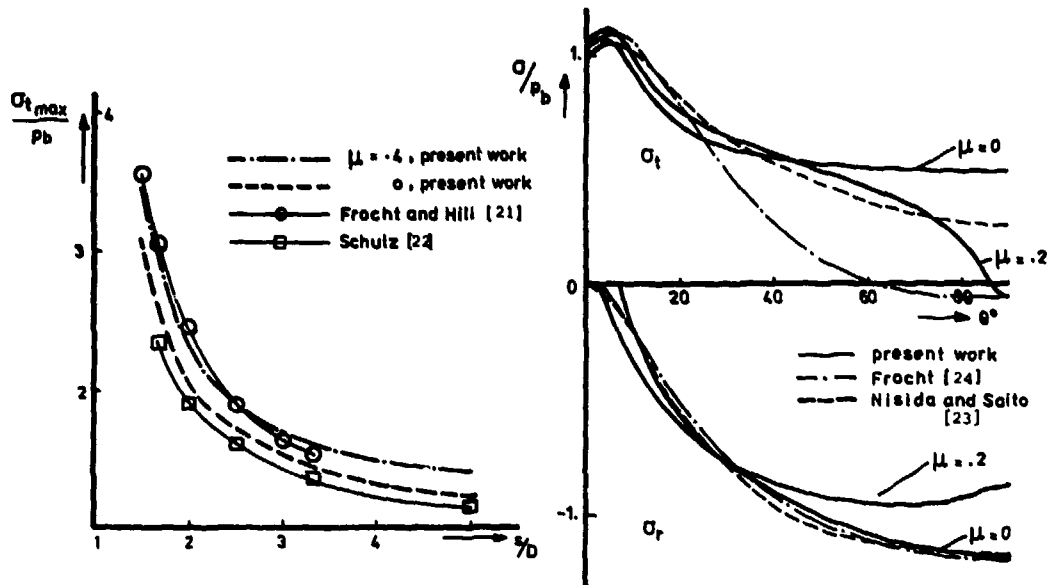


Figure 3: The maximum tangential stress concentration in a pin-loaded isotropic material as function of  $s/D$ .

Figure 4: The stresses along the edge of a pin-loaded hole in an isotropic material for  $s/D = 10$ .

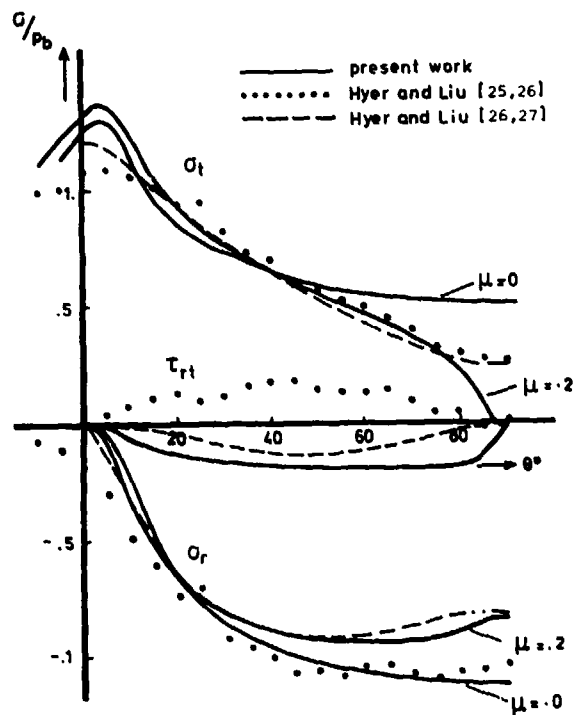


Figure 5: Comparison of present results with experimental values of Hyer and Liu; material (quasi-) isotropic and  $s/D = 4$ .

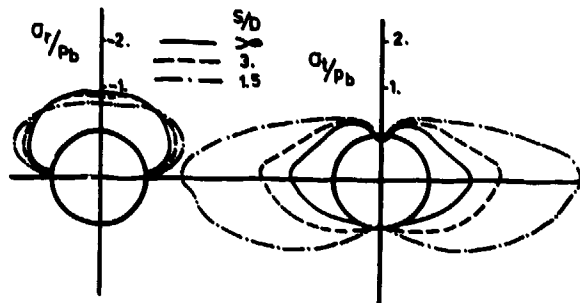


Figure 6: The stresses around a pin-loaded hole in an isotropic material in plane stress, friction coefficient  $\mu = .2$ .

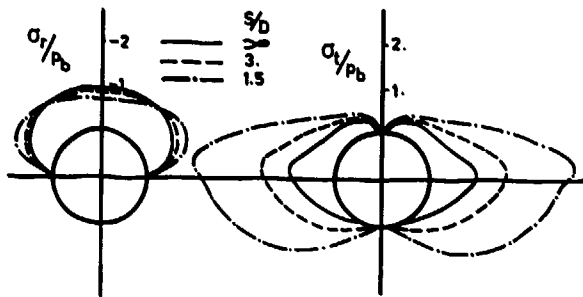


Figure 7: The stresses around a pin-loaded hole in an isotropic material in plane strain, friction coefficient  $\mu = .2$ .

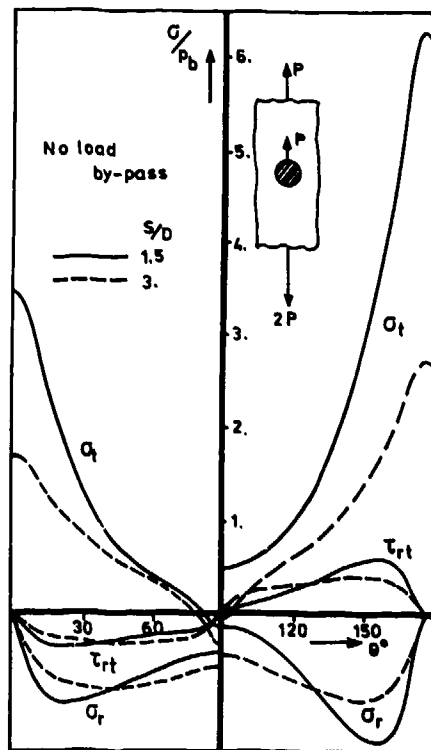


Figure 8: The effects of load by-pass on the stresses around a pin-loaded hole in an iso-

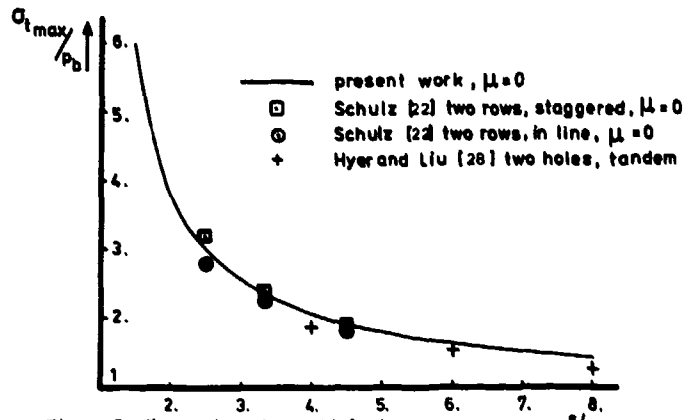


Figure 9: The maximum tangential stress concentration in an isotropic material as function of the ratio  $s/D$  in the case of load by-pass.

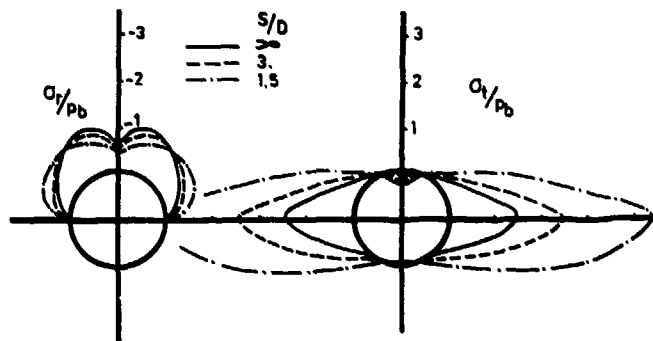


Figure 10: The effects of the ratio  $s/D$  on the stresses around a pin-loaded hole in the  $[0_4 / \pm 45]_s$  - laminate for  $\mu = .4$ .

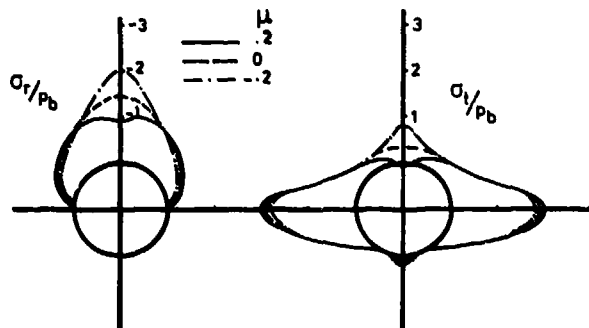


Figure 11: The effects of the friction coefficient  $\mu$  on the stresses around a pin-loaded hole in the  $[0_4 / \pm 45]_s$  - laminate for  $s/D = 3$ .

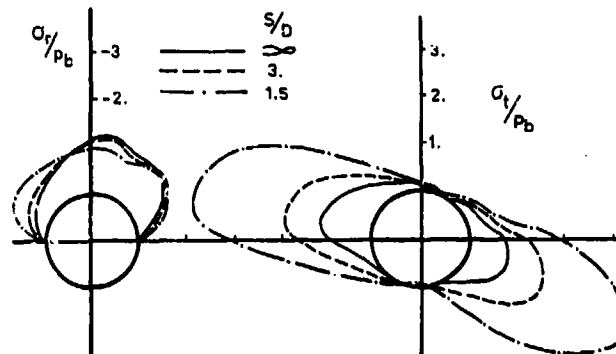


Figure 12: The effects of the ratio  $s/D$  on the stresses around a pin-loaded hole in the  $[0_4/\pm 45]_s$  - laminate for  $\mu = .4$  and  $\varphi = 30^\circ$ .

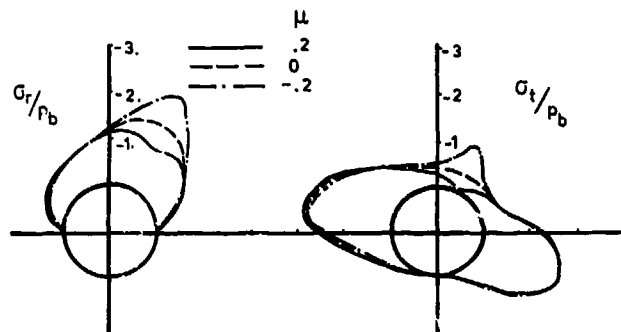


Figure 13: The effects of the friction coefficient  $\mu$  on the stresses around a pin-loaded hole in the  $[0_4/\pm 45]_s$  - laminate for  $s/D = 3$  and  $\varphi = 30^\circ$ .

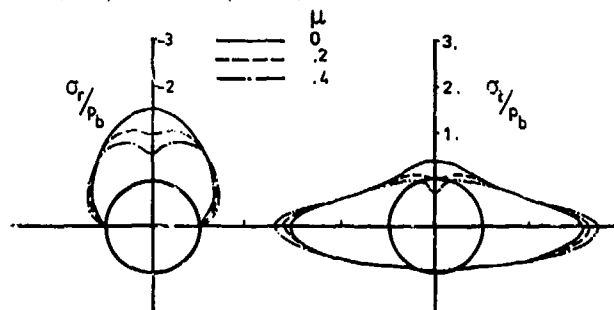


Figure 14: The effects of the friction coefficient  $\mu$  on the stresses around a pin-loaded hole in the  $[0_3/\pm 45]_s$  - laminate for  $s/D = 3$ .

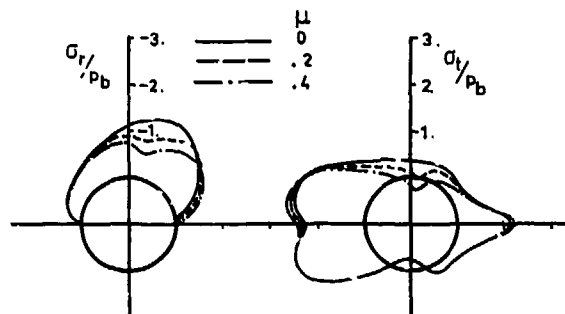


Figure 15: The effects of the friction coefficient  $\mu$  on the stresses around a pin-loaded hole in the  $[0_3/\pm 45]_s$  - laminate for  $s/D = 3$  and  $\varphi = 30^\circ$ .

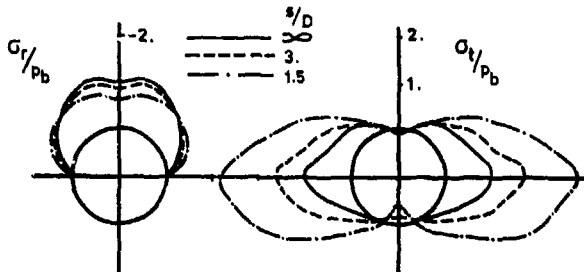


Figure 16: The stresses around a pin-loaded hole in the  $[0_s/\pm 45_s]$  - laminate for various values of the ratio  $s/D$  and  $\mu = .2$ .

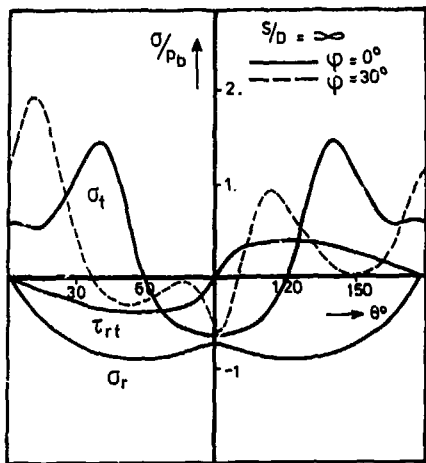


Figure 17: The stresses around a pin-loaded hole in an infinite  $[\pm 45_s]$  - laminate for two values of  $\phi$  and  $\mu = .4$ .

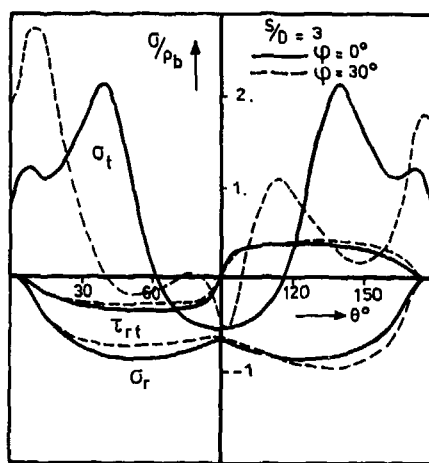


Figure 18: The stresses around a pin-loaded hole in a  $[\pm 45_s]$  - laminate for two values of  $\phi$ ,  $s/D = 3$  and  $\mu = .4$ .

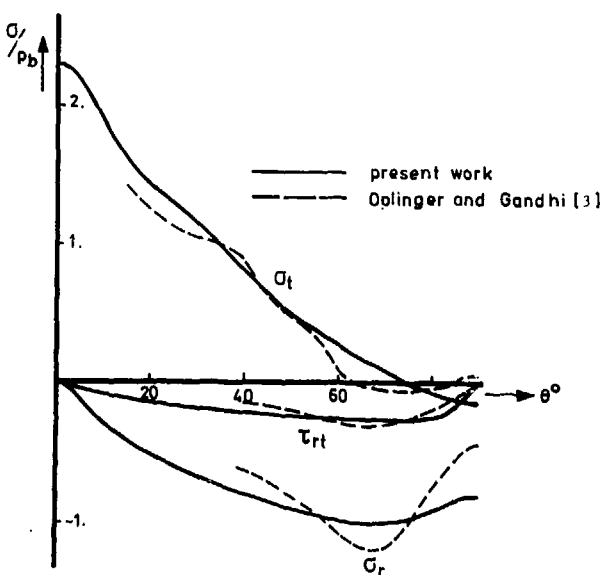


Figure 19: Comparison of present results with results of Oplinger and Gandhi for  $s/D = 2$  and  $\mu = .25$ .

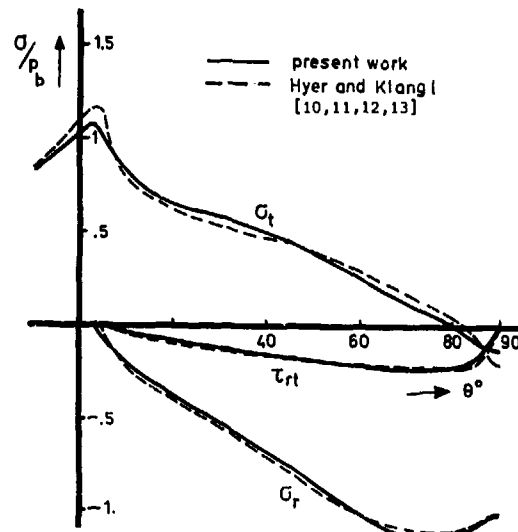


Figure 20: Comparison of present results with results of Hyer and Klang for the infinite  $[0_2/+45]_s$  laminate, friction coefficient  $\mu = .2$ .

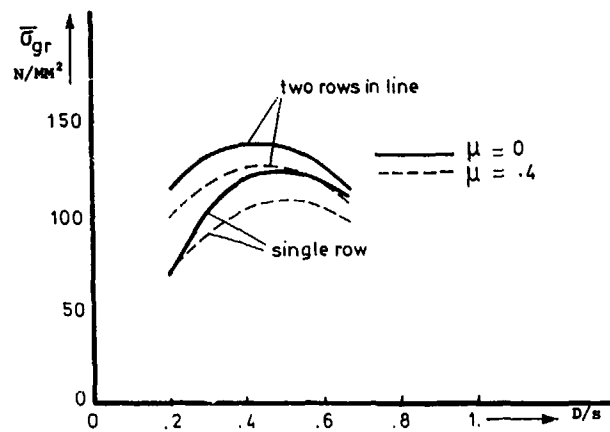


Figure 21: The maximum value of the gross stress in the far field as function of  $D/s$ . The calculation is based on first yielding of the duraluminium 7075-T6 plate material around the fastener holes.

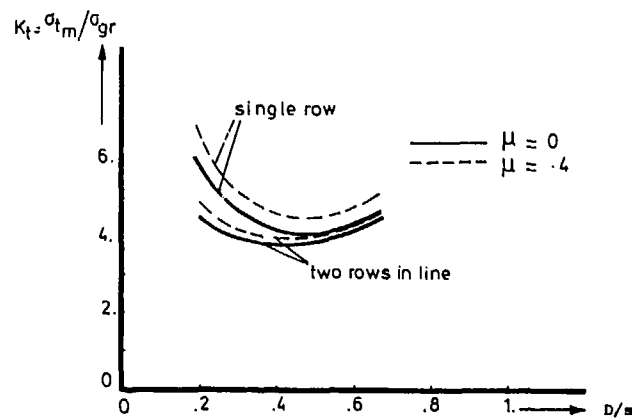


Figure 22: The maximum tangential stress concentration factor in a pin-loaded isotropic material as function of  $D/s$ .

## AN ANALYSIS METHOD FOR BOLTED JOINTS IN PRIMARY COMPOSITE

## AIRCRAFT STRUCTURE

Ingvar Eriksson

Saab-Scania AB, Saab Aircraft Division, Stress Department, S-58188 Linköping, Sweden.

and

The Royal Institute of Technology, Department of Aeronautical Structures and Materials, S-10044, Stockholm, Sweden.

## ABSTRACT

The analysis of bolted joints in composite structure requires, like structural analysis in general, methods for determining the stress distributions and relevant failure criteria. The stress analysis procedure discussed in this paper starts by addressing the joints as an integrated part of the overall structure. The stresses in the vicinity of the hole boundary are obtained through a series of finite element analyses, which starts with an overall load distribution analysis and ends with a 2-dimensional detailed contact stress analysis of the most highly stressed region in the joint. Strength is predicted for two basic failure modes occurring in a joint, net-tension and bearing failure. The failure hypotheses for these failure modes are described. Both the stress analysis and failure hypotheses are performed and established, respectively under certain idealizations. The conditions in a real joint in an aircraft may differ from these idealizations. Hence, further work is required and is also proposed in this paper. The analysis procedure described in this paper is based on today's powerful computer facilities and offer great advantages compared with more empirical procedures. The procedure is presently used at Saab Aircraft Division.

## CONTENTS

1	INTRODUCTION . . . . .	1
2	STRESS ANALYSIS . . . . .	2
2.1	Load distribution analysis . . . . .	2
2.2	Detailed stress analysis . . . . .	3
3	FAILURE CRITERIA . . . . .	4
3.1	Net-tension failure . . . . .	4
3.2	Bearing failure . . . . .	4
4	MISCELLANEOUS CONSIDERATIONS . . . . .	6
5	ACKNOWLEDGEMENTS . . . . .	6
6	REFERENCES . . . . .	7

## 1 INTRODUCTION

Most published work on the strength of bolted joints in composite structures deal with joints of simple geometry, which are subjected to uniaxial loads in double shear. The problem of predicting the strength of such joints is by no means a simple problem. On the contrary, it is well known that the characterization of the strength is complicated by the very large number of parameters involved, such as laminate layup (fibre pattern), stacking sequence, geometry, bolt torque, etc.

In spite of the amount of published work on the subject, the mechanical behaviour of such relatively "well defined" joints is yet not fully understood. In primary aircraft structures, the joints may be far more complicated. The loading conditions are generally complicated and usually it is a matter of multirow joints. The problem of determining the load distribution in general is statically undetermined. Because of the lack of appropriate analytical/numerical methods, empirical methods, which require large amount of data, have been used for analysis and design of joints. For several reasons, there are urgent needs for improved methods, which are based on today's powerful computer facilities:

- 1) The generating of such data bases has proved to be both costly and time-consuming.
- 2) New and improved materials are appearing on the market continuously, which means that the data bases must be regenerated.
- 3) An improved computational procedure will lead to a better understanding of the mechanical behaviour, which in its turn will lead to better designed structures as well as more efficiently designed test programs.

4) With an efficient computational procedure, design charts for desirable load cases are easily computed.

5) Last but not least, such a procedure would prevent the results of the analysis, to a higher extent, to be dependent on the judgements made by the individual analysts.

On the other hand such an improved computational procedure must not be so sophisticated and full of details that it becomes too time-consuming and expensive to use in the daily analysis work. The finite element method, FEM, has proved to be a powerful tool in order to determine load and stress distributions in structures. The disadvantage with FEM is that the modeling work has a tendency to be time-consuming. The execution time may also be long and costly. If FEM is adopted for the determination of load and stress distributions, it is essential to support such a procedure with efficient pre- and post-processors. If the analysis procedure is used frequently, it is necessary to have powerful computer facilities in order to reduce the execution time. Figure 1 shows the different stages in such an analysis procedure based on FEM.

First, the internal load distribution in the joint is calculated, see figure 1(b). The structural behaviour is for critical joints mechanically simulated by connecting the members with finite beam or spring elements, which are given a representative stiffness. Due to economic limitations, the fastener stiffness (flexibility) is, for ordinary joints, excluded at this stage. In that case it may be necessary to perform another analysis, before the final detailed stress analysis, figure 1(c), where the internal load distribution in the joint is determined.

Then, the stresses in the vicinity of the most highly stressed holes are computed by performing a detailed analysis, see figure 1(c). The procedure is supported by the two Saab-Scania developed computer programs GENCUT and COBOJ. GENCUT is a command-controlled program for transferring loads from a cut in one finite element model to the boundary of another. This is a time-saving processor, when a more detailed FE-analysis of a part of the structure is required. The program COBOJ generates a complete detailed FE-model and writes all necessary command files needed for control of the ASKA (1) analysis. COBOJ also evaluates the analysis according to selected failure criteria, described in later sections. The flowchart in figure 2 illustrates the complete bolted joint analysis procedure.

## 2 STRESS ANALYSIS

### 2.1 Load distribution analysis

The purpose of the discussion below is to point out some of the problems occurring in conjunction with such an analysis, rather than presenting obtained research results.

The analysis can, as mentioned, be an integrated part of the overall structural load distribution analysis, as outlined in figure 1(b), or be performed separately. A too detailed FE-model should be avoided for economic reasons, but must at the same time not be too coarse, making the results unreliable. Usually the contact between the joined members is ignored. Another approximation often used in the FE-model is to degenerate the hole to a point (node) and represent the fastener by either a beam or a spring element, see figure 3. For a correct prediction of the bolt load distribution, the finite fastener element must be given a representative stiffness (flexibility). It is desirable that the experimentally obtained displacement,  $\delta^{EXP}$ , is correctly predicted by the load distribution model, see figure 4. This displacement consists partly of the fastener deformation,  $\delta^{EXP,FAST}$ , partly of the contribution from the local deformations at the hole edges,  $\delta^{EXP,HOLE}$ , that is

$$\delta^{EXP} = \delta^{EXP,FAST} + \delta^{EXP,HOLE} \quad (1)$$

In equation (1)  $\delta^{EXP,HOLE}$  represent the total contribution from each member. (Practically,  $\delta^{EXP}$  is unseparable). The equivalent displacement obtained in the FE-analysis,  $\delta^{FEM}$ , consists in the same way partly of the deformation in the finite fastener element,  $\delta^{FEM,FAST}$  and partly of the local deformations of the including meshes in the vicinity of the fastener,  $\delta^{FEM,MESH}$ , that is

$$\delta^{FEM} = \delta^{FEM,FAST} + \delta^{FEM,MESH} \quad (2)$$

In equation (2)  $\delta^{FEM,MESH}$  represent the total contribution from each mesh. In order to obtain a correct prediction of the bolt load distribution, the finite fastener should be given a flexibility so that,

$$\delta^{EXP} = \delta^{FEM} \quad (3)$$

When determining this flexibility some difficulties occur. Usually,  $\delta^{EXP}$ , is unknown. An estimation based on empirically or semi-empirically determined formulas is another possibility, which is perhaps sufficient with access to a large empirical data base. Unfortunately, this estimated flexibility cannot represent the fastener flexibility in the finite element model. Because of the simulation of the connection in the model, the obtained displacement,  $\delta^{FEM,MESH}$ , is not equal to the experimentally obtained displacement,  $\delta^{EXP,HOLE}$ . A refined model is more flexible, which leads to a large displacement

contribution from the meshes. Hence, a stiffer fastener is required. Further, a mesh refinement is not necessarily leading to better predictions. On the contrary, a very fine mesh may lead to very large local deformations, which is schematically shown in figure 5. It is possible, with such a fine mesh, that even if the fasteners are modelled completely rigid, the calculated displacement will come out too large.

Of course it is not completely satisfactory to use a model showing such qualities. Extensive investigations need to be carried out in order to obtain methods for adjustment of the finite fastener flexibility with respect to the displacement contribution from the mesh. It would be desirable to use a model, which is much less sensitive to the size of the mesh and which has the quality that a refined mesh automatically would lead to improved results. One way to obtain such results is to take into account the holes in the model, e.g. as made by Edlund (2), see figure 6. The advantages with such a model is that the problem of adjusting the finite fastener flexibility with respect to displacement contribution from the mesh is significantly reduced. In addition, according to Edlund (2), the secondary bending of the laminate is much better predicted. (Secondary bending is currently neglected in the present method, but may be considered in the future). Approximative account could be taken to the through-thickness stress concentration caused by bolt tilting and deformation. It would even be possible to predict failure approximately if the holes are considered in the model without making the final detailed analysis (figure 1(c)). The disadvantage is of course that such an improved load distribution model is more expensive in terms of modelling costs and computer costs. The modelling cost, however, may be reduced to a minimum by developing an efficient pre-processor for generating such a model. Perhaps it is a much better idea to develop such a pre-processor compared with developing methods for the adjustment of the finite fastener flexibility so that acceptable results are obtained with a coarser model, which does not account for the holes.

## 2.2 Detailed stress analysis

In order to determine the stress distribution in the vicinity of the hole boundary, a detailed stress analysis is carried out with a refined model (see figure 1(c)) of the most highly stressed region. Loads acting on the edges of that model are transferred by GENCUT from the previous load distribution analysis, see figure 1(b). It was shown by Edlund (3) that the stress/strain state close to the fastener, in such a load distribution analysis, where no account is taken to the holes in the model, is erroneously predicted. This locally erroneous prediction of the stress/strain state close to the fastener, however, does not necessarily mean that the approach should be avoided. The loads transferred by GENCUT are obtained some distance away from the load transmission point. It is possible, in spite of the quite rough approximations which are made, that the load distribution at this distance away from the transmission point is acceptably predicted by the model.

There are several possible ways of treating the bolt/hole interaction problem in such a detailed analysis. Numerous studies have been made on this topic (4-17). Most analyses usually ignore the bolt/hole interaction and assume rather than evaluate a certain stress distribution on the boundary of loaded holes, e.g. a cosine distribution. In (17) the author used the FE-program ASKA to carry out a detailed parametric study of the stress distribution around a single hole loaded by a bolt. A membrane contact analysis was used, i.e. through-thickness variations in properties were ignored. The laminate elastic properties, bolt clearance, bolt stiffness and friction were varied. All of these parameters were found to affect the results, the bolt stiffness having only a small effect. For both economic and technical reasons, however, it is questionable if friction should be included in practical design cases. The frictional properties are also difficult to determine. The effects of laminate elastic properties were in (17) investigated by computing stresses on the hole boundary and in the vicinity of the hole boundary for three different laminates, defined in figure 7 and table 1. Here the frictionless contact problem was solved with a perfect fit between the bolt and the hole. The bolt used in the analysis is representative of a titanium bolt with Young's modulus  $E=110$  GPa and Poisson's ratio  $\nu=0.29$ . Also a cosine distribution was applied to laminate C. Since a membrane analysis is performed, the stacking sequence is unimportant. The stresses in figure 8 were normalized by the average bearing stress.

$$S = P/d \cdot t \quad (4)$$

Figures 8(a) and (b) show the radial stress, as a function of the angle  $\varphi$ , along the hole boundary and a distance ( $a_0=1.26$  mm) away from the hole boundary. The figures show that the radial stress strongly depends on the laminate properties. The peak stress moves off the center line for laminates with high stiffness in the y-direction. Of the contact distributions which were calculated, the one obtained for laminate B shows good agreement with the cosine distribution. The others differ considerably. The results presented in Figure 8 (a) are in general agreement with those presented by Hyer and Klang (15).

### 3 FAILURE CRITERIA

#### 3.1 Net-tension failure

##### Introduction

Collings (18) conducted an experimental program with single hole, loaded bolt specimens and found that the ultimate tensile strength was strongly dependent on the layup, hole diameter and specimen width. The best results were obtained for a (0/45)-laminate. It was assumed that the inclusion of  $\pm 45^\circ$  plies in the 0-laminate will introduce a degree of softening to the joint, i.e. decrease the stress concentration and increase the strength.

Quite a number of papers have been published on methods for predicting net tension failure in bolted joints, (4,5,7,9,19-23). In general, these methods include severe approximations and/or limitations. Usually, the contact problem between the bolt and the hole is ignored which may lead to significant errors in calculated stresses and strains. These erroneous results are then used in a failure criterion, which usually operates at a characteristic distance away from the stress concentration. (The characteristic distance, in its turn, may have been determined by the use of erroneous stresses). Under such circumstances it is very difficult to have a general opinion about the failure criteria which are proposed. Secondly, the experimental data which are published in conjunction with most of the studies are often very limited as far as the layup and loading conditions are concerned.

The point stress criterion, PSC, proposed by Whitney and Nuismer (24) is used here to predict tensile strength. The PSC requires knowledge of the stress distribution in the vicinity of the notch and assumes failure to occur when  $\sigma_v$  at some fixed distance,  $d_0$ , ahead of the hole first reaches the unnotched tensile strength,  $\sigma_0$ , of the material, see figure 9.

##### Experimental

The two fundamental parameters used in the criterion, the unnotched tensile strength,  $\sigma_0$ , and the characteristic distance,  $d_0$ , are determined from experiments. Laminates of different layups were processed according to table 2. (Only laminates with fibres in the basic directions (0/90/ $\pm 45^\circ$ ) are considered in this paper). Specimens with holes of different radii and widths were manufactured, see figure 10 and table 3 where also the test results are presented. All laminates were ultrasonically inspected to detect processing-related flaws. The laminates with holes were inspected with X-ray to detect any delaminations caused by drilling. All tests were performed in "hot-wet" conditions (100°C and 1X moisture content by weight).

##### Numerical results

The FE-system ABAQUS (25) was used to investigate the effects of layup, hole diameter and specimen width on  $d_0$ . The experimentally determined failure load was applied to the FE-model of the specimen. The complete contact problem, which includes both friction and clearance, was taken into account. As well known, the characteristic distance  $d_0$  takes different values for different layups. This also appears from figure 11 where the effect of layup on the variation of normal stress is plotted. ( $d_0$  is approximately 1.2 mm for laminate B and C and 3 mm for laminate A). In figure 12 the tangential stress concentration factor,  $K_T$ , derived for an infinitely large orthotropic plate with a hole is used for normalising  $d_0$  with respect to layup.

The effects of hole diameter and specimen width were, for the specimens included in this study, found to be of much less importance (5X).

In a general loading case it is assumed that failure initiation occurs at points on the hole boundary where fibres are either tangential or normal to the boundary, see figure 13. Net-tension failure is evaluated in each of these points at a radial distance,  $d_0$ , away from the boundary. The characteristic distance,  $d_0$ , is assumed to vary with the location around the hole according to figure 12.

Net-compression failure is predicted in a similar way, but no details are given in this paper.

#### 3.2 Bearing failure

##### Introduction

Bearing failure is another basic failure mode in bolted joints, which together with net-tension failure is the most important mode. It was experimentally shown by Collings (18) that the bearing strength is dependent on four main variables: degree of lateral constraint around the hole, layup, stacking sequence and laminate thickness. Large improvements in strength were observed by applying higher constraint. This phenomenon is also discussed by Hart-Smith (26) and Stockdale (27). Hart-Smith (26) presented the diagram shown in figure 14. He raised the question whether it is adequate or not to rely on the benefits of torquing beyond finger tightness. The drawback, he says, in taking advantage of the strength associated with the extra clampup is that it would take only one under-torqued bolt to impose a significant loss of static strength.

The effect of layup is clearly shown by Collings (18) and Hart-Smith (26). Collings (18) investigated the effect by introducing 0° plies into a ±45° laminate. (0° is the loading axis). The bearing strength was significantly increased. The effect of stacking sequence was shown (18) to have a significant influence on the magnitude of the ultimate bearing strength. The more homogeneous stacked laminate (a) was shown to have about 16X higher bearing strength compared with the less homogeneous laminate (b),

$$(a) (0 / +45 / 0_2 / -45 / 0_2 / -45 / 0_2 / +45 / 0)$$

$$(b) (0_2 / +45 / -45 / 0_4 / -45 / +45 / 0_2)$$

For the adequately clamped laminates investigated by Collings (18) the effect of thickness on the bearing strength was reported small.

Indeed there are other important parameters which affect the bearing strength as well. The choice of fastener, tolerance and washer are all important parameters. In the case of single shear joints, the effects introduced by bolt tilting and bending, which cause a through-thickness stress concentration may be severe. It is beyond the scope of this paper, however, to discuss the influence on the bearing strength from these parameters in detail. Many of them have, to the knowledge of the author, not been investigated to their full extent. In this paper, the objective has been to develop a failure hypothesis for finger-tight torqued joints in homogeneously stacked laminates of the (0/90/±45) layup family loaded in double shear. Only one type of fastener installation has been considered.

Various failure hypotheses and failure criteria are investigated in the literature (4-7,19,23). Most of them adopt a well known criterion (Tsai-Hill, Tsai-Wu, Yamada-Sun, max-stress...) at a characteristic dimension away from the hole boundary. Here a concept proposed by Chang et al. (5) was chosen. They proposed that failure occurs, when, in any of the plies, the combined stresses satisfy the Yamada-Sun failure criterion at any point on a characteristic curve. The Yamada-Sun criterion states that failure occurs when the following requirements are met in any one of the plies:

$$\left(\frac{\sigma_x}{X}\right)^2 + \left(\frac{\sigma_{xy}}{S}\right)^2 = e^2 \quad \begin{cases} e^2 > 1 & \text{failure} \\ e^2 < 1 & \text{no failure} \end{cases} \quad (5)$$

In equation (5),  $\sigma_x$  and  $\sigma_{xy}$  represent the longitudinal and shear stresses in a ply, respectively (x and y being the coordinates parallel and normal to the fibres in a ply). S is in this paper the shear strength obtained from a tension loaded (+45/-45) laminate. X is either the longitudinal tensile strength or the longitudinal compressive strength of a single ply. The tensile strength ( $X=X_t$ ) is used when the stress  $\sigma_x$  is tensile. Consequently, the compressive strength ( $X=X_c$ ) is used when  $\sigma_x$  is compressive. The characteristic curve (Figure 15) is specified by Chang et al. (5) by the expression:

$$r_c = D/2 + R_t + (R_c - R_t) \cos \Theta \quad (6)$$

$R_t$  and  $R_c$  are referred to as the characteristic lengths for tension and compression. These parameters are determined experimentally. Bearing failure is in (5) assumed to occur when the parameter e is equal to or larger than the unity at any point, in any of the plies, on the characteristic curve in the range of:

$$-15^\circ < \Theta < 15^\circ \quad (7)$$

#### Experimental procedure for determining the characteristic curve

Eriksson and Ireman (28) introduced some important differences compared with the approach proposed by Chang et al. (5). No restrictions are put on the shape of the curve. It is only assumed (in analogy with the assumptions in the PSC about the characteristic length,  $d_0$ ) that failure occurs when the parameter e is equal to, or larger than unity at some distance,  $r_c$ , from of the hole boundary. Further, it is assumed that  $r_c$  varies with layup, hole diameter and location along the hole boundary.

$$r_c = f(\text{layup}, d, \Theta) \quad (8)$$

Collings (18) stated that the layup has a definite influence on the position around the hole circumference (a) at which failure is initiated (0-45° to the loading axis). Therefore, in this study, bearing failure is assumed to initiate in the interval defined by the relation:

$$-45^\circ < \Theta < 45^\circ \quad (9)$$

Specimens of different layup and geometry were manufactured according to table 4 and figure 16 and were tested in "hot-wet" conditions (100% and 1X moisture content by weight) The characteristic curve  $r_c$  is determined by the following procedure: The failure load obtained in the experiments were applied to the corresponding FE-models of the specimen. A typical ASKA FE-model is shown in figure 17. The frictionless contact problem was solved. Lamina stresses were obtained through the use of laminated plate theory and the characteristic curve where e is equal to unity for each of the specimens could be determined. Failure data to be used in the Yamada-Sun failure criterion are shown below

$$\begin{aligned} X_1 &= 1894 \text{ MPa} \\ X_2 &= 1800 \text{ MPa} \\ S &= 76 \text{ MPa} \end{aligned} \quad (10)$$

#### Numerical results

In figure 18 the characteristic curves obtained for specimens no. (1-4) are plotted. As can be observed the shape of the characteristic curve is strongly dependent on layup. For practical reasons it would be desirable to replace all these curves with one equivalent characteristic curve, which should have such qualities that it could be used to predict the failure loads of all these specimens correctly. The requirement on such an equivalent curve is that it should at least in one point be tangent to each one of the original curves without crossing any of them. If such a curve exists, the failure load for all specimens investigated here would have been exactly predicted. The dotted curve in figure 18 almost fulfills these requirements.

Quasi-isotropic specimens were analysed in order to determine the effect of the hole size on  $r_0$ , see figure 19. As can be observed, the radial position of  $r_0$  is significantly influenced by the hole diameter. Even the shape is slightly changed. In figure 20 the parameter,

$$K = r_0(d) / r_0(d=6) \quad (11)$$

has been plotted as a function of the hole diameter,  $d$ , with the angle  $\varphi$  as parameter. It can be observed that the diameter influence upon  $K$  is strongly dominating over the angle influence. From here on the angle dependency is therefore disregarded. The "mean curve" to the curves in figure 20 is designed in figure 21 and denotes the radial translation of the characteristic curve for  $d > 6$  mm. Further on it is assumed that this translation is independent of the layup.

In a general loading case, the principal direction of the bolt load is determined. The characteristic curve,  $r_0$ , (the dotted curve in figure 18) is symmetrically located with respect to that direction, see figure 22. If the hole diameter is larger than 6 mm,  $r_0$  is radially translated according to the curve in figure 21.

#### 4 MISCELLANEOUS CONSIDERATIONS

Here it may be suitable to point out some important issues considering the analysis of bolted joints in real aircraft structures. Both the stress analysis and the failure hypotheses described in this study are performed and established, respectively, under certain idealizations. A membrane stress state is assumed in the stress analysis and the failure hypothesis for net-tension and bearing-failure are established by use of simple, "well-defined" joints. Certain conditions are prescribed in advance. In a real joint in an aircraft several differences to that "well-defined" joint may occur: The loading conditions are generally complex, through-thickness effects exist, the fasteners are torqued, some load will be carried by friction between the plates etc etc. Some of these effects will act to our advantage, whereas others will have the opposite effect. It is of course essential to improve both the stress analysis and the failure hypothesis so that the influence on the strength from these effects could be accounted for properly.

One obvious advantage with adopting FEM for the determination of stresses is that complex loading conditions can be accounted for properly. Complex loading conditions are difficult to handle with an analytical method.

Generally, the poorer theory used in an analysis procedure, the more test results are required to obtain sufficient design data. Another great advantage with the computational analysis procedure described in this paper is that such design data for desirable load cases easily can be computed. Such an example is the combined bearing types loading diagram shown in figure 23. The diagram was determined by Ireman (29) with the computational procedure described in figure 2. The right side of figure 23 shows tension results and the left side shows the corresponding compression results. Figure 23 also indicates the computed failure mode for each loading condition. The symbol NT indicates net-tension failure. The TRB and CRB indicates bearing failure for tension- and compression reacted bearing loads, respectively. Finally, NC indicates net-compression failure. A similar diagram was experimentally determined in (30).

#### 5 ACKNOWLEDGEMENTS

The work presented in this paper was supported by Saab-Scania Aircraft Division, Linköping, Sweden and the National Board for Technical Development, STU. The author also takes the opportunity to acknowledge his many colleagues and superiors at Saab-Scania aircraft division, The Royal Institute and elsewhere, who have been involved in this work.

## 6 REFERENCES

1. ABAQUS, A finite element system from SAAB-SCANIA AB and IKOSS GmbH, User's manual, Version 2, (1986)
2. Edlund, A., A nonlinear finite element analysis of the secondary banding in composite bolted joint, Saab-Scania paper TKH R-3472, Sweden, (1985)
3. Edlund, U., A linear finite element for simulation of a shear loaded fastener, Saab-Scania paper PKH R-3330, Sweden, (1981)
4. Waszczak, J.P. and Cruse, T.A., Failure mode and strength predictions of anisotropic bolt bearing specimens, Journal of Composite Materials, Vol.5 (1971), pp. 421-425
5. Chang, Fu-Kuo, Scott, Richard A. and Springer, George S., Failure of composite laminates containing pin-loaded holes—method of solution, Journal of Composite Materials, Vol. 18 (1984), pp. 255-278
6. Collings T.A., On the bearing strengths of CFRP laminates, Composites, July (1982), pp. 241-252
7. Wilson, D.W., Gillespie, J.W., York, J.L. and Pipes R.B., Failure analyses of composite bolted joints, Center of Composite materials, University of Delaware, USA, NASA-CR-163732, July 1980
8. Matthews, F.L., Wong, C.M. and Chryssafitis, S., Stress distribution around a single bolt in fibre-reinforced plastics, Composites, July (1982), pp. 316-322
9. Agarwal, B.L., Static strength prediction of bolted joint in composite materials, AIAA Journal, Vol 18 (11) (1980), pp. 1371-1375
10. Conti, Paolo, Influence of geometric parameters on the stress distribution around a pin-loaded hole in a composite laminate, Composite Science and Technology Vol. 25 (1986), pp. 83-101
11. de Jong, Theo, Stresses around pin-loaded holes in elasticity orthotropic or isotropic plates, Journal of Composite Materials, Vol. 11, (1977), pp. 313-331
12. Oplinger, D.W. and Gandhi, K.R., Analytical studies of structural performance in mechanically fastened composite plates, AMMRC MS 74-8, (1974), pp. 221-240
13. Mangalgiri, P.D. and Dattaguru, B., Unbonded smooth rigid circular pin in an orthotropic plate, Res Mechanics, Vol. 12 (1984), pp. 143-150
14. Zhang, Kai-da and Ueng, Charles, E.S., Stresses around a pin-loaded hole in orthotropic plates with arbitrary loading direction, Composite Structures Vol 3 (1985), pp. 119-43
15. Hyer, M.W. and Kiang, E.C., Contact stresses in pin-loaded orthotropic plates, Virginia Polytechnical Institute and State University, USA, NASA- CR-173475, April 1984
16. Rowlands R.E., Rahman, M.U., Wilkinson T.L and Chiang Y.I., Single- and multiple-bolted joints in orthotropic materials, Composites, July (1982), pp. 273-279
17. Eriksson L.I., Contact Stresses in bolted joints of composite laminates, Composite Structures Vol. 6 (1986) pp. 57-75
18. Collings, T.A., The strength of bolted joints in multi-directional cfrp laminates, Composites, Januari (1977), pp 43-55
19. Ueng, Charles E.S. and Zhang, Kai-da, Strength prediction of a mechanically fastened joint in laminated composites, AIAA Journal, Vol. 23 (11) (1985), pp. 1832-1834.
20. Garbo, S.P. and Ogonowski, J.M., Strength prediction of composite laminates with unloaded fastener holes, AIAA Journal Vol. 18 (5) (1980), pp 310-314
21. Garbo, S.P., Hong, S.W. and Kim, W., Strength evaluation of helicopter composite bolted joints, 27th SDM AIAA Conference, May(1986), pp. 486-494
22. Eisenmann, J.R., Bolted joint static strength model for composite materials, NASA TN-X-3377, April (1976), pp 563-602
23. Garbo, S.P. and Ogonowski, J.M., Effect of variances and manufacturing tolerances on the design strength and life of mechanically fastened composite joints, Flight Dynamics Laboratory, AFWAL-TR-81-3041, April 1981
24. Whitney, J.M. and Nuismer, R.J., Stress fracture criteria for laminated composites containing stress concentrations, Journal of Composite Materials, Vol 8. (1974), pp. 253-265
25. ABAQUS, A finite element system by Hibbit, Karlsson and Sorensen, User's manual, Version 4, (1982)
26. Hart-Smith, L.J., Design and analysis of bolted and riveted joints in fibrous composite structures, presented to international symposium on joining and repair of fibre-reinforced plastics, Imperial College, London September 10 and 11, 1986

27. Stockdale, J.H. and Matthews F.L., The effect of clamping pressure on bolt bearing loads in glass fibre-reinforced plastics, Composites, Januari (1976), pp. 34-38
28. Eriksson, I. and Irenan, T., Analysis of bearing failure in bolted joints of composite structure, Saab-Scania paper TRN R-3473, Sweden, 1985
29. Irenan, T., Bearing and combined bearing and bypass loading on a composite laminate, Saab-Scania paper TRN R-3612, Sweden, 1987
30. Crews, Jr., J.H and Naik, R.A., Combined bearing and bypass loading on a graphite/epoxy laminate, Composite Structures 6(1986)21-40.

Figure Captions:

- 1 Analysis procedure based on FEM
- 2 Computational stress analysis procedure
- 3 Connection of parts by a beam element
- 4 Load distribution model
- 5 Local effects in the vicinity of load transmission
- 6 Improved load distribution model, from (2)
- 7 Laminates studied in reference (17)
- 8 Radial stress versus  $\psi$
- 9 Plate with circular hole illustrating the Point Stress Criterion
- 10 Net-tension test specimen
- 11 The effect of laminate layup on  $d_0$
- 12  $d_0$  as a function of  $K_T$
- 13 Net-tension failure initiation points
- 14 Effect of bolt torque on bearing strength of fibrous composite laminates, from (26).
- 15 Description of the characteristic curve, from (5)
- 16 Bearing failure test specimen
- 17 ASKA FE-model
- 18 Influence of laminate layup on the characteristic curve
- 19 Influence of the hole diameter on the characteristic curve
- 20 Relative characteristic distance versus hole diameter with the angle  $\psi$  as parameter
- 21 Relative characteristic distance versus hole diameter
- 22 Evaluating of bearing failure in a general loading case
- 23 Bearing-bypass diagram, from (29).

TABLE 1

## Laminate Stiffnesses of T300/914C Graphite/Epoxy System

Percentage of plies in directions (0/90/ $\pm$ 45)	$E_x$ (GPa)	$E_y$ (GPa)	$G_{xy}$ (GPa)	$\nu_{xy}$
A: 25/25/50	51.4	51.4	19.3	0.33
B: 69/6/25	102	24.2	11.1	0.44
C: 6/69/25	24.2	102	11.2	0.10

TABLE 2

## Laminate configuration (T300/914C Graphite/epoxy system)

Laminate	Stacking sequence	No. of plies in directions (0/90/ $\pm$ 45)
A:	( $\pm$ 45/0 <sub>2</sub> /90/0 <sub>2</sub> /90/0 <sub>2</sub> ) <sub>S</sub>	(12/4/4)
B:	( $\pm$ 45/90 <sub>2</sub> /0/90 <sub>2</sub> /0/90 <sub>2</sub> ) <sub>S</sub>	(4/12/4)
C:	(( $\pm$ 45/0/90) <sub>3</sub> /0/90/ $\pm$ 45) <sub>S</sub>	(8/8/16)

TABLE 3

## Test results of T300/914C filled hole specimens

Laminate	w (mm)	w/d	t <sub>nom</sub> (mm)	$\sigma_N^{EXP}/\sigma_0$	Cv %	No off	Batch
A	36	6	2.54	0.82	1.0	5	1
A	36	6	2.54	0.78	4.7	5	2
B	36	6	2.54	0.63	4.6	7	2
C	36	6	4.06	0.57	1.9	7	2
C	48	6	4.06	0.55	2.3	6	2
C	60	6	4.06	0.53	1.8	7	2
C	36	3.6	4.06	0.49	0.8	4	1

Where Cv is the coefficient of variation,

$$Cv = S/\bar{x}$$

S in equation 12 is the standard deviation and  $\bar{x}$  is the meanvalue

$\sigma_0$  is determined from batch 1

TABLE 4

## Bearing failure specimens of T300/914C Graphite/Epoxy System

Type	No. of plies in directions (0/90/ $\pm$ 45)	d (mm)	w (mm)	e (mm)	Load
1	(4/12/4)	6	48	36	$P_t$
2	(8/8/16)	6	36	36	$P_c$
3	(4/12/4)	6	36	36	$P_c$
4	(12/4/4)	6	36	36	$P_c$
5	(8/8/16)	8	48	36	$P_c$
6	(8/8/16)	10	60	36	$P_c$

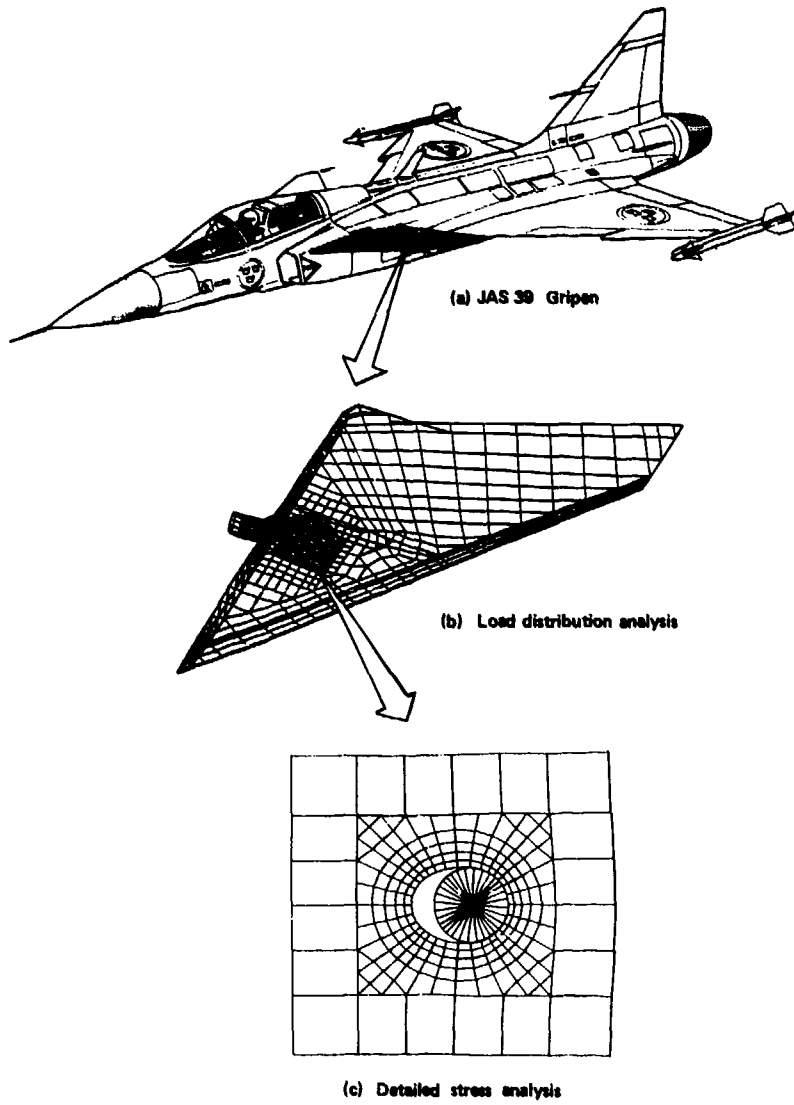


Figure 1.

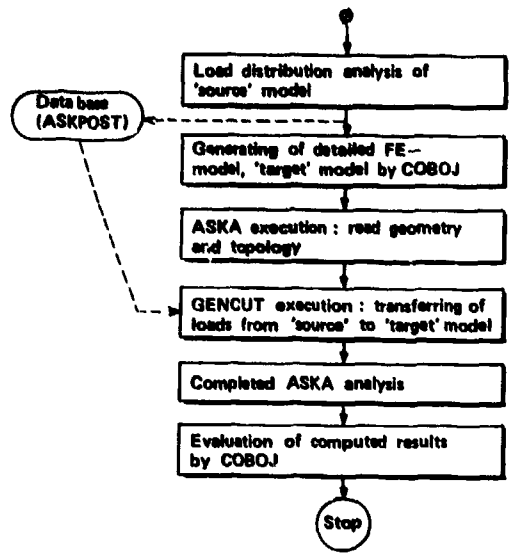


Figure 2.

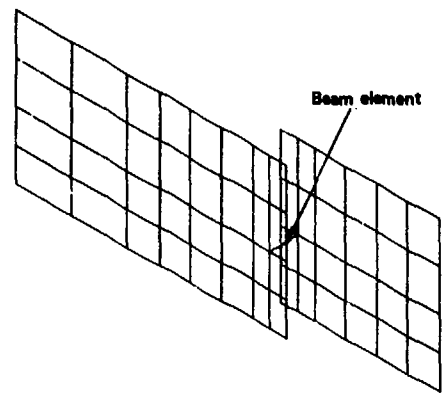


Figure 3.

6-12

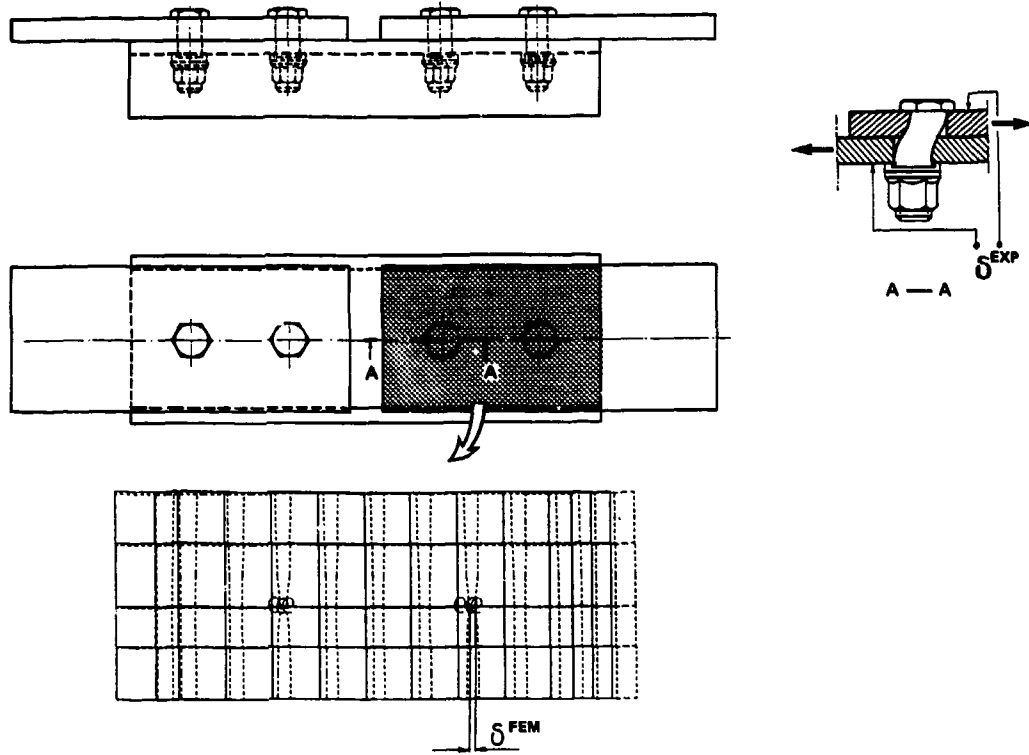


Figure 4.

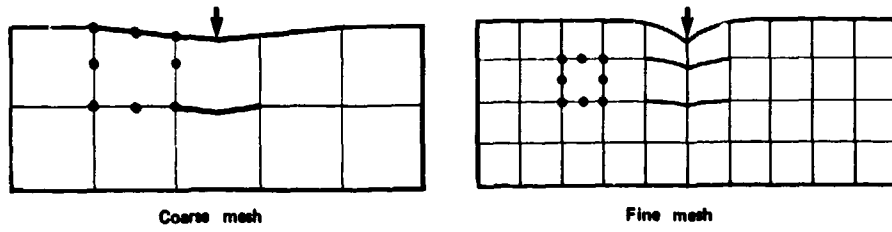


Figure 5.

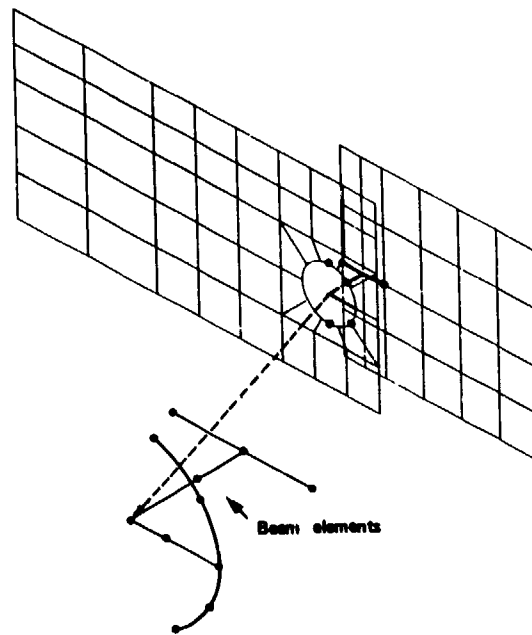


Figure 6.

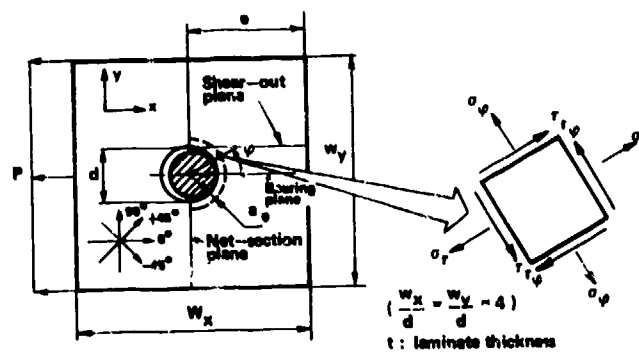


Figure 7.

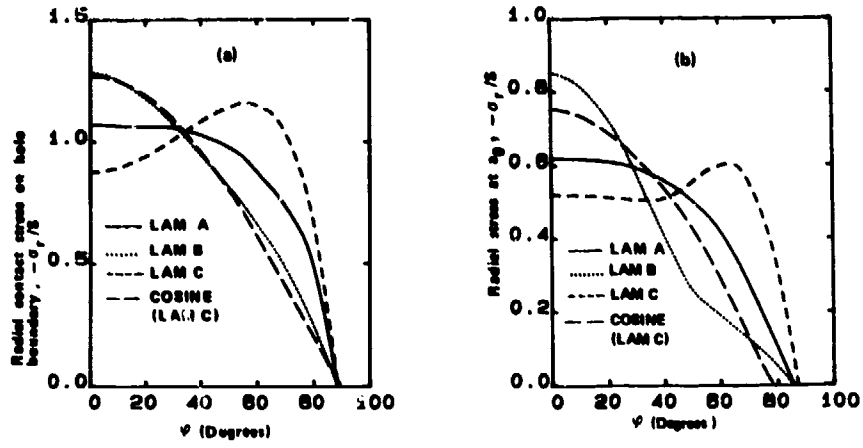


Figure 8.

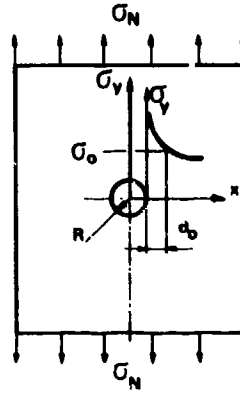


Figure 9.

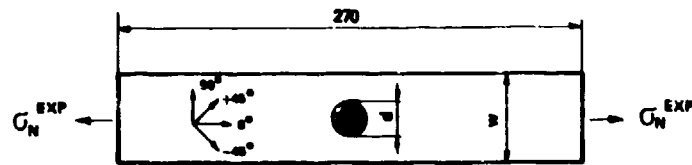
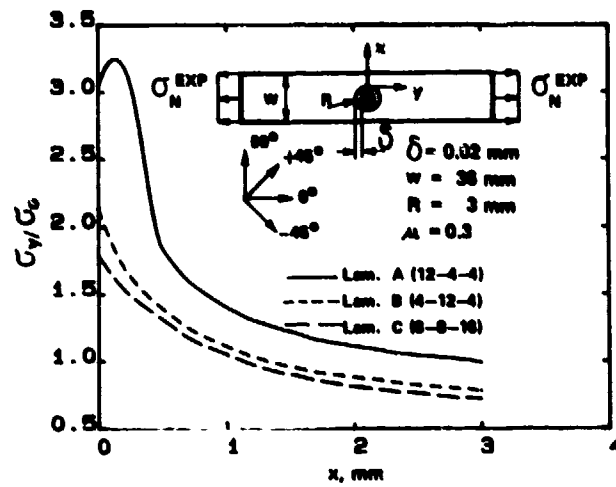
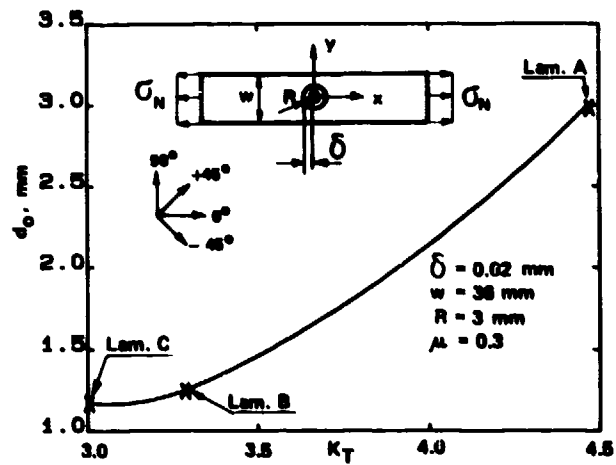


Figure 10.



Where  $\sigma_0$  is unnotched tensile strength

Figure 11.



Where

$$K_T = 1 + \sqrt{2 \left( \sqrt{\frac{E_x}{E_y} - \nu_{xy}} \right) + \frac{E_x}{G_{xy}}}$$

Figure 12.

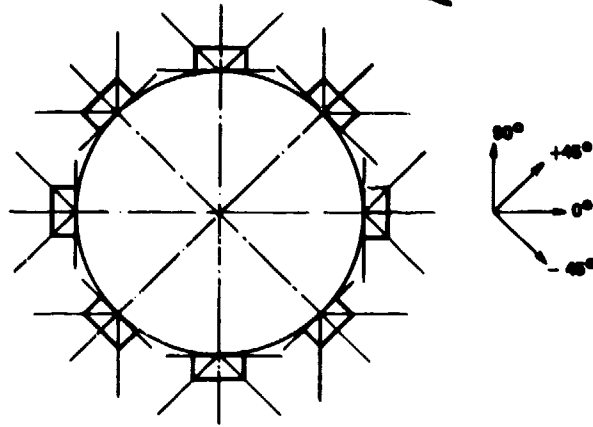


Figure 13.

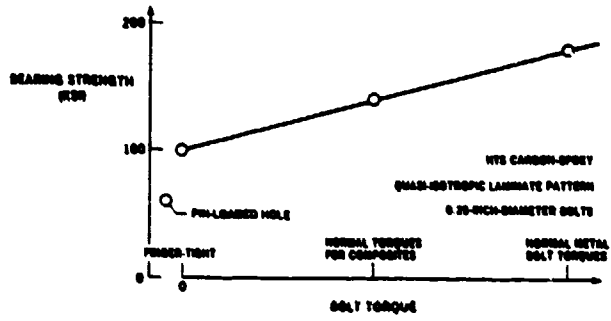


Figure 14.

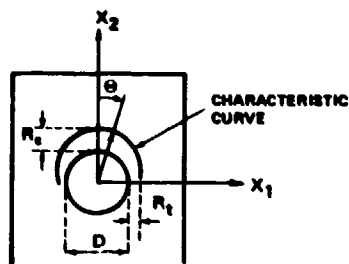


Figure 15.

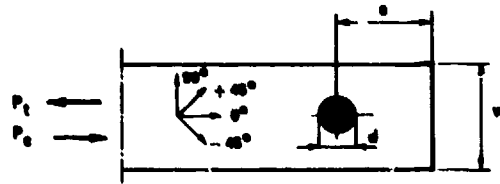


Figure 16.

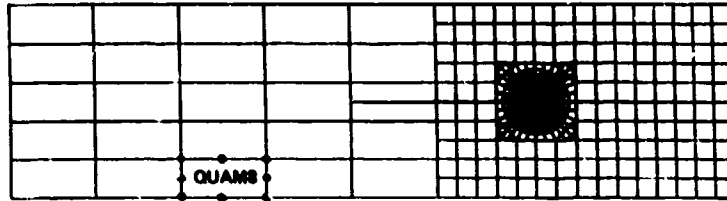


Figure 17.

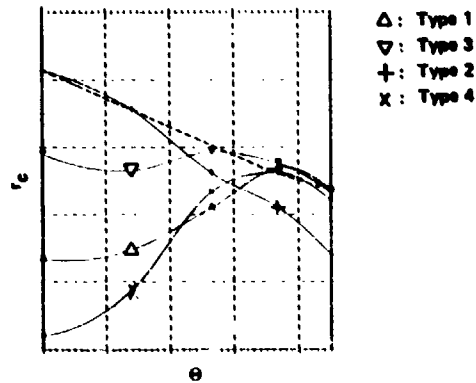


Figure 18.

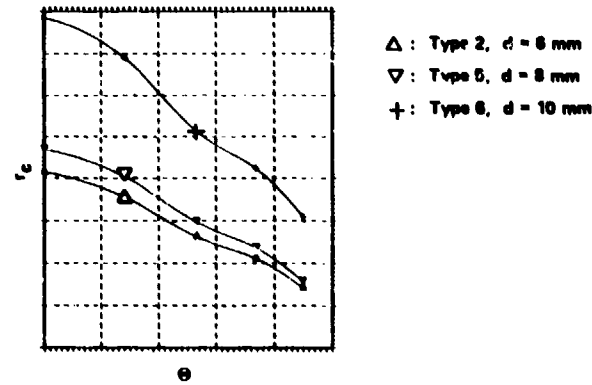


Figure 19.

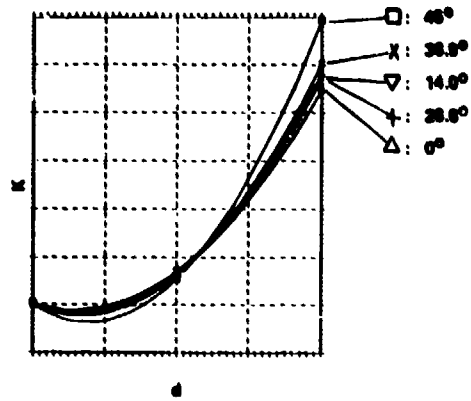


Figure 20.

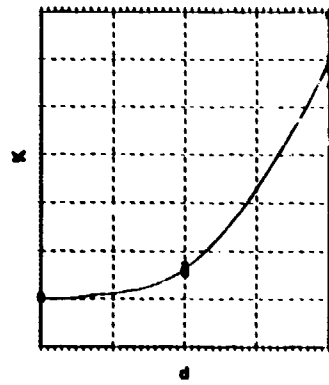


Figure 21.

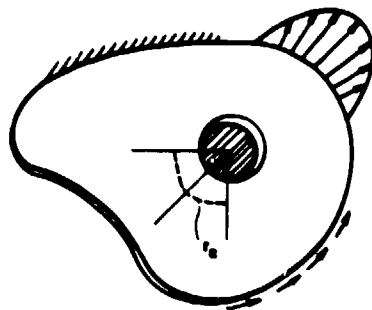


Figure 22.

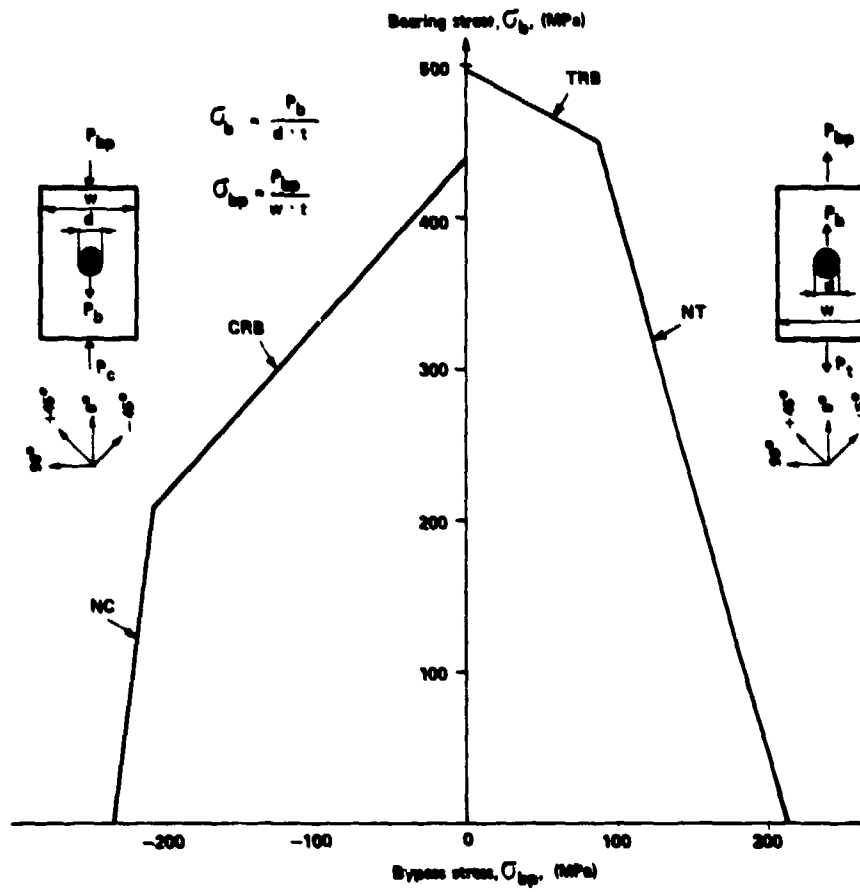


Figure 23.

**STRENGTH ANALYSIS OF MECHANICALLY FASTENED  
COMPOSITE STRUCTURES**

R. L. Rankumar, E. G. Saether and K. Appa

Northrop Corporation, Aircraft Division  
1 Northrop Avenue, Hawthorne, CA 90250, U.S.A.

and

V. B. Venkayya

AFWAL/FISRA, Flight Dynamics Laboratory

Wright-Patterson Air Force Base, Dayton, Ohio 45433, U.S.A.

**Abstract:**

An analysis is presented for the strength prediction of bolted composite structures, based on the average stress failure criterion. The analysis incorporates analytically derived special finite elements (loaded hole, unloaded hole, plain and effective fastener elements) into the SAMCJ (Strength Analysis of Multifastener Composite Joints) computer code. The loaded hole, unloaded hole and plain elements are derived from a doubly-connected laminate analysis that accounts for the effects of finite plate dimensions via a least squares boundary collocation solution procedure. The effective fastener element is derived from a fastener analysis that accounts for fastener shear and bending effects and through-the-thickness effects in the bolted laminates. The special finite elements in the SAMCJ code are developed using Argyris' natural mode method. The bolted plates are modeled using these elements, a conventional solution procedure yields the fastener loads and the stress state in each plate, and average stress failure criteria are used for strength prediction. The characteristic distances for net section, shear-out and bearing failures are assumed to be material constants obtained through limited testing. SAMCJ predictions account for the effects of fastener spacing, adjacent cut-outs, through-the-thickness effects at the fastener location, and taper in the bolted plate thickness. SAMCJ predictions of fastener loads, joint failure loads and failure modes demonstrate excellent correlation with available test results from single and double shear tests on graphite/epoxy-to-aluminum joints.

**1. Introduction**

An analysis was developed in Reference 1 to predict the strength of bolted composite structures. This paper presents details of the developed analysis, sample predictions, and a discussion on its validity and its application to structural design.

Prior to the initiation of the program in Reference 1, the strength of a bolted laminate was analytically predicted using approximate analyses and experimental results (References 2 to 4). The distribution of the applied load among the fasteners was initially obtained, and the most critical fastener location was subsequently analyzed to predict the joint strength. The fastener load distribution analysis was essentially one-dimensional, assuming that all the fasteners in a row (perpendicular to the load direction) carried equal loads. The load distribution among the various rows was predicted based on experimentally obtained "joint stiffness" values. The subsequent strength analysis at a fastener location was based on an infinite plate stress analysis and was incapable of accounting for neighboring stress concentrators (like a free edge, a cut-out or a neighboring fastener location).

The strength analysis developed in Reference 1 overcomes the major deficiencies that existed at program inception. The analysis incorporates special finite elements into a failure analysis procedure that predicts the fastener load distribution, the critical fastener location, the joint strength and its failure mode. Four special finite elements were developed using a fastener analysis and a stress analysis that accounts for finite laminate planform dimensions (References 5 and 6). These elements include a loaded hole element, an unloaded hole element, a plain element, and an effective fastener element. A finite element model of the bolted joint computes the fastener load distribution and averaged stresses at each fastener and cut-out location. The critical fastener or cut-out location, the joint failure load and the corresponding failure mode are predicted based on these computations.

The developed strength analysis has been programmed to be the SAMCJ (Strength Analysis of Multifastener Composite Joints) computer code. SAMCJ requires a definition of the geometry and the material properties of the bolted plates and fasteners as input. The presence of any cut-out is included in the finite element model as an "unloaded hole" element linked to adjacent "loaded hole" and plain elements. The input material properties of the bolted laminates include parameters that are required by the average stress failure criteria. These are distances from the fastener or cut-out hole boundaries, at selected locations, over which stresses are averaged and compared to plain laminate strengths, to predict failure (see Reference 7). SAMCJ computes the joint load values for net section, bearing and shear-out modes of failure at each fastener and cut-out location. Information corresponding to the least value provides the joint failure load, the critical fastener or cut-out location, and the failure mode.

In computing the fastener load distribution and the critical average stress values at every fastener/cut-out location, SAMCJ also accounts for fastener flexibility effects. The fastener analysis in Reference 8 (FDFA computer code) is used to compute the effective fastener stiffness, accounting for bolt torque and load eccentricity (single versus double shear transfer of the applied load). FDFA is employed twice to compute the effective transverse stiffnesses of the fastener, along and perpendicular to the load direction. The effective fastener stiffness matrix connects the bolted plates at the fastener locations, accounting for all significant joint parameters.

### 3. Two-Dimensional Analysis of a Finite Geometry Laminate With a Loaded or Unloaded Hole

A two-dimensional analysis of a finite bolted laminate is a primary requirement in the development of a strength analysis for bolted laminates. A brief description of the analysis (FIGCON computer code) developed in Reference 9 is presented below.

The two-dimensional stress field in a finite bolted plate is expressed in terms of the Airy stress function  $F(x, y)$  that automatically satisfies equilibrium equations everywhere in the plate domain (Figure 1). The corresponding displacement solution satisfies compatibility requirements when the following equation is satisfied by the stress function:

$$\begin{aligned} a_{22}F_{,xxxx} - 2a_{26}F_{,xxyy} + (2a_{12} + a_{66})F_{,xyyy} - 2a_{16}F_{,xyyy} + \\ a_{11}F_{,yyyy} = 0 \end{aligned} \quad (1)$$

where  $a_{ij}$  are laminate compliances as defined in Reference 9. Equation 1 is the governing equation for the problem of interest.

A complex variables approach, described in Reference 10, is undertaken to obtain the solution to Equation 1. This approach has been pursued by other investigators to solve similar problems (References 11 to 14). The solution to Equation 1 is dependent on the roots of the following characteristic equation:

$$a_{11}\mu^4 - 2a_{16}\mu^3 + (2a_{12} + a_{66})\mu^2 - 2a_{26} + a_{22} = 0 \quad (2)$$

For physically meaningful values of the constants  $a_{ij}$ , two solution types are possible:

(a) The roots of Equation 2 are two pairs of complex conjugates:

$$\mu_1 = \alpha + i\beta, \mu_2 = \gamma + i\delta, \mu_3 = \bar{\mu}_1, \text{ and } \mu_4 = \bar{\mu}_2 \quad (3)$$

where a bar denotes a complex conjugate, and  $\beta$  and  $\delta > 0$ .

(b) The roots of Equation 2 are pairwise equal:

$$\mu_1 = \mu_2 = \alpha + i\beta, \bar{\mu}_1 = \bar{\mu}_2 = \alpha - i\beta \quad (\beta > 0) \quad (4)$$

For an isotropic plate,  $\mu_1 = \mu_2 = 1$ .

Recognizing that the stress function is a real function of  $x$  and  $y$ , the general solution for  $F$  may then be written as:

$$F = 2Re [F_1(z_1) + F_2(z_2)] \text{ when the roots are different, (5)}$$

$$F = 2Re [F_1(z_1) + z_1 F_2(z_1)] \text{ when the roots are equal. (6)}$$

$$\text{where } z_1 = x + \mu_1 y, \quad z_2 = x + \mu_2 y, \quad \bar{z}_1 = x + \bar{\mu}_1 y, \quad \bar{z}_2 = x + \bar{\mu}_2 y. \quad (7)$$

and  $F_1$  and  $F_2$  are arbitrary functions of  $z_1$  and  $z_2$ , respectively.

In the computer code developed to do this analysis (FIGROM), the properties of an isotropic plate are perturbed very slightly so that only the solution case with unequal roots have to be considered. For this case, the following new complex functions are introduced for convenience:

$$\phi_1(z_1) = \frac{dF_1}{dz_1}, \quad \phi_2(z_2) = \frac{dF_2}{dz_2} \quad (8)$$

These provide the following expressions for stresses and displacements in the plate:

$$\sigma_x = 2Re [u_1^2 \phi_1'(z_1) + u_2^2 \phi_2'(z_2)] \quad (9)$$

$$\sigma_y = 2Re [\phi_1'(z_1) + \phi_2'(z_2)] \quad (10)$$

$$\tau_{xy} = -2Re [u_1 \phi_1'(z_1) + u_2 \phi_2'(z_2)] \quad (11)$$

$$u = 2Re [p_1 \phi_1(z_1) + p_2 \phi_2(z_2)] \quad (12)$$

$$v = 2Re [q_1 \phi_1(z_1) + q_2 \phi_2(z_2)] \quad (13)$$

where  $p_1$ ,  $p_2$ ,  $q_1$  and  $q_2$  are the complex constants defined below:

$$p_1 = a_{11} u_1^2 + a_{12} - a_{16} u_1, \quad p_2 = a_{11} u_2^2 + a_{12} - a_{16} u_2$$

$$q_1 = a_{12} u_1 + a_{22} / u_1 - a_{26}, \quad q_2 = a_{12} u_2 + a_{22} / u_2 - a_{26} \quad (14)$$

Any expression for  $F$ , in terms of the arbitrarily assumed functions in Equation 8, is a solution to the two-dimensional problem, provided these expressions satisfy the appropriate boundary conditions. Recall that these functions automatically satisfy the governing equation. The problem of interest involves a finite anisotropic plate with a loaded or unloaded circular or elliptical hole (see Figure 1). In general, for arbitrary geometry and boundary conditions, one cannot determine closed form solutions for  $\phi_1$  and  $\phi_2$ . One method of obtaining approximate solutions is to consider series expansions of the functions with unknown coefficients. These unknown coefficients are then determined by satisfying the boundary conditions approximately. In contrast to series expansions in  $z_1$  and  $z_2$ , faster convergence is obtained if series expansions are assumed in coordinates  $\zeta_1$  and  $\zeta_2$ , obtained by using the following mapping functions:

$$\zeta_1 = (z_1 + \sqrt{z_1^2 - a^2 - \mu_1^2 b^2}) / (a - i\mu_1 b) \geq 1 \quad (15)$$

$$\zeta_2 = (z_2 + \sqrt{z_2^2 - a^2 - \mu_2^2 b^2}) / (a - i\mu_2 b) \geq 1$$

In a laminate with a circular or elliptical hole, the internal boundary gets transformed to an ellipse in the  $z_1$ - $z_2$  plane (see Equation 7). The functions in Equation 15 map the internal boundary to a unit circle in the  $\zeta_1$ - $\zeta_2$  plane, and the physical region of the laminate to the exterior of the unit circle. The signs of the square root terms in Equation 15 are chosen such that the internal boundary is mapped on to the unit circle. Note that these mapping functions are analytic functions, and hence the mapping is conformal.

In the  $\zeta_1 - \zeta_2$  plane,  $\phi_1$  and  $\phi_2$  are assumed to be the following (truncated) modified Laurent series expansions:

$$\phi_1 = a_0 \ln \zeta_1 + \sum_{n=1}^N (a_{-n} \zeta_1^{-n} + a_n \zeta_1^n) \quad (16)$$

$$\phi_2 = b_0 \ln \zeta_2 + \sum_{n=1}^N (b_{-n} \zeta_2^{-n} + b_n \zeta_2^n)$$

In the above expressions,  $a_n$  and  $b_n$  are complex coefficients which are determined so as to satisfy the boundary conditions. The logarithmic terms drop out if the internal boundary is stress-free (see Reference 14). For infinite plates, the positive exponent terms drop out as the stresses are bounded at infinity.

In the general case of a finite anisotropic plate with a loaded or unloaded hole, the coefficients can be numerically calculated to satisfy the boundary conditions. The finite number of unknown coefficients may be determined by selecting the same total number of points on the inner and outer boundaries, and by computing the unknown coefficients by satisfying the boundary conditions exactly at these points. However, in this case, the calculated solutions at other boundary points are significantly different from the imposed boundary conditions (see Reference 11). A more desirable approach is to choose a large number of boundary points than the number of unknown coefficients, and to satisfy the boundary conditions at these points in a least squares sense. This solution procedure has been adopted for this analysis. Prior to applying the least squares boundary collocation procedure, the single-valuedness of the displacements and the rigid body rotational constraint are imposed (see References 5, 8).

Once the complex coefficients in Equation 16 are determined, the stresses and the displacements are calculated using Equations 9 to 13. The accuracy of the solution is determined by recalculating the stresses at the boundaries and comparing them to the imposed values. As discussed in References 5 and 8, an  $N$  value of 7 and approximately 100 points on the boundary are sufficient to recover the imposed boundary conditions within  $\pm 3$ .

If the anisotropic plate in Figure 1 has a loaded hole, the assumptions made in Reference 2 are retained. The fastener is assumed to be frictionless and is assumed to bear over half the hole boundary. The fastener/laminate contact problem is by-passed, and the contact solution is assumed to be a conical distribution of the radial stress around the hole (see Figure 1). The tangential stress is zero around the frictionless hole boundary. Results from recent investigations (References 12 and 13) indicate that the contact problem could affect the local stresses significantly. Nevertheless, the simplified contact stress expressions are assumed in this analysis.

Examples are presented in Reference 5 and 8 to demonstrate the capability of the FIGSOM computer code in computing the effect of plate geometry on the stress concentration at the boundary of the loaded or unloaded holes. Computed solutions are compared with infinite plate solutions to demonstrate the significant increase in the stress concentration when the outer plate boundaries are moved closer to the hole.

### 3. Fastener Analysis

In the computation of the two dimensional stress state in a bolted plate, it is generally assumed that the fastener is rigid and the fastener/plate displacement due to inplane loads does not vary in the plate thickness direction. In most of the practical situations, this assumption is not valid, and the stress field at the fastener location is complex and three dimensional in nature (see Reference 15 to 18). The three dimensional stress field at the fastener location in a bolted plate is influenced by many factors: fastener size, fastener stiffness, fastener end constraints, fastener torque, hole clearance, properties of the bolted plates, stacking sequence of the bolted laminate, load eccentricity induced by joint configuration, etc.

A single lap joint configuration, due to the eccentricity in the load path, will affect the local stress field more significantly than a double lap configuration. If the fastener modulus is large compared to the bolted plate modulus, and the fastener diameter is large compared to the plate thickness, the fastener bending and shear stiffnesses will be large enough to cause it to act like a rigid fastener. Otherwise, fastener bending and shear deformation will influence the local stress field significantly.

Fastener end constraints also have a significant effect in the local stress state. A protruding head fastener with a large applied torque value creates a nearly-fixed end boundary condition, a pin permits free rotation at the boundary, and a highly torqued countersunk fastener creates nearly-fixed and nearly-free constraints at the nut and head locations, respectively.

Intermediate torque values are represented by elastic constraint equations that quantify constraints between fixed and free conditions.

A brief summary of the fastener analysis approach is presented with the aid of Figure 2. For a single lap joint configuration subjected to a tensile load (Figure 2a), a typical fastener/bolted plate displacement variation is shown in Figure 2b. The distribution of the contact force is influenced by the many factors mentioned earlier and is not a continuous function in the plate thickness direction. Figure 2b shows a typical contact force distribution in bolted metallic plates. The resultant of the contact force distribution will be equal to the applied load (P) in magnitude, but will not, in general, lie along the line of action P. This is because its line of action is determined based on moment equilibrium considerations. A free body diagram of the fastener will include contact forces that are opposite in sense to those shown in Figure 2c. The spring constants represent the resistance offered by the bolted plate to fastener displacement. In a laminated plate, spring constants vary from ply to ply, and are dependent on ply fiber orientations. In a metallic plate, the spring constant will be invariant in the thickness direction. The various springs, with appropriate constants assigned to each, mathematically replace the bolted plates by an elastic foundation whose modulus is piecewise uniform in general.

The fastener is modeled as a Timoshenko beam to account for shear deformation effects. Figure 3 shows the deformed state of an infinitesimal segment of the fastener, and Figure 4 presents the assumed sign conventions for transverse shear (V) and bending moment (M) in the fastener. The coordinates along the fastener axis and the loading direction (in the plane of the bolted plate) are labeled  $z$  and  $x$ , respectively. Under load, a plane section undergoes a translational displacement  $u(z)$  in the  $x$  direction, a bending rotation  $\psi(z)$ , and shear deformation. While  $\psi$  is not a function of  $x$ , the shear strain due to  $V$  is, due to the variation of the transverse shear stress ( $\tau_{zx}$ ) in the  $x$  direction. This results in the curved shape for the deformed cross-section.

Representing the average cross-sectional shear distortion (rotation) by the symbol  $\phi$ , the following relationship is assumed (Timoshenko beam theory):

$$V = \int \tau_{zx} dA = \lambda GA \phi \quad (17)$$

where  $A$  is the fastener cross-sectional area,  $G$  is its shear modulus, and  $\lambda$  is a shear correction factor accounting for nonlinear  $\tau_{zx}$  distribution in the  $x$  direction. The total rotation of the section  $AB$  is denoted by  $u'$ , where the prime denotes differentiation with respect to  $z$ . From Figure 3, it follows that:

$$u' = \phi - \psi \quad (18)$$

The bending moment at any  $z$  location is expressed as follows:

$$M = \int \sigma_x x dA = \int (E \epsilon_x) x dA = \int E(x\psi') x dA = EI\psi' \quad (19)$$

where  $\sigma_x$  is the fastener bending stress,  $\epsilon_x$  is the axial strain in the fastener due to bending,  $E$  is the fastener Young's modulus, and  $I$  is the moment of inertia of the fastener cross-section about the  $y$  axis (normal to the  $xz$  plane).

If the fastener is subjected to a distributed transverse load  $q(z)$ , force and moment equilibrium considerations yield the following relationships (see Figure 4):

$$V' = -q \quad (20)$$

$$M' = V \quad (21)$$

Again, primes denote differentiation with respect to  $z$ . Equations 17 to 21 yield the following relationships for  $M$ ,  $V$  and  $\psi$ :

$$M = -EI [u'' + q/(\lambda GA)] \quad (22)$$

$$V = -EI [u''' + q'/(\lambda GA)] \quad (23)$$

$$\psi = -(EI/\lambda GA) [u''' + q'/(\lambda GA)] - u' \quad (24)$$

Equations 20 and 21 may be combined to yield the following equilibrium equation:

$$w'' = -q \quad (25)$$

Substituting Equation 22 into the above equation, the following governing equation is obtained:

$$u'''' + q''/(\lambda GA) - q/(EI) = 0 \quad (26)$$

This equation, where  $q = q(z)$ , governs the displacement of the fastener.

The effect of the bolted plate (metallic or laminated) on the fastener displacement is represented by the transverse loading term  $q(z)$  in the governing equation. The  $q(z)$  term is, in turn, linearly related to the fastener displacement  $u(z)$  through the foundation modulus  $k(z)$ . For the more general laminated foundation, the foundation modulus varies from ply to ply, and is uniform within a ply.  $k(z)$  is, therefore, piecewise uniform.

In the developed analysis, every ply is also assumed to be a bilinear elastic (Hencky) material (see Figure 5). This representation of the ply behavior permits the prediction of a local damage in the ply (when  $u = u_0$ ) that is not catastrophic. The ply modulus is  $k_1$  for  $0 < u < u_0$ . Depending on the type of damage predicted in the ply, its modulus ( $k_2$ ) beyond  $u = u_0$  is set to be greater than, equal to or less than zero. If  $k_2 > 0$ , the ply exhibits a hardening behavior; if  $k_2 < 0$ , it exhibits a softening behavior; and if  $k_2 = 0$ , the ply is an elastic-perfectly plastic material. When  $u$  takes the value of  $u^*$  (Figure 5), the ply loses its load-carrying capability. At this load level, the ply is assumed to have failed totally and its modulus and load are reset to zero. Adjacent unfailed plies share the load that is released by the totally failed ply.

The general ply load versus displacement behavior is expressed mathematically as:

$$q(z) = -ku - \bar{k}u, \quad \text{where} \quad (27)$$

$k = k_1$  for an undamaged ply

$k = k_2 = \alpha k_1$  for a partially damaged ply

$k = 0$  for a totally damaged ply

$$\bar{k} = k_1 - k_2 = (1-\alpha)k_1 \quad \text{for a partially damaged ply} \quad (28)$$

$\bar{k} = 0$  for a totally damaged ply

$\bar{u} = 0$  for an undamaged ply

$\bar{u} = u_0$  for a partially or totally damaged ply

$k_1$ ,  $u_0$ ,  $k_2$  and  $u^*$  or  $P_{\text{ultimate}}/P_{\text{initial}}$  fully define the general

ply behavior.  $u_0$  and  $u^*$  are dependent on the failure criteria used to predict partial and total ply damage.  $k_2 = \alpha k_1$  is established by assigning  $\alpha$  values for the various partial damage types. If the ply behavior can be adequately represented by a linear elastic approximation, a simplified form of Equation 27 may be used.

The initial foundation modulus ( $k_1$ ) for the  $j$ th ply type is computed using the following relationship:

$$k_1^j = P_{xj}/(h_j \delta_{eff}) \quad (29)$$

where  $\delta_{eff}$  and  $P_{xj}$  are computed using FIGEOM results and the principle of work (Reference 5), and  $h_j$  is the thickness of the  $j$ th ply type.

The boundary and continuity conditions on a fastener that bolts two plates in a single lap configuration are shown in Figure 6. The portion of the fastener in each plate is shown separately. The load ( $P$ ) in each plate is enforced as a shear boundary condition at the interfacial location, to satisfy force equilibrium requirement. The shear force values at the outer boundaries (the head and nut locations of the fastener) are set equal to zero, since the load transfer is effected between these locations. At the interface between the bolted plates, continuity of the bending slope and the bending moment are enforced. Continuity of displacement is not enforced at this location. This is because  $u(z)$  represents the fastener/plate displacement, and undergoes a finite discontinuity across this interfacial location in the joint.

At the fastener head location, the head type and the presence of washers, if any, influence the constraint against free rotation. A washer and a nut offer a similar constraint at the other boundary. The constraints at the fastener head and nut locations can be generalized as shown in Figure 6, where  $R_1$  and  $R_2$  quantify the elastic restraint. For a pin-connected joint, for example,  $R_1$  and  $R_2$  are set equal to zero.

Load transfer in a symmetric double lap configuration yields the boundary, symmetry and continuity conditions shown in Figure 17. The boundary condition at the fastener head location, and the shear and continuity conditions at the interface between adjacent plates, are identical to those discussed earlier (see Figure 6). Symmetry introduces a zero shear and a zero bending slope condition at the midplane of plate 2. It is noted that only half the fastener is analyzed for a symmetric double shear situation. A total of 8 boundary/continuity/symmetry conditions are identified for each joint configuration.

Incorporation of Equation 27 into Equation 26 will result in a fourth order, ordinary differential equation for  $u(x)$  with variable coefficients (because  $k$  is a function of  $x$ ). A finite (central) difference approximation of the governing equation, and the boundary and continuity conditions, is adopted to obtain the fastener/plate displacement and the corresponding fastener load distribution in the thickness direction of the bolted plates. This provides a rapidly executable solution scheme that can be economically executed many times to predict progressive failures in bolted joints.

Figure 8 describes how the continuous fastener is discretized into a finite number of nodal points. In the chosen example, plates 1 and 2 are assumed to be 5-ply and 4-ply laminates, respectively, bolted together in a single lap configuration. The portion of the fastener in each plate is represented by equally-spaced nodes located at the ply midplanes. If either plate is metallic, it is divided into  $m$  or  $n$  number of plies of the same properties. To enable the use of a central difference scheme for the governing equation and the boundary conditions, two 'false' nodes are assumed to be present on either side of a plate.

The governing equation is enforced at the  $n + m$  'physical' nodes, and the boundary/continuity/symmetry conditions are enforced at the boundary nodes (identified in Figure 9 as nodes 3 and  $n+2$  in plate 1, and nodes  $n+7$  and  $m+n+6$  in plate 2). This provides a system of  $m+n+8$  equations that are solved for the nodal displacements by using a standard matrix decomposition or a matrix inversion routine. The coefficient matrix to be inverted is banded in nature, and a special purpose Gaussian triangularization computer code was developed to solve for the nodal displacements. When the coefficient matrix size is large, this provides an economical means of obtaining solutions.

The number of actual plies in a bolted laminate determines the number of nodes in the portion of the fastener within that laminate. A physical ply can also be divided equally into two or more plies of smaller thicknesses, to improve the accuracy of the solution. Referring to Figure 9, if plate 1 is a laminate with  $n$  plies, the portion of the fastener within plate 1 can be divided into  $k \times n$  segments that are  $t_1/(k \times n)$  in thickness, where  $k$  is any integer  $\geq 1$ .

The effect of the number of nodes per bolted plate on the convergence of the displacement solution was studied in Reference 5. It is necessary to divide a metallic plate into at least 20 identical "plies" to obtain a converged displacement solution, which ensures an accurate prediction of the load distribution in the thickness direction. In laminated (non-metallic) plates, a minimum of 30 nodes per plate is required to obtain accurate solutions.

The finite difference formulation of the fastener analysis has been programmed to be the FDFA computer code. Convergence studies on the analysis, correlation of FDFA predictions with available analytical solutions, and sample predictions using FDFA are presented in Reference 5.

#### 4. Effective Fastener Element

Referring to Figure 10, the relative displacement between two bolted plates is computed using the fastener analysis described in section 3 (FDFA computer code). This enables the computation of the effective fastener stiffness value as follows:

$$k_x = P / (\bar{u}_T - \bar{u}_B) \quad (30)$$

where  $\bar{u}_t, \bar{u}_b$  are the average relative displacements (between the top and bottom surfaces) in the top and bottom plates, respectively.  $P$  is the load applied along the  $x$  direction in the  $xy$  plane of the bolted plates. When both the bolted plates are isotropic, the effective transverse fastener stiffnesses in the  $x$  and  $y$  directions are identical; i.e.,  $k_y = k_x$ . If either plate is a laminated composite, this analysis is performed twice for each fastener. The layup used to compute  $k_x$  is rotated by 90 degrees to obtain  $k_y$ .

As shown in Figure 10, the two-node effective fastener element allows two degrees of freedom (DOF) at each node, perpendicular to the axis of the element. Through the PDFA computation of  $k_x$  and  $k_y$ , a  $4 \times 4$  effective fastener stiffness matrix is generated. Hitherto, these stiffnesses, referred to as joint stiffnesses, have been experimentally measured quantities.

##### 5. Loaded Hole, Unloaded Hole and Plain Elements

In a general multiply-fastened panel, significant moments and out-of-plane forces can be generated by the applied loading, particularly in a single shear load transfer configuration. The present analysis assumes that the loaded hole, unloaded hole and plain elements behave essentially as membranes under plane stress conditions.

The characteristic feature of the loaded and unloaded hole elements is the presence of a stress concentrator (the hole) which complicates the process of determining stiffness coefficients. The FIGEOM code, described in Reference 5, is capable of computing the state of stress within a doubly-connected region of finite dimensions, under arbitrary inplane biaxial loading. The availability of FIGEOM motivated the adoption of a flexibility approach to computing the element stiffness matrix. The natural mode method, originally proposed by Argyris, is employed for this purpose (Reference 19).

The natural mode method was originally developed as a simpler alternative to the sometimes tedious matrix displacement method of determining element stiffness relationships. The natural mode method recognizes that the total number of kinematic degrees of freedom in an element can be separated into straining and rigid body modes. Only the straining modes give rise to stiffnesses that are referred to as natural or invariant stiffnesses. The natural stiffness matrix is of a lower order than the global stiffness matrix. The natural mode technique proceeds from a flexibility standpoint in which natural load cases are initially imposed to compute the natural flexibilities. The natural flexibility matrix is subsequently inverted to yield the natural stiffness matrix. The natural stiffness matrix is then expanded to yield the global stiffness matrix using relationships between the natural modes and the nodal displacements.

The natural flexibility coefficients are computed based on the principle of virtual work. When stresses are varied while strains are held constant, a calculus of variations definition of the virtual work is:

$$\delta W_c = \iiint_V (\epsilon)^T \delta (\sigma) dV \quad (31)$$

where  $V$  is the volume of the domain of interest. The stresses and strains introduced by the natural loads are defined as:

$$(\sigma) = [\sigma_x \ \sigma_y \ \tau_{xy}]^T = [\bar{\sigma}] \{P_N\} \quad (32)$$

$$(\epsilon) = [\epsilon_x \ \epsilon_y \ \gamma_{xy}]^T = h[A]^{-1} [\bar{\sigma}] \{P_N\} \quad (33)$$

where the states of stress and strain are at a point in the plate of thickness  $h$ ,  $\{P_N\}$  is a vector of natural or generalized loads,  $h[A]^{-1}$  is the inplane flexibility matrix for a laminated or metallic plate, and  $\{\bar{\sigma}\}$  contains the contribution of each natural load case to the total stress state in the plate. Equation 31 may then be written as:

$$\delta W_c = \{P_N\}^T \left\{ \iiint_V [\bar{\sigma}]^T h[A]^{-1} [\bar{\sigma}] dV \right\} \delta \{P_N\} \quad (34)$$

The natural flexibility matrix may then be defined as:

$$[F_N] = \iiint_V [\bar{\sigma}]^T h[A]^{-1} [\bar{\sigma}] dV \quad (35)$$

Integrating in the thickness direction,

$$[F_N] = h^2 \iint_S [\bar{\sigma}]^T [A]^{-1} [\bar{\sigma}] dS \quad (36)$$

where  $S$  is the area of the domain of interest. If  $\{P_N\}$  is the natural displacement vector, the flexibility relationship is expressed as:

$$\{P_N\} = [F_N] \{P_N\} \quad (37)$$

or

$$\{P_N\} = [F_N]^{-1} \{P_N\} = [K_N] \{P_N\} \quad (38)$$

where  $[K_N]$  is the natural stiffness matrix.

To relate the displacements in the natural and global coordinate systems, the global displacement vector can be represented as a combination of elastic and rigid body components. Assuming  $n$  nodes in the plate element, and two degrees of freedom ( $u$  and  $v$  in the  $x$  and  $y$  directions, respectively) at each node,

$$\{p\} = [u_1 \ v_1 \ u_2 \ v_2 \ \dots \ u_n \ v_n]^T = \{p_e\} + \{p_o\} \quad (39)$$

The elastic global displacements at the  $n$  nodes are related to the natural loads as follows:

$$\{p_e\} = [A_N] \{P_N\} \quad (40)$$

where  $[A_N]$  is a transformation matrix. Substituting Equation 38 into Equation 40, one obtains:

$$\{p_e\} = [A_N] [K_N] \{P_N\} \quad (41)$$

The rigid body components of the global displacements are expressed as:

$$\{p_o\} = [A_o] \{p_o'\} \quad (42)$$

where  $\{p_o'\}$  contains the rigid body translations in the  $x$  and  $y$  directions ( $u$  and  $v$ ), and the rigid body rotation about the  $z$  direction ( $\theta_z$ ). The matrix  $[A_o]$  is solely dependent on the element geometry, and an example for a five-node element is presented in Figure 11.

The relationships in Equations 41 and 42 are adjoined to yield the following expression for the global displacements (see Equation 39):

$$\{p\} = \begin{bmatrix} [A_N] & [K_N] \\ [A_o] \end{bmatrix} \begin{bmatrix} \{P_N\} \\ \{p_o'\} \end{bmatrix} \quad (43)$$

The inverse of Equation 43 yields a relationship between the displacements in the natural and global coordinate systems:

$$\begin{aligned}
 \{a_n, a_o\}^T &= \left[ [A_n] [K_n] ; [A_o] \right]^{-1} \{p\} \\
 &= \left[ [a_o] ; [a_n] \right]^T \{p\}
 \end{aligned}
 \tag{44}$$

$$\text{or, } \{a_n\} = [a_n]^T \{p\}
 \tag{45}$$

Incorporating Equation 45 into the principle of virtual work, the following relationship between nodal (global) loads and the natural loads is obtained:

$$\{P\} = [a_o]^T \{p_n\}
 \tag{46}$$

The global stiffness matrix is then related to the natural stiffness matrix  $[K_n]$  through the transformation matrix  $[a_o]$ , as follows:

$$[K_g] = [a_o]^T [K_n] [a_o]
 \tag{47}$$

The order of the natural flexibility matrix is less than the total number of degrees of freedom (DOF) in the element by three. The 5-node, 10-DOF loaded hole element, therefore, requires seven natural load cases that form an uncoupled, orthogonal set. These load cases fully interrogate nodal interactions, and represent the basic element deformation modes, including membrane stretching, shear and bending (see Figure 12). In computing the natural flexibility matrix, Equation 36 is evaluated numerically using a standard Gaussian integration scheme to approximate the surface integral.

The integration (summation) is performed by dividing the element into four regions. The stresses for each load case are computed in each region, at locations that correspond to fifth order Gaussian quadrature points, scaled to the geometry of the element. The computed stresses are summed and weighted to yield the natural flexibility coefficients.

In the loaded hole element, the first four load cases, in which the externally applied load is reacted at the boundary, cause a significant non-uniform distortion of the element edges (see Reference 6). These straining modes are not adequately represented by storing only the nodal displacements in the  $[A_n]$  matrix. To correct this problem, the average edge normal displacements are assigned to the nodes.

The generation of global stiffness matrices for the unloaded (open) hole and plain elements follows the procedure outlined above. These elements contain only four nodes (8 DOF) each. Therefore, only five natural load cases are required to generate their natural flexibility matrices. The transformation of the 5 x 5 natural flexibility matrices to the 8 x 8 global stiffness matrices for the two elements follows Equations 38 to 47. Since FIGEON was developed to analyze doubly-connected planform regions, the plain element stiffnesses are obtained using the open hole element algorithm, setting the hole radius to a very small value. This also provides the added benefit of using the same set of subroutines to generate the stiffness matrices for all the plate elements (loaded hole, unloaded hole and plain elements).

#### 6. Load Distribution Among Fasteners

A typical bolted joint is represented by interconnected special finite elements. The stiffness of each element is initially computed and stored. The global joint stiffness matrix is then formed by assembling the individual stiffness matrices for the loaded hole, unloaded hole, plain and effective fastener elements. The SAMCJ user only defines the type, geometry and properties of the individual elements. SAMCJ internally processes this information to generate the global joint stiffness matrix.

The assembled, global joint stiffness matrix is related to the nodal displacements and loads as follows:

$$\{P\} = [K_g] \{p\}
 \tag{48}$$

Each bolted plate contains  $M$  nodes, which include the fastener nodes. Each node has two degrees of freedom ( $u$  and  $v$  displacements). Therefore, the global joint stiffness matrix is  $4M \times 4M$  in size. The imposed boundary constraints reduce the size of the stiffness matrix that is eventually used to compute the nodal displacements and boundary constraint forces. Incorporation of the nodal displacements into element equilibrium equations yield the nodal forces in the individual elements. The loads at node 5 in each loaded hole element provide the  $x$  and  $y$  components of the fastener load in that element.

#### 7. Stress State in the Bolted Plate

The stress state at any internal point in an element is computed using a procedure similar to the computation of the natural flexibility matrix (see Reference 6). During the generation of element natural flexibility matrices, the stress states at locations within the element are computed and stored for unit values of every natural load case. Desired stress recovery locations are pre-selected for this purpose.

#### 8. Strength and Failure Mode Prediction

SAMCJ predicts the strength of a bolted plate using average stress failure criteria at the laminate level (see Figure 13). In Reference 5, the same criteria were applied at the lamina level to predict progressive ply failures in a singly-fastened laminate. The characteristic distances over which the stresses are averaged in SAMCJ are different from those used in Reference 5. Also, failure is assumed to be a one-step (catastrophic) process. The strength of a bolted plate corresponds to the initial failure at a fastener or cut-out location, in a bearing, shear-out or net section failure mode.

Appropriate failure sites are identified by SAMCJ in every element. These sites vary with the applied loading. The characteristic distances for the net section, shear-out and bearing modes of failure are divided into a finite number of regions. The appropriate stress components corresponding to a 1-kip joint load are computed in these regions, and their average values over the respective characteristic distances are stored. The ratios of these average stresses to the corresponding unnotched strengths are subsequently computed and relatively evaluated to predict the strength of the bolted plate, the failure site and the failure mode. Under tensile loading, the average  $\sigma_x$  value over  $a_x^*$  is divided by the unnotched tensile strength to predict net section tensile failure. Under compressive loading, the average  $\sigma_x$  value over  $a_x^*$  is divided by the unnotched compressive strength to predict net section compressive failure. The average  $\sigma_x$  value over  $a_x^*$  is divided by the unnotched compressive strength to predict bearing failure. The average  $\tau_{xy}$  value over  $a_s^*$  is divided by the unnotched shear strength to predict shear-cut failure.

The unnotched laminate strengths, under tension and under compression, are computed by SAMCJ based on input fiber-directional failure strain values (tensile and compressive). Laminate strengths under  $N_x$  and  $N_{xy}$  loadings (inplane normal and shear stress resultants, respectively) are assumed to correspond to first fiber failure in a ply. This simplistic strength prediction procedure introduces inaccuracies that have been acknowledged and discussed in the literature. Nevertheless, SAMCJ adopts this procedure for lack of a validated alternative.

SAMCJ assumes that a net section, shear-out or bearing failure of any element results in joint failure. This assumption results in a one-step strength, failure site and failure mode prediction for a multiply-fastened plate. A 1-kip tensile or compressive load is applied, and fastener loads and normalized averaged stresses corresponding to net section, shear-out and bearing failure modes are computed. The failure value of the applied load corresponds to a unit value of the maximum normalized average stress. An identification of the maximum normalized average stress, and its location, provides the joint failure mode and the critical fastener or cut-out location.

#### 9. Sample SAMCJ Predictions

In the experimental part of Reference 1, over 160 composite-to-aluminum multifastener joints were tested under static loading. Reference 20 contains results from these tests, including fastener load distribution measurements using strain-gaged bolts, failure loads, failure locations and failure modes. Sample test cases from Reference 20 are analyzed below using the SAMCJ computer code. Analytical predictions are compared with test results to establish the validity of the developed analysis.

Bolted laminates were fabricated using AS1/3501-6 graphite/epoxy unidirectional prepreg material containing approximately 35% resin by weight. These included 20 - and 40 - ply laminates with 50/40/10, 70/20/10, 30/60/10 and 25/60/15 (percentages of 0°, +45° and 90° plies, respectively) layups. The 20-ply, 50/40/10, 70/20/10 and 30/60/10 layups had [(45/0/-45/0)2/90]s, [45/0/-45/0/90/0]s and [45/0/-45/0/45/90/-45/0/+45]s stacking sequences, respectively. The 40-ply, 50/40/10 and 70/20/10 layups had [(45/0/-

45/0)2/0/90]2s and [45/0/-45/03/90/03]2s stacking sequence, respectively.

Aluminum plates were bolted to laminates to facilitate load transfer in single and double-shear configurations. The metallic plates were machined from 7075-T7 raw stock, and contained fastener hole arrangements that were compatible with those in the laminated specimens. The thickness of the metal plates in the section is denoted by  $t_m$ .

Most of the tests used 5/16-inch diameter, protruding head steel fasteners. Selected tests used 5/16-inch diameter, 100 degree countersunk (tension head) steel fasteners. The fasteners were torqued to 100 in-lb, prior to testing, unless otherwise specified.

### 9.1 Composite-to-Metal Joints with Four Fasteners in a Rectangular Pattern

Test cases 225, 229 and 230 in Reference 20 consider composite-to-metal joints in a single-shear configuration, with four fasteners in a rectangular pattern. The finite element model for each of the bolted plates contains four plain and four loaded hole elements.

Figure 14 compares SAMJC predictions with test results from Reference 20 for bolted 50/40/10 laminates. The predicted fastener load distribution is nearly equal, with the inner fasteners carrying a slightly larger fraction of the load (8%). This agrees with the test results in Reference 20. SAMJC predicts a shearout failure at the inner fastener location. The predicted shearout load levels corresponding to the two inner fasteners were 18.1 and 18.9 kips. In Reference 20, the same failure location (inner fasteners) and failure mode were observed in two out of three replicates. In the remaining replicate, though, a net section failure occurred across the inner fasteners. The shearout failures in two specimens were accompanied by delamination in the laminate. The failure load predicted by SAMJC (18.1 kips) is only 6% larger than the measured average value (17.1 kips).

SAMJC predictions for bolted 70/20/10 laminates are presented in Figure 15. The fastener load distribution is identical to that predicted for the 50/40/10 laminate, and agrees with the test results from Reference 20. The predicted failure location (inner fasteners) and failure mode (shearout) correlate well with the observations in Reference 20. As before, shearout is accompanied by delaminations in the failed laminate. The failure load predicted by SAMJC (11.8 kips) is 21% lower than the measured average value (14.9 kips).

SAMJC predictions for bolted 30/60/10 laminates are presented in Figure 16. In this case, the predicted loads in the inner fasteners (3, 4) are 17% larger than those in the outer fasteners (1, 2). SAMJC predicts a net section failure across the inner fastener holes (3, 4) at a load level of 12.4 kips. In Reference 20, the predicted net section failure was observed at the predicted site, accompanied by delaminations. The failure load predicted by SAMJC (12.4 kips) is 24% lower than the measured average value (16.4 kips).

### 9.2 Composite-to-Metal Joints with Six Fasteners and an Adjacent Circular Cut-Out in the Laminate

Test cases 243 and 246 in Reference 20 address a single-shear load transfer between 0.5-inch-thick aluminum plates (without a cutout) and 40-ply laminates of 50/40/10 and 70/20/10 layups, with a one inch diameter circular cut-out adjacent to the fasteners.

SAMJC predictions for the 40-ply, 50/40/10 laminate are presented in Figure 17. SAMJC predicts the applied load to be divided nearly equally among the six fasteners, with fasteners at locations 2 and 5 carrying the largest fraction. This correlates fairly well with the strain-gaged bolt measurements in Reference 20. SAMJC predicts failure to occur in a net section mode, across the 1-inch diameter circular cut-out. Two out of three test replicates failed in the predicted manner. One replicate, however, failed in a net section mode, across the inner fasteners (4, 5, 6). The failure load predicted by SAMJC (38.3 kips) is 9% lower than the measured average value (42.0 kips). SAMJC predicts a higher load level (53.7 kips) for a net section failure across the inner fastener holes, observed in one out of three replicates.

SAMJC predictions for the 40-ply, 70/20/10 laminate are presented in Figure 18. Predicted load distribution among the six fasteners is similar to that predicted for the 50/40/10 laminate, and is in fair agreement with test measurements. SAMJC predicts a shearout mode of failure at an inner fastener location (5), and tests revealed shearout failures at all the fastener locations (1 to 6), accompanied by delaminations. The failure load predicted by SAMJC (37.9 kips) is 12% lower than the measured average value (42.9 kips). It is also noted that SAMJC predicts a net section failure across the 1-inch-diameter circular cut-out at a slightly higher load level (38.8 kips).

### 9.3 Composite-to-Metal Joints with Five Fasteners in a Row

Test case 280 in Reference 20 considers load transfer between an aluminum plate and a 40-ply, 80/40/10 laminate in a double shear configuration. SAMCJ predictions for this test case are presented in Figure 19. The predicted load distribution among the fasteners qualitatively follows the trend indicated by the strain-gaged bolt measurements in Reference 20. The predicted peak fastener load fraction (0.293), however, is lower than the measured value (0.345). The innermost fastener (5) is predicted to carry this peak fractional load, in agreement with test results. SAMCJ predicts the laminate to fail in a net section mode across the innermost fastener hole (5). This prediction is also in agreement with the observations in Reference 20. The analytically predicted failure load (13.4 kips) is 24% lower than the measured average value (17.7 kips).

### 10. Design Application

The design of a bolted joint in composite structures involves the selection of the fastener type, size and arrangement (spacing between adjacent fasteners), and geometry changes in the bolted plates (layup change and change in the planform dimensions). SAMCJ can quickly interrogate the effects of all these parameters on the joint strength, independent of test measurements like "joint stiffnesses," and is, therefore, a rapidly useable analytical design tool. If the bolted laminate is to be fabricated using a new material, only the basic lamina properties and the characteristic distances for the average stress failure criteria have to be determined prior to performing the analysis.

### 11. Conclusions

The significant improvements offered by SAMCJ over the state-of-the-art at the inception of the program in Reference 1 are:

(1) SAMCJ performs a one-step analysis that computes the fastener load distribution, critical fastener location, joint failure load, and the corresponding failure mode. Hitherto, separate fastener load distribution and failure analyses were performed, requiring a two-step analytical procedure.

(2) SAMCJ only requires the geometric and material properties of the bolted plates and fasteners as input. SAMCJ internally computes the effective transverse fastener stiffness values that account for fastener size, fastener and bolted plate material properties, bolt torque, load eccentricity (single versus double shear load transfer), and the local three dimensional stress state at the fastener location. Hitherto, these effects could only be accounted for via experimentally measured "joint stiffnesses." SAMCJ eliminates the need for these experimental measurements, and is, therefore, the first multifastener bolted joint strength analysis that is devoid of dependence on test results.

(3) SAMCJ performs a two-dimensional load distribution analysis, and predicts the magnitude and orientation of the load at each fastener location via components of the fastener load along and perpendicular to the load direction. Hitherto, analyses only addressed the row-to-row load variation, or the axial components of the fastener loads, resorting to a one-dimensional analysis.

(4) SAMCJ accounts for stress concentration interaction effects that hitherto could not be accounted for. This includes the effects of adjacent free edges, cut-outs and proximate fastener locations.

(5) SAMCJ accounts for tapered bolted plate geometries that are commonplace in practical situations.

The primary limitations of the developed analysis include its inability to account for the effect of countersunk fasteners, its inability to predict the precipitation of delaminations, and the inaccuracies introduced by the five-node representation of a complex problem (a laminate with finite planform dimensions, a fastener hole, and a fastener load distribution around the hole boundary). The fastener analysis segment of SAMCJ can be modified to overcome the first limitation. The failure procedure can be modified to predict delaminations through approximate estimations of interlaminar stresses and an appropriate failure criterion. This task will be similar to that performed in Reference 5. The last limitation (inaccuracies introduced by the five-node element) can be overcome by developing a higher order element (nine-node element).

The presented (SAMCJ) analysis is a significant contribution to the design and analysis of bolted structural parts. It is, for most of the practical joint configurations, moderately conservative, and provides the user with a fairly accurate prediction of the failure location and the overall failure mode. As such, it will be very useful in rapidly and analytically evaluating many bolted joint concepts, and to identify the most efficient concept for a selected application.

**REFERENCES**

1. Rankumar, R. L., et al., "Bolted Joints in Composite Structures: Design, Analysis and Verification", Interim and Final Technical Reports Northrop/AFWAL Contract No. F33615-80-C-1217, Northrop Corporation, Aircraft Division, Hawthorne, California, August 1982 - September 1986.
2. Garbo, S. P. and Ogonowski, J. M. "Effect of Variances and Manufacturing Tolerances on the Design, Strength and Life of Mechanically Fastened Composite Joints", Volume 1, AFWAL-TR-81-3041, April 1981.
3. Hart-Smith, L. J., "Bolted Joints in Graphite-Epoxy Composites", NASA CR-144899, Jan. 1977.
4. Hart-Smith, L. J., "Design Methodology for Bonded-Bolted Composite Joints, Vol. 1, Analysis Derivations and Illustrative Solutions", AFWAL-TR-81-3154, Vol.1, Feb. 1982.
5. Rankumar, R. L., et al., "Strength Analysis of Composite and Metallic Plates Bolted Together by a Single Fastener", AFWAL-TR-85-3064, August 1985.
6. Rankumar, R. L., Saether, E. S., and Appa, K., "Strength Analysis of Laminated and Metallic Plates Bolted Together by Many Fasteners", AFWAL-TR-86-3034, January 1986.
7. Whitney, J. M. and Nuismer, R. J., "Stress Fracture Criteria for Laminated Composites Containing Stress Concentration", Journal of Composite Materials, Vol. 8, pp 253-265, July 1974.
8. Kudva, N. J. and Madenci, E., "Stress Analysis of Finite Geometry Composite Bolted Joints Using Modified Boundary Collocation Techniques", Northrop Corporation Report, NOR 83-198, October 1983.
9. Jones, R. N., Mechanics of Composite Materials, Scripta Book Company/McGraw Hill, 1975.
10. Lekhnitskii, S. G., Anisotropic Plates, Gordon and Breach, 1968.
11. Oplinger, D. W. and Gandhi, K. R., "Stresses in Mechanically Fastened Orthotropic Laminates", AFFEL-TR-74-103, September 1974.
12. Myer, M. W. and Klang, E. C., "Stresses Around Holes in Pin-Loaded Orthotropic Plates", Proceedings of the 25th Structures, Structural Dynamics and Materials Conference, Sponsored by AIAA/ASME/ASCE/AHS, Palm Springs, California, May 1984.
13. Mangalgiri, P. D., "Pin-Loaded Holes in Large Orthotropic Plates", AIAA Journal, Vol. 22, No. 10, pp. 1478-1484, October 1984.
14. Ogonowski, J. M., "Analytical Study of Finite Geometry Plates with Stress Concentrations," Proceeding of the 21st Structures, Structural Dynamics and Materials Conference, sponsored by AIAA/ASME/ASCE/AHS, Seattle, May 1980.
15. Harris, M. G. and Ojalvo, I. U., "Simplified Three-Dimensional Analysis of Mechanically Fastened Joints", Proceedings of the Army Symposium on Solid Mechanics: The Role of Mechanics in Design--Structural Joints, September 1974.
16. Harris, M. G., Ojalvo, I. U. and Hooson, R. E., "Stress and Deflection Analysis of Mechanically Fastened Joints", Air Force Flight Dynamics Laboratory Technical Report, AFFDL-TR-70-49, May 1970.
17. Barrois, W., "Stresses and Displacements due to Load Transfer by Fasteners in Structural Assemblies", Engineering Fracture Mechanics, Vol. 10, pp. 175-176, 1978.
18. Mecenyi, M., Beams on Elastic Foundation, University of Michigan Press, Ann Arbor, Michigan, 1946.
19. Prgyris, J. H. and Scharpf, D. W., "Some General Considerations on the Natural Mode Technique: Part 1, Small Displacements; Part 2, Large Displacements", The Aeronautical Journal of the Royal Aeronautical Society, Vol. 73, April 1969.
20. Rankumar, R. L. and Tossavainen, E.W., "Bolted Joints in Composite Structures: Design, Analysis and Verification; Task II Test Results--Multifastener Joints", AFWAL-TR-85-3065, August 1985.

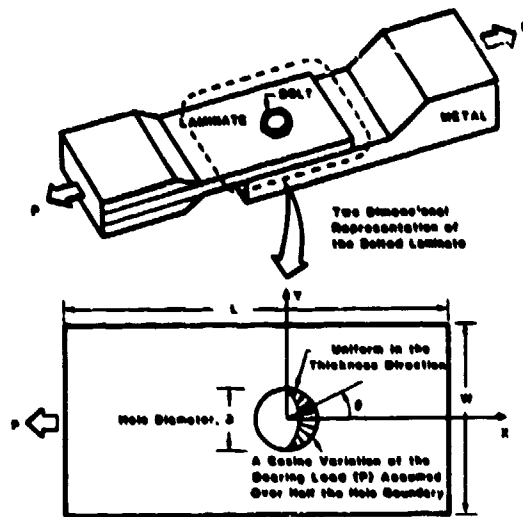


Figure 1. Schematic Representation of a Bolted Laminate with Finite Dimensions.

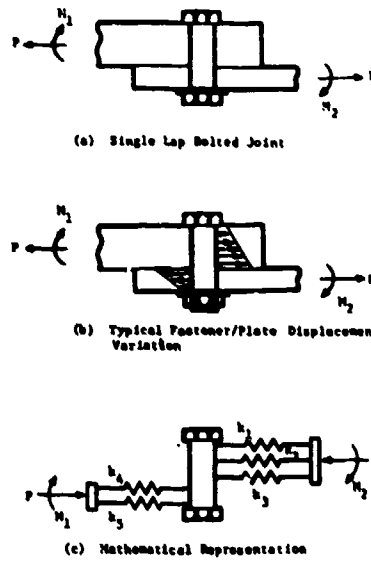


Figure 2. Representation of a Single Lap Configuration by an Equivalent Fastener Problem.

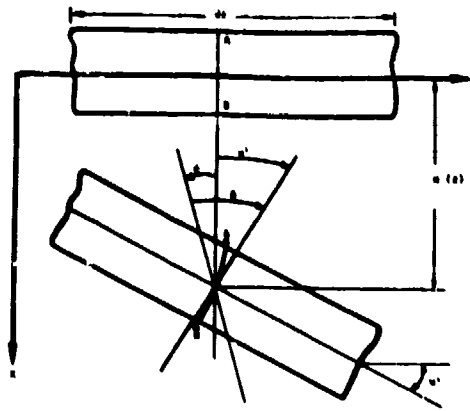


Figure 3. Deformation of an Infinitesimal Beam Element.

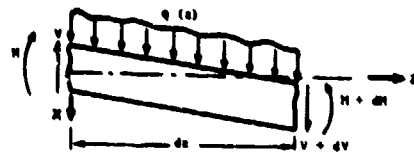


Figure 4. Positive Shear and Moment Conventions.

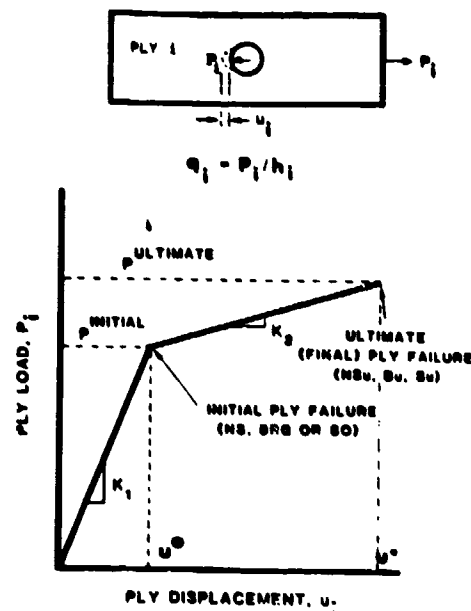


Figure 5. Bilinear Elastic Behavior of a Ply.

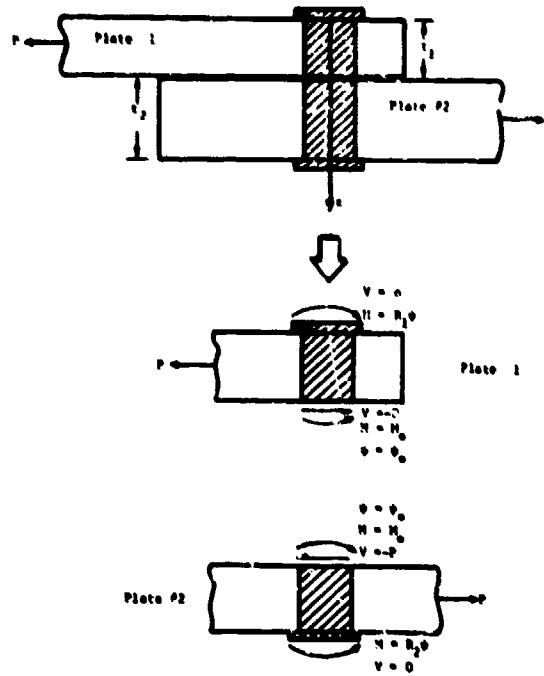


Figure 6. Boundary and Continuity Conditions for a Typical Single Lap Joint.

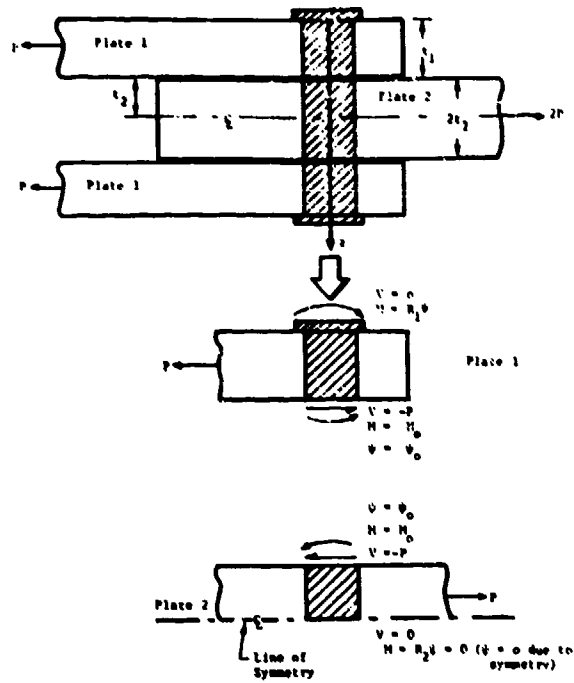


Figure 7. Boundary and Continuity Conditions for a Typical Double Lap Joint.

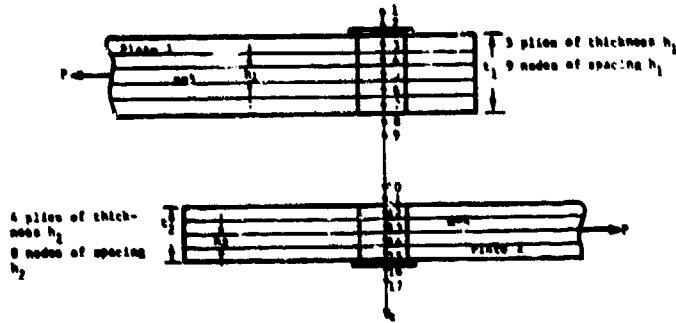


Figure 8. An Example of the Node Layout and Numbering Scheme in a Single Lap Shear Joint Configuration.

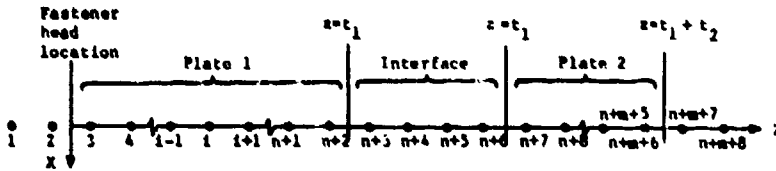


Figure 9. A General Node Arrangement with  $n$  Nodes in Plate 1 and  $m$  Nodes in Plate 2.

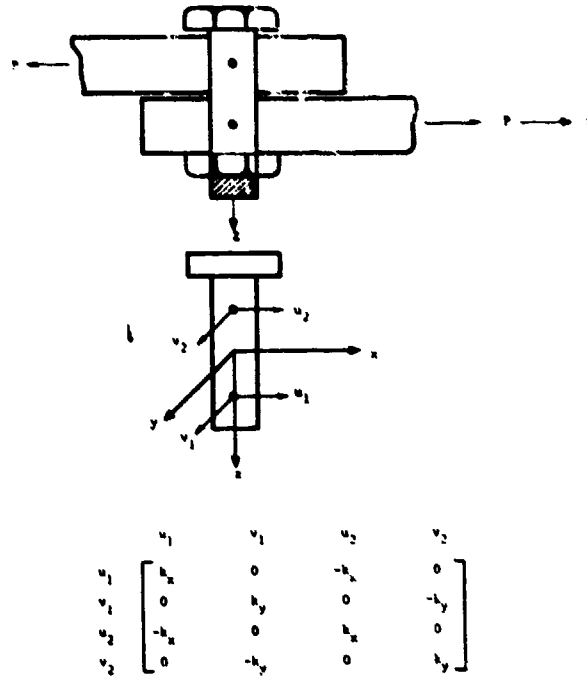


Figure 10. Effective Fastener Representation and Stiffness Matrix

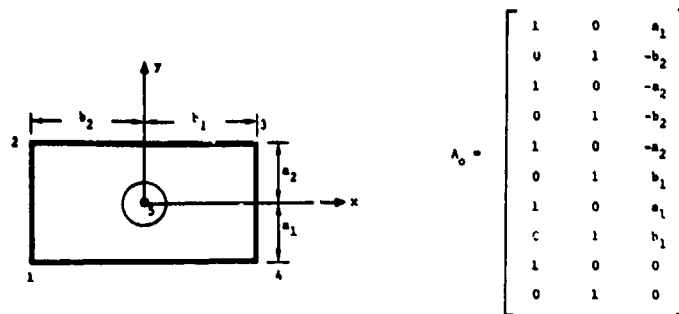


Figure 11.  $A_0$  Matrix for the five-Node Element Containing Element Rigid Body Modes.

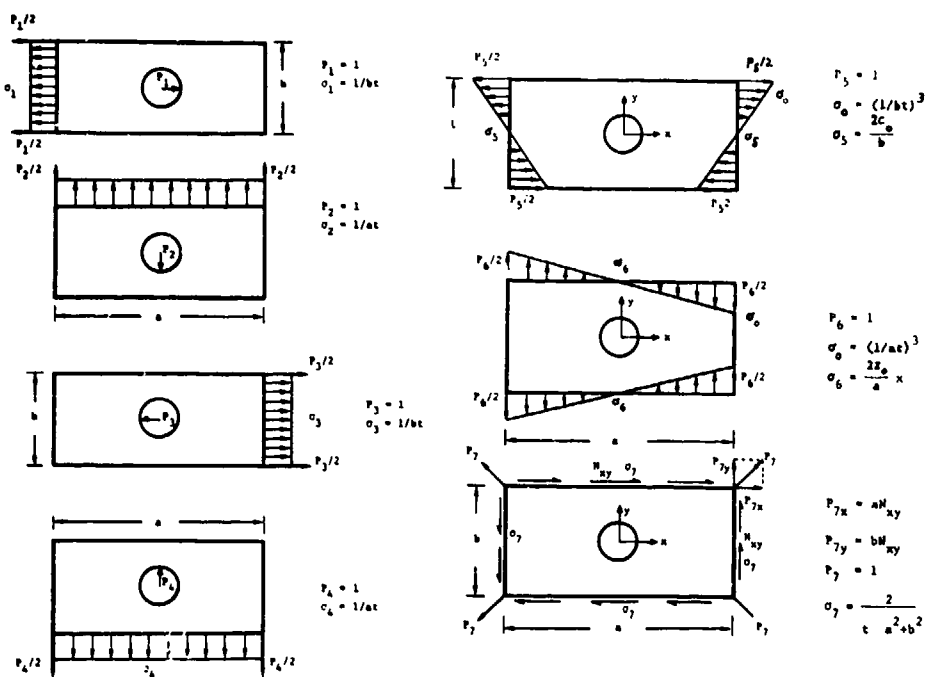


Figure 12. The Seven Natural Load Cases for the Loaded Hole Element.

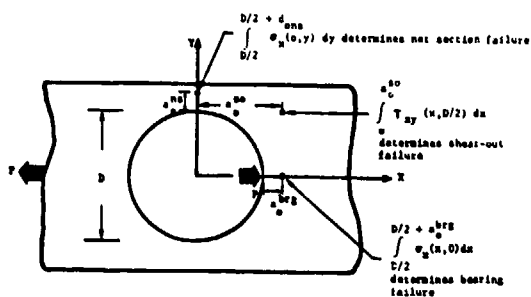
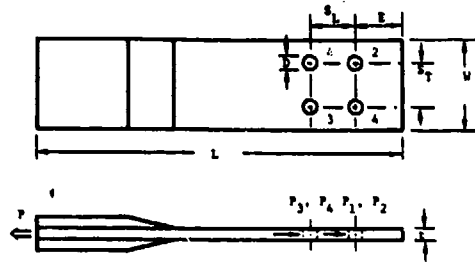


Figure 13. The Characteristic Distances Used in the Average Stress Failure Criteria.

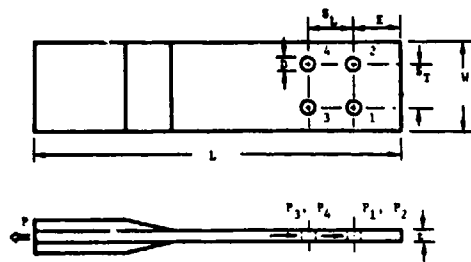
Test Case 225, Static Tension, Single-Shear  
 20-Ply, 50/40/10 Laminate  
 $D=5/16$  in.,  $t=0.117$  in.,  $t_{A1}=0.31$   
 $S_L/D=S_T/D=4$ ,  $W/D=10$ ,  $E/D=3$



	SAMCJ PREDICTION	TEST RESULTS
$P_1/P$	0.24	0.26
$P_2/P$	0.24	0.26
$P_3/P$	0.20	0.20
$P_4/P$	0.20	0.21
$P_{failure}$ (kips)	18.1 (18.0)	17.1
FAILURE LOCATION	4 (3)	3, 4
FAILURE MODE(S)	SHEAR-OUT	SHEAR-OUT, NET SECTION, DELAMINATION

Figure 14. SAMCJ Predictions and Test Results for Test Case 225 ( Ref.6 ).

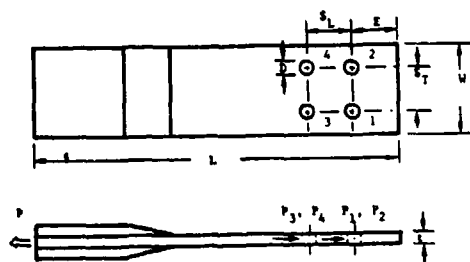
Test Case 229, Static Tension, Single-Shear  
 20-Ply, 70/20/10 Laminate  
 $D=5/16$  in.,  $t=0.105$  in.,  $t_{A1}=0.31$  in.  
 $S_L/D=S_T/D=4$ ,  $W/D=10$ ,  $E/D=3$



	SAMCJ PREDICTION	TEST RESULTS
$P_1/P$	0.24	0.26
$P_2/P$	0.24	0.24
$P_3/P$	0.20	0.20
$P_4/P$	0.20	0.22
$P_{failure}$ (kips)	11.8 (12.3)	14.0
FAILURE LOCATION	4 (3)	4, 3, 2, 1
FAILURE MODE(S)	SHEAR-OUT	SHEAR-OUT, DELAMINATION

Figure 15. SAMCJ Predictions and Test Results for Test Case 229 ( Ref.6 ).

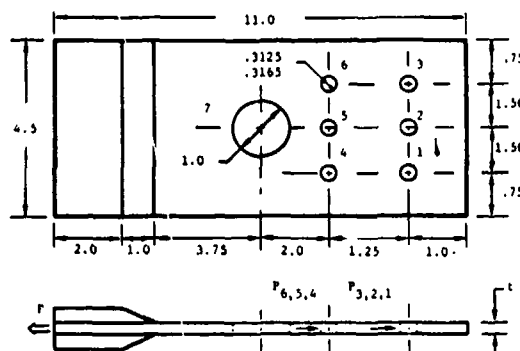
Test Case 230, Static Tension, Single-Shear  
 20-Ply, 30/60/10 Laminate,  $t=0.106$  in.,  $t_{AL}=0.31$  in.  
 $D=5/16$  in.,  $S_L/D=S_T=4$ ,  $W/D=10$ ,  $E/D=3$



	SAMCJ PREDICTION	TEST RESULTS
$P_1/P$	0.25	0.24
$P_2/P$	0.23	0.26
$P_3/P$	0.27	0.26
$P_4/P$	0.27	0.24
$P_{failure}$ (kips)	12.4 (12.8)	16.4
FAILURE LOCATION	4 (3)	3, 4
FAILURE MODE(S)	NET SECTION	NET SECTION, DELAMINATION

Figure 16. SAMCJ Predictions and Test Results for Test Case 320 ( Ref.6 ).

Test Case 243, Static Tension, Single-Lap  
 40-Ply, 50/40/10 Laminate,  $t=0.247$  in.,  $t_{AL}=0.50$  in.  
 $D=5/16$  in.,  $H_D=1$  in.,  $S_L/D=S_T/D=4$ ,  $W/D=14.4$ ,  $E/D=3.2$

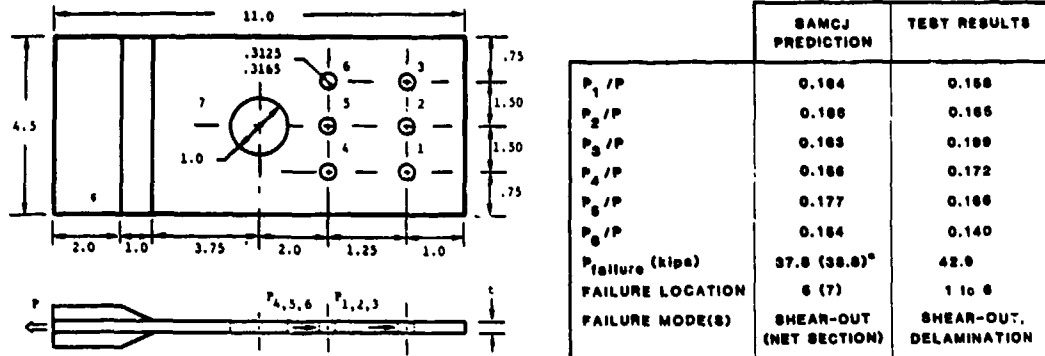


	SAMCJ PREDICTION	TEST RESULTS
$P_1/P$	0.164	0.162
$P_2/P$	0.161	0.160
$P_3/P$	0.163	0.168
$P_4/P$	0.168	0.177
$P_5/P$	0.178	0.161
$P_6/P$	0.167	0.165
$P_{failure}$ (kips)	38.3 (63.7)*	42.0
FAILURE LOCATION	7 (6)	7 and 4, 5, 6
FAILURE MODE(S)	NET SECTION (NET SECTION)	NET SECTION

\* Next possible failure mode and location at a higher load level

Figure 17. SAMCJ Predictions and Test Results for Test Case 243 ( Ref.6 ).

Test Case 246, Static Tension, Single-Lap  
 40-Ply, 70/20/10 Laminate,  $t=0.236$  in.,  $t_{AL}=0.50$  in.  
 $D=5/16$  in.,  $H_D=1$  in.,  $S_L/D=S_T/D=4$ ,  $W/D=14.4$ ,  $E/D=3.2$



\*Next possible failure mode and location at a higher load level

Figure 16. SANCJ Predictions and Test Results for Test Case 246 ( Ref.6 ).

Test Case 250, Static Tension, Double-Shear  
 40-Ply, 50/40/10 Laminate  $t=0.241$  in.,  $t_{AL}=0.38$  in.,  
 $D=5/16$  in.,  $S_L/D=4$ ,  $W/D=4.8$ ,  $E/D=3.2$

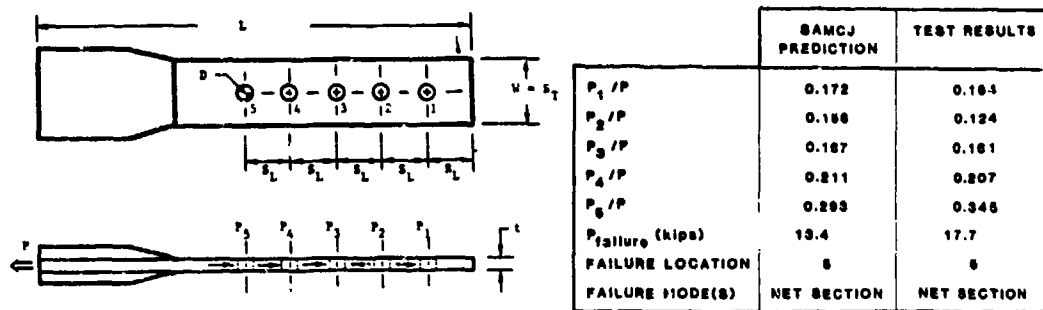


Figure 19. SANCJ Predictions and Test Results for Test Case 250 ( Ref.6 ).

## Typical Joints in a Wing Structure

Dieter Rose  
Manager of Technology Programs, Dornier GmbH

Dr. Manfred Rother  
Manager of Structural Analysis for Advanced Composites  
Dornier GmbH

Helmut Schelling  
Department Manager at the Institute for Structures and Design  
DFVLR Stuttgart

### Abstract

For the development of the Alpha-Jet CFRP wing typical connections between different components were examined both theoretically and experimentally; By doing this environmental conditions - component humidity and temperature - were considered mainly within the experimental work which was performed by the DFVLR-Stuttgart.

This paper covers typical joints such as:

- single-shear connection between skins and spars with low load transfer;
- joints between skins and ribs due to interior tank pressure;
- multi bolt joint between the CFRP skins and the fuselage attachment fittings with reference to
  - bolt strength distribution
  - bearing stresses

### Introduction

In a research contract, which was sponsored by the German Ministry of Defense Dornier developed and built a CFRP wing for the version "Close Air Support" of the Alpha-Jet for ground testing.

While the surrounding parts - leading edge, wing tip, trailing edge sections - and the mobile parts - flap, aileron - were taken from the series, the components of the torque box except for the metal ribs are from first generation composite materials Code 89/T300 with Fibre-rite 878/T300 as backup-system. The CFRP components are the stringer-stiffened upper and lower shells as well as the integrally stiffened front, middle and rear spars; all components were manufactured in-situ in monolithic construction method (fig. 1).

The wing-fuselage connection is made by a metallic multi-bolt joint ("Piano-Joint"). The attachment fittings are connected with the stringers and the skin with double-shear bolts.

The torque box comprises an integral tank, whose filling pressure amounts to 2,0 bar and its supply pressure to 0,83 bar; to the latter the liquid pressure from roll manoeuvres is to be overlaid, so that in the area of the tank endrib a resulting pressure of 2,24 bar is to be taken care of for the structure.

The requirements for the wing result from the requirements for the airplane. Environmental conditions result from the aircraft requirements which are to be considered

- Service temperature  $-55 < T [^{\circ}\text{C}] < 70$
- Component humidity : saturated humidity resulting from 85% relative humidity (conditioned state)

As critical were considered

- Joint between skin and spar with high by-pass or low load transfer ratio
- Joint between skin and ribs subject to interior tank pressure
- Joint between skin and fuselage attachment fitting

These were examined primarily experimentally in close collaboration with the DFVLR Stuttgart (fig. 2). All tests were performed with Zwick universal test equipment which is equipped with insertable climate chambers.

### Joint between Skin and Spars with Low Load Transfer

#### Introduction

This joint combines skins and sub-structure to a compound section. It prevents relative movements between the elements to be connected and thus enforces that the spars carry parts of the bending moments. A shear flow in the joint relieves the skin and loads the spar (fig. 3)

Fulfilling the equilibrium and deformation conditions for the skins and the wing sub-structure leads to the shear flow which is to be transferred by the joining elements. This shear flow and the normal force flow in the skins define the by-pass- or the load transfer ratios; the wing structural analysis performed by the FEM-method yields

- the by-pass-ratio to 80%
- the load transfer ratio to 20%

The load transmission behaviour of this single-shear joint for tension and compression loading was to be determined by a set of samples adapted to the designed framework and tested under different test conditions; these test conditions were derived from the environmental conditions:

- temperatures [°C]: -55; 23; 50; 70; 90; 110; 120;
- component humidity: unconditioned state (normal humidity),  
conditioned state.

#### Derivation of the Test Specimen

As laminate layups and thicknesses for skin and spar flange are given as well as bolt types the sample could be defined by its width and by its length only. The requirements for compatibility for the force equilibrium and the deformations lead to the sample presented in fig. 3. The realistic assembly conditions are represented by the installation of a shim-layer and a surface sealing in the joint area. The joint was accomplished by a titanium countersunk bolt with defined torque and a fit H7/f7 representing a play fit. For the check of the load distribution the sample was equipped with a sufficient number of strain gages.

#### Test Performance

In compression as well as in tension tests a strain gradient in the sample thickness which is due to the asymmetric structure of the sample, was observed. This indicates an inadvertent bending moment, caused by the eccentricity of the neutral axis in the sample. It could not even be prevented by the introduction of an antibuckling device /1/.

The influence of eccentricity and bending also expresses itself in a movement of the bolts. This is demonstrated by a pointer which is connected to the bolt in an extension of its axis (see fig. 4). This unexpected deformation was not taken into account in the design of the sample geometry. The additional flexibility of the joint leads to a reduction of load transfer.

#### Test Results

##### *Specimen under Compression*

The direct consequence of this sample insufficiency was an early failure of the samples subject to compression due to the bending load at the transition to the thickening of the skin laminate. Therefore no statement for load transmission under compression is possible (see fig. 5).

##### *Specimen under Tension*

The evaluation of the tension samples does not permit a statement with reference to the bearing failure, since all samples failed in the bonded area of the skin (see fig. 5). This result corresponds to the new conditions. The reduced rigidity of the joint causes a reduction of the load transfer of approximately 50% based on the evaluation of the strain measurements. Thus the bearing loads are reduced by also 50%, the by-pass-loads however increase by approximately 11% (see fig. 6). Therefore the bearing stresses reach an uncritical level, while the notch stresses rise to a critical level.

The obtained test data confirm the experiences, which were obtained from standard notched test specimen, showing that the rupture loads increase with increasing test temperature. The worst case proved to be at -55 C test temperature. It is notable that the failure load at high temperatures and with conditioned specimen does not decrease more clearly despite the proximity to the glass transition temperature  $T_G = 135^\circ\text{C}$  (fig. 7).

### **Joint between Skin and Ribs under Tank Pressure Load**

#### Introduction

The torque box is loaded by tank pressure (fig. 8). Due to the small airfoil curvature the tank pressure has to be transferred primarily by bending and shear from the skins to the ribs; the ribs balance the loads from the upper and lower shells. For stringer stiffened shells a girder grid can be used as a model for the load transmission behavior (fig. 9). This means that a continuous strip of the skin transfers the tank pressure to the stringer profiles which on their own are continuous bending members and transfer the proportional load to the ribs. Depending on the field between two neighbouring ribs and frames the connection forces of a stringer vary between 250 and 750 daN.

These loads must be transferred through the joint between skin and rib by riveting. On the one hand the bolts are subject to tension, on the other hand the laminate must have sufficient strength to prevent the pulling-through of the bolt.

#### Test Performance

An extensive test programme was performed for relevant combinations of bolt and laminate types (fig. 10) with the goals to determine

- influence of fiber material and bolt type
- temperature and ageing influence
- typical failure modes
- manufacturing influence
- design recommendations
- design allowables

For the basic investigations which were intended only to derive tendencies the number of samples was held deliberately small. On the other hand the design allowables were determined from the hardest test conditions from 6 samples each of 2 batches with a statistic security sufficient for this research programme.

### Test Facility and Test Specimen

The tests were carried out with simple flat test specimen for three different bolt types - screw bolt, sealing screw, lock bolt rivet. The specimen size depends on the bolt diameter, on the rivet pattern as well as on the flange width of the ribs; the sample thickness depends on the bolt diameter, in any case a minimum on the bolt shank should lie in the laminate (fig. 11/2/1).

### Test Results

Referring to the criteria mentioned above the results are commented in the following.

#### *Influence of the prepreg systems and the environment conditions*

In fig.12 the results of three different samples against the environmental conditions are presented. These samples are manufactured from Code 89 with 40 % prepreg resin content and Fiberite 878 with 40% or 34% prepreg resin contents.

The comparison between samples from the resin system Fiberite 878 with the two prepreg resin contents shows practically no difference in the results; bleeding off excessive resin at the 40%-system yields a resin content in the cured laminate which is similar to the one in the 34%-prepreg. A comparison between the resin systems Code 89 and Fiberite shows slight advantages for Code 89 with the exception of the test temperature -55°C. The most critical condition in the service spectrum proved to be the test temperature 70°C with conditioned samples; this can be explained with the larger flexibility and the reduced shear strength at high temperatures and with conditioned samples.

#### *Influence of bolt types and laminate thickness*

The influence of the bolt type - screwed rivet, sealing screw - is not very marked despite the clear differences in the shaping of the rivet heads (fig. 13); in tendency the screwed rivet appears to be more favorable.

#### *Failure Modes*

A comparison of the test results for screwed rivets of the 4 and 6 mm diameter in different laminate thicknesses (fig.14) shows some characteristic differences.

The failure takes place by delaminations between the individual plies, starting at the walls of the bolt holes, comparable to the shear failure of a short cantilever beam. Often the delaminations start at the transition from the cone-shaped to the cylindrical part of the drilling. Comparing the test results of specimens with the same diameter the laminate thickness is of major influence, especially the thickness in the cylindrical part of the drilling. The loadbearing capacity decreases with decreasing laminate thickness. This is in particular true for the thinnest 2.125 mm sample where after the first crack a pull-through of the bolt could be observed. After that the load could still be increased but to an insufficient level. With this sample practically no influence from environment conditions is recognizable due to the failure mode.

#### *Manufacturing Influence*

The features mentioned here are enhanced by the results of samples with defective drillings on the one hand and with drillings after second treatment on the other hand, in each case compared with intact drillings (fig.15). The pull-through strength is reduced substantially with defective drillings due to the roughness or the oversize in the countersink; additionally treated drillings do not reach pull-through strength of intact samples.

#### *Design recommendations and design allowables*

In principal there are the three failure modes

- laminate shear failure
- rivet head pull-in
- bolt shear-off

Bolt shear-off never occurred and is thus uncritical. The first two failure modes have to be taken care of by suitable choice of rivet diameter and laminate thickness.

The failure load for shear failure can fairly reliably be determined by the formula

$$F = \pi \times 3/2 \times T_{ILS} \times A \times t$$

Pull-in of the bolt can be prevented by a sufficient thickness of the cylindrical part of the drilling. Following the experience of this programme this can be achieved by fulfilling the following relation:

$$1 < d/t < 1.5 \\ 0.2 < (t - B)/t \text{ with } t \geq 0.6 \text{ mm}$$

Fig.16 lists the design allowables for the bolt types and laminates used for the CFRP wing. Finally it should be mentioned that for aluminum alloys with comparable dimensions the bolt pull-through values are much higher - up to factor 2 - than the values found here.

This design philosophy was realized and proved in a larger tank box which was tested at the DFVLR under tank pressure and compression and tension alternatively /3/.

### **Joins between CFRP-Skins and Al-Fittings**

Basic investigations have been performed in order to evaluate experimentally and theoretically the distribution of shear forces of multi row bolted joints/4/. Figure 17 shows the connection between the real panel- fitting-joint and the test specimen.

Three types of specimens of a double lap joint have been defined:

Type	Thickness	
	Laminate	Al-strips
I	constant	constant
II	constant	conical
III	conical	conical

The following two laminates were taken into account:

Material	Layup 0°/±45°/90°	Thickness mm	Application Type of spec.
T300	47/47/8	8,4	I, II
Code 88	28/50/28	8,0	I, III

So four configurations were available with at least three specimens in each case. For each specimen five bolts maximum were provided. Fig.18 shows the types of specimens and the arrangement of strain gauges. The bolt diameter and the distance between two neighboring bolts were equal in all cases. With that the remaining parameters were:

bolt number  
bolt fit  
bolt prestressing  
laminate layup

First of all two specimens of type I.1 and I.2 resp. were tested in order to study the influences of fit and prestressing. Finally some specimens were loaded in tension up to failure.

All tests were performed at normal humidity and room temperature.

The experimental results were compared with theoretical distributions of shear forces, evaluated by finite element method and a rod-model as well.

### Test performance

Except for the rupture tests, the load was limited to 30 KN in order to avoid premature damage. The tests were always started with five bolts and repeated with four and three bolts respectively. The normal forces in the Al-strips between every two bolts were evaluated by integrating the strains measured in the upper Al-strip:

$$F_B = \int E\epsilon(y) dy = f \times E I (b/11) \sum \epsilon_i$$

The factor  $f$  has been defined as

$$\text{e.g. } f = (\epsilon_{26} + \epsilon_{30})/2\epsilon_{26} \text{ (s.fig. 19) s.t.c.}$$

to correct any unavoidable bending effects. The shear forces result from the differences of the normal forces in the Al-strips on both sides of each bolt. These values were related to the overall tension load for better comparison of the results.

### First tests on two specimens

Two specimens of type I.1 and I.2 respectively were tested first in order to study the influence of fit and prestressing of the bolts. At the beginning the fit which had been chosen was

H11/7 i.e. 13./118µ tolerance

and the titanium bolts were not prestressed.

#### Variation of fit

The first results did not indicate any parabolic distribution of the shear forces as they had been expected to be. So all holes were measured and steel bolts (115 Cr V3) were manufactured in such a manner that the fits

H8/7 i.e., 13 ./ 50µ tolerance  
H7/h8 i.e., 0 ./ 24µ tolerance

could be realized. Fig.20 shows that the influence of the fit is small (the change of bolt material proved to be without any important influence too).

#### Influence of prestressing

Thereupon the bolts were prestressed by a torque of 12 Nm, and the tests were repeated. Fig.21 shows the results with and without prestressing for the same specimen: There can be seen clearly a parabolic shear force distribution.

#### Influence of the laminate layup

Fig.22 shows the shear force distribution of several specimens of type I.1 and I.2 respectively (mean values). The fit and the tightening torque were the same in all cases. The influence of the laminate layup proved to be small.

### Tests on all specimens

The further tests on all specimens were performed under the same conditions with regard to fit and prestressing. Fig.23 shows the mean values of all measurements at 30 KN and the curves enveloping all these distributions as well. The bandwidth including the specimen geometry as well as the two laminates is between 3% and 9% of the relative shear forces.

### Comparison of theory with experiment

Besides the investigation of shear force distribution by tests, comparisons with theoretical predictions have been done, that is prediction by means of

- finite element model
- rod-model

### Finite element model

A finite element model was built up for the type 1.1 specimen. The first calculations were carried out with the assumption of rigid bolts.

Subsequently the bolts were modeled by membrane elements with differentiation between the load carrying and the non load carrying side of the bolts. This model was applied to a specimen with five bolts. There were only small deviations compared with the assumption of rigid bolts. The results are shown in Fig.24

### Rod model

This one-dimensional model describes the compatibility between the deformed members of a joint within the distance of every two bolts  $/S/$ . In the case of  $n$  bolts this leads to  $n-1$  compatibility equations and one equilibrium equation. For a double lap bolted joint this can be written as

$$\begin{bmatrix} C_{m,n} \\ 0 \end{bmatrix} \cdot \begin{bmatrix} N_m \\ -N_n \end{bmatrix} = \begin{bmatrix} C_{L,m} \\ -0.5 \end{bmatrix} \cdot F$$

with

$C_{m,n}$  = compliances of the members of the joint  
 $C_{L,m}$  = compliances of the laminate only  
 $N_m$  = normal forces in each of the two Al-strips  
 $F$  = applied total force

This system of equations can be solved for the unknown forces  $N_m$ . The bolt forces will be received out of the difference of the forces  $N_m$ .

Because of the difficulty to estimate the bolt compliances  $C_B$ , the well-known compliances of the Al-strips and of the laminate were introduced into the equations for a three-bolt-joint of type 1.2 as well as the measured forces in the Al-strips. These equations were solved for the unknown values  $C_{B,n}$  ( $n = 1,2,3$ ). The mean value was

$$C_B = 9.1 \times 10^{-6} \text{ mm/N (steel bolts)}$$

This value was kept constant for all the bolts in re-calculating all test specimens. For comparison with the FEM calculation the results for type 1.1 specimen are figured in Fig.24 too. This figure also contains the bandwidth of the test results out of fig.23. The correspondence is satisfactory.

### Rupture tests

Some specimens were loaded up to rupture, which always occurred in the laminate, that is in the plane of the first bolt. The remaining parts were joined once more by two bolts (holes 4 and 5 of the laminate to holes 1 and 2 of the Al-strips). These additional specimens were also tested at 30 KN and at about 80 KN before being loaded up to rupture. The relative shear forces are listed in fig.25.

When the load increases, the shear force distribution becomes more well-balanced: the force transferred by the first bolt decreases while the share of the last one increases. In the case of two bolts only, the last bolt even transfers the higher load.

Figure 26 shows the ultimate loads of all the rupture tests. The stress concentration factors likewise being included in this figure group around two mean values; the larger one ( $\alpha = 1.83$ ) characterizes the orthotropic laminate, while the smaller value ( $\alpha = 1.58$ ) belongs to the quasi-isotropic laminate.

### Conclusion

In the beginning the tests led to shear force distributions which were unsatisfactory and in part hardly interpretable. Only the prestressing of the bolts led to the parabolic distribution that had been expected. All tests under the condition of a tightening torque of 12 Nm and the bolt fit H8/7 provided the following results:

- The influence of specimen geometry as well as of the laminate layup is small
- With increasing number of bolts the shear force transferred by each of the middle bolts decreases. At the same time there is a load reduction of the two outer bolts.
- At a moderate load level (i.e. linear strains) there is a satisfactory correspondence between tests and theory. At this level it is always the first bolt that transfers the highest load.

All types of specimen	Number of bolts	Shear force (%)		Number of tests
		1.bolt	last bolt	
specimen	2	80-58	42-30	5
	3	45-48	21-25	10
Moderate load level (30kN)	4	41-47	13-22	11
	5	40-44	9-15	12

- In approaching the ultimate load the shear force distribution becomes more balanced with decreasing load transfer of the first bolt and increasing load transfer of the last one. In the case of two bolts only, the last bolt even transfers the higher load

All types of specimen	Number of bolts	Shear force (%)		Number of tests
		1.bolt	last bolt	
specimen	2	42-49	51-58	5
	3	37-45	21-27	3
Ultimate load	4	38	18	1
	5	30-38	13-21	2

**References**

- 1/ H.Kraß/H.Schelling    Statische Belastungsversuche an gebolzten Fügungen mit 20%-igem Load Transfer  
DFVLR-Bericht IB 435-4/87
- 2/ H.Kraß/H.Schelling    Nietdurchzugsversuche an CFK-Verbundwerkstoffen  
DFVLR-Bericht IB 435 3/87
- 3/ D.Rose et al.          Design of a CFRP-Wing for the Alpha-Jet/Major Panel Tests  
Journal of Aircraft Vol.23/Number 6/June 1986
- 4/ M.Rother et al.        Dornier Report IB 3885/Mai 1982
- 5/                            Advanced Composites Design Guide Vol.II/1973

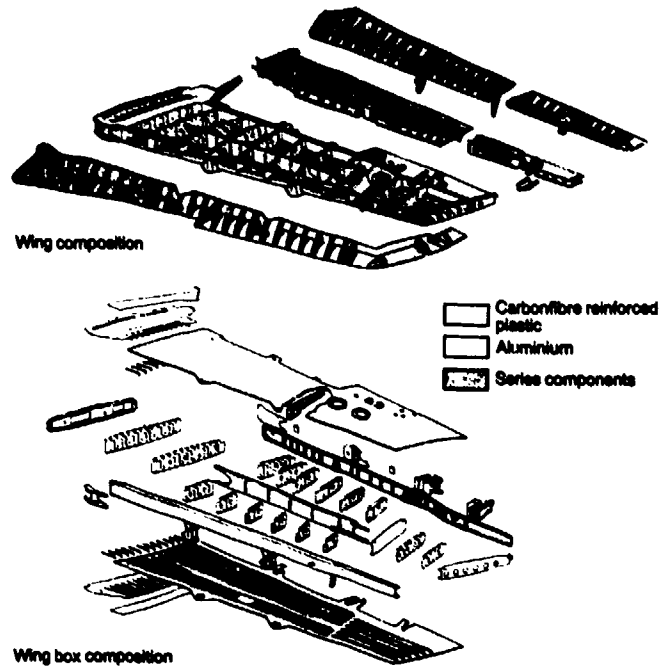


Fig. 1 Wing and Wing Box Composition

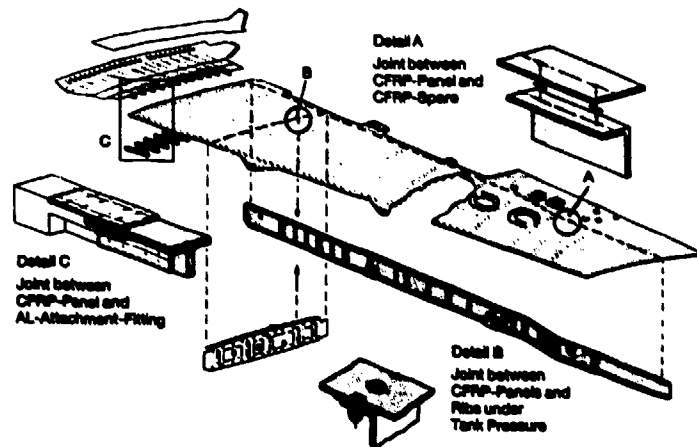


Fig. 2 Typical Joints at the Wing Structure



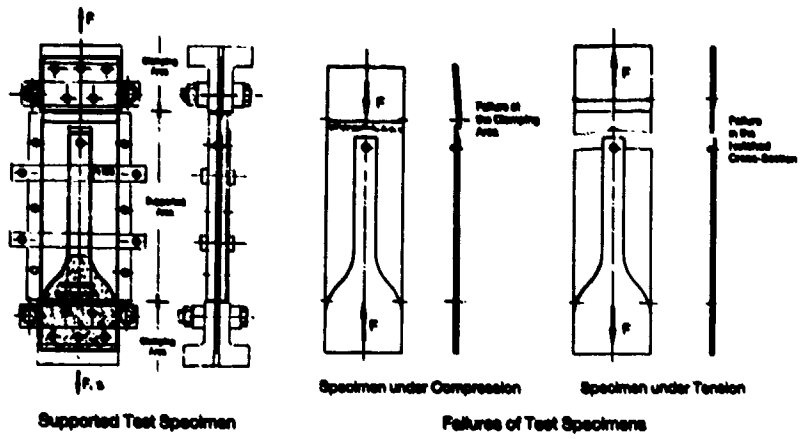


Fig. 5 Panel-Spar-Joint Supported Test Specimen and Its Failures

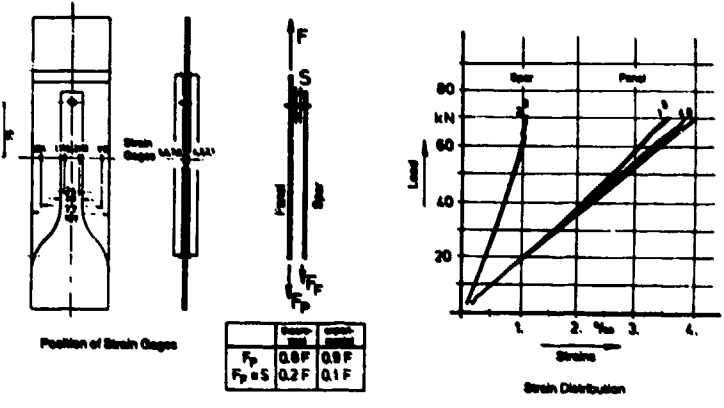


Fig. 6 Panel-Spar-Joint Evaluation of Load transfer

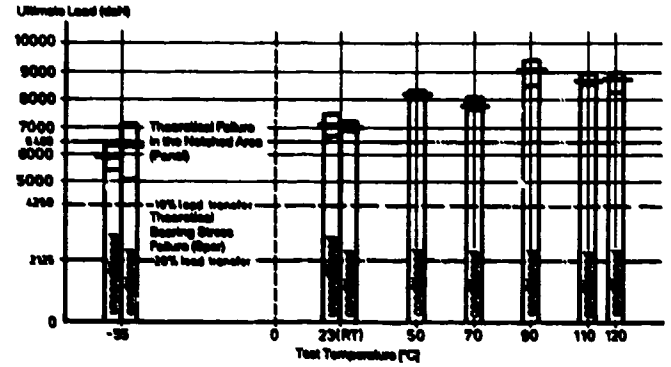


Fig. 7 Panel-Spar-Joint Test Result



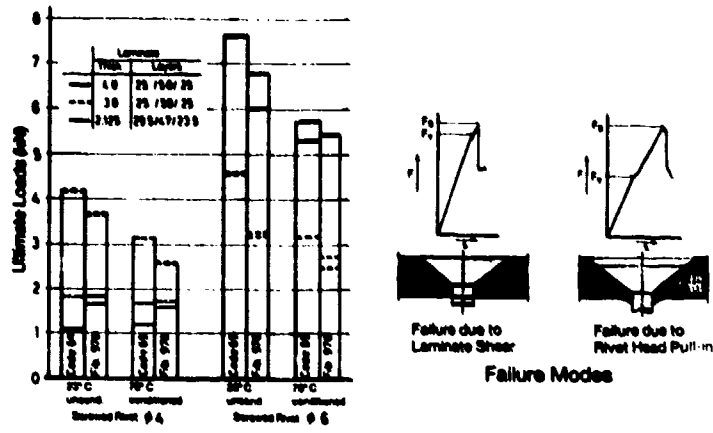


Fig. 14 Panel-Rib-Joint Comparison of Test Results for Bolt Diameter versus Thickness and Failure Mode

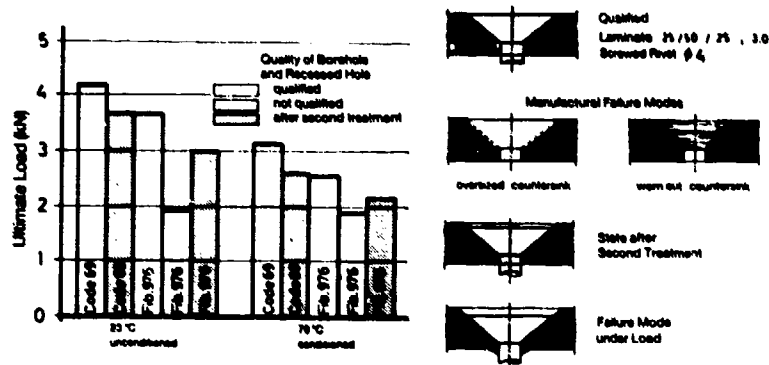


Fig. 15 Panel-Rib-Joint Influence of the Quality of Bore and Recessed Holes on Load Capacity

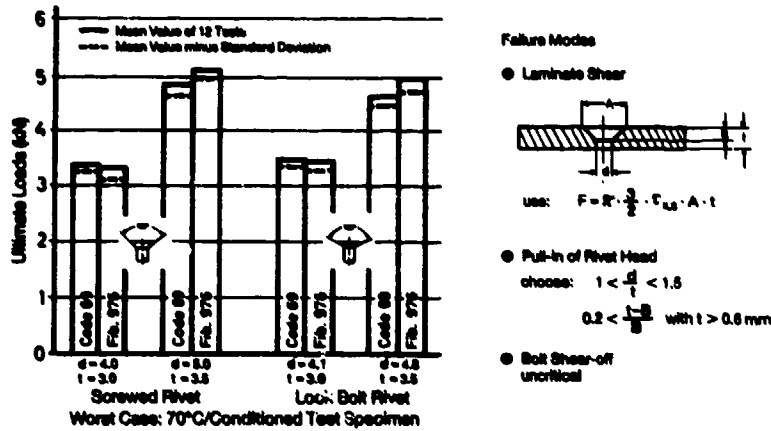


Fig. 16 Panel-Rib-Joint Design Allowables and Recommendations for Design

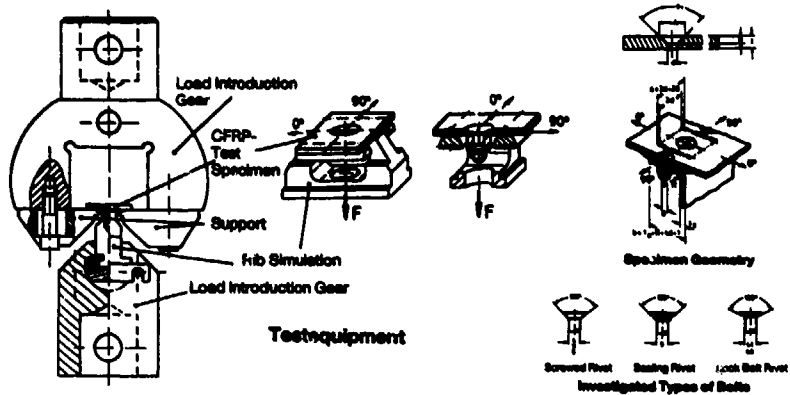


Fig.11 Panel-Rib-Joint Testequipment and Specimen Geometry

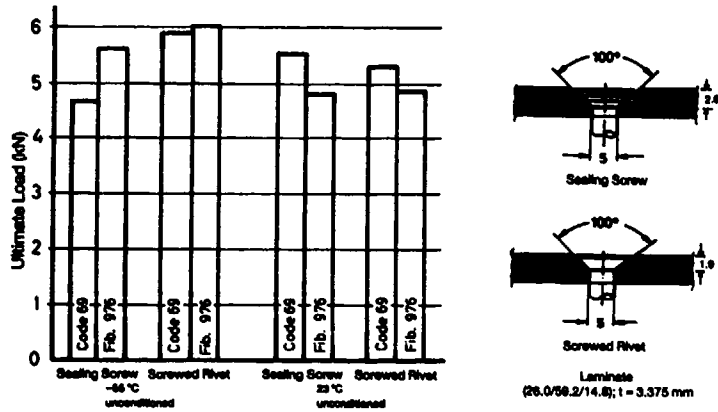


Fig.13 Panel-Rib-Joint Comparison of Test Results for Sealing Screw and Screwed Rivet

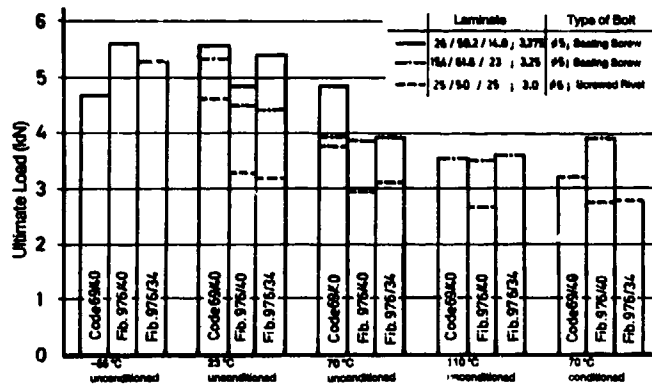


Fig. 12 Panel-Rib-Joint Influence of Resin-Systems with Different Test Specimens versus Test Conditions

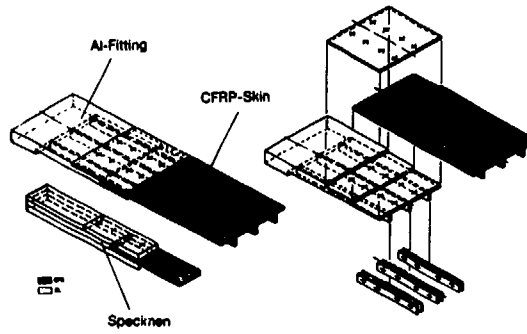


Fig. 17 Panel-Fitting-Joint Skin to Fitting Attachment (Schematic)

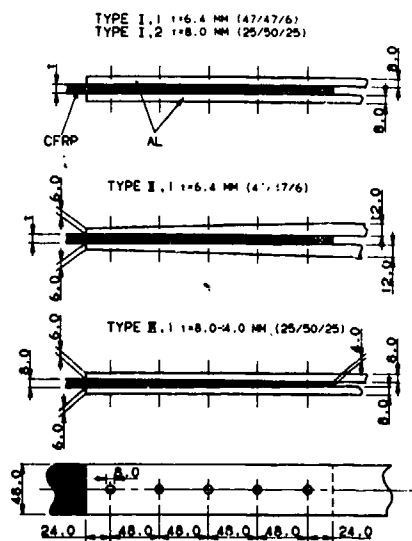


Fig. 18 Panel-Fitting-Joint Types of Specimen

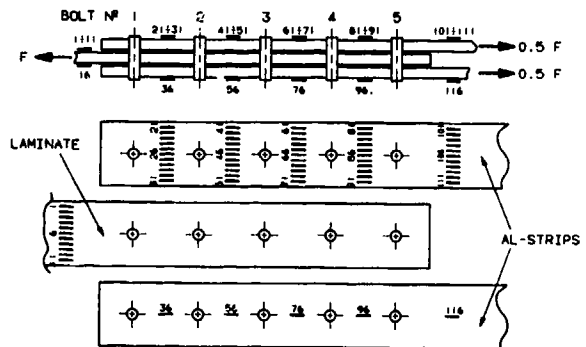


Fig. 19 Panel-Fitting-Joint Plan of Strain Gages

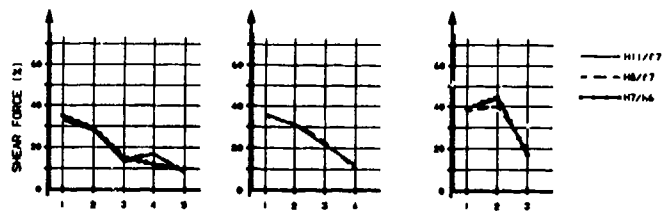


Fig. 20 Panel-Fitting-Joint Influence of Fit  
-Specimen Type I, 1  
-Torque = 0

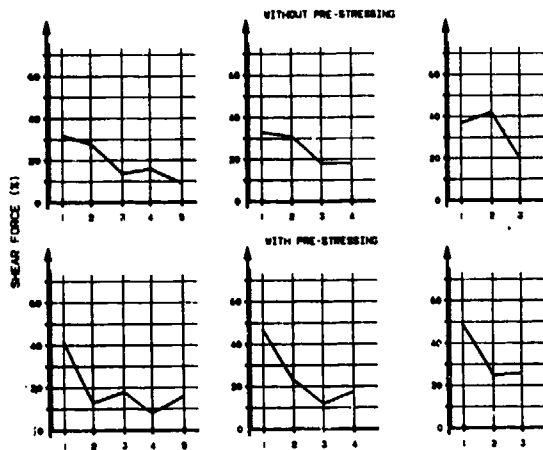


Fig.21 Panel-Fitting-Joint  
Influence of Pre-Stressing  
-Specimen Type I.2  
-Torque = 12 Nm

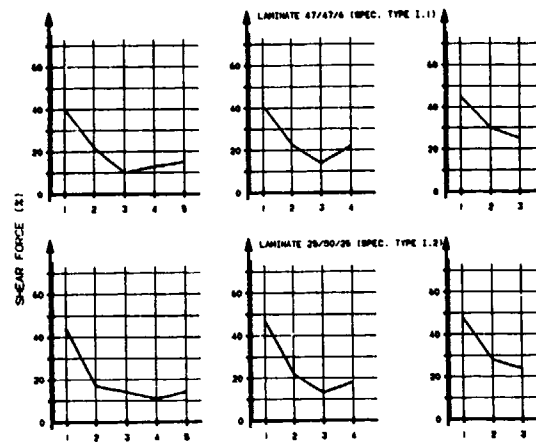


Fig.22 Panel-Fitting-Joint  
Influence of Laminate Layup (Mean Value)  
-Fit H8/I7  
-Torque = 12 Nm

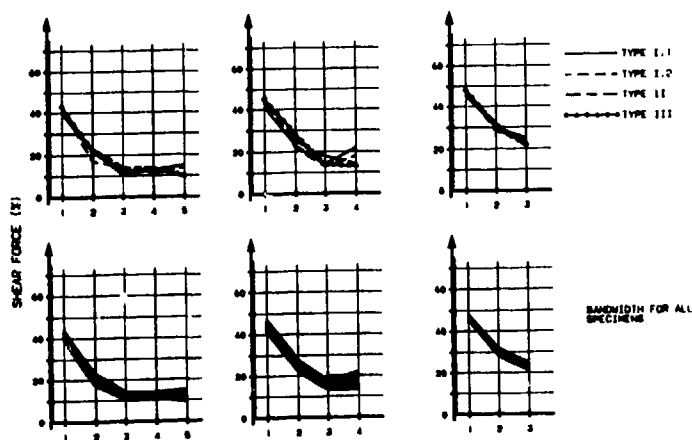


Fig.23 Panel-Fitting-Joint  
Influence of Specimen Geometry (Mean Values)  
-Fit H8/I7  
-Torque = 12 Nm

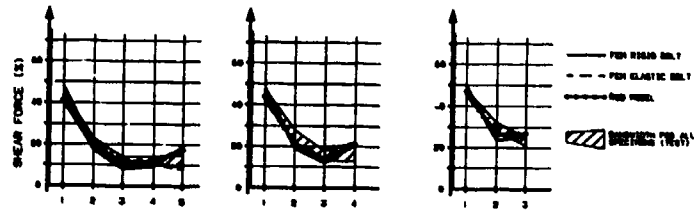


Fig.24 Panel-Fitting-Joint  
Comparison of Theory with Experiment  
-Fit H8/F7  
-Torque = 12 Nm

Type of Specimen	Test N°.	Load (kN)	Shear force (N)	
			1. Bolt	2. Bolt
I,1	1	30	80	80
		80	48	84
I,2	2	30	84	48
		80	42	80
I,2	3	30	80	42
		80	42	80
II	4	30	82	48
		80	45	88
II	5	30	77	80
		78.5	47	83
III	6	30	86	44
		70	49	81

Fig.25 Panel-Fitting-Joint  
Tests on Specimen with 2 Bolts

Type of Specimen	Test N°.	Number of bolts	F <sub>ul</sub> (kN)		F <sub>ul, Theor.</sub> / F <sub>ul, Test</sub>	σ̄
			Test	Theory <sup>*)</sup>		
I,1	1	3	80.7	181.8	1.71	1.83
	2	2	80.7		1.80	
	3	3	81.2		1.87	
	4	2	86.3		1.76	
II	5	4	81.5	1.86		
	6	2	77.8	1.85		
	7	3	80.1	1.78		
	8	2	81.8	1.86		
I,2	9	3	87.2	132.5	1.82	1.88
	10	2	82.3		1.81	
	11	3	85.0		1.88	
	12	2	82.4		1.88	
III	13	3	80.4	89.4	1.83	
	14	2	76.1	128.8	1.88	

<sup>\*)</sup> relative to net cross section

Fig.26 Panel-Fitting-Joint  
Ultimate Loads

MISE AU POINT D'ELEMENTS DE  
FIXATION SPECIFIQUES POUR ASSEMBLAGES DES  
STRUCTURES COMPOSITES

par Monsieur LOUIS Raymond - SERVICE TECHNIQUE DES PROGRAMMES

AERONAUTIQUES

4, Avenue de la Porte d'Issy - 75015 PARIS - FRANCE

RESUME

La réalisation des assemblages en matériaux composites doit tenir compte des singularités inhérentes à la nature des matériaux utilisés, par exemple, le délaminage, l'endommagement par choc et/ou gonflement, la corrosion galvanique etc...

Plusieurs actions ont été entreprises pour mettre au point des éléments de fixation spécifiques susceptibles de limiter certains des problèmes rencontrés dans ces assemblages. Elles concernent :

- le développement d'un rivet semi-tubulaire "anti-peeling" en titane T.40 pour structures "non travaillantes". Sa géométrie et ses caractéristiques permettent une pose facile tout en ménageant les matériaux assemblés.

- la réalisation d'écrous en cage interchangeable fixés par collage par l'intermédiaire d'une bande en fibre de verre. Les avantages sont d'éviter le perçage multiple et le rivetage, comme pour les bandes d'écrous prisonniers classiques, de s'adapter à des profils complexes et de permettre le remplacement aisé des écrous.

- la modification de fixation existantes (vis et rivets structuraux) afin d'améliorer les caractéristiques mécaniques des assemblages. En particulier la variation de l'angle de tête de 100° à 130 °permet un gain sur la tenue en cisaillement et en fatigue des assemblages.

L'utilisation d'éléments de fixation classiques pour l'assemblage des C.F.R.C. a révélé, dans les conditions habituelles de fabrication un certain nombre de difficultés liées à la spécificité des matériaux composites.

- délaminage des fibres, limitant les montages serrés ;
- endommagement dû au choc et/ou au gonflement, ce qui rend délicat l'utilisation de rivets ;
- corrosion galvanique, ce qui implique un choix de matériaux non corrodables par le composite carbone (titane ou aciers inoxydables) ;

- conductivité électrique et dilatation thermique différentielle.

Afin de résoudre certains de ces problèmes, le Service Technique des Programmes Aéronautiques a piloté plusieurs études ponctuelles destinées à mettre au point des éléments de fixation spécifiques pour l'assemblage des composites carbone-résine susceptibles de remédier, dans certains cas, aux difficultés rencontrées.

Parmi ces études, nous citerons :

- le développement d'un rivet semi-tubulaire "anti-peeling" en titane T-40 pour structures non travaillantes ;
- la réalisation d'écrous en cage interchangeables fixés par collage par l'intermédiaire d'une bande en fibre de verre ;
- la modification de fixations existantes (vis et rivets structuraux).

#### 1. - RIVET SEMI TUBULAIRE "ANTI-PEELING"

Il s'agissait de définir un rivet utilisé au niveau des assemblages considérés comme non-travaillants et ayant pour rôle essentiel un effet anti-peeling (figure 1).

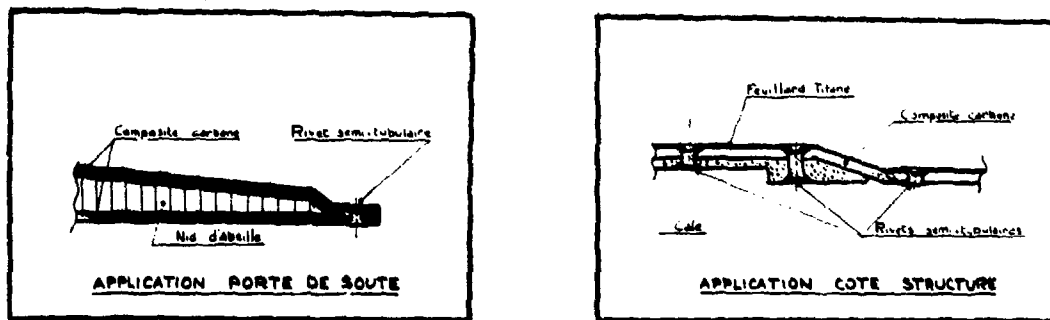


FIG. 1 : Exemples d'utilisation

Le rivet devait répondre en particulier aux impératifs

suivants :

- ne pas détériorer le composite au cours de la pose du rivet,
- avoir une bonne tenue en corrosion galvanique,

et sa géométrie devait permettre :

- une même forme d'usinage de chaque côté des éléments à assembler (fraisure),
- une plage de serrage de 1 mm environ,
- une résistance mécanique suffisante,
- une pose sans gonflement du rivet.

#### Définition

Le matériau choisi en fonction de sa bonne tenue en corrosion galvanique par rapport aux composites carbone-résine est le titane T-40, matériau déformable à froid.

La géométrie du rivet avant pose est donnée par la figure 2.

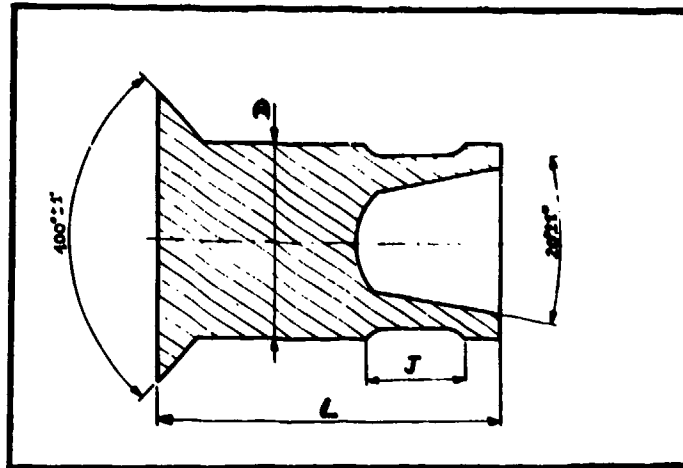


**FIG.2** : Géométrie du rivet

C'est un rivet tête fraisée 100°, hauteur réduite, qui présente deux particularités :

- un trou borgne conique, d'angle au sommet 20°, situé côté tête à former,
- une gorge périphérique sur la surface extérieure de la tige au niveau de la partie tubulaire.

L'évidement, côté tête à former, permet de diminuer l'effort de pose.

La gorge circulaire a deux fonctions :

- protéger l'angle de raccordement entre la fraisure et l'alésage du trou de rivet,
- déterminer la plage de serrage du rivet.

De plus la présence simultanée de la gorge et du perçage

conique a pour avantage de créer une toile de moindre épaisseur permettant de localiser le pliage lors de la formation de la seconde tête.

### Caractéristiques

Les caractéristiques présentées ci-après concernent les résultats d'essais effectués sur des rivets de diamètre nominal = 4 mm.

### Caractéristiques de pose du rivet

La pose du rivet est facilitée par :

- la grande tolérance de la plage de serrage (1mm),
- la grande plage de pression de pose ( $\pm 100$  daN)
- la géométrie particulière de la bouterolle (figure 3) adaptée à celle du rivet et qui permet la pose sans pratiquement aucun gonflement du rivet.

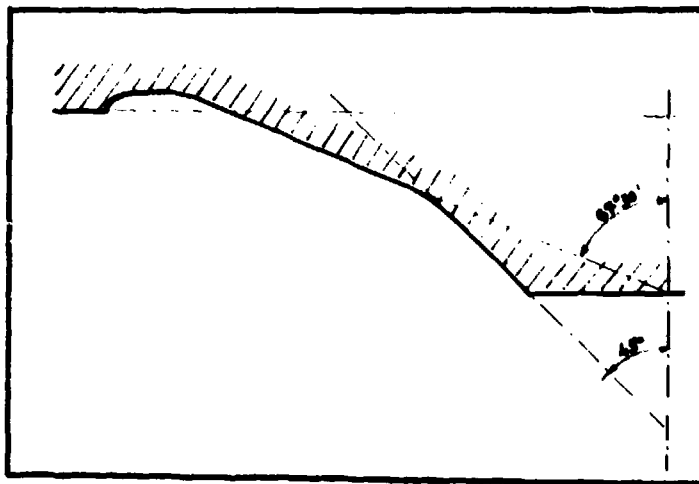


FIG.3 : Profil de la bouterolle

A noter que pour aider à la formation de la seconde tête du rivet il est recommandé de recouvrir les rivets d'un lubrifiant (alcool céthylique ou bisulfure de molybdène).

Pression de pose - Les essais de pose ont été effectués suivant une gamme de pression allant de 700 à 1100 daN.

On constate une bonne pose des rivets sans détérioration des matériaux composites, comme le montrent sur coupes micrographiques les figures 4-5-6 et 7 (seuls des défauts d'usinage du composite avant pose sont visibles).

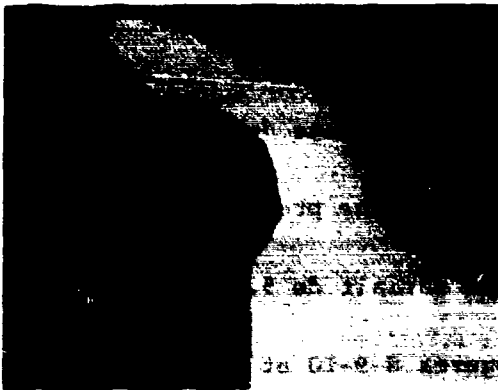


FIG.4 :

- pression = 700 daN  
- épaisseur = 5,1 mm

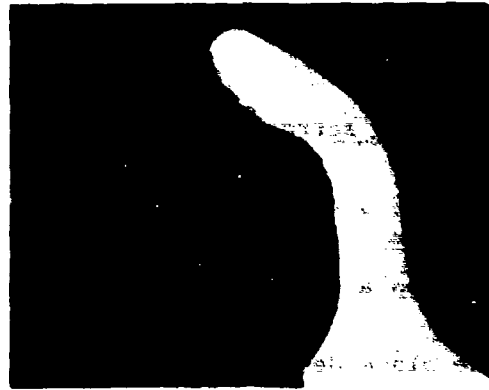
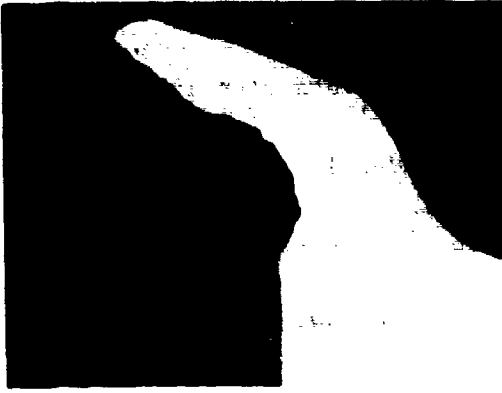


FIG.5 :

- pression = 700 daN  
- épaisseur = 6,1 mm



**FIG. 6 :**

- pression = 1000 daN  
- épaisseur = 5,1 mm



**FIG. 7 :**

- pression = 1000 daN  
- épaisseur = 6,1 mm

Suite à ces essais, la pression de pose retenue est de :

900 daN  $\pm$  100 daN.

Plage de serrage - La détermination de la plage de serrage

résulte d'essais de pose effectués, sous une pression de 900 daN, sur des assemblages dont l'épaisseur variait de 5,3 à 6,6 mm soit une plage de serrage de 1,3 mm (figures 8-9-10 et 11).

Les résultats sont satisfaisants pour les quatre épaisseurs, tant sur le plan de l'accostage que sur celui de l'endommagement du matériau composite.

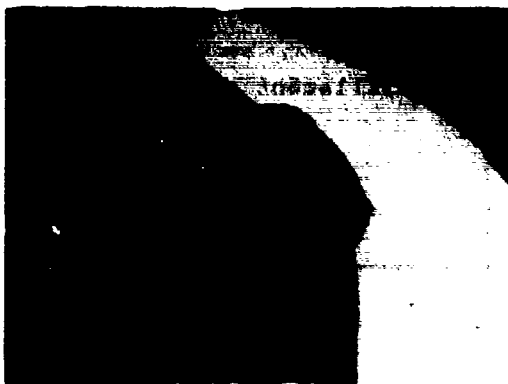


FIG.8 : épaisseur = 5,3mm



FIG.9 : épaisseur = 5,5 mm



FIG.10 : épaisseur = 6 mm



FIG.11 : épaisseur = 6,6 mm

Afin d'assurer dans tous les cas une pose correcte du rivet, la plage de serrage a été fixée à 1 mm.

Ceci permet en outre de définir des rivets dont l'épaisseur standard de pose est en millimètres (par exemple 4 - 5 ou 6 mm).

#### Caractéristiques mécaniques

Des essais de traction et de cisaillement ont été réalisés sur des plaquettes assemblées d'épaisseur dite faible, moyenne et forte, correspondant dans le cas présent à une épaisseur totale de 5,3 - 6 et 6,6 mm.

L'éprouvette de traction est définie figure 12. L'éprouvette de cisaillement est une éprouvette de cisaillement simple à 2 rivets.

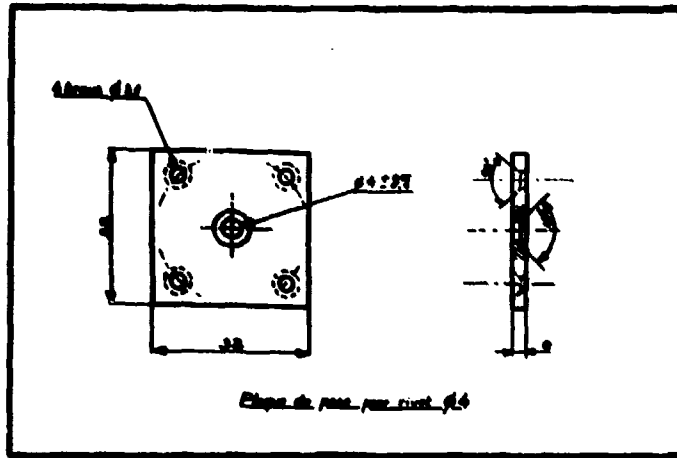


FIG.12 : Eprouvette de traction

Les caractéristiques propres du rivet sont déterminées sur des éprouvettes constituées de deux tôles en 2017 A.

Les résultats obtenus sont donnés dans le tableau I.

EPAISSEUR DES EPROUVETTES	CHARGE DE RUPTURE (daN)			
	TRACTION		CISAILLEMENT	
	MINI	MAXI	MINI	MAXI
FAIBLE : 5,3mm	260	285	895	940
MOYENNE : 6mm	220	238	795	850
FORTE : 6,6mm	162	192	750	778

TABLEAU I

De ces résultats on peut assurer comme caractéristiques du rivet les valeurs suivantes :

- charge de rupture en traction = 150 daN,
- charge de rupture en cisaillement = 350 daN.

Les caractéristiques de l'assemblage composite sont déterminées sur des éprouvettes en composite carbone T300-414 d'épaisseur 2,4 mm.

Les résultats obtenus sont donnés dans le tableau II.

EPAISSEUR DES EPROUVETTES	CHARGE DE RUPTURE (daN)			
	TRACTION		CISAILLEMENT	
	MINI	MAXI	MINI	MAXI
FAIBLE : 5,3mm	194	202	756	790
MOYENNE : 6mm	176	182	720	732
FORTE : 6,6mm	148	156	570	596

TABLEAU II

Les valeurs d'essais dépendent dans ce cas de la tenue du composite et non des rivets et on peut assurer comme valeurs limites :

- charge de rupture en traction = 110 daN
- charge de rupture en cisaillement = 260 daN.

A noter que le cisaillement dans l'assemblage n'est pas un cisaillement pur mais un compromis entre cisaillement et déboutonnage.

Parallèlement à l'étude du rivet, les outillages de pose ont été définis afin de vérifier la faisabilité des assemblages.

L'opération la plus importante est le centrage de la bouterolle de façon à éviter que celle-ci endommage le matériau composite.

La pose peut se faire soit :

- au Cé avec un vérin à double effet :
  - avance sous faible pression pour centrage,
  - déclenchement de la pression de pose lors du contact.
- avec un vérin à simple effet et une pièce désattelée permettant un centrage manuel avant la mise en pression.

Les rivets présentent d'autre part une très grande facilité de dépose à condition d'éviter la rotation du rivet. A cet effet un outillage spécifique a été conçu.

La gamme de rivets proposée comprend :

- les diamètres 3,2 - 4 - 4,6 et 5,6 mm, pour des longueurs de serrage comprises entre 4 et 25 mm,
- les diamètres 4/32 - 5/32 - 6/32 - 7/32 d'inch pour des longueurs de serrage comprises entre 5/32 et 1 inch .

L'étude a permis la mise au point d'un rivet qui convient bien à l'assemblage des composites. Les caractéristiques mécaniques obtenues montrent que c'est le composite qui dimensionne ces dernières.

La pose du rivet est extrêmement aisée et surtout celui-ci remplit parfaitement son rôle en ménageant les matériaux dans lesquels il est posé.

2. - ECROUS EN CAGE INTERCHANGEABLES FIXES PAR COLLAGE PAR

L'INTERMEDIAIRE D'UNE BANDE EN FIBRE DE VERRE

L'utilisation sur structures composites des écrous "non démontables" classiques (bandes à écrous prisonniers et écrous à river) se heurte, compte tenu des spécificités des matériaux composites, aux risques suivants :

- endommagement des composites, lors de la mise en place des fixations (perçages multiples pour les trous de rivet et pose des rivets),
- tenue en corrosion galvanique entre les écrous et les composites carbone.

Pour y remédier il fallait définir une géométrie de pièces permettant des reprises d'efforts adaptées aux composites carbone-résine et prévoyant un dispositif d'écrous démontables dont l'assemblage sur les structures soit différent d'un montage par rivetage. La solution adoptée est la mise au point d'écrous en cage interchangeables maintenus dans une bande en fibre de verre. Cette possibilité concerne aussi les écrous isolés

correspondant aux écrous à river classiques.

Le nouveau système de fixation est constitué de plusieurs éléments, (voir figure 13).

- un support en fibre de verre insérant la partie cage de l'écrou. Cette bande de fibre de verre, tout en maintenant les cages, réalise en même temps l'isolation galvanique de l'écrou par rapport aux composites carbone à assembler.
- un écrou, soit à freinage interne par déformation elliptique, soit élastique. Dans ce dernier cas le freinage se fait par un frein plastique, type ESLOK par exemple (dépôt de polyamide).
- un clip démontable permettant le maintien de l'écrou dans la cage.

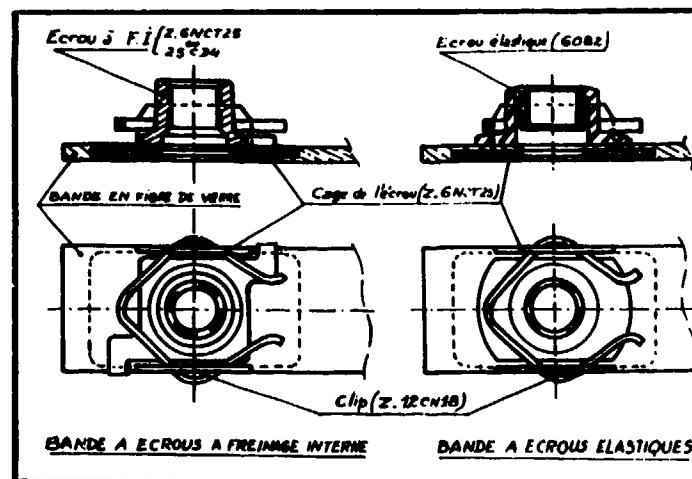


FIG.13 : Bandes à écrous

L'assemblage, sur les structures, des bandes à écrous ou des écrous isolés se fait par collage du support en fibre de verre sur le composite.

Le collage doit seulement pouvoir répondre aux sollicitations au montage ou au démontage des vis dans les écrous. Par contre il ne subit pratiquement aucune contrainte en fonctionnement.

Le système de fixation développé présente les avantages suivants :

- possibilité, à partir d'un même produit de base, de disposer de bandes à écrous multiples ou bien, après découpe adéquate de la bande, d'écrous isolés ;
- la bande étant fixée par collage, les opérations de perçage et de rivetage sont supprimées, évitant ainsi l'endommagement éventuel des composites ;
- la souplesse de la bande lui permet de s'adapter à des profils complexes. Elle peut également sur un même plan suivre, par découpe appropriée, un profil quelconque ;
- le maintien des écrous par clips facilite le remplacement d'écrous endommagés, mais offre en plus la possibilité de monter n'importe quel type d'écrou.

Plusieurs types d'écrou sont d'ailleurs prévus pour équiper les bandes :

- écrous élastiques en alliage d'aluminium 6082 anodisé,

écrous ayant la particularité de s'adapter aux variations éventuelles de prétension dans les assemblages. Les vis montées avec ces écrous sont également en alliage d'aluminium (7075) protégées par vernis époxy ;

- écrous à freinage interne par déformation elliptique, à découpe allégée :

- soit en acier inoxydable Z-6NCT25 (A286) avec des vis en T-A6V ou en aciers inoxydables,
- soit en acier faiblement allié 25CD4, les vis utilisées devant dans ce cas être elles-mêmes protégées par vernis.

Tous ces écrous sont à chambrage profond afin de faciliter en particulier l'usage de vis protégées par vernis (sauf le filetage).

A noter que, lorsque des surfaces non planes sont à assembler, ou pour éviter l'utilisation de fixations à river il est possible d'utiliser les bandes ou les écrous isolés pour des assemblages mixtes ou entièrement métalliques.

Les bandes peuvent être équipées d'écrous de :

- diamètres 4-5-6 et 8 mm en filetage MJ;
- diamètres 10/32" - 1/4" - 5/16" en filetage UNJF 32.

La bonne tenue à la corrosion des divers types de fixation a été vérifiée par des essais de 750 heures au brouillard salin. Aucune corrosion galvanique n'a été observée. De même les écrous satisfont aux spécifications techniques française (NFL 22500) ou internationale (ISO DIS 5858).

Les écrous à cage interchangeable doivent aussi répondre à des conditions de tenue en expulsion et à l'arrachement en torsion.

Toutefois, à cause de l'opération collage des bandes sur les structures composites, ces caractéristiques dépendent et de la fixation elle-même et de son implantation sur les structures (nature du collage, etc ...). Ces caractéristiques ne peuvent donc être définies qu'en fonction de l'utilisation.

### 3 - MODIFICATION DE FIXATIONS EXISTANTES - VIS ET RIVETS STRUCTURAUX

L'expérience acquise avec l'utilisation d'éléments de fixation structuraux "classiques" dans les assemblages composites carbone-résine a mis en évidence la nécessité de modifier la géométrie de ces fixations pour les adapter au comportement des matériaux composites.

Ces modifications ont porté principalement sur l'amélioration des surfaces d'appui, l'objectif étant de diminuer les pres-

sions de matage en :

- faisant varier l'angle des têtes fraisées, passage de 100° généralement utilisé à 120° et 130°, sur les vis et rivets type SL (lock-bolt);
- augmentant le diamètre de l'embase sur les bagues de rivet SL.

Sur les vis et rivets SL eux-mêmes, l'évolution de l'angle de fraisure, de 100 à 130°, augmente très sensiblement les surfaces de matage. Cette augmentation est également importante en faisant varier les diamètres d'embase des bagues de rivets SL.

Les tableaux III et IV donnent quelques valeurs relevées sur pièces.

DIAMETRE NOMINAL (mm)	ANGLE DE TETE	SURFACE DE MATAGE (mm <sup>2</sup> )	%
4	100°	29	—
	120°	48	+ 65
	130°	64	+120
5	100°	41	—
	120°	67	+ 63
	130°	90	+120
6	100°	53	—
	120°	88	+ 66
	130°	119	+124

TABLEAU III - Vis et rivet SL

DIAMETRE NOMINAL (mm)	DIAMETRE D'EMBASE (mm)	SURFACE DE MATAGE (mm <sup>2</sup> )	%
4	6,5	21	—
	8	38	+80
5	8,1	32	—
	10	59	+85

TABLEAU IV : Baque de rivet SL

L'évaluation des modifications a été vérifiée sur la tenue

des assemblages au niveau des caractéristiques :

- d'endommagement au montage,
- de déboutonnage,
- de cisaillement simple en traction,
- de fatigue.

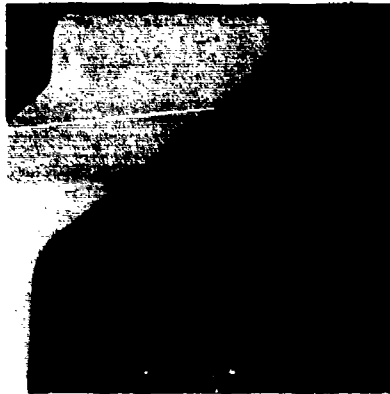
Compte tenu des épaisseurs des matériaux composites utilisés :

- plaque carbone T 300 - résine 5208 - épaisseur:3,83 à 4,05m<sup>m</sup>  
- 28 plis,
- plaque carbone T 300 - résine 914 - épaisseur:3,74 à 3,84m<sup>m</sup>  
- 30 plis,

les éléments de fixation avaient une capacité de serrage de 7,5 à  
8 mm.

Endommagement au montage

Sur coupes micrographiques on constate qu'au montage il n'y<sup>a</sup> pratiquement pas de ruptures ou de décohésions dangereuses de plis (figures 14-15-16-17 et 18).



Fraisure 100°



Fraisure 130°

FIG : 14 et 15 - VIS NFL 5mm et écrou.

Couple de serrage = 3,5 N.m



Fraisure 100°



Fraisure 130°



Bague

FIG . 16-17 et 18 - Rivets SL 5 mm

### Déboutonnage

Le dispositif d'essai est issu du test n°8 de la Norme MIL SDT 1312. Il s'agit d'un essai de traction indirecte par compression (voir éprouvette fig. 19). Le composite utilisé est le T 300-5208.

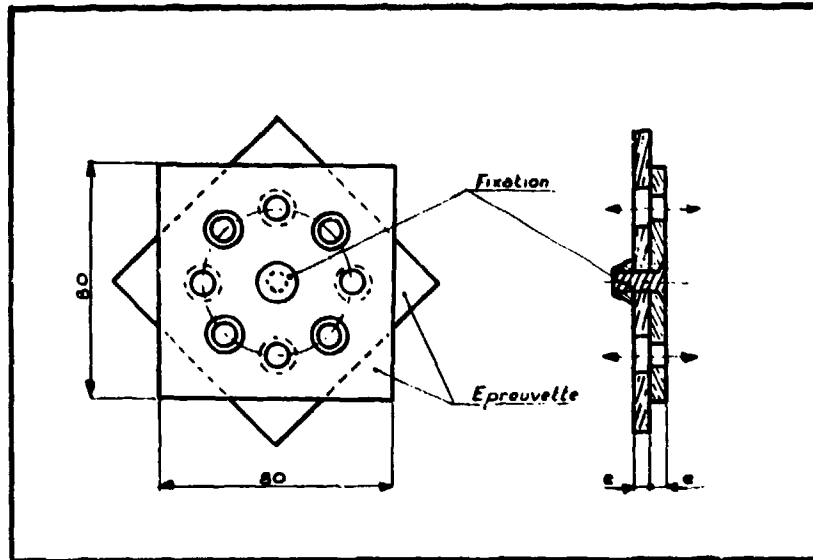


FIG. 19 - Eprouvette de déboutonnage

Les tableaux V et VI donnent quelques résultats d'essais. Dans ce cas seul l'angle de tête a été modifié.

TYPE DE FIXATION	ANGLE DE TÊTE	COUPLE DE SERRAGE (N.m)	CHARGE DE RUPTURE (KN)	Ø MATAGE AU NIVEAU TÊTE (mm)	OBSERVATIONS
VIS TP Ø 6 sans empreinte T.AGV - T.R.	15°	3,5	6,5	81	Débouillage de la tête
	30°	3,5	6,7	80	Débouillage de la tête
	45°	3,5	6,7	75	Débouillage de la tête
VIS TP Ø 6 avec empreinte EMAS T.AGV-T.R.	15°	3,6	7,4	81	Débouillage de la tête
	30°	3,6	6,7	80	Débouillage de la tête
VIS TP Ø 8/10 <sup>+</sup> avec empreinte TONG - SET T.AGV - T.R.	15°	2	5,8	137	Débouillage de la tête
	30°	2	6,2	140	Débouillage de la tête
	45°	2	6,7	95	Débouillage de la tête
	15°	2	6,8	80	Débouillage de la stabilité
	30°	2	5,4	65	Débouillage de la tête
	45°	2	7,4	80	Débouillage de la tête

**TABLEAU V : ESSAIS DE DEBOUTONNAGE**

Systeme vis - écrou

TYPE DE FIXATION	ANGLE DE TÊTE	CHARGE DE RUPTURE (KN)	Ø MATAGE AU NIVEAU TÊTE (mm)	OBSERVATIONS
RIVET SL Ø 4 TAGV-TR BAGUE 2004	15°	6,5	117	Débouillage de la bague
	30°	6,5	117	Débouillage de la bague
	45°	6,5	91	Débouillage de la bague
RIVET SL Ø 4 TAGV-TR BAGUE T 40	15°	4,6	80	Ø
	30°	4,6	80	Ø
	45°	4,6	75	Ø
RIVET SL Ø 6 TAGV-TR BAGUE 2004	15°	6,5	117	Débouillage de la tête
	30°	7,4	117	Ø
	45°	6,7	95	Débouillage de la bague
RIVET SL Ø 6 TAGV-TR BAGUE T 40	15°	6,5	117	Débouillage de la tête
	30°	7,4	117	Ø
	45°	7,4	80	Débouillage de la bague

**TABLEAU VI : ESSAIS DE DEBOUTONNAGE**

Systeme rivet SL - bague sertie

(1) Interposition sous l'écrou ou la bague d'une rondelle de diamètre 12 mm épaisseur 1,2 mm afin de pouvoir relever la charge de rupture acceptée par la modification de l'angle de tête.

D'une façon générale les charges de rupture supportées sont supérieures pour les fraises 120 et 130°. L'augmentation des portées sous tête nécessite de modifier dans le même sens celle de écrous et des bagues, car leur dimensionnement est insuffisant.

#### Cisaillement simple en traction

L'éprouvette d'essai (figure 20) est issue du test n°4 de la Norme MIL - SDT 1312.

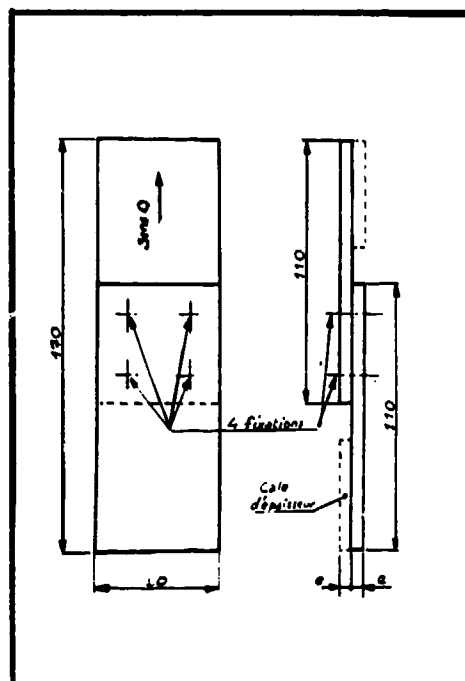


FIG. 20 - Epreuve de cisaillement

Outre la charge de rupture il a été également relevé la pénétration de la tête de l'élément de fixation dans le composite au fur et à mesure de la montée en charge.

Les tableaux VII et VIII donnent quelques valeurs de charges de rupture obtenues ainsi que les contraintes ramenées à la section

de rupture du composite S1 et à celle des fixations S2. Ces tableaux et les courbes effort-pénétration (figures 21 et 22) montrent que la résistance de l'assemblage est améliorée par l'utilisation de fixations à fraisure 130° ou 120°.

TYPE DE FIXATION	ANGLE DE TETE	COUPLE DE SERVAGE (kg)	RUPTURE (MPa)		OBSERVATIONS			
			COMPOSITE	FIXATION				
VIS T7 95 avec épave	130-914	100°	4,5	36,1	238	469	1	Rupture des 4 fibres à travers le composite
	120-914	120°		24,2	155	309	2	Rupture composite côté externe
	130-914	130°		41,9	276	536	3	" " "
VIS T7 95 avec épave	130-914	100°	4,5	38	251	486	4	Rupture des 4 fibres à travers le composite
		120°		42,1	278	538	5	" " "
		130°		43,4	286	555	6	Rupture composite du côté des fibres
BNA T-ABV-T R	130-914	120°	3,5	31,5	202	403	7	Rupture composite côté interne
		130°	4,5	31,9	204	408	8	Rupture composite côté externe

TABLEAU VII - Essai de cisaillement

Systeme vis-écrou

TYPE DE FIXATION	COMPOSITE	ANGLE DE TETE	CHARGE DE RUPTURE (K N)	σ RUPTURE (MPa)		COURBE N°	OBSERVATIONS
				COMPOSITE	FIXATION		
RIVET SL # 4 TASV-TR BAGUE 2024	T 300. 914	100°	28,8	181	576	NR	Écartement des bagues
		120°	30,9	194	618	NR	Pénétration partielle des 4 vis dans le composite
		130°	31,8	200	638	NR	Dv
RIVET SL # 4 TASV-TR BAGUE T-40		120°	27,5	173	550	9	Dv
RIVET SL # 5 TASV-TR BAGUE 2024		100°	38	251	486	10	Pénétration des 4 vis à travers le composite
		120°	41,8	278	538	11	rupture de composite au droit des fixations
		130°	42,1	278	538	12	Dv
RIVET SL # 5 TASV-TR BAGUE T-40		100°	39	257	499	13	Dv
		120°	41,8	278	538	14	Dv
		130°	41	271	524	15	Dv

TABLEAU VIII - Essai de cisaillement

Système rivets SL - bague sertie

NOTA : NR = Courbe non relevée

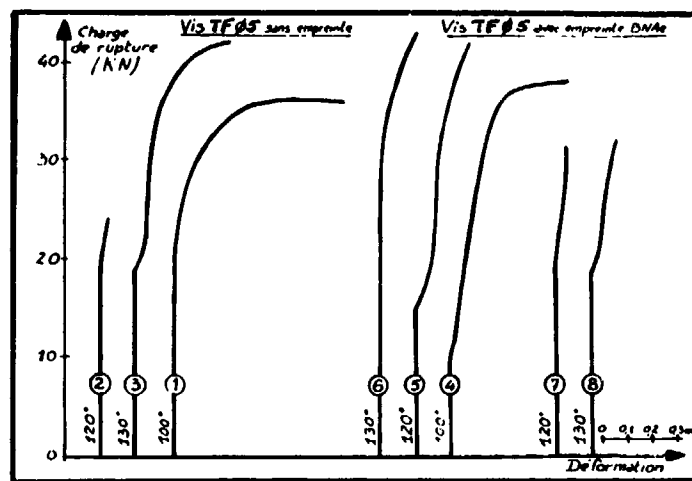


FIG. 21. Courbes effort-pénétration  
Système vis-écrou

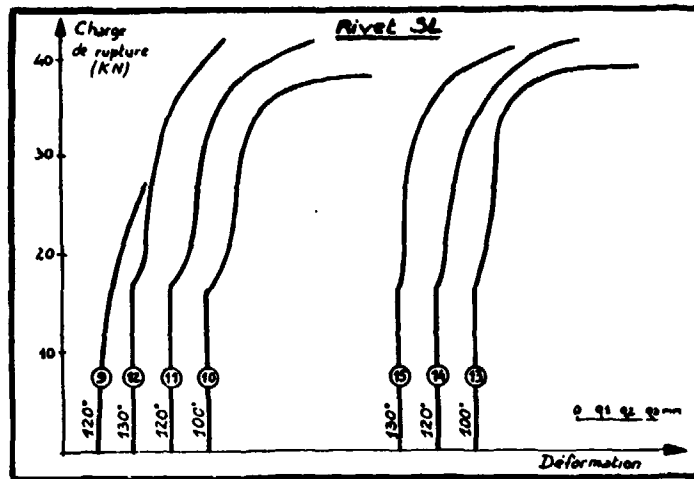


FIG 22 - Courbes effort - pénétration

Système rivet SL-bague sertie

Il apparaît, aux essais de cisaillement en traction, des gains sur la tenue en charge de rupture allant de 9 à 13%.

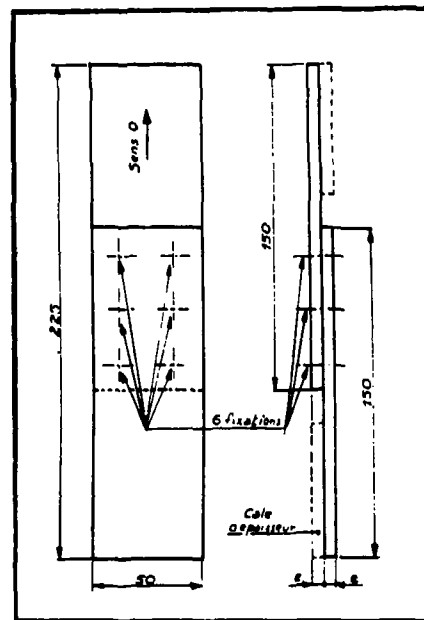


FIG 23 - Eprouvette de fatigue

Des résultats d'essais sont consignés dans les tableaux IX et X.

### Fatigue

L'éprouvette d'essai est définie par la figure 23 et les essais ont été effectués dans les conditions suivantes :

- charge en traction ondulée  $P - 0,1 P$ ,
- charge dynamique  $P = 65\%$  de la charge de rupture maximale relevée à l'essai de cisaillement simple,
- section travaillante du composite  $S_1 = (L - 2 D)e$ .

L'essai est considéré comme terminé lorsque la charge dynamique  $P$  chute à  $95\%$  de sa valeur initiale ou lorsque la durée de vie atteint 500 000 cycles.

TYPÉ DE PIERON	ANGLE DE TÊTE	COUPLE DE SERVAGE (kg)	$\sigma$ MAX DANS LE COMPOSITE (kg/cm <sup>2</sup> )	NOMBRE DE CYCLES à 10 <sup>3</sup>	OBSERVATIONS
Vis TFOAS1 avec empreinte TORO-BET TAG V-TR sans TAG V	100°	9,4	202	62	Pénétration importante des lattes
	120°	9,8		82	" "
Vis TFOAS1 avec empreinte TORO-BET TAG V-TR sans acier avec résille agglom	100°	4,5	162	49	Pénétration très importante des lattes
	120°			500	R.A.S
	130°			207	Pénétration des lattes
Vis TFOAS avec empreinte BNAo TAG V-TR sans acier	100°	3,5	186	17	Pénétration importante des lattes
	120°			24	" "
Vis TFOAS sans empreinte TAG V-TR sans acier	100°	4,5	180	173	Pénétration des lattes
	120°			500	R.A.S
	130°			370	Pénétration des lattes

TABLEAU IX - Essais de fatigue

- Système vis-écrou
- Eprouvettes en composite T 300-914

TYPE DE FIXATION	COMPOSITE	ANGLE DE TETE	$\sigma$ MAX DANS LE COMPOSITE (MPa)	NOMBRE DE CYCLES $\times 10^3$	OBSERVATIONS	
RIVET SL 84 TABV-TR BAGUE T 40	T300.914	100°	113	39	Pénétration des têtes	
		120°		225	DV	
		130°		345	DV	
RIVET SL 88 TABV-TR BAGUE T 40		100°	179	48	DV	
		120°		125	DV	
		130°		225	DV	
RIVET SL 88 TABV-TR BAGUE 2024		T300.5208	100°	181	105	DV
			120°		142	DV
			130°		170	DV
100°	111		500	R.A.S		
120°			500	R.A.S		
130°			500	R.A.S		

**TABLEAU X - Essais de fatigue**

Systeme rivet SL-bague sertie

Pratiquement toutes les éprouvettes périssent par pénétration des têtes après ovalisation des fraises, quel que soit le type de fixation, son diamètre et la contrainte appliquée.

Comme pour l'essai de cisaillement en traction statique la pénétration (p) des têtes (mesurée en fin d'essai) est plus faible avec les fraises 120° et 130° ( $p \leq 0,25$  mm) qu'avec la fraise à 100° ( $0,35$  mm  $\leq p \leq 0,7$  mm).

Les durées de vie comparatives montrent nettement l'intérêt d'augmenter les angles des têtes fraisées. Suivant les types de fixation essayés les gains obtenus varient de 40% à 10 fois.

L'intérêt, en particulier, de la modification de l'angle de fraisure des fixations sur la tenue des assemblages est démontrée. Il apparaît déjà aux essais de déboutonnage et plus nettement aux essais de cisaillement, mais la sélection est indiscutable avec les essais de fatigue.

#### 5 - CONCLUSIONS

La réalisation d'éléments de fixation spécifiques pour l'assemblage des structures composites permet de remédier d'une façon plus ou moins satisfaisante aux problèmes rencontrés avec les matériaux composites carbone-résine.

Les améliorations sont sensibles mais la mise au point de produits même simples nécessite souvent une étude appropriée aux divers types de fixation et aux cas d'utilisation.

Une concertation étroite entre fabricants d'éléments de fixation et utilisateurs potentiels est d'autant plus nécessaire afin que les produits définis correspondent le mieux aux possibilités de fabrication des uns et aux besoins des autres.

A STUDY TO OPTIMIZE THE CFRP-AL MECHANICAL JOINT IN ORDER  
TO REDUCE ELECTRICAL RESISTANCE

by

F. Cipri, M. Pelosi  
Combat Aircraft Group  
PERITALIA  
C.so Marco 41, 10100 Turin  
ITALY

SUMMARY

The aim of this paper is to show what could be the kind of joints that would reduce the electrical resistance when a carbon fiber reinforced structure has to be jointed with an aluminum part.

Assembly of specimens has been considered in fixed and removable configurations.

The materials used to prepare the specimens to be jointed were:

- Carbon fiber reinforced plastic F253-T300 Fabric 3K70PW
- Aluminum alloy 2024 - T3

1 INTRODUCTION

New difficulties are arising during the design of CFRP parts in comparison with aluminum ones. The main problem will be to verify the composite structure behaviour from the electrical point of view. It will be necessary to consider how the environment will affect the structures made of composite material.

Events such as lightning strike can have more dangerous effects on CFRP than on metallic parts.

The metallic structure itself is used as A.C. or D.C. systems return path with currents of hundreds of amperes, as a ground plane for antennas, and as shielding element for the external electromagnetic fields. A CFRP part can be used as an antennas ground plane and shielding element only if the frequencies involved are high; in this case the electromagnetic behaviour of the CFRP is similar to the aluminum one. Different solutions will be required on CFRP parts for low frequencies.

Moreover the structure has to be able to dissipate without problems the electrostatic charges. These charges could arise inside the aircraft for the movement of fluids (i.e. fuel) and outside for the motion of the aircraft in the atmosphere, therefore it is essential that all the parts of the aircraft and the aircraft itself should have the lowest electrical resistance. Particular attention has to be given to the increase of the structural weight and on the joints CFRP - Al.

A part with low resistivity for the presence of a metallized carbon ply and a bad electrical connection with other metallic elements will not solve the overall conductivity of the aircraft. Moreover the CFRP part with low resistivity will attract the lightning strike and will not be able to dissipate high currents. In this case the protected structure will be damaged more seriously than an unprotected one.

2 LIGHTNING STRIKE

The tips of the aircraft have high probability to be struck by lightning. The current will follow preferential paths as front fuselage-rear fuselage and half left wing - half right wing.

The current need a low resistivity and a sufficient cross section between all the extremities of the airframe (Fig.1).

The aircraft is subdivided in areas according the probability to be struck by lightning (Fig.2). A subdivision exists also in single parts like vertical fin (Fig.3).

Some CFRP structures have to be protected independently from the zone of the aircraft if there are inside devices susceptible to external currents and electromagnetic fields. Particular attention has to be paid on the fuel area (wet wing). The sparking between the bolts inside the wing is a problem when metallic structures are used; new different solutions will be required if the wing is manufactured with CFRP. The currents generated during lightning strike may reach values up to 200 kA in the most exposed aircraft structures; they can reduce the structural integrity of the hit part and can have consequences on the equipment.

Some phenomena can occur:

- shock waves that can produce delaminations;
- local increase of the temperature favoured by the low thermal conductivity of CFRP;
- hot spots in the attachment point of the lightning strike and in the junctions if they have high resistivity;

- erosions particularly dangerous in the fuel area;
- delaminations produced by a fast evaporation of the water usually inside CFRP;
- interference on the harnesses with troubles on transmitting systems, controlling instruments and equipment of the aircraft.

Several solutions as metallic meshes, metallized carbon fibers and plasma spray can be adopted to minimize the damage caused during lightning strike. Usually the protections adopted for the lightning strike are not useful for the shielding of electromagnetic fields; in any case the shielding problem needs a solution especially on new generation aircrafts with "fly by wire" systems. The potential differences have to be considered carefully when metallic materials have to be jointed with CFRP. If the materials are not compatible from a galvanic corrosion point of view, a fiberglass ply has to be used between the metallic protection and the carbon underlayer. In any case meshes will increase the weight of a CFRP part because they are added plies and are not structural materials. Metallized carbon fiber ply should be more useful; it is a structural material and could be used instead of the last ply of the laminate. In this case only the metal of the ply will slightly increase the weight of the part. The choice of a metallic protection has to be made taking into account thermo-mechanical distortion problems during cure cycle; metallic meshes on fabric carbon underlayer don't give particular problems while if unidirectional carbon fibers are used distortion problems can arise. The main factors are the lay up and the thickness of CFRP part, the cure cycle maximum temperature and the difference between thermal expansion coefficients of the metallic mesh and the carbon fibers used. These protections can be a problem during repairs because a good electrical continuity between the damaged area and the part is not easy to obtain.

### 3 JOINTS

Metal metal joints that fulfil mechanical requirements will be satisfactory also from the electrical point of view if a dry assembly is used. CFRP - CFRP and CFRP - Al joints will give particular problems also if the joint does fulfil mechanical requirements. CFRP - CFRP joints have to be avoided and if it is possible a cocuring kind of structure has to be chosen. When CFRP components have to be bonded (cobonding or secondary bonding) the low conductivity of the adhesive has to be considered. Sometimes the adhesives are filled with aluminum powder to improve mechanical properties but this is usually detrimental from the electrical point of view.

Bolts are widely used for the assembly of components because they can sustain high mechanical loads. Moreover a bonded joint between CFRP and metal is not mechanically reliable if the adhesive chosen needs a cure cycle; in this case the materials will be pre-stressed for the different coefficients of thermal expansion. Among the bolted joints there are fixed configurations with Hi - Loks and removable ones with nut plates. Fixed configurations are used mainly for the joining between primary structural parts (i.e. fin box - rear fuselage fittings). Removable configurations are used to join secondary structural parts (i.e. fin leading edge - fin box) that have to be removed for servicing. The bolt material has to be compatible with both parts to be assembled. A titanium bolt will be used for CFRP - Al joints in order to reduce the galvanic corrosion even if Ti resistivity is higher than aluminum one. Several solutions can be adopted to minimize the resistivity of a CFRP part; an electrical connection of the heads of the bolts with a metallic strip will be very useful. The total resistivity will be reduced and the current will have a new preferential path. If aerodynamic requirements don't permit to use metallic strips, plasma spray can be used for the electrical connection of the screws heads.

The current path in the bolt has to be considered carefully in order to improve the joint conductivity. The shank of the bolt does not play a large part in making contact between CFRP and Al. Several others factors contribute:

- incorrect drilling can produce over size holes;
- presence of non conductive sealant during a wet assembly will increase the resistivity;
- wrong speed drilling or feed rate can smear the resin over the ends of the fibers insulating them;
- a tenacious non conducting oxide film that the titanium bolts tend to have could also increase the resistivity.

The current will flow under the head of the pin and will reach the metallic part through the shank of the bolt.

The use of washers or metallic strips connecting more Hi Loks will improve the conducti-

vity by increasing the electrical cross section. If a Ti bolt is used, the higher resistivity of this material in comparison with the Al has to be taken into account for the cross section calculation.

Also the metal surface has to be unpainted and abraded in order to improve the conductivity but only in the bolt area. Nut plates not floating will also minimize the resistivity. The use of washers or metallic strips will improve the stresses around the hole but also the conductivity because the resistance decreases when the pressure of the bolt increases.

#### 4 EXPERIMENTAL WORK

Electrical conductivity tests have been performed in order to optimize the configuration fin box - fuselage fitting ribs for the ANX aircraft.

Fin box is a cocured carbon fiber reinforced plastic structure. External skins and spars are cocured simultaneously. The part does not need secondary bonding after the cure cycle. Only trimming, drilling and assembly with other parts are necessary (Fig.4).

The material used to manufacture the fin box is a prepreg with a 3K70PW fabric of Toray T300 fibers and an epoxy resin, F263 from Hexcel, with 177 C curing temperature.

The specimens for the conductivity tests simulate the fin box lay up and the aluminum alloy of the metallic parts.

Typical specimens configuration have been chosen in order to verify each bolt conductivity. The percentage of non conducting bolts has been calculated for each kind of assembly (Fig.5).

Two kinds of assembly have been considered. The first one is used in fixed configurations and it is as follows:

Hi Lok pin with countersunk head in titanium and an aluminum collar (Fig.6). The second one is used in removable configurations and it is as follows:

Titanium screw with a stainless steel washer on CFRP side and aluminum not floating nut plate with two lugs rivetted on the Al side (Fig.7).

First of all the electrical conductivity of CFRP specimen without Al parts has been evaluated. The lay up was 50% at 0/90 and 50% at +/-45. The holes of the specimens have been metallized with a nickel flash and a copper electrogalvanic deposition. Copper wires have been welded in the holes using a silver - tin alloy in order to connect the specimen with the measurement equipment.

In Tab.I are the results of D.C. and A.C. measurements and in Fig.8 are the R and Z curves against the frequency between 10 kHz and 10 MHz.

The resistivity of a CFRP specimen is affected by the lay up, the kind of fibers and, for the same fibers, if they are a fabric or a tape.

The ratio between the resistivity in 0 and 90 direction seems to be about 1:600 using 600x300 mm specimens with the same kind of unidirectional fibers and the same resin system between 0-50 kHz (Figs.9-10).

Tests performed on 3K70PW fabric and unidirectionals ((0,+45,-45,90)s lay up) specimens with the same dimensions have shown almost the same resistivity that is 57 mohm between 0-50 kHz.

The resistivity of the carbon yarn changes also with the graphitizing percentage. This percentage is in correlation with the heat treatment of the PAN fibers. Our tests have been performed on high strength fibers.

Assembly of specimens have been carried out on several kinds of protections and bolting types.

The metallic part of the specimens have been made according the following flow:

2024 T3 Aluminum sheet

Sulphocromic pickling

Chemical conversion coating  
Alodyne 1200

Epoxy primer

Epoxy topcoat

Non conductive sealant (PR 1436G B 1/2), epoxy adhesives filled with silver (Eccobond 56C and Scotchcast 105) and conductive paint (Eccoshield 341) have been used during the assembly.

#### Al - CFRP specimens results

The use oh Hi Lok bolts is associated with a very high junction uncertainty; bad contact can

achieve a resistivity of 2ohm (Tab.II). The conductivity and uncertainty of the joint will slightly improve only if a conductive paint (filled with silver) was used. Anyway the problem will not be solved because the conductivity improvements are too low. No improvement is achieved if the hole drilling tolerance decrease from H11 to H8. The only possible solution to minimize the resistivity is to use a removable configuration. Stainless steel washer will be bonded on the CFRP with conductive adhesive and nut plates will be rivetted on the aluminum. The Ti screw will join the CFRP and Al parts. This kind of solution cannot always be used. Different solutions have been considered in order to minimize the uncertainty of Hi Lok - Collar junctions.

#### Al - CFRP plus Al mesh specimens results

These specimens have been made using the same prepreg underlayer as above and adding a fiberglass ply, aluminum mesh and an adhesive ply. The mesh had 180 yarns/cm with a yarn diameter of 0.05 mm. This part has been cured simultaneously with a 177 C cure cycle. The fiberglass ply is necessary because the potential difference between 2024 Al alloy and CFRP is 0.9 V; this value is higher than +/- 0.25 V maximum allowable for galvanic compatibility.

Results of D.C. measurements on fixed and removable configurations are in Tab.III. The resistivity of fixed configurations is about 7 mhm, slightly improved than before. The percentage of efficient junctions has been bettered; the uncertainty was about 36% and with the Al mesh is decreased to 16%. This solution probably is not the best but an improvement on fixed configurations has been achieved.

Removable configuration resistivity is higher than before; but this is understandable because now there is no conductive adhesive under the washer of the screw. The use of conductive adhesive with this configuration will give the possibility to obtain values as before if not better. The Al mesh will partially solve the conductivity problem but will increase the weight of the protected part.

#### Al - CFRP plus Ni coated graphite fibers specimens results

Tape and fabric carbon fibers metallized with Ni have been added to a carbon underlayer as before.

In this case also Hi Lok and nut plates assemblies have been considered. Results of measurements are in Tab.IV.

The joints resistivity is about 2 mohm for both configurations and the uncertainty percentage is very low. This kind of solution seems to be promising; the resistivity and the uncertainty factors are very low and also the structural weight can be minimized. Metallized carbon ply is a structural material and it could be used instead of the last ply of carbon underlayer. Weight increase will be only due to the metallization of the last carbon ply.

Preliminary tensile mechanical tests performed on CFRP and CFRP plus Ni coated fabric specimens show that the failure stresses are very close; in particular the failure stresses variation is lower than the coefficient of variation.

#### Fin measurements results

A study on the best electrical configuration for the AMX fin has been performed following the indications on specimens results. AMX fin box has to be protected because its typical thickness is lower than 5 mm.

CFRP parts thicker than 5 mm do not require particular protections against lightning strikes. The carbon, also if not a good conductor, will be able to dissipate high currents if the cross section is sufficient. Obviously the joints have to work correctly. Some CFRP parts thicker than 5 mm will be protected if shielding requirements exist.

The original configuration of the vertical fin is as follows:

the Al mesh is 2/3 of the fin height and it works like an antenna ground plane; the leading edge is made of kevlar and it is fitted on the fin box with Ti screws and nut plates. The fin box is fitted on the upper and lower metallic ribs with Ti Hi Loks and Al collars. D.C. resistivity between the upper and lower ribs was 11 mohm. Some variations have been proposed in order to improve electrical conductivity as follows:

- change the kevlar leading edge with an Al one. This can be useful to have a preferential path from the fuselage to the rear extremity of the upper rib;
- cocure the Al mesh for all the fin box length. In this way the upper and lower Hi Loks rows will be connected;
- connect the bolts heads of each row with a thin stainless steel strip. The metallic strip will be drawn in order to have the best coupling with the hole countersunks.

Conductive adhesive will be used only in the hole countersink area; none conductive sealant will be used between metallic strip and CFRP far from holes.

A second vertical fin made with these new suggestions has had a resistivity of 2.5 mohm with the same measurement conditions of the first one. The current cross section with

these improvements is about 25 mm<sup>2</sup> (Fig.11).

Ni coated carbon fibers gave the best results on coupons but they have not yet been used as structural material. A study of their applicability is a subject of further investigation. Nevertheless mechanical performances have to be tested after the tearing of a Ni coated area struck by lightning.

Changes proposed for the fin configuration will partially solve the conductivity problem, but this will be only the first step to improve the performances of the vertical fin. Lightning strike tests on the AMX fin will be necessary to verify the new solutions. Ultrasonic inspection, static and fatigue tests will be also helpful.

Lightning strike tests have been performed on 550x280 mm panels according MIL STD 1757. Unprotected and protected laminates have been considered. The materials used for protection were Thorstrand TEF 5 and Ni coated graphite fibers fabric. The impedance values and maximum pulse currents are in Tab.V. The Ni coated graphite panels give, also in this case, the minimum of impedance. The unprotected CFRP fabric panel dissipated the highest current. Damage was rather serious because three plies have been damaged in the attach zone. Thorstrand TEF 5 ply tore with 110 kA current while an unprotected panel made of unidirectional fibers dissipated a 132 kA current with the tearing of the first ply. Ni coated graphite panel showed only surface burning with 184 kA current. The Ni coated CFRP seems to be able to discharge high currents, also if it is an attraction element for lightning strike.

#### 5 CONCLUDING REMARKS

Several suggestions can be proposed in order to minimize the resistivity between CFRP and light alloys.

They are:

- verify if the structure has preferential paths with enough cross section for the currents;
- foresee the drawing at design stage to obtain preferential paths;
- adopt metallic protections on CFRP parts; structural solutions will be more helpful for weight savings;
- pay particular attention to mechanical joints in order to minimize galvanic corrosion and in order to have the electrical continuity for each fastener;
- make an electrical connection between more fasteners in order to minimize total resistivity;
- consider carefully the sparking problem in the fuel area.

#### REFERENCES

1. J.M. Thomson  
The electrical properties of carbon fibre composites AGARD Lecture Series No.124 - Practical considerations of Design, Fabrication and Tests for Composite Materials
2. J. Rouchon, D. Gall  
Evaluation du comportement a la foudre de structures en materiaux composites haut module  
AGARD Conference Proceedings No.288-Effect of Service Environment on Composite Materials 14-17 April 1980 Athens, Greece
3. Vernon L. Bell  
The potential for damage from the accidental release of conductive carbon fibers from aircraft composites  
AGARD Conference Proceedings No.288 - Effect of Service Environment on Composite Materials 14-17 April Athens, Greece
4. S.D. Schneider  
Lightning protection considerations for graphite/epoxy aircraft structure  
AGARD Conference Proceedings No.288 - Effect of Service Environment on Composite Materials 14-17 April 1980 Athens, Greece
5. K.J. Lodge, J. Brettie  
A current dependent resistance effect in carbon fibre composites joints  
Composites, July 1982 pagg. 135-138

6. K.J. Lodge  
The electrical properties of joints in carbon fibre composites  
Composites, July 1982 pagg. 305-310
7. Military Standard  
Lightning qualification test techniques for aerospace vehicles and hardware  
17 June 1980
8. K.E. Crouch  
Simulated lightning strike tests on Cycom MCG fiber panels  
Lightning technologies Inc  
June 1982
9. D.W. Bigg  
The effectiveness of Nickel coated carbon fibers as a filler to provide EMI shielding in plastic composites  
Battelle Columbus Laboratories

#### ACKNOWLEDGMENTS

In preparing a paper such as this we have collected information from a variety of sources. These sources include the literature and personal contacts. We are deeply indebt to all the specialists that we met and we must specifically mention, for his freely given advice and cooperation, Mr. Vione, Combact Aircraft Group, System Department, Aeritalia.

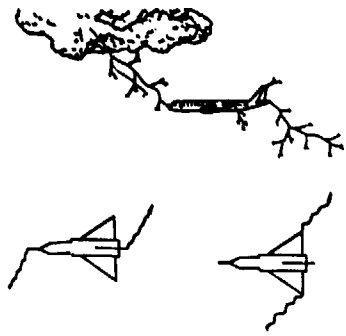


Fig.1  
Typical Lightning Strike paths

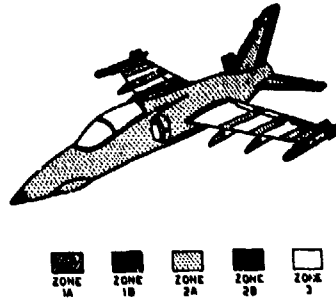


Fig.2  
Typical zoning for a tactical fighter according to MIL -STD - 1757A criteria

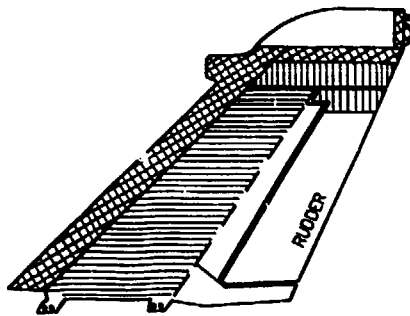
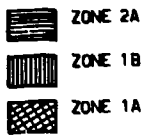


Fig.3  
Example of zoning criteria for a vertical fin structure

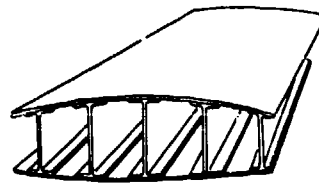


Fig.4  
Scheme of the AMX CFRP vertical fin torsion box

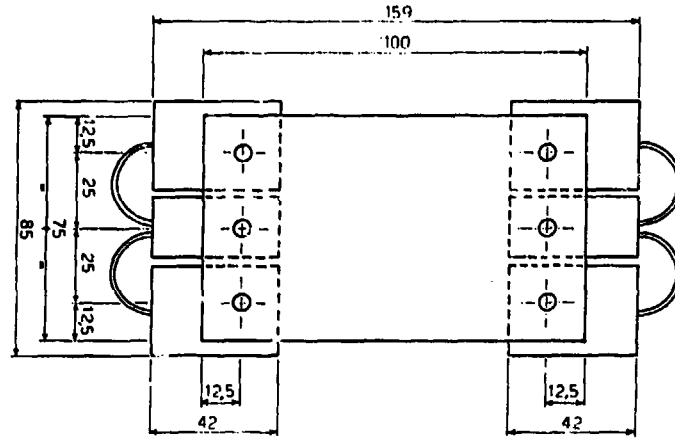


Fig. 5

CFRP specimen for conductivity testing

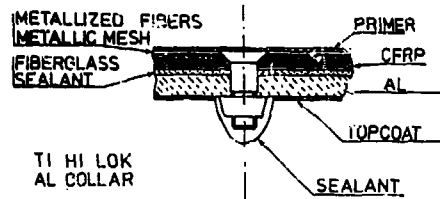


Fig. 6

Fixed configuration joint

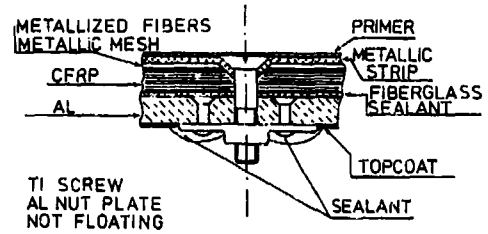


Fig. 7

Removable configuration joint

MATERIAL	DC MEASUREMENTS (mohm)	AC MEASUREMENTS (mohm)			% UNCERTAINTY
		10 kHz	1 MHz	10 MHz	
CFRP 50% 0/90 50% +/-45	8.26	95.97	139.3	95.0	b

Tab. 1

Conductivity results on CFRP fabric laminates without fasteners



MATERIAL	ASSEMBLY		DC MEASUREMENTS (mooh)	AC MEASUREMENTS (mooh)			% UNCERTAINTY
	Hi-Lok	Nut Plates Aux. Mat.		10 kHz	1 MHz	10 MHz	
AL - CFRP	H11 AL-collar	DRY	8.7				50
AL - CFRP	H 8 AL-collar	Kapton	11.3				39
AL - CFRP	H11 AL-collar	PR1436U	7.46	110.4	164	1260	29
AL - CFRP	H11 AL-collar	PR1436G Eccoshield 341	6.24	78.9	141	2070	17
AL - CFRP	H11 AL-collar	Eccobond 50C	7.02				28
AL - CFRP	H11 AL-collar	PR1436G Eccobond 50C	9.14				33
AL - CFRP	H11 Ti screw Inox washer	Eccobond 50C	4.94				0

Tab.2  
Conductivity results on CFRP/Al joints in fixed and removable configurations

MATERIAL	ASSEMBLY		DC MEASUREMENTS (mooh)	% UNCERTAINTY
	Hi-Lok	Nut Plates Aux. Mat.		
CFRP Al mesh FMS00 Fiberglass AL	H11 AL-collar	PR1436G	6.64	11
CFRP Al mesh FMS00 Fiberglass AL	H11 AL-collar	DRY	7.04	22
CFRP Al mesh FMS00 Fiberglass AL	H11 Ti screw Inox washer	DRY	8.05	16

Tab.3  
Conductivity results on CFRP plus Al mesh/Al joints

MATERIAL	ASSEMBLY		DC MEASUREMENTS (mooh)	AC MEASUREMENTS (mooh)			% UNCERTAINTY
	Hi-Lok	Nut Plates Aux. Mat.		10 kHz	1 MHz	10 MHz	
CFRP Ni-coated Tape 4 plies AL	H11 AL-collar	DRY	2.65				11
CFRP Ni-coated Tape 4 plies AL	H11 Ti screw Inox washer	DRY	1.72				6
CFRP Ni-coated Fabric 1 ply AL	H11 Ti screw Scotchcast Inox washer	105	2.57	26.02	97	1530	0

Tab.4  
Conductivity results on CFRP plus Ni coated graphite fibers/Al joints

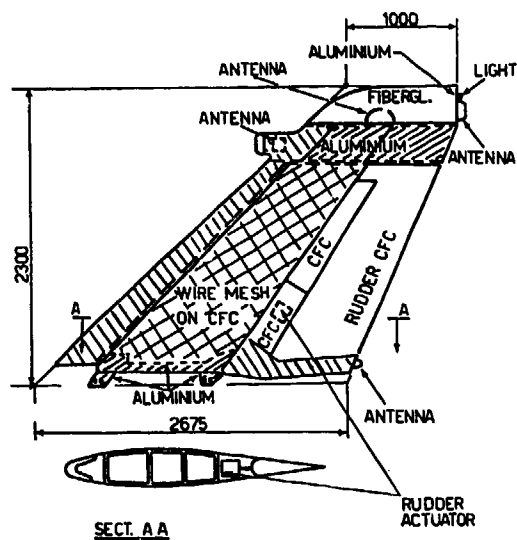


Fig.11

Vertical fin configuration to improve conductivity behaviour

MATERIALS	IMPEDANCE ( mohms )	CURRENT PULSES ( kA )	VISIBLE DAMAGE
CFRP F263-T300 FABRIC	58 0 + 50 kHz	46 ↓ 195	59 kA Tearing of the first ply  With the maximum current pulse three plies have been dama- ged in the attach zone
CFRP F263-T300 UNIDIRECTIONAL (0,+45,90,-45) <sub>2s</sub>	58 0 + 50 kHz	51 ↓ 132	90 kA Tearing of the first ply
CFRP F263-T300 FABRIC THORSTRAND TSP 5	64 0 + 50 kHz	94 ↓ 110	100 kA Tearing of the Thorstrand
CFRP F263-T300 FABRIC MI COATED GRAPHITE FIBERS FABRIC	17 0 + 10 kHz	37 ↓ 184	Burning of the surface

Tab.5

Simulated lightning strike test results on CFRP panels

TEST SPECIMENS FOR BEARING AND BY-PASS STRESS INTERACTION  
IN CARBON FIBRE REINFORCED PLASTIC LAMINATES

by  
M B Snell  
RARDE  
Christchurch  
Dorset

G P Burkitt  
Materials & Structures Department  
Royal Aircraft Establishment  
Farnborough  
Hampshire

SUMMARY

Compact test specimens for measuring the strength interaction behaviour of bolted joints subject to combined bearing and by-pass stresses have been studied. Multi-bolt specimens which have been successfully used to study these effects in aluminium alloy were found to be unsatisfactory because of the uncertainty in load transfer, and a new specimen based on parallel plates was developed. Bearing load at the holes is achieved through load transfer from the central CFRP coupon to the parallel plates. The maximum ratio of bearing to bypass loads is limited by the initial fit of the bolt and by subsequent bolt/hole deformation under load. However the specimens recommended are capable of applying a wide range of bearing/bypass load ratios.

Sample strength interaction envelopes were produced for a Hercules IM6 fibre and Ciba-Geigy Fibredux 6376 resin laminate on a typical wing skin lay-up, 5.5 mm thick. Both tension and compression quadrants were studied, with two hole sizes, in both double shear and single shear. The interaction behaviour was similar in both tension and compression for 6.35 mm holes in double shear, but in the case of 9.5 mm bolts there was less interaction in compression than in tension. Countersunk fasteners in tension appeared to suffer little reduction in net strength due to bearing stresses.

LIST OF CONTENTS

1	INTRODUCTION	
2	MULTIPLE HOLE JOINTS	
2.1	Prospects for analysis	
2.2	Exploratory tests	
2.3	Thermoelastic investigation using SPATE equipment	
3	PARALLEL PLATE SPECIMENS	
3.1	Specimen types and potential applications	
3.2	Test programme and results	
3.2.1	Trials with short specimens using aluminium alloy and steel side plates.	
3.2.2	Trials with long specimens.	
3.2.3	Single shear specimens.	
3.2.4	Specimens in compression.	
3.2.5	Conclusions from specimen trials	
4	STRENGTH INTERACTION CURVES	
4.1	Tension - bearing interaction, double and single shear, 6.35 mm hole	
4.2	Tension - bearing interaction for 9.5 mm bolts in double shear	
4.3	Compression - bearing interaction in double shear for 6.35 mm and 9.5 mm bolts	
5	DISCUSSION	
6	CONCLUSIONS	
	REFERENCES	
	ILLUSTRATIONS	FIGS 1-23
	TABLE 1	

## 1 INTRODUCTION

Mechanical joints in carbon fibre plate structures are widely used since they offer a reliable means of load transfer; bolts bearing against the supported axial fibres in multidirectional laminates have been shown to achieve bearing strengths close to the laminate compression strength (1). The efficiency of CFRP joints in bearing is well understood but, apart from a minority of jointing cases such as single hole joints at wing attachment fittings, bearing stress alone is a rare occurrence.

The general case found in mechanical joints is the transfer of load by bolt bearing into a stressed sheet. Examples abound, such as in aircraft wings where a combination of membrane stress due to bending and bearing stress due to transfer of shear load at the skin/substructure interface occurs. The ratio of bearing stress to membrane stress varies widely across the wing but will generally be low for the skin/substructure joints and high for the multi-hole joints at wing attachment fittings. Both membrane and bearing stresses will give rise to stress concentrations at the edge of the hole which may initiate failure and it is to be expected that some interaction of the stress concentrations will occur, leading to a reduction in strength.

The strength values used in aerospace structural design are the filled-hole notched strength and the bearing strength, both of which vary with lay-up and fibre/resin system. They are generally measured using separate coupon specimens designed to give representative failure modes and strengths. The interaction problem is often treated using assumed (conservative) factors to reduce the notched strength to account for additional bearing stress. In consequence a method is sought to obtain accurate design values for strength of notched laminates under combined membrane and bearing stress. The problem has been studied by others including Hart-Smith (2) who developed a semi-empirical design method. Strength measurements under combined stress have been carried out by Crews (3), who developed a servo-hydraulic test frame capable of applying membrane and bearing loads independently. This method shows great potential but requires complex testing equipment.

The aim of the present work is to develop a simple method for strength interaction measurement using coupon specimens in ordinary test machines. Two main types of specimen were investigated. One specimen depends on load sharing between the bolts of a multi-bolt joint and the other, more successful, specimen depends on load sharing between the CFRP coupon and parallel steel side plates which are loaded only via the bolts. This parallel plate method is applicable to double shear and single shear joints with plain or countersunk bolts. The bearing load achieved is dependent on the relative stiffness of the members and the initial bolt fit. These parameters can be controlled to give a wide range of bearing/membrane stress. The specimens were used to develop strength interaction curves for a laminate made from Hercules IM6 fibre and Giba-Geigy Fibredux 6376 resin. Both tension/bearing and compression/bearing quadrants were investigated, using plain (hexagonal headed) bolts in double shear and countersunk bolts in single shear. Test results to date are given in Table 1.

## 2 MULTIPLE HOLE JOINTS

## 2.1 Prospects for Analysis

The analysis of bolt groups depends critically on the local deformation of the holes and the bolts. Work by De Jong (4) using elasticity theory and conformal mapping has studied various configurations of bolt rows. Finite element methods can, of course, be applied, although complex and costly models are needed to represent the three-dimensional deformations and stresses. No elastic method has been found accurate for strength prediction of composite joints.

If bolt/hole deformation is ignored, a row of fasteners in double shear can be analysed simply. The following results apply to a three-hole joint shown in Fig 1.

$$P_1 = P_2 = \frac{(2A_1E_1)P}{2A_1E_1 + A_2E_2} \quad P_3 = P_4 = \frac{(A_2E_2)P}{2A_1E_1 + A_2E_2}$$

$$S_1 = \frac{(2A_1E_1)P}{2A_1E_1 + A_2E_2} \quad S_2 = 0 \quad S_3 = \frac{(A_2E_2)P}{2A_1E_1 + A_2E_2} \quad (1)$$

For a symmetrical joint,  $A_1E_1 = A_2E_2/2$ , then

$$P_1 = P_2 = P/2, \quad P_3 = P_4 = P, \quad S_1 = S_3 = P/2$$

These results apply to joints of similar configuration with any number of holes per row, is only the outer bolts are effective in load transfer and the sheet between the outer bolts is under constant stress. Provided the bolt clearances are matched, a symmetrical two-hole joint should, from equation (1), have equal bearing loads at each hole. This is the only case in which 50% load transfer can be assured.

For other configurations, deformation of the bolt/hole will clearly redistribute load between the bolts and, for ductile materials, experience has shown that shear equalisation can take place with plastic deformation (5). This is shown qualitatively in Fig 2. Given the occurrence of shear equalisation from local yielding, a multi-hole fastener would provide a convenient means of studying the bearing/membrane stress interaction problem, with a two hole specimen giving 50% load transfer, a three hole specimen 33% and so on.

Shear equalisation is less likely with the relatively brittle characteristics of CFRP and the high stiffness of the steel or titanium fasteners used. However, a number of exploratory tests were carried out to assess the multiple hole specimen.

## 2.2 Exploratory Tests

The laminate used for all the tests in the present report was 44 ply, nominally 5.5 mm thick, in a distributed lay-up of 18/20/6 plies at  $0^\circ/\pm 45^\circ/90^\circ$  respectively, in IN6-6376 material. For this thickness it was found that the diameter of high-tensile steel bolt required to give bearing failure in the composite without bolt bending was greater than 8 mm so the nearest standard size of 9.5 mm was used. The bolts in all tests were torque tightened to a moderate level (7 Nm) to provide a positive lateral constraint without significant friction. The specimens used are shown in Fig 3 as types B, C and D. Only one test was carried out in each configuration, to establish the basic behaviour. The results are shown as load-extension curves in Fig 4. Five curves are shown, one (CO7) a bearing strength test, one (CO4) a filled hole tension test and the remainder (CO3, CO5 and CO6) combined bearing/by-pass tests with four, three and two hole specimens respectively. The failure modes are shown in the photographs in Fig 5. CO7 and CO4 exhibit the normal bearing and notched tensile modes. Considering the multi-hole specimens, CO3 shows tensile failure at the first hole with evidence of additional bearing deformation at holes 1, 2 and 3 only. Hole 4 shows no visible sign of permanent bearing deformation. The three hole specimen, CO5, also failed in a tensile mode at hole 1, but in this case the bearing deformation is less and limited to hole 1. The two hole specimen, CO6, has the same failure mode, and shows evidence of bearing deformation at both holes.

Referring to Fig 4 it is clear that the multi-hole specimens all failed at virtually the same load, but less than that for the filled hole tensile specimen by 25%. This indicates that the notched tensile strength ( $s_{nt}$ ) is significantly reduced by bearing stress and the reduction does not necessarily vary with number of holes in a joint. From the visible evidence of the failure modes it appears that the bearing load was concentrated at the first hole. Equalisation of bolt loads did not occur so no accurate estimate of the bearing loads can be made.

## 2.3 Thermoelastic Investigation Using SPATE Equipment

An investigation of the load distribution in the steel side plates was carried out using the SPATE system at RAE, general details of which are given in Ref 6. This equipment detects adiabatic temperature changes, which for isotropic materials are proportional to the sum of the principal stresses, in structures undergoing cyclic loading. Specimens of type D were used, 30 mm wide, with 6 mm thick parallel steel plates either side fastened with four 6.35 mm bolts. Two specimens were tested, the first a static test and the second a residual strength test after fatigue "shake-down". In the second test emissions from the side plates were detected to obtain a measure of the stress variation, and resultant bearing loads at each hole. The fatigue test was carried out at 5 Hz at mean load of 33 kN and alternating load of 27 kN ( $R = 0.1$ ).

The fatigue tests were run up to 100,000 cycles to observe load redistribution resulting from local bearing deformation in the CFRP coupon. During this time several scans of the steel side plate were performed using SPATE. During the early stages the bearing load was concentrated at the first bolt, which failed in fatigue several times and was renewed. Towards the end of the test the first three bolts failed, and all four were replaced before the residual strength test. The residual strength test gave the net tensile strength as 572 MPa, 14.6% below the notched tensile strength result. The static strength test gave 72.2 kN compared with 76.2 kN for the residual strength test, so the bearing deformation under fatigue may have caused a significant equalisation of bearing load and a consequent increase in net tensile strength. It should be noted, however, that even in the absence of bearing effects the net tensile strength would be expected to increase slightly as a result of fatigue (7). Consequently the strength achieved was closer to the notched tensile strength than that for the 9.5 mm bolts discussed in section 2.2 (86% of  $s_{nt}$  for the 6.35 mm bolts and 75% of  $s_{nt}$  for the 9.5 mm bolts). A photograph of the failed residual strength specimen is shown in Fig 6. The bearing fatigue caused elongations of the holes of between 3.1% (1st hole) and 1% (4th hole).

Photographs of the SPATE scans in Fig 7 show some increase of stress away from the first hole between 30,000 and 100,000 cycles, indicating bearing redistribution. However the results so far have not given accurate values of the bearing load at each hole. Although it may be possible to use multi-hole specimens, the difficulty of measuring the bearing load at each hole is a major disadvantage. Paradoxically it appears that the strength of multi-hole joints can be improved by using "weak" fasteners which yield and so equalise the fastener shears.

### 3 PARALLEL PLATE SPECIMENS

#### 3.1 Specimen types and Potential Applications

The parallel plate specimen types used in this investigation are shown in Fig 8. Bearing load is generated at the CFRP hole by load transfer into the side plates. The model shown in Fig 9 gives the load distribution in terms of the member strains and stiffnesses for a symmetric three-plate specimen.

An upper limit to the bearing load, neglecting bolt/hole deformation is

$$P_b = P / (1 + (A_1 E_1 / 2A_2 E_2)) \quad (2)$$

A practical minimum ratio of  $A_1 E_1 / A_2 E_2$  is about 1/5 and this yields, neglecting bolt/hole deformation, a maximum bearing load of 12/13 of the applied load. As will be shown later, this upper limit could only be expected for extremely long specimens.

In practice the bearing loads can be determined from measured strains:

From measured side plate strains,

$$P_b = 2A_2 E_2 \epsilon_3$$

From measured CFRP coupon strains,

$$P_b = P - A_1 E_1 \epsilon_2$$

Thus, the true bearing load can be obtained from strain gauge measurements on either the side plates or the CFRP coupon, once the Youngs modulus is accurately known. The ratio of bearing/applied load will vary as bolt or hole deformation takes place so the strains must be continuously monitored to obtain the correct results at failure.

Initial bolt clearance and deformation under load reduce the achievable bearing loads. It was found that the short specimen (type E), with 100 mm bolt pitch, achieved load transfer of about 20%. This could be increased to about 85% using type F. In specimen type F, the initial bolt clearance is halved because only one bolt acts in load transfer. At the other end the CFRP strip is bonded and pinned to the side plates and this rigid joint is clamped in the hydraulic grips of the test machine. The combination of increased effective length and reduced clearance gives much higher load transfer ratios.

In practice, predictions of load transfer are difficult because of non-linear bearing deformation characteristics near failure. However, it has been found that the two specimens, types E and F give sufficient range to cover the relevant loading cases. For a given specimen type, variability in initial clearance and bolt/hole deformation will result in variability in load transfer at failure. This is no disadvantage since it expands the interaction data over the range studied.

Load transfer in single shear with countersunk fasteners can be studied using specimen type C, backed with an anti-bending plate if necessary. The single sided plate arrangement can also be used to study additional bending effects by adding spacers between the plate and coupon, with strain gauges attached to measure both load transfer and additional bending.

Approximately fifty specimens of various configurations were tested to develop the best type and to generate sample strength interaction curves for the CFRP laminate. An essential prerequisite was the Youngs modulus of the constituent plates. The laminate Youngs modulus in tension and compression was measured as 71.1 GPa and 70.3 GPa, respectively. Both aluminium alloy (L65) and steel (EN8) side plates were used in the trials, with modulus of 70 GPa and 210 GPa.

#### 3.2 Test Programme and Results

##### 3.2.1 Trials with short specimens using aluminium alloy and steel side plates

The first tests compared specimens with L65 and steel side plates, either 3 mm or 6 mm thick, strain gauged on the side plates only. The curves of load-extension and load-strain for 3 mm aluminium alloy and steel side plates are compared in Fig 10. Both strain curves show increasing side-plate strain per unit load as initial clearance is taken up and bearing pressure increases. The curves for 3 mm steel plates indicate a progressive localised failure just before final failure, with a step increase in extension and reduction in strain. The 3 mm aluminium alloy and steel specimens achieved bearing loads of 15% and 20% of  $P_{ult}$  respectively. The load-extension results for 3 mm and 6 mm aluminium alloy and 6 mm steel are shown in Fig 11. Despite the differences of up to 25% in total stiffness, assuming no bolt/hole deformation, there is very little difference in measured stiffness for the three specimens. In practice, clearance and local deformation have reduced the stiffness contribution of the side plates and limited the bearing loads to about 20% of  $P_{ult}$ .

### 3.2.2 Trials with long specimens

Long specimens using steel side plates either 3 mm or 10 mm thick were investigated to increase the achievable load transfer. The specimen type is shown in Fig 8, F. The first studied, CO1, was 30 mm wide with 3 mm side plates fastened with a 6.35 mm bolt. Strain gauges were attached to the side plates only. The load-extension and load-strain curves are shown in Fig 12. Neglecting deformation the theoretical maximum bearing load, from equation 2, is 76% of the applied load. The measured bearing loads achieved are shown in Fig 12, reducing from the initial value of 0.63P to 0.38P at failure. The reduction in bearing load ratio was caused by bolt bending and plastic elongation of the holes in the side plates. The bearing stress at failure in the CFRP coupon was 784 MPa, 71% of the bearing strength.

To overcome the bolt/hole deformation problem and increase the load transfer ratio a specimen, denoted CO2, 50 mm wide with 10 mm thick steel side plates fastened with a 9.5 mm bolt, was investigated. The load-extension and load-strain curves for CO2 are shown in Fig 13. The lower curve shows the variation of side plate strain with applied load. It is linear up to initial bearing failure in the CFRP and then increases more slowly. The theoretical maximum bearing load neglecting deformation is 0.91P, whereas the initial value, measured from Fig 13, is about 0.79P. At initial bearing failure the bearing load is 50.4 kN, 72% of the applied load and 73% of the bearing strength for a 9.5 mm hole. Beyond initial failure, progressive bearing failure occurred, resulting in the reduction in total stiffness and strain rate shown. The failure modes of specimens CO1 and CO2 are shown in the photographs in Fig 14. CO1 has mostly tensile failure with a small amount of bearing deformation whereas CO2 shows evidence of much more bearing deformation, corresponding with the load-strain curve.

### 3.2.3 Single shear specimens

Specimens of type G (Fig 8) were used to study strength interaction in single shear with 6.35 mm countersunk fasteners. The asymmetry of this specimen can cause secondary bending, and this was restricted by clamping the CFRP coupon to the side plates. A single strain gauge was attached to the centre of the coupon at both sides to monitor both load transfer and additional bending. The results from a specimen with a 6 mm steel side plate are given in Fig 15. Load transfer values of up to 15.9% were achieved, although local deformation reduced this to 12.9% at failure. The secondary bending strain was less than 5%.

### 3.2.4 Specimens in compression

The compression quadrant was studied using the same specimens as for tension, types E and F in Fig 8. The side plates used were 6 mm or 10 mm thick steel which gave adequate Euler buckling rigidity. Nevertheless, the specimens were lightly clamped using engineers clamps to prevent incipient buckling of the individual members. Strain gauges were attached to the plates.

The load, displacement and strain response for a typical short specimen (BO9, type E) is given in Fig 16. The strain curve shows three distinct phases, representing friction effects, bolt bearing load transfer and progressive failure. Before the bolt clearance is taken up a small amount of load is transferred to the side plates through friction. A linear phase of bolt bearing load transfer then occurs, followed by progressive failure during which the side plate strain increases rapidly. Final failure occurs at a strain level greater than that for bolt bearing load transfer alone, and an estimate must be made of the strain at initial failure due to combined bolt bearing and compression stress. This point is shown on the curve at 380µε side plate strain and 81 kN applied load. Above this point the side plate strain increases rapidly because lateral expansion of the composite material around the hole under progressive failure causes increased friction load transfer. Nevertheless, the point of initial failure is clearly identified from the strain curve.

The problem of friction effects in laterally constrained compression bearing tests is known to give high values of bearing strength (8), and this is shown by the strength values obtained at final failure from the present tests. The apparent increase arises from friction locking of material round the hole, over an increased diameter of about one bolt diameter.

### 3.2.5 Conclusions from specimen trials

The results from the specimen trials established confidence in the parallel plate method for combined bearing/by-pass strength measurement. For low load transfer the short specimen, type E, with steel side plates the same thickness as the CFRP coupon gives bearing loads of up to 0.2P, depending on the bolt fit. Steel side plates are preferred for greater resistance to hole deformation. For double shear testing, strain gauges on the side plates only are sufficient, and the same side plates can be used for several specimens with resulting economy. However, the strains measured are of the order of 100µε and sensitive measurement equipment is required for good accuracy. The strains in the CFRP coupon are much greater, of the order of 1000µε, and consequently easier to measure. For this reason it is preferable, but more expensive, to apply the strain gauges to either side of the CFRP coupon midway between the bolts. By clamping the assembly to prevent buckling effects the parallel plate specimen can be used for compressive loading, but friction effects must be considered. For single shear testing single sided plates can be used, and they appear to give the same amount of load transfer as in double shear.

The coupon must be strain gauged to monitor both load transfer and secondary bending.

The long specimen, pinned and bonded, was capable of achieving very high load transfer ratios. With side plates about twice the coupon thickness, and a bolt of sufficient diameter to prevent bending, load transfer of up to 0.79P could be achieved. The specimen was shown to give a combined failure mode with considerable bearing deformation before failure in a bearing/tensile mode. The specimens developed were used to produce the strength data for sample strength interaction curves.

#### 4 STRENGTH INTERACTION CURVES

##### 4.1 Tension-bearing Interaction, Double and Single Shear, 6.35 mm Hole

The results for tension-bearing interaction in double shear (plain hexagonal headed bolts) for 6.35 mm holes are shown in Fig 17. The mean net tensile strength, from five filled hole specimens, was 670 MPa with a coefficient of variation (CV) of 3.28%. The bearing strength was determined for a 7.9 mm (5/16 in) hole because 6.35 mm bolts had insufficient strength for the thickness of laminate. The value given of 1091 MPa is the result from one specimen.

The interaction points were obtained from seven specimens identified in the diagram. Specimen G01, discussed in section 3.2.2 achieved the highest bearing stress, limited by bolt bending and hole elongation. A06, A07 and A08 were discussed in section 3.2.1. The other three, B03, B04 and B05 were tested with the same pair of 6 mm steel slide plates. As can be seen the bearing stress varied considerably for this group, depending on the initial bolt fit and deformation characteristics. This has given a spread of data points useful in constructing the curve.

A tension-bearing interaction curve for 6.35 mm countersunk bolts in single shear is shown in Fig 18. As in the double shear case only the tensile failure mode is shown since it is impossible to achieve bearing failures with this bolt size. The stresses were calculated assuming plain hole area loss, ie ignoring the countersink area. With this included the tensile stresses based on true net area are 5% higher than those given. The mean of three filled-hole specimens was used to give the net tensile strength, 572 MPa with CV of 0.87%. Specimen type G was used for the interaction studies, with strain gauges attached either side of the CFRP coupon to monitor both load transfer and bending. All specimens were clamped to restrict bending and the strain results showed this to be less than 5% at the specimen centre. The lower group of points, B16 to B18, were obtained from a specimen with a 6 mm steel side plate whereas the upper group, G01 and G02 used a 10 mm steel side plate. As can be seen the points are grouped with little scatter and an interaction curve could be drawn easily through them.

##### 4.2 Tension-bearing Interaction for 9.5 mm Bolts in Double Shear

The limited amount of testing with 9.5 mm bolts gave just sufficient data to produce an interaction curve, given in Fig 19. This curve is based on results from a bearing test, a filled hole tensile test and two interaction tests. Of the latter, the upper point was obtained using specimen G02, discussed in section 3.2.2. For this specimen, as shown in Fig 13, a distinct initial failure occurred at 62% of ultimate load followed by progressive deformation up to break. Referring to Fig 4, it can be seen that the corresponding bearing strength specimen, G07, had the same type of progressive failure characteristics, with initial bearing failure occurring at the same bearing stress of about 950 MPa. Depending on the design philosophy, the allowable stress would be set between initial failure and break, and it can be seen from Fig 19 that widely differing strength envelopes could result. Specimen G06 was used to give the other interaction point, assuming equal bearing load at each hole. The tensile mode curve is therefore an estimate and more results are needed to confirm its position. It nevertheless gives a good indication of the strength interaction characteristics with high bearing stress. Both strength modes were significantly reduced by interaction, but the initial bearing failure characteristics were unchanged by the presence of by-pass stress. Thus it seems that the major strength interaction effect is the reduction of net tensile strength.

##### 4.3 Compression-bearing Interaction in Double Shear for 6.35 mm and 9.5 mm Bolts

The compression-bearing interaction curve for 6.35 mm bolts is given in Fig 20. The net section strength, from four filled hole specimens, was 702 MPa with CV of 3.14%. Three specimens of the type discussed in section 3.2.4 were used to give the interaction points. An estimated curve for the compression failure mode (initial failure) was drawn through the limited number of points. Comparing this with the tension mode failure in Fig 17 shows the behaviour in both quadrants to be virtually the same. The points shown for final failure show much higher bearing strengths but are unrepresentative of bearing/bypass interaction because of the "friction locking" mechanism discussed in section 3.2.4.

The compression-bearing interaction behaviour with 9.5 mm bolts is shown in Fig 21. This envelope was constructed from the mean of three net compression strength results, a bearing strength result and an interaction strength result using the specimens shown. Compared with the tensile quadrant (Fig 19) there is little apparent interaction in the compression mode. However, this may be masked by the high scatter present in the notched compression results. The CV from the three tests was 9%, considered high for fibre

controlled failure, although failures occurred in a satisfactory mode through the hole centre in each case. The mean compression strength was 543 MPa, 82% of the net tensile strength measured from one specimen.

The effect of bearing on net compression failure mode is shown in the photographs in Fig 22; the fracture zone has moved from the hole centre to a position outside the hole centred on the focus of bearing deformation.

## 5 DISCUSSION

The first part of the study compared test methods for measuring the strength interaction of bearing and by-pass stresses. Two major specimen types were studied: multi-hole specimens depending on load sharing between a number of bolts in a row and parallel plate specimens depending on load sharing between the CFRP coupon and the parallel plates. Multi-hole joints in aluminium alloy have been tested successfully and the bolt/hole deformation resulting from plasticity was found in the limit to "equalise" the bearing load on each bolt. This limiting case would be most useful in CFRP testing also since it would give a means of varying the ratio of bearing load to bypass load simply by varying the number of holes in a row.

This concept was assessed with CFRP/steel specimens but the relatively brittle nature of the material prevented appreciable equalisation of the bolt loads. It was found that specimens with two, three and four holes failed at virtually the same load, with the bearing stress concentrated at the first hole. A 4-hole specimen was fatigue tested to "shake-down" the stress concentrations, and simultaneously analysed using the SPATE system to monitor load redistribution among the bolts. Although there was some equalisation of the bolt loads, the effect was not readily quantifiable. By sophisticated design, such as tapering the loading plates and using "weaker" bolts, it may be possible to achieve a more even load distribution. This would nevertheless be uncertain and dependent on predictable bearing deformation characteristics in the CFRP laminate. In view of the uncertain bolt load distribution, the multi-hole specimen cannot be recommended for quantitative testing in combined bearing and by-pass stress.

The parallel plate specimen proved to be more successful. It was capable of applying a wide range of bearing/by-pass load ratios, and was economical of material. The best arrangement was given by steel plates, of the same thickness and width as the parallel CFRP coupon, which were varied in length to vary the bearing/by-pass load ratio. For double shear testing a symmetrical assembly of two steel plates was used, whereas for single shear testing a single steel plate was used, supported against bending if necessary. The load in the members was determined from measured strain, either in the side plates or in the CFRP coupon. In double shear testing the side plates only need be instrumented, and the same pair of plates can be used for many tests. For single shear tests the CFRP coupon must be strain gauged to monitor both load transfer and the incidence of secondary bending.

Using the two configurations of parallel plate specimen described in section 3, sample strength envelopes were produced for two bolt sizes in an IM6-6376 laminate. In practice the 6.35 mm bolts were not strong enough to cause bearing failure and the bearing stress was limited to about 70% of bearing strength. Consequently the study was limited to the effect of bearing stress on net tensile strength. In the tension-bearing quadrant for 6.35 mm holes, (double shear) bearing stress significantly reduced the net tensile strength, up to about 18% for this hole size. Similar interaction behaviour was shown for countersunk holes in single shear. The compression - bearing quadrant was also studied for 6.35 mm bolts in double shear. Friction effects after initial failure were significant giving rise to unrepresentatively high bearing stresses at failure. Nevertheless the initial failure point was clearly detected from the load-strain curves. The interaction curve obtained for compression mode failure was similar to that for tension mode failure.

A limited amount of testing was done using 9.5 mm bolts in double shear. In this case bearing mode failures could be achieved and the interaction studies covered the full envelope of bearing and by-pass strength. It was found that the interaction behaviour for high load transfer (bearing mode) was virtually identical in both quadrants. A difference occurred in notched strength, with compression strength significantly less than tension strength. Some of this can be attributed to scatter, but its effect is to reduce the strength interaction in compression compared with tension.

It is clear from all the results that the main effect of interaction is the reduction of notched strength due to bearing stress. This is shown for tension in Fig 23. Plain holes in double shear have the greatest strength reduction. Countersunk holes appear to show very little strength reduction up to 30% load transfer.

Clearly, more testing is required, both to confirm the shape of the interaction curves and to provide statistically significant data. Nevertheless the specimens developed provide a convenient method of little more complexity than simple coupons.

## 6 CONCLUSIONS

The parallel strip specimen, as described, provides a convenient means of experimentally studying the strength interaction of bearing and by-pass stresses. It is adaptable for use in double shear and single shear, with different fastener type. The bearing

load is most effectively controlled by varying the specimen length, since this reduces the effects of initial clearance and bolt/hole deformation. However, the important case of low load transfer can be studied with a short specimen which is economical of material.

A range of sample strength interaction curves were produced in IM6-8376 material, for two hole sizes in both tension and compression. It was concluded that the strength envelopes for 6.35 mm bolts in double shear were virtually the same in either stress quadrant. In the case of the larger bolts (9.5 mm) there appeared to be less interaction in compression than in tension, although some of the differences was accounted for by scatter in net compression strength. Single shear (countersunk fastener) joints in tension showed less reduction in net strength than double shear joints.

Further testing is underway at RAE to explore interaction behaviour over a range of parameters, including countersunk fasteners in compression and environmental testing.

#### REFERENCES

<u>No</u>	<u>Author</u>	<u>Title, etc</u>
1	T A Collings	The strength of bolted joints in multi-directional CFRP laminates. RAE Technical Report 75127 (1975).
2	L J Hart-Smith	Design and analysis of bolted and riveted joints in fibrous composite structures. International Symposium on Joining and Repair of Fibre-Reinforced Plastics, Imperial College, London, Sept 10, 1986.
3	J H Crews, Jr R A Naik	Combined bearing and bypass loading in a Graphite/Epoxy laminate. Journal of Composite Structures Sept 86 Vol 6 Nos 1-3, 1986.
4	Th de Jong E C Klang	Pinned connections in composite materials, theory and experiment. Delft University of Technology. Report LR-445 January 1985.
5	E H Green	Report on the stiffness of bolted and riveted joints. S.O.R.(P) 75, British Aerospace, Warton, Oct 1971.
6	N Harwood W M Cummings	Applications of thermoelastic stress analysis. Strain, February 1986.
7	S V Ramani D P Williams	Notched and unnotched fatigue behaviour of angle-ply graphite/epoxy composites. ASTM STP 636 1977 pp27-46.
8	T A Collings	On the bearing strengths of CFRP laminates. RAE Technical Report 82033 (1982).

#### LIST OF FIGURES

Fig 1	Load distribution in 3-hole joint
Fig 2	Effect of yielding in multi-hole specimens
Fig 3	Specimen configurations
Fig 4	Load extension curves for multiple hole joints C03-C07
Fig 5	Failure modes of multi-hole specimens
Fig 6	Failure mode of 4-hole residual strength specimen
Fig 7	SPATE scans of 4-hole specimen
Fig 8	Parallel plate specimen configurations
Fig 9	Load distribution in parallel plate specimen
Fig 10	Load extension and load strain curves for 3 mm Al and steel side plates
Fig 11	Load extension curves for S1 to S3
Fig 12	Load extension and load strain, C01
Fig 13	Load extension and load strain, C02
Fig 14	Failure modes, C01 and C02
Fig 15	Load extension and load strain characteristics single shear c/s B16
Fig 16	Compression-bearing specimen B09, load extension and load strain characteristics
Fig 17	Tension-bearing interaction, 6.35 mm hole
Fig 18	Tension-bearing interaction, 6.35 mm c/s hole
Fig 19	Tension-bearing interaction, 9.5 mm hole
Fig 20	Compression-bearing interaction, 6.35 mm hole
Fig 21	Compression-bearing interaction, 9.5 mm hole
Fig 22	Combined failure modes in high bearing stress
Fig 23	Effect of bearing stress on net tensile strength

Type	Spec ID	Geometry					Test Result and Comments	
		b	l	p	d	t2		
A	A00	30	160				Tension Compression	E = 71.1 GPa E = 70.3 GPa
B	A03	30	205	e/d=	6.35		Bolt Sheared	
B	A04	30	205	5	7.9		Pb = 49 kN	$\sigma_b = 1091 \text{ MPa}$
B	A05	64	205	5	9.5		Pb = 57.3 kN	$\sigma_b = 1069 \text{ MPa}$
B	C07	50	205	5	9.5		Pb = 69.5 kN	$\sigma_b = 1296 \text{ MPa}$
C	A09	30	160		6.35		$\sigma_{TT} = 676 \text{ MPa}$	
C	B06	30	160		6.35		$\sigma_{TT} = 687 \text{ MPa}$	
C	B07	30	160		6.35		$\sigma_{TT} = 631 \text{ MPa}$	
C	B08	30	160		6.35		$\sigma_{TT} = 692 \text{ MPa}$	
C	A12	30	160		6.35		$\sigma_{TT} = 574 \text{ MPa}$	(C/S)
C	A13	30	160		6.35		$\sigma_{TT} = 565 \text{ MPa}$	(C/S)
C	A14	30	160		6.35		$\sigma_{TT} = 566 \text{ MPa}$	(C/S)
C	C04	50	290		9.5		$\sigma_{TT} = 646 \text{ MPa}$	
C	A02	30	160		6.35		$\sigma_{TC} = -684 \text{ MPa}$	
C	B12	30	160		6.35		$\sigma_{TC} = -728 \text{ MPa}$	
C	B13	30	160		6.35		$\sigma_{TC} = -721 \text{ MPa}$	
C	B14	30	160		6.35		$\sigma_{TC} = -678 \text{ MPa}$	
C	A10	30	160		6.35		$\sigma_{TC} = -653 \text{ MPa}$	(C/S)
C	A11	30	160		6.35		$\sigma_{TC} = -663 \text{ MPa}$	(C/S)
C	B15	30	160		6.35		$\sigma_{TC} = -680 \text{ MPa}$	(C/S)
C	C09	50	290		9.5		$\sigma_{TC} = -529 \text{ MPa}$	
C	H01	50	290		9.5		$\sigma_{TC} = -491 \text{ MPa}$	
C	H02	50	290		9.5		$\sigma_{TC} = -609 \text{ MPa}$	
D	A15	30	205	4d	6.35	6 St	$\sigma_{TT} = 541 \text{ MPa}$	4 HOLE
D	B01	30	205	4d	6.35	3 St	Test Stopped ( $\sigma_{TT} = 430 \text{ MPa}$ )	4 HOLE
D	B02	30	205	4d	6.35	6 St	$\sigma_{TT} = 572 \text{ MPa}$	4 HOLE
D	C03	50	205	4d	9.5	10St	$\sigma_{TT} = 490 \text{ MPa}$	4 HOLE
D	C05	50	205	4d	9.5	10St	$\sigma_{TT} = 476 \text{ MPa}$	3 HOLE
D	C06	50	205	4d	9.5	10St	$\sigma_{TT} = 490 \text{ MPa}$	2 HOLE
E	A06	30	160	100	6.35	3 Al	$\sigma_{TC} = 586 \text{ MPa}$	$\sigma_b = 298 \text{ MPa}$
E	A07	30	160	100	6.35	6 Al	$\sigma_{TC} = 602 \text{ MPa}$	$\sigma_b = 239 \text{ MPa}$
E	A08	30	160	100	6.35	3 St	$\sigma_{TC} = 542 \text{ MPa}$	$\sigma_b = 419 \text{ MPa}$
E	B03	30	160	100	6.35	6 St	$\sigma_{TC} = 568 \text{ MPa}$	$\sigma_b = 461 \text{ MPa}$
E	B04	30	160	100	6.35	6 St	$\sigma_{TC} = 564 \text{ MPa}$	$\sigma_b = 377 \text{ MPa}$
E	B05	30	160	100	6.35	6 St	$\sigma_{TC} = 581 \text{ MPa}$	$\sigma_b = 638 \text{ MPa}$
E	B09	30	160	100	6.35	6 St	$\sigma_{TC} = 621 \text{ MPa}$	$\sigma_b = 802 \text{ MPa}$
E	B10	30	160	100	6.35	6 St	$\sigma_{TC} = 626 \text{ MPa}$	$\sigma_b = 863 \text{ MPa}$
E	B11	30	160	100	6.35	6 St	$\sigma_{TC} = 672 \text{ MPa}$	$\sigma_b = 873 \text{ MPa}$
E	F07	30	160	100	6.35	6 St	$\sigma_{TC} = 615 \text{ MPa}$	$\sigma_b = 718 \text{ MPa}$
F	C01	30	540		6.35	3 St	$\sigma_{TT} = 543 \text{ MPa}$	$\sigma_b = 779 \text{ MPa}$
F	C02	50	580		9.5	10St	$\sigma_{TT} = 503 \text{ MPa}$	$\sigma_b = 1175 \text{ MPa}$
F	C08	50	580		9.5	10St	$\sigma_{TC} = -514 \text{ MPa}$	$\sigma_b = 1213 \text{ MPa}$
G	B16	30	160	100	6.35	6 St	$\sigma_{TT} = 553 \text{ MPa}$	$\sigma_b = 636 \text{ MPa}$
G	B17	30	160	100	6.35	6 St	$\sigma_{TT} = 566 \text{ MPa}$	$\sigma_b = 589 \text{ MPa}$
G	B18	30	160	100	6.35	10St	$\sigma_{TT} = 535 \text{ MPa}$	$\sigma_b = 597 \text{ MPa}$
*	G01	30	585		6.35	10St	$\sigma_{TT} = 517 \text{ MPa}$	$\sigma_b = 914 \text{ MPa}$
*	G02	30	585		6.35	10St	$\sigma_{TT} = 496 \text{ MPa}$	$\sigma_b = 869 \text{ MPa}$

\*Single side plate specimen of type F (C/S)

TABLE 1

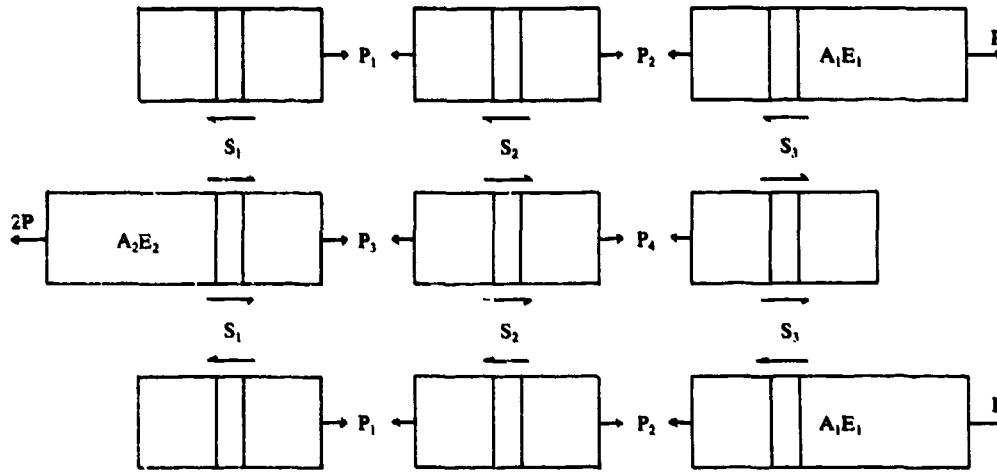
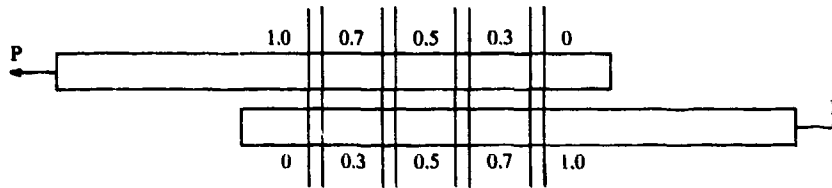


FIG.1 LOAD DISTRIBUTION IN 3 HOLE JOINT

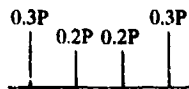
MULTI-HOLE SPECIMENS



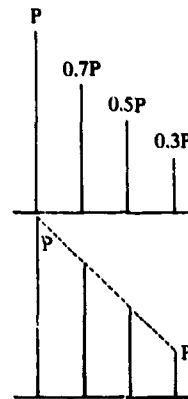
BOLT BEARING AND SHEET BEARING FLEXIBILITY IN ALUMINIUM SHEET GIVE TYPICAL LOAD DISTRIBUTION AS

1

BOLT SHEAR



SHEET TENS



IN METALS, YIELDING EQUALISES BOLT SHEARS, GIVING

2



LESS BEARING DEFORMATION IN COMPOSITES MAY NOT GIVE SHEAR EQUALISATION AS IN METALS — UNQUANTIFIED LOAD TRANSFER

FIG.2 EFFECT OF YIELDING IN MULTI-HOLE SPECIMENS

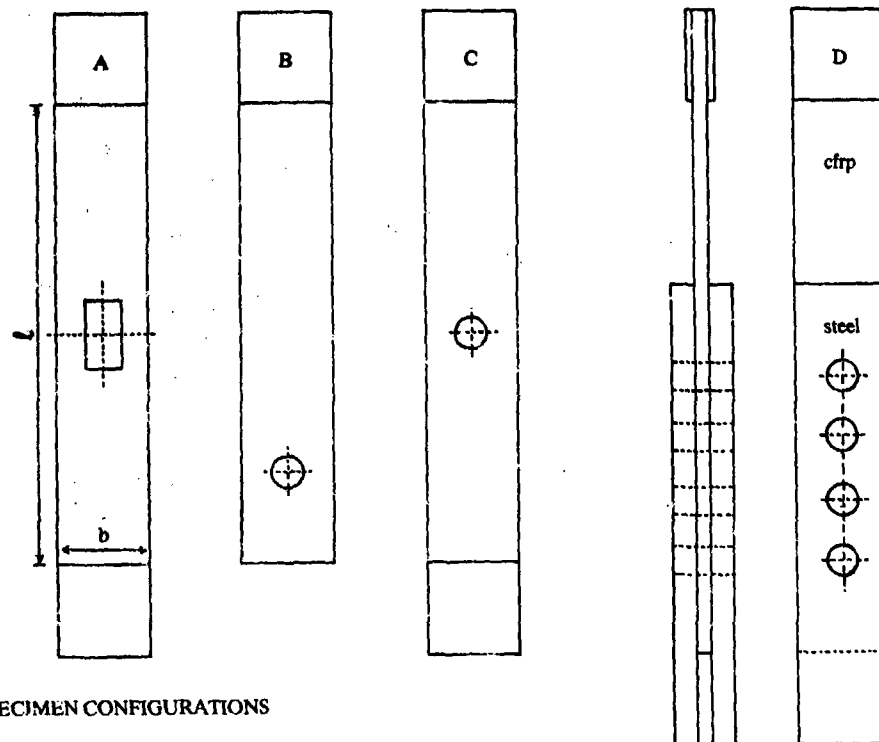


FIG.3 SPECIMEN CONFIGURATIONS

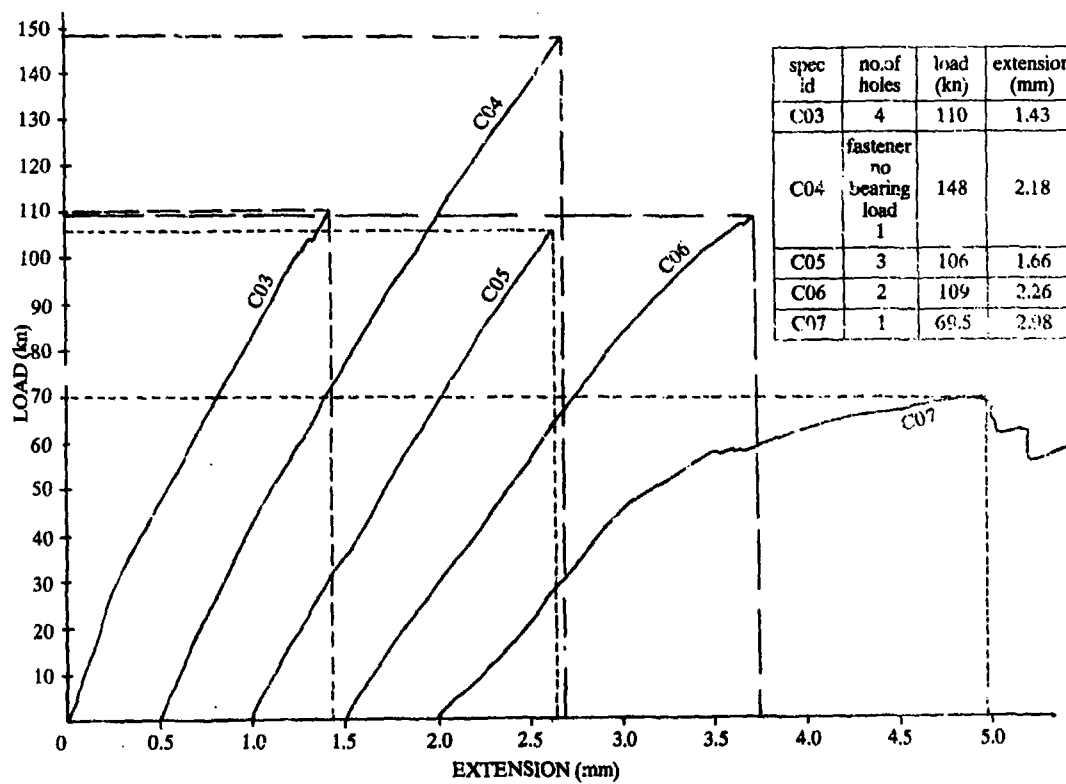


FIG.4 LOAD—EXTENSION CURVES FOR MULTIPLE HOLE JOINTS C03—C07

11-12



C07  
BEARING



C04  
TENSION



C03



C05



C06

FIG.5 FAILURE MODES OF MULTI-HOLE SPECIMENS



FIG.6 FAILURE MODE OF 4-HOLE RESIDUAL STRENGTH SPECIMEN

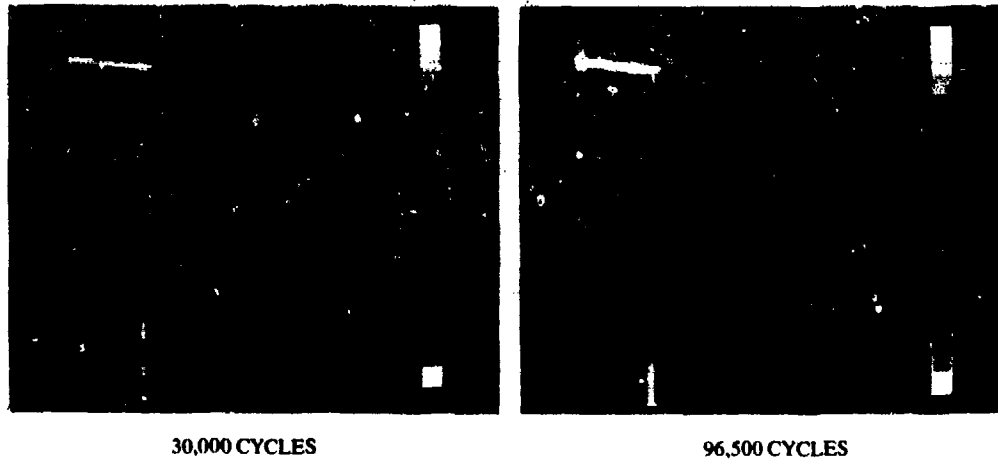


FIG.7 SPATE SCANS OF 4-HOLE SPECIMEN

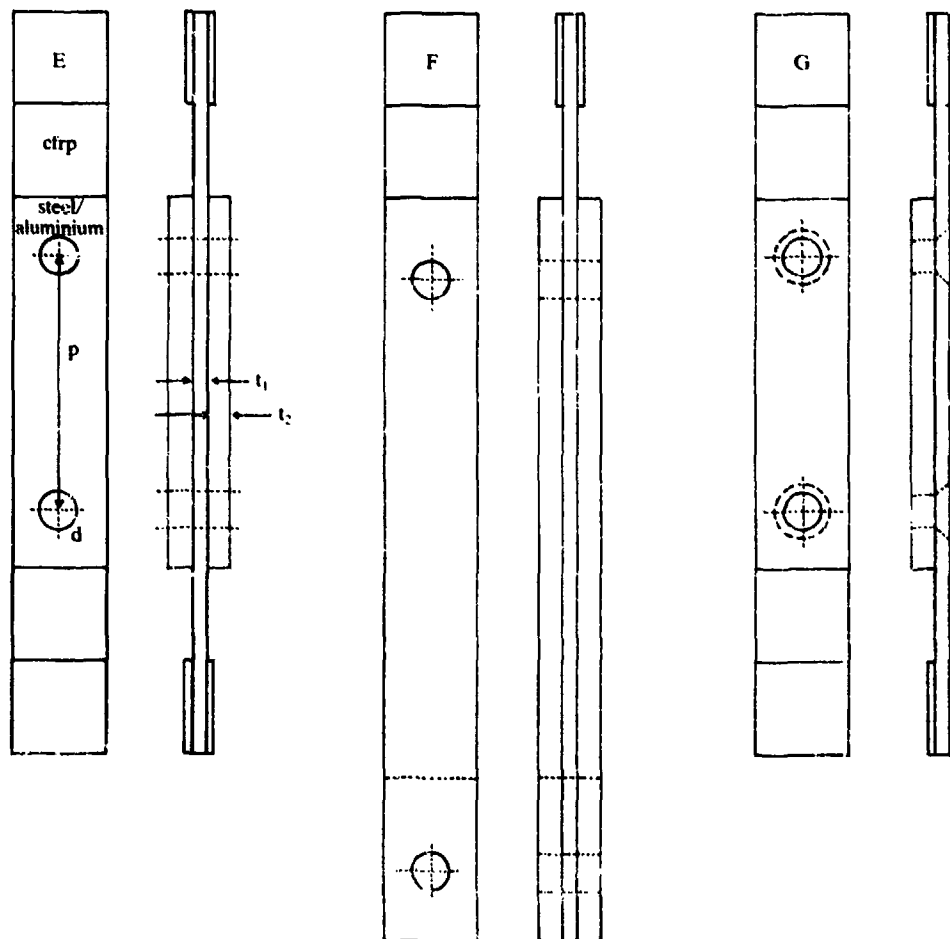


FIG.8 PARALLEL PLATE SPECIMEN CONFIGURATIONS

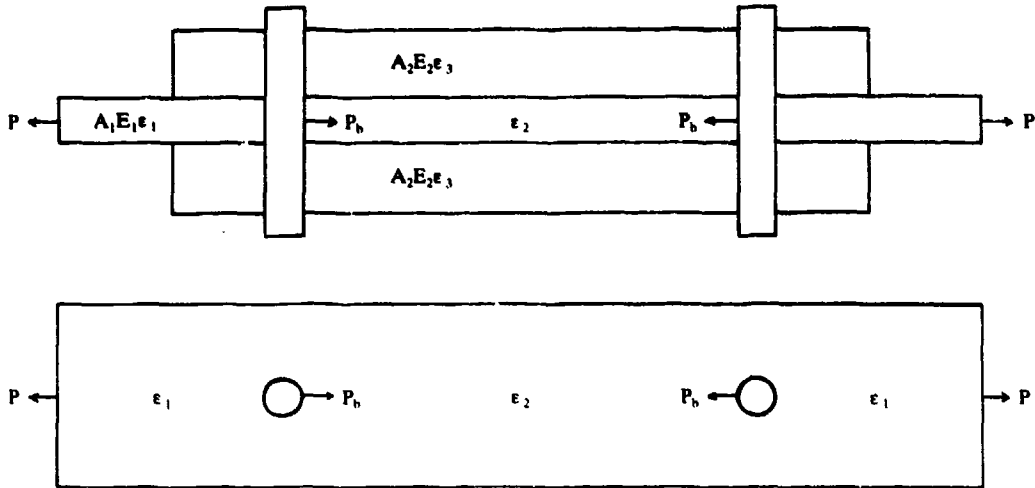


FIG.9 LOAD DISTRIBUTION IN PARALLEL PLATE SPECIMEN

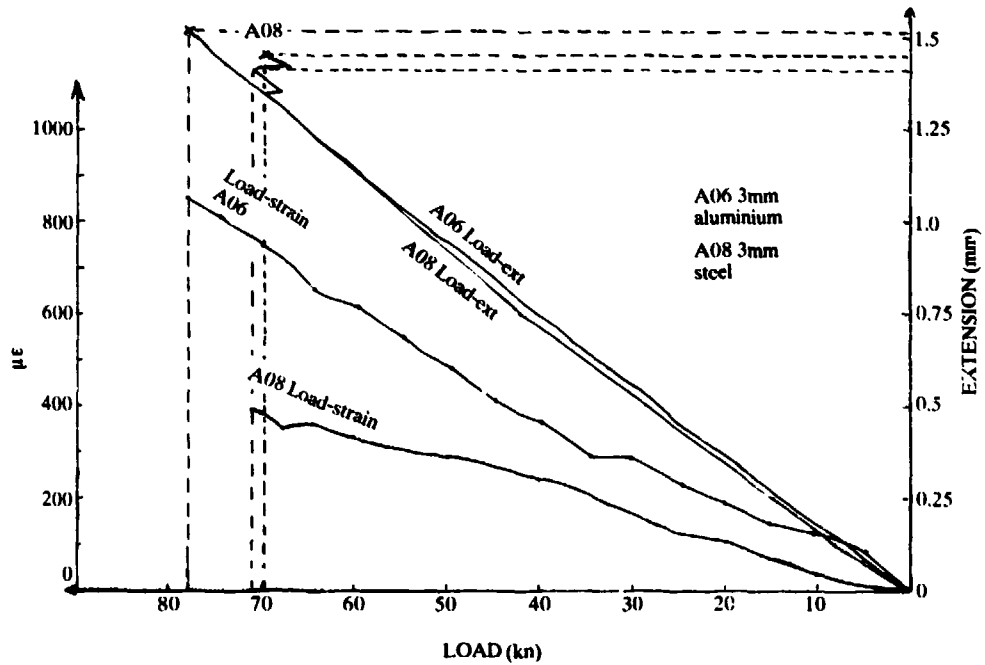


FIG.10 LOAD-EXTENSION AND LOAD-STRAIN CURVES FOR 3mm ALUMINIUM AND STEEL SIDE PLATES

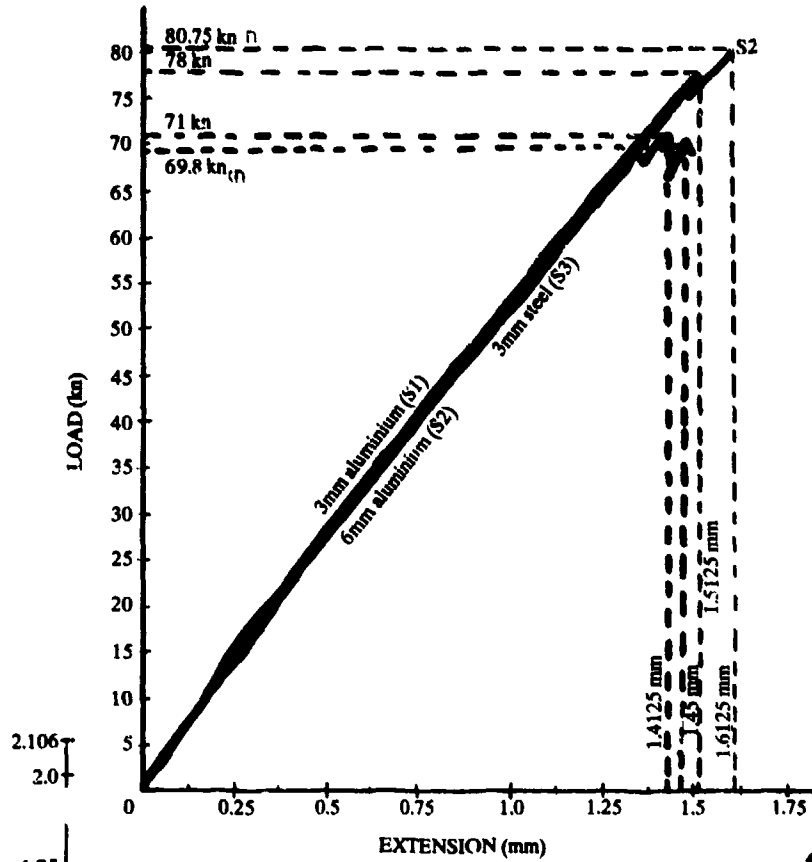


FIG.11 LOAD EXTENSION CURVES FOR S1 TO S3 (A06 TO A08)

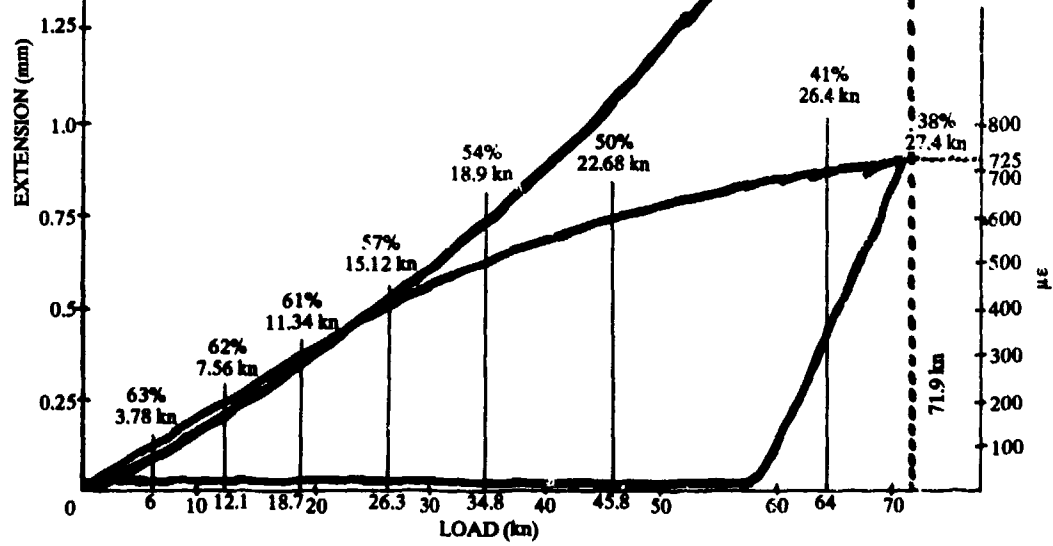


FIG.12 LOAD EXTENSION CURVE & LOAD STRAIN CO1

11-16

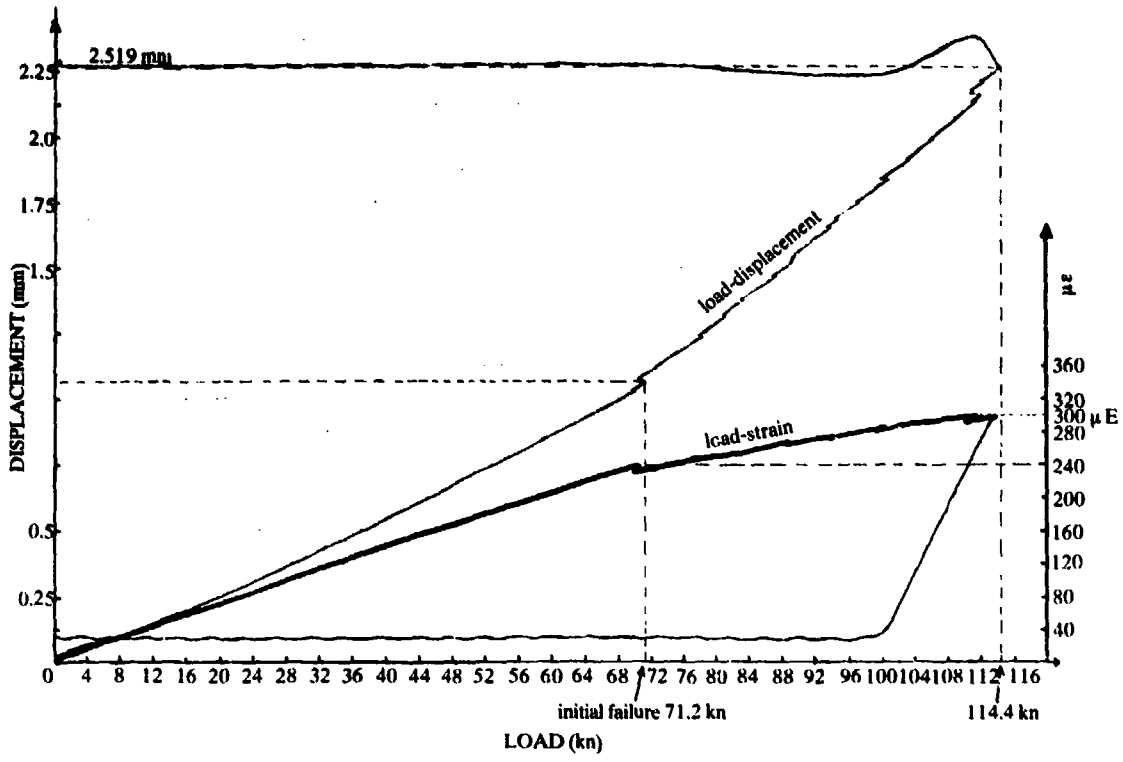


FIG.13 LOAD EXTENSION & LOAD STRAIN, CO2

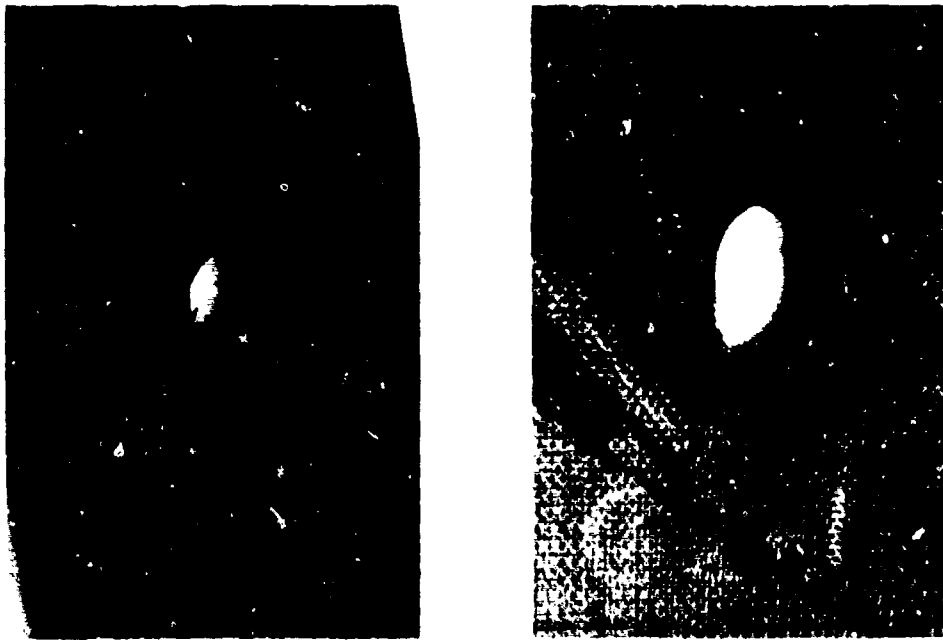


FIG.14 FAILURE MODES, CO1 AND CO2

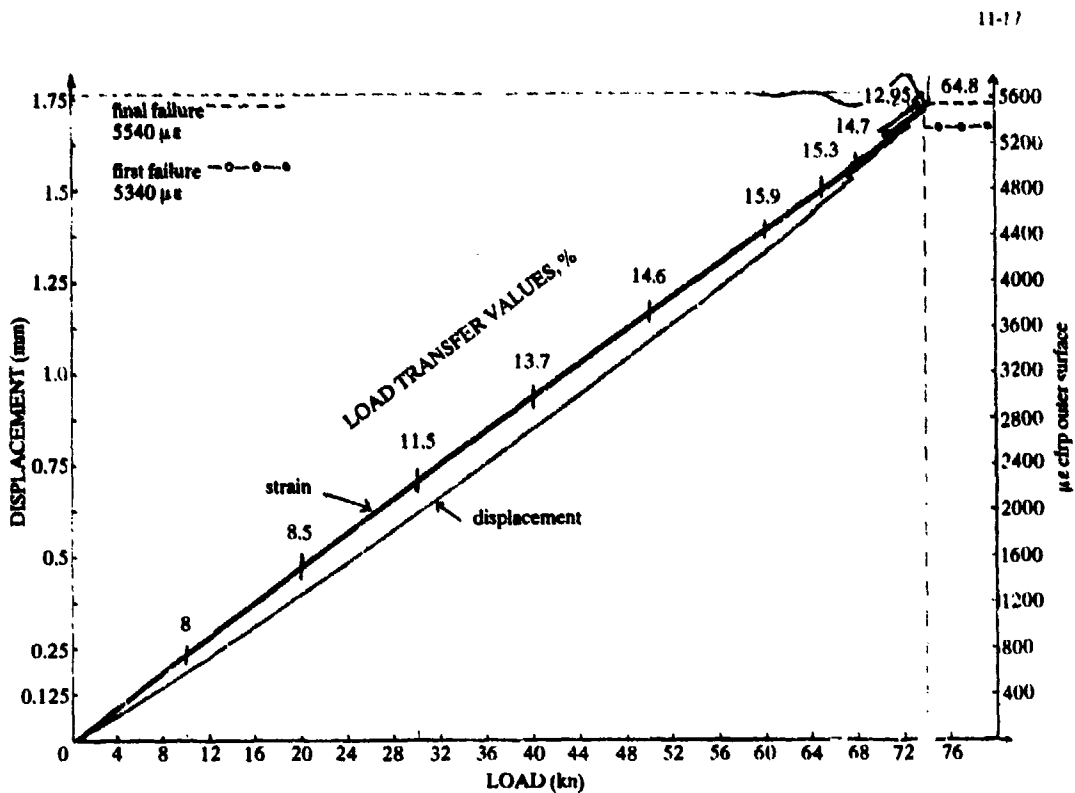


FIG.15 LOAD-EXTENSION AND LOAD-STRAIN CHARACTERISTICS, SINGLE SHEAR C/S B16

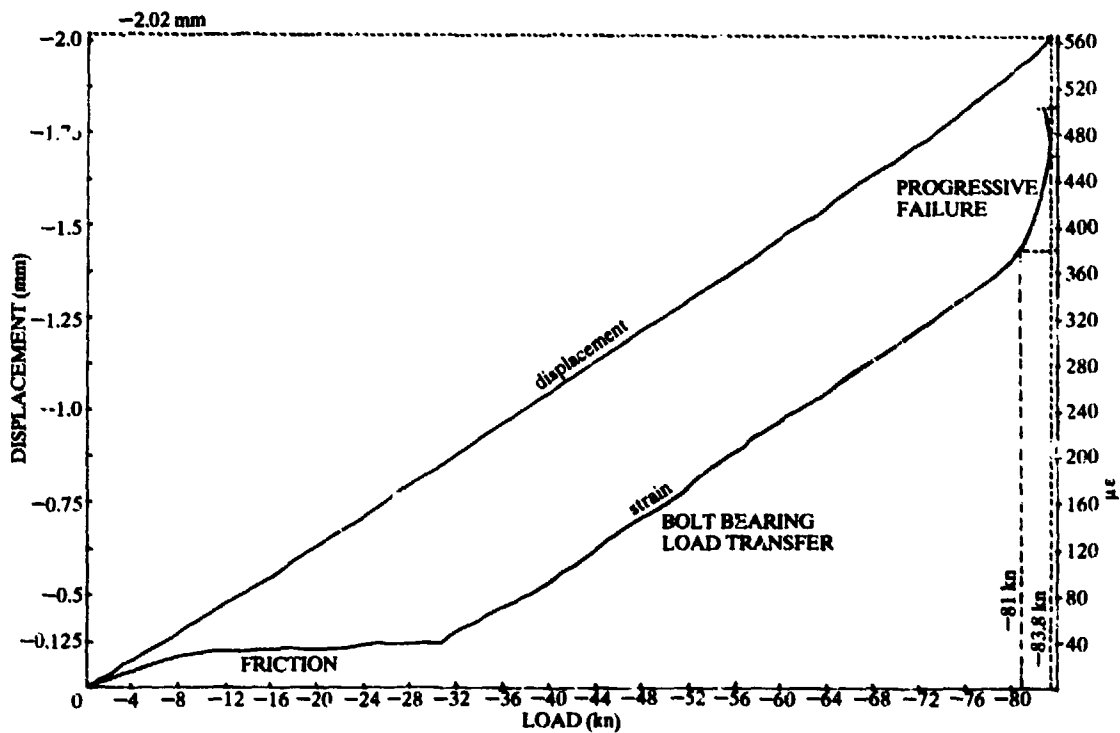


FIG.16 COMPRESSION-BEARING SPECIMEN B09, LOAD EXTENSION AND STRAIN CHARACTERISTICS

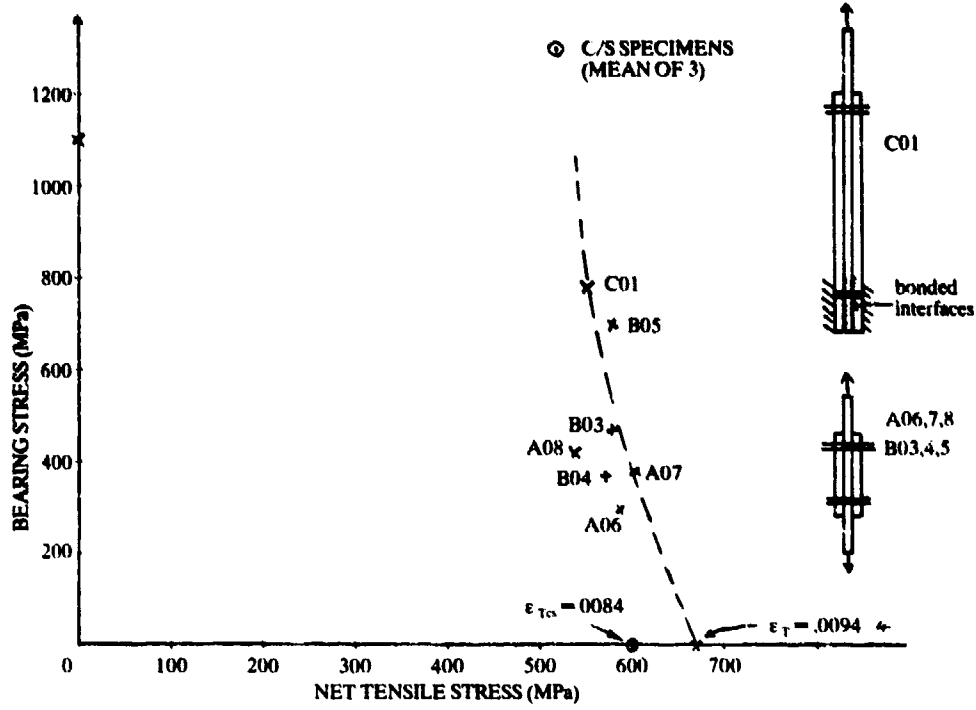


FIG.17 TENSION-BEARING INTERACTION, 6.35 mm HOLE

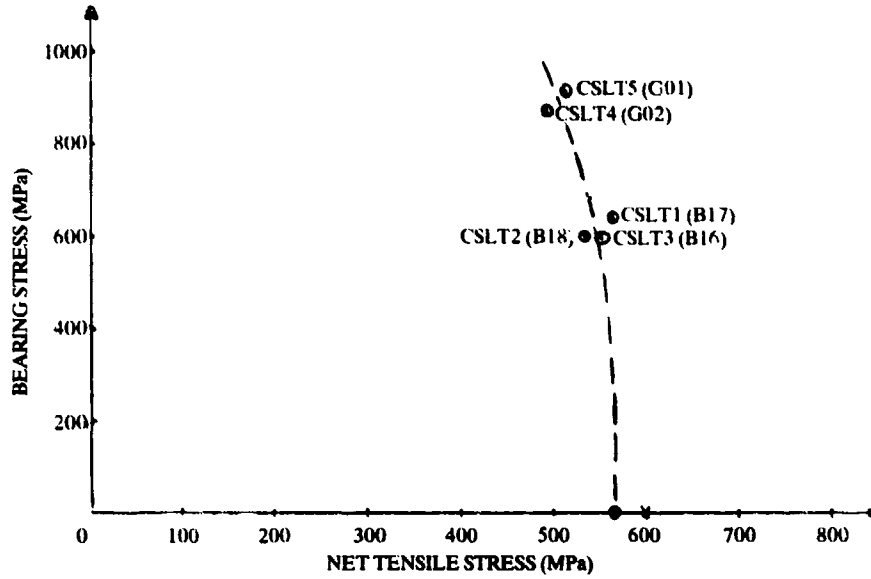


FIG.18 TENSION-BEARING INTERACTION 6.35 mm C/S HOLE

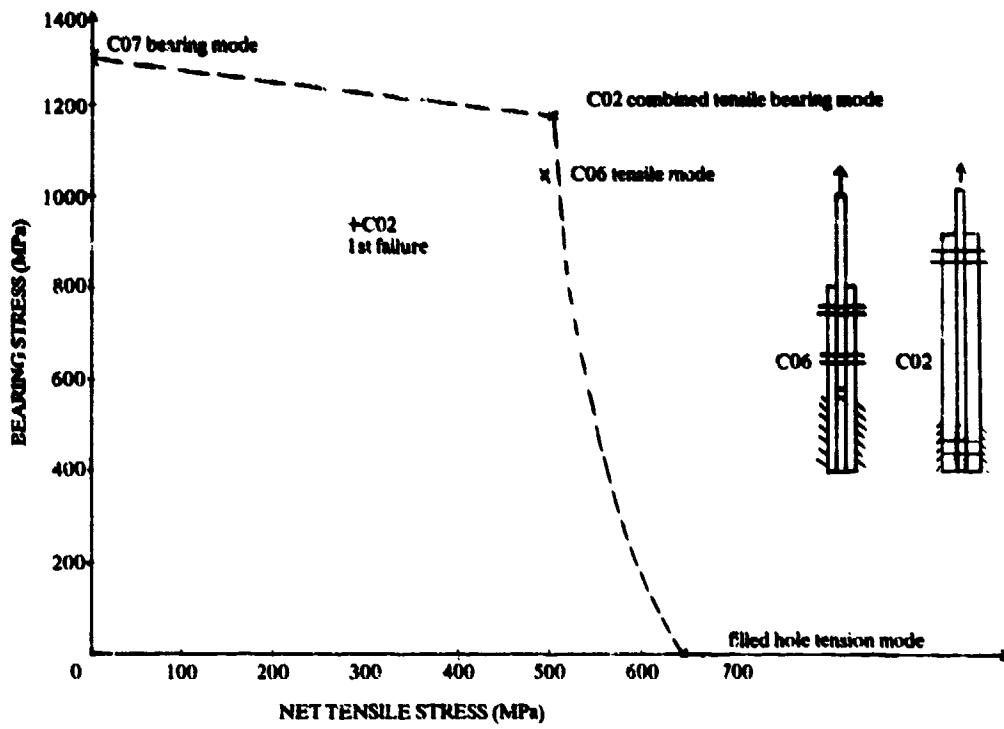


FIG.19 TENSION-BEARING INTERACTION 9.5 mm HOLE

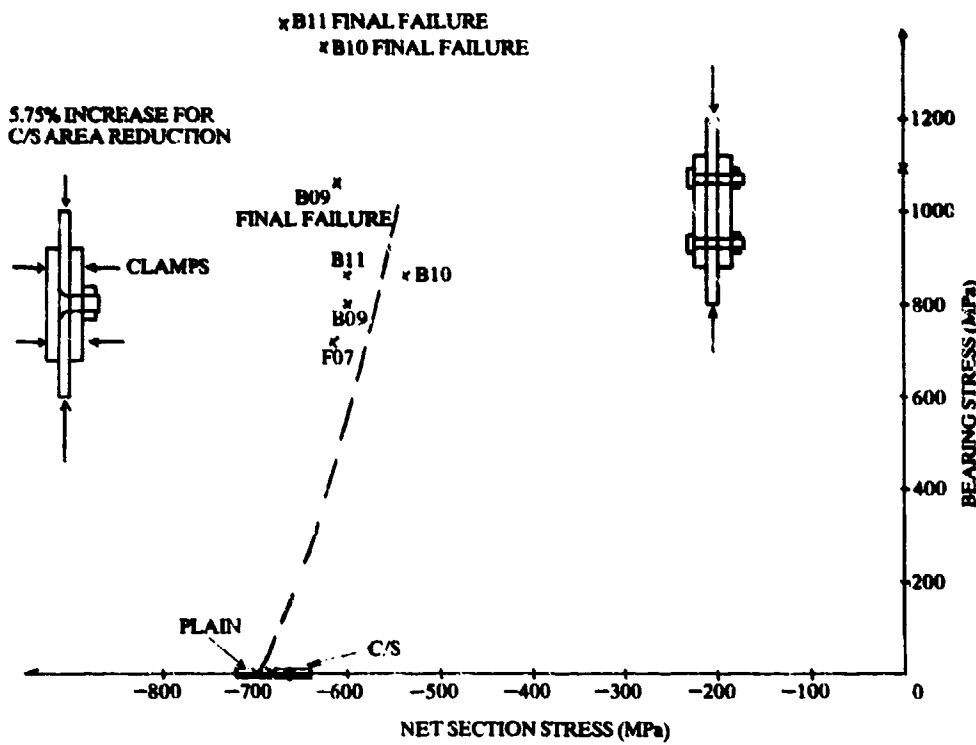


FIG 20 COMPRESSION BEARING INTERACTION, 6.35 mm HOLE

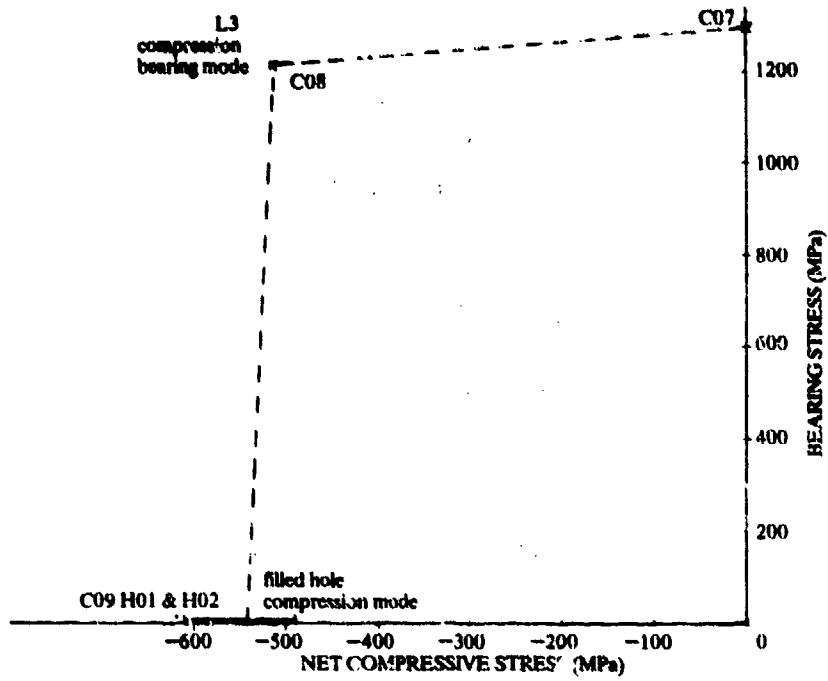


FIG.21 COMPRESSION BEARING INTERACTION 9.5 mm HOLE

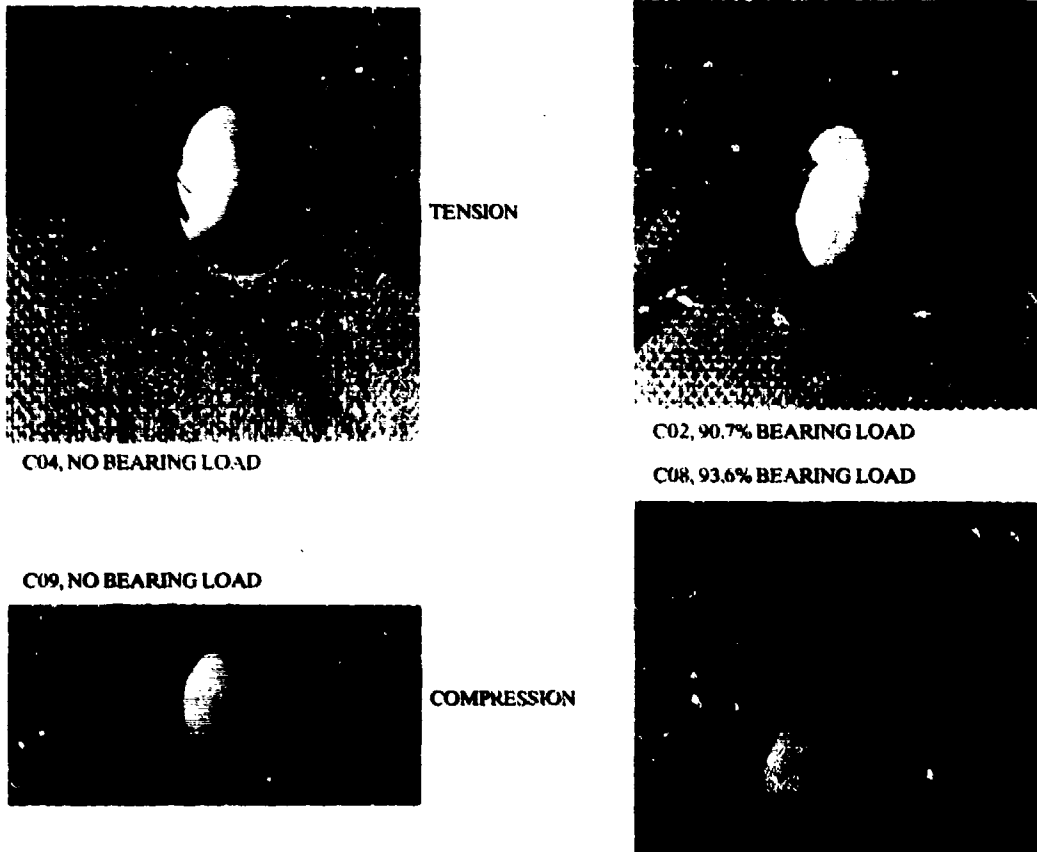


FIG.22 COMBINED FAILURE MODES IN HIGH BEARING STRESS

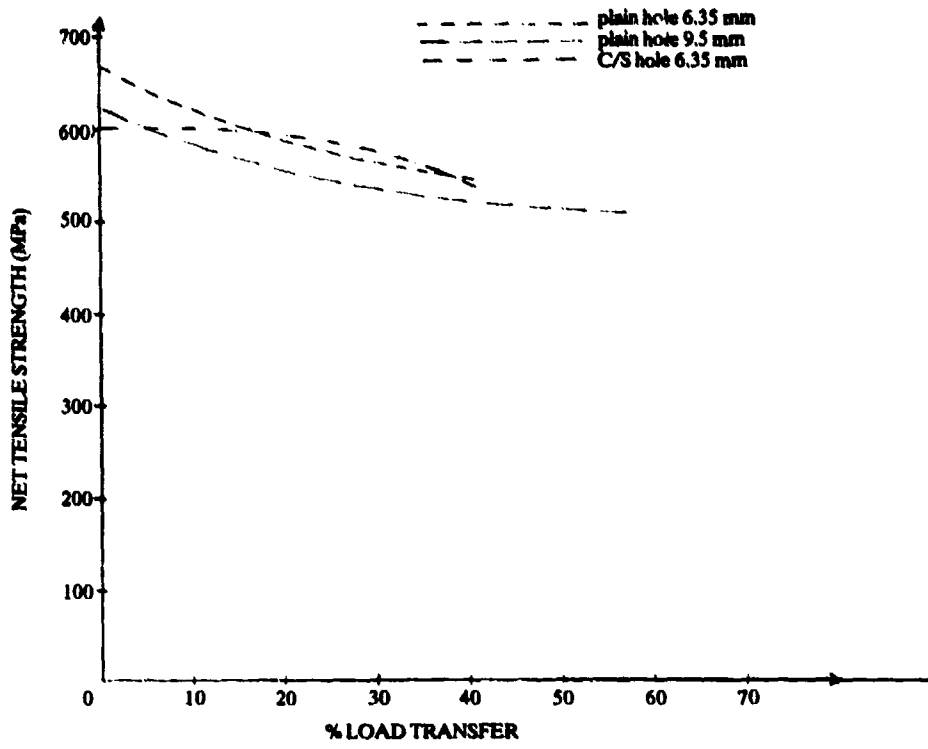


FIG.23 EFFECT OF BEARING STRESS ON NET TENSILE STRENGTH

## BEARING-BYPASS LOADING ON BOLTED COMPOSITE JOINTS

by  
 J. H. Crews, Jr.  
 NASA Langley Research Center  
 Mail Stop 188E  
 Hampton, Virginia 23665, U. S. A.

and  
 R. A. Naik  
 PRU Kentron, Inc.  
 303 Butler Farm Road  
 Hampton, Virginia 23666, U. S. A.

## SUMMARY

A combined experimental and analytical study has been conducted to investigate the effects of simultaneous bearing and bypass loading on a graphite/epoxy (T300/3208) laminate. Tests were conducted with a test machine that allows the bearing-bypass load ratio to be controlled while a single-fastener coupon is loaded to failure in either tension or compression. Test coupons consisted of 16-ply quasi-isotropic graphite/epoxy laminates with a centrally-located 6.35-mm bolt having a clearance fit. Onset-damage and ultimate strengths were determined for each test case. Next, a finite element stress analysis was conducted for each test case. The computed local stresses were used with appropriate failure criteria to analyze the observed failure modes and strengths. An unexpected interaction of the effect of the bypass and bearing loads was found for the onset of compression-reacted bearing damage. This interaction was caused by a decrease in the bolt-hole contact arc and a corresponding increase in the severity of the bearing loads. The amount of bolt-hole contact had a significant effect on local stresses and, thus, on the calculated damage-onset and ultimate strengths. An offset-compression failure mode was identified for laminate failure under compression bearing-bypass loading. This failure mode appears to be unique to compression bearing-bypass loading and, therefore, cannot be predicted from simple tests.

## LIST OF SYMBOLS

$C$	bolt-hole clearance, m
$d$	hole diameter, m
$P_A$	applied load, N
$P_b$	bearing load, N
$P_p$	bypass load, N
$S_b$	nominal bearing stress, MPa
$S_{np}$	nominal net-section bypass stress, MPa
$r, \theta$	polar coordinates, m, deg
$t$	specimen thickness, m
$w$	specimen width, m
$x, y$	Cartesian coordinates, m
$\beta$	bearing-bypass ratio
$\theta_1$	bolt-hole contact half-angle for single contact, deg
$\theta_2$	secondary bolt-hole contact half-angle for dual contact, deg
$\sigma_{rr}$	radial stress component, MPa
$\sigma_{\theta\theta}$	tangential stress component, MPa

## INTRODUCTION

In the past, composite joints have often been designed using rather simple metals-based procedures without encountering serious problems. In most such cases, the structural design strains have been limited by damage-tolerance considerations, and at low structural strain levels, the joints have been adequate. However, as tougher composites come into use, the design strains will rise and structural joining requirements will become more critical. Analytical design procedures for joints should be based on a sound understanding of the response of composite materials under loading conditions similar to those in multi-fastener joints.

Within multi-fastener joints, fastener holes may be subjected to both bearing loads and loads that bypass the hole, as shown in figure 1. The ratio of the bearing load to the bypass load depends on the joint stiffness and configuration. As the joint is loaded, this bearing-bypass ratio at each fastener remains nearly constant until damage begins to develop. In general, different bearing-bypass ratios produce different failure modes and strengths for each fastener hole. The laminate response can be studied by testing single-fastener specimens under bearing bypass loading, but such tests are usually difficult. The first objective of the present paper is to describe a relatively simple approach for the bearing-bypass testing of single-fastener coupons. This approach uses two hydraulic servo-control systems to apply proportional bearing and bypass loads to a specimen with a central hole. The second objective

of this paper is to present bearing-bypass strength data for a wide range of bearing-bypass ratios in both tension and compression. Previous data in the literature have been rather limited, especially for compression. The test specimens were made of T300/5208 graphite/epoxy in a 16-ply quasi-isotropic layup. The bearing loads were applied through a clearance-fit steel bolt having a nominal diameter of 6.35 mm. The test results are presented as bearing-bypass diagrams for damage-onset strength and for ultimate strength. The corresponding damage modes were determined by radiographing each specimen after testing.

The third objective of this study was the analysis of the bearing-bypass test results using the local stresses around the bolt hole, computed for combined bearing and bypass loading. These stresses were calculated using a finite element procedure that accounted for nonlinear bolt-hole contact. The corresponding contact angles were calculated, as well as the local stress distributions. The stresses were used to compute the damage-onset and ultimate strengths for the range of bearing-bypass test conditions. The computed strengths were used to discuss the test trends.

## BEARING BYPASS TESTING

### Test Procedure

The test specimen configuration and loading combinations are shown in figure 2. The graphite/epoxy specimens were machined from a single [0/45/90/-45]<sub>2s</sub> panel. The bolt holes were machined using an ultrasonic diamond core drill. They were then carefully hand-reamed to produce a clearance of 0.076 mm with the steel bolts. This clearance, 1.2 percent of the hole diameter, is typical of aircraft joints.

The test system used in this study is shown schematically in figure 3. The center of the specimen is bolted between two bearing-reaction plates that are attached to the load frame using two load cells. The ends of the specimen are then gripped and loaded independently by two servo-control systems (called "upper" and "lower" in figure 3). Any difference between these two end loads produces a bearing load at the central bolt hole. This bearing load is measured by the load cells under the bearing-reaction plates. The end loads are synchronized by a common input signal; as a result, a constant bearing-bypass ratio is maintained throughout each test.

A photograph of the apparatus is shown in figure 4. This photograph shows the friction grips that load each end of the specimen and the head of the steel bolt that attaches the specimen to the bearing-reaction plates. Only a small portion of the specimen edge is visible. Notice that the bearing-reaction plates are bolted to the bearing load cells, allowing either tension or compression bearing loads. During compression, the bearing-reaction plates prevent specimen buckling. Although not visible in this photograph, hardened steel bushings were used between the bolt and the bearing-reaction plates. These 12.7-mm bushings were machined for a sliding fit, allowing the bolt clamp-up force to be transmitted to the local region around the bolt hole. This arrangement was equivalent to having a clamp-up washer directly against the side of the specimen, as was used in references 1, 2, and 3. For the present tests, the bolt was finger tightened (about 0.2 Nm torque) to produce a very small clamp-up force against the specimen.

The loading notations for tension and compression testing are shown in figure 2(b). All tests were conducted at a rather slow loading rate of 3.75 N/s. The results are reported in terms of nominal bearing stress  $S_b$  and nominal net-section bypass stress  $S_{np}$ , calculated using the following equations:

$$S_b = F_b / td$$

$$S_{np} = P_p / t(w - d)$$

where  $t$  is specimen thickness and  $w$  is the width. The bearing-bypass ratio  $\beta$  is defined as

$$\beta = S_b / S_{np}$$

Throughout each test, the specimen deformation was measured by displacement transducers. These transducers were mounted symmetrically on the front and back of the bearing-reaction plates, see figure 4. (These plates were made from nonmagnetic 347 stainless steel so they would not affect the transducers.) The transducer rods rested on small bars that were cemented to the specimen slightly above the grip line. This arrangement provided a measurement of the relative displacement between the bearing-reaction plates and the specimen. These measurements were used to determine the onset of damage.

The bearing and bypass loads were plotted against the specimen displacement, shown for a typical case in figure 5. Both the bearing and bypass curves have a small initial nonlinearity (probably due to varying bolt-hole contact) but gradually develop a nearly linear response. At higher load levels, the curves gradually develop a second nonlinearity, which indicates damage at the bolt hole, as mentioned in reference 3. An offset of  $0.001d$  was selected to define the

damage-onset load, as indicated in figure 5. Some specimens were unloaded after the damage-onset load level and were then treated with an X-ray opaque dye-penetrant and radiographed to determine the damage-onset mode.

#### Test Results

Figure 6 shows radiographs of four damage-onset modes. For tension dominated loading, the damage developed in the net-section tension (NT) mode, figure 6(a). The gray shadows show delaminations and the dark bands indicate ply splits. The tension-reacted bearing (TRB) and compression-reacted bearing (CRB) damage modes are quite similar, as expected, and appear to be delamination dominated. The net-section compression (NC) mode involves rather discrete damage zones extending from the hole. This damage was probably caused by microbuckling in the 0° plies.

The measured  $S_b$  and  $S_{np}$  values corresponding to damage onset are plotted against one another in figure 7, as a so-called bearing-bypass diagram. Each open symbol represents the average of three tests and the tick marks indicate the range of the measured strengths, plotted along lines of constant  $\beta$ . The data in figure 7 is also given in Table 1. The right side of figure 7 shows tension results for four  $\beta$  values (0, 1, 3,  $\infty$ ). The symbol on the  $S_{np}$  axis represents the all bypass loading in tension ( $\beta = 0$ ). The NT next to the symbol indicates net-section tension damage. As expected, all the test cases with NT damage can be represented by a straight line and, thus, show the linear interaction discussed in references 3 and 4. This linearity suggests that the local stresses due to bearing loading and those due to bypass loading each contribute directly to failure. The "bearing-cutoff" line was drawn through the  $\beta = \infty$  data point. The damage-onset strengths for the all bearing tension case ( $\beta = \infty$ ) and the all bearing compression case ( $\beta = -\infty$ ) differ by about three percent. However, the bearing-cutoff line used for tension does not appear to apply for compression. The CRB damage mode was found at  $\beta = -1$  for a much lower strength level. The compressive bypass load had a somewhat unexpected effect on the onset of bearing damage. The bearing failure for combined bearing and bypass loading was analyzed in reference 3 and resulted from a decrease in the bolt-hole contact angle caused by the compressive bypass load. For the all bypass compressive loading ( $\beta = -0$ ), NC damage initiated at -422 MPa, which is much larger than the expected compression strength for this laminate. This suggests that "dual" bolt-hole contact developed, allowing the load to transfer across the hole, and, therefore, produced a higher strength. This will be discussed later in an analysis of the bolt-hole contact.

The bearing-bypass diagram for the ultimate strengths (solid symbols) is shown in figure 8. To evaluate the progression of damage from onset to ultimate failure, the damage-onset curves are replotted from figure 7. A general comparison of these two sets of results shows that the specimens failed immediately after damage onset when an all bypass loading ( $\beta = 0$  and  $-0$ ) was used. In contrast, for the all bearing loading ( $\beta = \infty$  and  $-\infty$ ), the specimens failed at considerably higher loads than required to initiate damage. Also, when bearing and bypass loads were combined, the specimens showed additional strength after damage onset, more so in compression. A comparison of the damage modes indicated in figure 8 shows that the onset-damage mode was the ultimate failure mode in most cases. The exception occurred for the compressive bearing-bypass loading. For  $\beta = -3$ , the damage initiated in the CRB mode but the specimen failed in a different mode, referred to here as the offset-compression (OSC) mode. Figure 9 shows a specimen that failed in the OSC mode. The failure is typical of a compression failure but developed away from the specimen net-section. The light region near the fracture is a solid film lubricant that transferred from the bearing-reaction plate when the specimen failed. The offset of the failure from the net section is believed to be caused by the CRB delamination damage extending beyond the clamp-up area around the hole, thereby initiating a compression failure away from the hole. This transition from the CRB damage-onset mode to the OSC failure mode could also happen in multi-fastener joints and, therefore, may be an additional complication when joint strength predictions are made for compressive loadings.

#### STRESS ANALYSIS

In this section, first, the stress analysis procedures are briefly described. Then, stresses at the hole boundary are shown for selected combinations of bearing-bypass loading in tension and compression. These stress results are then used in the next section to calculate the specimen strengths for the various damage modes observed in the bearing-bypass tests.

#### Finite Element Procedures

The finite element procedures used in this study were presented and evaluated in reference 5. When a bolt clearance is used, as in the present study, the contact angle at the bolt-hole interface varies with applied load, as shown in figure 10. Using the inverse technique described in reference 5, this nonlinear problem is reduced to a linear problem. In this technique, for a simple bearing loading, a contact angle is assumed and the corresponding bearing load is calculated. This procedure is repeated for a range of contact angles to establish a relationship between contact angle and bearing load. In the present study, this technique was extended to include combined bearing and bypass loading. For each bearing-bypass ratio  $\beta$ , the combined bearing and bypass loading was expressed in terms of bearing stress  $S_b$  and  $\beta$ . Thus, for a given  $\beta$ , the procedure was identical to that used in reference 5. This procedure was repeated to establish a relationship between contact angle and bearing-bypass loading for each  $\beta$  value in the test program.

These calculations were done using the NASTRAN finite element code. This code is well suited for the inverse technique because the contact of the bolt and the hole can be represented using displacement constraints along a portion of the hole boundary. Displaced nodes on the hole boundary were constrained to lie on a circular arc corresponding to the bolt surface. This represents a rigid bolt having a frictionless interface with the hole. A very fine two-dimensional mesh was used to model the test specimen. Along the hole boundary, elements subtended less than  $1^\circ$  of arc. As a result, the contact arc could be modeled very accurately.

#### Stress Results

Figure 11 shows the hole-boundary stress distributions for three tension loading cases. The first case is an all bypass tension loading ( $\beta = 0$ ); the hole-boundary tangential stress  $\sigma_{\theta\theta}$  is shown as a dash-dot curve. It has the expected peak at  $\theta = 90^\circ$ , the specimen net-section. The value of this  $\sigma_{\theta\theta}$  peak can be used to predict the applied load for damage onset in the NT mode, as demonstrated in reference 2. The second case in figure 11 represents an all bearing tension loading ( $\beta = \infty$ ) of 400 MPa with zero clearance between the bolt and the hole;  $\sigma_{\theta\theta}$  and  $\sigma_{rr}$  are shown as dashed curves. The peak value of the  $\sigma_{rr}$  curve governs the bearing damage onset. The  $\sigma_{rr}$  curve also indicates a contact angle of about  $82^\circ$ ; the peak value in the  $\sigma_{\theta\theta}$  curve occurs slightly beyond the end of the contact angle. The third case in figure 11, the solid curves, also represents an all bearing case with  $S_b = 400$  MPa, but with the 0.076 mm clearance used in the tests. Comparison of the  $\sigma_{rr}$  curves for the two all bearing cases shows that the clearance reduced the contact angle by about  $20^\circ$  and increased the  $\sigma_{rr}$  bearing stress. Thus, clearance tends to decrease bearing strength.

Hole-boundary stresses for tension bearing-bypass loading are shown in figure 12. These results correspond to a bearing stress  $S_b$  of 400 MPa with three tension bypass stress  $S_{np}$  levels. The  $\sigma_{rr}$  curves show that increasing  $S_{np}$ , the bypass load, caused the contact angle to increase. However, the peak  $\sigma_{rr}$  value changed very little for increasing  $S_{np}$ , suggesting that tension bypass loading has little influence on the bearing strength. In contrast, increasing the tension bypass stress levels produced higher  $\sigma_{\theta\theta}$  peaks, which corresponds to lower net-section tension strengths.

Hole-boundary stresses for compression bearing-bypass loading are shown in figure 13. Again, the bearing stress  $S_b$  was 400 MPa. The  $\sigma_{rr}$  curves show that increasing the compressive  $S_{np}$  value produced smaller contact angles and correspondingly higher peak  $\sigma_{rr}$  values. This shows that the value of  $S_{np}$  influences the bearing strength, as shown previously in figure 7. The  $\sigma_{\theta\theta}$  tensile peaks were nearly the same for the range of  $S_{np}$  values but the  $\sigma_{rr}$  compressive peaks varied widely. The curve for  $S_{np} = 500$  MPa illustrates dual contact; notice the  $\sigma_{rr}$  contact stress near  $\theta = 180^\circ$ .

The contact angle trends discussed in figures 12 and 13 are summarized in figure 14. The contact angles,  $\theta_1$  and  $\theta_2$  defined by the insert, are shown for a range of tension and compression bypass loadings with  $S_b = 400$  MPa. Increasing the tensile bypass loading increased  $\theta_1$ , while increasing the compressive bypass loading had the opposite effect. The small jog in the curve at  $S_{np} = 0$  is caused by the small difference between tension-reacted bearing and compression-reacted bearing. Notice that dual contact initiated for a compressive bypass stress of about 450 MPa. The secondary contact angle  $\theta_2$  increased rather abruptly as the compressive  $S_{np}$  exceeded this value. Additionally, the decreasing trend for  $\theta_1$  reversed when dual contact developed. Dual contact provides a path for the applied load to "bridge" across the hole rather than divert around it. This reduces the stress concentration in the net section and produces higher net-section compression strength than with no dual contact.

#### STRENGTH CALCULATIONS

As previously mentioned, laminate strengths for bearing-bypass loading were calculated using the local stresses at the bolt hole. These calculations were used to study the strength trends for the range of loading combinations and the different failure modes. The damage-onset strengths were calculated using the peak hole-boundary stresses, as in reference 2. The onset of damage was assumed to occur when the peak hole-boundary stress reached a critical value for each damage mode. For each measured damage-onset strength, the peak stress was calculated and the average of the peaks in each damage mode was assumed to be the critical value for that damage mode. The following critical values were calculated for each damage mode: 869 MPa for NT; -750 MPa for TRB; -808 MPa for CRB; and -817 MPa for NC. The solid curves in figure 15 represent the damage-onset strengths calculated in this manner. The average damage-onset

strength data from figure 7 are replotted as open symbols in figure 15. The calculated curves agree with the data trends for strength. Also, the calculated damage modes agree with those discussed earlier. This demonstrates that damage-onset strengths can be predicted from the peak hole-boundary stresses if a critical stress value is known for each damage mode.

The ultimate strengths for bearing-bypass loading were calculated using the well-known point-stress criterion (reference 6). The stress distribution calculated along the observed direction of damage growth near the hole was compared with the laminate strength to determine a characteristic dimension. This failure theory was fit to the test data for each failure mode to determine an average characteristic dimension. The following characteristic dimensions were determined for each failure mode: 2.44 mm for NT; 2.22 mm for TRB; 3.87 mm for CRB; 8.89 mm for OSC; and 2.54 mm for NC. The strength calculations must agree with the data averages for each failure mode. As expected, the calculations also agreed with the trends for the strength data, as shown by the dash-dot curves and solid symbols in figure 15.

The correlation between the strength calculations and the strength measurements in figure 15 suggests that a combined analytical and experimental approach could be used to predict bearing-bypass diagrams from a few tests. Such tests could be conducted for the all bypass ( $\beta = 0$ ) and the all bearing ( $\beta = \infty$ ) cases to determine the critical material strength parameters, which could then be used with stress analysis to construct curves for the more complicated cases of bearing-bypass loading. This approach seems viable for tension bearing-bypass loading because only two failure modes are involved. But for compression loading, there are three ultimate failure modes. The OSC mode occurs only for combined bearing and bypass loading, so this failure mode cannot be evaluated using simple loading. Therefore, strength calculations for compression would require bearing-bypass tests for at least one  $\beta$  value to find the OSC material strength parameter.

#### CONCLUDING REMARKS

A combined experimental and analytical study has been conducted to investigate the effects of combined bearing and bypass loading on a graphite/epoxy (T300/5208) laminate. Tests were conducted on single-fastener specimens loaded in either tension or compression. Test specimens consisted of 16-ply, quasi-isotropic graphite/epoxy laminates with a centrally-located hole. Bearing loads were applied through a steel bolt having a clearance fit. Onset damage, ultimate strengths, and the corresponding failure modes were determined for each test case. A finite element procedure was used to calculate the local stresses around the bolt hole.

A dual-control test system, described in this paper, was used to successfully measure laminate strengths for a wide range of bearing-bypass load ratios in both tension and compression. The tension data showed the expected linear interaction for combined bearing and bypass loading where the damage developed in the net-section tension mode. However, the bearing damage-onset strengths in compression showed an unexpected interaction of the effects for the bearing and bypass loads. Compressive bypass loads reduced the bearing onset strength. The compressive bypass loading decreased the bolt-hole contact arc, which increased the severity of the compressive bearing loads. Compressive bearing-bypass loading also produced an off-set compression (OSC) failure mode, not previously reported in the literature.

The present stress analyses showed that combined bearing and bypass loading can have a significant influence on the bolt-hole contact angles. These contact angles had a strong influence on the local stresses around the hole; they must, therefore, be accurately represented in strength calculation procedures that are based on local stresses.

Although the trends in the bolt-hole strength for combined bearing and bypass loading were accurately calculated using local stresses together with failure criteria, some bearing-bypass testing is required to predict the compression response. The laminate response under compression bearing-bypass loading involved the OSC failure mode, which cannot be evaluated by simple loading conditions. Therefore, predictions of laminate bearing-bypass strengths may need to be combined with selected bearing-bypass testing to account for the off-set compression failure mode.

#### REFERENCES

1. Crews, J. H., Jr.: "Bolt-Bearing Fatigue of a Graphite/Epoxy Laminate," *Joining of Composite Materials*, ASTM STP 749, K. T. Kedward, Ed., American Society for Testing and Materials, 1981, pp. 131-144.
2. Crews, J. H., Jr. and Naik, R. A.: "Failure Analysis of a Graphite/Epoxy Laminate Subjected to Bolt-Bearing Loads," *Composite Materials: Fatigue and Fracture*, ASTM STP 707, H. T. Hahn, Ed., American Society for Testing and Materials, 1986, pp. 115-133.
3. Crews, J. H., Jr. and Naik, R. A.: "Combined Bearing and Bypass Loading on a Graphite/Epoxy Laminate," *Composite Structures*, Vol. 6, 1986, pp. 21-40.
4. Hart-Smith, L. J.: "Bolted Joints in Graphite/Epoxy Composites," NASA CR-144899, National Aeronautics and Space Administration, January 1977.
5. Naik, R. A. and Crews, J. H., Jr.: "Stress Analysis Method for a Clearance-Fit Bolt under Bearing Loads," *AIAA Journal*, Vol. 24, No. 8, August 1986, pp. 1348-1353.
6. Whitney, J. M. and Nuismer, R. J.: "Stress Fracture Criteria for Laminated Composites Containing Stress Concentrations," *J. Composite Materials*, Vol. 8, July 1974, pp. 253-265.

Table 1 Laminate strengths for bearing-bypass loading.

Bearing-bypass ratio, $\beta$	Damage-Onset			Ultimate Failure		
	$S_b$ (MPa)	$S_{np}$ (MPa)	Mode	$S_b$ (MPa)	$S_{np}$ (MPa)	Mode
<b>Tension</b>						
0	0	304	NT	0	330	NT
1	237	237	NT	263	263	NT
3	468	156	NT	648	216	NT
$\infty$	542	0	TRB	812	0	TRB
<b>Compression</b>						
-0	0	-422	NC	0	-422	NC
-1	314	-314	CRB/NC	461	-461	OSC
-3	498	-166	CRB	759	-253	OSC
$-\infty$	528	0	CRB	853	0	CRB

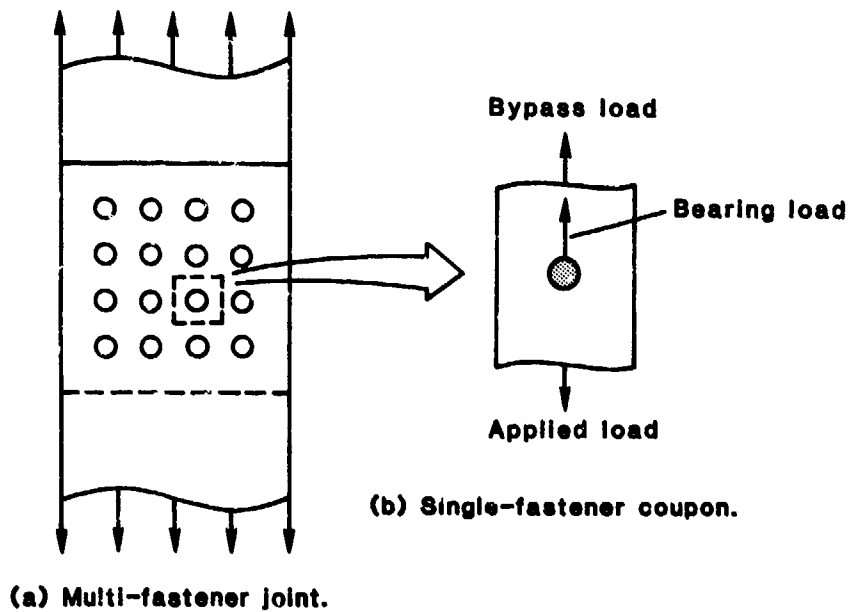


Figure 1 Bearing-bypass loading within a multi-fastener joint.

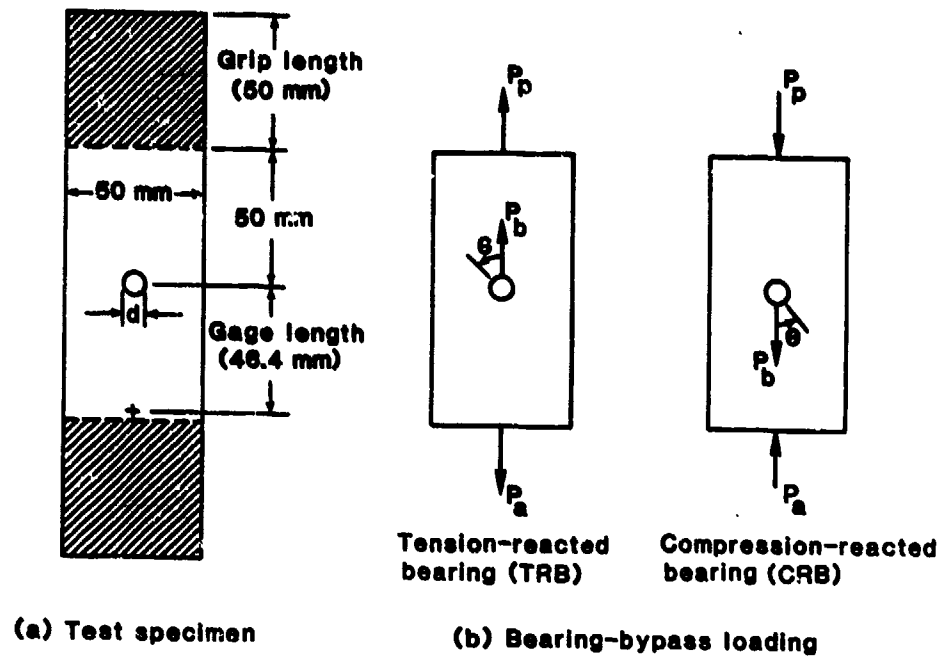


Figure 2 Specimen configuration and bearing-bypass loading.

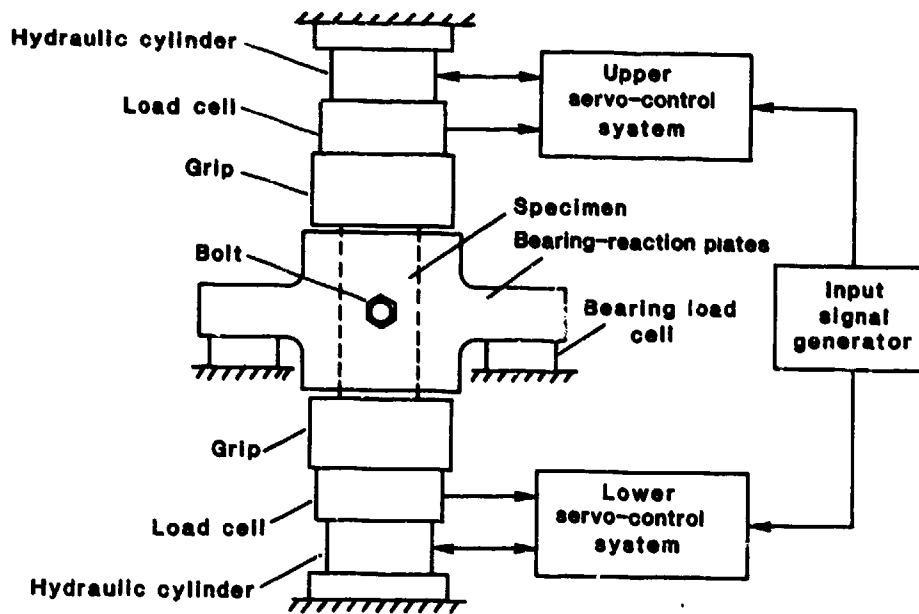


Figure 3 Block diagram of the bearing-bypass test system.



Figure 4 Photograph of bearing-bypass test apparatus.

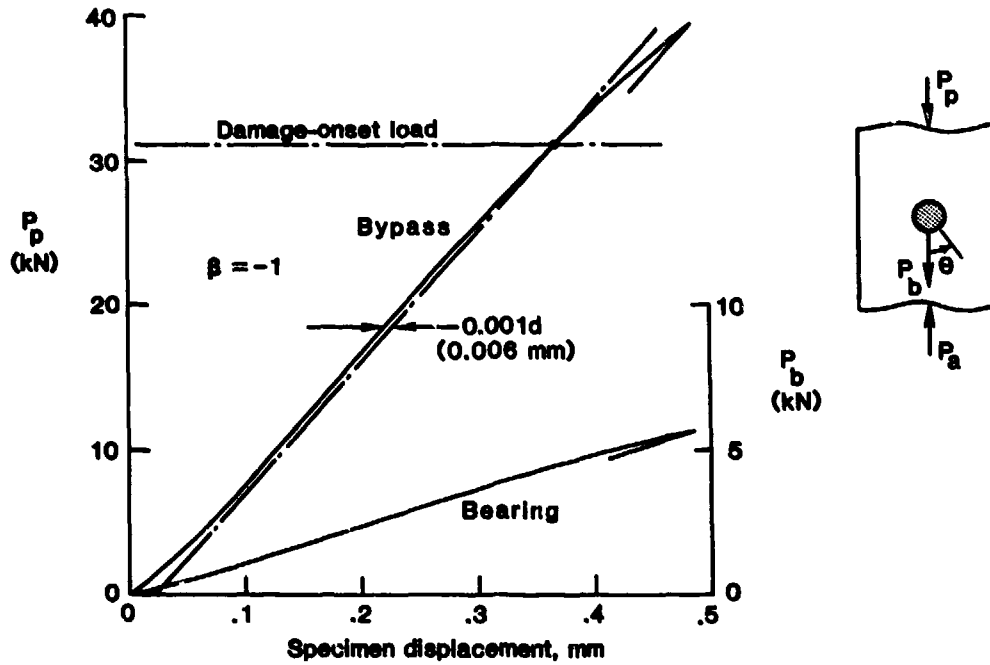


Figure 5 Typical load-displacement curves.

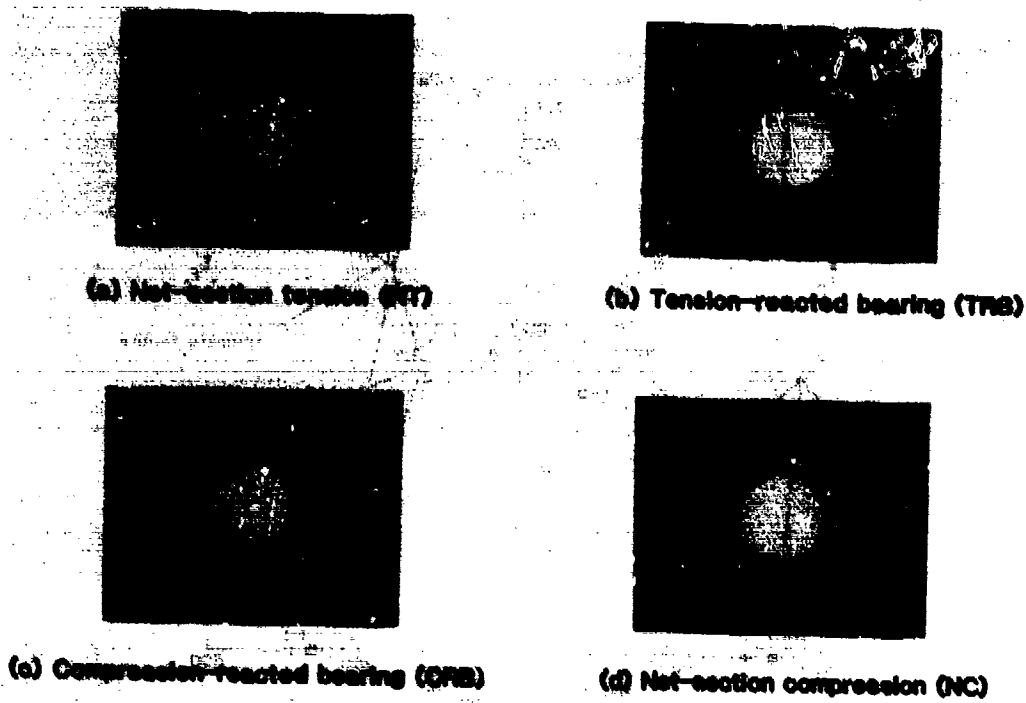


Figure 6 Radiographs of damage at fastener hole.

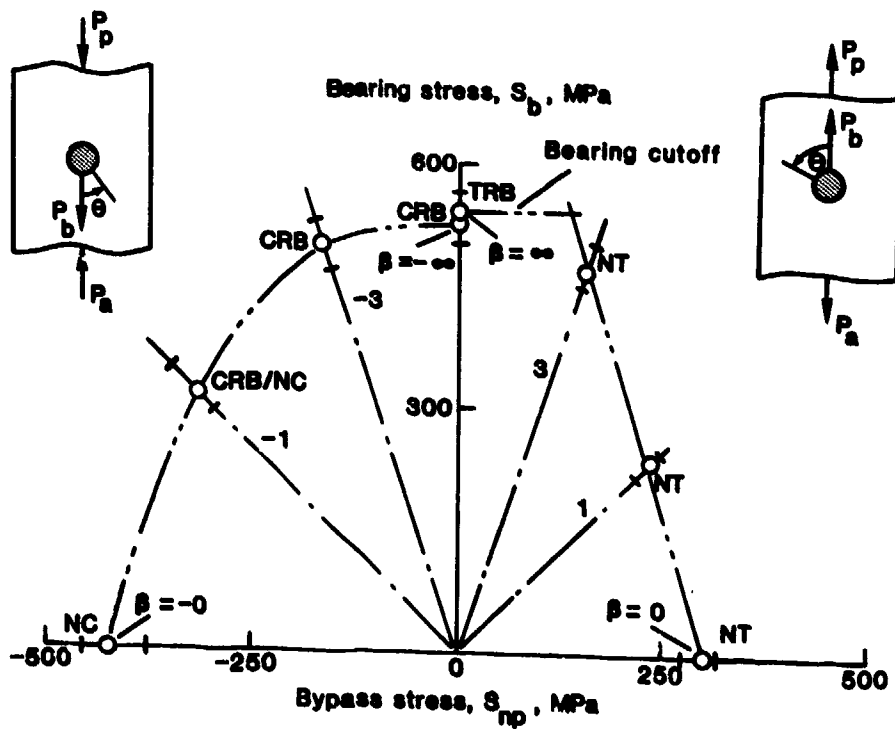


Figure 7 Bearing-bypass diagram for damage-onset strength.

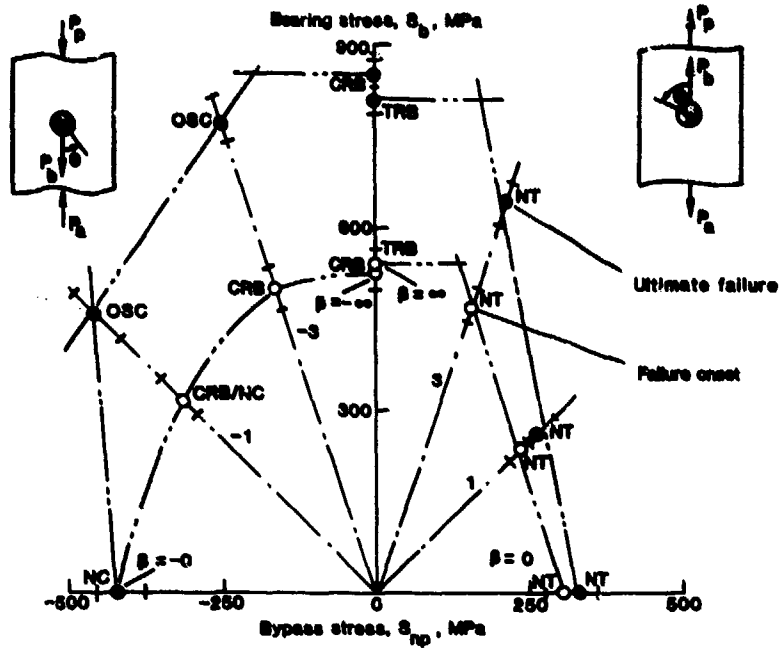


Figure 8 Bearing-bypass diagram for ultimate and damage-onset strengths.



Figure 9 Photograph of a failed specimen showing an offset-compression (OSC) failure.

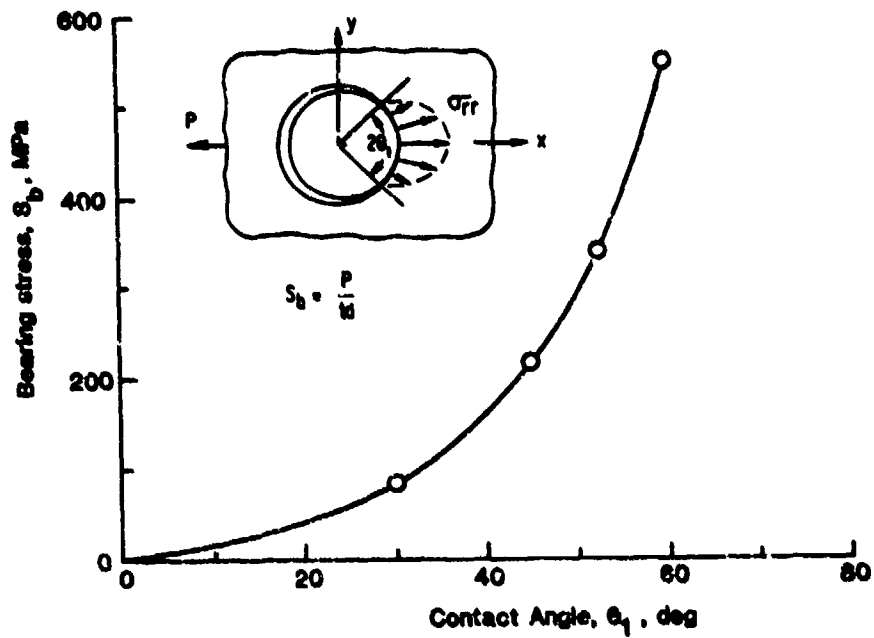


Figure 10 Nonlinear relationship between bearing stress and contact angle.

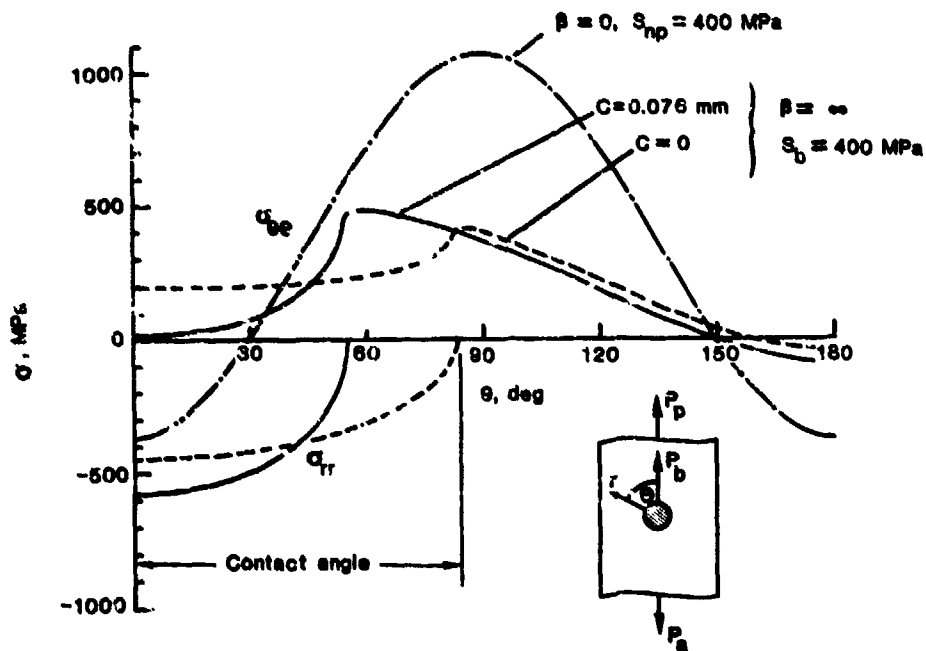


Figure 11 Stress distributions along hole boundary for all bearing and all bypass tension loads.

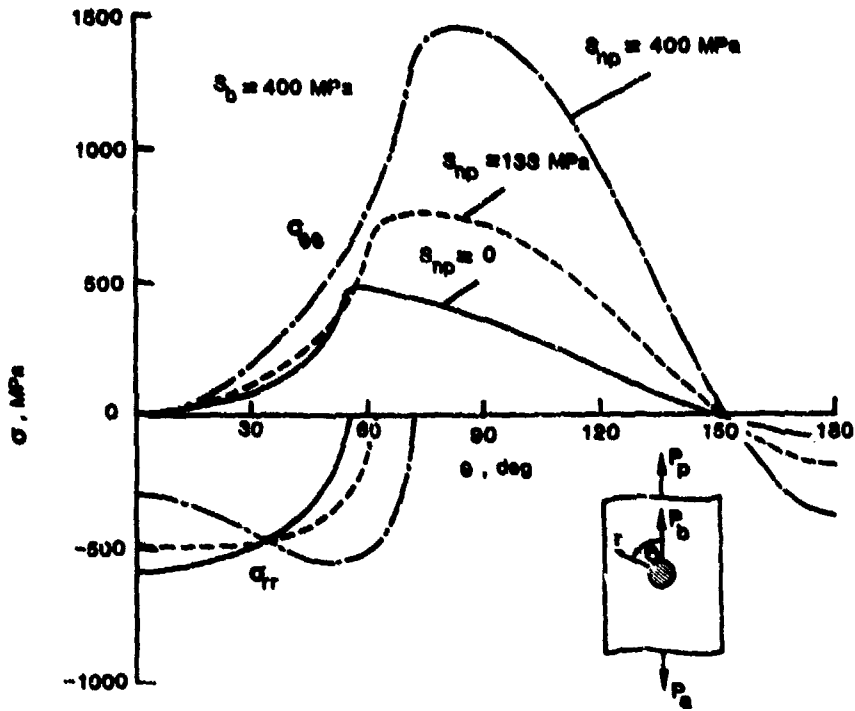


Figure 12 Stress distributions for tension bearing-bypass loadings.

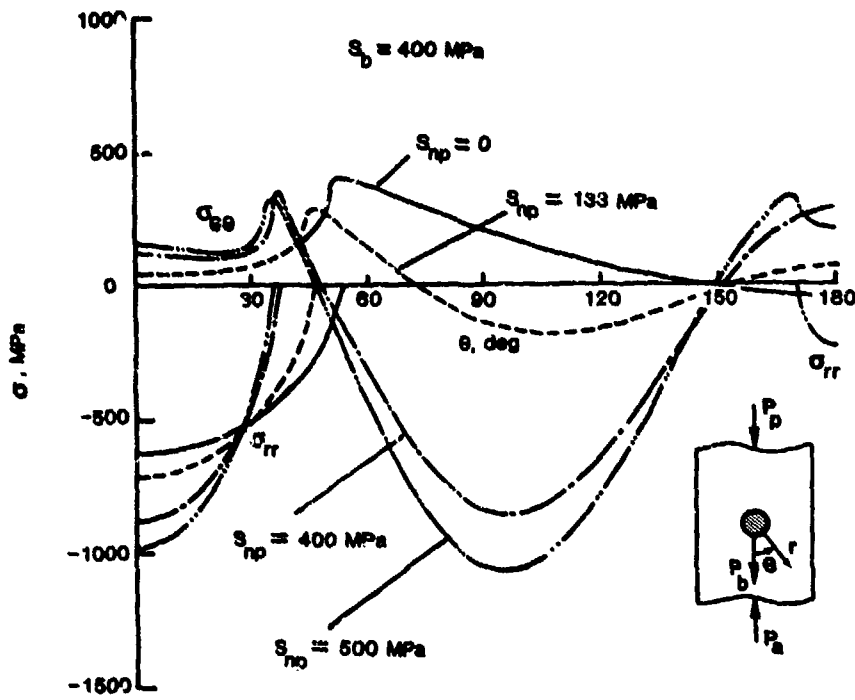


Figure 13 Stress distributions for compression bearing-bypass loadings.

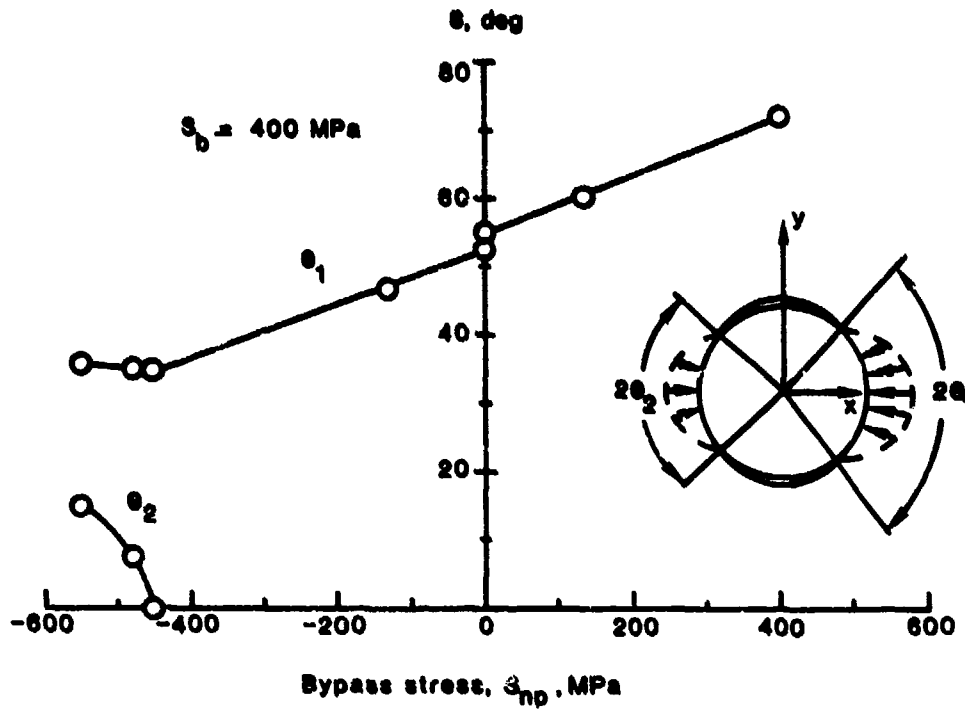


Figure 14 Contact angles for bearing and a range of bypass loadings.

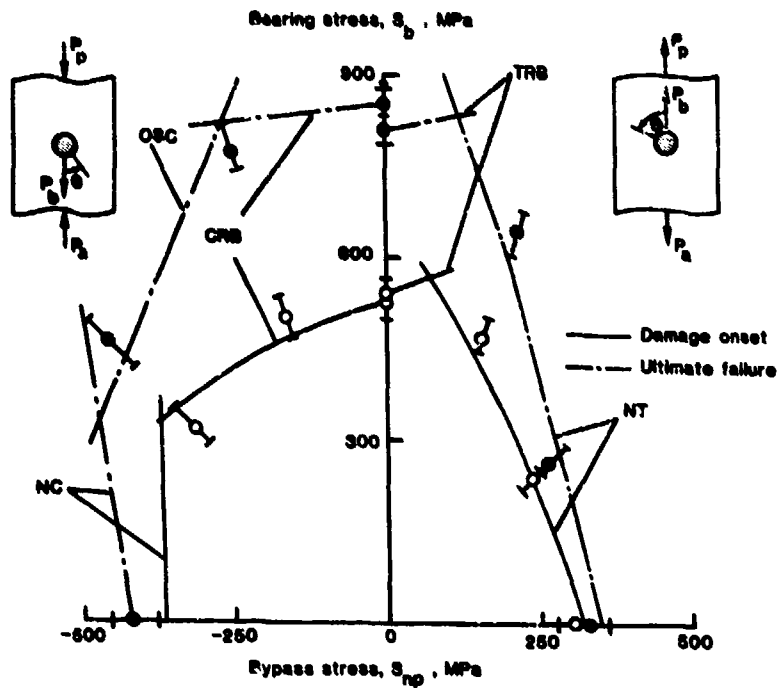


Figure 15 Strength calculations for damage-onset and ultimate failure strengths.

Bolted Joints in Composites  
Primary Structures

by  
A. Ruiz  
CASA D.P.  
Avda. John Lennon s/n, Cetafe, Madrid, Spain

**ABSTRACT**

In the design of composite parts in primary structures, it is necessary to use bolted joints because of inspection requirements and the need for partial disassembly, repairability, access to the structure and for manufacturing breaks.

The proven methodology for bolted joints in metallic structures cannot directly be applied to bolted joints in composites because of: material anisotropy, susceptibility to the environment and, specially, due to the brittle behaviour of typical carbon/epoxy joint members up to ultimate failure.

In typical highly loaded multirow joints, a tension type failure generally occurs. Peak tangential stresses at the edge of fastener hole produces fibres break-out. Stress concentration factors governs the failure, as in metal joints under fatigue loads.

A methodology for composite bolted joints analysis must be able to size any particular joint design, avoiding the need for detail design tests. The approach under the present work is based on a methodology developed by J.L. Hart-Smith (Douglas, Long Beach) which correlates stress concentration factors in elastic-isotropic materials with those which appear in composites, by means of an empirically determined "relief" factor.

CASA has developed a test plan which includes several hundreds of coupons. Basically, bearing strength allowables and stress concentration factors, are investigated. The plan covers double and single shear specimens, environmental effects (cold-dry and hot-wet), different resin systems and fasteners, and various loading conditions. Provisions for evaluating hole size effect are also made.

**LIST OF SYMBOLS AND SUBSCRIPTS**

**Symbols**

C : Correlation coefficient between stress concentration factors in composites and elastic isotropic materials.

d : diameter

e : End margin (measured from the center of the hole to the plate end perpendicular to the load).

K : Stress concentration factor.

- elastic isotropic materials (e)

$K_{bne}$  : tensile stress concentration factor due to bearing load and based on net tension stress.

$K_{tne}$  : tensile stress concentration factor due to tension bypass load and based on net stress.

- composites

$K_{bn}$  : tensile stress concentration factor due to bearing load and based on net tension stress.

$K_{tn}$  : tensile stress concentration factor due to tension bypass load and based on net stress.

P : Load

t : Laminate thickness

w : Width

Subscripts

b : Bearing

t : Tension bypass

INTRODUCTION

The increased application of advanced composites in aircraft structures has resulted in a substantial reduction of the "part count" and subsequently a reduction of attachments and joints. However, joints, and specially bolted joints, are still required because of inspection requirements and the need for partial disassembly, repairability, access to the structure and for manufacturing breaks.

While methodology for bolted joints in METAL structures is well-established and supported by many years of tests and hardware experience, a direct adaptation of design policies and analysis procedures to COMPOSITE bolted joints is not possible, mainly because of: material anisotropy, influence of layup, different failure modes and environmental susceptibility.

Due to the comparatively brittle behaviour of typical carbon epoxy joint members up to ultimate failure, the "forgiving" features of metal joints at ultimate load are missing, i.e. high ductility and local redistributions and essentially no stress risers. The load-sharing analysis for composite joints at ultimate load therefore requires a careful modelling of the joint under consideration, of joint members and fastener stiffness, conceptually similar to the analysis of metal joints under operating (fatigue) loads.

KNOW YOUR LOADS

Many aircraft structures, specially those made of composite materials, are currently being analyzed using finite element modelling. This structural analysis account for gross element stiffness to solve redundant internal load distribution. It is common, in such analysis, to model bolted joints areas without including fasteners and associated flexibilities, because of economic limitations and the small contribution of local joint structure to overall structural deformation.

Once external loads which act on joints are obtained, a conventional analysis will determine the load distribution at fasteners. It could require, as in the particular multibolt joint in Fig. 1, a load sharing analysis which can use analytic close form procedures or finite element modelling for more complex joints.

This analysis will account for the flexibility of each fastener as a function of fastener stiffness, joint member stiffness and load eccentricity.



FIG. 1 LAMINATE DETAIL LOADS

The load sharing analysis will provide the analyst with the load transferred by the fastener ( $P_b$ ) and the bypass loads ( $P_t$ ) on the laminate. Then, a detailed stress analysis must be performed. This analysis deals with the determination of the stress distribution at the vicinity of the hole.

## STATE-OF-THE-ART ON JOINT ANALYSIS

### Stress analysis

The work under Reference 1 considers theoretical and empirical approaches to determine stress distribution.

State-of-the-art theoretical approaches include analytic, finite element and strength of materials approximation methods.

The analytical methods are formulated from a two-dimensional anisotropic elasticity theory. One of these methods is the "Bolted Joint Stress Field Model (BJSFM)" which has been developed at McDonnell Aircraft. This method accounts mainly for material strength anisotropy, stiffness anisotropy, general biaxial inplane loadings and arbitrary fastener hole sizes. A cosine distribution of radial stresses at the fastener hole represents bolt bearing loads.

The finite element methodology has a limited use due to the costs. Sometimes analytic methods are used for parametric studies while finite element are only used for cases of complex geometries or through-the-thickness effects.

Theoretical methods based on strength of material approximations (beam theory, shear lag theory, ...) are limited to account for complex loading and material anisotropy. Accounting for fastener flexibility, head rotation and non-uniform through-the-thickness stress distribution can be made within this approach.

Empirical approaches are an alternative to the theoretical ones. The main difference between empirical and theoretical approaches is the establishing of failure directly by test in the first case while in the second one a failure criteria must be assessed. An empirical approach based on Hart-Smith's method will be widely commented later in this paper.

### Failure analysis

The previous paragraph dealt with procedures to determine stress distribution around the hole. Once it is known, a failure analysis must be performed. Criteria such as Tsai-Hill, Max. strain, Tsai-Wu, etc., are generally used for unnotched material failure.

Detailed analysis at the hole location combining theoretical elastic stress distribution analysis with a theoretical failure criteria, gives highly conservative results. This is due to the behaviour of composites up to failure, at the vicinity of the hole, which is not completely elastic. Microdamages at the resin level, produce a stress relaxation before failure. It introduces a "relief" factor on the effective stress concentration as compared with the theoretical (elastic) stress concentration.

Several procedures to account for this composite "relief" factor have been established:

- Finite element modelling
- To use a "progressive" failure criteria instead of a "first-ply" failure. (Reference 2)
- A "characteristic dimension" failure hypothesis which correlates, by testing, the effective point stress at failure with a theoretical value situated at a certain "distance" on the stress distribution curve. (Reference 3).
- A linear elastic fracture mechanics model which assumes an "intense energy region" must be stressed to a critical level before fracture occurs. (Reference 4).

The "characteristic dimension" approach have widely been followed all over the world. The methodology under Reference 1, uses this approach. Springer developed an experimental work (Reference 5) to evaluate the influence of several parameter on the "characteristic length". A "characteristic length" in tension ( $R_t$ ) and in compression ( $R_c$ ) must be determined.

The use of theoretical approaches to determine stress distribution is associated with the need for establishing a theoretical failure criteria and a composite "relief" factor. None of the existing failure criteria is adequate to cover all possible loading conditions (Reference 6). Likewise, to assess the "relief" factor, an adequate number of tests is needed.

Empirical approaches establish the failure directly through testing. An empirical procedure has been followed by CASA to develop its Bolted Joints Methodology.

### THE EMPIRICAL APPROACH

The approach used here is based on the L.J. Hart-Smith's work (References 7, 8) which is mainly supported by experimental observations. The elastic stress concentrations at holes are well established in

the literature. Tests on composite materials permit the assessment of composite "relief" factor to account for the effective stress concentration at failure. Influence of material anisotropy on that factor is also empirically deduced.

Limited test data are generalized to other geometries, evaluating the interaction between stress concentrations caused by bearing and bypass loads in an uniaxial load case. This methodology is also extended, with adequate limitations to the biaxial load cases.

Stress concentration factors in elastic isotropic materials are well known, specially for fatigue analysts. Peterson (Reference 9) attributes to Heywood an empirical formula for stress concentration at unloaded holes in a strip (bypass load).

$$K_{tne} = 2 + (1-d/w)^3$$

Some corrections are introduced when a hole in a row of an infinite plate.

In case of a loaded hole in a finite strip (bearing load) the above equation is reexpressed in Reference 7 (by Frocht and Hill), as:

$$K_{bne} = (w/d + 1) - 1.5 \frac{(w/d - 1)}{(w/d + 1)} \textcircled{+}$$

being H defined as:

$$\begin{aligned} \textcircled{+} &= 1.5 - 0.5/(e/w) \text{ for } e/w \leq 1 \\ \textcircled{+} &= 1 \text{ for } e/w \geq 1 \end{aligned}$$

Once elastic isotropic stress concentration factors are established, the next step is to correlate these factors with those which are observed at ultimate load in composite. In other words, to calculate the composite "relief" factor (C).

A linear relationship between these factors has empirically been observed. Figure 2, borrowed from Reference 7, shows this relationship.

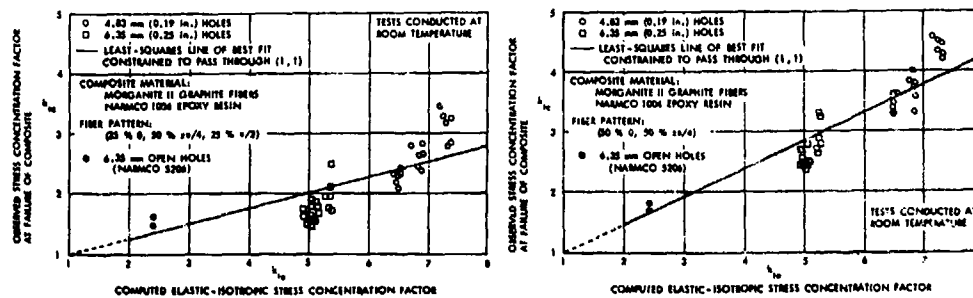


Fig. 2 CORRELATION BETWEEN STRESS CONCENTRATION FACTORS

Experimental observations suggest the invariability of C for loaded and unloaded holes.

Likewise this factor is layup dependant, as is clearly shown in Figure 2. Also the absolute hole size and the eccentricity influence C. A typical value of C, for Double Shear Joints, have been found to be in the vicinity of 0.25.

A linear interaction between tangential stresses has been demonstrated to occur in the case of combining a bearing load with a bypass load (Figure 3).

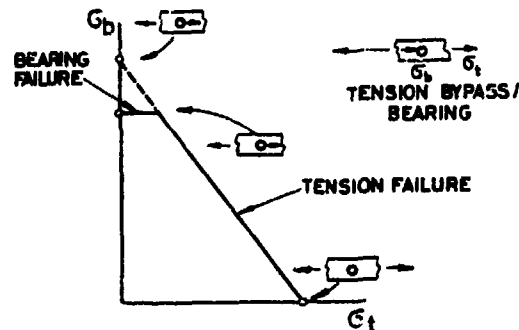


Fig. 3 INTERACTION BETWEEN BEARING AND BYPASS LOADS

Biaxial load cases are more complex than the uniaxial ones, because simple combinations of critical stresses do not apply. Biaxial cases require superposition of full hoop stress fields to determine the final result. Likewise, the lack of biaxial test results imposes the need of having adequate caution when an analysis is done in this field.

#### CASA TEST PLAN

Empirical factors under the methodology described above have been obtained from in-house tests. The CASA Test Plan is described in Reference 10. Tests were performed during the year 1985. A total of 500 specimens were tested.

This Plan is divided into two parts. The main body of the plan applies to resin system (T300/F594) and fasteners (HILOK, 6.35mm) commonly used in main CASA structural applications. As an appendix to the main body, specific aspects such as big bolt size, highly matrix dominant layup, blind fasteners and different resin system, are also included.

The programme covers Bearing (loaded hole,  $w=8d$ ), Bypass (unloaded hole,  $w=4d$ ) and "Tension-Through-the-Hole" (loaded hole,  $w=3d$ ) tests.

#### Bearing Tests

A bearing type failure is desired in the Bearing Tests. The maximum bearing strength will be achieved with the Double Shear specimen. Several layups are tested, maintaining the same specimen configuration, to detect the influence of layup on the strength.

Once maximum bearing strength is determined, parameters affecting strength are tested for quasi-isotropic layup. These parameters are listed below:

- . Single shear
- . Bolt head
- . Eccentricity
- . Short end distance
- . Environment
- . Torque

#### Bypass Tests

A second type of tests, Bypass, are conducted on a notched Specimen under bypass tension loads (unloaded hole). The aim is to assess composite "relief" factor for this load case. The following parameters are investigated:

- . Layup
- . Open/filled hole
- . Torque
- . Bolt head
- . Environment

### Tension-Through-the-Hole Tests

A narrow, loaded hole, specimen ( $w=3d$ ) is tested to determine the composite "relief" factor corresponding to this load case. A tension type failure under bearing loads is desired. Several layups are investigated with the Double Shear specimen. Additional parameters are then also investigated:

- . Single shear
- . Bolt head
- . Torque
- . Environment

Some compression bypass tests, open and filled hole, are also performed. Additionally, "pull through" tests are included.

Specimens configuration and test fixtures, extensively described in Reference 10, are not contained in this paper.

Test programme finished in October 85. Test results have been reported in Reference 11.

### TEST RESULTS EVALUATION

Analysis of Test Plan Results will permit, by means of adequate data reduction to achieve the appropriate understanding on how design variables affect performance of bolted joints in composites.

In this paper only main conclusions and general trends will be included. A detailed description of test results (under Reference 12) is not the aim of this publication.

Two main types of failures appear in bolted joints: bearing and tension. Therefore derivations must be addressed to obtain bearing strength values and stress concentration factors.

### Bearing Strength Allowables

Cloth material is used for testing. Empirical evidence shows that bearing strength, for double shear specimens, remains constant within a wide range of layups around quasi-isotropic. Average values are always over  $900 \text{ N/mm}^2$ , when tests are performed under room temperature.

Bearing strength is tremendously affected by eccentricity and environment. Strength can drop up to 50% when hot-wet is combined with a high eccentricity.

A bearing failure is very easy to analyse and is not a methodology type dependant analysis.

### Stress Concentration Factors

Under the Empirical Approach a composite "relief" factor which correlates elastic-isotropic materials and non-elastic-anisotropic ones (composites) must be derived from tests.

Test results show (Figure 4) a linear relationship between stress concentration factor in metals and composites. For the same layup (quasi-isotropic) and bolt diameter, the results of the tests carried out under different load conditions (bearing and bypass) and geometries ( $w/d = 3,4,8$ ) follow a straight line. The slope of that line is the "relief" factor  $C$ . Hole size effect produces higher slope, which means higher peak stresses, when 12.70mm diameter specimens are tested.

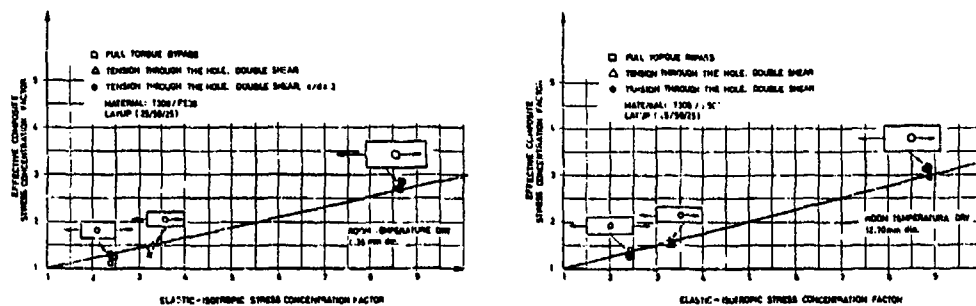


Fig. 4 CORRELATION BETWEEN STRESS CONCENTRATION FACTORS (CASA TESTS)

Correlation factor  $C$  is layup dependant. So, fiber dominant layups produce higher  $C$  values than those produced with matrix dominant layups.

Average  $C$  values derived from tests, on cloth material, show a linear relationship when plotted against  $0^\circ$  fiber percentage (Figure 5). Scatter associated to these tests is considered to be usual in composites. This linear behaviour is found when bypass load (unloaded hole) and also when bearing load (loaded hole).

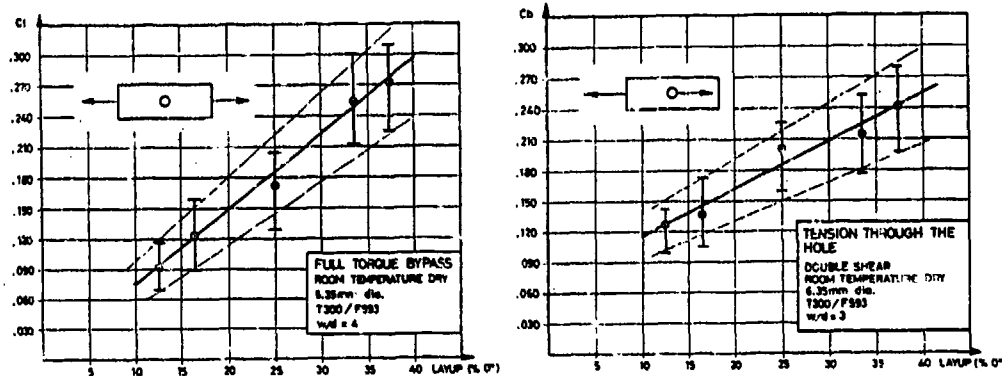


Fig. 5 COMPOSITE RELIEF FACTOR (C) VERSUS LAYUPS (CASA TESTS)

The above conclusions permit the derivation of stress concentration factors in composites, based on those which appear in elastic-isotropic materials, for any geometry ( $w/d$ ), layup and bolt diameter, within a range typically used in structural design. This derivation, in case of bearing loads, will be governed by the following formula:

$$(K_{bn} - 1) = C (\%b_{ne} - 1)$$

A similar formula applies for stress concentration factors due to tension bypass loads.

For uniaxial load cases combining bearing and bypass loads, a linear superposition is considered.

Environmental conditions greatly affect stress concentration factors. Critical values for  $C_b$  have been obtained with a cold-dry environment.

Another parameter affecting significantly  $C_b$  is eccentricity. Tests carried out under single shear specimens with high  $t/d$  values have shown  $C_b$  values twice those found under double shear tests. Influence of this parameter is specially significant when countersunk head fasteners are combined with high eccentricities.

Analysis under biaxial loads requires knowledge of not only the critical peak stress, but all the hoop stress distribution around the hole, in order to find the hole location where stress combination becomes critical. Based on test results under single load cases, it is possible to determine stress concentration at several locations around the hole.

#### BOLTED JOINTS DESIGN MANUAL

Many times, researchers need a wide range of test programmes to provide them with the answers they need for having an adequate understanding of a particular phenomenon. Test results will permit them to support theoretical assumptions, establishing a design methodology.

Sometimes, major efforts are dedicated in defining a test plan, testing and deriving conclusions, but these conclusions are not stated in a user friendly way for non-expert engineers working on hardware.

In the programme, under this paper, big efforts have been made in developing a Design Manual easy to use for engineers having a relatively little experience in bolted joints on composites.

The Manual provides:

- Guidelines for composite bolted joint design.
- Basic sizing and analysis procedures for initial design and trade-off studies.
- Complete methodology for final analysis.
- Analysis examples illustrating the use of the methodology.

The arrangement of the manual accommodates the groups of users, design and stress engineers, during different stages of design, from preliminary studies to formal analysis for certification.

A computer code is also being developed. This code performs bolted joints final analysis. The code, interactive and tutorial, is very user friendly.

#### CONCLUSIONS

More relevant theoretical and empirical approaches which represent state-of-the-art on composite Bolted Joints Analysis are evaluated in this paper.

The empirical approach, based on an empirically determined composite "relief" factor (C) is widely discussed.

A CASA Test Plan, with 500 test specimens, has permitted C value derivations for CASA materials and fastener systems. C is geometry-non-dependant, while varies linearly with the 0° fiber percentage. Eccentricity and environment significantly affect C.

The methodology derived from the Test Plan is condensed in a Design Manual and a computer code.

#### REFERENCES

1. GARBO, S.P. "Effect of Variances and Manufacturing Tolerances on the Design Strength and Life of Mechanically Fastened Composite Joints". AFFDL-TR-78-179, McDonnell Douglas Corp., December 78.
2. Chou, S., "Post-Failure Behaviour of Laminates: II-Stress Concentration". Journal of Composite Materials, Volume II, January 77.
3. Withney, J.M. and Nuismer, R.J., "Stress Fracture Criteria for Laminated Composites Containing Stress Concentrations", Journal of Composite Materials, Volume 8, July 74.
4. Eisenmann, S.R., "Bolted Joints Static Strength Model for Composite Materials", NASA-TM-X-3377, 1975.
5. Springer, G.S., et. al., "The Effect of Laminate Configuration on Characteristic Lengths and Rail Shear Strength". Journal of Composite Materials, Volume 18, May 84.
6. Cole, B.W., and Pipes, R.B., "Filamentary Composite Laminates Subjected to Biaxial Stress Fields". AFFDL-TR-73-115, 1974.
7. Hart-Smith, L.S., "Mechanically Fastened Joints for Advanced Composites. Phenomenological Considerations and Simple Analysis", DP6748A, McDonnell Douglas Corporation, November 78.
8. Hart-Smith, L.J., "Bolted Composite joints with Orthogonal Load Components", MDC J2907, McDonnell Douglas Corporation, October 83.
9. Peterson, R.E., "Stress Concentration Factors", John Wiley and Sons, New York, 1974.
10. Ruiz, A. and Walker, K., "Composite Material Bolted Joints Test Plan". C/MC/84-041, CASA internal report, 1985.
11. Redondo, E. and Oltra, J., "Ensayos Mecánicos de taladros y uniones remachadas en laminados de fibra de carbono". I-125/85, CASA internal report, October 85.
12. Ruiz, A. and Walker, K.: "Composite Bolted Joints Analysis Methodology". C/MC/85, CASA internal report, 1986.

## THE STATIC STRENGTH OF BOLTED JOINTS IN FIBRE REINFORCED PLASTICS

F.L. MATTHEWS  
Department of Aeronautics and  
Centre for Composite Materials  
Imperial College of Science & Technology  
Prince Consort Road, London SW7 2BY, UK.

### SUMMARY

Joints in glass fibre/epoxy (GFRP) and 'Kevlar' fibre/epoxy (KFRP) laminates show similar characteristics to those in carbon fibre/epoxy (CFRP) but with differences brought about by the low elastic modulus of glass fibres, and the low compressive strength of 'Kevlar' fibres. The current paper presents data for GFRP laminates manufactured from layers of unidirectional fibre prepreg, and for KFRP laminates manufactured from layers of balanced, bi-directional, woven fabric prepreg. Comparative data for CFRP are also given.

As far as GFRP is concerned, tests on single-hole joints show that the effects of width, end distance, hole size, bolt clamping pressure and stacking sequence are similar to those in CFRP. In general, strength levels for GFRP are about 20% below those for CFRP. The best lay-up is judged to be  $0/\pm 45^\circ$ , with 60% of the plies at  $\pm 45^\circ$ . A stronger interaction between failure modes is found for GFRP, which also shows a greater tendency to delaminate rather than showing in-plane shear or tensile cracking.

Due to the nature of the prepreg the range of possible lay-ups for KFRP is restricted; only  $0/90, \pm 45^\circ$  are tested. Bearing strengths are generally in the range 500-600 MN/m<sup>2</sup>, i.e. 25-30% below GFRP. Overall behaviour is found to be similar to other FRP although the ultimate failure mode is almost invariably tensile. There is evidence that the inherent compressive characteristics of 'Kevlar' fibre contribute to the low bearing strength. Surprisingly, although very large hole distortions are seen at failure there is very little evidence of resin cracking.

The strengths obtained for CFRP are of a similar level to CFRP.

### INTRODUCTION

It is well known that the mechanical characterisation of fibre-reinforced plastics (FRP) is complicated by the very large number of variables involved. The situation is, of course, very much worse for joints since, in addition to the material variables, the nature of the fastener and the geometry of the joint must also be considered. In spite of these difficulties a considerable body of literature now exists on the failure behaviour of mechanically fastened joints in FRP. In particular carbon and glass fibre-reinforced epoxy resin (CFRP and GFRP) have been studied extensively [1,2,3] and 'Kevlar' fibre-reinforced epoxy rather less so [4,5]. There is little data available on carbon fibre-reinforced PEEK (CFRPEEK) [6]. Collings [7] presents an excellent survey of the topic.

Because the number of variables for each fibre/resin system under evaluation precludes, on economic grounds, a complete characterisation, experimental programmes have concentrated on single hole joints with a few fastener types in a restricted range of lay-ups and stacking sequences. The general behaviour can conveniently be described by considering three sets of parameters:

#### a) Material Parameters

For optimum bearing properties there should be between 30 and 60% of  $\pm 45^\circ$  fibres, depending on the fibre type, the balance being oriented at  $0^\circ$ , i.e. parallel to the load. Stacking sequence also influences joint strength, although to a lesser extent than lay-up. Fibre volume fraction, fibre type and form (woven, unidirectional, etc), matrix type all affect strength.

#### b) Fastener Parameters

The fundamental choice is between rivets and bolts. Riveted joints can give satisfactory performance in laminates up to 3mm thick. The strength is limited by the small head and tail size, which in turn limits the clamping force imposed by the rivet in the through-thickness direction. This clamping force has a significant influence on joint strength. As might, then, be expected, countersunk rivets are inferior to round-head rivets.

The need for a high clamping force indicates that using bolts will provide the strongest joints. Normal levels of tightening usually provide adequate clamping force. Factors such as bolt size, washer size and bolt-to-hole fit are relatively unimportant.

#### c) Design Parameters

Overall considerations, such as load magnitude, will generally decide the joint type (single lap, double lap or step). Laminate thickness is clearly related to the load for a given material combination and lay-up. The most important parameters are then joint geometry (pitch, width, end distance, etc). Tensile failure can, normally, be eliminated if the joint is sufficiently wide and shear out eliminated if the end distance is large enough. However enforcing bearing failure, the most benign mode, may not provide the most efficient joint.

Other factors that may influence strength are load direction, loading rate and load type (static or dynamic).

Whilst it is true that FRP can be considerably weakened by the introduction of holes, adequate performance of mechanical joints can be achieved if allowance is made for the anisotropic nature of the material and the associated, complex, failure mechanisms. The major factors influencing joint strength are reviewed in the current paper. Most data will refer to double-ended specimens similar to that shown in Figure 1, the load being applied by a linkage such as that shown in Figure 2, where the load cell is used to monitor bolt clamping force. Unless otherwise stated laminates will have been made from preimpregnated warp sheet.

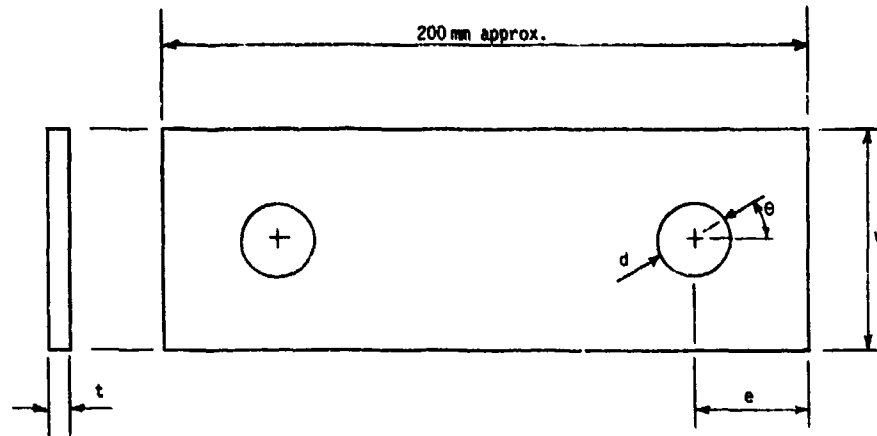


Figure 1. Specimen Configuration and Definition of Dimensions

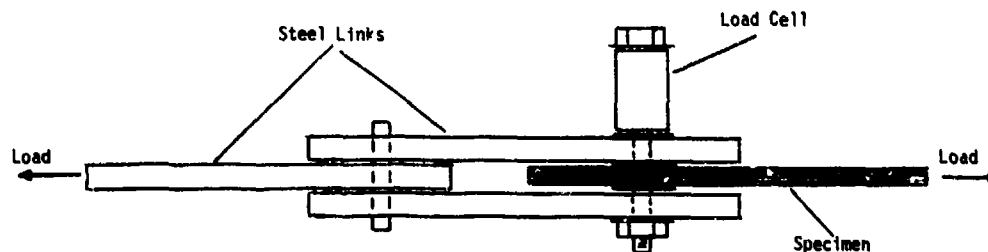


Figure 2. Representation of Loading Mechanism

### FAILURE MODES

Mechanically fastened joints in composites display the same basic failure modes as in metals, i.e. tension, shear out and bearing. Failure is also possible by pull-out or in a combined tension/bending mode referred to as cleavage. These modes are illustrated in Figure 3.

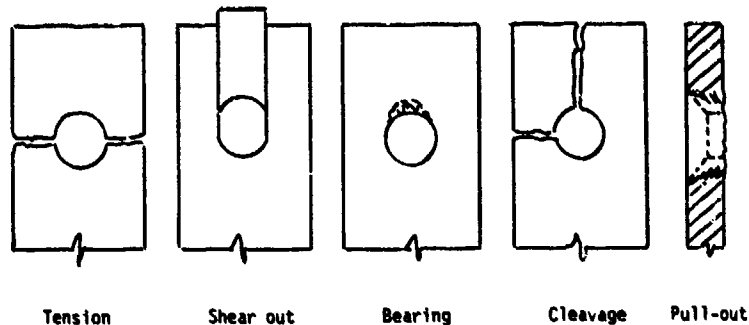


Figure 3. Failure Modes

#### a) Tension

As with conventional materials the tensile load required to fail a laminate through a section at which holes occur (the net section) is less than at a section with no holes (the gross section).

The corresponding failure stresses may be defined by:

$$\sigma_N = \frac{P}{(w - nd)t}$$

and

$$\sigma_G = \frac{P}{wt}$$

where  $P$  is the maximum load,  $n$  the number of holes and the width  $w$ , diameter  $d$  and thickness  $t$  are defined in Figure 1. It is conventional to express the above stresses in the form of stress concentration factors

$$k_N = \sigma_{ult}/\sigma_N \quad \text{and} \quad k_G = \sigma_{ult}/\sigma_G \quad \text{respectively,}$$

where  $\sigma_{ult}$  is the ultimate tensile strength of the plain laminate.

Because FRP are essentially elastic to failure they cannot take advantage of yielding at the hole edge and hence the stress concentration will lead to a low net failure stress. The latter depends strongly on the degree of anisotropy, and hence fibre orientation, in the vicinity of the hole.

For CFRP and CFRPeek laminates tensile failure will be governed by the  $0^\circ$  fibres, i.e. those parallel to the applied load. GFRP failures are more complex due, mainly, to the low modulus of the fibre resulting in higher shear strains being imposed on the laminate. As a consequence failure propagates by in-plane shearing between  $0^\circ$  and  $45^\circ$  plies, leaving only the  $45^\circ$  fibres to react the load.

'Kevlar' fibres have high tensile strength and it is thought that fibrillation of the fibres may provide a mechanism for the relief of stress concentrations at the hole edge.

## b) Shear Out

The shear out strength of a bolted joint is usually given by:

$$\sigma_s = \frac{P}{2et}$$

where the end, or edge, distance  $e$  is defined in Figure 1. Because of the difficulty of measuring the appropriate shear strength, it is unusual to quote shear stress concentration factors.

It is clear that, as with tensile strength, fibre orientation will play an important part in determining shear out strength. A unidirectional specimen, for example, has a low strength, whereas the strength of  $0/\pm 45^\circ$  lay-ups can be very high. Obviously the degree of anisotropy affects the stress concentration.

## c) Bearing

Bearing of a fastener in a hole gives rise to compressive stresses around the loaded portion of the circumference. These compressive stresses cause tensile stresses in the through-thickness direction which, because of the low strength in that direction, can lead to early failure if adequate restraint is not provided. For this reason pin joints have the lowest and bolted joints the highest strengths, with rivets in between.

The compressive strength of the  $0^\circ$  plies is a vital determinant of the joint's bearing strength, as is the stiffness of the fibres.

Bearing stress is defined by:

$$\sigma_b = \frac{P}{dt}$$

## d) Other

Cleavage, a combined bending and transverse tension failure, can be avoided if sufficient non-axial ( $\pm 90^\circ$ ) fibres are included in the lay-up.

Pull-out failure is normally associated with rivets, particularly those with a counter-sunk head; it should not occur with bolted joints.

## MAIN FACTORS AFFECTING FAILURE

## a) Fibre Orientation

The importance of fibre orientation has already been mentioned. As might be expected the ratio of  $0^\circ$  to off-axis ( $45^\circ$  and  $90^\circ$ ) fibres is a key factor. At low concentrations of  $0^\circ$  fibres shear out failure will predominate. The shear strength will increase with the inclusion of off-axis material (say,  $\pm 45^\circ$ ) until bearing becomes the critical mode. Continued increase in the proportion of  $\pm 45^\circ$  layers will change the failure mode to tension with a consequent drop in strength.

Fortunately for design considerations, joint performance is reasonably insensitive to lay-up over quite a wide range of composition. As a general recommendation the  $0^\circ$  plies should constitute between 35 and 65% of the total [7,3].

Contrary to what might be expected from the compressive behaviour of  $\pm 45^\circ$  laminates, the bearing strength of such laminates is high. This is due to the constraint offered by the washers. In  $0/\pm 45^\circ$  lay-ups the  $\pm 45^\circ$  plies enhance bearing performance by inhibiting longitudinal splitting in the  $0^\circ$  layers [7].

## b) Through-Thickness Constraint

It is well known that the bearing strength of a plain pin is very low. This is because the 'brooming' of the laminate on the loaded side of the pin is not prevented. Even a bolt with a finger-tight nut produces, at least, a 100% increase in strength because the washer suppresses the through-thickness failure. Tightening the bolt produces further increase in strength until a 'plateau' is reached, for most materials, at a clamping pressure of around 20 MN/m<sup>2</sup>. Such pressures are achieved with bolts tightened to normally-recommended torques.

## c) Stacking Sequence

The bearing strength of pinned joints in quasi-isotropic GFRP is very sensitive to stacking sequence [8], and that of CFRP rather less so [9]. The effect is related to the associated stress distributions. For a fully tightened bolt the failure can change from local bearing at the hole edge to 'remote-bearing' [9] at the edge of the washer. The latter mode is essentially one of buckling of the surface ply (or plies) and will again be related to the stacking sequence.

The above comments apply to 8 or 16-ply laminates (with  $0/90/\pm 45^\circ$  plies) in which the plies are 'intimately mixed'. With thicker laminates, or those with high proportions of fibres in one direction, it is possible to produce a 'blocked' configuration, i.e. one in which several similarly oriented plies are grouped together. Such an arrangement can have a lower strength (possibly by as much as 50%) than a laminate with an intimately mixed or 'homogeneous' sequence [3,7,10]. Although wider considerations make the use of a blocked lay-up unlikely, the above remarks about strength loss could be important when dealing with local reinforcement.

## d) Joint Geometry

## i) Width

The essentially linear elastic behaviour of FRP means that net tensile strength is strongly dependent on width. Also, gross strength is related to hole size and both net and gross strengths depend on lay-up. The effect of width is most marked for  $0/90^\circ$  laminates and least for  $\pm 45^\circ$  lay-ups.

For design it is usual to choose a geometry ( $w/d$ ) which gives equal likelihood of failure in tension or bearing. Precise values will depend on the material and it could be that the tensile mode will be the stronger [10].

Whatever the failure mode, strength is normally expressed in terms of the bearing stress. Typical curves of experimental data [7,6] are shown in Figures 4-6, where it is seen that the behaviour of the various materials is essentially the same. Thus, failure changes from tensile at low values of  $w/d$  to bearing at high  $w/d$ . The change over point and the 'plateau' value depend on fibre, matrix and lay-up.

## ii) End Distance

Varying end distance has the same effect on shear out strength as varying width has on tensile strength. Curves of bearing stress variation with  $e/d$  are, hence, similar to those for  $w/d$  and only data for CFRP are shown to illustrate the situation (Figure 7) [7].

An interesting feature of woven KFRP laminates is that, even for high values of  $w/d$  and  $e/d$ , failure was always in a tensile mode for bolted joints. Pinned joints, in contrast, showed mode changes as described above [4].

## iii) Hole Size and Thickness

Net tensile strength is largely insensitive to hole size although gross strength reduces as hole size is increased [1,3,6].

Shear out strength appears not to be sensitive to hole diameter, as does the bearing strength of CFRP and CFRP/epoxy. However, the bearing strength of both GFRP [3] and KFRP [4] are reduced at large diameters (or small thicknesses for a given diameter). The reduction is due to gross bending of the laminate on the loaded side of the hole, in what is effectively an instability phenomenon. The effect is most marked for pinned joints but is also present in bolted joints, becoming marked if  $d/t > 3$ . A further source of strength reduction, at high  $d/t$  ratios, is brought about by bending of the fastener imposing high stresses on the surface plies.

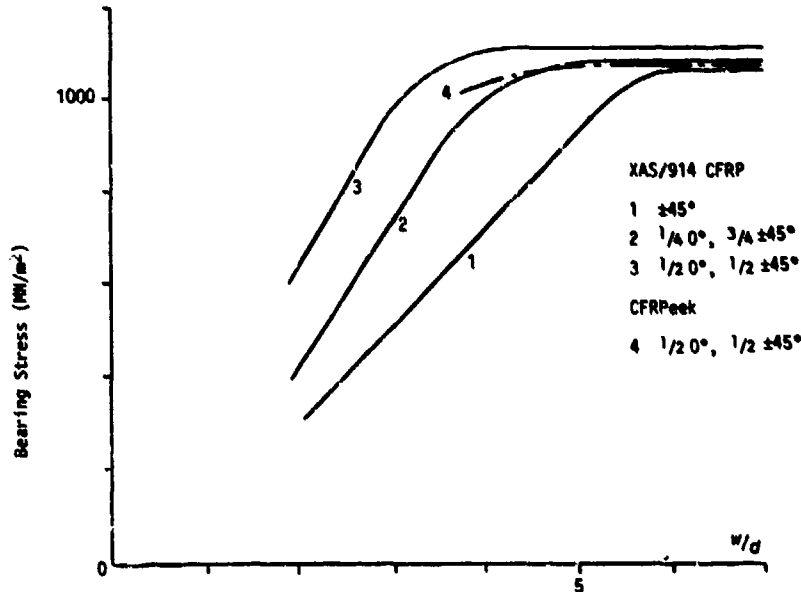


Figure 4. Variation of Failure Bearing Stress with  $w/d$  for Carbon Fibre Laminates

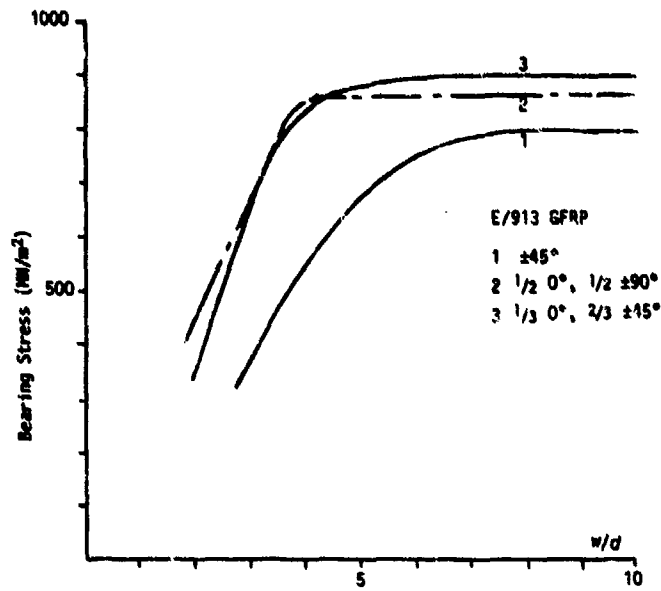


Figure 5. Variation of Failure Bearing Stress with  $w/d$  for Glass Fibre Laminates

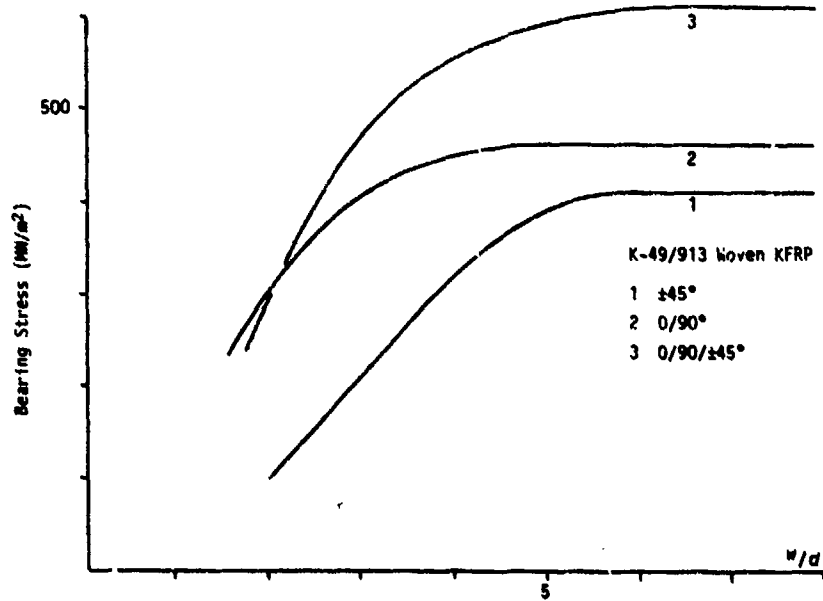


Figure 6. Variation of Failure Bearing Stress with  $w/d$  for 'Kevlar' Fibre Laminates

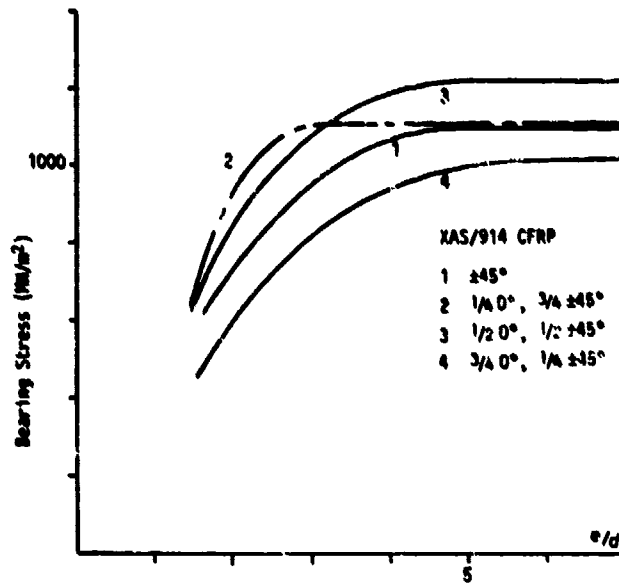


Figure 7. Variation of Failure Bearing Stress with  $a/d$  for Carbon Fibre Laminates

#### STRESS DISTRIBUTIONS

Many workers have investigated the stress distributions around a loaded hole and attempted to relate these to failure. A particularly detailed discussion is given by Smith [9], who also reviews the work of other investigators.

The important average stresses in the laminate plane around the hole edge will be: maximum compression at  $\theta = 0^\circ$  (see Figure 1 for definition of  $\theta$ ), maximum tension at  $\theta = \pm 90^\circ$ , maximum shear on radii at  $\theta = \pm 45^\circ$ . These maxima clearly play an important part in determining failure.

The details of the failure process are, however, related more to the through-thickness direct and shear stresses. These stresses are closely linked to the lay-up, stacking sequence, bolt clamping force and, of course, ply mechanical properties.

Such stress analyses illustrate clearly why bearing failure at the hole edge (at  $\theta = 0^\circ$ ) for a pinned joint changes to remote bearing (at the washer edge) for a bolted joint [9,11]. Also the way in which stacking sequence can change the through-thickness direct stress from tension to compression correlates well with experimental results and indicates that the fibres in the two plies nearest the surface should not be oriented at  $0^\circ$  [9].

Further development of such stress analyses is important as they offer the possibility of strength prediction, once the failure process and associated failure criteria can be more accurately modelled [12].

#### OTHER FACTORS

##### a) Joint Configuration

The experimental data quoted above derives from single hole specimens loaded in double shear, by an arrangement similar to that shown in Figure 2, where the bolt clamping force is transmitted to the laminate via washers. Apart from the question of symmetry of loading, this situation is relevant to a laminate which forms the outer component of a joint.

Also of interest are double shear arrangements where the laminate is sandwiched (without intervening washers) either between metal plates or similar laminates. Stress analyses performed by Smith [9] indicate that the first arrangement should bring about an increase in strength of 5-10% and the second somewhat less, but still higher than the washer arrangement. This latter assessment is confirmed by experimental data.

A further consideration is the joint type, i.e. single or double lap. Experimental results here are scarce but there is evidence that for CFRP and CFRP/PEEK [6 & 7], a single hole single lap joint is about 10% weaker than the double shear arrangement. The reduction is rather less for two-hole (parallel to the load) single lap joints. For KFRP the strength reduction for single laps is closer to 20% [8], and it appears that the strength hierarchy of lay-ups can change compared to joints loaded in double shear.

#### b) Multiple Fasteners

For a row of fasteners (i.e. normal to the load) there is generally no interaction between holes provided the spacing (pitch) is greater than  $4d$ . This means that test data for single hole specimens of width  $4d$  can be used to design such multi-hole joints.

Joints with lines of fasteners (i.e. parallel to the load) are more complicated because of the presence of the by-pass stress. As noted by Hart-Smith [10], it is difficult in such circumstances to improve on the optimum single hole joint without resorting to considerable complexity, such as a stepped or tapered lap joint.

#### c) Bearing Strains

Although irreversible damage is apparent well before final failure, probably at about 60% of ultimate load for CFRP [2], the load-carrying capability of the laminate is not impaired. Because significant bearing strain (hole elongation) occurs before failure, careful consideration must be given to choice of design strain levels. This is especially so if hammering in fatigue is to be avoided. A factor of 2 on ultimate stress is probably adequate. Even at the associated stress levels FRP are still competitive with metals on a strength-to-weight basis (see below).

### GENERAL COMMENTS

It is clear from the information already presented, Figures 4-7, that CFRP and CFRP/PEEK have virtually identical bearing strength with GFRP about 20% weaker and KFRP about 50% weaker than the carbon fibre materials.

Because of the large number of variables involved there is a requirement for a predictive capability that will reduce the need for extensive testing. Collings [2] fulfills this requirement for CFPP with a semi-empirical approach which gives expressions for bearing strength of various lay-ups, in terms of basic strengths of individual plies. This approach should also work for CFRP/PEEK. Unfortunately the method adopted by Collings does not appear to work for GFRP, a more complicated description of failure seems to be needed [13].

It is interesting to note that FRP compare well with metals on a strength-to-weight basis [7]. Typical values for bearing strength are shown in Table 1.

Material	Bearing Strength (MN/m <sup>2</sup> )	Specific Gravity	Specific Bearing Strength
Steel S96	973	7.85	124
Aluminium Alloy L71	425	2.70	157
CFRP XAS/914 50% 0°, 50% ±45°	1070	1.54	695
GFRP E/913 33% 0°, 67% ±45°	900	1.90	473
KFRP Woven/913 0/90°	450	1.35	333

Table 1. Comparison of Specific Bearing Strengths  
(i.e. strength ÷ specific gravity)

### CONCLUSIONS

a) Carbon fibre-reinforced epoxy and PEEK are equally strong, with a bearing strength around 1000 MN/m<sup>2</sup>. Glass fibre-reinforced epoxy has about 80%, and 'Kevlar' fibre-reinforced epoxy about 50%, of the strength of the carbon fibre materials.

b) For a given fibre/matrix combination, lay-up is a key factor in determining strength. Lay-ups should not be strongly anisotropic. A 0/±45° combination is generally to be preferred, with between 35 to 65% 0° fibres.

c) The stacking sequence should be as homogeneous as possible, i.e. plies of the same orientation should not be grouped together.

d) Through-thickness clamping strongly influences behaviour. Bolts must be fully tightened if maximum strength is to be obtained.

- e) As a general rule width (or pitch) and end distance should be approximately  $4d$  to obtain optimum performance.
- f) For GFRP and KFRP  $d/t$  should be less than 3.
- g) Single lap joints are from 10 to 20% weaker than joints loaded in double shear.
- h) Design stresses limited to about 50% of ultimate should provide adequate protection against permanent damage, whilst still offering a strength-to-weight advantage over metals.

#### REFERENCES

1. Collings, T.A., Royal Aircraft Establishment, Farnborough, UK, The strength of bolted joints in multidirectional CFRP laminates, 1975, TR 75127.
2. Collings, T.A., On the bearing strengths of CFRP laminates, *Composites*, Vol 13, No 3, 1982, pp 241-252.
3. Kretsis, G. and Matthews, F.L., The strength of bolted joints in glass fibre/epoxy laminates, *Composites*, Vol 16, No 2, 1985, pp 92-102.
4. Matthews, F.L. and Kalkanis, P., The strength of mechanically fastened joints in 'Kevlar' fibre-reinforced epoxy resin, Proc. 5th Int. Conf. on Composite Materials (ICCM-V), San Diego, USA, July/August 1985: The Metallurgical Soc. Inc., Warrendale, Pa., USA, pp 1297-1314.
5. Hodgkinson, J.M., de Beer, D.L. and Matthews, F.L., The strength of bolted joints in 'Kevlar' RP, Proc. Workshop: Composites Design for Space Applications, ESTEC, Noordwijk, The Netherlands, October 1985, ESA SP-243, February 1986, pp 53-61.
6. Hodgkinson, J.M., Centre for Composite Materials, Imperial College, London, UK, The strength of mechanically fastened joints in carbon fibre-reinforced PEEK, March 1986.
7. Matthews, F.L. (Editor), *Joining Fibre Reinforced Plastics*, Barking, Essex, UK, Elsevier Applied Science Publishers, 1986, Chapter 2.
8. Quinn, W.J. and Matthews, F.L., The effect of stacking sequence on the pin-bearing strength in glass fibre reinforced plastic, *J. Composite Mater.*, Vol 11, No 3, 1977, pp 139-145.
9. Smith, P.A., St Catherine's College, University of Cambridge, UK, Aspects of the static and fatigue behaviour of composite laminates, including bolted joints, December 1985, PhD Thesis.
10. Hart-Smith, L.J., McDonnell Douglas, Long Beach, California, USA, Design and analysis of bolted and riveted joints in fibrous composite structures, August 1986, Douglas Paper 7739; presented at Int. Symp: Joining and Repair of Fibre-Reinforced Plastics, Imperial College, London, UK, September 1986.
11. Matthews, F.L., Wong, C.M. and Chryssafitis, S., Stress distribution around a single bolt in fibre-reinforced plastic, *Composites*, Vol 13, No 3, 1982, pp 316-322.
12. Matthews, F.L. (Editor), *Joining Fibre Reinforced Plastics*, Barking, Essex, UK, Elsevier Applied Science Publishers, 1986, Chapter 3.
13. Kretsis, G., Department of Aeronautics, Imperial College, London, UK, The strength of bolted joints in GFRP laminates, September 1983, MSc Project Report.

## MECHANISM OF SINGLE SHEAR FASTENED JOINTS

J. Bauer

MESSERSCHMITT-BÜLKOW-BLOHM GMBH  
Helicopter and Airplane Division  
8000 Munich 80, P.O.Box 801160, W-Germany

## SUMMARY

The problems arising with the strength of single shear fastened joints are considerably greater than those of double shear joints. The additional (or secondary) bending moment loads not only the cover plates, but also causes considerably bending in the fasteners. If one of the cover plates is of composite material its brittleness and relatively low bearing strength lead to new problems.

Experimental data were produced with a 100 % load transfer specimen using a CFRP to metal joint. Taking the specimen configuration as a basis, the interaction of bolt bending and local load introduction into the two plates is shown in form of diagrams based on theoretical investigations.

## INTRODUCTION

Mechanically fastened single shear joints are used extensively in any aircraft structure. With the increasing use of composites, the question of the strength of these joints with CFRP becomes more and more important. Single shear bolted joints are used to connect spars, ribs or frames to skins. Concentrated load introductions, like fitting joints, are usually carried out in double shear. Single shear joints can nevertheless offer extensive advantages in aircraft structures in respect to weight, aerodynamic, costs, design and production purposes. To make more use of these advantages, even for high load transfers, a more detailed knowledge about the mechanism and the strength of those joints is necessary. The final target is, to find a reliable method, considering strength requirements, which separates clearly, whether it is possible to use a single shear bolted joint or a double shear one has to be used. Until now, this question was answered, more or less, by experience and previous data from metal structures. It is doubtful, that this gives sufficient accuracy and reliability. The low bearing strength of CFRP, together with its brittleness, leads to increased thicknesses and to a different elastic behaviour. The engineer using COMPOSITES needs more detailed information about these phenomena acting together. To be able to make use of advantages a more sophisticated method for joining single shear joints is necessary.

## BASIC REALIZATIONS OUT OF TESTS

To investigate the problems of single shear bolted joints with CFRP-laminates, a test program was performed. The objectives of the tests had been to clarify the basic mechanism with special respect to the behaviour of the CFRP. We wanted to produce as much information as possible, to create a data-base for the development of a prediction method for the strength of single shear bolted joints.

The test method/configuration was designed to avoid any effects, which could influence the behaviour of the CFRP during the static and dynamic tests. As shown in Figure 1 we used a CFRP-lap fastened onto a steel plate, which was chosen to be relatively thick. The bolt is therefore supported very stiff. During the tests this prevents, that the bolt fails before the CFRP-plate was damaged.

The secondary bending moments introduced into the plates, tended to raise the edge of the CFRP-specimen from the steel plates. It seemed reasonable to avoid such bending by a clamping ring, because in application of aircraft structures this cannot take place in most cases. To simulate the worst case, the bolts were only finger-tightened.

Measurements were carried out, to investigate the load displacement behaviour of the joint in an accurate way. Therefore the displacements between the two plates were measured in the vicinity of the bolt. Typical load displacement curves are shown in Figure 2. Three different physical events are characterizing the slope:

- 1.) First nonlinearity
- 2.) Beginning of nonlinear behaviour
- 3.) Ultimate Failure.

The first nonlinearity is the sign of the first failure at the inner side of the CFRP-plate and it marks the end of the initial linear behaviour. This effect leads to a more uniform load distribution in the CFRP-plate and results in a new range of linear behaviour in the load displacement curve. Finally a range of nonlinearity occurs, superimposed by plastic bolt bending and destruction of the laminate. The result of

such a destruction is given in Figure 3 as photomicrograph. The example shows a counter-sink drilling after final bearing failure. The laminate is destroyed by fibre failures, transverse cracks and large delaminations in bolt-load direction. It is remarkable, that the opposite side of the drilling remains undisturbed.

#### THEORETICAL INVESTIGATION

The main problem of single shear bolted joints results from non-symmetry. The load transfer, from the first plate into the bolt and then into the second plate, produces secondary bending moments within the plates and leads to a significant bending of the bolt. The mechanism taking place, is understood as an interaction of the three participating parts. In other words, the non-symmetry of the joint leads to a non-uniform load introduction into the plates and causes bending of the bolt. But the bended bolt itself influences the distribution of the load introduction into the plates. Out of this basic understanding the governing parameters of the mechanism can be determined:

Properties of Plate 1 :	Thickness :	$t_1$
	Modulus of Elasticity :	$E_2$
Properties of the Bolt :	Diameter :	$d$
	Modulus of Elasticity :	$E_f$
Properties of Plate 2 :	Thickness :	$t_1$
	Modulus of Elasticity :	$E_2$

With these six parameters the interaction of bolt bending and load introduction into the plates can be mathematically described within the linear elastic range of the problem. Such an analytical solution can be found in the literature. It was developed by William Barrois and published in 1978 in Engineering Fracture Mechanics, Vol. 10. With some minor modifications it is possible to use this approach for our problem of fastening a CFRP-part onto a metal one.

It should be mentioned, that one parameter is not included in the theory, the bolt torque. It has some influence, but here it can be neglected with good conscience as it does not influence the principle of the investigation. Figure 4 shows the results of a re-calculation of our specimen, with protruding head.

The overall impression of the bolt bending and the local load introduction into the two plates is not surprising. The example of our test specimen shows, that the highest local bearing load acts on the thick metal plate at the contact surface. This can be seen as evidence, that thickness alone will not protect from uncritical loading and local damages.

Further information is offered by the theory, the bending of the bolt is described in detail. It should render possible the prediction of the working life of the fastener from its bending stresses.

As a final conclusion from this example, we can see that anyone of the three different participating parts could possibly initiate the failure of the joint. The important advantage of such a calculation, is the possibility to quantify the effects and be able to vary the six parameters which influence the interaction between bolt bending and load introduction into the plates. Six different parameters are not easily represented. We are forced to treat the problem step by step keeping several parameters constant. As a basis our single shear specimen is used and then the following properties are found to remain constant:

Thickness of the CFRP-plate :	$t_1 = 6 \text{ mm}$
Diameter of the bolt :	$d = 8 \text{ mm}$
Material of the bolt :	$E_f = 210000 \text{ N/mm}^2$
Material of the metal plate :	$E_2 = 210000 \text{ N/mm}^2$

This means we fasten a CFRP-plate with a 8. mm dia steel bolt onto a steel plate and vary its thickness. To show the effects clearly the maximum local bearing stresses have to be normalized:

- For the CFRP-plate the maximum local bearing is normalized by the average bearing stress:

$$k_1 = \frac{\sigma_{1bmax}}{\sigma_{1b}}$$

- The maximum local bearing stress of the steel-plate with variable thickness is divided by the transferred load:

$$s_2 = \frac{\sigma_{2bmax}}{P}$$

These two factors give a representative value for the maximum bearing stress, independent from the loading.

The bolt bending moment can be separated from the loading of the joint by the factor:

$$b_m = \frac{M_{bolt,max}}{P}$$

In Figure 5 the behaviour of these three parameters ( $k_1$ ,  $s_2$ ,  $b_m$ ) is shown.

We are starting with a thickness of 15. mm and try to reduce the weight of our specimen configuration by sizing the steel plate with smaller thicknesses. It is obvious that the maximum bearing stress does not increase extensively, as long as the thickness remains above about 7. mm. With a smaller steel plate the local maximum bearing stresses increase steadily in both laps.

To proceed to light weight constructions Figure 6 was created. The steel plate is changed to light alloy and the bolt material becomes titanium. In comparison to the heavy metal configuration, the CFRP-plate is then subjected to a higher loading. Both, the weaker bolt and the worse support of the bolt by the light metal plate lead to higher maximum local bearing stresses within the CFRP-plate.

The light metal plate itself distributes loading in a more optimal way than the stiffer but heavy configuration. And the titanium bolt does not carry as large a bending moment as the stiffer steel bolt.

#### CONCLUSION

The example shown confirms, that everyone of the three geometric and three elastic properties influences the load transfer. It is not possible to neglect any of them. This knowledge is necessary for the interpretations of test results and helpful, if a test program for single shear fastened joints has to be created.

Some general rules for the design of mechanically fastened single shear joints can be established from the theoretical results shown:

- The strength of a CFRP-plate, fastened onto a metal plate, is dependent upon the geometric dimensions of the joint.
- A good design of a single shear fastened joint seems to be when both plates, the metal and the CFRP-plate are of about the same thickness.
- Increasing the plate thicknesses results in higher bending moments of the bolts, but does not affect the strength of the two plates.
- Smaller bolt diameters lead to higher local bearing stresses for the CFRP-plate, but also to higher bending moments of the bolt.
- A CFRP-plate with a low modulus of elasticity is not affected by such high local bearing stresses, but the other plate has to withstand higher local bearing loads.
- For the bolt the slope of  $b_m$  (Figure 5+6) shows, that for a thinner metal plate, its maximum bending moment decreases.
- A CFRP to metal joint can transfer the highest loads, if the metal parts, both bolt and plate, are as stiff as possible.

As a summary, the theoretical investigations confirm, that large thicknesses of the two laps result in less than ideal conditions for the bolt. Alternatively, if the two laps are designed too thin then the local bearing stresses are allowing only a small load to be transferred.

#### REFERENCES

- 1) William Barrois  
Stresses and Displacements due to Load Transfer by Fasteners  
in Structural Assemblies  
Engineering Fracture Mechanics 1978, Vol. 10  
pp. 115-176, Pergamon Press
- 2) D. Schutz, H. Lowak  
Die Berücksichtigung des Einflusses der Sekundär-Biegung  
auf die Schwingfestigkeit von Fügungen  
Bericht Nr. FB-113 (1974)

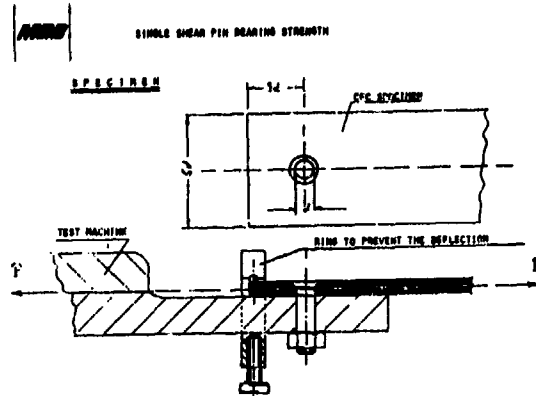


Figure 1 : Specimen Configuration

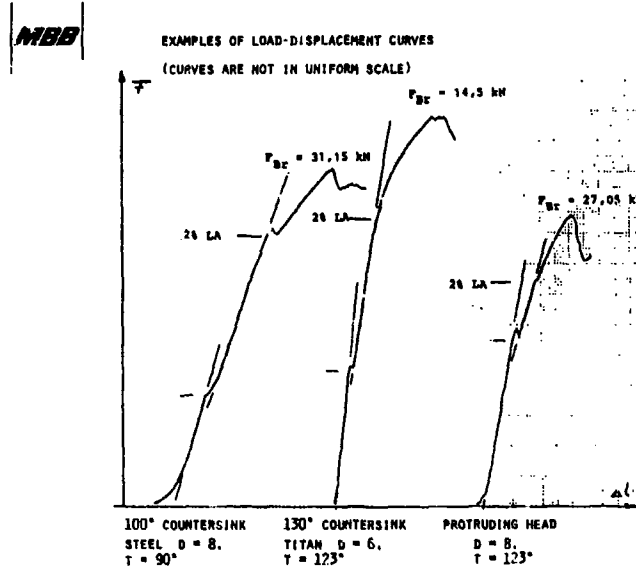


Figure 2 : Typical Load Displacement Curves of Single Shear Bolted Joints

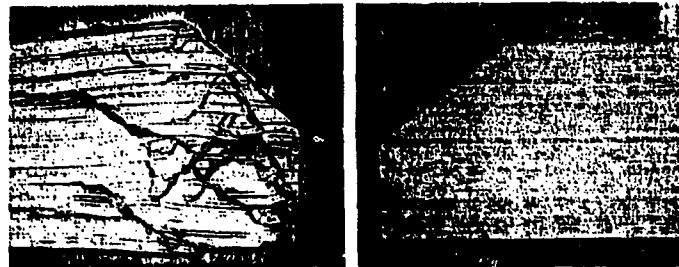


Figure 3 : Photomicrograph of a Countersink Drilling after Test

**MBB**

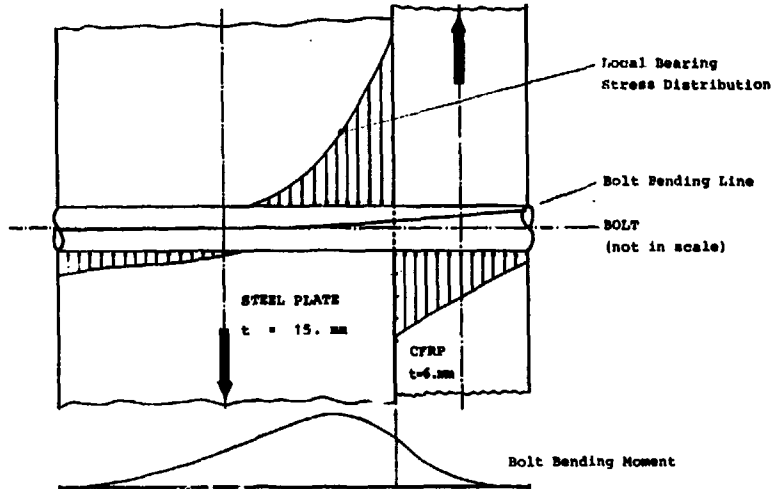


Figure 4 : Load Transfer of the Specimen Configuration

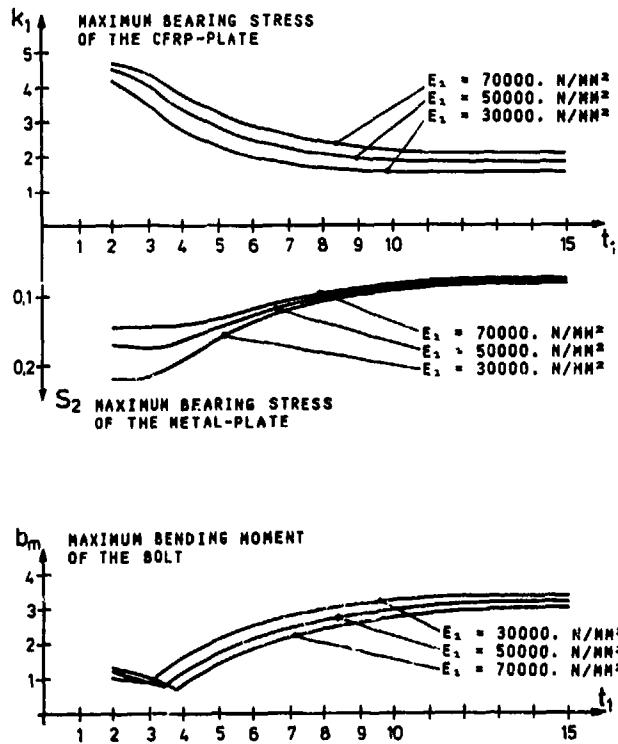


Figure 5 : Maximum Bearing Stresses and Maximum Bending Moments of the Bolt for Various Steel Thicknesses

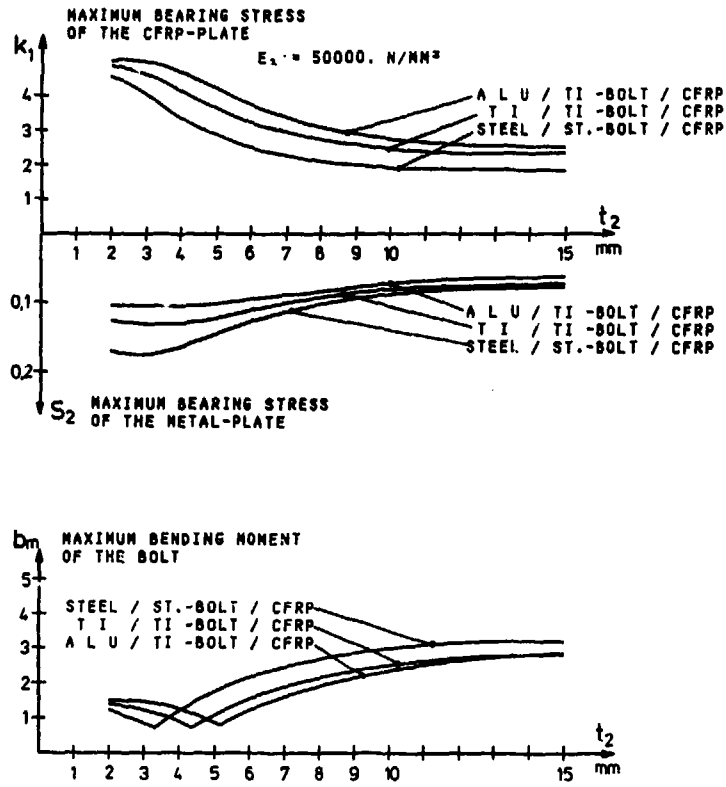


Figure 6 : Difference between Steel and Light Alloy Configuration

JOINING OF CARBON FIBER  
COMPOSITE WITH FASTENERS

by  
Salvatore Pagliuso  
AERITALIA GVT  
Viale dell'Aeronautica  
80038 Pomigliano d'Arco(Napoli)  
Italy

SUMMARY

This paper deals with the Aeritalia experience on drilling techniques and fastener selection for advanced composite assembly. Details are provided on fabrication techniques. Informations are given on corrosion prevention.

1. INTRODUCTION

Aeritalia's experience pertaining to carbon composite structures going back to the early 70's when curing of lab-scale carbon composites was started followed by experimental G 222 spoilers. Aeritalia's knowledge was built-up on several programs. An important step came from the participation to the Boeing B 767 program. Aeritalia's involvement in the development work was ample and essential to the utilization of carbon/epoxy in the program.

The production phase, which is still going on, gave Aeritalia a deep experience in the area of large C./EP. components fabrication and assembly and contributed to the development of both engineering and production knowledge that, combined with internal research activity, have given Aeritalia a leading position in the area of advanced composite structures.

This experience was completed and furtherly enhanced through the development of Aeritalia ATR 42 program and participation to the MD 80 and Rohr CFM 56-5 programs, which have given Aeritalia a widely recognized knowledge of the state-of-the art technology for C./EP. aerospace structures.

2. DRILLING

A few basic recommendations must be taken into account, during drilling operations, to guarantee good quality. Clamping pressures should be well distributed to avoid damaging parts.

Once the cut is started, it should not be stopped since this may leave tool marks on the surface.

Tools shall always be kept as sharp as possible. Dull tools create more heat than sharp one.

Since all plastics are poor conductors, heat builds up on the cutter causing tools to break down rapidly.

Besides dull tools generate edge delaminations, chipping, crazing, and tearing of fibers.

In fact, dull tools generate higher cutting forces that will tend to delamination.

Back-up strips are helpful in preventing delamination, mainly with unidirectional tapes.

A fiberglass layer, used as a corrosion protection layer, is also helpful in preventing delamination during drilling. During drilling, it is generally recommended a frequent retraction of the cutter to prevent drill binding and tapered holes.

In deep holes, coolants are helpful to prevent tip overheating. Feeds should be reduced near the end of the cut to prevent chipping or break through.

Different shapes of tools are utilized in drilling C./EP. parts. Aeritalia's experience and manufacturing research selected a tungsten carbide drill patented by Aeritalia and shown in Fig.1

The minimum drilling speed utilized with this cutter is 4500 R.P.M.

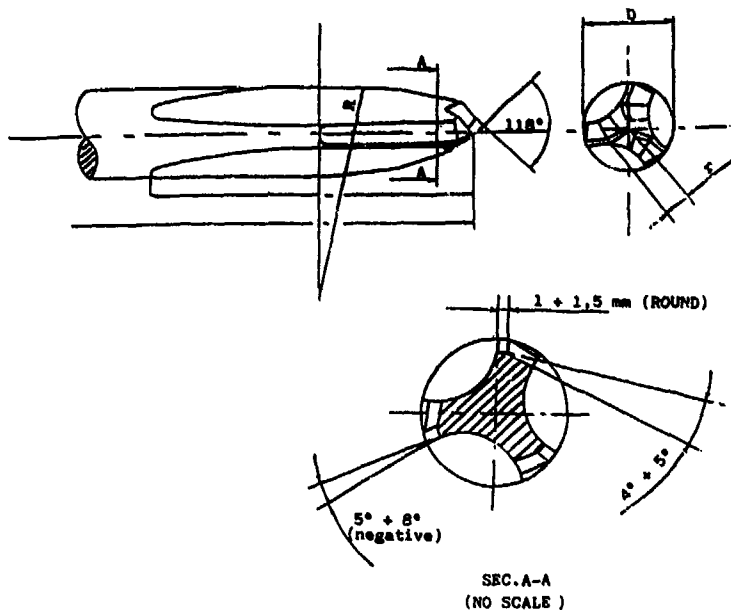
C./EP. parts must often be drilled together with the structure components made in aluminum or titanium material to avoid holes misalignment.

To drill these assemblies traditional helix drills in tungsten carbide are used starting from the C./EP. side and using a drilling template.

The metal is used as back-up to avoid the delamination.

Aluminum - C./EP. assemblies are drilled at 4000 - 4500 RPM. Titanium - C./EP. assemblies are drilled at 150 - 300 RPM. Close tolerance holes are made with a 0,8 mm minor drill point and then completed by reaming. A peculiar problem is the drilling operation of a sandwich structure for blind fasteners installation ( see Fig.2 ). The drilling operation is accomplished with the same technique plus an inside cleaning operation to provide a suitable mating surface for the blind fastener head.

The cleaning operation is accomplished with a special tool developed by Aeritalia for which a patent request is pending.



L = 100 mm  
 T = 50 mm  
 R = 250 mm  
 r = D/2 x 15 mm  
 D TOLERANCES = +0,025 - 0,000 mm

FIG.1  
 AERITALIA'S PATENTED CARBON/EPOXY MATERIAL DRILL POINT

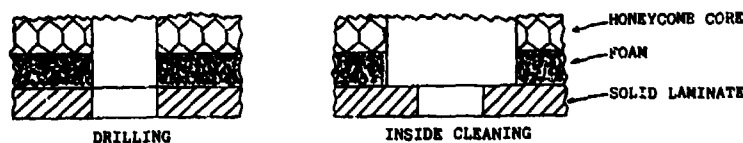


FIG.2  
 DRILLING OPERATIONS IN SANDWICH STRUCTURES  
 FOR BLIND FASTENER INSTALLATION

### 3. FASTENERS

Three types of fasteners are generally utilized for C./EP. assemblies : typical, blind and hollow ended. Typical fasteners are very similar to the ones utilized for metallic assemblies. Particularly interesting is the utilization of fasteners with a hi-lok type pin on K-fast type nut.

In fact this type of fastener has the following advantages respect the traditional hi-lok :

- K fast nuts generally have lower purchase prize than collars.
- There is no broken collar or pin to contend with.
- The low profile allows easier installation in limited access areas.
- K fast nuts are reusable according to military specification MIL-N-25077.
- The oversized nut counterbore configuration allows standard K-fast nuts to be used on either standard or oversized pins, eliminating the need for duplicate inventory.
- Closely controlled setting torque eliminates possible surface damage and gives a more consistent pre-load.
- They can be retorqued after sealant setting.

Blind fasteners for composites must provide a large blind side upset to reduce possible delamination. The large blind side permits the fastener to exert very clamp-up loads to the structure, without damage. The two mostly used types of blind fasteners are the "big foot" and the one with an expandible washer. The "big foot" is shown in Fig.3 and its installation procedure shown in Fig.4 is :

- 1) The fastener is inserted into the prepared hole. The installation tool is placed over the screw to simul

simultaneously engaging the wrench flats and the drive nut.

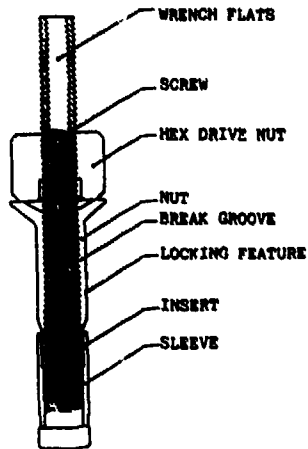


FIG. 3

"BIG FOOT" FASTENER

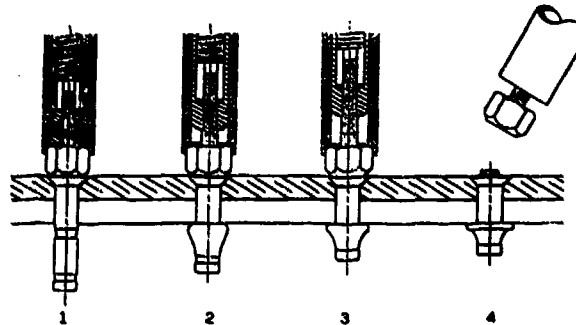


FIG. 4

"BIG FOOT" FASTENER INSTALLATION

- 2) Torque is applied to the screw while the drive is held stationary. Screw advances through nut body to cause sleeve to be drawn up over the tapered nose of the nut. Blind head formation is started.
- 3) Continued tightening removes sheet gap, completes the large blind head and clamps the sheets tightly together.
- 4) When the sleeve forms tightly against the blind side of the structure, the screw will fracture in the break groove. The tool is pulled away and the pintail drive nut assembly is discarded.

In this fasteners the sleeve buckling is accomplished directly against the composite structure; this could result in local crushing of the composite material, but this has never been experienced by Aeritalia. Very critical is the formation of the correct head on the blind side. Aeritalia's experience is that the installation of "big foot" fasteners is reliable providing that a constant driving tool is used without action interruption to allow the thermoplastic ring correct fusion. If during the installation the driving is interrupted, the head formation can be affected and dissymetry will result (see Fig. 5).

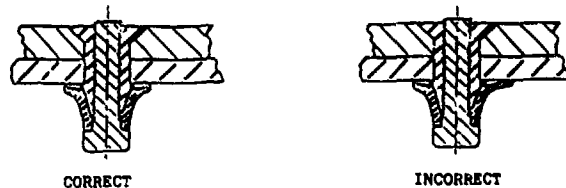


FIG. 5

POTENTIAL PROBLEM FOR "BIG FOOT" FASTENER INSTALLATION

The installation shall be accomplished by hand or automated machine at 30 RPM minimum. The "expendible washer fastener" is shown in Fig. 6, its installation procedure is :

- 1) The fastener is inserted into the prepared hole and the installation tool is placed over it.
- 2) The advance of the corebolt forces the washer and sleeve over the taper, expanding and uncoiling the washer to its maximum diameter.
- 3) Continued advance of the corebolt draws the washer and sleeve against the joint surface, preloading the structure. At a torque level controlled by the break groove, the slabbed portion of the corebolt separates, and installation is complete.

Though this type of fastener has not given the potential problems of the "big foot", it is not being utilized at Aeritalia. In fact the following problems were encountered during its laboratory valuation ( on 4 mm diameter fasteners ):

-Shank bearing over the head

- Shank breaking below the head
- Shank breaking without gripping

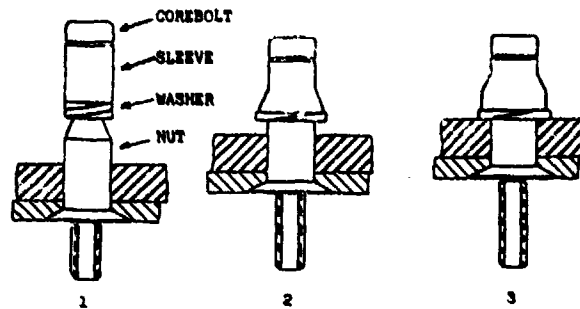


FIG. 6

## EXPENSIBLE WASHER FASTENER INSTALLATION

The hollow ended fasteners are shown in Fig. 7

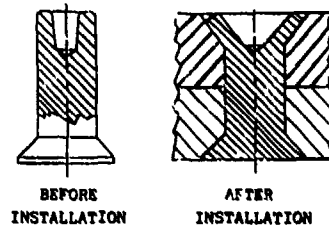


FIG. 7

## HOLLOW ENDED FASTENERS

They are utilized in areas where double side aerodynamic surfaces must be ensured. They are made out of annealed titanium-columbium alloy or bimetallic materials (body heat treated titanium alloy and tail annealed titanium - columbium alloy) so that after positioning the fastener from the countersunk head side, the manufactured head can be easily swaged to its required shape.

They are mainly utilized at Aeritalia to join trailing edges of control surfaces whose parts are mechanically assembled. No particular problem is caused by their installation.

## 4. CORROSION PROBLEMS

Joining C./EP. parts gives galvanic compatibility problem. This problem has been reduced with the right selection of fastener materials and insulating with particular care the elements of the joints. The fasteners material must be as less dissimilar as possible to C./EP., from a galvanic stand point. The mostly used type is titanium, which couples the specific strength characteristics to the low galvanic dissimilarity with carbon.

The fastener is also insulated with an organic coating.

The biggest potential corrosion problem is encountered when a carbon structure is joined to a metallic one, mainly aluminum components that is strongly anodic to the carbon.

The solution was to insulate both the carbon structures (that usually are a large cathod) and the aluminum parts fastened to them. The insulation of the C./EP. parts is guaranteed by a ply of fiberglass applied during the lay-up on the side coupled to the aluminum component.

The aluminum parts are insulated by a layer of primer and one layer of enamel and installed to the mating surfaces with faying sealant. Fasteners going through the joining surfaces will be wet installed with sealant. Laboratory tests and mainly service experience certified the reliability of this protection.

### 5. CONCLUSION

Mechanical assembly of carbon/epoxy components is an operation that appears not too far from the traditional one. Obviously it requires the knowledge of some essential precautions and the need of following some recommendations that only can guarantee the reliability consistency and quality of the parts.

**ENTURES BOULONNÉES EN MATERIAUX COMPOSITE CARBONE  
COMPARAISON ENTRE MONTAGES A INTERFERENCE ET MONTAGE A JEU**

Par Denis CHAUMETTE  
Avions Marcel Dassault - Breguet-Aviation  
Saint-Cloud - FRANCE

**RESUME**

Des essais ont été effectués de tenue d'assemblage carbone avec viseries montées avec ou sans interférence. Les résultats montrent que, contrairement à ce que des calculs de surcontrainte élastique auraient laissé espérer, l'interférence n'a pas d'influence significative sur la résistance statique des éprouvettes, même après chargement en fatigue.

Ce résultat peut s'expliquer par le mode de rupture réel des pièces en composite trouées qui fait intervenir une adaptation par délaminage.

**1 - GENERALITES**

Dans le cadre des différents programmes de structures composite qu'elle a conduit, du MIRAGE 3 au démonstrateur RAFALE (voir planche 1), la Société Avions Marcel Dassault-Breguet Aviation a été amenée à développer des méthodes de calcul très complètes intégrant les assemblages chargés (contraintes et critères de rupture), les calculs de flambage post-critique en compression, les méthodes d'optimisation automatique, et les composites dits de deuxième génération (fibres à moule intermédiaire (IM), à matrice bismaléimide (BMI)).

Le présent papier présente, extrait de cette base d'expérience, les résultats d'études et d'essais sur les performances d'assemblages par viseries montées à interférence.

**2 - LE ROLE DE L'INTERFERENCE DANS LES ASSEMBLAGES METALLIQUES**

L'intérêt du montage à interférence pour la tenue en fatigue des assemblages métalliques est connu depuis très longtemps et cette méthode est pratiquée de façon extensive sur un certain nombre de structures.

La méthode la plus souvent utilisée est le montage de viseries cylindriques standard de diamètre supérieur au trou, mais aussi de viseries spécialisées (par exemple vis coniques) et de systèmes axe conique-bague pour les chapes.

Le rôle de l'interférence est double :

- . de limiter le fretting en limitant les micromouvements
- . de réduire la contrainte maximale et l'amplitude du cycle de fatigue.

Ce deuxième point est explicité dans la planche 2 (tirée de la référence (1)) qui montre le résultat du calcul par éléments finis d'un trou criqué avec différentes longueurs de crique (calcul par éléments finis non linéaires avec contact variable entre la fixation et le trou).

Cette planche montre clairement qu'à partir d'une certaine charge, l'interférence réduit la contrainte en bord de trou. Par ailleurs, elle réduit aussi l'amplitude de variation de contraintes.

Sur les matériaux métalliques, cet effet ne joue qu'en tenue en fatigue et propagation de criques, et non en tenue statique du fait de l'adaptation plastique de ces matériaux.

Pour les matériaux composites qui n'ont pratiquement pas d'adaptation plastique, l'interférence pourrait donc se présenter comme une solution pour améliorer aussi la tenue statique. C'est ce qui a fait l'objet d'une vérification expérimentale sur éprouvettes à fixations non chargées.

Le matériau utilisé est une fibre de carbone à module intermédiaire (IM) dans une matrice bismaléimide (BMI).

Les viseries utilisées sont montrées en planche 3.

On compare le cas de base de la vis fraisée avec les fixations à interférence HUCK TITE. Ces fixations utilisent une bague lubrifiée pour éviter de délaminer le composite lors du montage.

Des essais sont aussi faits avec des rivets MLGPL à tête fraisée, similaires au HUCK TITE mais montés à jeu et sans bague.

Ces résultats seront aussi comparés des résultats d'essais statiques faits il y a quelques années sur des éprouvettes en T300-914 et utilisant des vis à tête hexagonale montées soit à jeu, soit à interférence avec bague.

**3 - ESSAIS AVEC INTERFERENCE DANS LES COMPOSITES : CAS DES TROUS NON CHARGES**

L'éprouvette utilisée est une éprouvette standard 23 plus du standard AMD-BA montrée planche 4.

La planche 5 montre l'éprouvette utilisée lors d'essais antérieurs en T300-914.

La planche 6 montre les résultats d'essais en traction et compression sur éprouvettes neuves. On constate que, contrairement aux espérances, l'interférence n'apporte rien, et même est légèrement défavorable à la résistance en traction ceci aussi bien sur IMI-BMI que sur T300-914.

L'influence de l'interférence sur la tenue en fatigue a aussi été étudiée :

Le cycle de fatigue appliqué est un cycle vol par vol standard "MIRAGE 2000" modifié par le rajout de 1 pic à 10 g tous les 600 vols.

La charge de référence 1 g est prise égale à la charge de rupture statique de l'éprouvette du type considéré divisée par 12 (en traction pour les éprouvettes fatigue-traction, en compression pour les éprouvettes fatigue-compression). 25000 vols sont appliqués, ce qui fait que ce chargement en fatigue est très sévère tant au niveau de contraintes qu'en nombre de vols.

Aucune éprouvette n'ayant été rompue lors de ces essais de fatigue, elles ont été cassées en statique résiduel, dans trois cas de chargement : résiduel en traction sur éprouvette fatigue en traction, résiduel en compression sur éprouvette fatigue en traction (pour mettre en évidence une éventuelle influence de délaminage) et résiduel en compression sur éprouvette fatigue en compression.

Les résultats de ces essais sont montrés planche 7, en comparaison avec les éprouvettes non fatiguées.

On constate que malgré la sévérité du chargement de fatigue appliqué, la fatigue n'a que très peu d'influence et peut même dans certains cas améliorer légèrement la résistance résiduelle.

#### 4 - ESSAIS AVEC INTERFERENCE DANS LES COMPOSITES : CAS DES ENTURES

Les essais ont porté sur des entures du standard AMD-BA (voir planche 8) adaptées aux matériaux composites IMI-BMI.

Les essais ont été faits avec vis à jeu, rivets HUCK TITE montés avec deux niveaux d'interférence et rivets MLGPL montés à jeu.

La planche 9 montre les résultats de tenue statique en traction sur éprouvettes neuves (ni vieilles, ni fatiguées).

On constate que les éprouvettes HUCK TITE tiennent nettement mieux que les éprouvettes avec vis (le mode de rupture étant le montage, avec déversement et rupture de la vis).

Mais cet écart n'est pas dû à l'interférence. En effet les éprouvettes équipées de rivets MLGPL (semblables aux rivets HUCK-TITE mais montées à jeu sans bague) tiennent encore mieux.

Cette constatation est recoupée par des résultats d'essais plus anciens sur entures en T300-914 à vis hexagonales (voir planche 10) qui montrent qu'à iso-fixation, l'interférence ne joue pratiquement pas.

La planche 11 montre les résultats en compression.

On constate là aussi que l'interférence n'a pas d'influence sur la tenue statique.

La planche 12 montre l'influence de la fatigue.

Les cycles de fatigue appliqués sont définis de la même façon que pour les éprouvettes monotrou de la planche 7.

On constate que le cycle de fatigue appliqué qui est pourtant très sévère n'a aucune influence défavorable sur la tenue statique résiduelle et souvent même l'améliore, dans certains cas de 10 %.

#### 5 - INTERPRETATION ET CONCLUSIONS

Contrairement à ce que l'étude du champ de contrainte élastique en bord de trou peut laisser penser, le montage à interférence de fixations dans des assemblages composite-composite n'apporte aucun bénéfice significatif en tenue statique, que ce soit sur pièce neuve ou sur pièce fatiguée.

Ce résultat est décevant (encore qu'il reconferme la remarquable tenue en fatigue des matériaux composite carbone). Il peut cependant s'interpréter si l'on considère le mécanisme particulier de la rupture au bord d'un trou en traction.

Une étude effectuée par AMD-BA (référence (2)) a porté sur l'identification des dommages et délaminages en bord d'un trou à un niveau de chargement très près de la rupture statique, dans différents cas de drapage.

La planche 13 présente dans un cas particulier une schématisation de la nature et de l'étendue des délaminages en bordure de trou. On constate, autour des plis à 0° la présence simultanée de délaminages interlaminaires entre plis à 0° et plis d'autres directions et de délaminages translaminaires dans les plis à 0°.

L'ensemble de ces délaminages a pour effet pratique de décharger partiellement les fibres à 0° tangentielles au trou.

Ceci est démontré par la planche 12, qui présente les calculs par éléments finis faits à partir de la planche 11 (avec différents degrés de simplification).

On constate que la fibre à 0° est déchargée de façon notable par les délaminages, et ce calcul recoupe de façon très correcte la valeur expérimentale de la rupture.

Compte tenu de ce mécanisme d'adaptation, on peut penser que l'effet du montage à interférence est en fait masqué par le mécanisme d'adaptation à rupture.

En compression, on peut penser que de toutes façons une partie importante de la charge passe en appui sur la fixation, qu'elle soit montée à jeu ou non, et que l'interférence a peu de rôle.

Il en résulte que le montage à interférence n'a pas d'intérêt dans le cas de liaison carbone-carbone. Par contre, il reste probablement intéressant dans le cas de liaison carbone-dural chargée en fatigue, du fait de son effet bénéfique sur la tenue en fatigue de la partie dural.

#### REFERENCES

- (1) Interference fit and crack growth prediction by D. CHAUMETTE, R. CAZES and C. CZINCZENHEIM - AMD-BA 12 th ICAF SYMPOSIUM - Toulouse - May 25-27 1983.
- (2) Calcul des délaminages dans les composites - D. GUEDRA - V. POGGI - AMD-BA - Actes du Troisième Colloque Tendances Actuelles en calcul de structures - Bastia - 6-8 Nov. 1985.

### COMPOSITE MATERIAL IN AMD-BA AIRCRAFT FROM "MIRAGE III" "RAFALE" TO "HERMES"

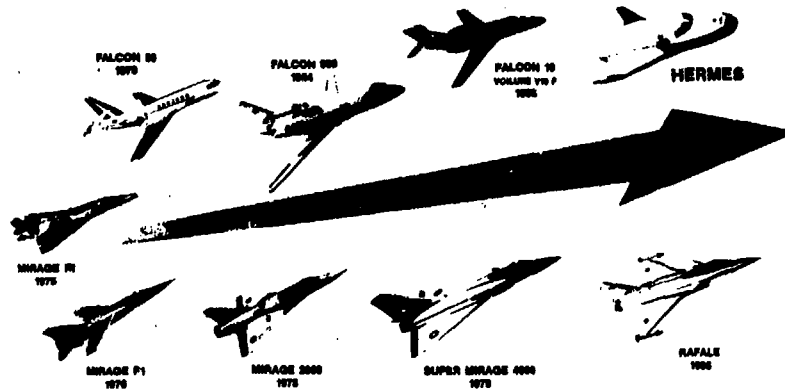


Planche 1 - Programmes de structures composites aux AMD-BA.

#### EFFECT OF INTERFERENCE

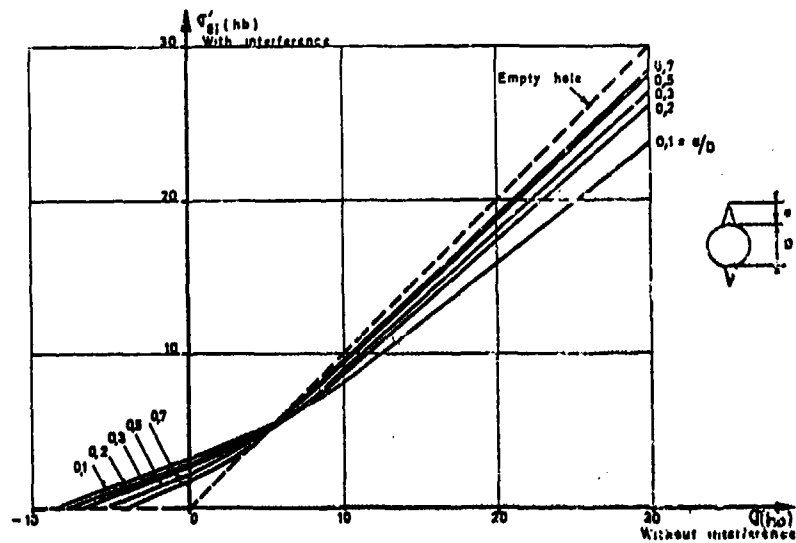


Planche 2 - Effet de l'interférence sur les contraintes en bout de craque d'un trou criqué.

**FIXATIONS UTILISEES**

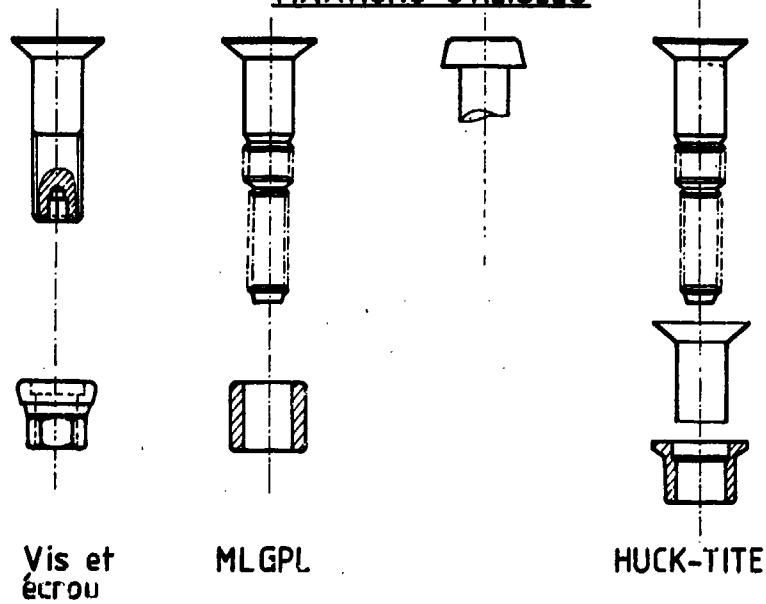


Planche 2 - Type de vis utilisées dans l'étude.

**COMPRESSION SUR DRAPE TROUE  
(# 6 TF HABITE)**

Eprouvette type : **S. 22**  
 Nappage : 28 plis - 12.6.6.4

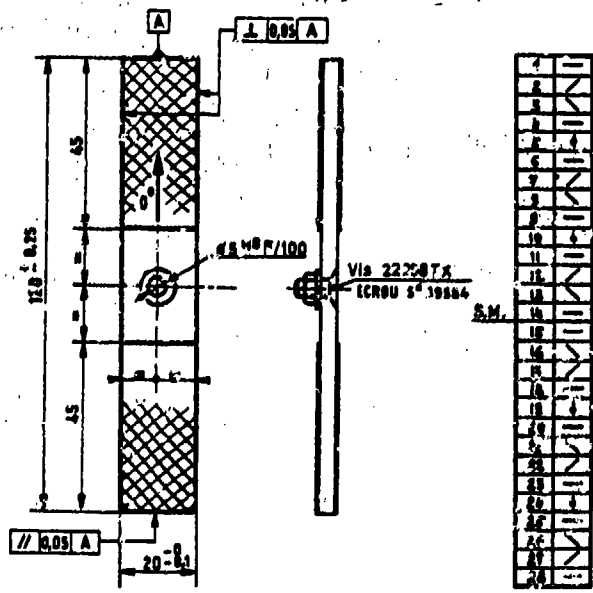
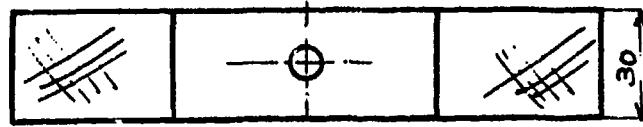


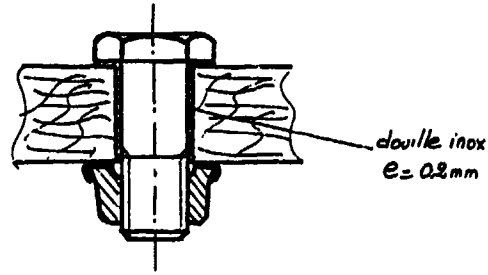
Planche 4 - Eprouvette de trou non chargé 28 plis.

18-6



Vis  $\phi$  6 mm tête H.

$e = 6 \text{ mm}$ .



*douille inox*  
 $e = 0.2 \text{ mm}$

Planche 5 - Eprouvette et fixation utilisées pour des essais antérieurs en T300-914.

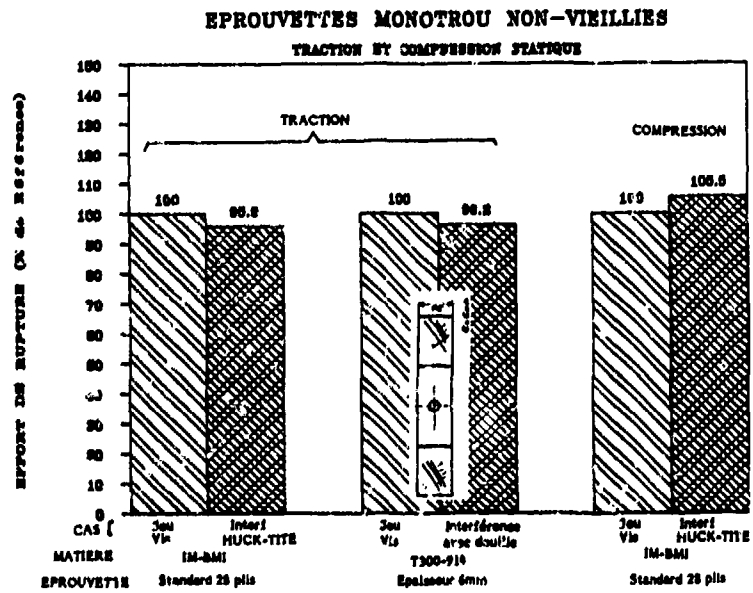


Planche 6 - Résultats d'essais de traction et compression (sans fatigue).



**ENTURES EN TRACTION STATIQUE**

IM-BMI NON-VIEILLI MAPAGE 18-8-0-4

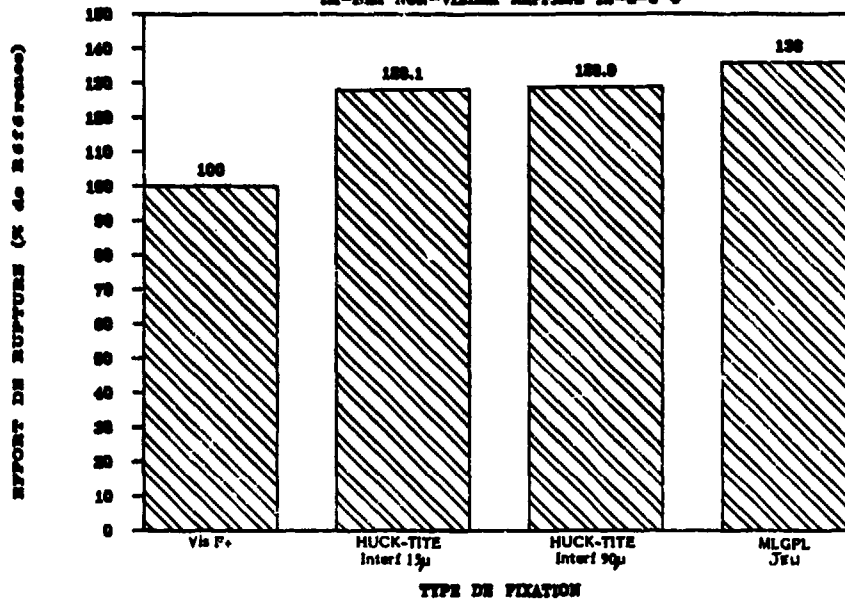
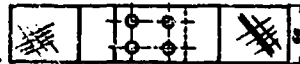


Planche 9 - Essais en traction sur entures IM-BMI.

**ENTURES EN TRACTION**

MATERIAU T300-914



Ø = 51 mm - 700 N

2-4,0

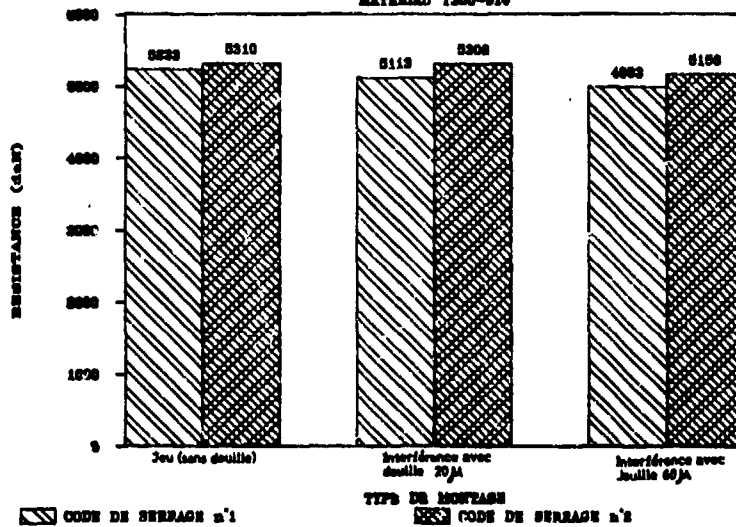


Planche 10 - Essais en traction sur entures T300-914.

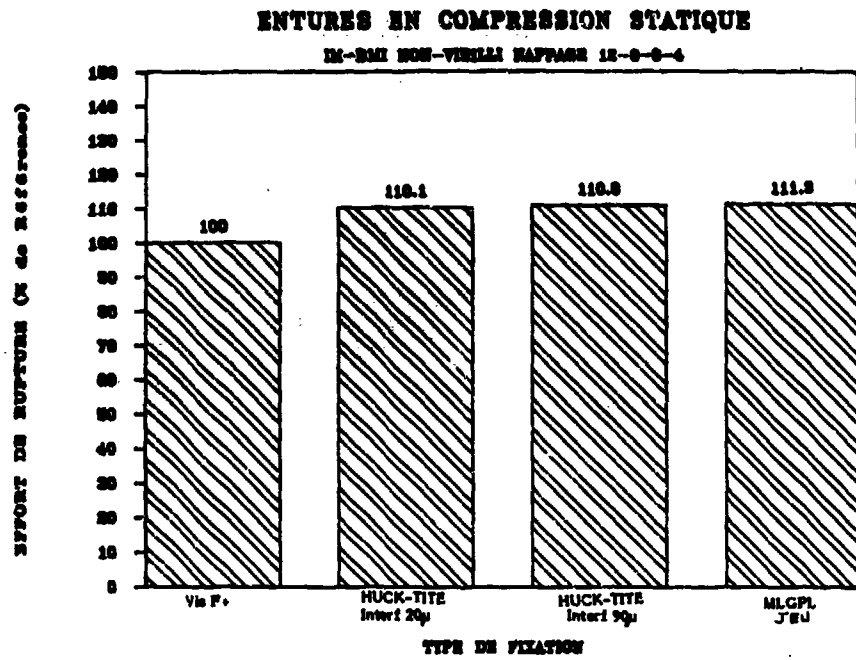


Planche 11 - Essais en compression sur entures IM-BMI.

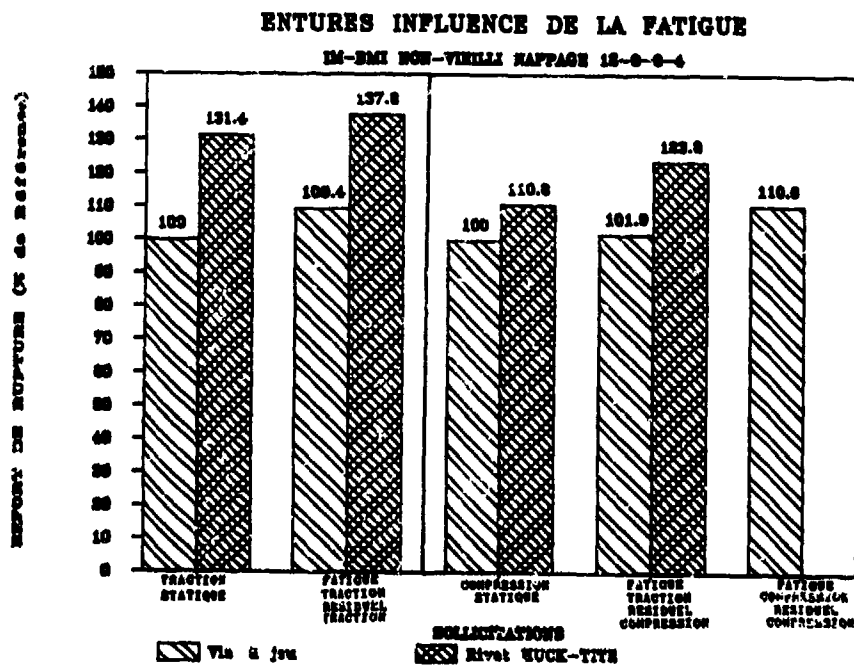


Planche 12 - Influence de la fatigue sur entures IM-BMI.

**DELAMINAGE EN BORDURE DE TROU**  
(Eprouvette type B)

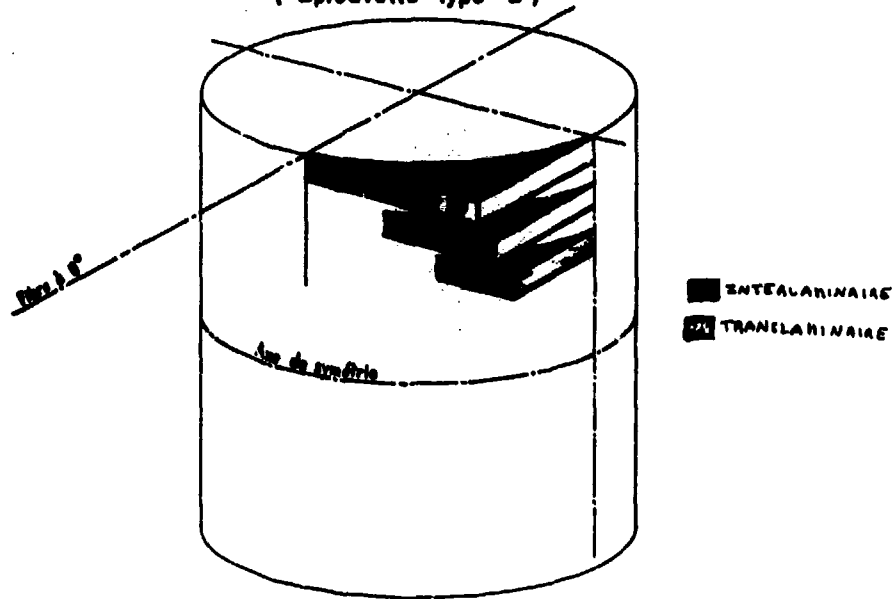


Planche 13 - Schématisation des délaminages au bord d'un trou en traction.

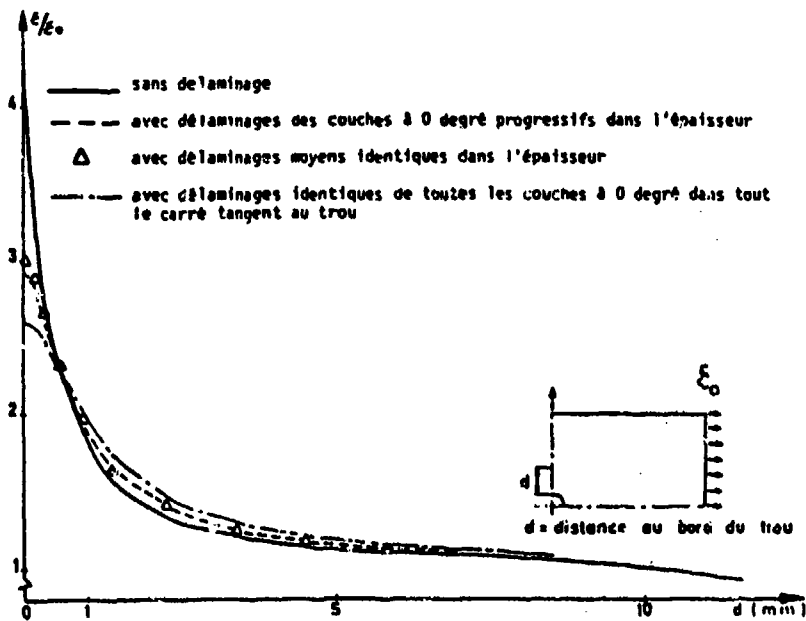


Planche 14 - Surcontraintes dans la fibre à 0° au bord d'un trou en traction.

**Effect of Environment and Improvement Measures on  
Static and Fatigue Strength of Bolted CFRP-Joints**

by  
J. J. Gerharz and H. Muth  
Fraunhofer-Institut für Betriebsfestigkeit (LBF)  
Bartlingstr. 47  
6100 Darmstadt  
Germany (FRG)

**Summary**

This paper documents effects of environment, preloading, bushings, local reinforcements and joint laminate tailoring on the efficiency of CFRP-joints. Thereby joint efficiency at static, residual and fatigue strength is considered. The laminate lay-up, the fastener system, fastener fit and clamping stresses were not changed. The material used was 914C/T300 or Fiberite 974/T300. Critical hot/wet condition expected in service reduced joint efficiency but preloading on fatigue design load level with superimposed temperature cycle per flight did not. Installation of metal bushings into fastener holes, local reinforcement by adding layers to the hole section, and joint laminate tailoring through strip design were introduced to reveal their ability to improve composite joint efficiency. They proved to be successful depending on design constraints and required joint performance.

**Introduction**

As in metal structures mechanically fastened joints are critical elements in composite structures too. From numerous experimental and theoretical investigations / 1; 2; 3; 4 / optimal geometry parameters (a/d; d/w; d/t) and laminate lay-up structure have evolved. However, joint strength still remained low compared to the strength of the basic laminate. This is represented by the so called Joint Efficiency (JE) which is the ratio of gross section joint strength to laminate strength away from the hole. This paper considers JE as a function of cycles to failure, where the JE at N = 1 is the ratio of static strength data. The effects of fatigue loading with and without superimposed environmental conditions and of methods to increase JE are presented. These improvement measures include

- bushings installed in fastener holes,
- local reinforcements by adding layers to the basic laminate in the hole area, and
- joint laminate tailoring by dividing the laminate in to soft and stiff strips running parallel to the local direction.

The laminate used contained 47 percent 0°, 47 percent ± 45° and 6 percent 90° layers.

The investigation of joint tailoring began with stress analysis by a finite element method to provide a nearly optimal strip geometry for the specimens. The analytical and experimental results are documented.

**Joint Efficiency as a Function of Cycles to Failure**

The SN-curves in Fig. 1 and Fig. 2 show typical results of laminate and joint fatigue testing respectively / 5 /. Corresponding to definition of joint efficiency (JE):

$$JE = \left( \frac{\text{Strength of Joint}}{\text{Strength of Basic Laminate}} \right)_N = \left( \frac{S_J}{S_{\text{plain}}} \right)_N$$

the "joint efficiency curve" in Fig. 3 was derived, representing the fatigue strength ratios which may also be expressed as 1/K<sub>f</sub>. A comparable JE-curve for metal joints is added to illustrate the most important difference in static strength at N = 1, where composite joints exhibit the lowest and metal joints the largest JE. With increasing number of cycles to failure the JE of metal joints typically decreases. The increasing JE of the composite joint seems to be specific for this joint configuration. JE-curves for 100 percent load transfer composite joints for example show a nearly constant JE / 6 /.

**The Influence of Environment on Joint Efficiency**

For two conventional carbon/epoxy systems the effect of environment and flight-by-flight loading on JE was investigated / 7 /. Both the environmental and fatigue loading conditions corresponded to design criteria for composite structure in a fighter aircraft. Fig. 4 shows the JE's at N = 1 for the loading conditions:

- RT; "as received",
- + 120° C; equilibrium moisture content corresponding to 85 percent relative humidity (hot/wet) and
- hot/wet after preloading.

The preloading was four times (16000 flights) with FALSTAFF loading sequence and superimposed temperature cycles per flight.

Note that tensile loading is critical; it leads generally to lower joint efficiencies than compressive loading. There is a significant drop in joint efficiency due to the hot/wet condition but no further reduction due to the additional preloading; instead it seems that preloading at fatigue design load level was beneficial. This correlates to with often observed increase of residual strength after preloading of notched composite laminate specimens, see for example / 8 /.

#### The Effect of Bushings on Joint Efficiency of CFRP-Joints

Installation of bushings in fastener holes was originally introduced as a repair measure and as a cost saving alternative to close tolerance holes / 9 /. Cylindrical and tapered bushing are shown on Fig. 5 were bonded (EA-934, Hysol) into the hole. Besides bonding, cylindrical bushings were cold worked to receive an interference fit of the bushing in the hole. The installed bushing had been expanded by pushing a tapered mandrel through the bushing. The expansion was such that the low alloy steel bushing received a tight fit in the CFRP laminate and there was just enough clearance to install the fastener by hand.

Fatigue testing of CFRP-joints with and without bushing led to the joint efficiency data shown in Fig. 5. The results revealed that bushings had increased JE of 100 percent load transfer joints (pure bearing) at  $N = 10^5$  and  $N = 10^6$  and the beneficial effect was enlarged with tighter fitting bushings. Joints with by-pass loading showed equal or somewhat less joint efficiency when bushings are installed. It should be noted that bolt diameters were kept constant and therefore holes in joints with bushings were larger corresponding to the wall thickness of the bushings which were .75 to 1.15 mm. It appears that bushings tightly installed in fastener holes have the ability to improve the JE of 100 percent load transfer joints permanently.

#### The Effect of Local Reinforcement on the Joint Efficiency of CFRP-Joints

Local reinforcement in the area of high stress concentration is a conventional method to improve performance of the overall structure. It can also be practiced with composite structures by adding layers in the critical region. The reinforcing layers are either cured with the laminate curing process or bonded to the cured laminate. With respect to geometry the additional layers are either placed symmetrically on both sides or just on one side of the laminate, see Fig. 6.

Fatigue and static testing of composite joints with and without local reinforcements / 6 / revealed the JE improvements shown in Fig. 6. The upper part of the figure shows the improvement by additional  $\pm 45^\circ$  and  $0^\circ$ -layers increasing the critical section by a factor of 1.5. At  $N = 1$  the improvement factor is close to reinforcement factor; however, at  $N = 10^6$  the local reinforcement had become less effective as the improvement factors had dropped to 1.2. This correlates with the shape of the SN-curves in Fig. 7 showing larger slopes with reinforced joints. Thus it appears that the beneficial effect of local reinforcement diminishes with increasing number of cycles to failure. But the improvement remaining at  $N = 10^6$  is stress-wise and life-wise still larger than that reached by bushings. From the literature even larger improvements are known when the critical section is more rigorously enlarged as for example by a factor of 4.0. This led to an improvement factor of 2.5 at  $N = 1$  as illustrated in the lower part of Fig. 6. Here all reinforcing layers were added on one side of the quasi-isotropic laminate. This may have contributed to the failure mechanism through detachment of the reinforcement with subsequent secondary net section fracture. It is assumed that symmetrical reinforcement would increase the improvement efficiency; however it should also be remembered that in the quasi-isotropic laminate stress concentration is less than in the more anisotropic laminate / 2 / applied so far. Generally improvements are more easily reached with details of high stress concentration than with details of lower stress concentration.

#### The Effect of Joint Laminate Tailoring

Local reinforcement is not always practicable because of design constraints with respect to available space or aerodynamic requirements. Fortunately, designing composite laminates allows tailoring along the width of the joint resulting in a so called "strip laminate" which is schematically illustrated in Fig. 8. In essence the  $0^\circ$ -layers of the basic laminate were transferred outside the hole area, where they took the place of  $\pm 45^\circ$ -layers which were concentrated in the hole area. Between the stiff strips containing the  $0^\circ$ -layers and the soft strip with the loaded holes, strips of basic laminate were introduced. The widths of the strips were such, that basic and strip laminate had the same compliance (strain/load) and thickness. This measure aims at an improvement through reduction of stress concentration. To prove this and to establish an optimal strip design for the specimens a stress analysis, applying an experimentally verified FE-method was conducted first. Fig. 9 shows the FE-model at the critical hole; load was introduced through the central nodal point of the bolt mesh. Load distribution was calculated through simulation of outer joint parts by a simple rod element. Special contact elements were placed between adjacent nodal points across the bolt-laminate interface. These contact elements could only transfer radial compressive loads; thereby a frictionless interface was produced and developing gap between bolt and hole surface determined.

Fig. 10 and 11 show results of such a FE-stress analysis in form of stress contour lines around the critical hole in the basic laminate and the strip laminate with optimal strip widths. The strip design is easily recognized by the pattern of the stress contour lines displaying that the strips pick up loads corresponding to their stiffnesses.

Through the strip design the maximum stress in the joint was reduced by a factor of 1.8. Taking into account the difference in joint width the stress concentration factor was reduced from  $K_t = 3.0$  to  $K_t = 2.0$ . It was found that load was more uniformly distributed to the holes in the strip laminate but hole deformation was twice of that in the basic laminate as demonstrated by the difference in gap sizes shown in Fig. 10 and 11.

The results of the stress analysis and the originators of the joint laminate tailoring method / 11 / suggest that the efficiency of this improvement measure increases with the number of fastener rows. Therefore experimental investigation on the effect of optimal strip design on joint strength comprised double shear joints with two, three and four fasteners. Strength and ultimate load of basic and strip laminate joints were plotted in Figs. 12 and 13. The results confirmed increasing efficiency with increasing number of fasteners. The experimental results so far indicate that joint tailoring successfully increased the load transfer capacity of bolted composite joints as shown in Fig. 12. However, it did not exhibit much advantage when JE is to be improved, as shown by the data in Fig. 13.

Investigations should continue to disclose more details of the effects of joint laminate tailoring on the mechanical behaviour of composite joints.

#### Conclusions

Effect of expected environmental service conditions and of improvement measures on static and fatigue strength of composite joints was judged (whenever feasible), by changes of joint efficiency (JE).

- In contrast to metal joint behaviour JE of CFRP-joints was found to be low at static strength ( $N = 1$ ) and in the low life region.
- JE dropped at hot/wet service condition of fighter aircraft.
- Preloading on fatigue design load level with superimposed temperature cycle per flight did not cause a further drop of JE.
- Metal bushings with a tight fit improved JE of 100 percent load transfer joints in the high life region ( $N > 10^5$ ).
- Local reinforcement by adding  $0^\circ$ - and  $\pm 45^\circ$ -layers to the basic laminate in the hole region improved JE first of all at  $N = 1$  (static strength), at  $N = 10^5$  improvement was less but still larger than that reached with bushings.
- Joint laminate tailoring reduced stress concentration and improved load transfer capacity; the efficiency of this measure increases with number of fastener rows.

#### References

- / 1 / Collings, T. A.: On the Bearing Strengths of CFRP Laminates, Composites, Juli 1982, pp. 241 - 252
- / 2 / Crews, Jr., J. H.; Hong, C. S.; and Raju, I. S.: Stress Concentration Factors for Finite Orthotropic Laminates with a Pin-Loaded Hole, NASA Technical Paper 1842, May 1981
- / 3 / Godwin, E. W.; Matthews, F. L.: A Review of the Strength of Joints in Fibre-Reinforced Plastics, Part 1, Mechanically fastened Joints, Composites, July 1980, pp. 155 - 160
- / 4 / N. N.: Fastening and Joining, Mil-Mdbk - 17A, Jan. 1971
- / 5 / Schütz, D.; Gerharz, J. J. and Alschweig, E.: Fatigue Properties of Unnotched, Notched, and Jointed Specimens of a Graphite/Epoxy Composite, in: Fatigue of Fibrous Composite Materials, ASTM STP 723, American Society for Testing and Materials, 1981, pp. 31 - 47
- / 6 / Gerharz, J. J. and Schütz, D.: Fatigue Properties of Bolted Double Shear Composite Joints (in German), Forschungsbericht aus der Wehrtechnik, BMVg-FBWT 82-7, 1982
- / 7 / Berg, M. and Rott, D.: Investigation of the Effect of Environment on the Mechanical Behaviour of CFRP-Specimens Subjected to Combined Flight-by-Flight Loading and Flight-by-Flight Temperature Changes (in German), LBF Report No. 4845, March 1985
- / 8 / Huth, H.; Peter, O. and Schütz, D.: Damage Growth - and Residual Strength Testing with CFRP-Laminates (in German) Forschungsbericht aus der Wehrtechnik, BMVg-FBWT 82-5, 1982
- / 9 / Gerharz, J. J. and Schütz, D.: The Effect of Bushings on the Fatigue Properties of Composite Joints (in German), LBF-Report No. 4848, Febr. 1984
- / 10 / Gerharz, J. J.; Idelberger, H.; and Huth, H.: Measures to Improve Strength Behaviour of Composite Joints (in German), LBF Report No. 5938, to be released 1987
- / 11 / Eisenmann, J. R. and Leonhardt, J. L.: Improving Composite Bolted Joint Efficiency by Laminate Tailoring, in: Joining of Composite Materials, ASTM STP 749, K. T. Kedward, Ed., American Society for Testing and Materials, 1981, pp. 171 - 130

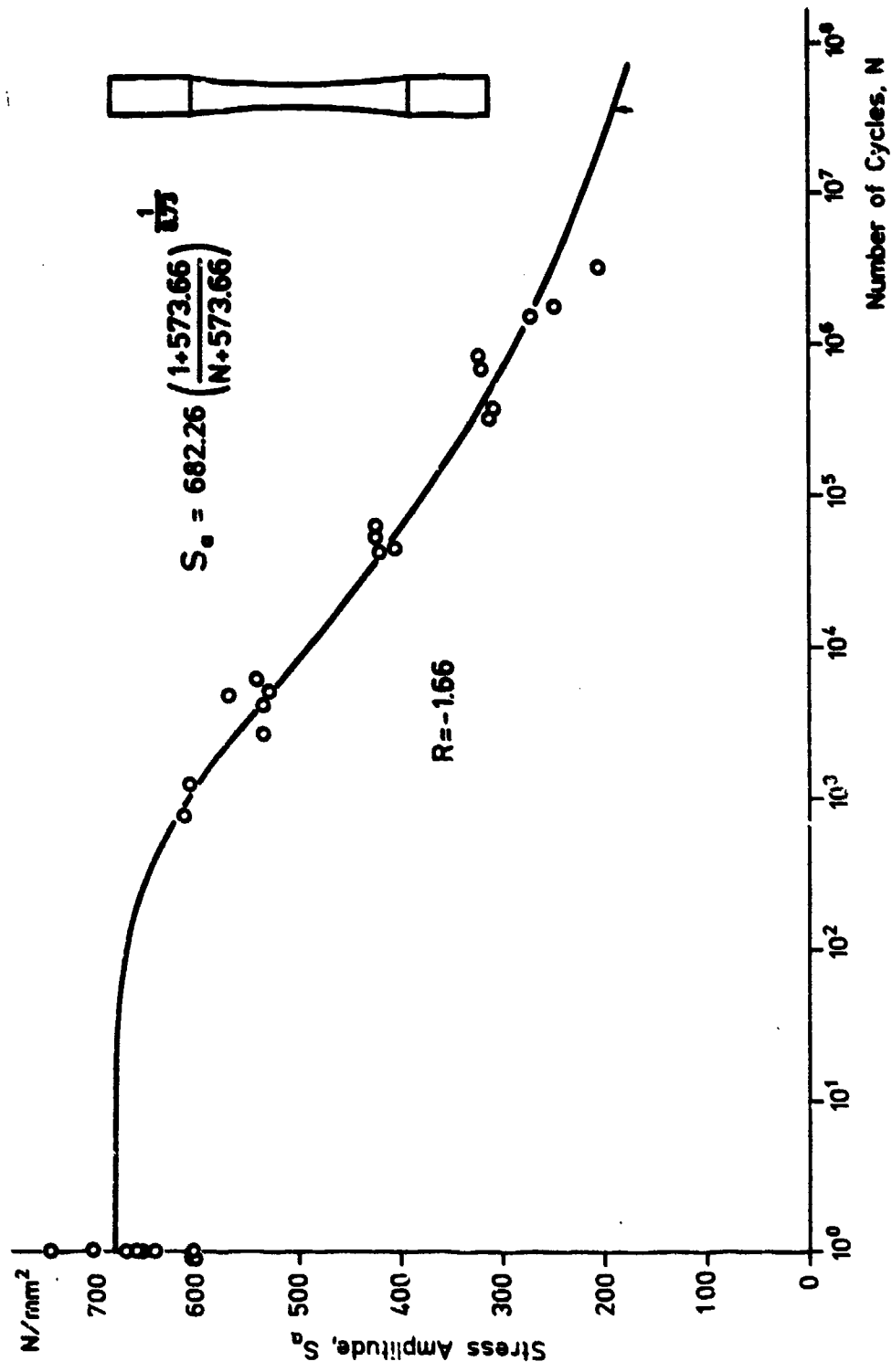


Fig. 1: SN-Curve of Unnotched Basic Laminate (Ciba 914C/T300)

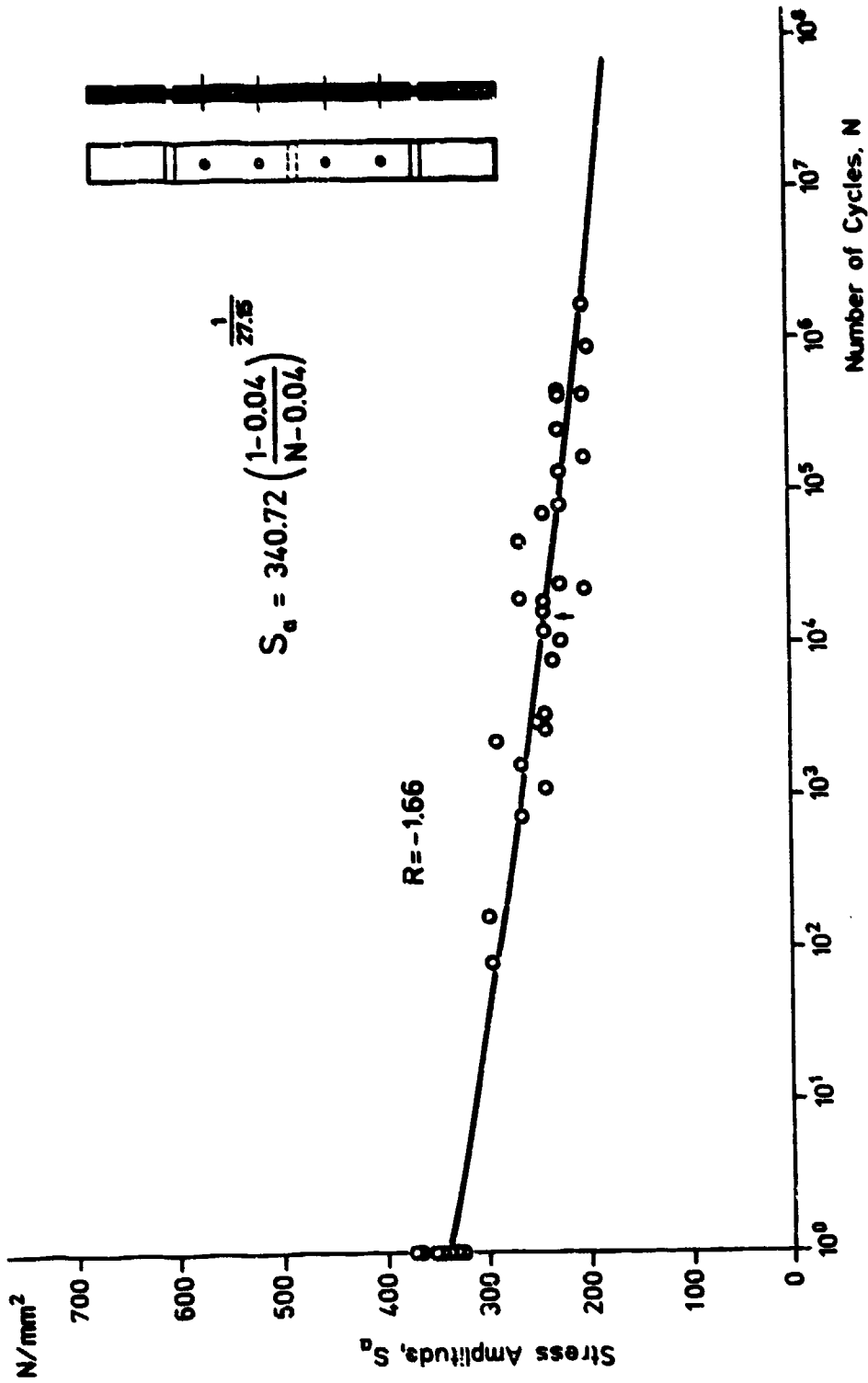


Fig. 2: SN-Curve of Composite/Composite Joint (50% Load Transfer)

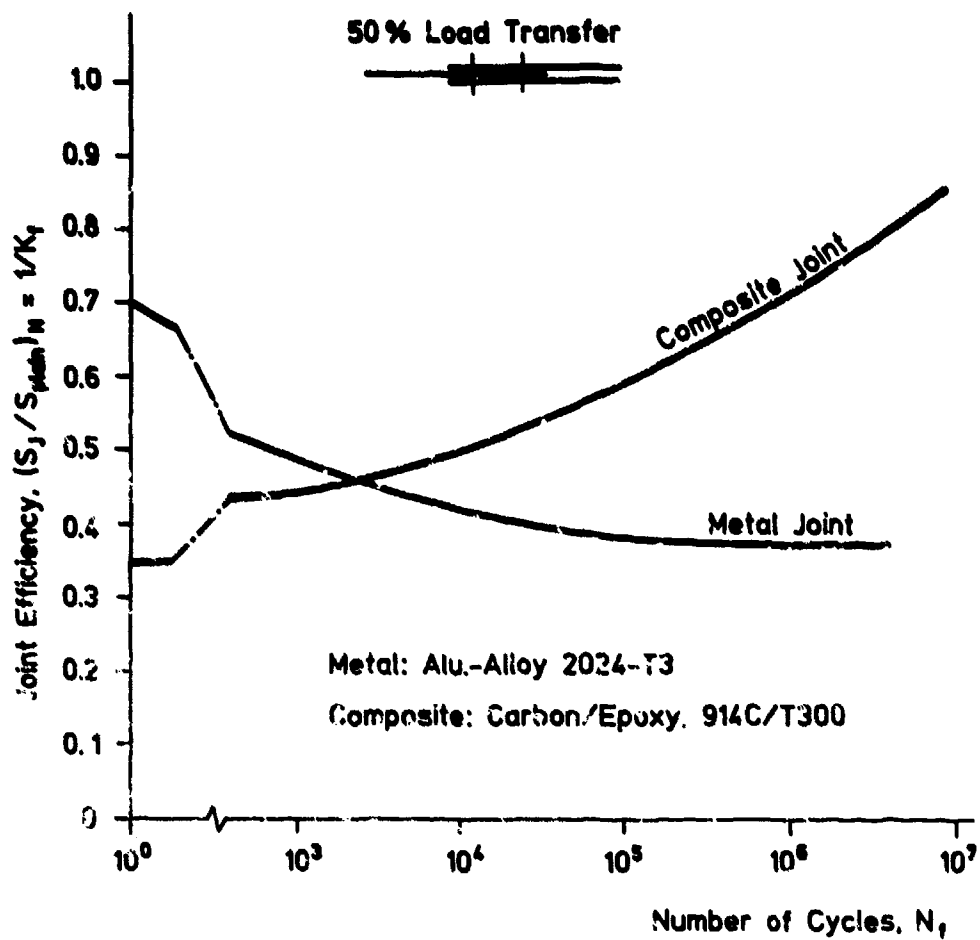
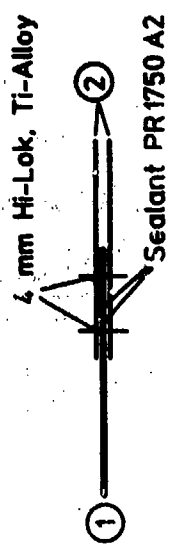


Fig. 3: Joint Efficiency at Cycles to Failure of Composite and Metal Joints



- ①  $[0_2/\pm 45]_2/90$
- ②  $[0_2/\pm 45/0_2/\pm 45/90]$

T = Tension  
 C = Compression  
 EM - Equilibrium Moisture  
 a four Lives FALSTAFF  
 + Temperature Cycle/Flight  
 Fatigue Design Load Level

	$S_{u, plmn, RT/AR}$
Ciba 914C/T300	800 N/mm <sup>2</sup>
Fiberite 1076/T300	785 N/mm <sup>2</sup>

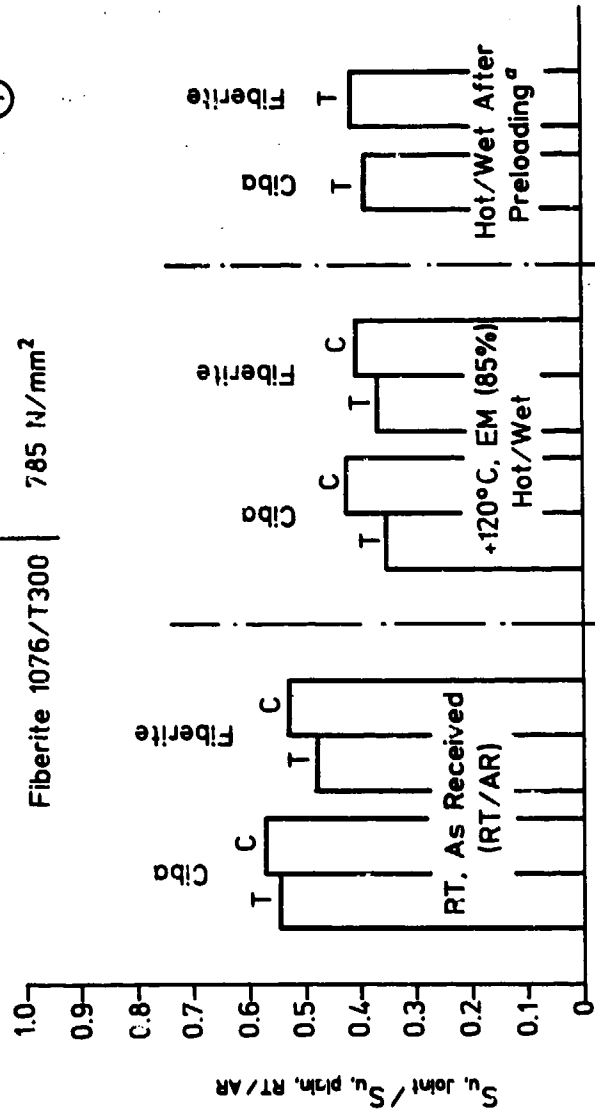


Fig. 4: Joint Efficiency at Hot/Wet Condition with and without Preloading

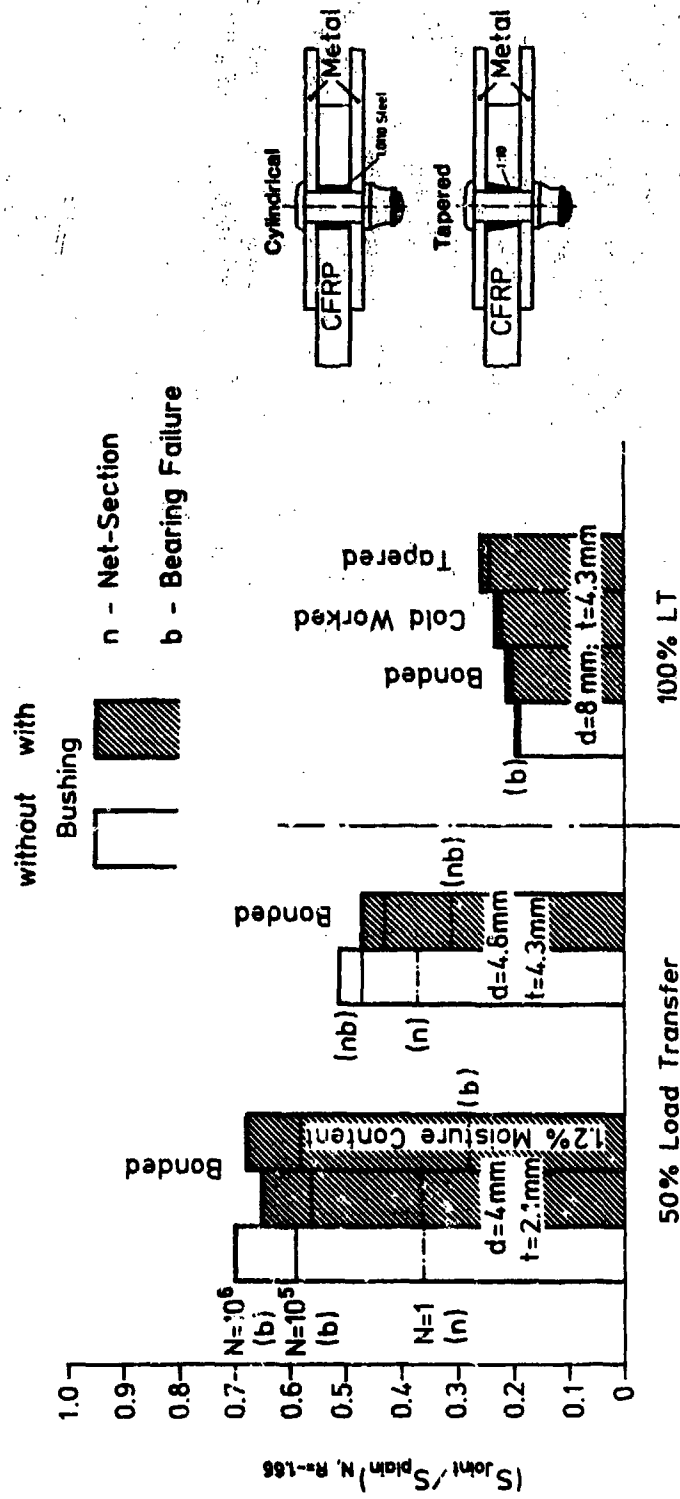
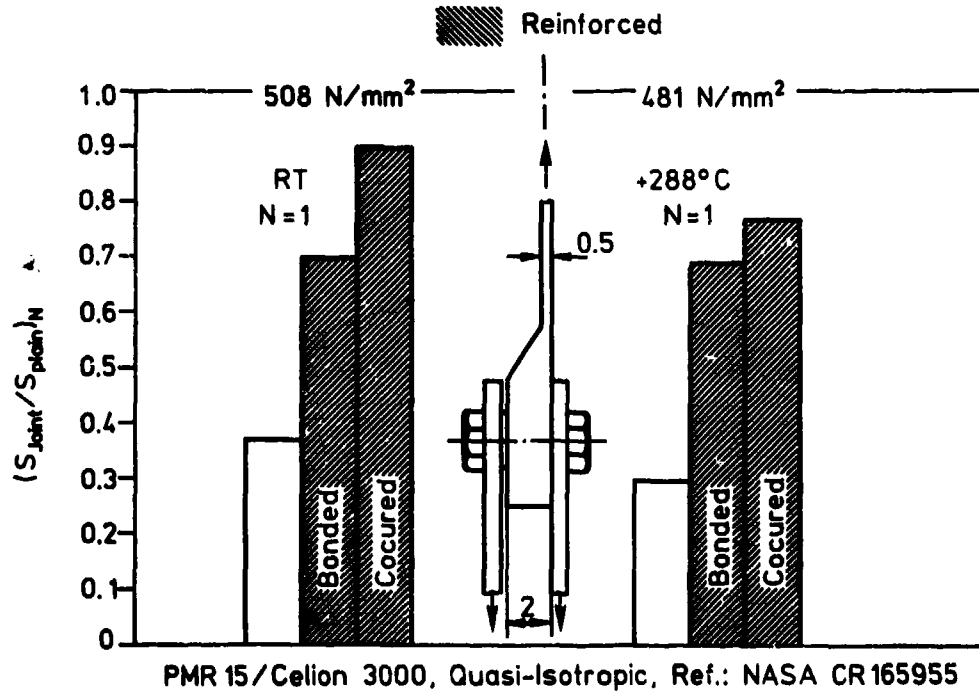
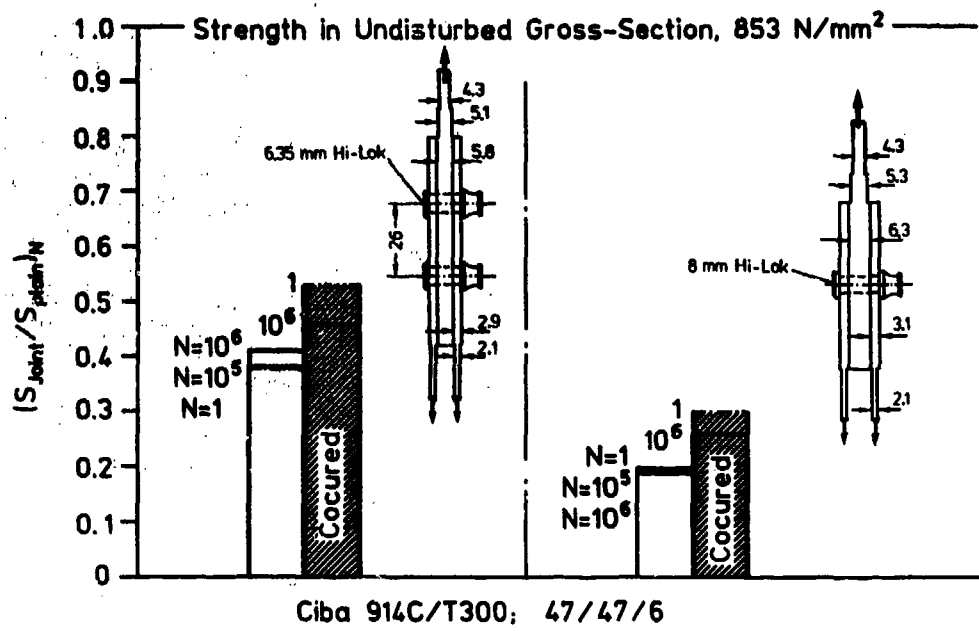


Fig. 5: Efficiency of Composite Joints without and with Bushing



**Fig. 6: Efficiency of Composite Joints with Local Reinforcement**

19-10

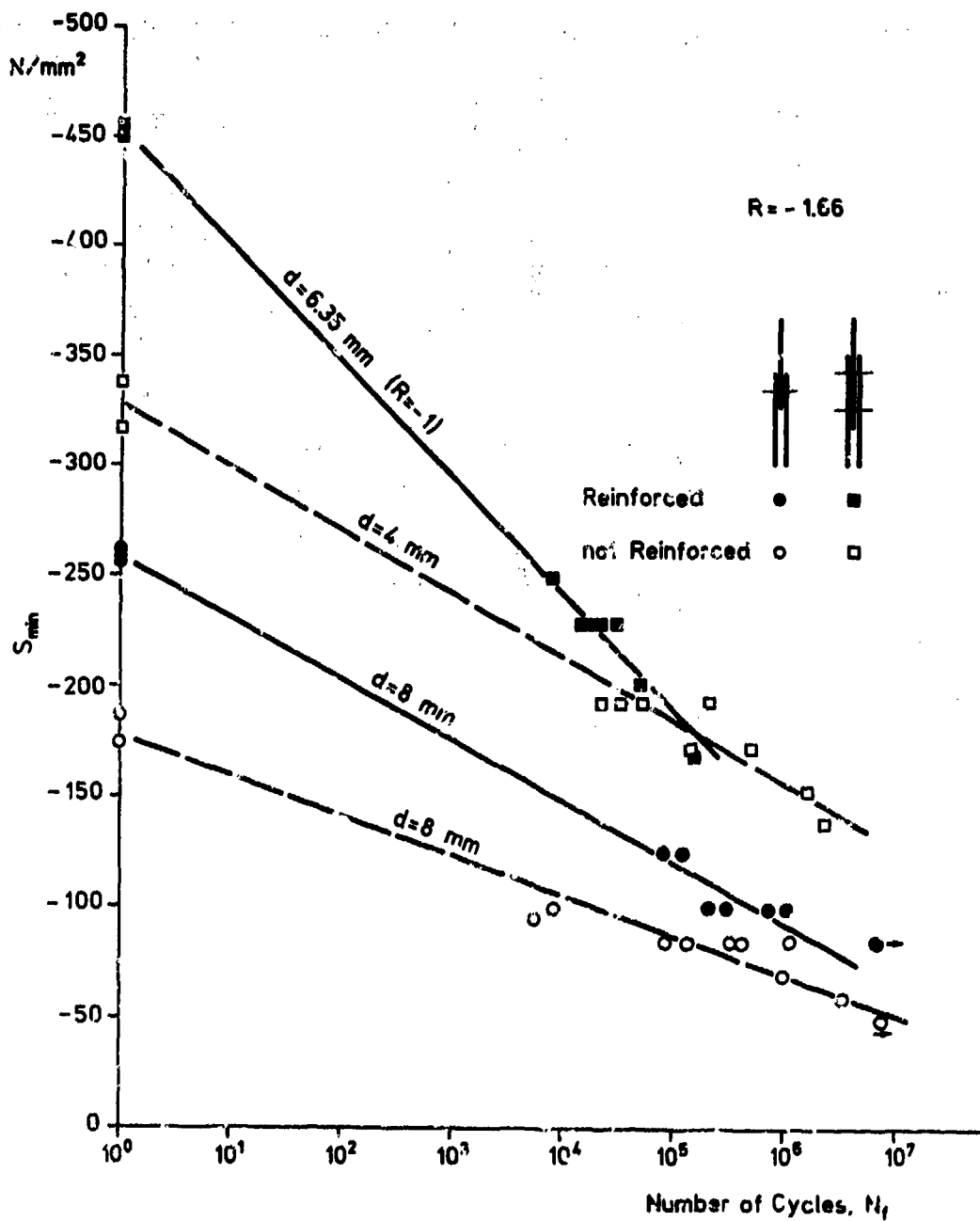
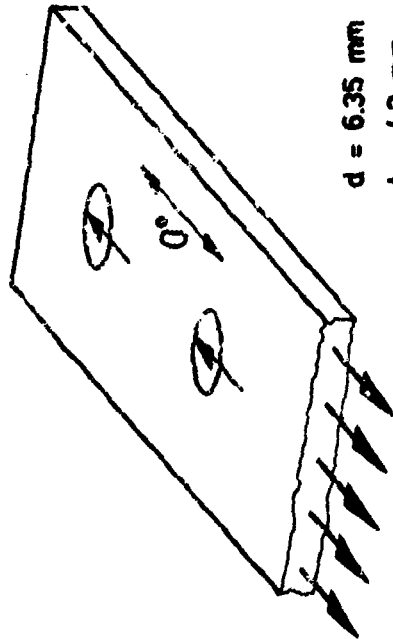


Fig. 7: S-N-Curves of Composite Joints with and without Reinforced Hole Areas

Basic Laminate



$d = 6.35 \text{ mm}$   
 $t = 4.3 \text{ mm}$

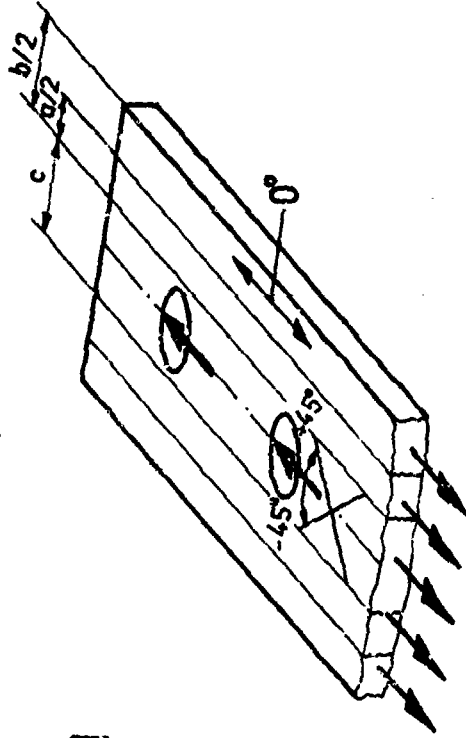
$[(0_2/\pm 45/0_2/\pm 45)_2]_s$   
 $w = 32 \text{ mm}$

Basic and Strip Laminate  
of Same Thickness and  
Compliance (Percent Strain/Load)

$k_t = 3.0$

$\sigma_{max,y} / \sigma_{gross}$

Strip Laminate



—  $\pm 45^\circ$  in the Central Strip (Loaded Hole Area) in Place of  $0^\circ$ -Layers of the Basic Laminate;  $c = 15 \text{ mm}$

—  $0^\circ$  in the Edge Strips in Place of the  $\pm 45^\circ$ -Layers of the Basic Laminate;  $b = 24 \text{ mm}$

— Basis Laminate Built-up in the Transition Area;  $a = 18 \text{ mm}$

$k_t = 2.0$

Fig. 8 : Composite Joint Tailoring to Improve Joint Performance

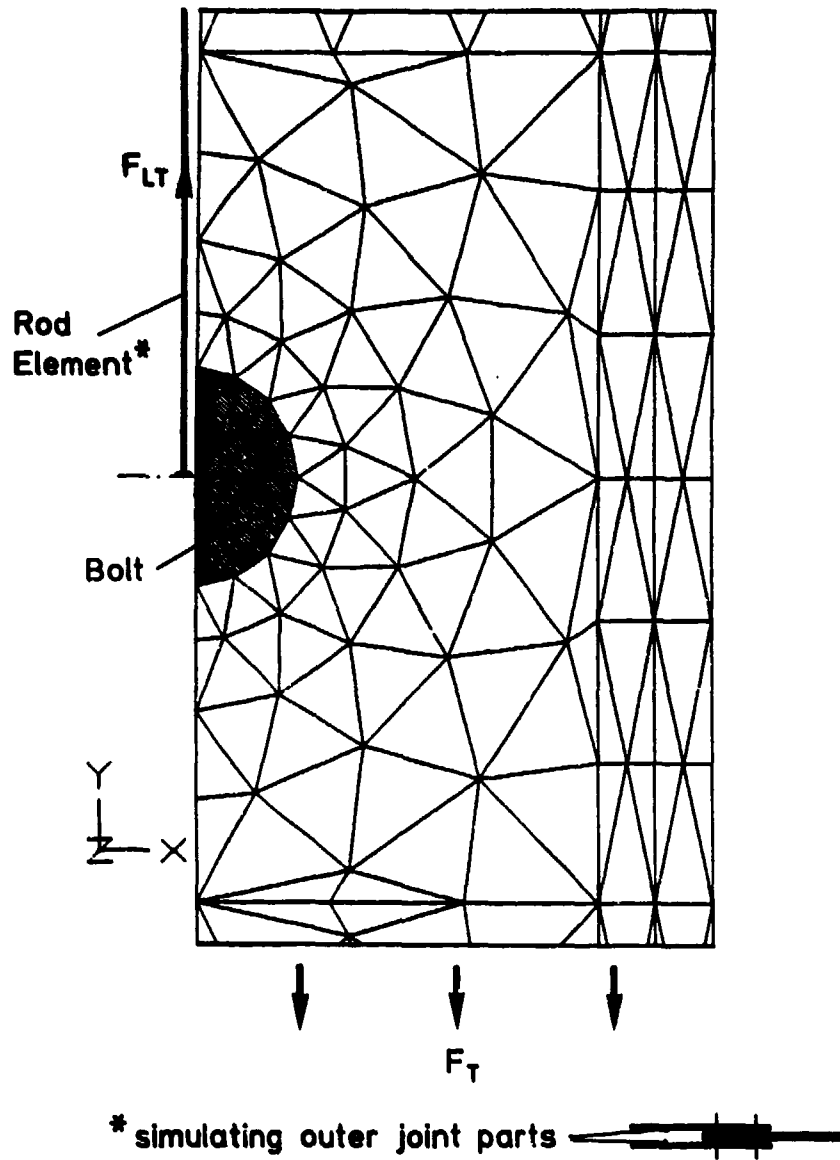


Fig. 9: Finite Element Model

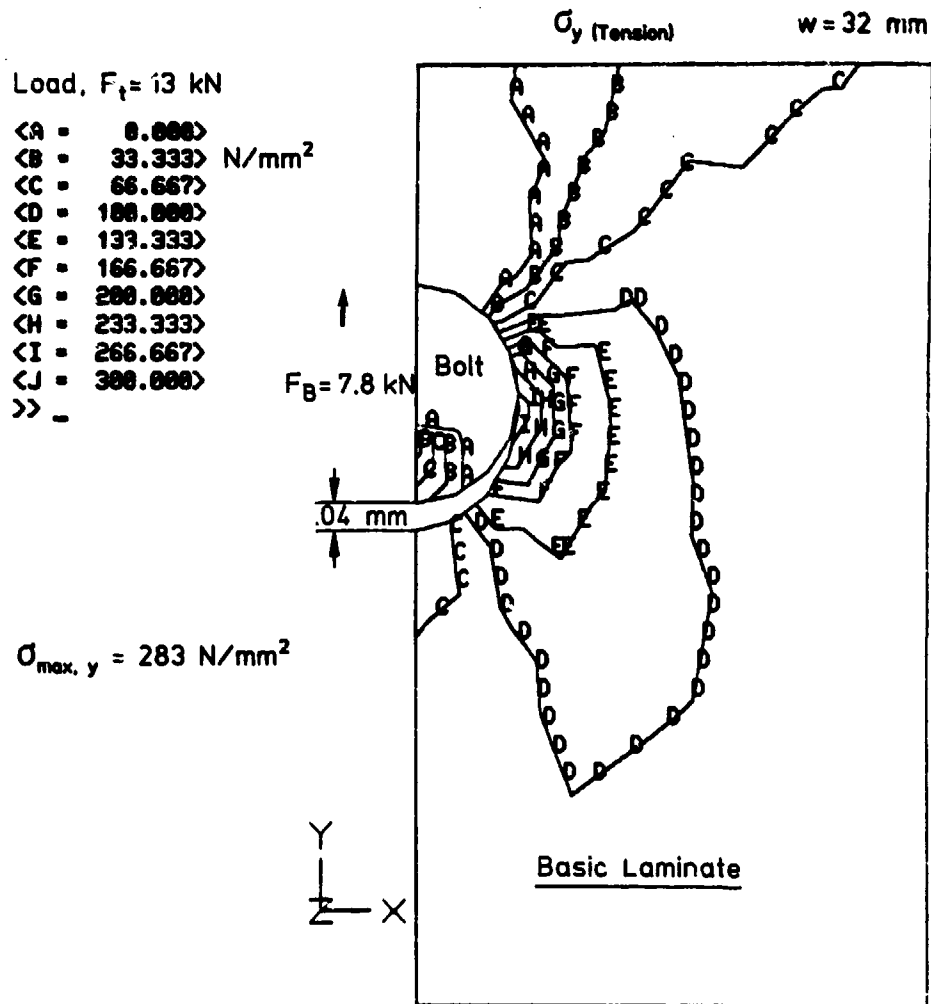


Fig. 10: Contour Lines of Stresses at Critical Hole

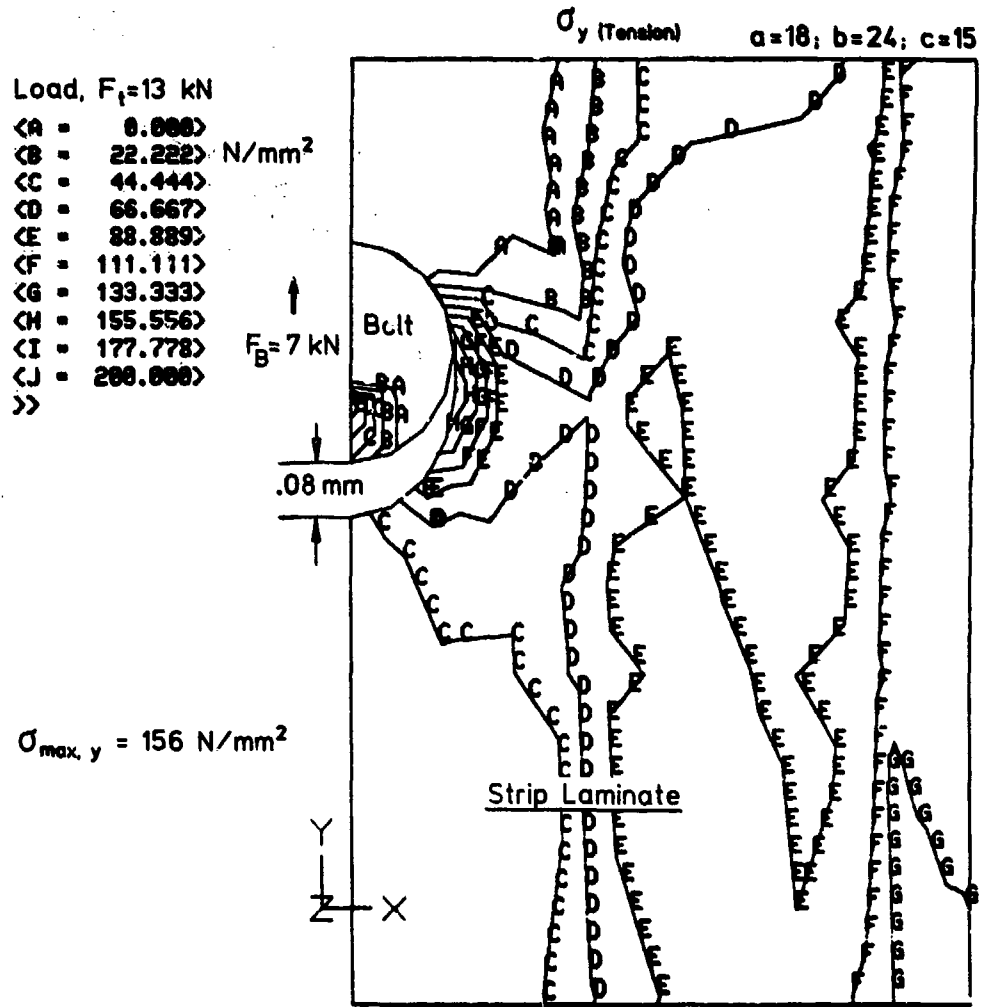


Fig. 11: Contour Lines of Stresses at Critical Hole

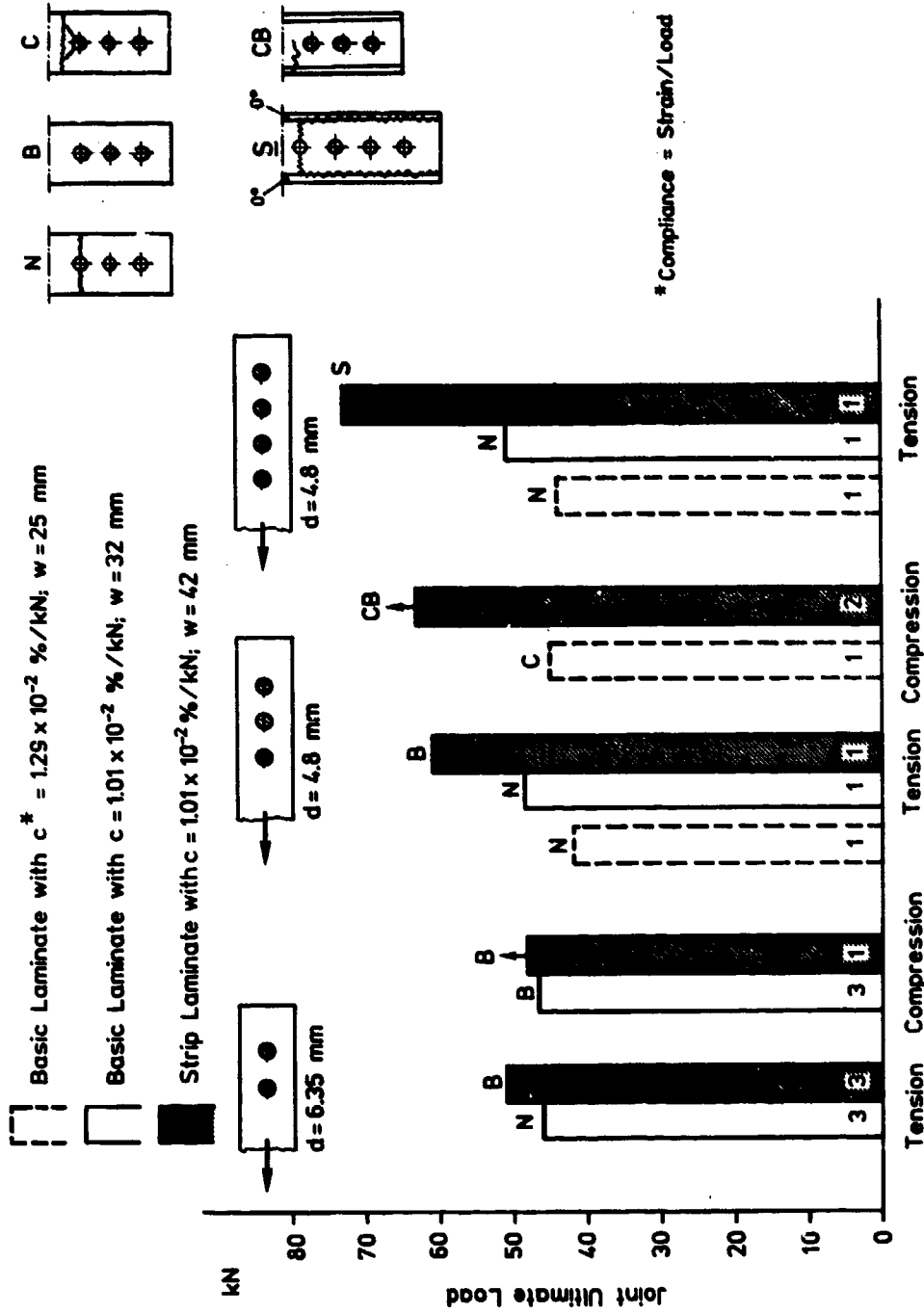


Fig. 12: Effect of Composite Joint Tailoring on Ultimate Load  
(Equal Compliance of Basic and Strip Laminate)

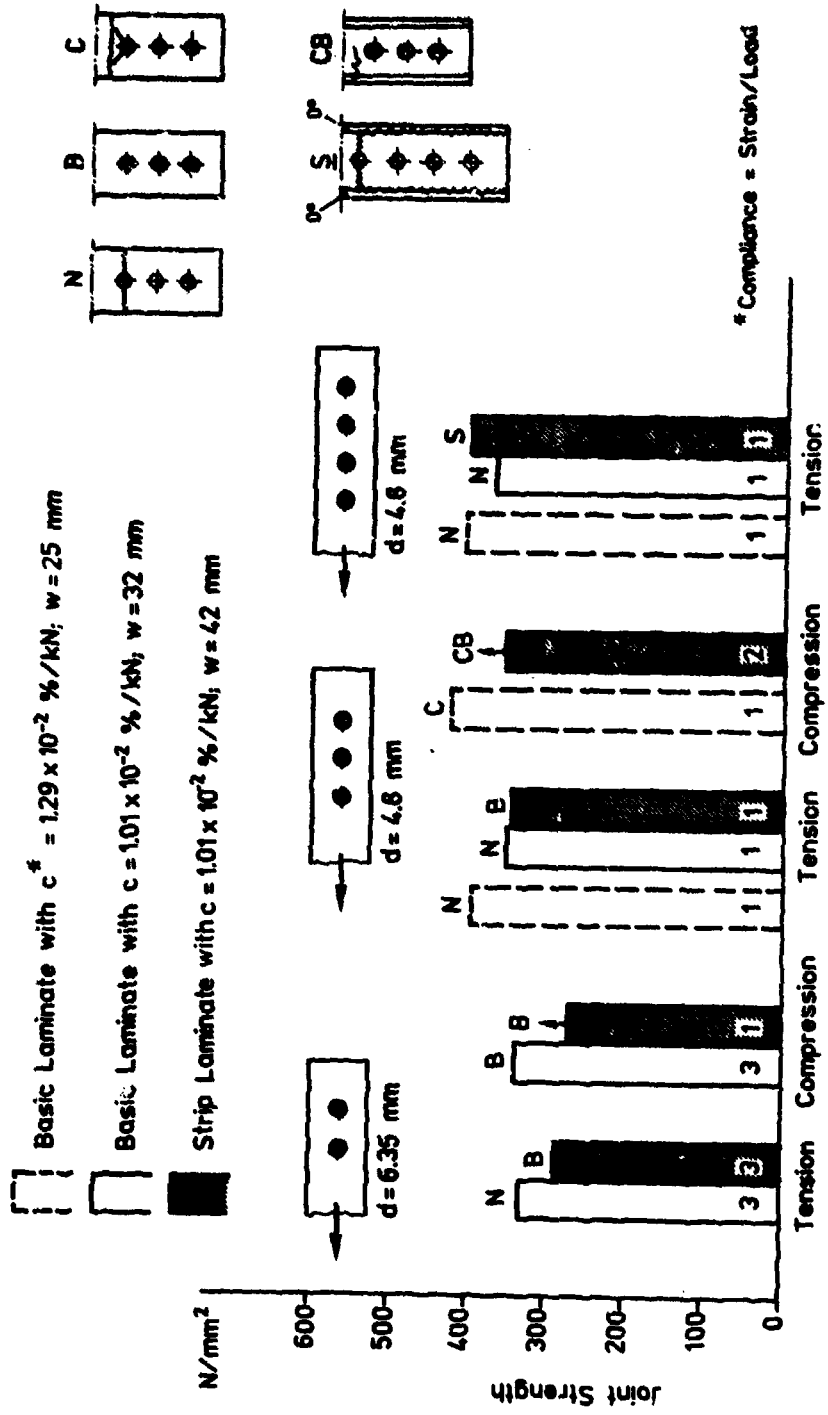


Fig. 13: Effect of Composite Joint Tailoring on Static Strength  
(Equal Compliance of Basic and Strip Laminate)

**STIFFNESS AND RESIDUAL STRENGTH VARIATIONS  
ON MECHANICAL JOINTS  
IN CFRP SPECIMENS IN CYCLING LOADING**

by

C. Caprile - G. Sala  
Dipartimento di Ingegneria Aerospaziale - Politecnico di Milano - Italy

**Summary**

An experimental study of the fatigue behaviour of jointed specimens made of carbon fibre reinforced plastic has been carried out. Four different configurations and four laminations have been taken into account, to point out the influence of by-pass load / transfer load ratio and stacking sequence on specimen fatigue behaviour. Loading frequency has been maintained at 20 C.P.S. in tension-tension tests at room temperature with dry test conditions. Fatigue loads have consisted in an alternate component (20% of failure load) superimposed on a constant tensile force (60% of failure load). The influence of different sequences of constant amplitude load blocks have been also investigated. Residual strength and stiffness versus number of load cycles have been compared for the same stacking sequence by varying specimen configuration, and for different stacking sequences and equal configuration. Elastic and tensile characteristics have been monitored on-line by means of load-cells, LVDT transducers and strain gauges. Damage growth has been inspected by making use of N.D.T. like X-rays radiography with opaque enhanced penetrant liquids and electronic microscope photography. The final results have consisted in a correlation between damage growth and residual strength and stiffness of jointed specimens.

**INTRODUCTION**

Nowadays, the relatively poor static strength of composite joints forces the designers to keep stresses at low levels, so that joints fatigue does not emerge as a design problem (1).

It is well known that important role may be played by many parameters, as the nature of material, the load amplitude and frequency, the specimen and notch geometry, the stacking sequence, the type of fasteners, the ratio of by-pass to transfer load, the test temperature and moisture (2), and the load history (3), (4).

In order to understand the influence of such parameters, some of them has been taken into account separately, assigning different values only to few quantities and keeping constant the other ones (5), (6), (7).

During the present investigation only two basic parameters have been taken into account, namely stacking sequence and general arrangement of the specimen (presence or absence of holes, with or without fasteners installed, and percentage of by-pass load (8)).

Other parameters, like the type of material, load amplitude and frequency, temperature, moisture, clamping torque, bolt clearance or interference, have been kept constant, in order to observe only consequences of stacking sequence and specimens general arrangement.

Some specimens have been subjected to static tests, to measure stiffness and strength in order to normalize residual values.

Then residual strength and stiffness have been plotted versus the number of load cycles, in order to show the influence of stacking sequence and specimen configuration.

**MATERIAL, SPECIMENS AND FATIGUE LOADS**

All specimens, supplied by C.A.G. AGUSTA S.p.A., have been made from the same pre-preg system, that is graphite-epoxy T300-5208, with 0.18 mm layer thickness.

Laminates have been produced by pressure bagging technology, and specimens by sawing. So some initial edge delamination may have occurred; anyway this damage has been detected by X-rays inspection on specimens before any static or fatigue test.

Four different symmetrical stacking sequences have been taken into consideration, each one made of eight layers:

- (0°/90°/0°/90°)<sub>s</sub> (cross-ply)
- (+45°/-45°/+45°/-45°)<sub>s</sub> (angle-ply)
- (0°/0°/+45°/-45°)<sub>s</sub> (stringer type)
- (0°/90°/+45°/-45°)<sub>s</sub> (quasi-isotropic)

with a total of thickness of 1.44 mm.

These different stacking sequences have been chosen first to compare the different behaviour of matrix dominated fatigue loads, and then to point out how typical "joint lamination" quasi-isotropic (0°/90°/+45°/-45°)<sub>s</sub> or typical "stringer lamination" (0°/0°/+45°/-45°)<sub>s</sub> behave if notched, bolted and subjected to cyclic loading.

Geometry of specimens is shown in Fig.1; these are plain, notched, with idling fastener installation, and 100% load transfer with two laps of the same thickness and lamination.

All specimens were 280 mm in length and 28 mm in width, with end reinforcements made of glass fiber NARMCO 3200-7781, 2.5 mm in thickness and 65 mm in length, bonded to specimen surface with NARMCO 1113 adhesive.

Hole for notched specimens was 5 mm in diameter, resulting in a ratio of the hole diameter to the specimen width of 0.18.

After drilling and seat reaming, the fastener was installed with a clamping torque for the HL 86 nut of 5 Nm, corresponding to a pre-loading for the HL 20 tension head equal to 5000 N.

Mounting of the hy-lock was carried out with a slight clearance, equal to 1.5% of nominal hole diameter (9), (10).

Values of static and alternate loads generally met in literature have been used (11), (12), (13), (14).

Loading frequency was 20 c.p.s. with room temperature dry test conditions.

Such a frequency level is high enough to allow relatively short test time, but not too high to reach the glassy temperature of the resin.

In fact the maximum level of temperature measured during tests at 20 c.p.s. has been of 35 °C.

#### EXPERIMENTAL ARRANGEMENTS

Loads were provided by a servocontrolled hydraulic system able to apply forces up to 50,000 N.

Loads were monitored by strain gauge load cells, and specimen elongation by differential transformer transducers.

Inspections were carried out by means of a GILARDONI radiolight Be X-rays tube, making use of opaque enhanced dye penetrants techniques (15), (16), (17).

The arrangement of the load application system is shown in fig.2.

Tab.1 shows longitudinal elastic modulus E and ultimate tensile strength as statically measured on plain specimens.

For every kind of specimen, characterized by a particular combination of stacking sequence and geometry, fifteen samples were available.

Each group of such specimen was divided in five sub-groups, to be subjected respectively to 0., 0.25E6, 0.75E6 and 1.00E6 cycles at constant amplitude fatigue loading varying between 40% and 80% of static failure load.

A larger number of specimens was tested for shorter lives (0.25E6 and 0.50E6 cycles), because the greater scatter typical of these conditions requires a larger base (18), (19).

Tab.2 shows the percentages of specimens that have been subjected to the different number of load cycles.

Elastic modulus and tensile strength were measured and then reduced to non-dimensional form dividing by the corresponding static values, to obtain residual elastic characteristics.

Then, for each set of residual stiffness, corresponding to a specified number of cycles, the mean value was computed together with its confidence limits (for sets containing at least 3 values), assuming Student distribution and small samples theory (Tab.3).

Such mean values were best fitted to obtain plots of the residual stiffness versus the number of load cycles, for each stacking sequence and geometrical configuration (20), (21).

After each static and fatigue test an opaque dye penetrant enhanced radiography was carried out, to monitor and to evaluate damage growth (16).

Finally a correlation between stiffness and strength decrease and damage growth was investigated by means of micrographs (22), (23), (24).

## RESULTS

### Residual stiffness

The residual stiffness of (+45°/-45°/+45°/-45°)s lamination does not decrease strongly with an increasing number of load cycles in the case of plain specimens, while for notched specimens, such decrease reaches a value of about 20% at one million cycles.

On the other hand, specimens with no load transfer show a slight improvement in stiffness (Fig.3), while the load transfer ones show a large decrease.

As far as jointed specimens with load transfer are concerned, decreasing in stiffness is greater than previous cases.

Anyway the scatter of results suggests a wider investigation, on a larger statistical basis, in order to obtain more reliable results.

The (0°/90°/0°/90°)s lamination shows a behaviour qualitatively similar to the (+45°/-45°/+45°/-45°)s one (Fig.4).

It has to be noted that, in general, (0°/90°/0°/90°)s lamination seems to be less sensitive to fatigue than other stacking sequences.

Stringer-type and quasi-isotropic laminations have a behaviour different from the previous ones: in fact a slight increase in elastic modulus was observed at 1.00E6 cycles for notched (0°/0°/+45°/-45°)s, for load transfer (0°/90°/+45°/-45°)s and for no load transfer specimens of both laminations (Fig.5).

From the previous results it appears that, for each stacking sequence, plain specimens do not suffer considerable consequences from fatigue cycling (Fig.6).

Viceversa, nearly any kind of notched sample shows an increase in compliance; this phenomenon seems to be directly dependent on the number of +45°/-45° plies in the stacking sequence: in fact stiffness reduction is about of 10% for (0°/90°/0°/90°)s laminate, and 20% for (+45°/-45°/+45°/-45°)s (Fig.7).

Finally, for jointed specimens, the scatter in results is much greater than for plain and notched ones, and the trend of residual stiffness versus the number of cycles is more strongly non linear.

In any case, no load transfer specimens are less sensitive to fatigue (Fig.8), than load transfer specimens, the latter being much more sensitive than the plain and the notched ones.

Moreover such sensitivity depends on the number of +45°/-45° oriented plies. In particular the stiffness reduction at one million cycles reaches about 25% of static stiffness for (+45°/-45°/+45°/-45°)s ply and 5% for (0°/90°/0°/90°)s ply; viceversa elastic modulus of quasi-isotropic specimens seems to increase of about 5%, as shown in Fig.9.

### Residual strength

The residual strength of each kind of specimen considered is only slightly dependent on lamination: it mostly depends on specimen type.

In particular, for (+45°/-45°/+45°/-45°)s stacking sequence, specimens seem to be slightly influenced by fatigue if plain, while the notched ones show a slight increase in static strength, about 4% at one million cycles (Fig.10).

The same qualitative behaviour is shown by stringer-type, quasi-isotropic and (0°/90°/0°/90°)s specimens.

As far as fastened specimens are concerned, a small decrease in static strength has been observed, for all the stacking sequences. In load and no load transfer cases a slight decrease in residual strength has been observed (Fig. 11-12).

On the other hand, also for residual strength, (+45°/-45°/+45°/-45°)s lamination is more sensitive to tension-tension fatigue than (0°/90°/0°/90°)s, stringer-type and quasi-isotropic.

In fact, in the case of plain specimens, while (+45°/-45°/+45°/-45°)s lamination at one million cycles shows a decrease in residual strength of about 3%, (0°/90°/0°/90°)s lamination shows a slight increase (Fig.13). This trend holds also in the case of notched specimens (Fig.14).

On the other hand, for load transfer specimens, a decrease in static strength has been noted, both for (+45°/-45°/+45°/-45°)s and (0°/90°/0°/90°)s, respectively of 7% and 5%, while, for quasi-isotropic lamination, the same decrease was about 9% (Fig.15).

It must be observed that the presence of "fiber dominated behaviour" plies, in some way mitigates the negative effects of fatigue cycling. This is true also for no load transfer specimens (Fig.16).

Finally it must be pointed out that, also for residual strength, scatter in results is much greater for jointed specimens than for plain and notched ones.

#### INFLUENCE OF INCREASING AND DECREASING AMPLITUDE LOAD BLOCKS

A test program is now going on to investigate the influence of increasing and decreasing amplitude load blocks, taking into consideration transfer load specimens of four different stacking sequences.

Built-up load sequences include 5 equal blocks of 200,000, each of 4 increasing and decreasing sub-blocks (Fig.17a,b).

Related results are not yet completely available, but, only for some quasi-isotropic specimens, it is possible to note that increasing load sequences have a stronger influence on fatigue behaviour, especially over 500,000 cycles (Fig.18).

#### CONCLUDING REMARKS

In conclusion it can be asserted that, in general, tension-tension fatigue for plain CFRP specimens, does not modify in a considerable way neither the residual strength nor the residual stiffness, up to one million load cycles.

Notched specimens subjected to fatigue loading undergo two different kinds of modification in elastic characteristics, opposite in sign. A strong decrease in longitudinal stiffness has been observed, 10% for (0°/90°/0°/90°)s lamination and 20% for (+45°/-45°/+45°/-45°)s.

On the contrary, the same kind of specimen has shown a slight but appreciable increase in residual strength, qualitatively similar for each stacking sequence and quantitatively stronger for (0°/90°/0°/90°)s and stringer-type.

Also notched specimens with fastener installed and no load transfer show the same stiffness decreasing trend with load cycles.

On the other hand specimens with load transfer show a great sensitivity to fatigue cycling: in particular both residual strength and residual stiffness decrease for each lamination, except for the quasi-isotropic one.

To sum up it seems apparent that tension-tension fatigue on CFRP specimens does not lead to considerable negative effects if specimens are plain. On the contrary, if specimens are notched, they undergo remarkable fatigue consequences, but opposite in sign as far as residual strength and residual stiffness are concerned: in fact increasing the number of fatigue cycles, the residual stiffness strongly decreases and the residual strength slightly increases. Such a behaviour may be justified examining Fig.19a,b,c,d,e and micrographs 20a,b,c,d,e,f, which show delamination growth with the number of cycles. Such delamination, near the hole contour, firstly increases the longitudinal compliance and, at the same time, seems to play a stress peak smoothing role similar to plasticity for metallic notched specimens (25), (26), (27), especially near an empty hole, where the fibers are free to move to reduce their strain.

The change in specimen shape due to this effect is shown in Fig.21.

Examining Fig.22a,b, different failure modes, corresponding to different fatigue lives, seem to confirm this hypothesis.

The most sensitive stacking sequence for tension-tension fatigue is (+45°/-45°/+45°/-45°)s: its loss in stiffness is impressive, while the corresponding gain in strength is not significant.

Thanks to these observations it appears that the presence of "matrix-dominated behaviour" layers holds a notable influence on global fatigue behaviour of laminates, that is: the more CFRP specimen has +45°/-45° plies, the more it suffers fatigue (28).

In general it is possible to assert that "fiber dominated behaviour" seems to confer good fatigue performances to plain and notched specimens, while quasi-isotropic stacking sequence is more suitable for jointed specimens, as damage growth shows (fig.22a,b,c, 23a,b,c, 24a,b,c).

#### REFERENCES

- (1) L.LAZZERI: Sul comportamento a fatica di provini intagliati realizzati in carbonissima. Atti VIII Congresso Nazionale AIDAA, Torino 22-27/9/1986.
- (2) G.C.GRINES, L.L.JEANS, E.DEMUTS: Sensitivity of bonded and bolted joints in composites to load/environmental spectrum variations, conference on Fibrous Composites in Structural Design, San Diego - California, 1978.
- (3) L.JARPALL: Shear loaded fasteners installations, SAAB SCANIA Report KD-R-3360, 1983.
- (4) K.HELLBOM: A summary of SAAB SCANIA experience on mechanically fastened joints in composite materials, SAAB SCANIA report FKHK-I-82.063, 1982.
- (5) L.LAZZERI: La sperimentazione a fatica dei materiali compositi, stato delle

- conoscenze e problematiche, Atti VII Congresso Nazionale AIDAA, Napoli 25-28/10/1983.
- (6) O.BUXBAUM, D.SCHUTZ: Review of investigations on aeronautical fatigue in the Federal Republic of Germany, ICAF Conference, 1977.
  - (7) T.KAMFYAMA, T.SHIMOKANA: Review of aeronautical fatigue investigations in Japan, XVII ICAF Conference, Noordwijkerhout, the Netherlands, 5/1981.
  - (8) J.M.McKINNEY: A crack stopped concept for filamentary composite laminates, Journal of Composite Materials, vol.6, pp. 420-424, 1972.
  - (9) R.T.COLE, E.J.BAWEH, J.POTTER: Fasteners for composite structures, Composites, 7/1982, pp. 233-240.
  - (10) C.Y.KAM: Bolt hole growth in graphite-epoxy laminates for clearance and interference fits when subjected to fatigue loads, ASTM Symposium, San Francisco 22-23/5/1979.
  - (11) D.SCHUTZ, J.J.GERHARW: Fatigue strength of a fibre reinforced material, Composites, 10/1977, pp. 245-250.
  - (12) D.SCHUTZ, J.J.GERHARZ, E.ALSCHWEIG: Fatigue properties of unnotched, notched and joined specimens of a graphite epoxy laminate, ASTM Symposium, San Francisco 22-23/5/1979.
  - (13) J.D.WHITCOMB: Experimental and analytical study of fatigue damage in notched graphite-epoxy laminates, ASTM Symposium, San Francisco 22-23/5/1979.
  - (14) J.M.WHITNEY: Fatigue characterization of composite materials, ASTM Symposium, San Francisco, 22-23/5/1979.
  - (15) A.F.BLOM, P.A.GRADIN: Use of radiography for non destructive testing and evaluation of fibre reinforced composites, ICAF Doc No.1507, FFA TN 1985-53, Stockholm 1985.
  - (16) G.P.SENDECKYJ: E techniques for composite laminates, AGARD Conference Proceedings No.355.
  - (17) L.IAZZERI: Sul comportamento a fatica di provini intagliati realizzati in carboresina, L'Aerotecnica, Missili e Spazio, 6/1984, pp. 73-80.
  - (18) Z.GAO: The confidence level and determination of the minimum of specimens in fatigue testing, communication of Beijing Institute of Aeronautics and Astronautics.
  - (19) A guide for fatigue testing and the statistical analysis of fatigue data - Supplement to Manual of fatigue testings STP No.91, ASTM Special Technical Publication No.91-A.
  - (20) H.FU, Z.GAO: Probability density function of fatigue strength, communication of Beijing Institute of Aeronautics and Astronautics.
  - (21) H.T.HAHN: Fatigue behaviour and life prediction of composite laminates, USAF Technical Report, AFML-TR-78-43 1978.
  - (22) A.F.BLOM: Fracture mechanics analysis and prediction of delamination growth in composite structures, ICAF doc No.1447, FFA TN 1984-1985, Stockholm 1984.
  - (23) R.PRINZ: Growth of delamination under fatigue loading, AGARD Conference Proceedings No.355.
  - (24) W.GEIGER, J.VILSMETER, D.WEISGERER: Experimental investigation of delaminations in carbon fibre composite, AGARD Conference Proceedings No.355.
  - (25) L. ART-SMITH: Mechanically-fastened joints for advanced composites. Phenomenological consideration and simple analyses, Conference on fibrous Composites in structural Design, San Diego - California, 1978.
  - (26) D.J.WILKINS: The engineering significance of defects in composite structures, AGARD Conference Proceedings No.355.
  - (27) M.E.WADDOUPS, J.R.EISENMANN, B.E.KAMINSKY: Macroscopic fracture mechanics of advanced composite materials, Journal of Composite Materials, vol.5, 1972.
  - (28) R.D.JAMISON: Advanced fatigue damage development in graphite-epoxy laminates, Ph.D. Thesis, Virginia Polytechnic Institute and State University, 1982.

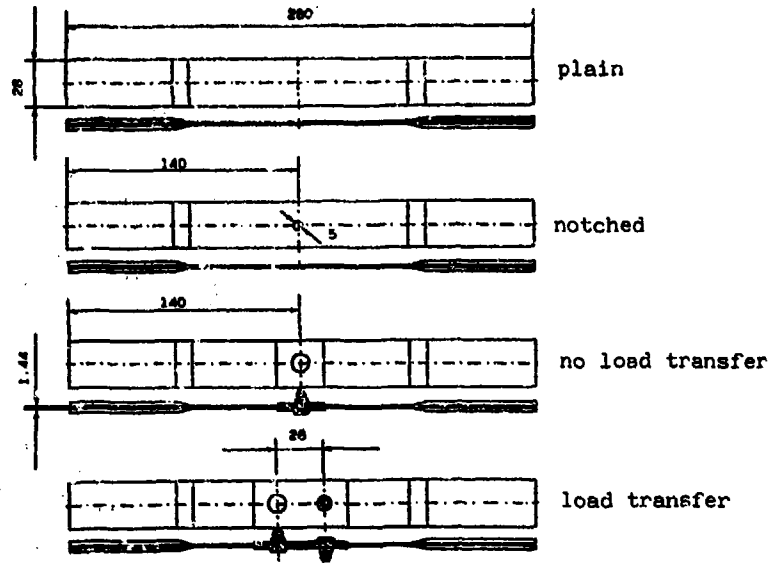


Fig.1 Specimen configuration

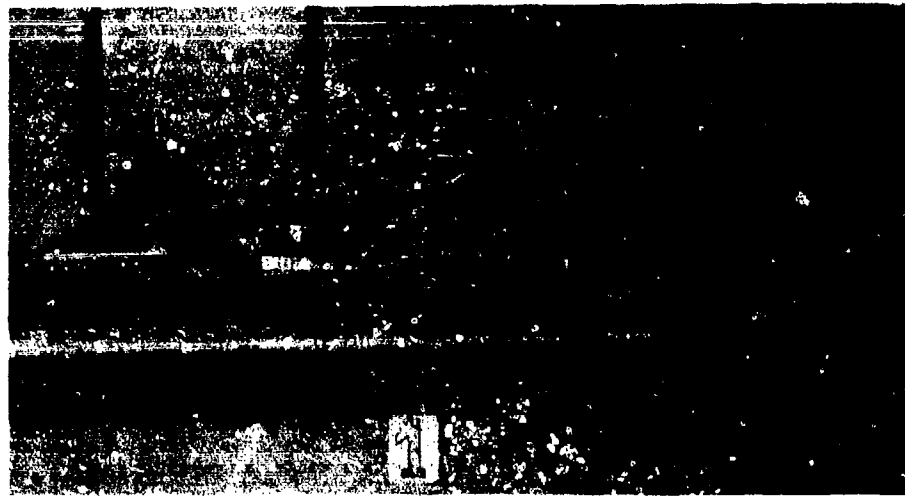


Fig.2 Experimental arrangement

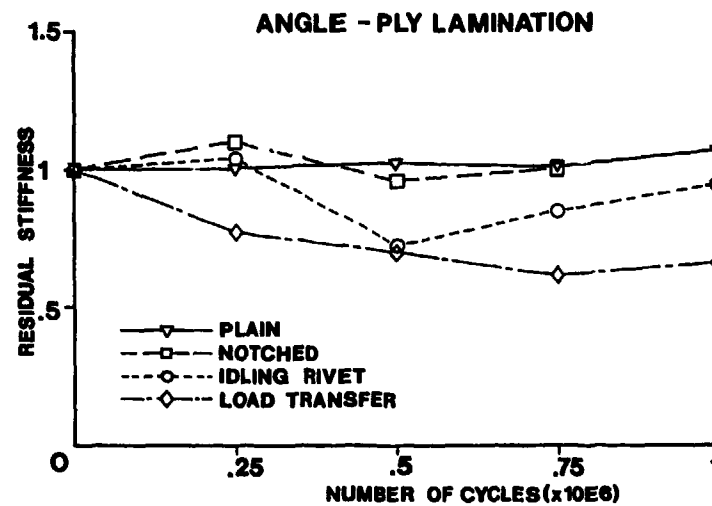


Fig.3 Residual stiffness for angle-ply lamination

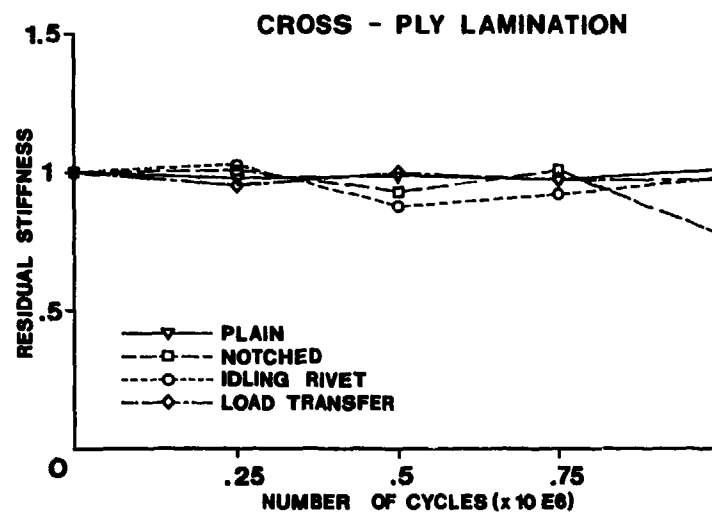


Fig.4 Residual stiffness for cross-ply lamination

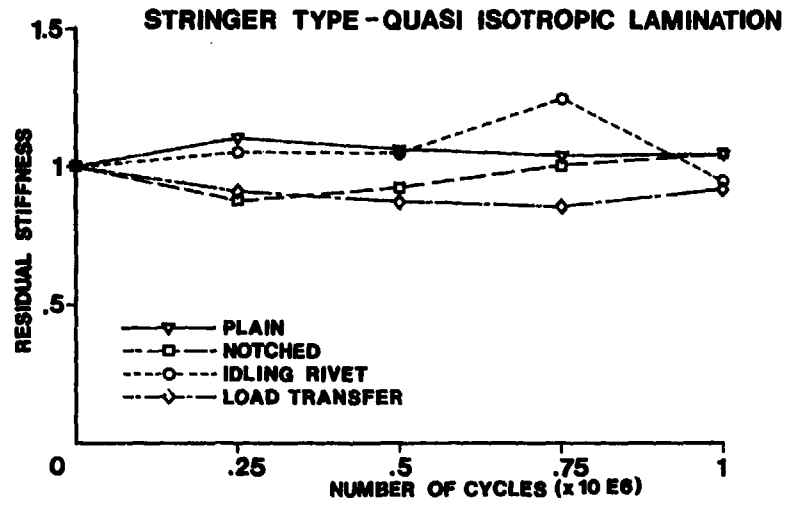


Fig.5 Residual stiffness for stringer-type and quasi-isotropic laminations

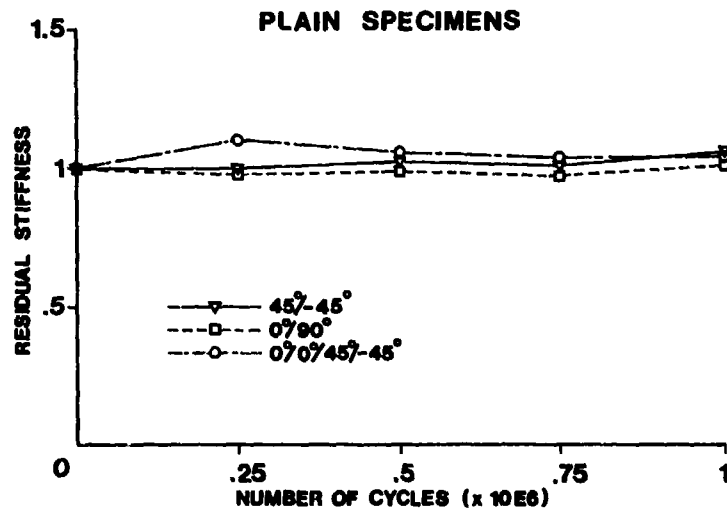


Fig.6 Residual stiffness for unnotched specimens

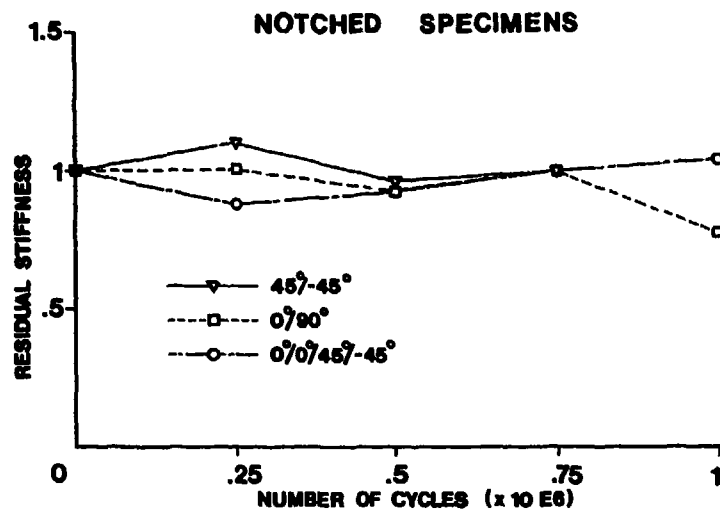


Fig.7 Residual stiffness for notched specimens

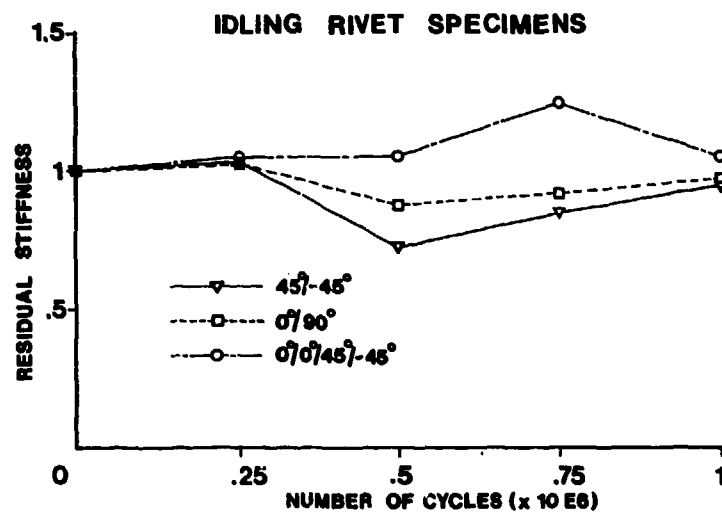


Fig.8 Residual stiffness for 100% by-pass load specimens

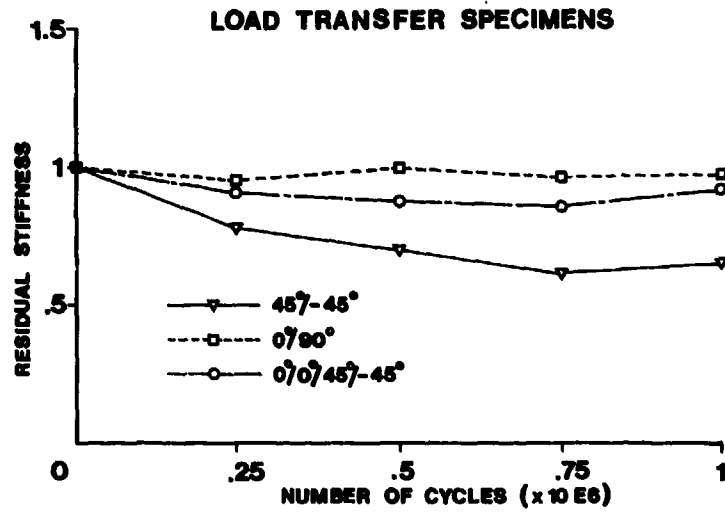


Fig.9 Residual stiffness for 100% transfer load specimens

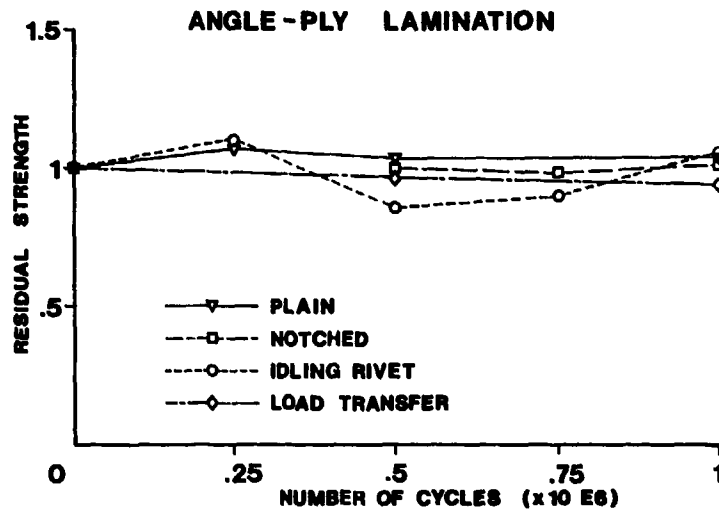


Fig.10 Residual strength for angle-ply lamination

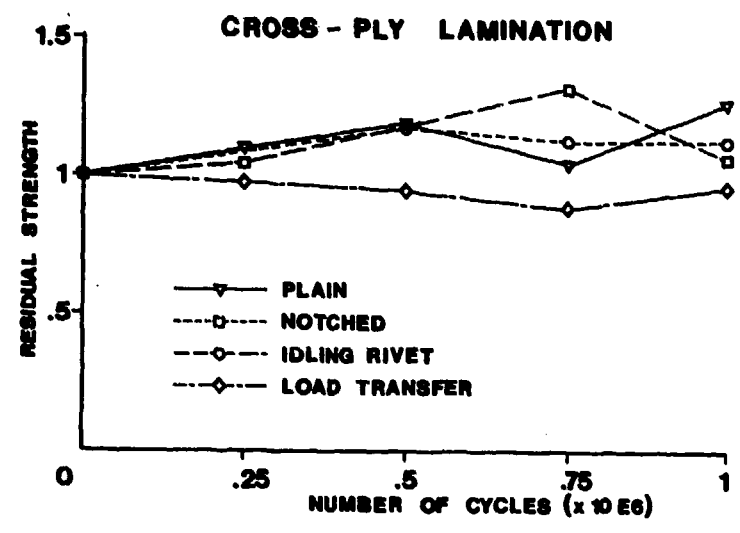


Fig.11 Residual strength for cross-ply lamination

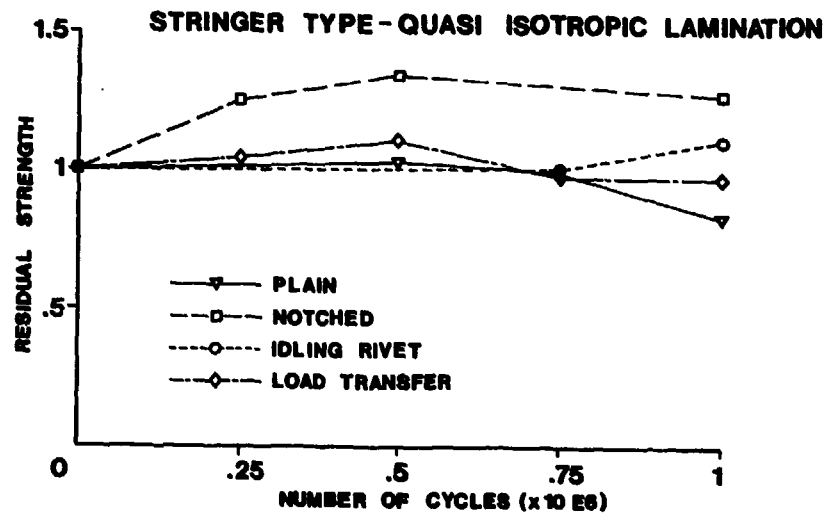


Fig.12 Residual strength for stringer-type and quasi-isotropic laminations

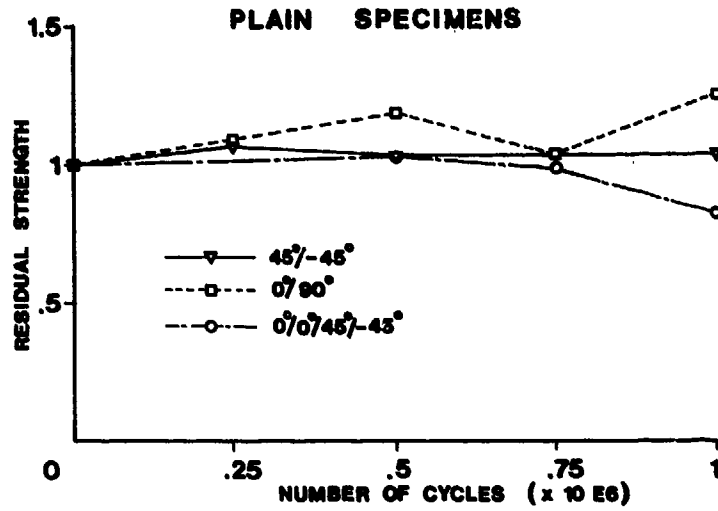


Fig.13 Residual strength for unnotched specimens

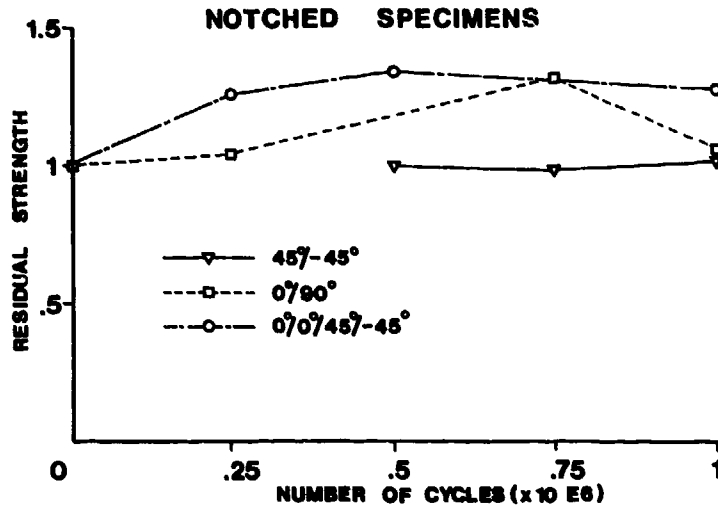


Fig.14 Residual strength for notched specimens

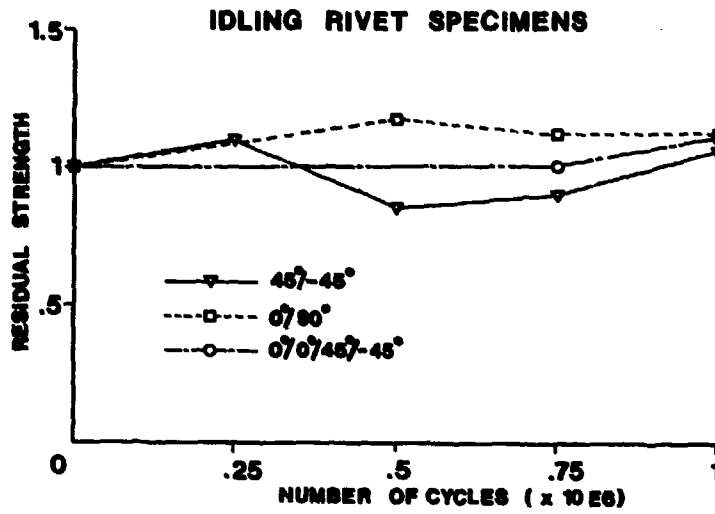


Fig.15 Residual strength for 100% transfer load specimens

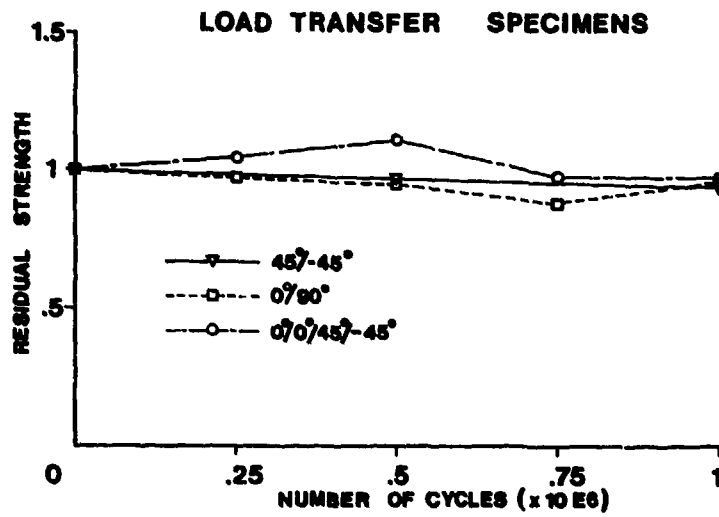


Fig.16 Residual strength for 100% by-pass load specimens

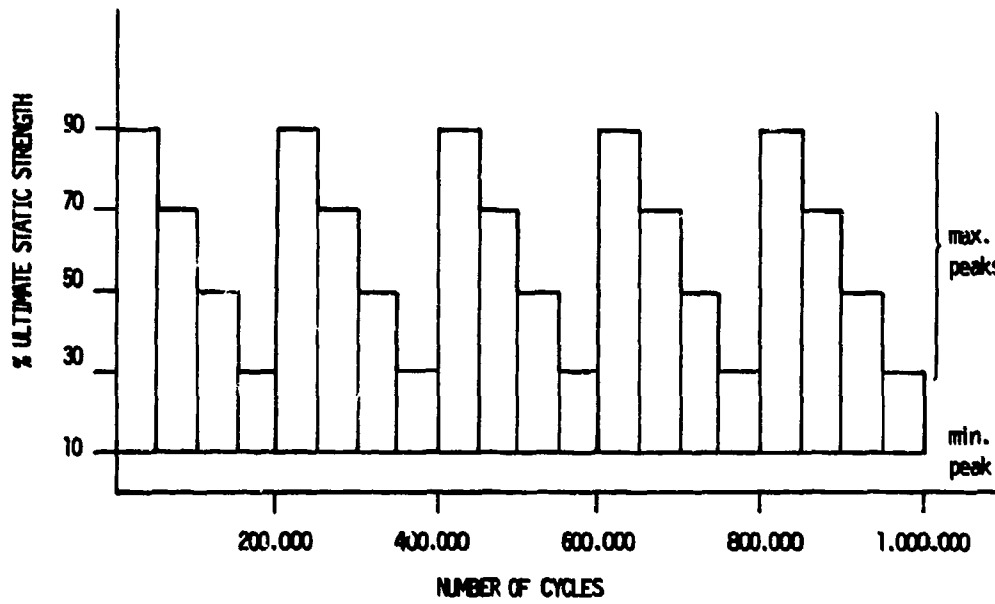
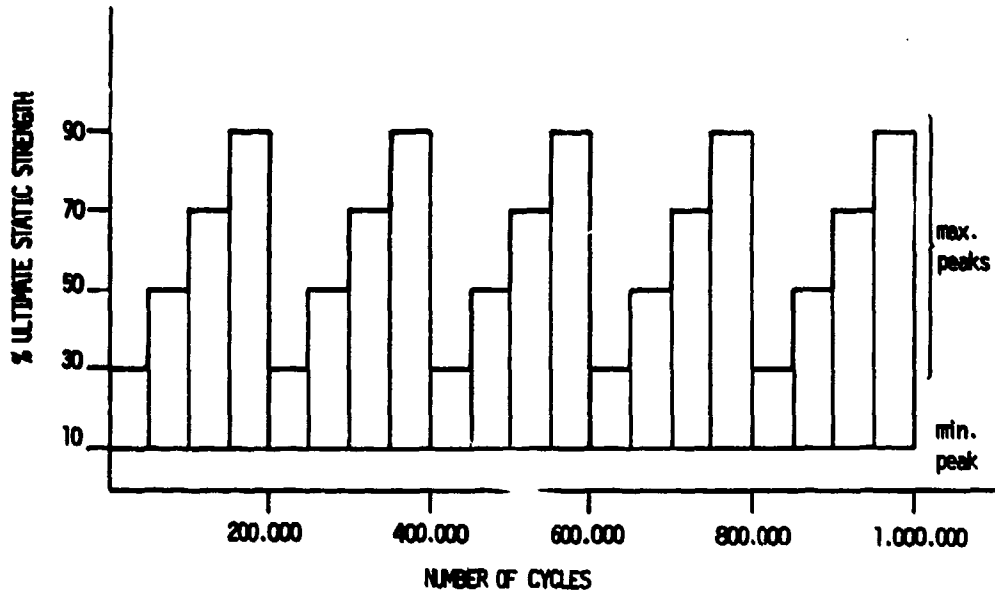


Fig.17a-b Increasing and decreasing built-up load specimens

### 100% TRANSFER LOAD SPECIMENS

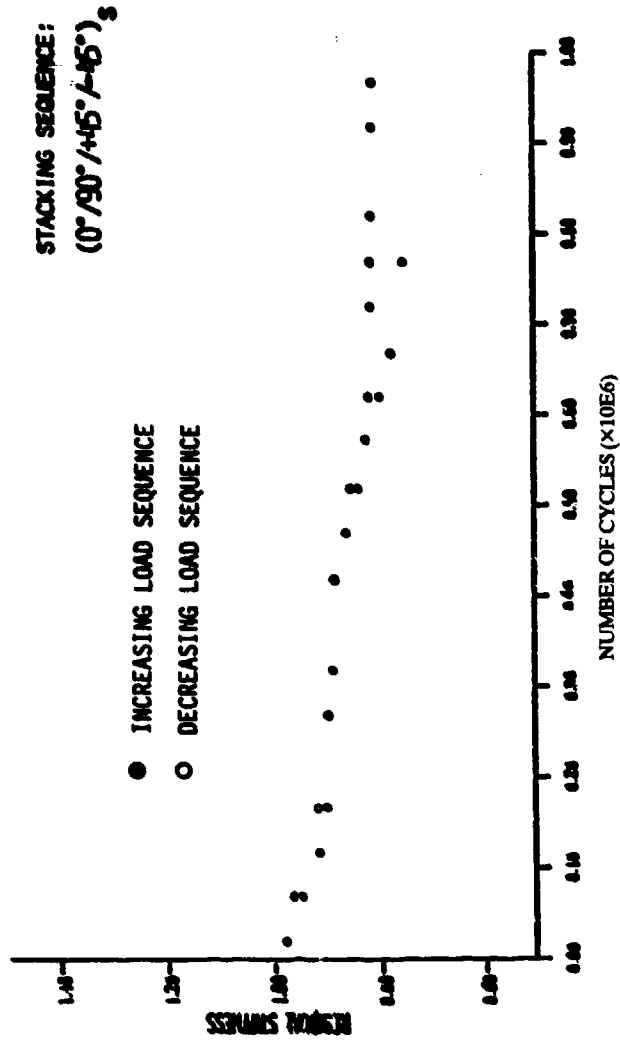


Fig.18 Behaviour of jointed specimen subjected to increasing and decreasing built-up load sequences

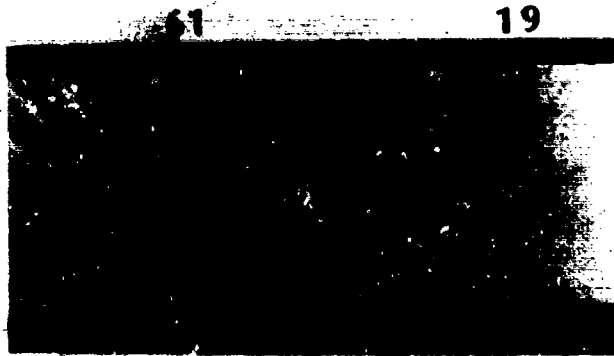


Fig.19a

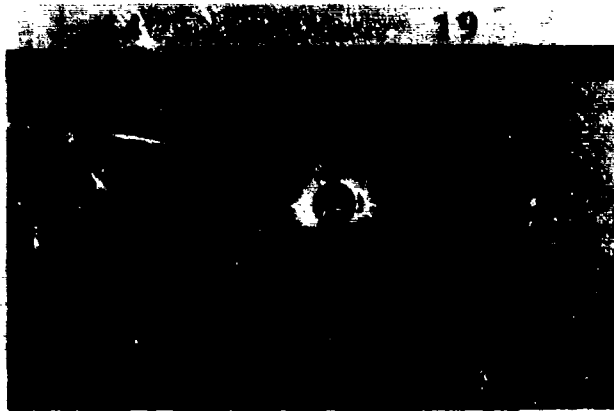


Fig.19b



Fig.19c



Fig.19d



Fig.19e

Fig.19a-c Damage growth for quasi-isotropic notched specimens (.00, .25E6, .50E6, .75E6, 1.00E6 cycles)



Fig.20a



Fig.20b



Fig.20c



Fig.20d



Fig.20e

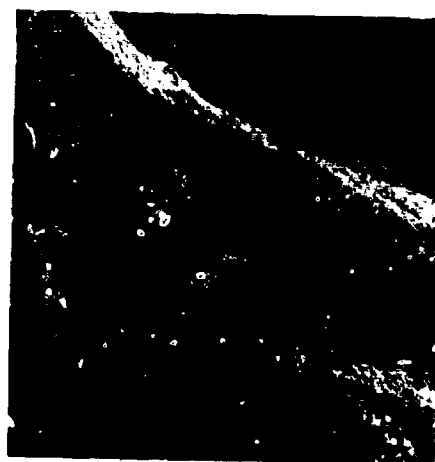


Fig.20f

Fig.20a-f Micrographs (48X) showing point of view, non cristallizing penetrant liquid and damage growth for quasi-isotropic jointed specimens at .25E6, .50E6, .75E6, 1.00E6 cycles



1 A

Fig.21 Change in shape for angle-ply specimen subjected to 1.00E6 cycles



Fig.22a



Fig.22b

Fig.22a-b Different failure modes for .00 and 1.00E6 cycles



Fig. 23a



Fig. 23b



Fig. 23c

Fig. 23a-c Damage growth for quasi-isotropic jointed specimens (.50E6, 1.00E6 cycles)

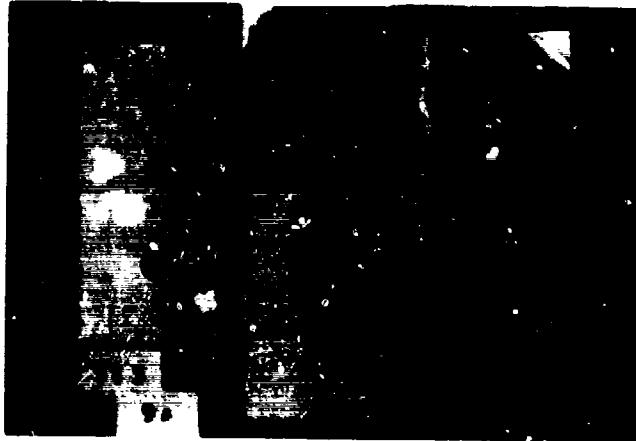


Fig.24a

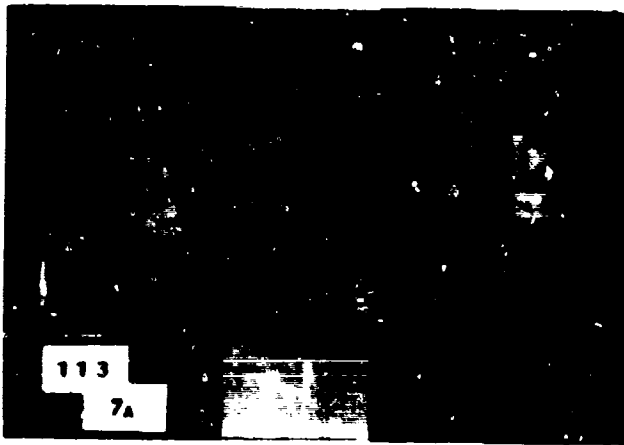


Fig.24b

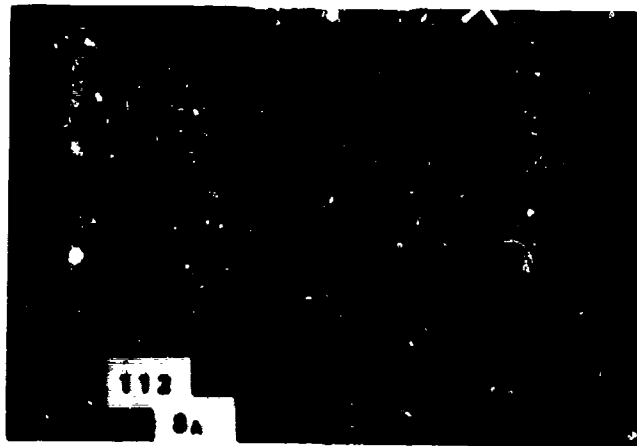


Fig.24c

Fig.24a-c Damage growth for cross-ply jointed specimens (.00, 50E6, 1.00E6 cycles)

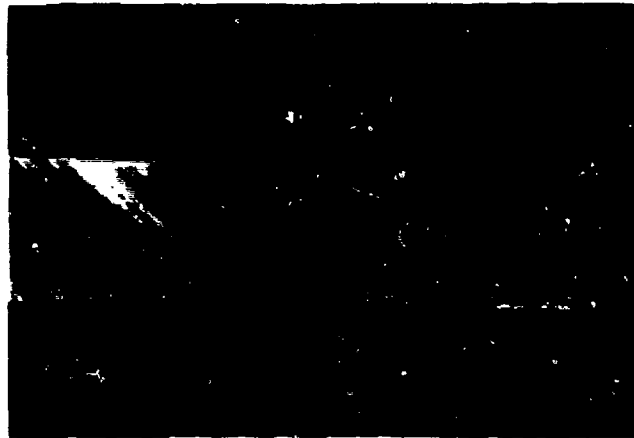


Fig.25a

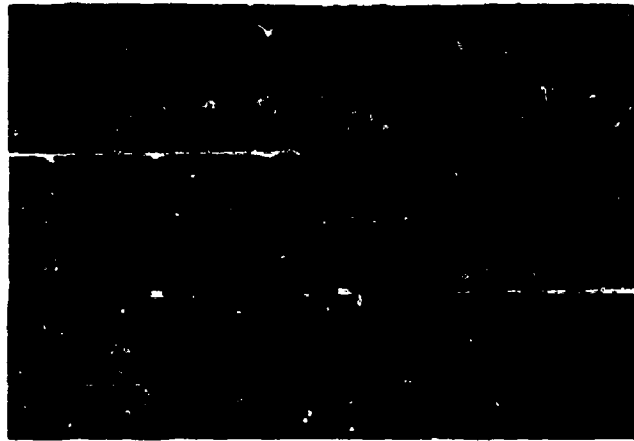


Fig.25b

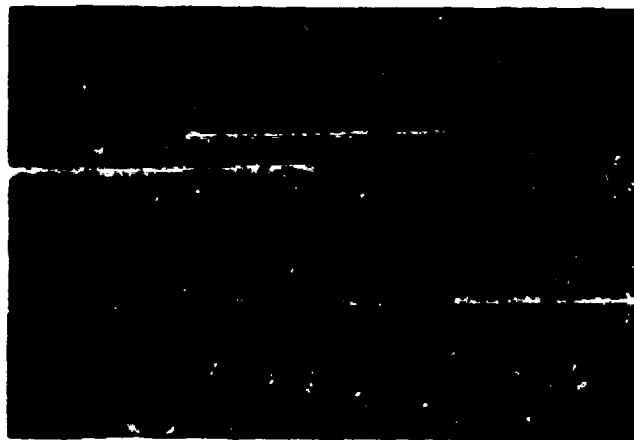


Fig.25c

Fig.25a-c Damage growth for angle-ply jointed specimens (.00, 50E6, 1.00E6 cycles)

Table 1 Static characteristics

LAMINATIONS	(0°/90°) <sub>n</sub>	(+45°/-45°) <sub>n</sub>	stringer type
E (MPa)	88954	19015	91776
σ (MPa)	221	121	641

Table 2 Number of specimens for various life steps

NUMBER OF CYCLES	0.00	0.25E6	0.50E6	0.75E6	1.00E6
No. of SPEC. (%)	33	27	20	13	7

Table 3 Mean values and confidence levels for elastic moduli (MPa)

	NUMBER OF LOAD CYCLES											
	0.				250000				500000			
	Mean value and confidence levels											
	N.V.	99%	95%	90%	N.V.	99%	95%	90%	N.V.	99%	95%	90%
<b>PLAIN</b>												
0/90	107272	-	-	-	102956	4415	2403	1776	102142	11144	4827	3375
±45	16393	2962	1795	1373	15156	3532	2962	2207	15873	13106	2609	1295
0/0/±45	96383	9912	5862	4258	102289	37661	16324	11085	94863	20346	8819	5984
<b>NOTCHED</b>												
0/90	112481	32010	17432	12881	111187	-	-	-	11472	-	-	-
±45	21906	6435	3502	2580	25584	11968	7750	5208	21543	14087	6102	4140
0/0/±45	134838	9506	5730	4395	118014	33452	18217	13459	122448	28214	12223	8299
<b>BY PASS</b>												
0/90	137163	33864	18443	13626	123145	-	30578	20768	123214	-	25506	17316
±45	25496	3993	2168	1599	23613	13734	7475	5523	21866	-	-	-
0/0/±45	144325	19031	11497	8809	136948	42448	23112	17079	133639	-	-	-
<b>TRANSFER</b>												
0/90	82708	20199	13881	11183	80874	25653	17295	13930	83277	24290	16039	12704
±45	17952	2099	1462	1177	14274	1589	1010	795	13008	3689	2011	1481
0/90/±45	81560	13911	9378	7554	72839	16481	10536	8280	73349	20434	12351	9457

## Behaviour of Mechanically Fastened Joints in Advanced Composites

by

C. Pean and R. Gould

Structures and Materials Laboratory  
National Aeronautical Establishment  
National Research Council Canada  
Ottawa, Ontario K1A 0R6

### SUMMARY

In this report, experimental results obtained to date from an on-going test program are presented. The purpose of this program is to evaluate the performance of mechanical fastener systems in Narmco IM6/5245C, a high strain/tough resin composite identified as a promising material system for new aircraft designs. Preliminary results obtained from tensile tests on open-hole specimens and double-lap joints were used to characterize the notch strength and the bearing strength as influenced by the effect of design parameters involving geometric ratios, hole size and fastener torque. A constant amplitude tension-compression ( $R = -1$ ) fatigue test was performed on a double-lap composite joint to assess a simple and effective technique based on hysteresis measurements for monitoring progressive elongation of a fastener hole. It was found that the hysteresis measurement technique underestimates the actual hole elongation by as much as 26% at the end of the fatigue test. This was explained by the observation that graphite particles formed during the fatigue test reduce the clearance between the hole and the pin. Single-shear composite/titanium joints were tested to evaluate three fastener systems designed specifically for composite applications. Four single-shear joints were tested to date to the ultimate tensile strength. It was found that the Huck interference fit lockbolt fastener system provides a single-shear joint strength 30% higher than that provided by the Cherry Maxifoot blind fastener system and 44% higher than that provided by the SPS COMP-TITE blind fastener system respectively. The single-shear specimens tested were strain-gauged for the purpose of measuring the load transfer and secondary bending. However, the analysis of the strain gauge data has not been completed and the results are not reported in this paper.

### 1.0 INTRODUCTION

The use of composites in aircraft structures has increased considerably over the past decade. Composite structural components can be found in the fuselage, wing and empennage of modern aircraft. A major requirement for the assembly of composite structural components, especially in primary structures where the load transfer is high, is the usage of mechanical fastener systems. This poses a challenge for efficient joint design because of the inherent interlaminar shear and compression weaknesses in composites which not only render them extremely susceptible to bearing and delamination failures but also render them much less capable to resist secondary bending resulting from eccentric load paths.

Attempts to reduce the stress concentration produced in a loaded fastener hole of a composite joint by including  $90^\circ$  plies in the lay-up and to minimize interlaminar stresses in the fastener hole by adopting a more homogeneous stacking sequence have successfully resulted in improved properties<sup>(1)</sup>. But these design measures, when applied to first generation composites which consist of low strain carbon reinforcing fibers and brittle epoxy resin, are not producing optimum results as evidenced by the low design strain levels in the range of 0,000 to 3,000  $\mu\text{m/m}$  imposed on the composite wings of the F-14 and the advanced Harrier aircraft (AV-8B)<sup>(2)</sup>. These design strain levels have been developed to accommodate stress concentration effects of fastener holes and environmental effects. They also serve to provide an inherent damage-tolerant structure.

Improvements in the structural efficiency (load transfer per unit weight) of a mechanically fastened composite joint can be realized by increasing the allowable design strain level. One promising way to achieve this is by selecting high strain/tough resin composites for structural components. A survey conducted by Canadair Ltd.<sup>(3)</sup> on the types of advanced composite material systems currently being investigated by the aircraft industry indicated that both the tensile and compressive properties of these second generation tough composites are significantly higher than those of the conventional baseline systems. The most important improvement of these newer composites over the conventional composites appears to be in damage-tolerance. A recent literature review<sup>(4)</sup> found that there is a lack of data for mechanically fastened joints in these newer composites. Also, improvements in both static and fatigue properties of a composite joint can be achieved by optimizing the fastener system. Important design parameters to be considered include interference fit, clamping pressure and configuration of the fastener.

State-of-the-art design analysis procedures for mechanically fastened composite joints are highly dependent upon empirical data. Thus, it is important to establish a data base for these advanced composites. A test program<sup>(5)</sup> was launched at the Structures and Materials Laboratory for this purpose. Experimental data collected to date from testing of mechanical fastener systems in IM6/5245C are presented and discussed in this short contribution.

### 2.0 SPECIMEN PREPARATION

The composite material selected for this test program was IM6/5245, a high strain/tough resin composite manufactured by Narmco Materials Inc. The resin system, Narmco Rigidite 5245C, is a 169° to 190°C curing modified bismaleimide resin with an intended service temperature range of -39° to 177°C. Neat resin physical and mechanical properties provided by the manufacturer are presented in Table 1. The Hercules Magnarite IM6 is a continuous and intermediate-modulus carbon fiber which can be used in prepreg systems. Typical fiber properties are given in Table 2. Typical mechanical properties of IM6/5245C are given in Table 3. This material was procured in unidirectional tape prepreg form for use in this program. Mechanical properties of the procured material obtained by an in-house characterization program are also presented in Table 3.

Table 1 Typical Resin Properties for Narco Rigidite 5243C  
(Manufacturer's Published Data)

Cured density	1.25 gm/cc		
T <sub>g</sub> , dry	227°C		
Gel time at 177°C	8 ± 3 minutes		
Heat distortion temperature	199°-210°C (dry) 163°C (wet)		
Moisture pickup	1.7% (72 hr boil)		
Tensile strength (R.T.)	83 MPa		
Tensile modulus (R.T.)	3.3 GPa		
Elongation (R.T.)	2.9%		
	Temperature	Dry	Wet (40 hr boil)
Flexure strength	R.T.	145 MPa	112 MPa
	93°C	115 MPa	97 MPa
	132°C	107 MPa	83 MPa
Flexure modulus	R.T.	3.4 GPa	3.1 GPa
	93°C	3.2 GPa	3.0 GPa
	132°C	2.8 GPa	2.7 GPa
Strain energy rate, G <sub>IC</sub>	0.157 kJ/m <sup>2</sup>		
Unnotched Izod impact energy	10.4 J		

Table 2 Typical Properties for Hercules Magnamite IM6 Fiber  
(Manufacturer's Published Data)

Typical Fiber Properties	SI Units
Tensile strength	4,378 MPa
Tensile modulus	278 GPa
Ultimate elongation	1.50%
Carbon content	94.0%
Density	1.77 g/cm <sup>3</sup>
Specific heat at 75°C	0.22 cal/g (°C)
Specific heat at 175°C	0.27 cal/g (°C)
Electrical resistance	0.52 ohm/cm
Electrical resistivity	1400 x 10 <sup>-6</sup> ohm-cm

Table 3 Typical Properties for Narco IM6/5243C Composite  
(Manufacturer's Published Data Compared with NAE Data)

Properties	Temperature			
	R.T.	93°C	163°C	177°C
<b>Elastic Constants</b>				
0° tensile modulus, GPa	170(173)*	168	167	165
0° compressive modulus, GPa	150	-	-	-
90° tensile modulus, GPa	8.3(8.5)*	8.3	-	-
<b>Allowables</b>				
0° tensile strength, MPa	2620(2606)*	2634	2379	2206
0° compressive strength, MPa	1613	1517	965	896
90° tensile strength, MPa	61(60)*	55	-	-
0° tensile strain, m/m	14000	16300	14200	13300
0° compressive strain, m/m	10100	11300	-	-
In-plane shear strength, MPa	119(118)*	107	-	-

\* Data obtained from an in-house characterization program (Ref. 9)

Panels were fabricated by first cutting the prepreg tape into plies with the required fiber orientations and dimensions. These plies were laid up by hand and vacuum-bag cured by an autoclave process. During the lay-up, the plies were compacted using a temporary vacuum-bag process at room temperature. After curing, the panels were inspected by an ultrasonic C-scan system. Specimen blanks were cut from each panel using an abrasive cutting wheel. Fastener holes were prepared by first drilling the hole undersize and then reaming it to the required diameter. Carbide tools were used for both drilling and reaming. A drill speed of 1300 rpm was used in conjunction with a slow feed rate of 6.33 cm/min. No coolant was used during drilling and reaming. Composite laminates were clamped between two plexiglass plates during hole preparation to prevent damaging the laminate. After completing all machining work, the laminates were again C-scanned to determine if any damage was introduced during machining.

Three types of specimens have been tested to date. The first type, illustrated in Figure 1, was a flat plate with a 6.35 mm diameter hole. The lay-up of the laminate was quasi-isotropic with a stacking sequence of  $(0^\circ/90^\circ/-45^\circ/90^\circ)_{16S}$ . The second type of specimens, illustrated in Figure 2, was a double-lap joint with a single fastener. The steel plates were made by using the Starrett No. 496 precision-ground flat stock oil hardened to R-41. The lay-up of the laminate was fiber-dominated and was composed of 30%, 40% and 10% of  $0^\circ$ ,  $45^\circ$  and  $90^\circ$  plies respectively. The stacking sequence was  $(0^\circ/0^\circ/-45^\circ/0^\circ/90^\circ/0^\circ/45^\circ/0^\circ/-45^\circ/0^\circ)_{123}$ . Either dowel pins or hexagonal head steel fasteners (NAS 464-4, UTS = 1240 MPa) were used in the double-lap joints. The third type, illustrated in Figure 3, was a single-shear composite/titanium joint with two fasteners in tandem. The composite plate had the same lay-up and stacking sequence as that used for the double-lap joint. The composite/titanium joint was used to evaluate mechanical fastener systems designed for composite applications. Three fastener systems were selected for testing. Fastener system (1) was the SPS COMP-TITE titanium blind fastener with a  $100^\circ$  countersunk head configuration; fastener system (2) was the Cherry Maxifor A-286 stainless steel blind fastener with a  $130^\circ$  countersunk head configuration, and fastener system (3) was the Huck titanium interference-fit lockbolt with a  $100^\circ$  countersunk head configuration. All fasteners were installed using equipment and procedures provided by the fastener manufacturers.

Only one strain gauge was mounted on the open-hole tension specimen or on the double-lap joint for measuring the gross strain in the composite. Six strain gauges were mounted on the single shear composite/titanium joint. Their locations are indicated in Figure 4.

### 3.0 TEST PROCEDURE

Both static and fatigue tests were conducted on a 300 kN capacity MTS 880 test system equipped with hydraulic grips. Gripping pressure can be increased to a maximum level of 69 MPa. For all composite joint tests, both static and fatigue, a gripping pressure of 21 MPa was found to be adequate against specimen slipping. For open-hole tensile tests, the gripping pressure was increased to 45 MPa because of the much higher failure loads. The composite appeared to resist this clamping pressure very well and not a single failure occurred in the gripped region. The MTS 880 test system is fully computer automated and has nine A/D channels for data acquisition. The first three channels were used for load cell, extensometer and hydraulic actuator LVDT data gathering. The remaining six channels were used for strain data gathering. All data collected were stored on floppy disks. Software was developed to control the testing process and to perform data acquisition during the test. For the static tests, specimens were loaded to the ultimate tensile strength at a loading rate of 750 kN/second or less. For the constant amplitude fatigue tests, specimens were subjected to cyclic loads at a frequency of two cycles/second.

### 4.0 RESULTS AND DISCUSSION

Three open-hole tensile tests were performed. Specimens illustrated in Figure 1 were loaded until tensile failure occurred in the notched section. The average notched tensile strength at the net section for IM6/5245C laminates with quasi-isotropic lay-up and a 6.35 mm diameter hole was found to be 330.8 MPa. The unnotched tensile strength was calculated based on classical lamination theory<sup>(6)</sup> and found to be 875.3 MPa. Basic unidirectional laminate properties obtained by the in-house characterization program were used in calculating the unnotched strength. The net stress concentration as defined by Collings<sup>(7)</sup> was determined to be 1.59 by dividing the unnotched strength with the notched strength. When compared to a conventional graphite/epoxy system, Narmco T300/5208, with notched strength and unnotched strength of 230.3 MPa and 494.4 MPa (calculated) respectively (stress concentration factor = 1.59), IM6/5245C was found to possess much improved notched tensile strength and similar stress concentration factor.

Twenty-eight double-lap joints (Fig. 2) were tested under static tensile loading at room temperature to investigate the effects of geometric ratio, fastener size and fastener torque on the bearing strength of IM6/5245C. An extensometer, with a gauge length of 102 mm, was attached across the fastener to measure the relative deflection between the steel plate and the composite plate. A typical load versus deflection plot is given in Figure 5. A method was proposed to measure the initial failure load in a consistent manner. The slope of the linear portion of the load versus deflection curve was determined. This linear portion of the curve was extended to intersect the horizontal axis at point A as shown in Figure 5. Then a straight line, with a slope equal to 95% of that of the linear portion of the curve, was drawn from point A until it intersected the load versus deflection curve. The load value at this intersection point was the initial failure load,  $P_i$ . Although this method is arbitrary, it may indicate the onset of failure of the first ply which is typically used as an analytical failure criterion. In the case shown in Figure 5, as well as in most other cases,  $P_i$  identified by the above method corresponds to the first load reversal. At this load level, acoustic emissions from the specimen were often heard during testing. After the first load reversal, the laminate was able to sustain higher loads, but its stiffness was reduced. As the fastener plowed further into the laminate, more load reversals occurred along the way which indicated progressive failures of remaining plies. At this stage, the load level only increased slightly. At the ultimate failure load,  $P_u$ , gross laminate failure or fastener failure had occurred which was indicated by a sharp drop in load level. The bearing strengths are calculated as follows:

$$\sigma_{t,i} = \text{initial bearing strength} = \frac{P_i}{D \cdot T}$$

$$\sigma_{t,u} = \text{ultimate bearing strength} = \frac{P_u}{D \cdot T}$$

where  $D$  = hole diameter  
 $T$  = laminate thickness

The effect of the specimen width to hole diameter (W/D) ratio on the bearing strength of IM6/5245C is shown in Figure 6. The edge distance to hole diameter (E/D) ratio was 3 and the diameter of the hole was 6.33 mm. A single hexagonal head steel fastener was used. The clamping pressure was kept reasonably constant by a fastener torque of 3.6 N.m. It is difficult to draw any conclusion because of the limited sample size tested to date and the large scatter in the data, however, it appears that the W/D ratio of 6 resulted in the highest bearing strength. An examination of the failure mode found that all specimens tested for W/D ratio effects failed in a shear-out/bearing mode (see Fig. 10(a)).

The effect of E/D ratio on the bearing strength of IM6/5245C is shown in Figure 7. Again, the limited sample size tested to date had made it difficult for firm conclusion to be drawn. Specimens with E/D ratio = 2 had the lowest ultimate bearing strength and failed in total shear-out mode (see Fig. 10(b)) and there is a falling off at higher E/D ratios.

The effect of hole size on the bearing strength of IM6/5245C is presented in Figure 8. Specimens with hole size = 9.33 mm had the highest ultimate bearing strength. Again, this conclusion is only preliminary because of the limited number of samples tested.

The effect of fastener torque on the ultimate bearing strength of IM6/5245C is presented in Figure 9. A dowel pin was used to transfer load in the double-lap joint for zero fastener torque test cases where the steel plates maintained a small gap between the composite laminate. Even though the sample size was small, a trend was obvious: composite laminate loaded by a dowel pin without lateral constraint had the lowest ultimate bearing strength; while increasing the fastener torque also increased the ultimate bearing strength but at a diminished rate. The trend for the effect of fastener torque on the initial bearing strength was less obvious (Fig. 9). The highest initial bearing strength was obtained when the fastener torque of 16.9 N.m was used.

Only one constant amplitude fatigue test has been performed to date on a double-lap joint with fastener hole size = 6.383 mm, W/D ratio = 8 and E/D ratio = 3. A dowel pin with a diameter = 6.330 mm was used for load transfer in the double-lap joint. This resulted in a hole clearance of only 0.333 mm. A bolted joint was simulated by using a C-clamp and two hexagonal nuts. Lateral clamping pressure in the dowel pin region was applied by clamping the nuts against the steel plates. The end of the screw in the C-clamp was modified so that a torque wrench could be used to apply a clamping load approximately equivalent to that obtained from using a torque level of 3.6 N.m on a similar size fastener. Maximum cyclic load level of 13.6 kN with a R ratio (minimum load/maximum load) of -1 was used to test the double-lap joint. The test was conducted in laboratory air environment. An extensometer with 102 mm gauge length was mounted on the specimen for hysteresis measurements before the start of the fatigue test and at predetermined numbers of cycles after the start of the fatigue test. The purpose of the hysteresis measurement was to determine the amount of hole elongation under cyclic loading. The amount of hole elongation was determined as follows:

$$\Delta_i = \text{hole elongation at } i\text{th cycle} = \delta_i - \delta_1$$

where  $\delta_1$  = total deflection measured at 1st cycle

$$\delta_i = \text{total deflection measured at } i\text{th cycle}$$

A summary of the constant amplitude fatigue test results is presented in Figure 11. A plot of hole elongation,  $\Delta$ , versus the number of cycles,  $N$ , is presented in Figure 12. Significant hole elongation (0.13 mm) was measured by hysteresis measurement technique at 83,000 cycles. At this point the joint was disassembled and the hole was measured. It was observed that the hole was elliptical with the major axis parallel to the loading direction. The length of the major axis was found to be 6.541 mm or a hole elongation (6.541 mm - 6.383 mm) of 0.158 mm. The actual hole elongation was 0.028 mm or 22% higher than that determined by hysteresis measurement. At this point, the composite laminate was C-scanned and bearing damage was found around the fastener hole. The fatigue test was continued until the hole elongation was found to be more than 10% of the hole diameter. At this stage, the fatigue test was stopped. Again, the joint was disassembled and the hole was measured. The length of the major axis of the elongated hole was found to be 7.303 mm. The actual hole elongation was determined to be 0.92 mm. The hysteresis measurement indicated an elongation of 0.73 mm which was 0.19 mm or 26% lower than the actual value. Again, the specimen was C-scanned which indicated the bearing damage had grown by approximately 30% since the last measurement at 83,000 cycles.

When the joint was disassembled, it was observed that graphite powder formed during the fatigue test was compressed into "flakes" that stuck to the pin surface as well as to the fastener hole surface. This graphite had reduced the clearance between the pin and the hole. When the joint was disassembled, these graphite layers "flaked" off the surface before the hole was measured. Consequently, the actual hole elongation is always less than that measured by the hysteresis measurement technique because of debris accumulation. However, the hysteresis measurement technique can detect hole elongation reasonably well and it is a good technique to use in cases where the joint cannot be disassembled.

Three fastener systems designed specifically for composite applications were selected for static testing in this program. The single-shear composite/titanium joint shown in Figure 3 was used for evaluating these fastener systems. Figure 13 shows the characteristics of fastener systems after installation in the composite laminate. The fastener systems selected are designed for galvanic compatibility with graphite-fiber composite. To accomplish this titanium or A-286 stainless steel are used in these fasteners. The SP3 COMP-TITE and the Cherry Maxifoot are blind fasteners with significantly improved blind head diameters which are essential to develop high clamping loads without crushing or delaminating the composite material during installation. Also, enlarged blind heads are required in composite fastening to resist pull-through loads and to resist fastener cocking associated with eccentric loads. The Huck titanium lockbolt is a two-piece fastener system designed specifically for interference fit installation in composites. The fastening principle is based on a swaging action which fills the locking grooves on the lockbolt with collar material to form a permanent lock. The sleeve expansion process in the hole during installation is the key to developing an interference fit. When applying this fastener system using 0.0762 mm tolerance holes, an interference fit range of 0.0254 mm to 0.1524 mm is possible. Tests performed at Huck<sup>(8)</sup> demonstrated that no damage occurred in the composite when this fastener system was installed with interferences up to 0.1778 mm on the diameter. Fastener removal tests demonstrated

that there was no significant plastic deformation or crushing in the hole as the hole returned to within 0.0254 mm of its original diameter for all interference levels. Interference fit is now becoming an important design consideration in mechanically fastened composite joints for a number of potential performance gains such as improved structural static and fatigue properties, improved load transfer in multi-fastener joints, electrical continuity and water/fuel tightness with no sealant.

Four composite/titanium joints have been tested to date. These four specimens were tested in static mode up to the ultimate tensile strength. Six strain gauges were mounted on these specimens as per the locations indicated in Figure 4(b). The two strain gauges on the composite plate measured the total strain while the two strain gauges on each titanium plate indicated the total load transfer as a result of fastener bearing and plate friction. Analysis of these strain gauge data have not been completed, so the results are not included in this short contribution. A constant amplitude fatigue test with tension-compression cyclic loading ( $R = -1$ ) is now underway. This test is on a joint fabricated with the SPS COMP-TITE fasteners. This joint was strain gauged according to the locations shown in Figure 4(a) to determine the amount of secondary bending.

The ultimate tensile strength for the joints using the two-piece Huck interference-fit fasteners was by far the highest. The average failure load of the two joints with Huck fasteners was 54.2 kN. This was 30% and 44% higher than the failure load of the blind joints using Cherry Maxifoot fasteners and SPS COMP-TITE fasteners respectively. The ultimate failure of all the joints tested was caused by shear failure of the fastener at the junction of the countersunk head and the fastener shaft. Significant fastener cocking under high tensile loading was observed for all fasteners which ultimately led to failure. Also both titanium plates were observed to bend outward at the free end under the influence of eccentric loading. Examination of the composite plates after the failure of the joints revealed bearing damage at both fastener holes. Crushing damage and delamination of the 45° surface ply with breakage of fibers were observed on the blind side or the collar side of the composite plate in the neighbourhood of the fastener hole (see Fig. 14).

### 5.8 CONCLUSIONS

Experimental data obtained to date from an on-going test program evaluating the performance of mechanical fastener systems in IM6/5205C were presented in this short contribution. Preliminary conclusions are as follows:

- (1) The notched strength of IM6/5205C was found to be higher (71%) than that of the conventional T300/5208 graphite/epoxy system.
- (2) Results from double-lap tensile tests indicated that the bearing strength was the highest when W/D ratio = 6. Decreasing the E/D ratio to 2 resulted in a change in failure mode from shear-out/bearing to total shear-out and also a decrease in bearing strength by 22%.
- (3) The bearing strength was found to be slightly higher for joints with a hole diameter of 9.35 mm than those with a hole diameter of 6.35 mm or 12.7 mm. The lowest ultimate bearing strength was obtained by loading with a dowel pin and without any lateral clamping constraint. The bearing strength was found to increase by increasing the fastener torque.
- (4) A technique based on hysteresis measurements was found to be a simple and effective way to measure the amount of hole elongation under cyclic loading. This technique is extremely useful in cases where the joint cannot be disassembled during testing.
- (5) The Huck interference-fit lockbolt fastener system was found to provide a single-shear joint strength 30% and 44% higher than that provided by the Cherry Maxifoot blind fastener system and that provided by the SPS COMP-TITE blind fastener system respectively.
- (6) A method based on the concept of 5% offset slope was proposed to obtain the initial failure load from a load versus deflection curve of a tensile joint test.

### ACKNOWLEDGEMENT

This work is accomplished by the support of the Department of National Defence Canada through Financial Encumbrance No. 325-F-093. The Cscan inspection services provided by Mr. T. Chapman, the technical support provided by Mr. T. Benak and the assistance provided by Mr. M. Tratt of Canadair for the installation of Huck interference fit fasteners are gratefully acknowledged. Also, services provided by the NAE Materials Laboratory and machine shop are acknowledged.

### REFERENCES

1. Collings, T.A., "The Strength of Bolted Joints in Multi-Directional CFRP Laminates", *Composites*, Vol. 8, No. 1, January 1977, pp. 43-55.
2. Weinberger, R.A., Somoroff, A.R. and Riley, B.L., "U.S. Navy Certification of Composite Wings for the F-18 and Advanced Harrier Aircraft", AIAA Paper, No. 77-466, 1977.
3. Lee, A., "A Material Selection Review for the MILP Contract on Development of Advanced Composite Materials Technology", Canadair Memorandum No. MCM-000-118, November 1984.
4. Poon, C., "Literature Review on the Design of Mechanically Fastened Composite Joints", National Research Council Canada, Report No. 23442, February 1986.
5. Poon, C., "Evaluation of Mechanical Fastener Systems in Advanced Composites", National Aeronautical Establishment, Laboratory Memorandum, ST-411, April 1986.

6. Butler, R.J. and Butler, A.L., "LAMANAL: A Program for the Design and Analysis of a Laminated Plate", Cranfield Institute of Technology, Cranfield, UK, 1986.
7. Collings, T.A., "The Strength of Bolted Joints in Multi-Directional CFRP Laminates", ARC CP No. 1380, December 1975.
8. Phillips, J.L., "Manual and Automated Fastening of Composite Structures", SME Paper No. AD85-07, 1985.
9. Scott, R. and Leo, S., unpublished report.

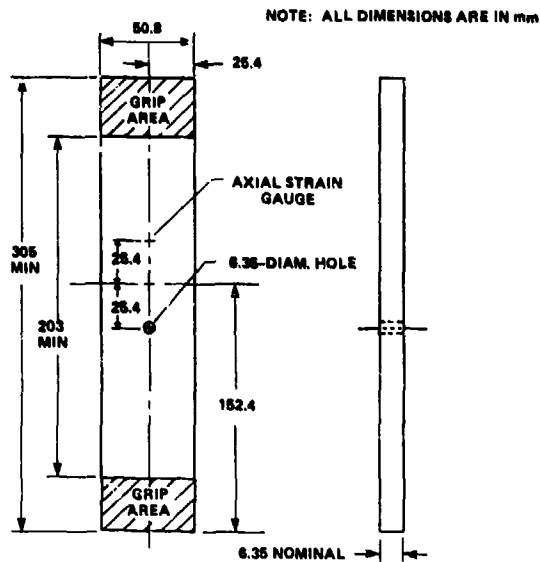
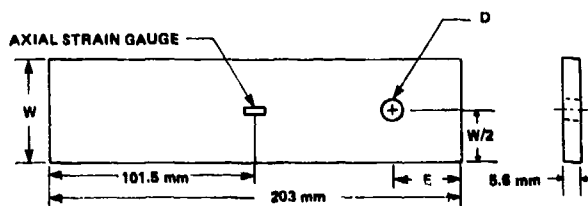
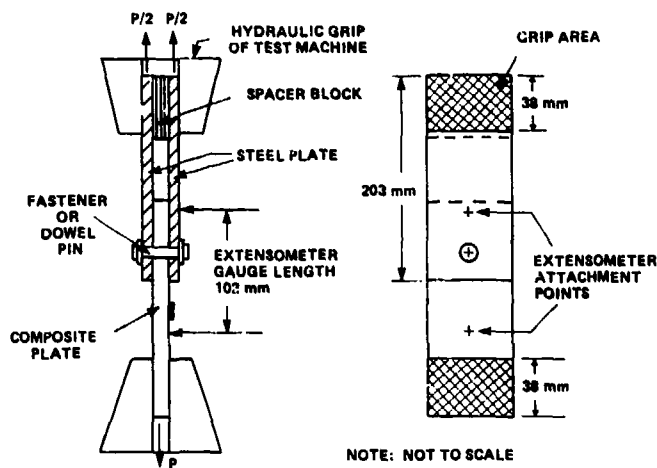


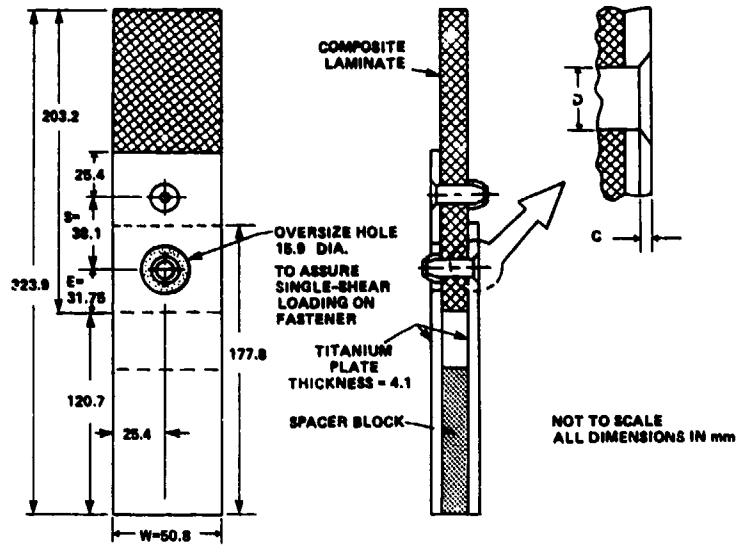
FIG. 1: OPEN-HOLE TENSION TEST SPECIMEN



IM6/5245C, (45°/0°/-45°/0°/90°/0°/45°/0°/-45°/0°)<sub>2S</sub>

GEOMETRIC RATIO DIMENSIONS, mm				
W/D	E/D	W	E	D
4	5	25.4	31.8	6.35
4	5	38.1	47.8	9.53
4	5	50.8	63.5	12.70
6	5	38.1	31.8	6.35
6	5	50.8	31.8	6.35
8	3	50.8	19.1	6.35
8	2	50.8	12.7	6.35

FIG. 2: DOUBLE-LAP JOINT FOR EVALUATING BEARING STRENGTH



MATERIAL SYSTEM: IM6/S248C  
 LAY-UP: 50/40/10  
 STACKING SEQUENCE: (+45°/0°/-45°/0°/90°/0°/45°/0°/-45°/0°)<sub>25</sub>  
 THICKNESS: 5.18 mm (40 PLIES)  
 TITANIUM ALLOY: ASTM B265 GRADE 5 (Ti 6Al-4V)

FASTENER SYSTEM	HEAD CONFIGURATION	HOLE DIAMETER	FASTENER DIA.	DIMENSION C
SPS COMP-TITE CT-410-S-400	100° FLUSH	6.804 - 6.680	6.563 - 6.591	2.64
HUCK CIL-8SC-VCDS-06	100° FLUSH	6.680 - 6.756	6.642 - 6.668	2.85
CHERRY MAXIFOOT CR-8686-S-6	130° FLUSH	6.617 - 6.680	6.541 - 6.604	1.45

FIG. 3: SINGLE-SHEAR COMPOSITE/TITANIUM JOINT FOR FASTENER EVALUATION

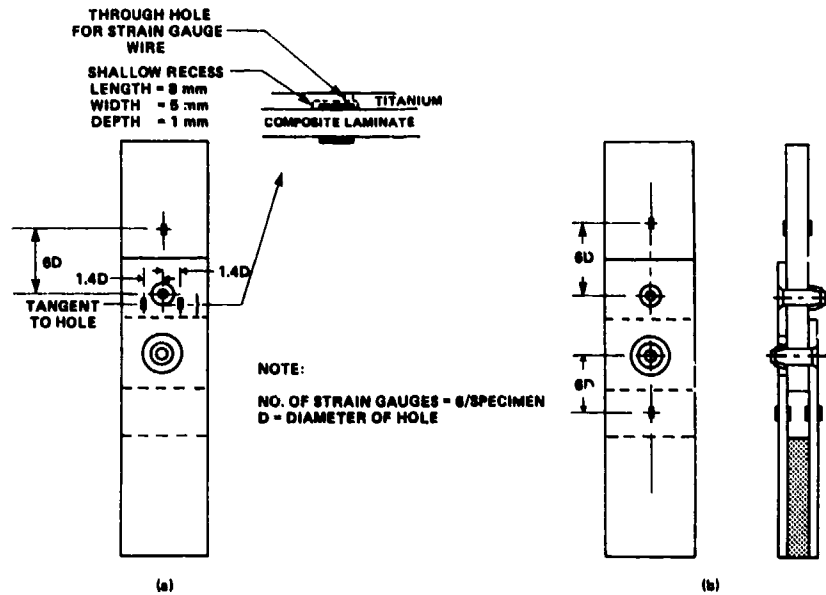


FIG. 4: LOCATION OF STRAIN GAUGES FOR COMPOSITE/TITANIUM JOINT

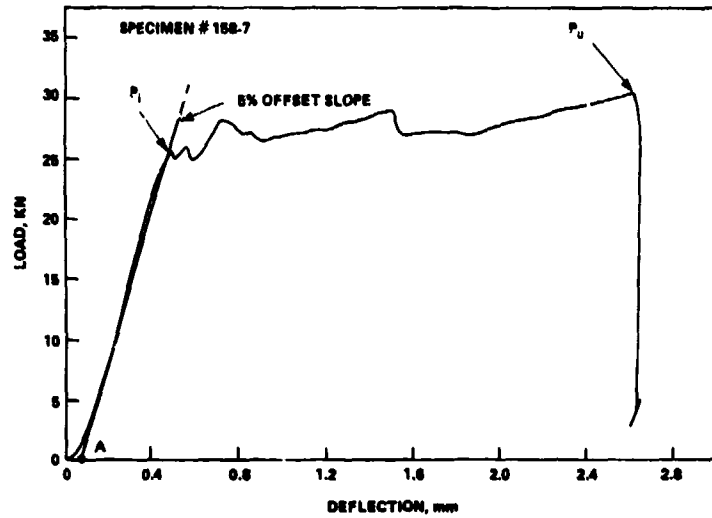


FIG. 5: LOAD vs DEFLECTION CURVE FOR DOUBLE-LAP JOINT

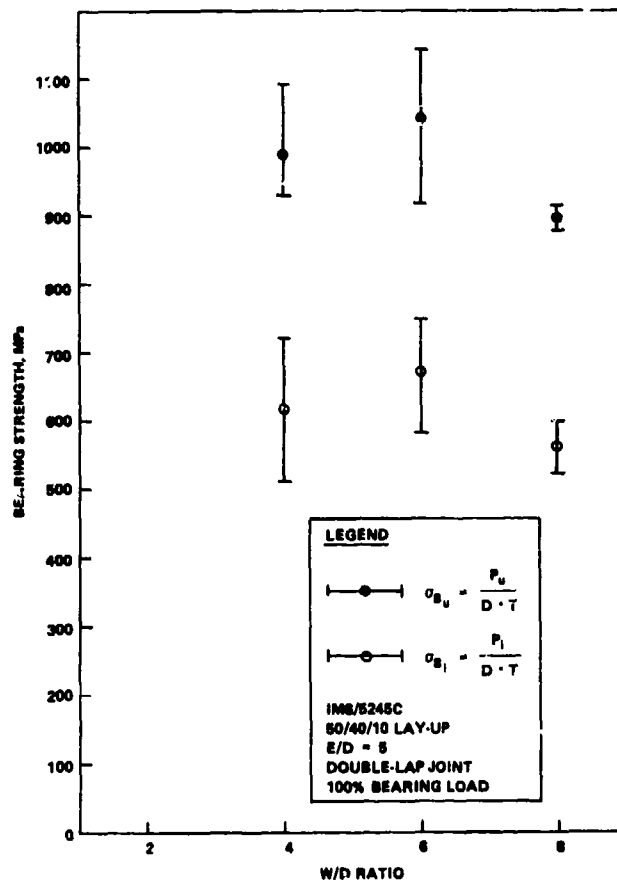


FIG. 6: EFFECT OF W/D RATIO ON BEARING STRENGTH

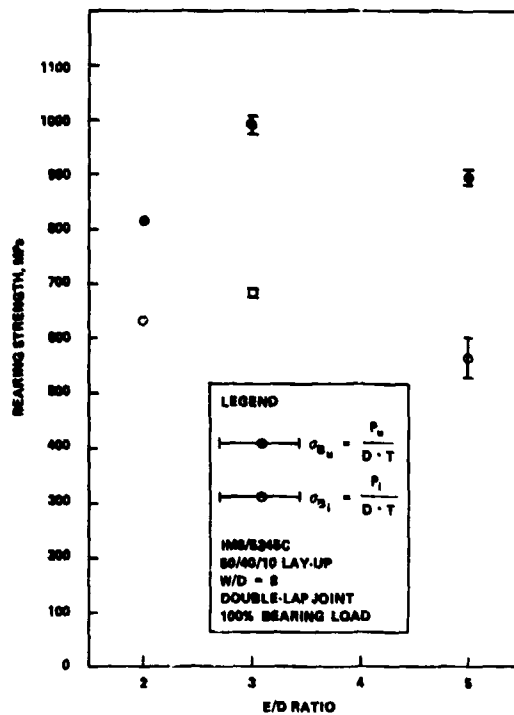


FIG. 7: EFFECT OF E/D RATIO ON BEARING STRENGTH

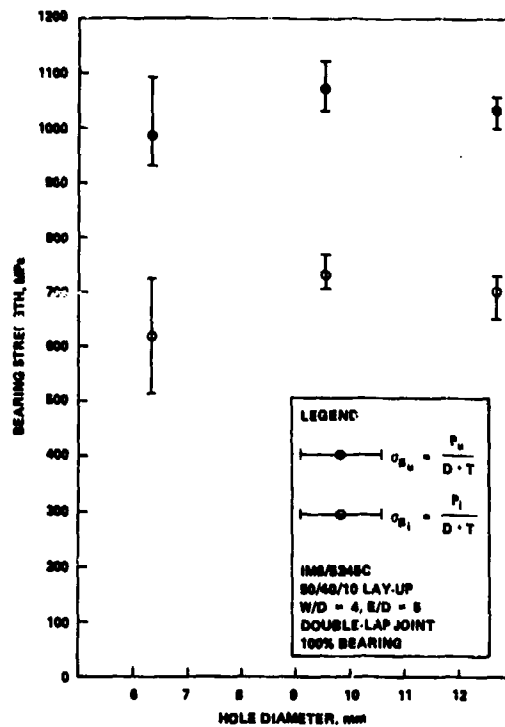


FIG. 8: EFFECT OF HOLE SIZE ON BEARING STRENGTH

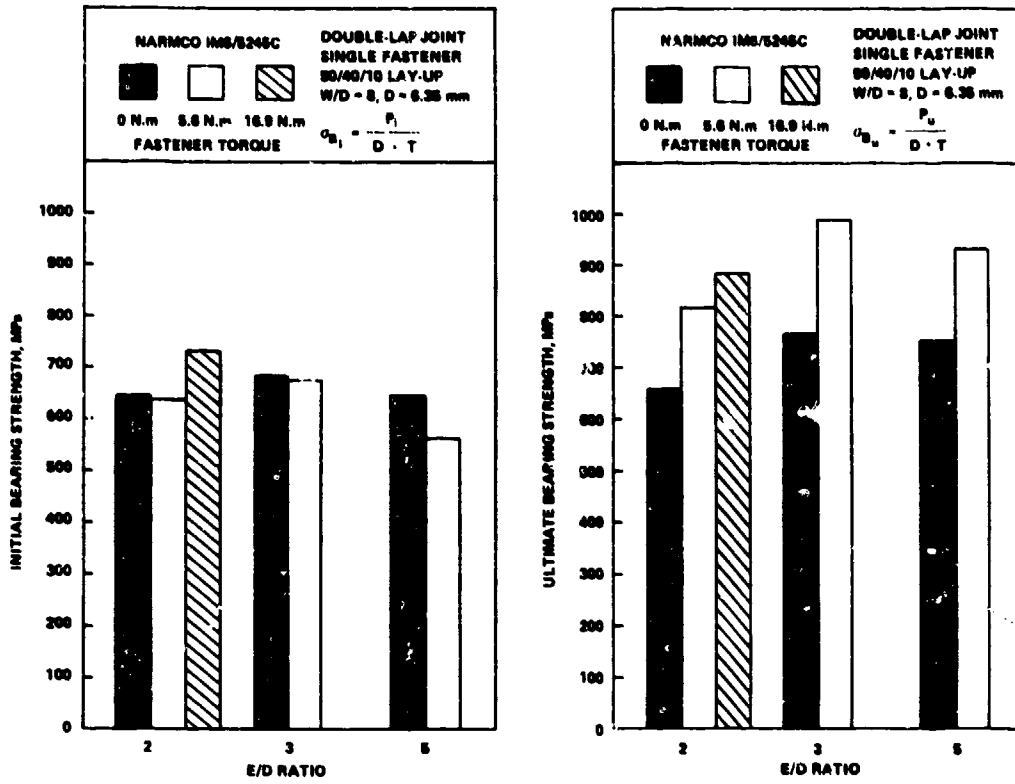


FIG. 9: EFFECT OF FASTENER TORQUE ON BEARING STRENGTH

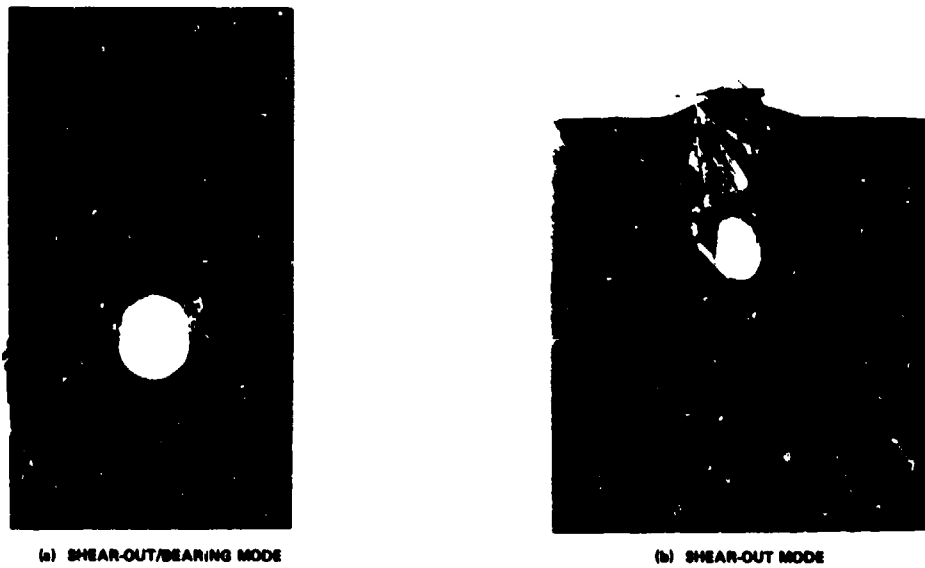
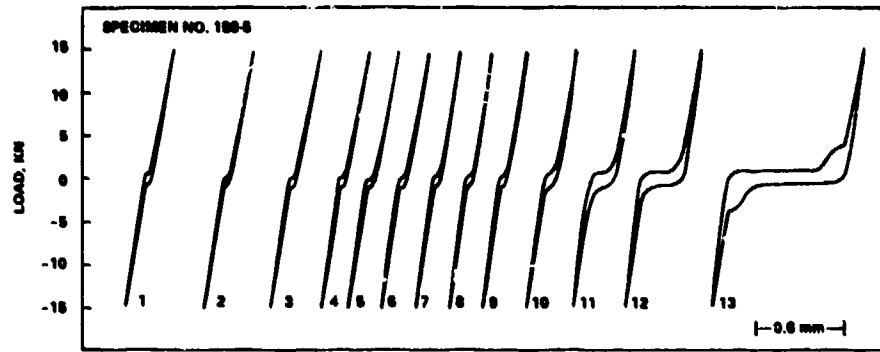


FIG. 10: FAILURE MODES FOR IM6/5248C DOUBLE-LAP JOINT



NARMCO IM8/S248C, LAY-UP (45°/0°/-45°/0°/90°/0°/45°/0°/-45°/0°) 20, DOUBLE-LAP JOINT												
HYSTERESIS CURVE #	1	2	3	4	5	6	7	8	9	10	11	13
1 <sup>st</sup> CYCLE	1	10	100	1,000	5,000	10,000	20,000	30,000	40,000	60,000	80,000	120,000
DEFLECTION, $\delta_1$ , mm	0.33	0.33	0.33	0.33	0.33	0.33	0.33	0.33	0.36	0.37	0.46	0.88
HOLE ELONGATION $\delta_1 - \delta_1$ , mm	0.00	0.00	0.00	0.00	0.00	0.00	0.70	0.00	0.02	0.04	0.13	0.73

FIG. 11: CONSTANT AMPLITUDE FATIGUE TEST RESULTS

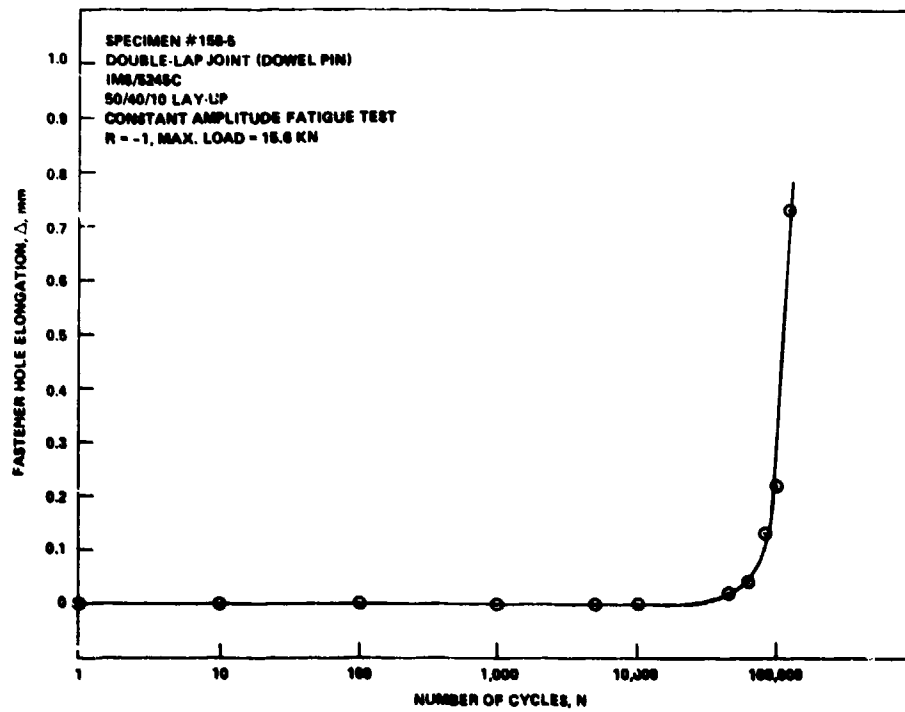
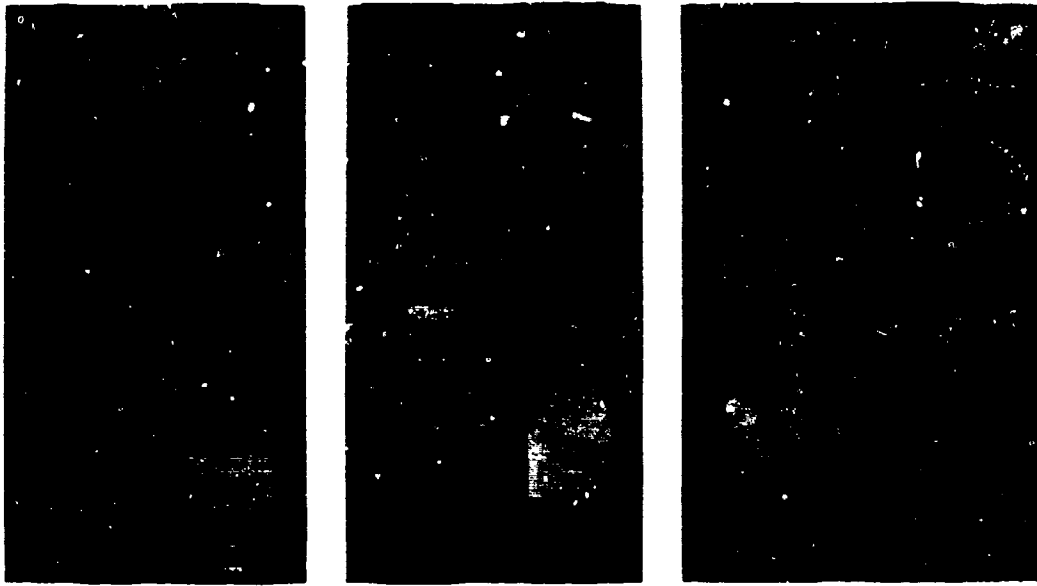


FIG. 12:  $\Delta$  vs N CURVE



(a) HUCK INTERFERENCE-FIT  
LOCKBOLT

(b) CHERRY MAXIFOOT FASTENER

(c) SP6 COMP-TITE FASTENER

FIG. 13: SINGLE-SHEAR COMPOSITE/TITANIUM JOINTS FOR FASTENER EVALUATION



FIG. 14: COMPOSITE DAMAGE ON THE  
BLIND-HEAD SIDE

REPORT DOCUMENTATION PAGE			
1. Reclplant's Reference	2. Originator's Reference	3. Further Reference	4. Security Classification of Document
	AGARD-CP-427	ISBN 92-835-0431-3	UNCLASSIFIED
5. Originator	Advisory Group for Aerospace Research and Development North Atlantic Treaty Organization 7 rue Ancelle, 92200 Neuilly sur Seine, France		
6. Title	BEHAVIOUR AND ANALYSIS OF MECHANICALLY FASTENED JOINTS IN COMPOSITE STRUCTURES		
7. Presented at	the Structures and Materials Panel Specialists' Meeting held in Madrid, Spain on 27-29 April 1987.		
8. Author(s)/Editor(s)	Various		9. Date March 1988
10. Author's/Editor's Address	Various		11. Pages 316
12. Distribution Statement	This document is distributed in accordance with AGARD policies and regulations, which are outlined on the Outside Back Covers of all AGARD publications.		
13. Keywords/Descriptors	<p>→ Joints (junctions), Composite materials, Mechanical properties,</p> <p>Life (durability), Mechanical tests, Research projects. (JES) ←</p>		
14. Abstract	<p>↙</p> <p>The rapidly increasing use of composite structures in NATO aerospace has intensified interest in methods of strength, and life analysis. At the same time the introduction of new tough resins has increased the static strength of composite joints with implications for the corresponding strength in fatigue. A number of NATO nations have built up data bases and developed methods for strength and life analyses; in order to take advantage of these resources the Structures and Materials Panel held a Specialists' Meeting, in conjunction with the 64th Panel Meeting, at Madrid, Spain on 27th-29th April 1987, under the chairmanship of Professor Vittorio Giavotto, to provide a focus for methods of analysis and the identification of research needs. This volume contains the papers presented at this Specialists' Meeting.</p>		

<p>AGARD Conference Proceedings No.427 Advisory Group for Aerospace Research and Development, NATO <b>BEHAVIOUR AND ANALYSIS OF MECHANICALLY FASTENED JOINTS IN COMPOSITE STRUCTURES</b> Published March 1988 316 pages</p> <p>The rapidly increasing use of composite structures in NATO aerospace has intensified interest in methods of strength, and life analysis. At the same time the introduction of new tough resins has increased the static strength of composite joints with implications for the corresponding strength in fatigue. A number of NATO nations have built up data bases and developed methods for strength and</p> <p>P.T.O.</p>	<p>AGARD-CP-427</p> <p>Joints (junctions) Composite materials Mechanical properties Life (durability) Mechanical tests Research projects</p>	<p>AGARD Conference Proceedings No.427 Advisory Group for Aerospace Research and Development, NATO <b>BEHAVIOUR AND ANALYSIS OF MECHANICALLY FASTENED JOINTS IN COMPOSITE STRUCTURES</b> Published March 1988 316 pages</p> <p>The rapidly increasing use of composite structures in NATO aerospace has intensified interest in methods of strength, and life analysis. At the same time the introduction of new tough resins has increased the static strength of composite joints with implications for the corresponding strength in fatigue. A number of NATO nations have built up data bases and developed methods for strength and</p> <p>P.T.O.</p>	<p>AGARD-CP-427</p> <p>Joints (junctions) Composite materials Mechanical properties Life (durability) Mechanical tests Research projects</p>
<p>AGARD Conference Proceedings No.427 Advisory Group for Aerospace Research and Development, NATO <b>BEHAVIOUR AND ANALYSIS OF MECHANICALLY FASTENED JOINTS IN COMPOSITE STRUCTURES</b> Published March 1988 316 pages</p> <p>The rapidly increasing use of composite structures in NATO aerospace has intensified interest in methods of strength, and life analysis. At the same time the introduction of new tough resins has increased the static strength of composite joints with implications for the corresponding strength in fatigue. A number of NATO nations have built up data bases and developed methods for strength and</p> <p>P.T.O.</p>	<p>AGARD-CP-427</p> <p>Joints (junctions) Composite materials Mechanical properties Life (durability) Mechanical tests Research projects</p>	<p>AGARD Conference Proceedings No.427 Advisory Group for Aerospace Research and Development, NATO <b>BEHAVIOUR AND ANALYSIS OF MECHANICALLY FASTENED JOINTS IN COMPOSITE STRUCTURES</b> Published March 1988 316 pages</p> <p>The rapidly increasing use of composite structures in NATO aerospace has intensified interest in methods of strength, and life analysis. At the same time the introduction of new tough resins has increased the static strength of composite joints with implications for the corresponding strength in fatigue. A number of NATO nations have built up data bases and developed methods for strength and</p> <p>P.T.O.</p>	<p>AGARD-CP-427</p> <p>Joints (junctions) Composite materials Mechanical properties Life (durability) Mechanical tests Research projects</p>

<p>life analyses; in order to take advantage of these resources and Structures and Materials Panel held a Specialists' Meeting, in conjunction with the 64th Panel Meeting, at Madrid, Spain on 27th-29th April 1987, under the chairmanship of Professor Vittorio Ciavotto, to provide a focus for methods of analysis and the identification of research needs. This volume contains the papers presented at this Specialists' Meeting.</p> <p>ISBN 92-835-0431-3</p>	<p>life analyses; in order to take advantage of these resources and Structures and Materials Panel held a Specialists' Meeting, in conjunction with the 64th Panel Meeting, at Madrid, Spain on 27th-29th April 1987, under the chairmanship of Professor Vittorio Ciavotto, to provide a focus for methods of analysis and the identification of research needs. This volume contains the papers presented at this Specialists' Meeting.</p> <p>ISBN 92-835-0431-3</p>
<p>life analyses; in order to take advantage of these resources and Structures and Materials Panel held a Specialists' Meeting, in conjunction with the 64th Panel Meeting, at Madrid, Spain on 27th-29th April 1987, under the chairmanship of Professor Vittorio Ciavotto, to provide a focus for methods of analysis and the identification of research needs. This volume contains the papers presented at this Specialists' Meeting.</p> <p>ISBN 92-835-0431-3</p>	<p>life analyses; in order to take advantage of these resources and Structures and Materials Panel held a Specialists' Meeting, in conjunction with the 64th Panel Meeting, at Madrid, Spain on 27th-29th April 1987, under the chairmanship of Professor Vittorio Ciavotto, to provide a focus for methods of analysis and the identification of research needs. This volume contains the papers presented at this Specialists' Meeting.</p> <p>ISBN 92-835-0431-3</p>

**AGARD**

**NATO OTAN**

**7 rue Ancoille • 92100 NEUILLY-SUR-SEINE  
FRANCE**

**Telephone (1)47.38.87.80 • Telex 610 178**

**DISTRIBUTION OF UNCLASSIFIED  
AGARD PUBLICATIONS**

AGARD does NOT hold stocks of AGARD publications at the above address for general distribution. Initial distribution of AGARD publications is made to AGARD Member Nations through the following National Distribution Centres. Further copies are sometimes available from these Centres, but if not may be purchased in microfiche or Photocopy form from the Purchase Agencies listed below.

**NATIONAL DISTRIBUTION CENTRES**

**BELGIUM**

Coordonnateur AGARD - VSL  
Euse-Major de la Force Aérienne  
Quartier Reine Elisabeth  
Rue d'Evre, 1140 Brussels

**CANADA**

Director Scientific Information Services  
Dept of National Defence  
Ottawa, Ontario K1A 0K2

**DENMARK**

Danish Defence Research Board  
Ved Idraetsparken 4  
2100 Copenhagen Ø

**FRANCE**

O.N.E.R.A. (Direction)  
29 Avenue de la Division Leclerc  
92320 Châtillon

**GERMANY**

Fachinformationszentrum Energie,  
Physik, Mathematik GmbH  
Karlsruhe  
D-7514 Eggenstein-Leopoldshafen 2

**GREECE**

Hellenic Air Force General Staff  
Aircraft Support Equipment Directorate  
Department of Research and Development  
Holargos, Athens, 15500

**ICELAND**

Director of Aviation  
c/o Flugrad  
Reykjavik

**UNITED STATES**

National Aeronautics and Space Administration (NASA)  
Langley Research Center  
M/S 180  
Hampton, Virginia 23665

**THE UNITED STATES NATIONAL DISTRIBUTION CENTRE (NASA) DOES NOT HOLD STOCKS OF AGARD PUBLICATIONS, AND APPLICATIONS FOR COPIES SHOULD BE MADE DIRECT TO THE NATIONAL TECHNICAL INFORMATION SERVICE (NTIS) AT THE ADDRESS BELOW.**

**PURCHASE AGENCIES**

National Technical  
Information Service (NTIS)  
5285 Port Royal Road  
Springfield  
Virginia 22161, USA

ESA/Information Retrieval Service  
European Space Agency  
10, rue Mario Nikis  
75015 Paris, France

The British Library  
Document Supply Division  
Boston Spa, Wetherby  
West Yorkshire LS23 7BQ  
England

Requests for microfiche or photocopies of AGARD documents should include the AGARD serial number, title, author or editor, and publication date. Requests to NTIS should include the NASA accession report number. Full bibliographical references and abstracts of AGARD publications are given in the following journals:

Scientific and Technical Aerospace Reports (STAR)  
published by NASA Scientific and Technical  
Information Branch  
NASA Headquarters (NIT-40)  
Washington D.C. 20546, USA

Government Reports Announcements (GRA)  
published by the National Technical  
Information Service, Springfield  
Virginia 22161, USA



Printed by Specialized Printing Services Limited  
40 Chigwell Lane, Loughton, Essex IG10 3TZ

ISBN 92-835-0431-3